Carbohydrate Functionalized Gold Nanoparticles Encode Bacterial Targeting and Immunomodulation

A Thesis

Submitted in partial fulfilment of the requirements

for the degree of

Doctor of Philosophy

By

Suraj Toraskar

Registration ID – 20153377

Under the guidance of

Dr. Raghavendra Kikkeri

Indian Institute of Science Education and Research, Pune – 411008

This thesis is dedicated to my parents.

For their love, encouragement and blessings

CERTIFICATE

This is to certify that the work incorporated in this thesis entitled "**Carbohydrate Functionalized Gold Nanoparticles Encode Bacterial Targeting and Immunomodulation**" submitted by **Suraj Toraskar** was carried out by a candidate at the Indian Institute of Science Education and Research, Pune under my supervision. The work presented here or any part of it has not been included in any other thesis submitted previously for the award of any degree or diploma from any other university or institution.

Date: 01-11-2021

Dr. Raghavendra Kikkeri
Associate Professor
IISER, Pune

DECLARATION

I hereby declare that the thesis entitled "**Carbohydrate Functionalized Gold Nanoparticles Encode Bacterial Targeting and Immunomodulation**" submitted for the Doctor of Philosophy in Chemistry Department at Indian Institute of Science Education and Research, Pune, has not been submitted by me to any other university or institution. This work presented here was carried out at the Indian Institute of Science Education and Research, Pune, India, under the supervision of **Dr. Raghavendra Kikkeri**.

Date: 01/11/2021

Suraj Toraskar

ID: 20153377

Acknowledgement

Foremost, I would like to express my sincere gratitude to my thesis advisor Dr Raghavendra Kikkeri for his incredible support during my PhD journey. His continuous support, encouragement, patience, enthusiasm and valuable insights helped me all the time. I could not have imagined having a better advisor and mentor for my PhD. Working in your lab has been an honour and privilege, and I have been enjoying it.

I would like to thank my Research Advisory Committee sincerely: Dr Krishanpal Karmodiya from IISER Pune and Dr Chepuri V Ramana from NCL Pune for their motivation, insightful comments, and fruitful discussions. I would like to thank Prof Dr Peter H Seeberger from MPIKG for hosting me as an EMBO Short Term Fellow and providing excellent research facilities.

My sincere thanks to our collaborators, Prof. Dr Peter H Seeberger from Germany, Dr Vered Padler-Karavani from Tel-Aviv University, Israel, Dr Mattan Hurevich from the Hebrew University of Jerusalem, Israel and Dr H. V. Thulasiram from NCL Pune for their kind cooperation, efforts and valuable time.

I would like to thank CSIR-INDIA for providing me with financial support and EMBO for Short Term Fellowship. My sincerest thanks to Director IISER Pune and Chair Chemistry for providing excellent research facilities. Many thanks to faculty, technician and instrument operators at the Department of Chemistry and Biology IISER Pune for helping me in crucial departmental activities and accelerating our research work.

I would like to thank my lab mate (RK Group) for help, adventure trips, parties, and stimulating discussions throughout the process. Special thanks to Dr Preeti, Dr Raghavendra Murthy, Dr Rohan, Dr Harikrishna, Dr Sivakoti and Dr

Madhuri for enlightening me with the first glance of Chemistry and Biology. A big thanks to Chathan, Balamurugan, Prashant and Trimbak for their incredible support and always being there. Huge thanks to Sandhya, Vijendra, Rakesh, Saurabh, Sharath, Virendra, Ankita, Deepak and Remya for a joyful and healthy environment at the lab. My warm thanks to Keerthana TV for having a great time and beautiful memories.

I am very grateful for having unique and stunning friends in my life. Many thanks to Santosh Panchal, Pradeep Desale, Gulab Walke, Rahul Jagtap, Madan Ambhore, Rahul Bhosale, Shankar Surle, and Avi Sapkal. I sincerely appreciate your constant guidance, your spirit and making the ordinary moments in life extraordinary. Thanks to cricket teams Resonance and Radical, I am lucky to be part of these teams. Thanks to IISER friends and community for their generous support.

I feel lucky to have you as my life partner to my caring and thoughtful wife, Akanksha. Thanks for your support, patience, encouragement, and your love. I am very grateful and proud to have such a lovely and compassionate family that cares about me and loves me. You have always helped me accomplish my goals and dreams. Thank you, god, for all your blessing to me.

Suraj Toraskar

Table of Contents

Chapter-3: Gold Nanoparticles Mediated Immune modulation of N-Glycolylneuraminic acid Glycans

Chapter-4: Shapes of Nanostructures Encode Immunomodulation of Carbohydrate Antigen and Vaccine Development

Abbreviations

A

Ac	Acetyl
Ac_2O	Acetic anhydride
AcOH	Acetic acid
All	Allyl
AuNPs	Gold Nanoparticles

B

BDAC	Benzyldimethylhexadecylammonium chloride
Bn	Benzyl
Boc	tert-Butyloxycarbonyl
BSA	Bovine Serum Albumin
Bu	Butyl
Bz	Benzoyl

C

CAM	Cerium Ammonium Molybdate
Cbz	Benzyl chloroformate
CPIs	Carbohydrate Protein Interactions
ConA	Concanavalin A
CRM 197	Cross Reacting Material 197
CTAB	Cetyltrimethylammonium bromide

D

DAPI	4′,6-diamidino-2-phenylindole
DBU	1,8-Diazabicyclo[5.4.0]undec-7-ene
DCs	Dendritic Cells
DCC	N,N′-dicyclohexylcarbodiimide
DCM	Dichloromethane
DIPEA	N,N-Diisopropylethylamine

DMAP	4-Dimethylaminopyridine
DMEM	Dulbecco's Modified Eagle's Medium
DMF	Dimethylformamide
DTT	Dithiothreitol

E

ECM	Extracellular Matrix
EDTA	Ethylenediaminetetraacetic acid
ELISA	Enzyme Linked Immunosorbent Assay

F

FACS	Fluorescence Activated Single Cell Sorting
FBS	Fetal Bovine Serum
FDA	Food and Drug Administration
FITC	Fluorescein isothiocyanate
Fmoc	Fluorenylmethoxycarbonyl

G

GAGs	Glycosaminoglycans
Gal	Galactose
GalN	Galactosamine
GM	Monosialodihexosylganglioside

H

HBTU	(2-(1H-benzotriazol-1-yl)-1,1,3,3-tetramethyluronium hexafluorophosphate, Hexafluorophosphate Benzotriazole Tetramethyl Uronium)
HEPS	(4-(2-hydroxyethyl)-1-piperazineethanesulfonic acid)
HCA	Hierarchical Cluster Analysis
HOBT	Hydroxybenzotriazole
HR-ESI-MS	High Resolution Electrospray Ionization Mass Spectroscopy
HRP	Horseradish Peroxidase
HR-SEM	High Resolution Scanning Electron Microscopy

HR-TEM	High Resolution Transmission Electron Microscopy

I

IFN-γ	Interferon gamma
IL	Interleukin
IMDM	Iscove's Modified Dulbecco's Media

M

MACS	Magnetic-activated Cell Sorting
MALDI-TOF	Matrix-Assisted Laser Desorption/Ionization-Time of Flight
mDC	Murine Dendritic Cell
MS	Molecular Sieves
MUC	Mucus

N

NHS	N-Hydroxysuccinamide
NIS	N-Iodosuccinimide
NMP	N-Methyl-2-pyrrolidone
NMR	Nuclear Magnetic Resonance
NPs	Nanoparticles

P

PBS	Phosphate Buffered Saline
PFP	Pentaflurophenol
PhOH	Phenol
PTSA	*p*-Toluenesulfonic Acid
py	Pyridine

R

RFU	Relative Fluorescence Units
RP-HPLC	Reverse Phase High Performance Liquid Chromatography

RPMI	Roswell Park Memorial Institute
RT	Room Temperature

S

SAR	Structure-Activity Relationship
SD	Standard Deviation
SDS	Sodium Dodecyl Sulfate
SSPS	Solid Phase Peptide Synthesis
STol	4-Mercaptotoluene

T

TACAs	Tumor Associated Carbohydrate Antigens
TBAF	Tetrabutylammonium Iodide
TBDPS-Cl	tert-Butyldiphenylsilyl Chloride
TD	T Cell Dependent
TCEP	(tris(2-carboxyethyl)phosphine)
TFA	Trifluroacetic Acid
TfOH	Trifluoromethanesulfonic acid
THF	Tetrahydrofuran
TIPS	Triisopropyl Silane
TLC	Thin Layer Chromatography
TLR	Toll Like Receptor
TMB	3,3′,5,5′-Tetramethylbenzidine
TMSOTf	Trimethylsilyl Trifluoromethanesulfonate
TNF-α	Tumor Necrosis Factor Alpha
Troc	2,2,2-Trichloroethoxycarbonyl

Abstract

Carbohydrates play a pivotal role in the maintenance of the structure and function of cells, and their importance is particularly evident during the course of cell development and differentiation. Nevertheless, carbohydrate-protein interactions (CPIs) are feeble; hence, nature uses the multivalent display of carbohydrates (so-called 'glycocalyx') to increase the avidity of the carbohydrate interactions. Following the glycocalyx structure, researchers decorated monovalent carbohydrate ligands on multivalent probes such as nanoparticles, polymers, dendrimers, and liposomes to study carbohydrate-carbohydrate and carbohydrate-protein interactions. In my thesis, I have investigated the role of different sizes and shapes of nanoparticles constructed from gold materials and carbohydrate ligands and their applications in bacterial biosensors, immune modulation, and vaccine development.

Chapter 1 summarizes different multivalent carbohydrate probes and their major biological and medical applications. More specifically, we address synthetic strategies used for decorating the different types of multivalent systems, ranging from nanoparticles to supramolecular structures of different shapes, to fine tune the spatial arrangement of carbohydrate ligands to improve the avidity of CPIs. Finally, we discuss Kikkeri lab findings on the shape of the nanoparticles' mediated modulation of carbohydrate-protein interactions.

Chapter 2 describes the synthesis of multivalent probes composed of heterogeneous carbohydrate ligands and different topologies of gold nanoprobes for selective targeting and inhibiting bacterial infection. The α-D-mannose and β-D-galactose were successfully conjugated to the homo and heterogenous glycodendrons, followed by functionalizing these ligands on sphere- and rod-shaped gold nanoparticles to generate dual-functional probes. Bacterial binding and inhibition assays were examined in FimH-expressed and knockout *E. coli* bacteria. Noticeably, the multivalent display and shape of the nanoprobes showed remarkable sensitivity and selectivity for FimH-mannose-mediated *E. coli* binding. At the same time, the heterogeneity of the dendrons showed the least impact on bacterial adhesion. This trend continued even with the inhibition of bacterial infection of HeLa cells, revealing new insight into the role of gold nanoparticles (AuNPs) shapes and heterogeneity in carbohydrate-protein interactions.

Chapter 3 deals with deciphering the size of gold nanoparticles that mediate immune modulation of sialic acid antigens. As a prototype, we synthesized Neu5Gc antigen ubiquitously expressed on human tissues, and interaction with anti-Neu5Gc antibodies

enhanced inflammation, which could facilitate tumor progression. In this project, we functionalized Neu5Gc glycan on gold nanoparticles of different sizes and immunized the Cmah-knockout mice. As a control, Neu5Gc glycan was also functionalized on CRM197 protein and immunized with an alum adjuvant. We found that carbohydrates were not able to induce effective immune responses compared to the CRM197 conjugated system. To facilitate better immune responses of Neu5Gc glycans. We have synthesized a tripartite system composed of synthetic TLR7/8 adjuvant, Neu5Gc glycopeptides, and cholesterol moiety. Covalent linkage of these three components is expected to drive the Neu5Gc antigen to the lymph node and modulate T-cell-dependent immune responses.

Chapter 4 demonstrate the design and synthesis of CpG-adjuvant coated sphere-, rod-, and star-shaped AuNPs were conjugated to the tripodal Tn-glycopeptide antigen to study their DC uptake and the activation of T-cells in the DCs/T-cell co-culture assay. Our results showed that sphere- and star-shaped AuNPs displayed relatively weak receptor-mediated uptake, endosomal sequestration induced a high level of T helper-1 (Th1) biasing immune responses compared with rod-shaped AuNPs, showing that receptor-mediated uptake and cytokine secretion of nanostructures are two independent mechanisms. Significantly, the shapes of AuNPs and antigen/adjuvant conjugation synergistically work together to modulate the effective anti-Tn-glycopeptide immunoglobulin (IgG) antibody response after *in vivo* administration of the AuNPs. These results show that by varying the shape parameter, one can alter the immunomodulation, leading to the development of carbohydrate vaccines.

Publications

1. Sangabathuni, S.; Murthy, R. V.; Chaudhary, P. M.; Subramani, B.; **Toraskar, S**.; Kikkeri, R. Mapping the Glyco-Gold Nanoparticles of Different Shapes Toxicity, Bio-Distribution and Sequestration in Adult Zebrafish. *Sci. Rep.* **2017**, *7*, 4239.
2. **Toraskar, S**.; Gade, M.; Sangabathuni, S.; Thulasiram, H. V.; Kikkeri, R. Exploring the Influence of Shapes and Heterogeneity of Glyco-Gold Nanoparticles on Bacterial Binding for Preventing Infections. *ChemMedChem*. **2017**, *12*, 1116-1124.
3. Sangabathuni, S.; Murthy, R. V.; Gade, M.; Bavireddi, H.; **Toraskar, S**.; Sonar, M. V.; Ganesh, K. N.; Kikkeri, R. Modeling Glyco-Collagen Conjugates Using a Host-Guest Strategy to Alter Phenotypic Cell Migration and *in Vivo* Wound Healing. *ACS Nano*. **2017**, *11*, 11969-11977.
4. Yadav, R.; Chaudhary, P. M.; Subramani, B.; **Toraskar, S**.; Bavireddi, H.; Murthy, R. V.; Sangabathuni, S.; Kikkeri, R. Imaging and Targeting of the α(2-6) and α(2-3) Linked Sialic Acid Quantum dots in Zebrafish and Mouse Models. *Acs Appl Mater Interfaces.* **2018**, *34*, 28322-28330.
5. Chaudhary, P. M.; **Toraskar, S**.; Yadav, R.; Hande, A.; Yellin, R. A.; Kikkeri, R. Multivalent Sialosides: A Tool to Explore the Role of Sialic Acids in Biological Processes. *Chem Asian J*. **2019**, *9*, 1344-1355.
6. **Toraskar S**, Chaudhary, P. M.; Kikkeri, R. Shapes of Nanostructures Encode Immunomodulation of Carbohydrate Antigen and Vaccine Development. *Manuscript submitted.*
7. Ganesh, D.; Jain, P.; Shanthamurthy, C. D.; **Toraskar, S**.; Kikkeri, R. Targeting Selectins Mediated Biological Activities with Glyco-nanoparticles. *Frontieres in Chemistry*.**2021**.

CHAPTER-1

Glyco-nanoparticles and its Multimodal Applications

Abstract

Glyco-nanoparticles are interesting nano-probes to decipher carbohydrate-mediated biological activity. The inherent chemical and physical properties of nanoparticles, such as optical, electronic, and magnetic properties, are useful to design biosensors, imaging tools, as well as for vaccination and drug delivery. Chapter 1 briefly describes the work on glyco-nanoparticles reported by several research groups and focuses on the shape of the gold-nanoparticles that contribute to this field.

1.1 Introduction:

Carbohydrates are the major constituents of cell surfaces for a wide variety of structures, including *N*- and *O*-glycans, glycosphingolipids, and proteoglycans. These glycans are involved in cell-cell interactions that play a pivotal role in several important physiological and pathological processes.[1, 2] However, most of the monovalent carbohydrate-based interactions have been reported to have generally weak binding (from the millimolar to the micromolar range). Hence, nature compensates for weak monovalent binding by the multivalent display of carbohydrate ligands, which provide combined strength for biological recognition.[3-6] Many research groups imitate the multivalent recognition by using various multivalent scaffolds, including dendrimers, polymers, liposomes, and nanoparticles (Figure 1).[7-9] Detailed studies of these multivalent glycoprobes suggested several key mechanisms for designing smart probes to alter carbohydrate-mediated interactions. The multivalent representation of the carbohydrate-ligands signification increases the binding affinity compared to the individual ligands. However, the size, geometry, and shapes of the multivalent probes are critical to fine-tuning the binding affinity.[10-12] This chapter pays special attention to the carbohydrate-based multivalent system based on gold nanoparticles that shows unique tunable size and shape properties for modulating the binding of glycans and proteins. We first present a systematic overview of various nanoparticles used in carbohydrate research with some specific examples, followed by the importance of gold glyconanoparticles in studying carbohydrate-protein and carbohydrate-carbohydrate interactions. Finally, we present the significance of the shapes of gold nanoparticles on molecular recognition behaviour.

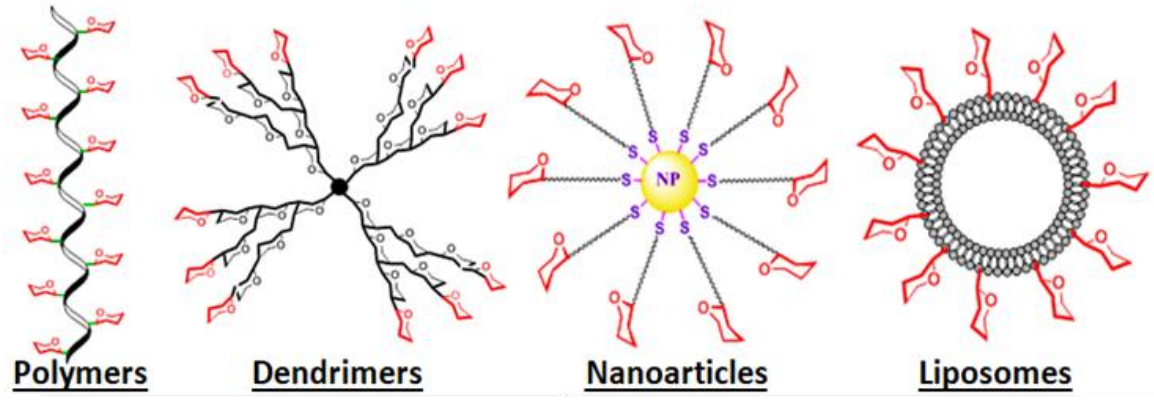

Figure 1. Multivalent carbohydrate scaffolds. (Adapted with permission from reference 22)

1.2 Polymer based nanoparticles:

Glyco-polymers are one of the earliest known multivalent probes to study carbohydrate-protein interactions, as they offer a wide range of molecular weight, cheaper, biocompatible and readily scalable materials. There are two different approaches mainly employed to synthesis glycopolymers; (a) convergent strategy, where free-radical polymerizing group such acrylate was conjugated to the monovalent ligand and polymerized. (b) Divergent method, where monovalent ligands were conjugated to polymeric templates such as polylysine, gelatin etc. In 1995, the Whiteside′s group reported a convergent free-radical-based polymerization method to synthesize acrylamide-based Sia copolymers.[13] They tested various adjuvants, such as ionic, hydrophobic/hydrophilic, and bulky substituents, with Sia ligands to modulate influenza-virus-mediated hemagglutinin activity and found that the presence of hydrophobic and charged species in the sialo-polymers enhanced the virus–protein binding affinity. Furthermore, the number of pendant Sia residues on the polymer backbone had a direct influence on the agglutination and illustrated the importance of multivalency in interfering with the viral binding to cell surfaces. Later a wide range of glycopolymers was synthesized using a convergent strategy to study CPIs (Figure 2). However, cell-surface glycans contain functional groups, such as sulfate or acid groups, which may quench the free radicals and lower free-radical polymerization efficiency. Hence, an effective method for the synthesis of structurally well-defined glycopolymers is still required. Alternatively, carbohydrate ligands are conjugated on polymer scaffolds to develop wide range of glycopolymers (Figure 3). Savasta and co-workers explored a divergent strategy for synthesizing GM3-ganglioside-based polymers to alter cell signalling, thereby modulating cell-proliferation.[14] The galactose/lactose ceramide ligands were coupled with an acrylic acid polymer scaffold in different stoichiometric ratios to generate lactose–ceramide polymers. These polymers were enzymatically reacted with a Sia precursor to synthesize GM3 polymers. The cell-proliferation assay and cell-signalling assay in the presence of these polymers revealed that the number of GM3 units per polymer and hydrophobic residue of GM3 directly influenced the inhibition of cell proliferation. Despite a broad range of methods developed to synthesize glycopolymers, these convergent and divergent strategies failed to produce well-controlled glycopolymers with end-group functionalization, essential for cell-surface engineering.

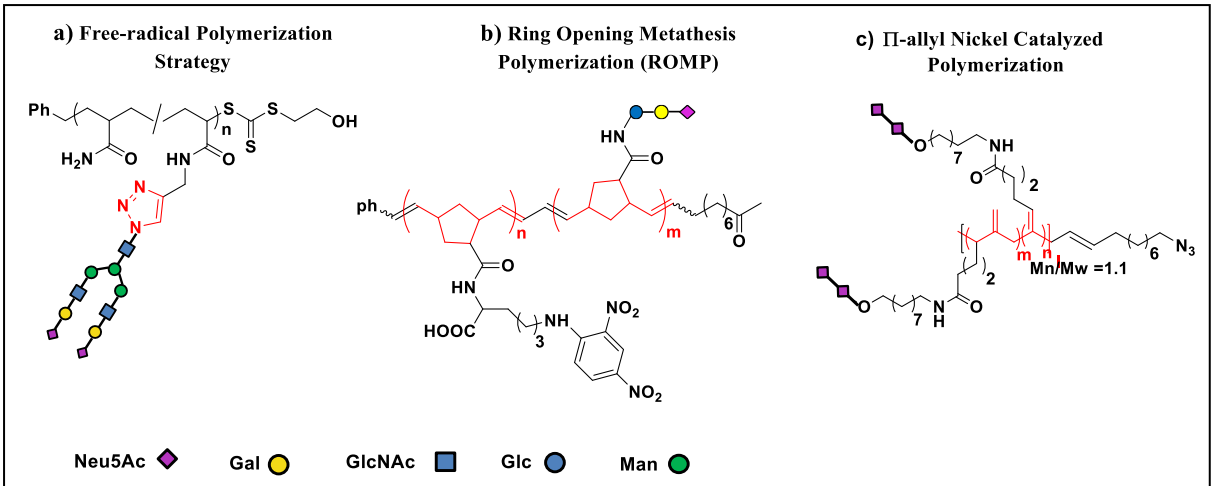

Figure 2. Structures of glyco-polymers that were synthesized by using a convergent strategy. Gal=galactose, GlcNac=*N*-acetylglucosamine, Glc=glucosamine, Neu5Ac=*N*-acetylneuraminic acid, Man=mannose.

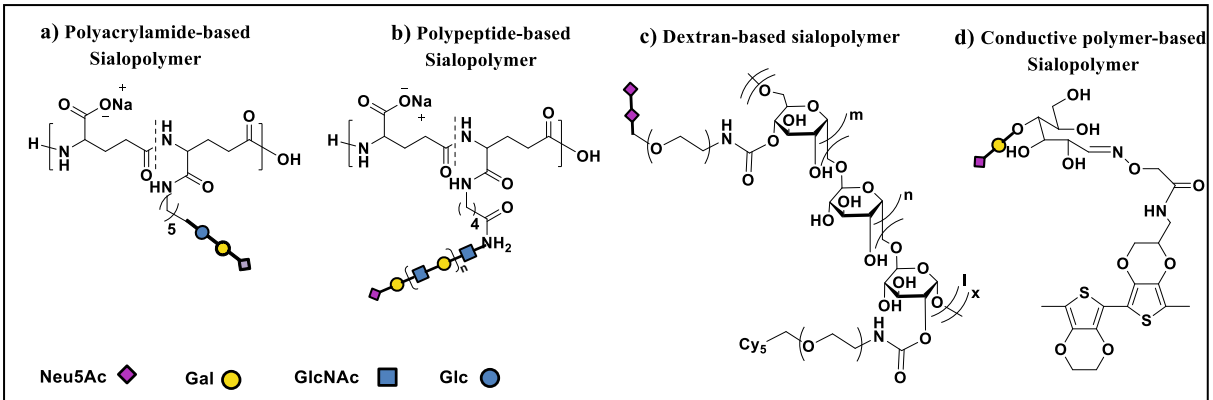

Figure 3. Structures of glyco-polymers that were synthesized by using a divergent strategy. Neu5Gc=*N*-glycolylneuraminic acid, Gal=galactose, GlcNac=*N*-acetylglucosamine, Glc=glucosamine,

1.3 Dendrimers:

Dendrimers are hyperbranched architecture that stemmed from the central core and radically emanates. Dendrimers represent one of the best three-dimensional nanoparticles. Dendrimers display reactive surface groups that can be functionalized in many biomolecules, including carbohydrates, peptides, photosensitizers, and redox units to develop biomedical probes. In addition, dendrimers can also host hydrophobic drug molecules and fluorescent probes between the braches, resulting in a potential multivalent probe for drug delivery. Dendrimers are classified based on the number of repeating units branching at the surfaces.[15-18] Apart from pure organic-based dendrimers, Metallo-glycodendrimers were also used in carbohydrate research. Ru(II) and Ir(III) complexes are preferential metal complexes, as they offer optical,

magnetic, and redox properties to monitor specific carbohydrate-protein interactions. Seeberger et al. have synthesized Ru(II) complexes appended with 14, 28 and 42 mannosepyranosyl units using host-guest chemistry to target ConA lectin by surface plasmon resonance (SPR).[19-21] Also,

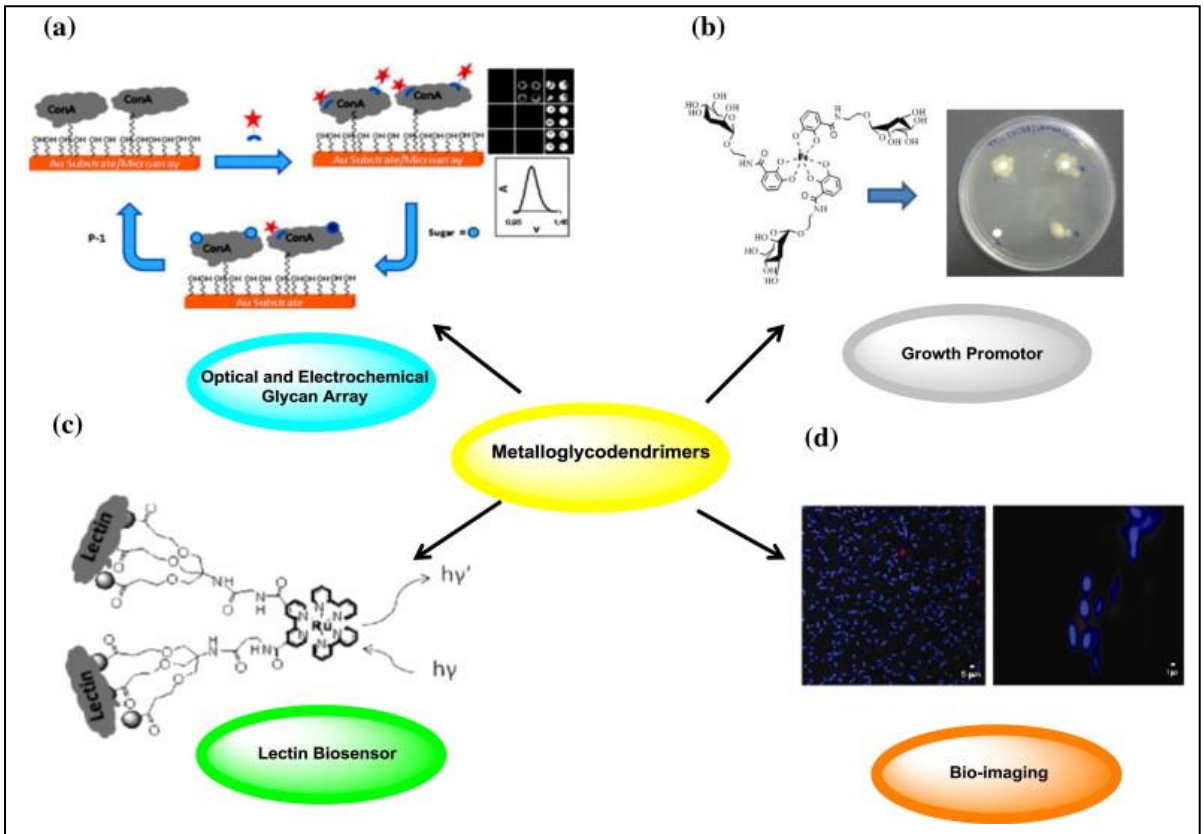

Figure 4. Potential applications of metalloglycodendrimers. (Adapted with permission from reference 9)

these systems allowed direct imaging of mannose-associated FimH lectin binding on *E. Coli* (stain ORN178). Recently, we have synthesized catechol-Fe(III) glycodendrimers to develop FimH receptor-mediated iron delivery and propagate growth promotion.[22] Overall, metal-glycodendrimers have shown a great prospect to decode several carbohydrate-mediated biological activities (Figure 4). However, most synthetic dendrimers are toxic due to their ability to disturb cell membranes. Hence we need a better multivalent probe to target carbohydrate-mediated interactions.

1.4 Nanoparticles:

Nanoparticles are usually referred to the particles size of between 1 to 100 nm in diameter. At this tiny size, particles start behaving differently from that of bulk materials. Nanoparticles display unique features such as the relatively large surface area to functionalize compounds

such as fluorescent probes, drug molecules, and proteins. Nanoparticles also possess inherent optical, electronic, and magnetic properties to generate imaging and biomedical applications.[23, 24] Nanoparticles are classified based on their one, two, or three-dimensional arrangements. Among them, three-dimensional nanoparticles are extensively used in carbohydrate research, as they closely resemble the cell-surface glycocalyx structure. The most prevalent 3D-nanoparticles used in carbohydrate research are quantum dots, dendrimers, polymer-based nanoparticles, liposomes and gold or silver nanoparticles.[25, 26]

1.4.1 Quantum dots:

Quantum dots are colloidal semiconductor nanoparticles of size ranging from 2-10 nm in diameter. The core of the QDs composed of either cadmium selenide (CdSe), cadmium telluride (CdTe), and Indium arsenide (InAs) and it is coved by ZnS or CdS shall prevent the surface quenching and leakage of nanocluster. QDs absorb white light and reemit a specific fluorescent light based on the bandgap of the materials. The semiconductor nature and the size-dependent fluorescent of the QDs have made them an attractive target of bioimaging studies. Our group and other researchers used carbohydrate-capped QDs for *in-vitro* and *in-vivo* imaging of specific carbohydrate-protein interactions.[27, 28] For example, Kim et al. synthesized hyaluronic acid-capped QDs to study CD44 mediated cancer cell targeting.[29] Seeberger et al. functionalized galactosamine-QDs to target asialoglycoprotein receptors expressed on liver cells.[30] We have recently used sialic acid oligosaccharide functionalized QDs to study the in-vivo biocompatibility of the zebrafish (*Danio rerio*) model.[31] As a prototype, we have synthesized Neu5Acα(2-6), and α(2-3)Gal conjugated quantum dots and performed toxicity, biodistribution, and sequestration of these nanoparticles in zebrafish and mouse model (C57BL). We showed that α(2-6)-linked sialic acid glycans displayed prolonged blood circulation and broad biodistribution in both models. In contrast, Neu5Ac α(2-3) glycan showed short blood circulation and sequestration in the liver. These results demonstrate that zebrafish can be used as a simple *in vivo* model to target carbohydrate-protein interaction (Figure 5).

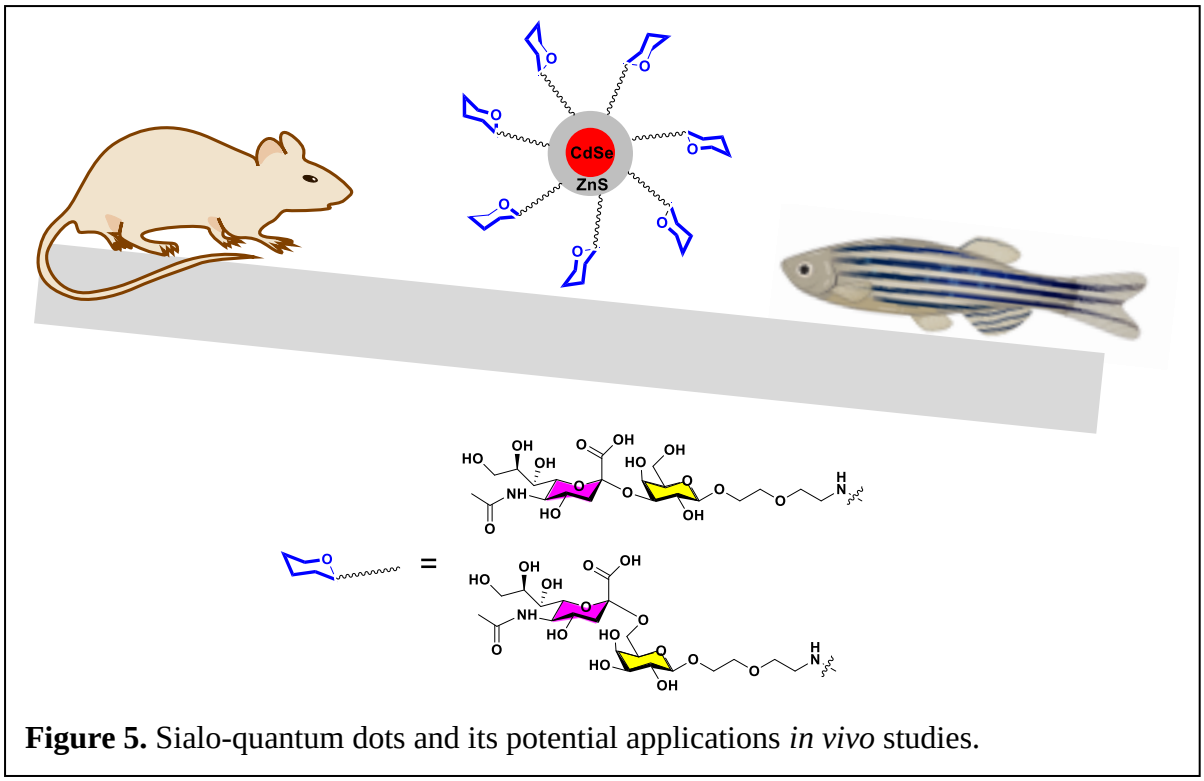

Figure 5. Sialo-quantum dots and its potential applications *in vivo* studies.

1.4.2 Liposomes:

Liposomes are one of the most attractive nanocarriers for controlled cargo delivery, composed of lipid bilayers in a discrete aqueous environment. They can host both hydrophilic drug molecules in the aqueous centre and hydrophobic molecules between the lipid bilayers and display a large surface area to functionalize biological ligands, including carbohydrates, peptides, and protein (Figure 6).[32, 33] Liposomes are extensively used to design selectin-mediated drug delivery and imaging systems to target various diseases. Li et al. synthesized sialic acid-modified doxorubicin-based liposomes to target and kill peripheral blood neutrophils via sialic acid-L-selectin interaction to reduce the accumulation of neutrophiles at rheumatoid arthritis (RA) disease site.[34] Similarly, Matsumura et al. synthesized sialyl lewis ^{X}-modified doxo-liposomes to target injured vessel walls to prevent stenosis after angioplasty (Tsuruta et al., 2009).[35] Meanwhile, Zalipsky et al. reported silyl lewis^{X} liposomes to develop antiadhesion molecules (DeFrees et al., 1996).[36] Azab et al. prepared bone marrow microenvironment destructing inhibitor modified P-selectin glycoprotein ligand-1 conjugated liposome to target multiple myeloma-associated endothelium (AK et al., 2012).[37]

However, single-ligands often fail to target the dynamic microenvironment of the tumor, particularly metastasis cancer cells. To improve the accuracy in targeting metastasis cancer cells, multi-ligand embedded liposomal nanoparticles have been synthesized. Here, P-se

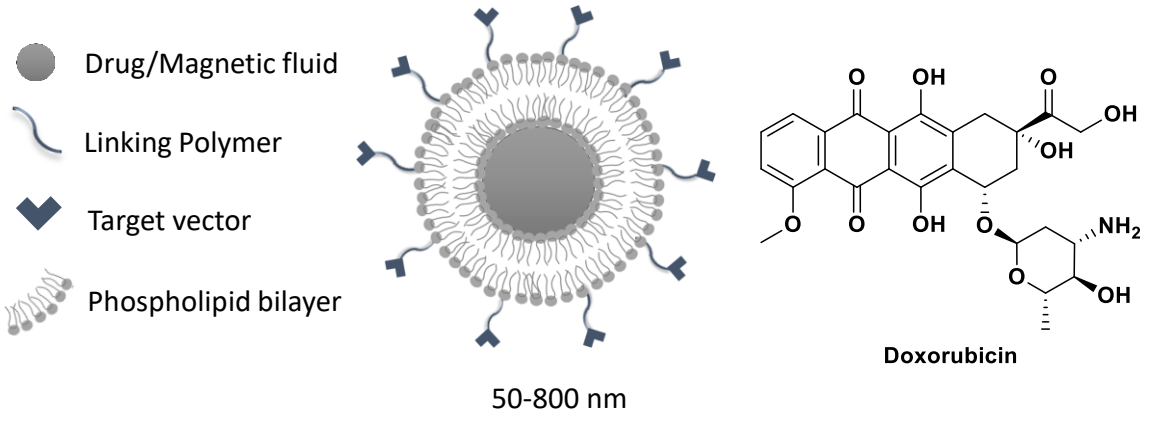

Figure 6. Structure of liposome. Liposome functionalized with target groups, hydrophilic drugs in bilayer and hudrophobic drugs in core

lectin-specific ligands, integrin-targeting peptides, fibronectin targeting peptides, and epidermal growth factor receptor (EGFR) targeting peptides were assembled on a single liposome to target more than one receptor overexpressed on cancer cells (Peiris et al., 2018). By employing such multi-ligand strategies, highly sensitive and precise imaging of early-stage cancer cells metastasis was achieved (Doolittle et al., 2015; Covarrubias et al., 2018). However, the poor cost-effectiveness of liposome-based drug-delivery limited its clinical translation.

1.4.3 Gold Nanoparticles:

Gold nanoparticles (AuNPs) are versatile, non-toxic, and extraordinarily stable nanomaterials with many potential applications. AuNPs exhibit unique surface-enhanced Raman scattering (SERS) for bio-sensing and bio-imaging studies and are easy to synthesize and functionalize as different sizes and shapes. A typical synthetic strategy involves the reduction of gold chloride in the presence of thio, citrate, or phosphine surfactants. Finally, gold nanoparticles can be functionalized with various bio-active ligands using the ligand exchange method.[38-42] In 2001, Penadesa et al. first reported the synthesis of glyco-gold nanoparticles to study carbohydrate-protein interactions using a direct ligand mixing process, resulting in 100%-coating of the glycoconjugates on AuNPs.[43] This facile method can be used to synthesize various other functional AuNPs, including DNA-, RNA- and peptides- conjugated AuNPs. However, the direct synthetic method showed difficulties in controlling the size of the core AuNPs. Hence, it was replaced by a multi-step synthetic strategy. Here, stable AuNPs were synthesized and then treated with carbohydrate ligands with a suitable functional group to perform ligand exchange reactions, resulting in well-defined glyco-gold nanoparticles (Figure

7). This method improves the prospect of controlling the ligand density on the AuNPs and can synthesize hetero-functional AuNPs, including fluorescent or drug conjugated glyco-AuNPs.[44, 45]

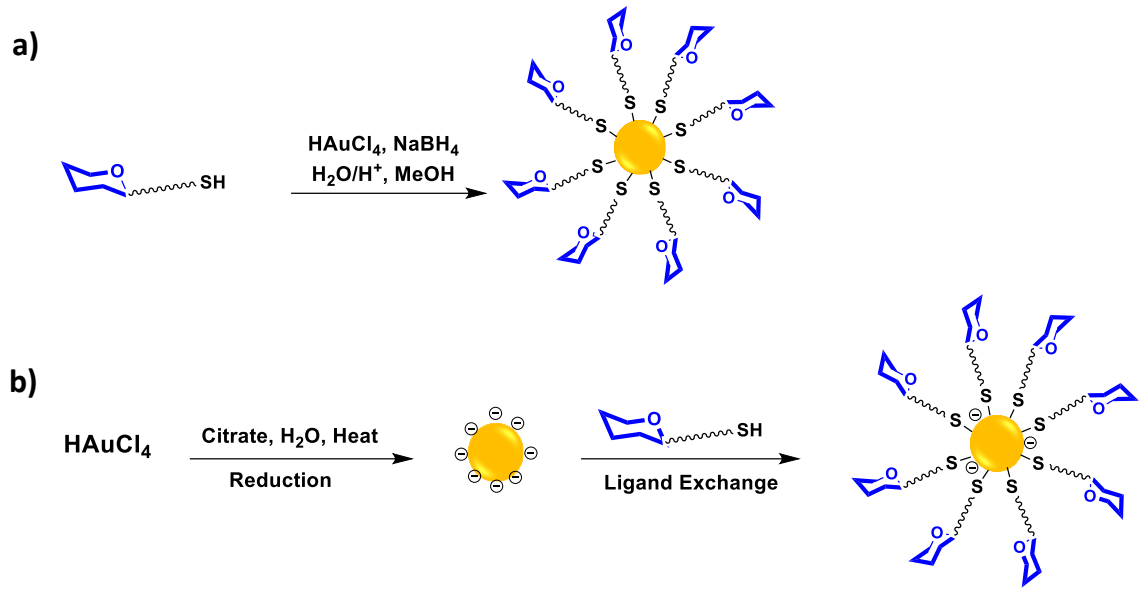

Figure 7. AuNP formulation by a) direct synthesis of glyco-gold nanoparticles b) two step synthesis of glyco-gold nanoparticles (reduction followed by ligand exchange reaction).

1.4.3.1 Recent developments in the use of glycogold-nanoparticles:

1.4.3.1.1 Protein Binding Studies:

Glyco-gold nanoparticles (GNPs) are one versatile tool for studying carbohydrate-protein interactions (CPIs). In general, colourimetric assays have been employed to study specific binding between glyco-AuNPs and lectin. This method is a highly versatile and simple way to characterize the binding affinity. The specific aggregation of glycol-AuNps by lectin was characterized by taking advantage of the UV-visible spectra of colloidal metallic elements. Previously, Katoka and coworkers employed this method to characterize lactose-Ricinus communis agglutinin (RCA_{120}) interaction.[46, 47] Similarly, Russell and coworkers characterized mannose-ConA selectivity using this assay.[48] However, Chen and coworkers performed a competitive colourimetric assay using the Mannose-GNPs-ConA complex and thyroglobulin to establish protein-protein interactions.[49] Penades and coworkers used Man-GNPs to target DC-SIGN. Here they used surface plasmon resonance (SPR) to characterize the specific glycosidic linkage essential to target DC-SIGN ubiquitously expressed on dendritic cells.[50]

1.4.3.1.2 Antiadhesion Properties:

Glycocalyx plays a pivotal role in normal and pathogenic cell adhesion a role in which, GNPs can intervene. In 2004, Penades et al. reported the first example of the anti-adhesion properties of lactose-AuNPs against lung metastasis in mice models.[51] Similarly, Gianvicezo reported that synthetic glucose-GNPs interact with gp120 of HIV and block the viral entry processes. In another development, the Penades group reported oligomannose appended GNPs as a potential blocker of HIV-Dendritic cells interactions.[52]

1.4.3.1.3 Cellular and Molecular imaging:

GNPs offer an outstanding contribution to understand molecular level biological activity and in the development of imaging and therapeutic applications. Recently, our group has reported the synthesis of synthetic heparin sulfate conjugated fluorescent gold nanoparticles to target cancer cells in 2D and 3D-cell culture systems.[53] Here, author constructed a multivalent fluorescent glyco-gold nanovehicle to target the epidermal growth factor receptors (EGFR) present on triple-negative breast cancer cells (TNBCs). A series of confocal images using HT-6S-NAc- and HT-6P-modified nanovehicles showed that HT-6S-NAc-capped gold nanoparticles in the two-dimensional cell culture model had preferential uptake compared with that of HT-6P. Also, this preferential uptake was in good agreement with the cell-surface EFGR expression on the TNBCs, with MDA-MB-468 (which had the highest EGFR expression) showing remarkably high uptake compared to that of SK-Br-3 (which had the lowest EGFR expression). Furthermore, the results were validated by selectively targeting cancer cells in the tumor microenvironment using the three-dimensional cell culture technique. Overall, the results support the use of HT ligands in targeted cancer therapy (Figure 8).

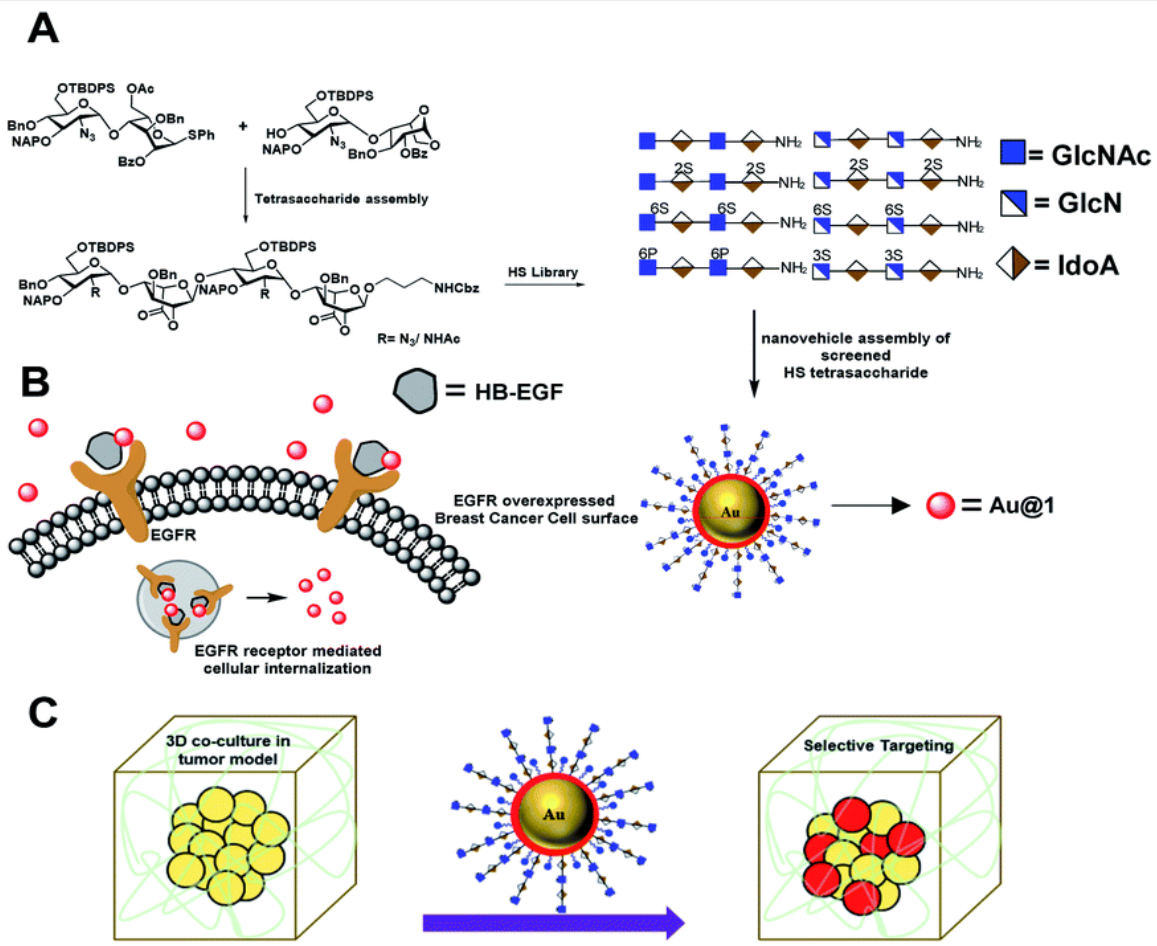

Figure. 8. a) Synthesis of heparan sulfate oligosaccharides using divergent strategy. b) Assembly of glyco-gold AuNps based nanovehicle targeting *via* EGFR overexpressed cancer cells in 2D and 3D-coculture models. c) Schematic representation of the tumor microevnivorment and selective targeting of cancer cells in the presence of stromal cells and an extracellular matrix. (Reproduced from Ref. 53 with the permission of the Royal Society of Chemistry)

1.4.3.1.4 Carbohydrate-Carbohydrate Interactions:

Carbohydrate-carbohydrate interactions (CCIs) are one of the initial steps of all biological recognition, and their binding affinity is much weaker than that of CPIs. Detecting such weak interactions is a daunting task. Multivalent glyco-gold nanoparticles are an essential tool to studying CCIs. Although the role of CCIs in cell-adhesion has been well established, the molecular level details were first established by Penades et al. They functionalized gold nanoparticles with Lewis^{x} and lactose trisaccharide ligands to study calcium-dependent CCIs. The aggregation of lactose and lewis^{x}-gold AuNPs was monitored in TEM imaging in the presence of Calcium ions, and the addition of EDTA showed a reversible effect. In the case of Lewis^{X} –conjugated AuNPs calcium-dependent aggregation was stronger than lactose, indicating that the fucose-residue is important to calcium mediated CCIs. Isothermal

calorimetry titration and SPR binding affinity studies of Lewis^x-Lewis^x mediated CCIs clearly showed micromolar range binding.[54]

1.4.3.1.5 Vaccine Development

Antigen conjugated gold nanoparticles showed a significant contribution to immune modulation and vaccine development. Multivalent displays of antigens on AuNPs substantially improve antigen delivery to immune cells and modulate IgG-specific antibody responses.[55, 56] Recently, Penades et al. synthesized high-mannose conjugated nanoparticles to dendritic cells to target HIV-gp120 to produce the anti-HIV antibody 2G12. However, carbohydrates-conjugated AuNPs failed to produce IgG responses. Hence, the synthesized V3 variable region peptides of HIV-gp12- on gold nanoparticles were immunized. The peptide-conjugated nanoparticles elicit antibody responses against gp120.[57, 58] Similarly, Barchi and co-workers synthesized Mucin-1 (MUC1) glycopeptide antigen conjugated AuNPs and immunized the mice (Figure 9). The anti-bodies titration showed that the multivalent presentation of MUC1-glycopeptides stimulates the immune system and anti-body responses.[59] In another study, AuNPs were conjugated with capsular polysaccharide of serogroup A of Neisseria meningitides and immunized. The results showed that the nanoparticles could stimulate nanoparticles size dependent T-cell proliferation and modulate immune responses .[60] Similarly, Compastella et al. synthesized CPS of *S.pneumoniae* type 19F and 14 conjugated nanoparticles and immunized them. The ELISA plate analysis showed that NPs enhanced the titer of IgG antibodies toward type 14 polysaccharides. These results indicated that gold nanoparticles could be applied to immunomodulate carbohydrate antigens and vaccine development.[61]

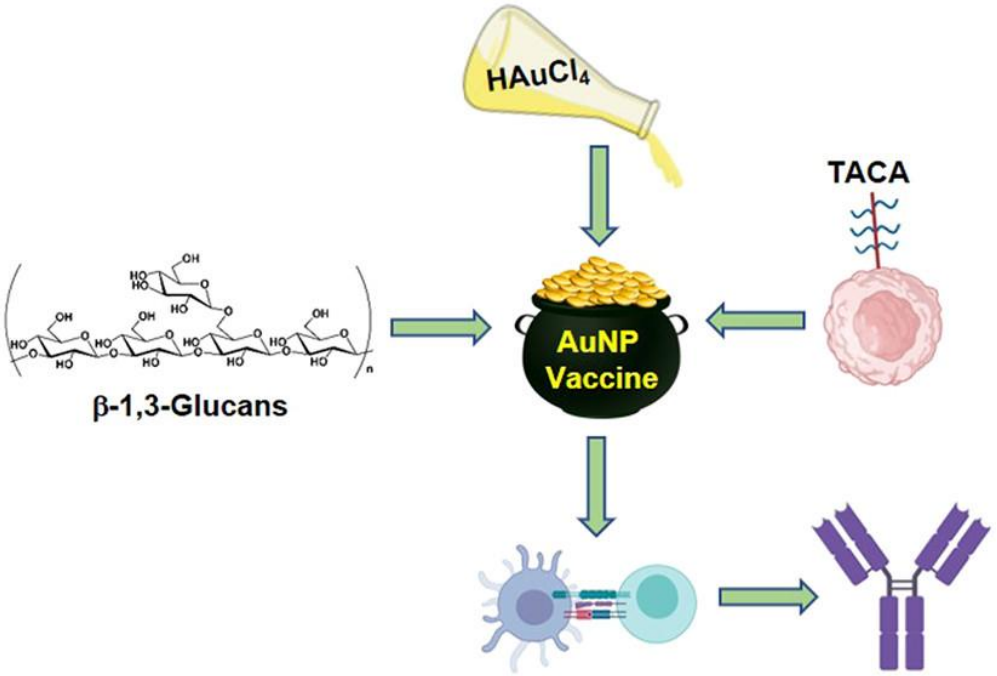

Figure 9. Schematic representation of glyco-AuNPs as T-Cell specific immune modulators. (Adapted with permission from reference 59)

1.4.3.1.6 Shape-dependent glyco gold-nanoparticles applications

As reported earlier, multivalent glycoprobes were extensively used to study the carbohydrate-protein interactions. However, in all these studies, the shape of multivalent glycoprobes were kept constant to validate the binding with bacteria, cells or organs, limiting the assessment of the role of different shapes of nanoparticles involved in specific CPIs. The latter is of fundamental importance for understanding the CPIs and developing new biomaterials. Various targeting units, such as antibodies, peptides, aptamers have been functionalized on different shapes of AuNPs to enhance their specificity for tumors, immune responses and biosensing processes. However, a systematic investigation of shape dependent CPIs with the same volume and sugar density and its potential applications have not been reported. Hence, our group first reported the use of three distinct shapes of glyco-AuNps in bacterial recognition and inhibiting bacterial infection.

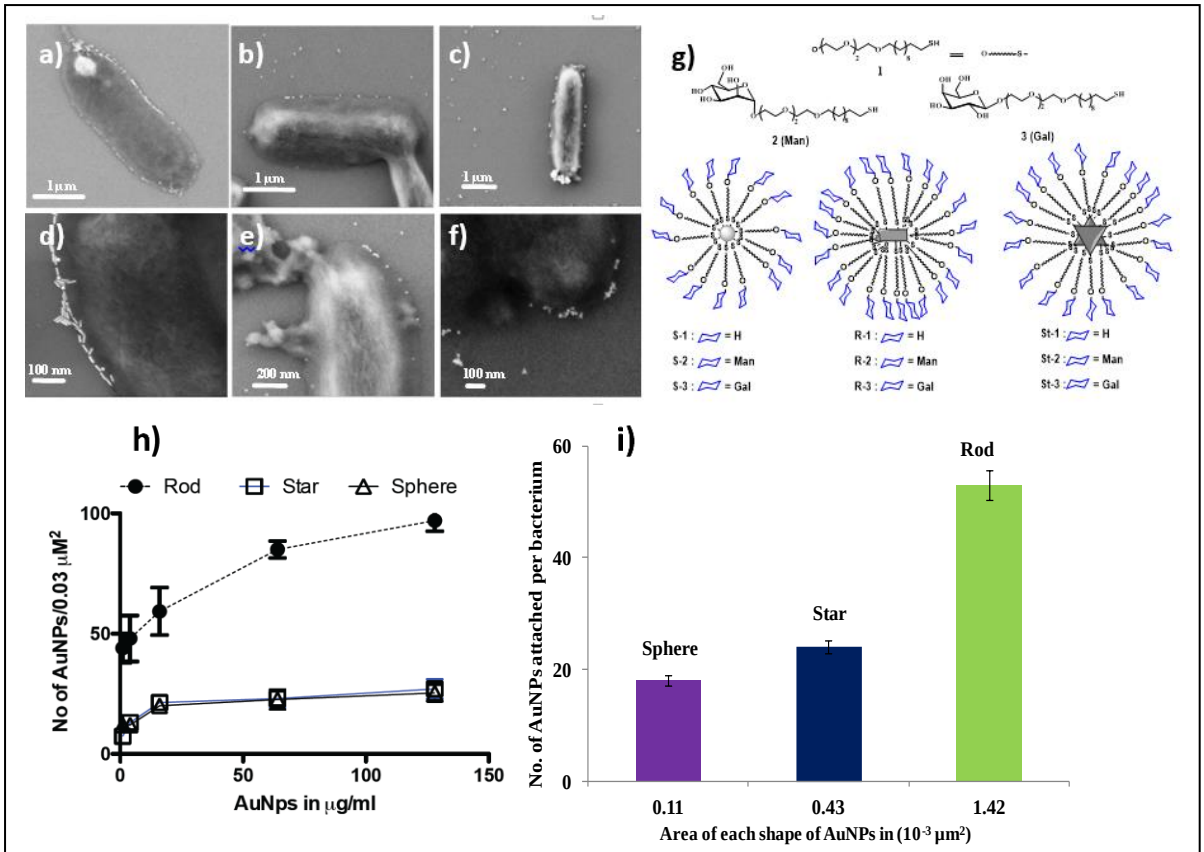

Figure 10. (a-f) SEM images of mannose functionalized AuNPs (Man-AuNPs) with *E. coli* ORN 178 stain: (a)-(d) Rod; (b)-(e) Sphere; (c)-(f) Star; (g) Quantification of attachment of Man-AuNPs on the surface of bacteria. Data represent the mean number of nanoparticles on the surfaces of bacteria (n =10); (h) Man-AuNPs bound to the surface of bacteria according to the surface availability; Conc of AuNPs = 0.8 μg/ml (n=5). (Note: While quantifying the bound AuNPs and area, the surface of the bacteria was assumed as flat surface) (Reproduced from Ref. 62 with the permission of the Royal Society of Chemistry.)

Three different shapes (rod, sphere and star) of gold nanoparticles coated with mannose and galactose sugar substrates and PEG were used to quantify the binding affinity with *E. coli* (Figure 10).[62] To profile the potential applications of the shape dependent CPIs, inhibition of *E. coli* infection of HeLa cells was quantified. Our studies showed that the rod-shaped AuNPs functionalized with mannose had substantial sensitivity compared to that of star-shaped and spherical shaped AuNPs. Factors such as self-assembly and effective surface contact are critical for sensitive adhesion. In a more general perspective, blockage of *E.coli* infection by rod mannose-AuNPs may open opportunities to develop efficient medicines for urinary or digestive tract infections.

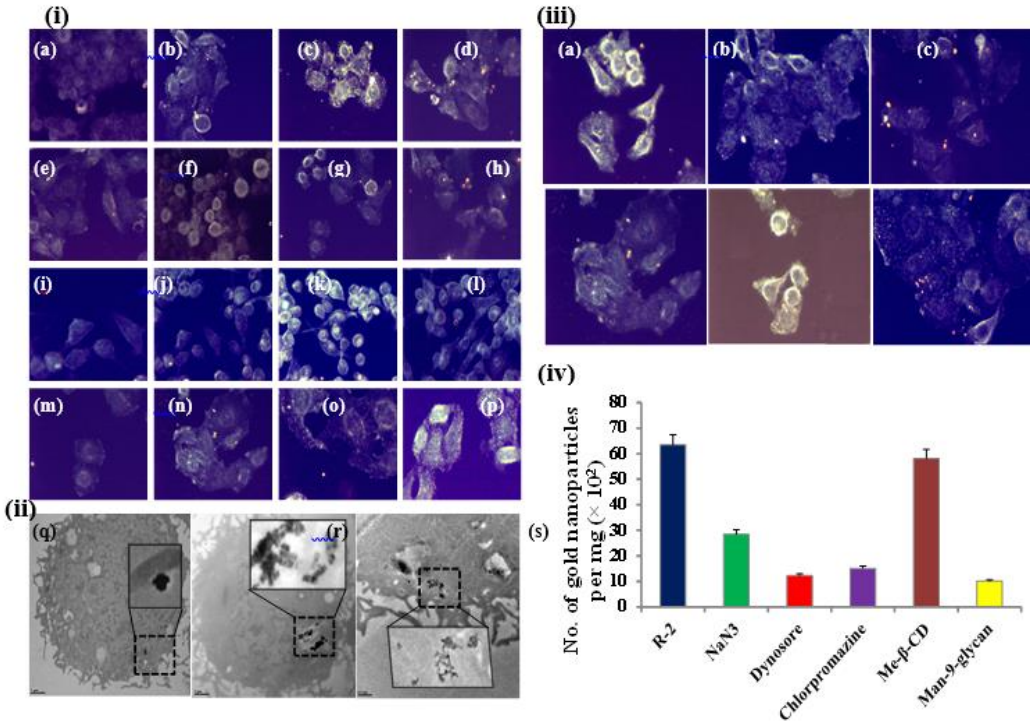

Figure 11. (i) Dark field microscopic images of rod shape nanoparticles incubated with HeLa (DC-SIGN transfected), HeLa (DC-SIGN knockdown), MDA-MB-231 and HepG2 cells for 24 h at 37 °C. (a) HeLa-control; (b) HeLa, R-1; (c) HeLa, R-2; (d) HeLa, R-3; DC-SIGN knockdown of (e) HeLa-control; (f) HeLa, R-1; (g) HeLa, R-2; (h) HeLa, R-3; (i) MDA-MB-231-control; (j) MDA-MB-231, R-1; (k) MDA-MB-231, R-2; (l) MDA-MB-231, R-3; (m) HepG2-control; (n) HepG2, R-1; (o) HepG2, R-2; (p) HepG2, R-3; (ii) TEM images of HeLa cells contain (q) S-2; (r) R-2; (s) St-2 after 24 h. (iii) Dark field microscopic images of HeLa cells treated with inhibitor for 30 mins followed by **R-2** after 4 h. (a) control **R-2** after 4 h; (b) NaN_3 (50 mM); (c) dynosore (50 µM); (d) chlorpromazine (25 µM); (e) Me-β-cyclodextrin (10 mM); (f) Mannose-9-glycan (50 mM). (iv) Statistical analysis of ICP-MS data in presence and absence of inhibitor after 4 h. Data are presented as mean ±SEM for three independent experiments. (Reproduced from Ref. 63 with the permission of the Royal Society of Chemistry)

We next investigated the shape dependent uptake of glyco-gold nanoparticles (G-AuNPs) in different cancer cell lines. *In vitro* experiments showed that rod-AuNPs exhibited the highest uptake than that of the star and spherical counterparts. Further investigation of the mechanism of uptake clearly demonstrated clathrin mediated endocytosis of the specific G-AuNPs (Figure 11).[63]

Finally, we investigated the bio-distribution of different shapes of glyco-gold nanoparticles (G-AuNPs) in a zebrafish model. *In vivo* experiments showed that rod-AuNPs exhibited fast uptake, while star-AuNPs displayed prolonged sequestration, demonstrating its potential therapeutic efficacy in drug delivery (Figure 12).[64] Overall, these results revealed the benefits

of different shapes in carbohydrate-mediated interactions and also illustrate zebrafish as a potential *in vivo* system to study carbohydrate-mediated interactions in quick time.

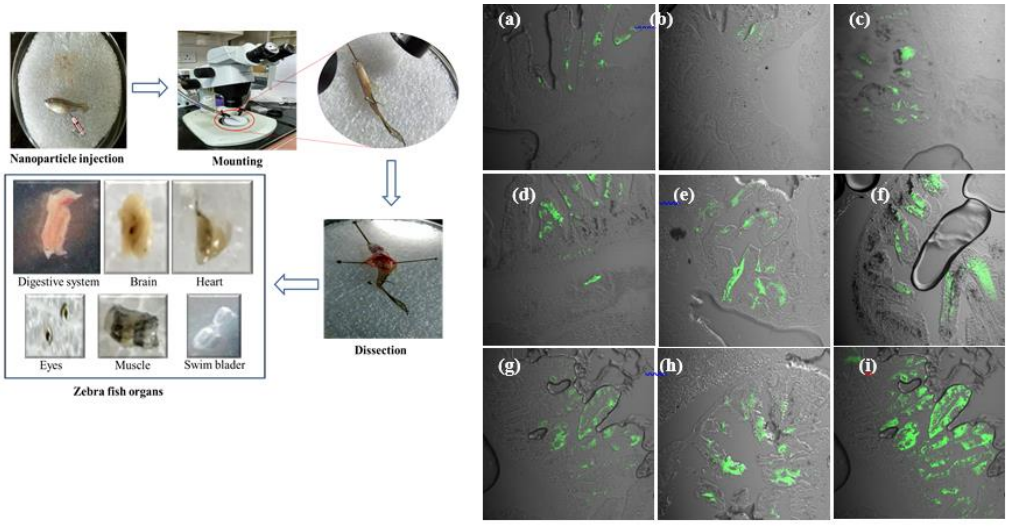

Figure 12. Schematic diagram of injection of nanoparticle to zebrafish, mounting for dissection and collecting of respective organs; Confocal images of zebrafish digestive system injected with FITC conjugated G-AuNPs after 6 h: (a) S-1; (b) R-1; (c) St-1; (d) S-2; (e) R-2; (f) St-2; (g) S-3; (h) R-3; (i) St-3.

1.5 Conclusion:

Multivalent carbohydrate scaffolds have demonstrated potential roles in the understanding, recognition, and modulation of biological processes. Recently, we have shown how different shapes of multivalent glycoprobes modulate specific carbohydrate-protein interactions. The motivation for this research comes from the realization that the inherent shapes of different cell types directly influence the glycocalyx. Therefore, rational design of the different shapes of glyco-AuNPs should be linked with future potent use.

1.6 References:

1. Varki, A. Biological roles of glycans. *Glycobiology*. **2017**, *27*, 3-49.
2. Varki, A.; Esko, J. D.; Freeze, H. H.; Stanley, P.; Bertozzi, C. R.; Hart, G. W.; Etzler, M. E. Eds. *Essentials of Glycobiology*; Cold Spring Harbor: New York, 2009.
3. Lee, Y. C.; Lee, R. T. Carbohydrate-Protein Interactions: Basis of Glycobiology. *Acc. Chem. Res.* **1995**, *28*, 321-327.
4. Lundquist, J. J.; Toone, E. J. The Cluster Glycoside Effect. *Chem. Rev*. **2002**, *102*, 555-578.
5. Lee, Y. C. Biochemistry of carbohydrate-protein interaction. *FASEB J*. **1992**, *6*, 3193-200.

6. Williams, S. J.; Davies, G. J. Protein--carbohydrate interactions: learning lessons from nature. *Trends Biotechnol*. **2001**, *19*, 356-62.
7. Jimenez Blanco, J. L.; Ortiz Mellet, C.; Garcia Fernandez, J. M. Multivalency in Heterogeneous Glycoenvironments: Hetero-Glycoclusters, -Glycopolymers and -Glycoassemblies. *Chem. Soc. Rev*. **2013**, *42*, 4518−4531.
8. Delbianco, M.: Bharate, P.; Varela-Aramburu, S.; Seeberger, P. H. Carbohydrates in Supramolecular Chemistry. *Chem Rev*. **2016**, *116*, 1693-752.
9. Chaudhary, P. M.; Toraskar, S.; Yadav, R.; Hande, A.; Yellin, R. A.; Kikkeri, R. Multivalent Sialosides: A Tool to Explore the Role of Sialic Acids in Biological Processes. *Chem Asian J*. **2019**, *14*, 1344-1355.
10. Gestwicki, J. E.; Cairo, C. W.; Strong, L. E.; Oetjen, K. A.; Kiessling, L. L. Influencing receptor-ligand binding mechanisms with multivalent ligand architecture. *J Am Chem Soc*. **2002**, *124*, 14922-33.
11. Cairo, C. W.; Gestwicki, J. E.; Kanai, M.; Kiessling, L. L. Control of multivalent interactions by binding epitope density. *J Am Chem Soc*. **2002**, *124*, 1615-9.
12. Cecioni, S.; Imberty, A.; Vidal, S. Glycomimetics versus multivalent glycoconjugates for the design of high affinity lectin ligands. *Chem Rev.* **2015,** *115*, 525-61.
13. Mammen, M.; Dahmann, G.; Whitesides, G. M. Effective inhibitors of hemagglutination by influenza virus synthesized from polymers having active ester groups. Insight into mechanism of inhibition. *J Med Chem*. **1995**, *38*, 4179-90.
14. Woerly, S.; Fort, S.; Pignot-Paintrand, I.; Cottet, C.; Carcenac, C.; Savasta, M. Development of a sialic acid-containing hydrogel of poly[N-(2-hydroxypropyl) methacrylamide]: characterization and implantation study. *Biomacromolecules*. **2008**, *9*, 2329-37.
15. Turnbull, W. B.; Stoddart, J. F. Design and synthesis of glycodendrimers. *J Biotechnol*. **2002**, *90*, 231-55.
16. Roy, R.; Shiao, T. C. Glyconanosynthons as powerful scaffolds and building blocks for the rapid construction of multifaceted, dense and chiral dendrimers. *Chem Soc Rev*. **2015**, *44*, 3924-41.
17. Chabre, Y. M.; Roy, R. Multivalent glycoconjugate syntheses and applications using aromatic scaffolds. *Chem Soc Rev*. **2013**, *42*, 4657-708.
18. Abbasi, E.; Aval, S. F.; Akbarzadeh, A.; Milani, M.; Nasrabadi, H. T.; Joo, S. W.; Hanifehpour, Y.; Nejati-Koshki, K.; Pashaei-Asl, R. Dendrimers: synthesis, applications, and properties. *Nanoscale Res Lett*. **2014**, 9, 247.

19. Kikkeri, R.; García-Rubio, I.; Seeberger, P. H. Ru(II)-carbohydrate dendrimers as photoinduced electron transfer lectin biosensors. *Chem Commun (Camb)*. **2009**, *2*, 235-7.
20. Kikkeri, R.; Kamena, F.; Gupta, T.; Hossain, L. H.; Boonyarattanakalin, S.; Gorodyska, G.; Beurer, E.; Coullerez, G.; Textor, M.; Seeberger, P. H. Ru(II) glycodendrimers as probes to study lectin-carbohydrate interactions and electrochemically measure monosaccharide and oligosaccharide concentrations. *Langmuir*. **2010**, *26*, 1520-3.
21. Kikkeri, R.; Liu, X.; Adibekian, A.; Tsai, Y. H.; Seeberger, P. H. Facile synthesis of size dependent Ru(II)-carbohydrate dendrimers via click chemistry. *Chem Commun (Camb)*. **2010**, *46*, 2197-9.
22. Khan, A. S.; Adak, A.; Murthy, R. V.; Kikkeri, R. Recent Advances in the metalloglycodendrimers and its potential applications. *Inorganic Chimica Acta*. **2014**, *409*, 26-33.
23. Khan, I.; Saeed, K.; Khan, I. Nanoparticles: Properties, applications and toxicities. *Arab. J. Chem.* **2019**, *12*, 908–931.
24. Mitchell, M. J.; Billingsley, M. M.; Haley, R. M.; Wechsler, M. E.; Peppas, N. A.; Langer, R. Engineering precision nanoparticles for drug delivery. *Nat Rev Drug Discov*. **2021**, *20*, 101-124.
25. Reichardt, N. C.; Martín-Lomas, M.; Penadés, S. Glyconanotechnology. *Chem Soc Rev*. **2013**, *42*, 4358-76.
26. Hernando, P. J.; Dedola, S.; Marín, M. J.; Field, R. A. Recent Developments in the Use of Glyconanoparticles and Related Quantum Dots for the Detection of Lectins, Viruses, Bacteria and Cancer Cells. *Front Chem*. **2021**, *9*, 668509.
27. Wagner, A. M.; Knipe, J. M.; Oriv, G.; Peppas, N. A. Quantum dots in biomedical applications. *Acta Biomater*. **2019**, *94*, 44-63.
28. Valizadeh, A.; Mikaeili, H.; Samiei, M.; Farkhani, S. M.; Zarghami, N.; Kouhi, M.; Akbarzadeh, A.; Davaran, S. Quantum dots: synthesis, bioapplications, and toxicity. *Nanoscale Res Lett*. **2012**, *7*, 480.
29. Bhang, S. H.; Won, N.; Lee, T. J.; Jin, H.; Nam. J.; Park, J.; Chung, H.; Park, H. S.; Sung, Y. E.; Hahn, S. K.; Kim, B. S.; Kim, S. Hyaluronic acid-quantum dot conjugates for in vivo lymphatic vessel imaging. *ACS Nano*. **2009**, *3*, 1389-98.
30. Kikkeri, R.; Lepenies, B.; Adibekian, A.; Laurino, P.; Seeberger, P. H. In vitro imaging and in vivo liver targeting with carbohydrate capped quantum dots. *J Am Chem Soc*. **2009**, *131*, 2110-2.

31. Yadav, R.; Madhukar, Chaudhary P.; Subramani, B.; Toraskar, S.; Bavireddi, H.; Murthy, R. V.; Sangabathuni, S.; Kikkeri, R. Imaging and Targeting of the α(2-6) and α(2-3) Linked Sialic Acid Quantum Dots in Zebrafish and Mouse Models. *ACS Appl Mater Interfaces*. **2018**, *10*, 28322-28330.
32. Akbarzadeh, A.; Rezaei-Sadabady, R.; Davaran, S.; Joo, S. W.; Zarghami, N.; Hanifehpour, Y.; Samiei, M.; Kouhi, M.; Nejati-Koshki, K. Liposome: classification, preparation, and applications. *Nanoscale Res Lett*. **2013**, *8*, 102.
33. Sercombe, L.; Veerati, T.; Moheimani, F.; Wu, S. Y.; Sood, A. K.; Hua, S. Advances and Challenges of Liposome Assisted Drug Delivery. *Front Pharmacol*. **2015**, *6*, 286.
34. Li, L.; Fu, J.; Wang, X.; Chen, Q.; Zhang, W.; Cao, Y.; Ran, H. 1. Biomimetic "nanoplatelets" as a Targeted Drug Delivery Platform for Breast Cancer Theranostics. *ACS Appl. Mater. Interfaces*, **2021**, *13*, 3605–3621.
35. Tsuruta, W.; Tsurushima, H.; Yamamoto, T.; Suzuki, K.; Yamazaki, N.; Matsumura, A. Application of liposomes incorporating doxorubicin with sialyl Lewis X to prevent stenosis after rat carotid artery injury. *Biomaterials*. **2009**, *30*, 118-25.
36. DeFrees, S. A.; Phillips, L.; Guo, L.; Zalipsky, S. Sialyl Lewis x liposomes as a multivalent ligand and inhibitor of E-selectin mediated cellular adhesion. *J. Am. Chem. Soc.* **1996**, *118*, 6101–6104.
37. Azab, A. K.; Quang, P.; Azab, F.; Pitsillides, C.; Thompson, B.; Chonghaile, T.; Patton, J. T.; Maiso, P.; Monrose, V.; Sacco, A.; Ngo, H. T.; Flores, L. M.; Lin, C. P.; Magnani, J. L.; Kung, A. L.; Letai, A.; Carrasco, R.; Roccaro, A. M.; Ghobrial, I. M. P-selectin glycoprotein ligand regulates the interaction of multiple myeloma cells with the bone marrow microenvironment. *Blood*. **2012**, *119*, 1468-78.
38. Yeh, Y. C.; Creran, B.; Rotello, V. M. Gold nanoparticles: preparation, properties, and applications in bionanotechnology. *Nanoscale*. **2012**, *4*, 1871-80.
39. Hu, X.; Zhang, Y.; Ding, T.; Liu, J.; Zhao, H. Multifunctional Gold Nanoparticles: A Novel Nanomaterial for Various Medical Applications and Biological Activities. *Front Bioeng Biotechnol*. **2020**, *8*, 990.
40. Elahi, N.; Kamali, M.; Baghersad, M. H. Recent biomedical applications of gold nanoparticles: A review. *Talanta*. **2018**, *184*, 537-556.
41. Thanh, N. T.; Maclean, N.; Mahiddine, S. Mechanisms of nucleation and growth of nanoparticles in solution. *Chem Rev*. **2014**, *114*, 7610-30.
42. Wuithschick, M.; Birnbaum, A.; Witte, S.; Sztucki, M.; Vainio, U.; Pinna, N.; Rademann, K.; Emmerling, F.; Kraehnert, R.; Polte, J. Turkevich in New Robes: Key

Questions Answered for the Most Common Gold Nanoparticle Synthesis. *ACS Nano*. **2015**, *9*, 7052-71.

43. de la Fuente, J. M.; Barrientos, A. G.; Rojas, T. C.; Rojo, J.; Cañada, J.; Fernández, A.; Penadés, S. Gold Glyconanoparticles as Water-Soluble Polyvalent Models To Study Carbohydrate Interactions. *Angew Chem Int Ed Engl*. **2001**, *40*, 2257-2261.
44. Fyrner, T.; Ederth, T.; Aili, D.; Liedberg, B.; Konradsson, P. Synthesis of oligo(lactose)-based thiols and their self-assembly onto gold surfaces. *Colloids Surf B Biointerfaces*. **2013**, *105*, 187-93.
45. Combemale, S.; Assam-Evoung, J. N.; Houaidji, S.; Bibi, R.; Barragan-Montero, V. Gold nanoparticles decorated with mannose-6-phosphate analogues. *Molecules*. **2014**, *19*, 1120-49.
46. Otsuka, H.; Akiyama, Y.; Nagasaki, Y.; Kataoka, K. Quantitative and reversible lectin-induced association of gold nanoparticles modified with alpha-lactosyl-omega-mercapto-poly(ethylene glycol). *J Am Chem Soc*. **2001**, *82*, 26-30.
47. Takae, S.; Akiyama, Y.; Otsuka, H.; Nakamura, T.; Nagasaki, Y.; Kataoka, K. Ligand density effect on biorecognition by PEGylated gold nanoparticles: regulated interaction of RCA120 lectin with lactose installed to the distal end of tethered PEG strands on gold surface. *Biomacromolecules*. **2005**, *6*, 818-24.
48. Reynolds, A. J.; Haines, A. H.; Russell, D. A. Gold glyconanoparticles for mimics and measurement of metal ion-mediated carbohydrate-carbohydrate interactions. *Langmuir*. **2006**, *22*, 1156-63.
49. Ding, L.; Qian, R.; Xue, Y.; Cheng, W.; Ju, H. In situ scanometric assay of cell surface carbohydrate by glyconanoparticle-aggregation-regulated silver enhancement. *Anal Chem*. **2010**, *82*, 5804-9.
50. Martínez-Avila, O.; Hijazi, K.; Marradi, M.; Clavel, C.; Campion, C.; Kelly, C.; Penadés, S. Gold manno-glyconanoparticles: multivalent systems to block HIV-1 gp120 binding to the lectin DC-SIGN. *Chemistry*. **2009**, *15*, 9874-88.
51. Barrientos, A. G.; de la Fuente, J. M.; Rojas, T. C.; Fernández, A.; Penadés, S. Gold glyconanoparticles: synthetic polyvalent ligands mimicking glycocalyx-like surfaces as tools for glycobiological studies. *Chemistry*. **2003**, *9*, 1909-21.
52. Gianvincenzo, P. D,; Calvo, J.; Perez, S.; Álvarez, A.; Bedoya, L. M.; Alcamí, J.; Penadés, S. Negatively charged glyconanoparticles modulate and stabilize the secondary structures of a gp120 V3 loop peptide: toward fully synthetic HIV vaccine candidates. *Bioconjug Chem*. **2015**, *26*, 755-65.

53. Jain, P.; Shanthamurthy, C. D.; Chaudhari P. M.; Kikkeri, R. Rational designing of glycol-nanovechicles to target cellular heterogeneity. *Chem Sci*. **2021**, *12*, 4021-4027.
54. de la Fuente, J. M.; Eaton, P.; Barrientos, A. G.; Menéndez, M.; Penadés, S. Thermodynamic evidence for Ca2+-mediated self-aggregation of Lewis X gold glyconanoparticles. A model for cell adhesion via carbohydrate-carbohydrate interaction. *J Am Chem Soc*. **2005**, *127*, 6192-7.
55. Dykman, L. A. Gold nanoparticles for preparation of antibodies and vaccines against infectious diseases. *Expert Rev Vaccines*. **2020**, *19*, 465-477.
56. Dykman, L. A.; Khlebtsov, N. G. Immunological properties of gold nanoparticles. *Chem Sci*. 2017, *8*, 1719-1735.
57. Chiodo, F.; Enríquez-Navas, P. M.; Angulo, J.; Marradi, M.; Penadés S. Assembling different antennas of the gp120 high mannose-type glycans on gold nanoparticles provides superior binding to the anti-HIV antibody 2G12 than the individual antennas. *Carbohydr Res*. **2015**, *405*, 102-9.
58. Gianvincenzo, P. D.; Calvo, J.; Perez, S.; Álvarez, A.; Bedoya, L. M.; Alcamí, J.; Penadés, S. Negatively charged glyconanoparticles modulate and stabilize the secondary structures of a gp120 V3 loop peptide: toward fully synthetic HIV vaccine candidates. *Bioconjug Chem.* **2015**, *26*, 755-65.
59. Trabbic, K. R.; Kleski, K. A.; Barchi, J. J. Jr. A. Stable Gold-Nanoparticles-Based Vaccine for the Targeted Delivery of Tumor-Associated Glycopeptide Antigens. *ACS Bio & Med Chem Au*. **2021**.
60. Manea, F.; Bindoli, C.; Fallarini, S.; Lombardi, G.; Polito, L.; Lay, L.; Bonomi, R.; Mancin, F.; Scrimin, P. Multivalent, saccharide-functionalized gold nanoparticles as fully synthetic analogs of type a *Neisseria meningitidis* Antigens. *Adv Mater*. **2008**, *20*, 4348–4352.
61. Vetro, M.; Safari, D.; Fallarini, S.; Salsabila, K.; Lahmann, M.; Penadés, S.; Lay, L.; Marradi, M.; Compostella, F. Preparation and immunogenicity of gold glyco-nanoparticles as antipneumococcal vaccine model. *Nanomedicine (Lond)*. **2017**, *12*, 13-23.
62. Chaudhary, P. M.; Sangabathuni, S.; Murthy, R. V.; Paul, A.; Thulasiram, H. V.; Kikkeri, R. Assessing the effect of different shapes of glyco-gold nanoparticles on bacterial adhesion and infections. *Chem Commun (Camb)*. **2015**, *51*, 15669-72.
63. Sangabathuni, S.; Murthy, R. V.; Chaudhary, P. M.; Surve, M.; Banerjee, A.; Kikkeri R. Glyco-gold nanoparticle shapes enhance carbohydrate-protein interactions in

mammalian cells. *Nanoscale*. **2016**, *8*, 12729-35.

64. Sangabathuni, S.; Murthy, R. V.; Chaudhary, P. M.; Subramani, B.; Toraskar, S.; Kikkeri, R. Mapping the Glyco-Gold Nanoparticles of Different Shapes Toxicity, Biodistribution and Sequestration in Adult Zebrafish. *Sci Rep*. **2017**, *7*, 4239.

CHAPTER-2

Exploring the Influence of Shapes and Heterogeneity of Glyco-Gold Nanoparticles on Bacterial Binding for Preventing Infections

Abstract:

To investigate the effects of the heterogeneity and shape of glyco-nanoprobes on carbohydrate–protein interactions (CPIs), α-D-mannose- and β-D-galactose-linked homo- and heterogeneous glycodendrons were synthesized and immobilized on spherical and rod-shaped gold nanoparticles (AuNPs). Lectin and bacterial binding studies of these glyco-AuNPs clearly illustrate that multivalences and shape of AuNPs contribute significantly to CPIs than the heterogeneity of glycodendrons. Finally, a bacterial infection of HeLa cells was effectively inhibited by the homogeneous glycodendron-conjugated rod-shaped AuNPs relative to their heterogeneous counterparts. Overall, these results provide insight into the role of AuNP shape and multivalency as potential factors to regulate CPIs.

2.1 Introduction:

It is widely accepted that carbohydrate–protein interactions (CPIs) play an important role in determining biological complexity.[1-3] However, the ability of carbohydrate ligands to participate in biological activities is related to their multivalent binding, as monovalent CPIs are extremely weak.[4-6] To understand the fundamental basis of these interactions, multivalent probes, including glycopolymers, glycodendrimers, glycoliposomes, glycopeptides, janus-glycodendrimers, and glyconanoparticles have been synthesized.[6-41] In addition to multivalency, a consistent body of results has demonstrated that symmetry, shape, and heterogeneity of the glycodendrimers are important parameters to fine tune the avidity of CPIs. For example, glycodendrimers of C_5 symmetry of GM1 and C_3 symmetry of GM3 ganglioside were found to inhibit cholera toxin binding and influenza virus hemagglutination selectively over the linear analogues.[42,43] Hartmann and co-workers synthesized programmable sequences of monodispersed homo- and heteroglyco-oligomers and they observed that heterogeneity in the glyco-oligomers enhanced the relative binding affinity.[44] Similarly, Lindhorst and co-workers synthesized heteroglycoclusters carrying mannose, fucose, and lactose to determine the binding affinity with bacterial type1 fimbriae (FimH) lectin.[45] In addition to heterogeneity in the glycodendrimers, we recently reported that different shapes of the glyco-gold nanoparticles exert disparity in CPIs and influence bacterial adhesion.[46,47] Although the shape of the glyconanoparticles and heterogeneity of the glycodendrimers independently contribute to multivalent lectin–carbohydrate interactions, the combined action could be interesting to improve the sensitivity and selectivity of CPIs. To study this aspect, herein we present the synthesis of a new set of glyco-AuNPs carrying homo- and heterogeneous glycodendrons of mannose and galactose carbohydrate scaffolds. Lectin binding and bacterial agglutination assays were performed to optimize the parameters essential for the highest CPIs. Finally, bacterial cell infection was inhibited in the presence of glyco-AuNPs to understand the significance of multivalency, shape, and heterogeneity in CPIs.

2.2 Results and Discussion:

2.2.1 Synthesis of Tripod Molecules:

Homo- and heteroglycodendrons **1–4** were synthesized by using a slightly modified procedure of a published protocol (Scheme 1 and 2) .[52] Briefly, pentafluorophenol active ester **7** was reacted with various stoichiometric amounts of 2-aminoethoxy ethanol derivatives of mannose or galactose (**5** or **6**) to obtain tri- and di-substituted dendrons **8–11**. Compounds **9** and **10** were treated with 1.2 equivalent of **5** or **6** to yield heterogeneous glycodendrons **12** and **13**

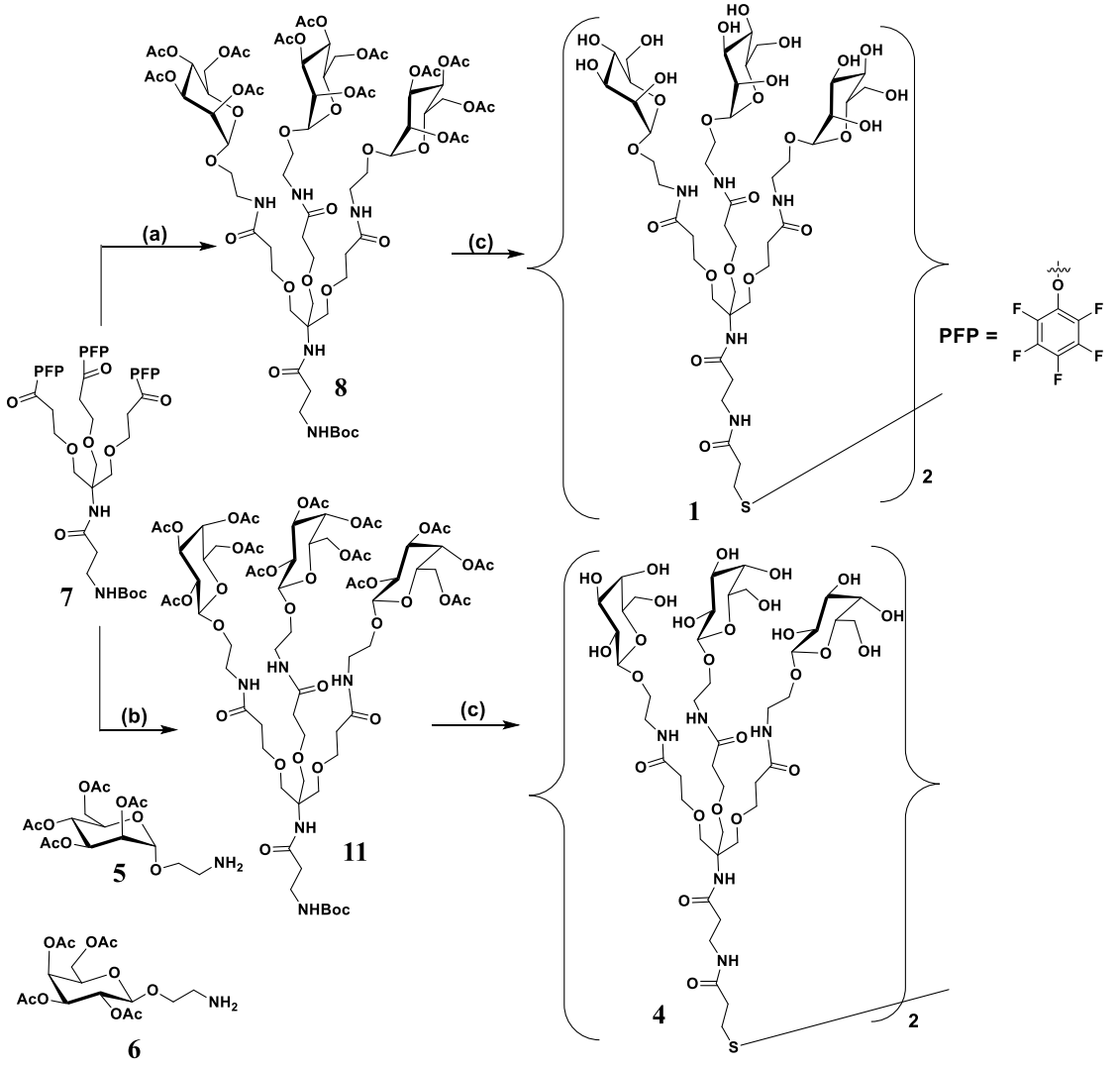

Scheme 1. Synthesis of glycodendrons **1** and **4**: a) **5**, Et_3N, DCM, RT, 12 h; b) **6**, Et_3N, DCM, RT, 12 h; c) i) DCM/TFA (4:1), ii) dithiobis(succinimidyl propionate), Et_3N, DMF, 45 °C, 4 h, c) NaOMe, MeOH, RT, 12 h.

(Scheme 2). These dendrons were deprotected and coupled with dithiobis(succinimidyl propionate) followed by deacetylation with sodium methoxide to yield compounds **1–4** (Scheme 1 and 2).

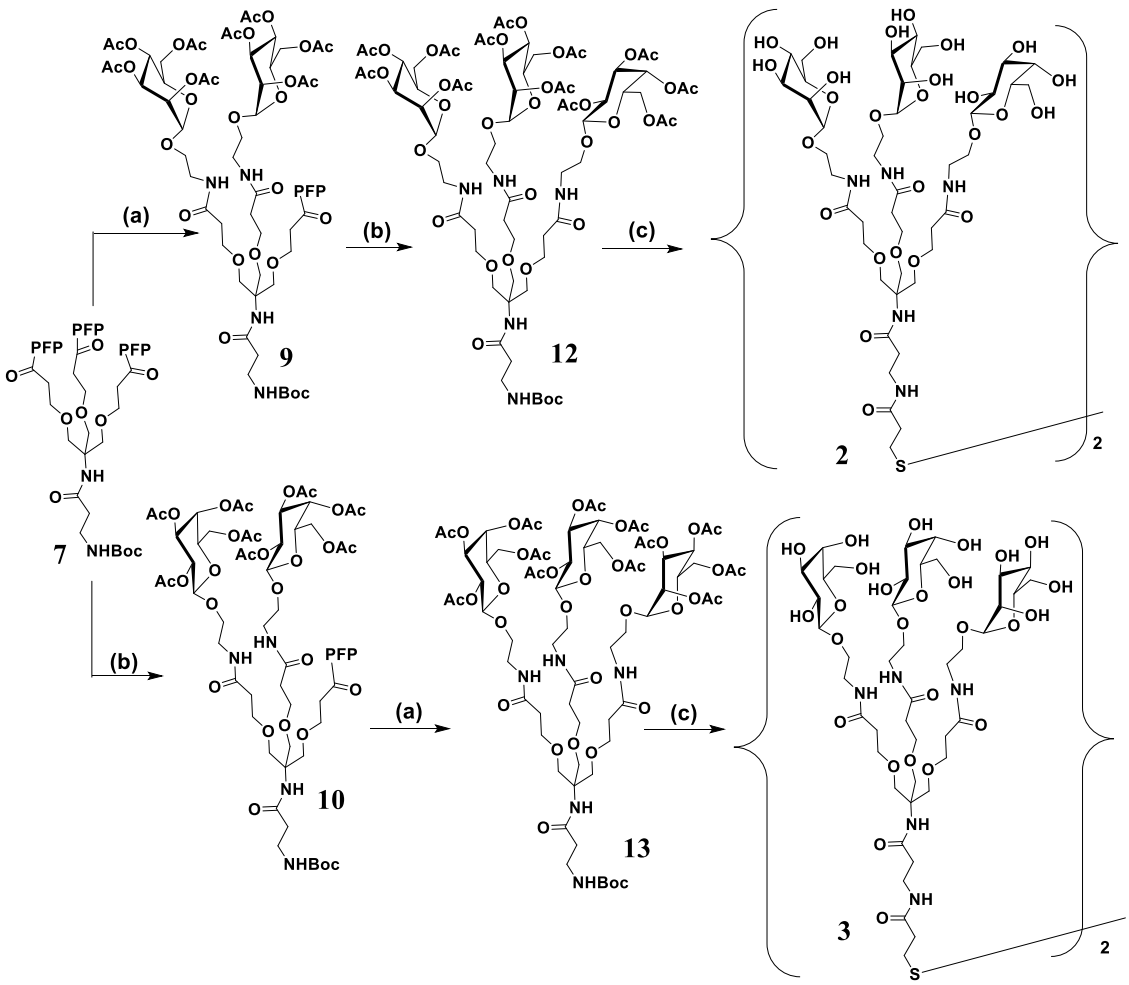

Scheme 2. Synthesis of glycodendrons **2** and **3**: a) **5**, Et_3N, DCM, RT, 12 h; b) **6**, Et_3N, DCM, RT, 12 h; c) i) DCM/TFA (4:1), ii) dithiobis(succinimidyl propionate), Et_3N, DMF, 45 °C, 4 h, c) NaOMe, MeOH, RT, 12 h.

2.2.2 Synthesis of Glyco-gold Nanoparticles:

Spherical and rod-shaped AuNPs were synthesized by reducing chloroauric acid with sodium citrate and seeding growth method as reported previously.[46, 47] The shape and size of the glyco-AuNPs were confirmed by transmission electron microscopy (TEM) and UV/Vis ab-sorption spectroscopy (Figure 1). Finally, glycodendrons **1–4** were immobilized on AuNPs by a ligand-exchange process (R-1 to R-4 and S-1 to S-4, Scheme 3). Further, shape and size of the glyco-AuNPs were confirmed by UV/Vis ab-sorption spectroscopy (Figure 1-i and 1-ii). The glycodendrons functionalization on the surface of gold nanoparticles were confirmed by the changes in zeta potential values (Table 1). The zeta potentials of spherical AuNPs changed from -29.7 to +3.3, indicating the sugar ligands displaced the negatively charged citrate ligands.

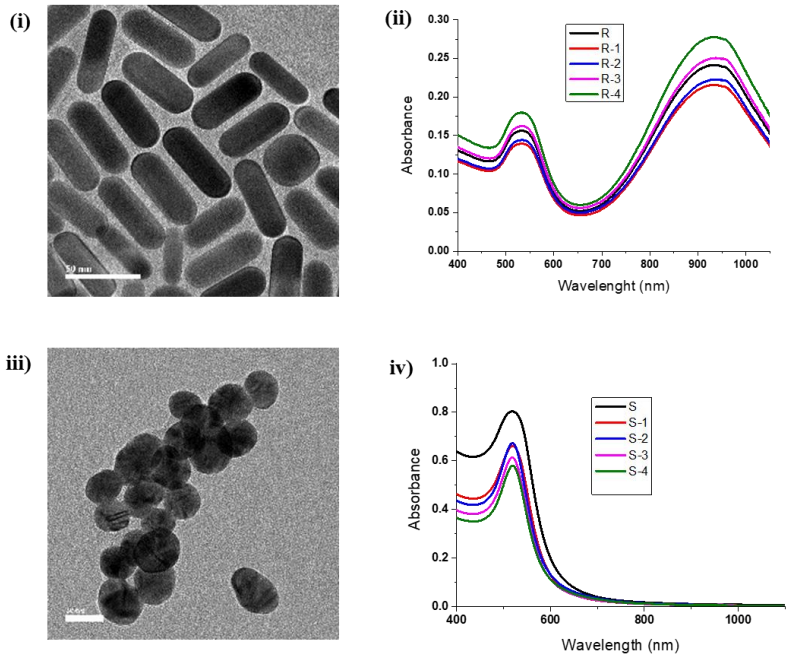

Figure 1. HR-TEM images and UV/Visible spectra of gold nanoparticles. i) HR-TEM image of rod gold nanoparticles (scale bar 50 nm). ii) UV/Visible spectra of non-conjugated (R) and dendrons conjugated (R-1, R-2, R-3 and R-4) gold rod nanoparticles. iii) HR-TEM image of sphere gold nanoparticles (scale bar 15 nm) iv) UV/Visible spectra of non-conjugated (S) and dendrons conjugated (S-1, S-2, S-3 and S-4) sphere gold nanoparticles.

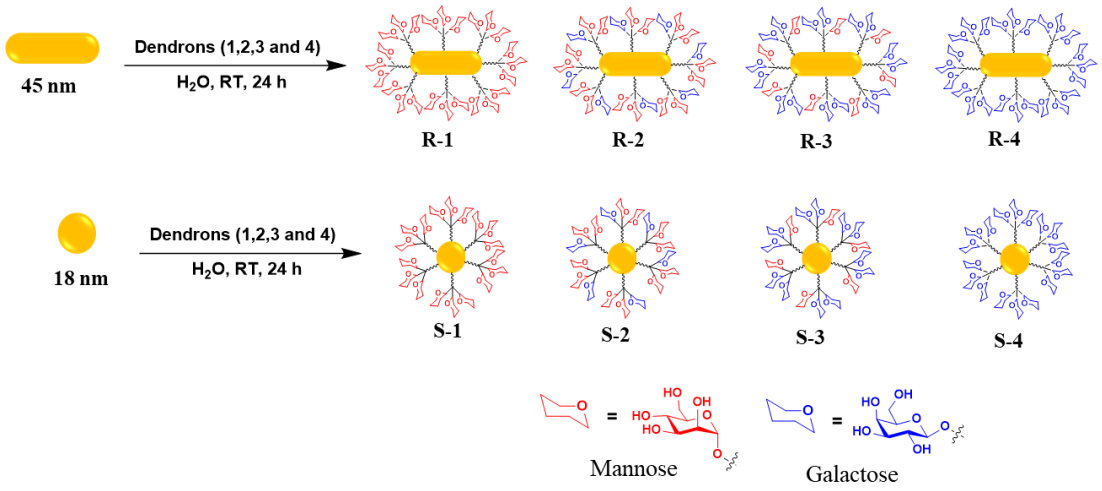

Scheme 3. Synthesis of glyco-gold nanoparticles. Glycodendrons (**1-4**) were functionalised on rod and sphere shaped nanoparticles.

Similarly, a decrease in the zeta potentials of glyco-conjugated rod-AuNPs relative to their native form indicates a ligand-exchange mechanism between the cetyltrimethylammonium bromide (CTAB) surfactant and glycodendrons (Table 1). The quantification of sugar scaffold on AuNPs was done by the phenol–sulfuric acid method (Table 1).[48]

Table 1. The physical characteristic of gold nanoparticles.

Sr. No.	Nanoparticles (Nps)	Zeta-potential (mv)	Sugar Concentration (mg/mL)	ConA binding IC_{50} (NPs/mL)
1	Rod	27.8 ± 1.4	-	-
2	Sphere	-29.7 ± 1.1	-	-
3	S-1	-7.8 ± 0.9	1.12 ± 0.14	4.3×10^5
4	S-2	5.2 ± 0.7	1.08 ± 0.09	6.1×10^5
5	S-3	3.3 ± 1.1	1.17 ± 0.11	6.9×10^5
6	S-4	5.3 ± 0.5	1.05 ± 0.07	-
7	R-1	12.7 ± 1.1	1.34 ± 0.23	2.1×10^5
8	R-2	7.64 ± 0.6	1.21 ± 0.21	5.2×10^5
9	R-3	8.1 ± 0.7	1.27 ± 0.15	6.3×10^5
10	R-4	5.8 ± 0.4	1.30 ± 0.17	-

2.2.3 ELISA lectin inhibition assay:

To establish carbohydrate–protein mediated interactions, we selected concanavalin (ConA) lectin binding and *E. coli* strains ORN 178 and ORN 208 for bacterial adhesion studies.[11-20] These two *E. coli* strains were selected because they had previously been shown to display antagonist and agonist activities against mannose multivalent interactions.[15]

To address the biological significance of glyco-AuNPs, their binding affinity to ConA lectin was established.[50] We performed inhibition studies for the binding of these lectins to mannose–BSA in the presence of homo- and hetero-glyco-AuNPs and quantitation was reported as the IC_{50} value (Table 1 and Figure 2). As expected, all mannose glycodendrons exhibited strong inhibition relative to galactose-capped glyco-AuNPs. Among the mannose-AuNPs, we observed two distinct types of binding patterns. Between the homo- and heteroglyco-AuNPs, homo-glycodendrons conjugated AuNPs showed strong binding affinity over their hetero-glyco-AuNPs analogues, indicating that the homo-multivalency is an important factor to

increase the binding affinity of CPIs compared to heterogeneity. Rod-shaped homo-glyco-AuNPs showed 1.5 to 2 fold higher sensitivity to their spherical glyco-AuNPs counterparts, indicating that spatial arrangement and aspect ratio of AuNPs are the determinants for high binding affinity.

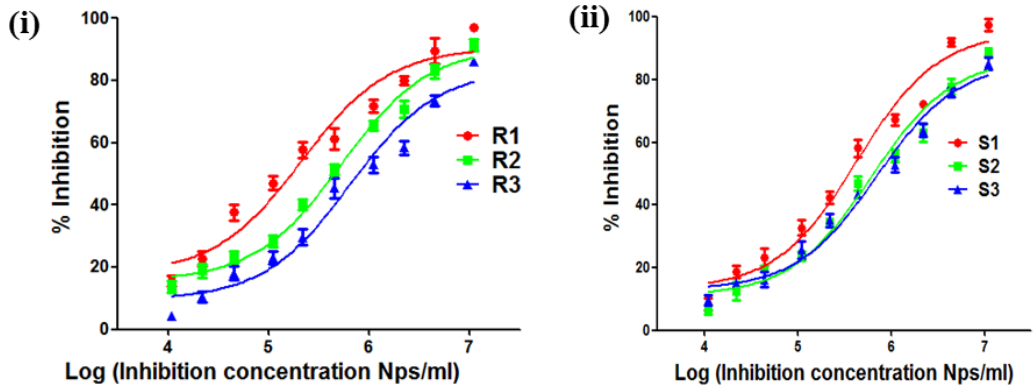

Figure 2. ConA lectin inhibition assay of glycogold nanoparticles. i) IC_{50} values for rod nanoparticles ii) IC_{50} values of sphere nanoparticles.

2.2.4 Bacterial aggregation experiment:

After studying mannose-specific lectin binding, our next experiment was to establish bacterial binding affinity. In this experiment, we incubated homo- and hetero-glycodendroncapped AuNPs (500 µg/mL) with *E. coli* ORN 178 and ORN 208 for 1 h in PBS. Bacterial media was then centrifuged, and the aggregates formed by the bacteria in the presence of glyco-AuNPs were imaged and quantified. As expected, a large amount of bacterial aggregation was observed with mannose-coated AuNPs relative to galactose-coated AuNPs (Figure 3). To determine the sensitivity of bacterial recognition, we performed bacterial aggregation assays using different concentrations of homo- and hetero-mannose glyco-AuNPs (R-1 to R-3 and S-1 to S-3; Figure 4 and 5). We observed two phases of fluorescence aggregation: a shape-dependent aggregation, which can be interpreted as shape-mediated CPIs, and a homo- and heterogeneous glyco-microenvironment on top of the AuNPs, which is expected to fine tune the bacterial aggregation. The rod-shaped mannose-AuNPs displayed 5 to 10 fold higher bacterial aggregation at different concentrations than their spherical counterparts. These results correlate well with previous bacterial binding studies.[46] R-1 revealed similar or nearly 1.5 fold higher bacterial aggregation relative to hetero-mannose AuNPs.

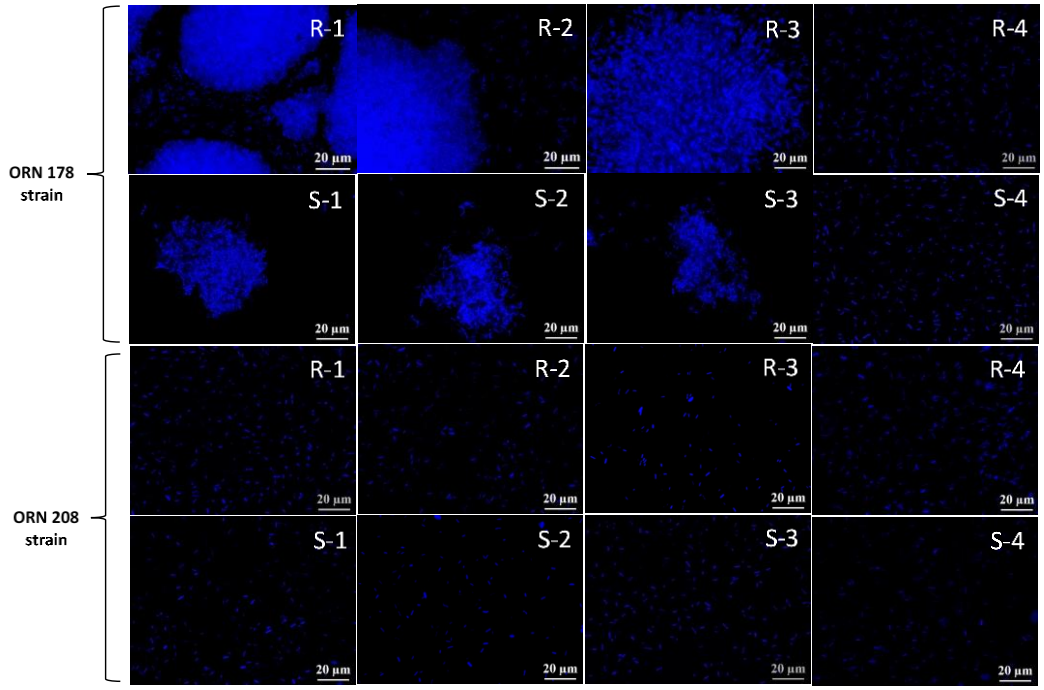

Figure 3. Confocal microscopy images of bacterial aggregation (*E. coli* ORN 178 and *E. coli* ORN 208) with glycogold nanoparticles (scale bar 20 µm). Sugar concentration 500µg/mL.

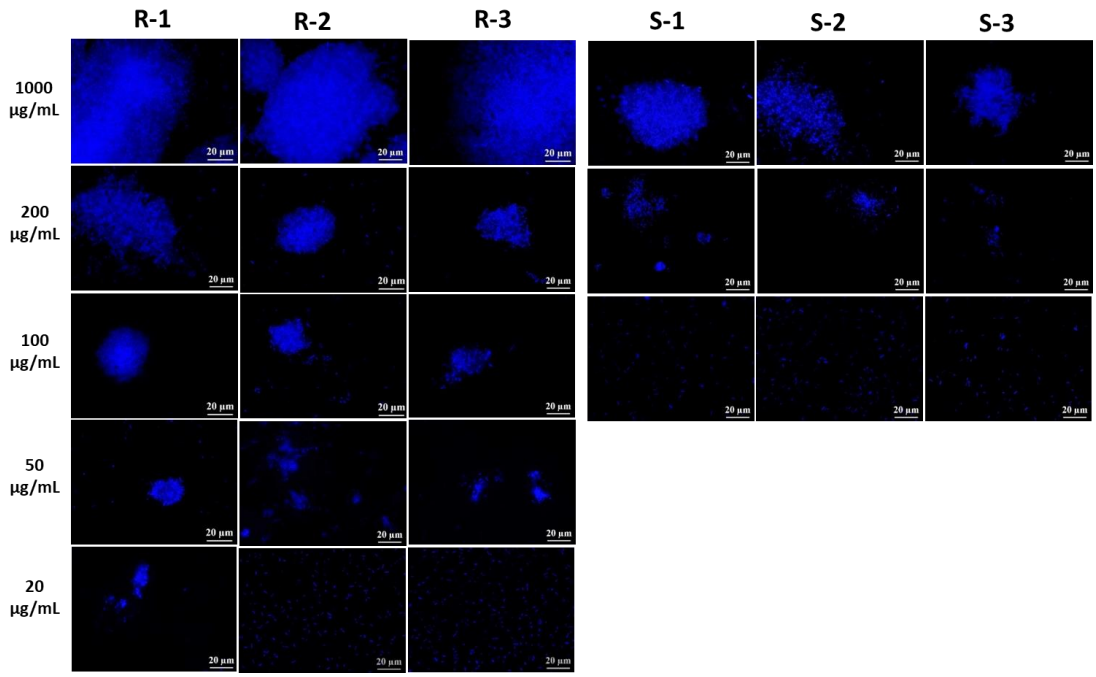

Figure 4. Confocal microscopy images of bacterial aggregation (*E. coli* ORN 178) with glycogold nanoparticles at different concentration (scale bar 20 µm).

At the highest concentration of AuNPs used (1000 µg/mL), the difference between homo and hetero-glyco-AuNPs was nearly 1.5-fold. However, as the concentration of AuNPs decreased,

the fluorescent intensities of the bacterial aggregations was similar to each other and displayed a detection limit of 20 µg/mL.

Interestingly, the spherical AuNPs displayed no such significant difference in the fluorescence intensity between S-1 to S-3 at different concentrations and displayed 200 µg/mL detection limits. Based on these results, we can hypothesize that factors such as aspect ratio and effective available surface area of rod-AuNPs contribute to strong aggregation over their spherical counterparts, while the heterogeneous form of dendrons displayed the least impact on bacterial aggregation. To further validate the above results, SEM images were obtained for *E. coli* ORN 178 treated with various concentrations (500 and 100 µg/mL) of glyco-AuNPs

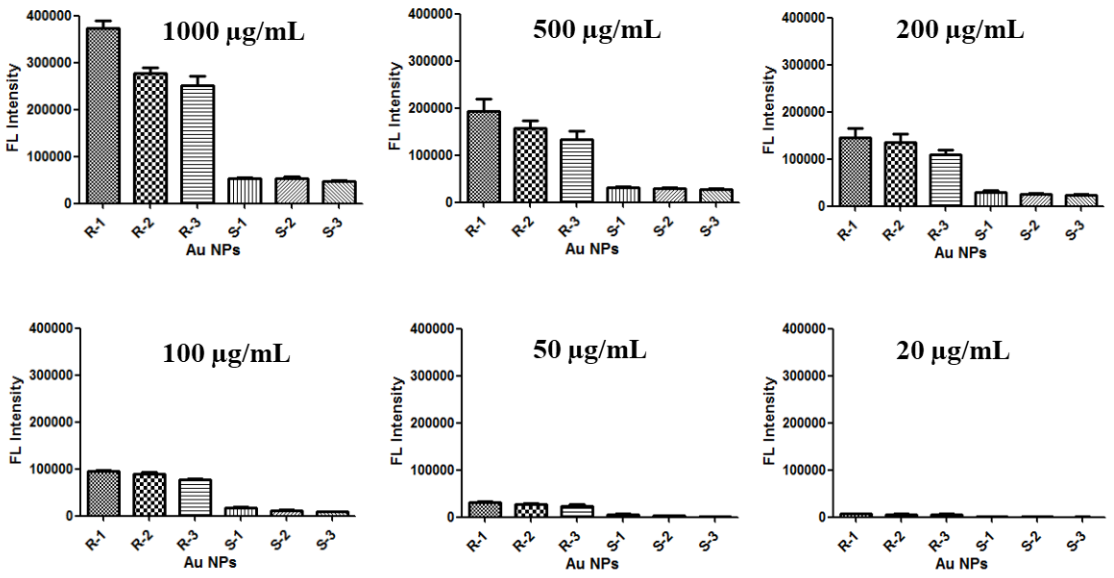

Figure 5. Relative fluorescence intensity graphs of bacterial aggregation (*E. coli* ORN 178) experiment at different concentration of glycogold nanoparticles.

(Figure 6). As expected, the relative amount of mannose rod-shaped AuNPs involved in effective CPIs is higher than spherical AuNPs.[51] On close examination of the rod-shaped AuNPs, we observed monodispersed rod AuNPs throughout the bacterial cell surfaces. In contrast, spherical AuNPs under the same conditions resulted in minimal aggregation, indicating that the large surface area of rod AuNPs is crucial for strong binding and sensitivity. All these results correlate well with the mathematical modelling and flow chemistry experiments reported by Kohlar et al.[52]

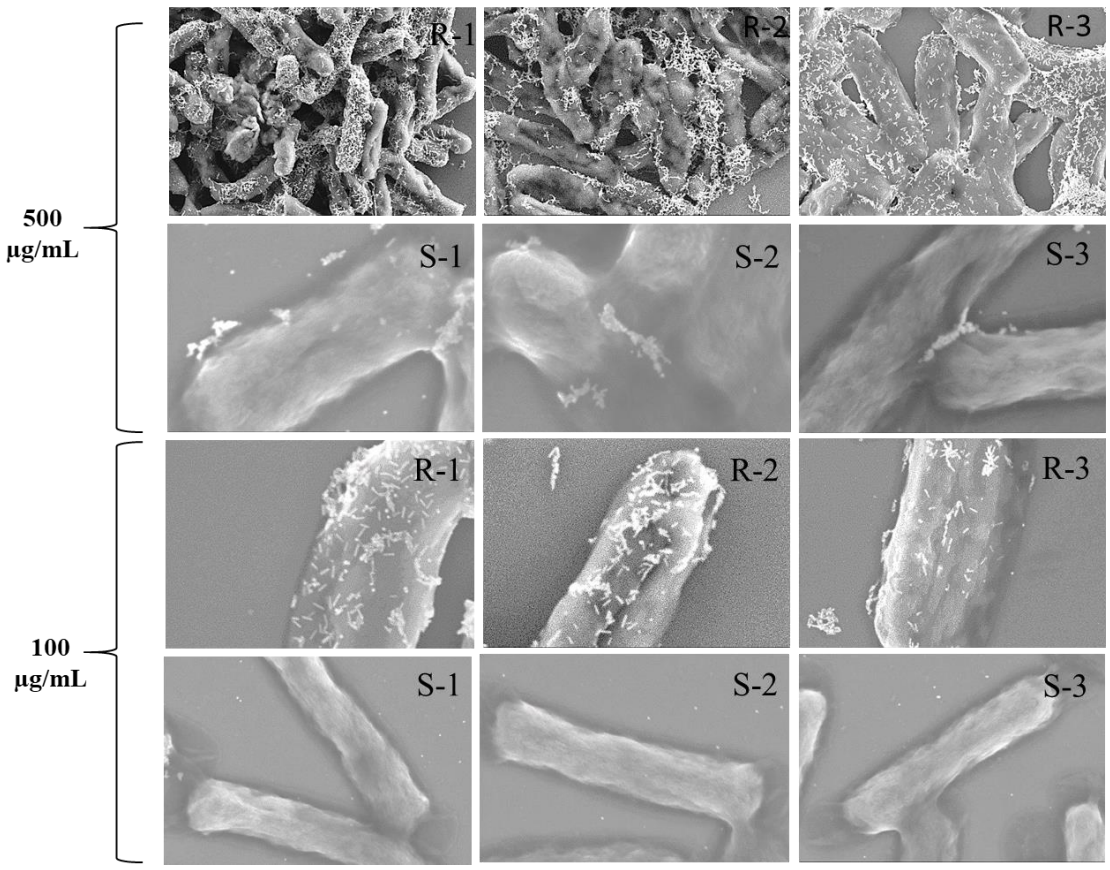

Figure 6. FE-SEM images of bacteria (*E. coli* ORN 178) with glyco-gold nanoparticles at different concentration.

2.2.5 Bacterial inhibition experiment:

Finally, the potential applications of these glyco-AuNPs in the inhibition of bacterial infection of HeLa cells was established. Before performing the inhibition assay, we first evaluated the toxicity of the glyco-AuNPs in Hela cells. Concentration dependent toxicity assays showed that glyco-AuNPs are nontoxic and biocompatible for cellular assay (Figure 7-i). HeLa cells have been reported to express high levels of mannose at the cell surface. It is expected that *E. coli* ORN 178 infect HeLa cells via specific CPIs, and addition of glyco-AuNPs inhibit the process via blocking strong affinity toward FimH receptors on the ORN 178 strain. Glyco-AuNPs of rod and spherical shapes at six different concentrations (5–100 µg/mL) were treated with bacteria before treating with HeLa cells. After 1 h of infection, unbound bacteria were separated and quantified by measuring the fluorescence intensity of DAPI. We observed that rod-shaped glyco-AuNPs and high-mannose inhibited bacterial infection more efficiently than their spherical counterparts (Figure 7-ii) and heterogeneous glyco-gold nanoparticles (R-2 to R-3 and S-2 to S-3) (Figure 7-ii). All these results correlated to our previous work.[46, 47] Moreover, this study further refined the factors that will preferentially influence CPIs.

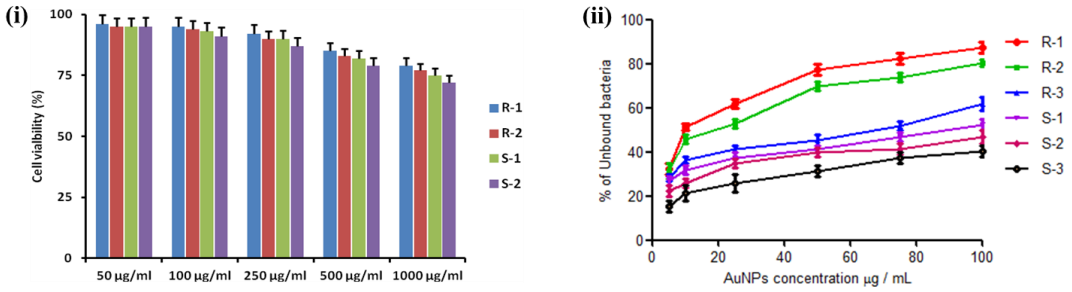

Figure 7. i) MTT assay of glyco-AuNPs with HeLa cell for 24 h. ii) Glyco-AuNPs mediate the inhibition of *E. coli* ORN 178 infection of HeLa cells. Quantification was determined with respect to DAPI fluorescence intensity, which was calculated from the average of three independent experiments.

2.3 Conclusion:

In summary, we have synthesized a fused system containing homo- and hetero-glycodendrons on two different shapes of gold nanoparticles. In a first step, mannose or galactose units were stoichiometrically conjugated on tripod active ester followed by a second substitution. The fourth arm of the tripod was further functionalized with a thiol linker for glycoconjugation on AuNPs. The lectin binding studies clearly displayed mannose multivalences and shape as an important parameter to fine tune CPIs, while the heterogeneity of the dendrons showed least impact on CPIs. This trend continued even with bacterial aggregation and detection and infection. Overall, these results propose new parameters to design smart glycoprobes to target specific CPIs more efficiently.

2.4 Experimental Section:

2.4.1 General information:

All chemicals were of reagent grade and, unless otherwise noted, were used as supplied. TLC was performed with Merck silica gel 60 F_{254} plates (0.25 mm) and visualized by dipping in CAM/ninhydrin solution and heating. Column chromatography was carried out on Fluka 22 Kieselgel 60, mesh 100–200. UV/Vis measurements were performed on an Evolution 300 UV/Vis spectrophotometer (Thermo Fisher Scientific, USA). ^{1}H and ^{13}C NMR spectra were recorded on a Jeol 400 MHz instrument. Chemical shifts (δ) are reported in ppm, coupling constants (J) in Hz. Residual solvents, for $CDCl_3$ δ_H: 7.26 ppm, δ_C: 77.3 ppm, and D_2O δ_H: 4.75 ppm are used as an internal reference.

2.4.2 Synthesis of dendrons:

General synthetic procedure A: In a solution of pentafluorophenol active ester **7** (1.0 equiv) and amino-linked sugar (3.2 equiv) in anhydrous DCM then Et_3N (3.2 equiv) was added in the reaction solution, and the reaction mixture was stirred at RT for 12 h. After completion of the reaction, the solvent was evaporated, and the residue was purified by silica gel column chromatography (1:10, MeOH:DCM) to afford the desired compound as a colorless solid.

General synthetic procedure B: In a solution of pentafluorophenol active ester **7** (1.o equiv) and amino-linked sugar (2.0 equiv) in anhydrous DCM then Et_3N (2.0 equiv) was added in the reaction solution, and the reaction mixture was stirred at RT for 12 h. After completion of the reaction, the solvent was evaporated and resulting residue was purified by silica gel column chromatography (2:3, acetone:ethyl acetate) to afford desired compound as colorless solid.

General synthetic procedure C: In a solution of di-substituted glycodendron (1.0 equiv) and amino-linked sugar (1.1 equiv) in anhydrous DCM then Et_3N (1.1 equiv) was added in the reaction solution, and the reaction mixture was stirred at RT for 12 h. Then the solvent was evaporated, and the residue was purified by silica gel column chromatography (1:10, MeOH:DCM) to afford the desired compound as a colourless solid.

General synthetic procedure D: Homo- or hetero-glycodendron (1.0 equiv) was dissolved in DCM/TFA (4:1) and stirred at RT for 2 h. Then solvent was removed, and the residue was co-evaporated with toluene. The crude residue was mixed with dithiobis(succinimidyl propionate) (0.4 equiv) in DMF, Et_3N (1.0 equiv) was added to the reaction mixture, and stirred at 45 $^{\circ}$C for 4 h. Next, the solvent was evaporated, and the residue was diluted with EtOAc and extracted with a saturated solution of $NaHCO_3$ (2×10 mL) and washed with water, brine, then organic layer dried on Na_2SO_4 and concentrated. To this crude compound, methanol (10 mL) and NaOMe (30 equiv) were added at 0 $^{\circ}$C and stirred at RT for 12 h. The reaction mixture was neutralized with acidic resin (IR-120), filtered, and concentrated. The residue was purified by BOND ELUT LRC-C18 column using water as eluent, and the purified fraction was lyophilized to afford the final compound.

Synthesis of compound **8**: General procedure **A** using PFP active ester **7** (300 mg, 0.29 mmol) and **5** (373 mg, 0.95 mmol) in 10 mL anhydrous DCM and Et_3N (128 mL, 1.0 mmol) and purification by column chromatography yielded **8** (245 mg, 51%). ^{1}H NMR (400 MHz,

$CDCl_3$); δ = 6.79 (bs, 2H), 6.43 (s, 1H), 5.37 (bs, 1H), 5.28–5.23 (m, 9H), 4.82 (d, J=1.4 Hz, 3H), 4.25 (dd, J=12.2, 5.4 Hz, 3H), 4.09 (dd, J=12.2, 2.4 Hz, 3H), 3.99–3.97 (m, 3H), 3.79–3.76 (m, 3H), 3.70 (t, J=5.8 Hz, 6H), 3.71-3.68 (m, 6H), 3.56–5.53 (m, 6H), 3.41–3.32 (m, 6H), 2.46–2.38 (m, 8H), 2.13 (s, 9H), 2.08 (s, 9H), 2.03 (s, 9H), 1.98 (s, 9H), 1.41 ppm (s, 9H). ^{13}C NMR (101 MHz, $CDCl_3$); δ = 171.74, 170.79, 170.23, 169.77, 156.14, 97.72, 69.44, 69.27, 68.76, 67.43, 67.21, 66.15, 62.53, 39.07, 36.54, 29.38, 28.54, 20.98, 20.85, 20.81 ppm. HRMS, ESI-MS: m/z calcd for $C_{69}H_{106}N_5O_{39}$ $[M+H]^+$; 1628.6466, found 1628.6462.

Synthesis of compound **9**: General procedure **B** using PFP active ester **7** (300 mg, 0.29 mmol) and **5** (233 mg, 0.59 mmol) in 10 mL anhydrous DCM and Et_3N (82 mL, 0.6 mmol) and purification by column chromatography yielded **9** (160 mg, 38%). ^{1}H NMR (400 MHz, $CDCl_3$) δ = 6.71 (bs, 1H), 6.38 (s, 1H), 5.29–5.24 (m, 8H), 4.81 (s, 2H), 4.25 (dd, J=12.2, 5.4 Hz, 2H), 4.10 (d, J=12.2 Hz, 2H), 3.99–3.94 (m, 2H), 3.81–3.76 (m, 7H), 3.72–3.63 (m, 9H), 3.56–3.52 (m, 4H), 3.39–3.52 (m, 4H), 2.91 (t, J=6.0 Hz, 2H), 2.45 (t, J=5.4 Hz, 4H), 2.14 (s, 6H), 2.09 (s, 6H), 2.04 (s, 6H), 1.98 (s, 6H), 1.41 ppm (s, 9H). ^{13}C NMR (101 MHz, $CDCl_3$) δ = 171.79, 170.81, 170.24, 169.78, 167.79, 156.11, 97.68, 69.38, 69.20, 68.73, 67.38, 67.19, 66.08, 62.48, 39.04, 36.48, 29.77, 29.31, 28.47, 20.94, 20.87, 20.77 ppm. HRMS, ESI-MS: m/z calcd for $C_{59}H_{82}F_5N_4O_3$ $[M+H]^+$; 1421.4935, found 1421.4936.

Syntheis of compound **10**: General procedure **B** using PFP active ester **7** (300 mg, 0.29 mmol) and **6** (233 mg, 0.59 mmol) in 10 mL anhydrous DCM and Et_3N (82 mL, 0.6 mmol) and purification by column chromatography yielded **10** (143 mg, 34%). ^{1}H NMR (400 MHz, $CDCl_3$); δ = 6.44 (bs, 2H), 5.39–5.37 (m, 2H), 5.34 (s, 1H) 5.15 (dd, J=10.4, 7.8 Hz, 2H), 5.03–4.99 (m, 3H), 4.48 (d, J=7.8 Hz, 2H), 4.20–4.09 (m, 6H), 3.92 (t, J=6.6 Hz, 2H), 3.89–3.85 (m, 2H), 3.82–3.79 (m, 3H), 3.69–3.3.64 (m, 10H), 3.45–3.42 (m, 5H), 3.34 (dd, J=12.2, 6.2 Hz, 2H), 2.90 (t, J=6.0 Hz, 2H), 2.42–2.39 (m, 4H), 2.14 (s, 6H), 2.05 (s, 6H), 2.03 (s, 6H), 1.97 (s, 6H), 1.41 ppm (s, 9H). ^{13}C NMR (101 MHz, $CDCl_3$); δ = 170.52, 170.29, 170.18, 169.87, 169.85, 156.08, 101.48, 70.91, 70.80, 69.03, 68.97, 67.44, 67.08, 66.22, 61.31, 39.28, 36.60, 36.57, 29.35, 28.50, 20.91, 20.76, 20.73, 20.66 ppm. HRMS, ESI-MS: m/z calcd for $C_{59}H_{82}F_5N_4O_3$ $[M+H]^+$; 1421.4935, found 1421.4946.

Synthesis of compound **11**: General procedure **A** using PFP active ester **7** (300 mg, 0.29 mmol) and **6** (373 mg, 0.95 mmol) in 10 mL anhydrous DCM and Et_3N (128 mL, 1.0 mmol) and purification by column chromatography yielded **11** (231 mg, 48 %). ^{1}H NMR

(400 MHz, $CDCl_3$) δ = 6.49 (bs, 3H), 5.40 (d, J=2.6 Hz, 3H), 5.17 (dd, J=10.4, 7.8 Hz, 3H), 5.04 (dd, J=10.4, 3.4 Hz, 3H), 4.51 (d, J=7.8 Hz, 3H), 4.18–4.12 (m, 6H), 3.95 (t, J=6.6 Hz, 3H), 3.90–3.86 (m,3H), 3.73–3.69 (m, 16 H), 3.47–3.34 (m, 6H), 3.39–3.35 (m, 3H), 2.43–2.41 (m, 8H), 2.17 (s, 9H), 2.08 (s, 9H), 2.06 (s, 9H), 1.99 (s, 9H), 1.42 ppm (s, 9H). ^{13}C NMR (101 MHz, $CDCl_3$) δ = 171.41, 170.49, 170.27, 170.15, 169.81, 156.09, 101.47, 70.91, 70.83, 68.99, 67.47, 67.10, 61.33, 39.31, 36.63, 28.54, 20.94, 20.78, 20.76, 20.67 ppm. HRMS, ESI-MS: m/z calcd for $C_{69}H_{106}N_5O_{39}$ $[M+H]^+$; 1628.6466, found 1628.6445.

Synthesis of compound **12**: General procedure **C** using compound **9** (150 mg, 0.11 mmol) and **6** (49 mg, 0.13 mmol) in 10 mL anhydrous DCM and Et_3N (17 mL, 0.13 mmol) and purification by column chromatography yielded **12** (60 mg, 35 %). ^1H NMR (400 MHz, $CDCl_3$) δ = 6.82 (bs, 2H), 6.45 (bs, 1H), 5.39 (d, J=2.6 Hz, 1H), 5.30–5.25 (m, 6H), 5.16 (dd, J=10.4, 7.8 Hz, 1H), 5.03 (dd, J=10.5, 3.2 Hz, 1H), 4.83 (s, 2H), 4.50 (d, J=7.8 Hz, 1H), 4.27 (dd, J=12.4, 5.4 Hz, 2H), 4.16–4.09 (m, 4H), 3.98–3.96 (m, 2H), 3.91–3.87 (m, 1H), 3.80–3.77 (m, 3H), 3.71–3.67 (m, 14 H), 3.58–5.54 (m, 5H), 3.43–3.35 (m, 6H), 2.45–2.41 (m, 8H), 2.16 (s, 3H), 2.15 (s, 6H), 2.10 (s, 6H), 2.07 (s, 3H), 2.05 (s, 9H), 1.99 (s, 6H), 1.97 (s, 3H), 1.42 ppm (s,H). ^{13}C NMR (101 MHz, $CDCl_3$) δ = 170.83, 170.55, 170.30, 170.26, 169.82, 156.17, 101.53, 97.76, 70.96, 70.86, 69.48, 69.30, 69.05, 68.79, 67.49, 67.26, 67.15, 66.19, 62.56, 61.37, 39.37, 39.09, 36.58, 28.58, 21.05, 21.02, 20.89, 20.85, 20.72 ppm. HRMS, ESI-MS: m/z calcd for $C_{69}H_{106}N_5O_{39}$ $[M+H]^+$; 1628.6466, found 1628.6503.

Synthesis of compound **13**: General procedure **C** using compound **10** (150 mg, 0.11 mmol) and **5** (49 mg, 0.13 mmol) in 10 mL anhydrous DCM and Et_3N (17 mL, 0.13 mmol) and purification by column chromatography yielded **13** (64 mg, 37%) as colorless solid. ^1H NMR
(400 MHz, $CDCl_3$) δ = 6.85 (bs, 1H), 6.49–6.46 (m, 2H), 5.38 (d, J=2.6 Hz, 2H), 5.28–5.23 (m, 3H), 5.15 (dd, J=10.5, 7.8 Hz, 2H), 5.02 (dd, J=10.2, 3.6 Hz, 2H), 4.82 (d, J=1.2 Hz, 1H), 4.49 (d, J=7.8 Hz,2H), 4.25 (dd, J=12.3, 5.4 Hz, 2H), 4.15–4.11 (m, 4H), 3.98–3.92 (m,3H), 3.89–3.85 (m, 2H), 3.78–3.76 (m, 1H), 3.71–3.66 (m, 15 H), 3.56–3.54 (m, 3H), 3.45–3.42 (m, 4H), 3.37–3.33 (m, 3H), 2.44–2.39 (m, 8H), 2.15 (s, 6H), 2.14 (s, 3H), 2.09 (s, 3H), 2.06 (s, 6H), 2.04 (s,9H), 1.98 (s, 3H), 1.97 (s, 6H), 1.41 ppm (s, 9H). ^{13}C NMR (101 MHz, $CDCl_3$) δ = 170.80, 170.52, 170.28, 170.23, 170.17, 169.84, 169.79, 156.13, 101.49, 97.72, 70.92, 70.84, 69.45, 69.27, 69.01, 68.76, 67.46, 67.23, 67.11, 66.16, 62.53, 61.44, 61.34, 60.39, 59.92, 39.33, 39.05,36.65, 36.54, 29.80, 28.55, 20.99, 20.95, 20.86, 20.82, 20.79, 20.77, 20.69 ppm. HRMS, ESI-MS: m/z calcd for $C_{69}H_{106}N_5O_{39}$ $[M+H]^+$; 1628.6466, found 1628.6492.

Synthesis of compound **1**: General procedure **D** using compound **8** (100 mg, 0.06 mmol), dithiobis(succinimidyl propionate) (10 mg, 0.02 mmol) in 5 mL anhydrous DMF and Et_3N (11 mL, 0.1 mmol), NaOMe (101 mg, 1.8 mmol) yielded **1** (40 mg, 32%) as a white solid. ^{1}H NMR (400 MHz, D_2O) δ = 4.86 (d, J=1.6 Hz, 6H), 3.93 (dd, J=3.4, 1.8 Hz, 6H), 3.87 (dd, J=12.2, 1.8 Hz, 6H), 3.80–3.71 (m, 32 H), 3.67 (s, 12H), 3.62–3.60 (m, 18H), 3.51–3.45 (m, 6H), 3.42–3.38 (m, 8H), 2.96–2.93 (m, 4H), 2.67–2.63 (m, 4H), 2.51 (t, J=5.8 Hz, 12 H), 2.45 ppm (t, J=6.6 Hz, 4H). ^{13}C NMR (101 MHz, D_2O) δ = 174.21, 174.03, 173.57, 99.71, 72.88, 70.56, 70.06, 67.54, 66.72, 65.84, 60.93, 60.25, 39.03, 34.95 ppm. HRMS, ESI-MS: m/z calcd for $C_{86}H_{152}N_{10}O_{52}S_2$:1133.4396 found $[M+2Na]^{2+}$ 1133.4384.

Synthesis of compound **2**: General procedure **D** using compound **12** (100 mg, 0.06 mmol), dithiobis(succinimidyl propionate) (10 mg, 0.02 mmol) in 5 mL anhydrous DMF and Et_3N (11 mL, 0.1 mmol), NaOMe (101 mg, 1.8 mmol) in MeOH, yielded **2** (36 mg, 29 %). ^{1}H NMR (400 MHz, D_2O) δ = 4.86 (d, J=1.4 Hz, 4H), 4.40 (d, J=7.8 Hz, 2H), 3.99–3.97 (m, 2H), 3.94–3.93 (m, 6H), 3.87 (dd, J=12.2, 1.8 Hz, 4H), 3.80–3.72 (m, 32H), 3.67 (s, 12 H), 3.65–3.58 (m, 14H), 3.55–3.36 (m, 18H), 2.95 (t, J=6.8 Hz, 4H), 2.66 (t, J=6.7 Hz, 4H), 2.52 (t, J=5.6 Hz, 12 H), 2.45 ppm (t, J=6.6 Hz, 4H). ^{13}C NMR (101 MHz, D_2O) δ = 174.15, 173.50, 170.65, 102.96, 99.64, 75.13, 72.81, 72.65, 70.72, 70.49, 69.98, 68.56, 68.45, 68.34, 67.47, 66.65, 65.77, 60.94, 60.86, 60.18, 39.37, 38.96, 36.05, 35.82, 34.89, 33.07 ppm. HRMS, ESI-MS: m/z calcd for $C_{86}H_{152}N_{10}O_{52}S_2$:1133.4396, found $[M+2Na]^{2+}$:1133.4430.

Synthesis of compound **3**: General procedure **D** using compound **13** (100 mg, 0.06 mmol), dithiobis(succinimidyl propionate) (10 mg, 0.02 mmol) in 5 mL anhydrous DMF and Et_3N (11 mL, 0.1 mmol), NaOMe (101 mg, 1.8 mmol) yielded **3** (35 mg, 28%) as white solid. ^{1}H NMR (400 MHz, D_2O) δ = 4.88 (s, 2H), 4.41 (d, J=7.8 Hz, 4H), 4.08–3.93 (m, 12H), 3.90–3.71 (m, 32H), 3.68–3.62 (m, 24H), 3.56–3.52 (m, 6H), 3.49–3.41 (m, 14H), 2.96 (t, J=6.8 Hz, 4H), 2.67 (t, J=6.8 Hz, 4H), 2.54 (t, J=5.7 Hz, 12H), 2.47 ppm (t, J=6.6 Hz, 4H). ^{13}C NMR (101 MHz, D_2O) δ = 174.25, 174.03, 173.56, 103.03, 99.70, 75.20,72.86, 72.71, 70.79, 70.54, 70.47, 70.05, 68.62, 68.47, 68.41, 67.54,66.70, 65.83, 61.01, 60.26, 39.43, 39.02, 36.13, 35.89, 34.95, 33.13 ppm. HRMS, ESI-MS: m/z calcd for $C_{86}H_{152}N_{10}O_{52}S_2$:1111.4577, found $[M+2H]^{2+}$: 1111.4512.

Synthesis of compound **4**: General procedure **D** using compound **11** (100 mg,0.06 mmol), dithiobis(succinimidyl propionate) (10 mg, 0.02 mmol) in 5 mL anhydrous DMF and Et_3N (11 mL, 0.1 mmol), NaOMe (101 mg, 1.8 mmol) yielded **4**, (36 mg, 29%). ^{1}H NMR (400 MHz, D_2O) δ = 4.40 (d, J=7.8 Hz, 6H), 3.99–3.96 (m, 6H), 3.94–3.91 (m, 6H), 3.78–3.72 (m, 32H), 3.67–3.63 (m, 21H), 3.54–3.50 (m, 7H), 3.48–3.39 (m, 16H), 2.98–2.93 (m, 4H), 2.67–2.64 (m, 4H), 2.52 (t, J=5.8 Hz, 12 H), 2.45 (t, J=6.4 Hz, 4H).^{13}C NMR (101 MHz, D_2O) δ = 175.17, 174.27, 173.58, 103.04, 75.20, 72.73, 70.80, 68.63, 68.42, 67.54, 61.02, 39.44, 36.13, 35.69, 33.58, 33.24, 32.35. HRMS, ESI-MS:m/z calcd for $C_{86}H_{152}N_{10}O_{52}S_2$:1111.4577, found $[M+2H]^{2+}$:1111.4576.

2.4.3 Synthesis of dendrons conjugated AuNPs:

Synthesis of spherical AuNPs

Spherical shape AuNPs were synthesized by mixing 1 mL of 0.5 wt% sodium citrate with 20 mL of 0.2 mM $HAuCl_4$ aqueous solution at 100 °C till the solution turned pale red. After centrifugation at 18500×g for 10 min, the Au nanospheres were re-dispersed in deionized water.[46]

Synthesis of rod AuNPs

Rod-shaped gold nanoparticles coated with cetyltrimethylammonium bromide (CTAB) were synthesized via the seeding growth method.[49]

Seed solution: 5 mL, 0.20 M CTAB solution was mixed with 5 mL of 0.5 mM $HAuCl_4$. To the stirred solution, 0.60 mL of ice-cold 0.010 M $NaBH_4$ was added; this forms a brownish-yellow solution. After 2 min of the vigorously stirring solution was stored at 25 °C.

Growth solution: First, 5 mL of 0.15 M BDAC and 0.2 M of CTAB were mixed and dissolved mixture by sonication at 40 °C for 20 min. To this solution was added 200 mL of 4 mM of $AgNO_3$ followed by the addition of 5.0 mL of 1 mM of $HAuCl_4$ solution, and after gentle mixing of the solution, 70 mL of 0.0778 M ascorbic acid was added. The growth process starts with the addition 12 mL of seed solution, and it completes in 1 h. After centrifugation at 9800×g for 10 min, the nanorods were re-dispersed in deionized water.

Synthesis of dendron-conjugated AuNPs

Prior to conjugation, disulfide bond of the tripods was reduced to thiol by using TCEP (5 equivalent) in water and triopods were purified. Next, 0.5 mL of 1 mmol of the reduced tripods

in double-distilled water was added to 0.5 mL of the AuNPs solution. After incubation at room temperature for 12 h, the modified Au nanostructures were separated by centrifugation and re-dispersed in deionized water.

2.4.4 Zeta potential measurement:

We used the zeta-potential analyzer to measure the surface potential of AuNPs. The electrostatic potential on the particle surface is called the zeta-potential. In the measurement, we applied unit field strength (1 $Vm^{-}1$) to the AuNP solution.

2.4.5 Phenol-sulfuric acid method to quantify sugars on AuNPs:

The concentration of mannose/galactose sugars on AuNPs was determined by the phenol-sulfuric acid method. Sugar-functionalized AuNPs (100 mL) were mixed with concentrated sulfuric acid (750 mL, 100%) and aqueous phenol solution (5% w/v, 100 mL) in the 1.5 mL centrifuge tube and heated at 80 °C. After 5 min, the solution was cooled to room temperature, and the absorbance coefficient at 490 nm was measured. AuNPs as such in sulfuric acid was used as a control. The sugar concentration was estimated by comparing the absorption of the sample with a standard curve.

2.4.6 Lectin inhibition assay:

Mannose-BSA (50 µg/$mL^{-}1$) was immobilized on 96-well ELISA plates for overnight at 48 °C as reference ligand and incubated with horseradish peroxide (HRP) labelled ConA lectin (25 µg $mL^{-}1$) in the presence of various concentrations of glyco-gold nanoparticles (1.09×10^{4} to 1.09×10^{7} NPs) in HEPES buffer (pH 7.2 containing 0.15 M NaCl and 20 mM $CaCl_2$). After incubation for 2 h, wells were washed with HEPES buffer, and HRP-ConA was quantified by HRP-catalyzed color reaction using 2,2'-azi-nobis(2-ethylbenzothiazoline-6-sulfonic acid) diammonium salt (ABTS) as substrate. ConA concentration was determined by optical density at 480 nm. Prism software was used to plot the logarithmic curve of inhibition quantification of IC_{50} values.

2.4.7 Bacterial aggregation assay:

E. coli strains ORN 178 and ORN 208 were kindly provided by Prof. Orndorff (North Carolina State University, College of Veterinary Medicine, Raleigh, NC, USA). The *E. coli* strains were

grown overnight at 37 °C until they reached an approximate OD_{600} of 1.0. For aggregation assay 2 mL aliquots of bacteria of approximate OD_{600}. of 1.0 was centrifuged at 6500×*g* for 10 min to obtain a bacterial pellet. The resulting pellet was washed twice with PBS buffer and re-suspended in 1 mL PBS, and the concentration was adjusted to 10^8 bacteria in 1 mL. Bacterial PBS solution (100 mL) was mixed with different shapes and different sugar-coated AuNPs (500 µg mL^{-1}) and incubated at room temperature for 1 h with gentle shaking. Then, bacteria conjugated with nanoparticles were incubated with organic dye 4',6-diamidino-2-phenylindole dihydrochloride, (DAPI) at a dilution of 1:1000 for 15 min. Bacteria were then centrifuged at 6500×*g* for 10 min, and the pellet was washed twice with 100 mL of PBS. Pellet was dissolved in PBS and fixed with 4% (w/v) paraformaldehyde for 15 min. A drop of fixed solution was mounted on microscopic slides and imaged. The relative fluorescence intensity of bacterial aggregates was calculated by measuring the fluorescence intensity of 50 random aggregations using image J software.

2.4.8 FE-SEM images of nanoparticles and bacterial binding:

E. coli ORN 178 (approximate 10^8) were treated with various concentrations of glycogold nanoparticles for 1 h. Then bacterial pellet was dehydrated in ethanol gradient (10, 30, 70, 95, and 100%) and fixed with 4% glutaraldehyde for 2 h. These bacteria were placed on small piece of silicon wafer and dried under a vacuum in a desiccator. Before imaging, samples were coated with gold (Polaron SC 502 sputter coater) and SEM images were performed in FE-SEM instrument.

2.4.9 Cell viability assay:

HeLa (1×10^5 cells per well) were seeded in 96- well microtiter plate and incubated overnight in a 5% CO_2 incubator at 37 °C for attachment. Cells were then treated with glycogold nanoparticles (**R-1**, **R-2**, **S-1** and **S-2**) at different concentrations (50, 100, 250, 500 and 1000 µg mL^{-1}) for 24 h. The medium was removed, and 20 mL of MTT reagent (5 µg mL^{-1}) and 100 mL of fresh medium was added to each well and incubated for 4 h at 37 °C. Formazan crystals were then solubilized in 100 mL of the solubilisation buffer (10% SDS in 0.01 M HCl) and incubated overnight. Absorbance was measured with a spectrophotometer at 550 nm. The percent cell viability was calculated considering the untreated cells as 100% viability.

2.4.10 Inhibition of bacterial binding to HeLa cells:

HeLa cells (1×10^5 cells per well) were seeded in a 96-well plate and incubated overnight in a 5% CO_2 incubator at 37 ˚C. Bacteria ORN 178 were stained with DAPI. Then ORN 178 (0.25×10^8 cells per mL⁻1) and 100 mL of (5–100 µg mL⁻1) different concentrations of rod and spherical mannose-AuNPs incubated. Pre-incubated mannose- AuNPs and bacteria were added to the Hela cells. After 60 min, the plate was centrifuged at 200×*g* for 5 min and the supernatant was collected, and DAPI fluorescence was measured in a fluorescent.

2.5 References:

1. Cohen, M.; Varki, A. Modulation of glycan recognition by clustered saccharide patches. *Int Rev Cell Mol Biol*. **2014**, *308*, 75-125.
2. Bertozzi, C. R.; Kiessling, L. L. Chemical glycobiology. *Science* **2001**, *291*, 2357-64.
3. Lis, H.; Sharon, N. Lectins: Carbohydrate-Specific Proteins That Mediate Cellular Recognition. *Chem Rev.* **1998**, *98*, 637-674.
4. Chabre, Y. M.; Roy, R. Multivalent glycoconjugate syntheses and applications using aromatic scaffolds. *Chem Soc Rev*. **2013**, *42*, 4657-708.
5. Gingras, M.; Chabre, Y. M.; Roy, M.; Roy, R. How do multivalent glycodendrimers benefit from sulfur chemistry? *Chem Soc Rev*. **2013**, *42*, 4823-41.
6. Bojarová, P.; Rosencrantz, R. R.; Elling, L.; Křen, V. Enzymatic glycosylation of multivalent scaffolds. *Chem Soc Rev*. **2013**, *42*, 4774-97.
7. Krannig, K. S.; Schlaad, H. Emerging bioinspired polymers: glycopolypeptides. *Soft Matter*. **2014**, *10*, 4228-35.
8. Krannig, K. S.; Sun, J.; Schlaad, H. Stimuli-responsivity of secondary structures of glycopolypeptides derived from poly(L-glutamate-co-allylglycine). *Biomacromolecules*. **2014**, *15*, 978-84.
9. Allen, J. R.; Harris, C. R.; Danishefsky, S. J. Pursuit of optimal carbohydrate-based anticancer vaccines: preparation of a multiantigenic unimolecular glycopeptide containing the Tn, MBr1, and Lewis(y) antigens. *J Am Chem Soc.* **2001**, *123*, 1890-7.
10. Kramer, J. R.; Deming, T. J. Glycopolypeptides via living polymerization of glycosylated-L-lysine N-carboxyanhydrides. *J Am Chem Soc.* **2010**, *132*, 15068-71.
11. Horan, N.; Yan, L.; Isobe, H.; Whitesides, G. M.; Kahne, D. Nonstatistical binding of a protein to clustered carbohydrates. *Proc Natl Acad Sci U S A.* **1999**, *96*, 11782-6.

12. Matsuura, K.; Hibino, M.; Yamada, Y.; Kobayashi, K. Construction of glyco-clusters by self-organization of site-specifically glycosylated oligonucleotides and their cooperative amplification of lectin-recognition. *J Am Chem Soc.* **2001**, *123*, 357-8.
13. Cairo, C. W.; Gestwicki, J. E.; Kanai, M.; Kiessling, L. L. Control of multivalent interactions by binding epitope density. *J Am Chem Soc.* **2002**, *124*, 1615-9.
14. Polizzotti, B. D.; Kiick, K. L. Effects of polymer structure on the inhibition of cholera toxin by linear polypeptide-based glycopolymers. *Biomacromolecules.* **2006**, *7*, 483-90.
15. Godula, K.; Bertozzi, C. R. Synthesis of glycopolymers for microarray applications via ligation of reducing sugars to a poly(acryloyl hydrazide) scaffold. *J Am Chem Soc.* **2010**, *132*, 9963-5.
16. Ruff, Y.; Buhler, E.; Candau, S. J.; Kesselman, E.; Talmon, Y.; Lehn J. M. Glycodynamers: dynamic polymers bearing oligosaccharides residues-generation, structure, physicochemical, component exchange, and lectin binding properties. *J Am Chem Soc.* **2010**, *132*, 2573-84.
17. Ponader, D.; Wojcik, F.; Beceren-Braun, F.; Dernedde, J.; Hartmann L. Sequence-defined glycopolymer segments presenting mannose: synthesis and lectin binding affinity. *Biomacromolecules.* **2012**, *13*, 1845-52.
18. Kiessling, L. L.; Grim, J. C. Glycopolymer probes of signal transduction. *Chem Soc Rev.* **2013**, *42*, 4476-91.
19. Jiménez Blanco, J. L.; Ortiz Mellet, C.; García Fernández, J. M. Multivalency in heterogeneous glycoenvironments: hetero-glycoclusters, -glycopolymers and -glycoassemblies. *Chem Soc Rev*. **2013**, *42*, 4518-31.
20. Ponader, D.; Maffre, P.; Aretz, J.; Pussak, D.; Ninnemann, N. M.; Schmidt, S.; Seeberger, P. H.; Rademacher, C.; Nienhaus, G. U.; Hartmann, L. Carbohydrate-lectin recognition of sequence-defined heteromultivalent glycooligomers. *J Am Chem Soc.* **2014**, *136*, 2008-16.
21. Turnbull, W. B.; Kalovidouris, S. A.; Stoddart, J. F. Large oligosaccharide-based glycodendrimers. *Chemistry*. **2002**, *8*, 2988-3000.
22. Woller, E. K.; Walter, E. D.; Morgan, J. R.; Singel, D. J.; Cloninger, M. J. Altering the strength of lectin binding interactions and controlling the amount of lectin clustering using mannose/hydroxyl-functionalized dendrimers. *J Am Chem Soc.* **2003**, *125*, 8820-6.

23. Thomas, B.; Berthet, N.; Garcia, J.; Dumy, P.; Renaudet, O. Expanding the scope of oxime ligation: facile synthesis of large cyclopeptide-based glycodendrimers. *Chem Commun (Camb).* **2013**, *49*, 10796-8.
24. Munoz, E. M.; Correa, J.; Riguera, R.; Fernandez-Megia, E. Real-time evaluation of binding mechanisms in multivalent interactions: a surface plasmon resonance kinetic approach. *J Am Chem Soc*. **2013**, *135*, 5966-9.
25. Appelhans, D.; Klajnert-Maculewicz, B.; Janaszewska, A.; Lazniewska, J.; Voit, B. Dendritic glycopolymers based on dendritic polyamine scaffolds: view on their synthetic approaches, characteristics and potential for biomedical applications. *Chem Soc Rev.* **2015**, *44*, 3968-96.
26. Roy, R.; Shiao, T. C. Glyconanosynthons as powerful scaffolds and building blocks for the rapid construction of multifaceted, dense and chiral dendrimers. *Chem Soc Rev.* **2015**, *44*, 3924-41.
27. Voskuhl, J.; Stuart, M. C.; Ravoo, B. J. Sugar-decorated sugar vesicles: lectin-carbohydrate recognition at the surface of cyclodextrin vesicles. *Chemistry.* **2010**, *16*, 2790-6.
28. Jayaraman, N.; Maiti, K.; Naresh, K. Multivalent glycoliposomes and micelles to study carbohydrate-protein and carbohydrate-carbohydrate interactions. *Chem Soc Rev*. **2013**, *42*, 4640-56.
29. Chmielewski, M. J.; Buhler, E.; Candau, J.; Lehn, J. M. Multivalency by self-assembly: binding of concanavalin A to metallosupramolecular architectures decorated with multiple carbohydrate groups. *Chemistry*. **2014**, *20*, 6960-77.
30. Loka, R. S.; McConnell, M. S.; Nguyen, H. M. Studies of Highly-Ordered Heterodiantennary Mannose/Glucose-Functionalized Polymers and Concanavalin A Protein Interactions Using Isothermal Titration Calorimetry. *Biomacromolecules.* **2015**, *16*, 4013-4021.
31. Zhang, S.; Xiao, Q.; Sherman, S. E.; Muncan, A.; Ramos Vicente, A. D.; Wang, Z.; Hammer, D. A.; Williams, D.; Chen, Y.; Pochan, D. J.; Vértesy, S.; André, S.; Klein, M. L.; Gabius, H, J.; Percec, V. Glycodendrimersomes from Sequence-Defined Janus Glycodendrimers Reveal High Activity and Sensor Capacity for the Agglutination by Natural Variants of Human Lectins. *J Am Chem Soc.* **2015**, *137*, 13334-44.
32. Percec, V.; Leowanawat, P.; Sun, H. J.; Kulikov, O.; Nusbaum, C. D.; Tran, T. M.; Bertin, A.; Wilson, D. A.; Peterca, M.; Zhang, S.; Kamat, N. P.; Vargo, K.; Moock, D.; Johnston, E. D.; Hammer, D. A.; Pochan, D. J.; Chen, Y.; Chabre, Y. M.; Shiao, T. C.;

Bergeron-Brlek, M.; André, S.; Roy, R.; Gabius, H. J.; Heiney, P. A. Modular synthesis of amphiphilic Janus glycodendrimers and their self-assembly into glycodendrimersomes and other complex architectures with bioactivity to biomedically relevant lectins. *J Am Chem Soc.* **2013**, *135*, 9055-77.

33. Zhang, S.; Moussodia, R. O.; Sun, H. J.; Leowanawat, P.; Muncan, A.; Nusbaum, C. D.; Chelling, K. M.; Heiney, P. A.; Klein, M. L.; André, S.; Roy, R.; Gabius, H. J.; Percec, V. Mimicking biological membranes with programmable glycan ligands self-assembled from amphiphilic Janus glycodendrimers. *Angew Chem Int Ed Engl.* **2014**, *53*, 10899-903.
34. Zhang, S.; Moussodia, R. O.; Murzeau, C.; Sun, H. J.; Klein, M. L.; Vértesy, S.; André, S.; Roy, R.; Gabius, H. J.; Percec, V. Dissecting molecular aspects of cell interactions using glycodendrimersomes with programmable glycan presentation and engineered human lectins. *Angew Chem Int Ed Engl.* **2015**, *54*, 4036-40.
35. Zhang, S.; Moussodia, R. O.; Vértesy, S.; André, S.; Klein, M. L.; Gabius, H. J.; Percec, V. Unraveling functional significance of natural variations of a human galectin by glycodendrimersomes with programmable glycan surface. *Proc Natl Acad Sci U S A.* **2015**, *112*, 5585-90.
36. Reichardt, N. C.; Martín-Lomas, M.; Penadés, S. Glyconanotechnology. *Chem Soc Rev.* **2013**, *42*, 4358-76.
37. Marradi, M.; Chiodo, F.; García, I.; Penadés, S. Glyconanoparticles as multifunctional and multimodal carbohydrate systems. *Chem Soc Rev.* **2013**, *42*, 4728-45.
38. El-Boubbou, K.; Huang, X. Glyco-nanomaterials: translating insights from the "sugar-code" to biomedical applications. *Curr Med Chem.* **2011**, *18*, 2060-78.
39. Kikkeri, R.; Lepenies, B.; Adibekian, A.; Laurino, P.; Seeberger, P. H. In vitro imaging and in vivo liver targeting with carbohydrate capped quantum dots. *J Am Chem Soc.* **2009**, *131*, 2110-2.
40. Huang, L. D.; Adak, A. K.; Yu, C. C.; Hsiao, W. C.; Lin, H. J.; Chen, M. L.; Lin, C. C. Fabrication of highly stable glyco-gold nanoparticles and development of a glyco-gold nanoparticle-based oriented immobilized antibody microarray for lectin (GOAL) assay. *Chemistry.* **2015**, *21*, 3956-67.
41. Fallarini, S.; Paoletti, T.; Battaglini, C. O.; Ronchi, P.; Lay, L.; Bonomi, R.; Jha, S.; Mancin, F.; Scrimin, P.; Lombardi, G. Factors affecting T cell responses induced by fully synthetic glyco-gold-nanoparticles. *Nanoscale.* **2013**, *5*, 390-400.

42. Isobe, H.; Cho, K.; Solin, N.; Werz, D. B.; Seeberger, P. H.; Nakamura, E. Synthesis of fullerene glycoconjugates via a copper-catalyzed Huisgen cycloaddition reaction. *Org Lett.* **2007**, *9*, 4611-4.
43. Ohta, T.; Miura, N.; Fujitani, N.; Nakajima, F.; Niikura, K.; Sadamoto, R.; Guo, C. T.; Suzuki, T.; Suzuki, Y.; Monde, K.; Nishimura, S. Glycotentacles: synthesis of cyclic glycopeptides, toward a tailored blocker of influenza virus hemagglutinin. *Angew Chem Int Ed Engl.* **2003**, *42*, 5186-9.
44. Gerke, C.; Ebbesen, M. F.; Jansen, D.; Boden, S.; Freichel, T.; Hartmann, L. Sequence-Controlled Glycopolymers via Step-Growth Polymerization of Precision Glycomacromolecules for Lectin Receptor Clustering. *Biomacromolecules.* **2017**, *18*, 787-796.
45. Lindhorst, T. K.; Bruegge, K.; Fuchs, A.; Sperling, O. A bivalent glycopeptide to target two putative carbohydrate binding sites on FimH. *Beilstein J Org Chem.* **2010**, *6*, 801-9.
46. Chaudhary, P. M.; Sangabathuni, S.; Murthy, R. V.; Paul, A.; Thulasiram, H. V.; Kikkeri, R. Assessing the effect of different shapes of glyco-gold nanoparticles on bacterial adhesion and infections. *Chem Commun (Camb)*. **2015**, *51*, 15669-72.
47. Sangabathuni, S.; Vasudeva Murthy, R.; Chaudhary, P. M.; Surve, M.; Banerjee, A.; Kikkeri, R. Glyco-gold nanoparticle shapes enhance carbohydrate-protein interactions in mammalian cells. *Nanoscale*. **2016**, *8*, 12729-35.
48. Masuko, T.; Minami, A.; Iwasaki, N.; Majima, T.; Nishimura, S.; Lee, Y. C. Carbohydrate analysis by a phenol-sulfuric acid method in microplate format. *Anal Biochem.* **2005**, *339*, 69-72
49. Nikoobakht, B.; El-Sayed, M. A. Preparation and Growth Mechanism of Nanorods (NRs) Using Seed-Mediated Growth Method. *Chem. Mater.* **2003**, *15*, 1957–1962.
50. Yadav, R.; Kikkeri, R. Carbohydrate functionalized iron(III) complexes as biomimetic siderophores. *Chem Commun (Camb).* **2012**, *48*, 1704-6.
51. Cho, E. C.; Liu, Y.; Xia, Y. A simple spectroscopic method for differentiating cellular uptakes of gold nanospheres and nanorods from their mixtures. *Angew Chem Int Ed Engl.* **2010**, *49*, 1976-80.
52. Kolhar, P.; Anselmo, A. C.; Gupta, V.; Pant, K.; Prabhakarpandian, B.; Ruoslahti, E.; Mitragotri, S. Using shape effects to target antibody-coated nanoparticles to lung and brain endothelium. *Proc Natl Acad Sci U S A.* **2013**, *110*, 10753-8.

2.6 NMR and HRMS Spectra:

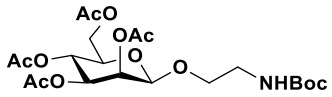

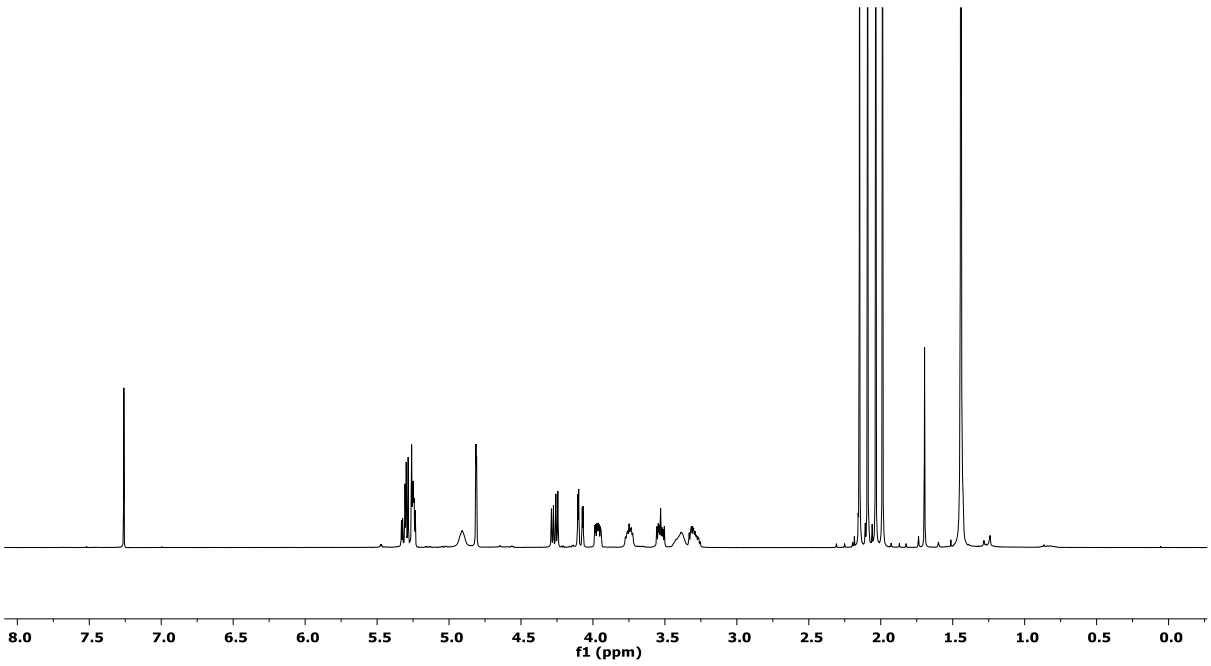

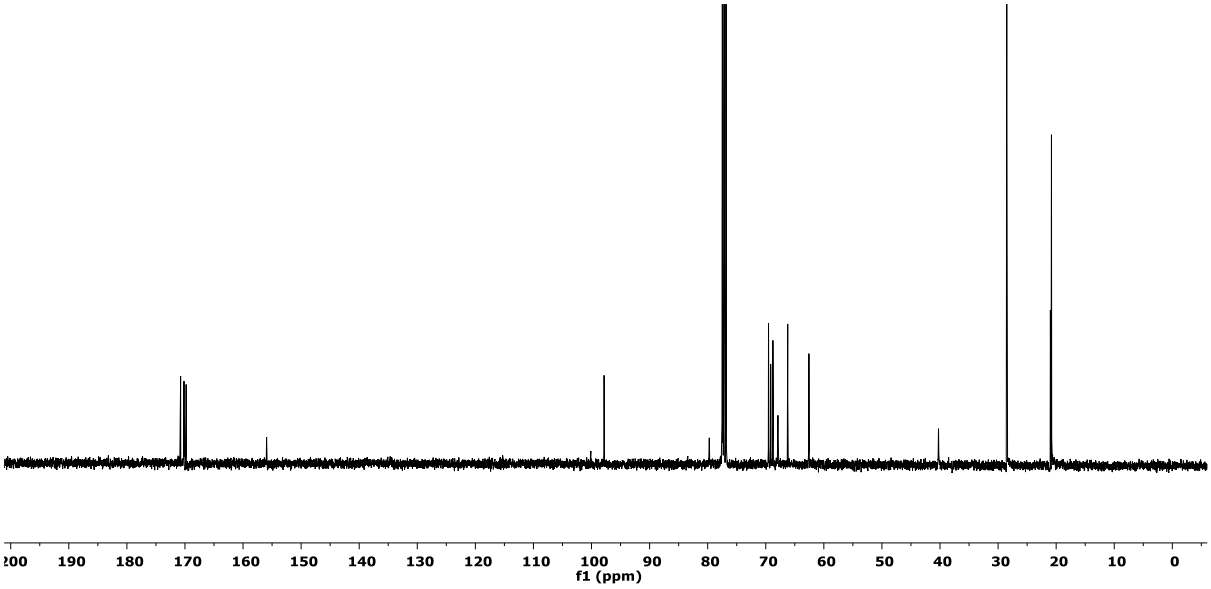
200 190 180 170 160 150 140 130 120 110 100 90 80 70 60 50 40 30 20 10 0
f1 (ppm)

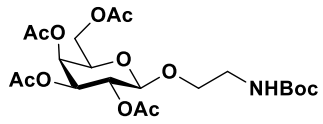
AcO
OAc
O
O
AcO
NHBoc
OAc

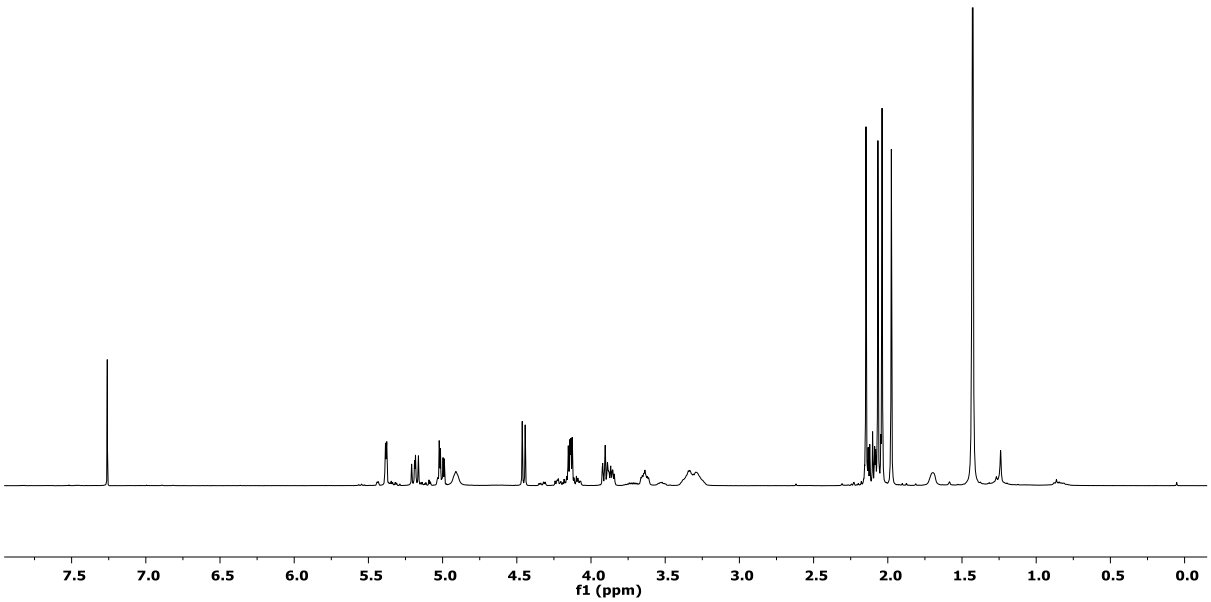
7.5 7.0 6.5 6.0 5.5 5.0 4.5 4.0 3.5 3.0 2.5 2.0 1.5 1.0 0.5 0.0
f1 (ppm)

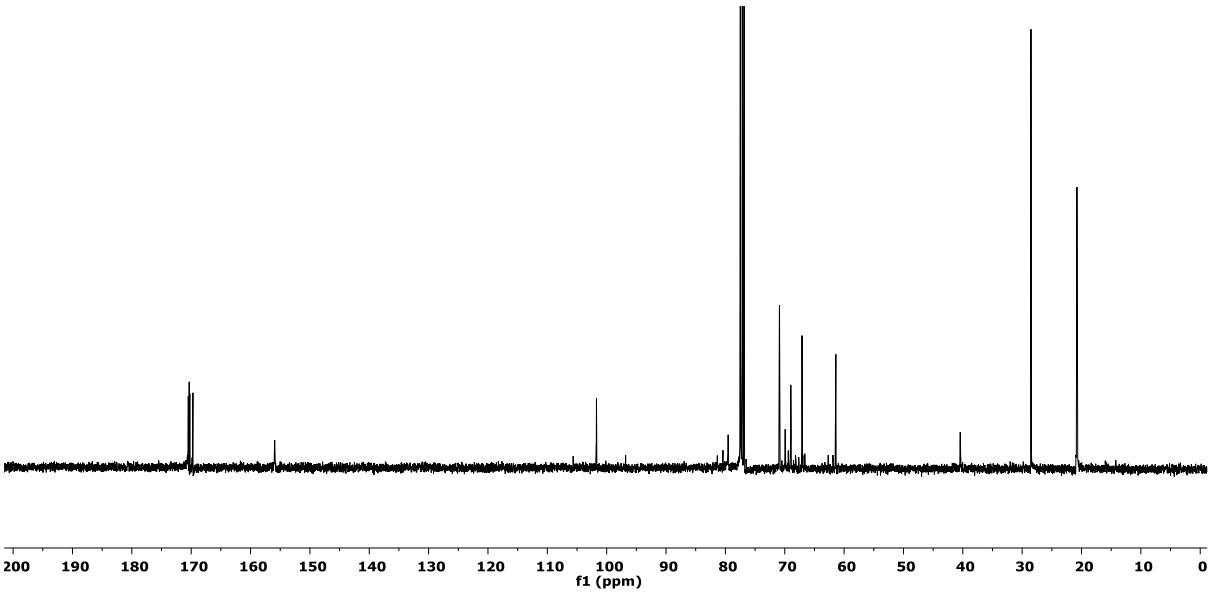
200
190
180
170
160
150
140
130
120
110
100
90
80
70
60
50
40
30
20
10
0
f1 (ppm)

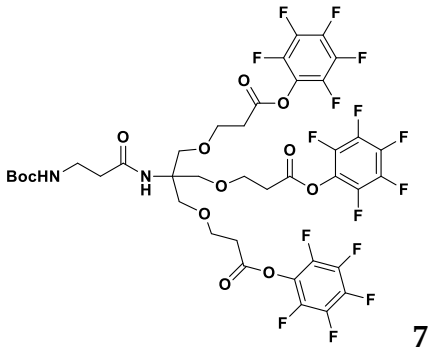
BocHN
N
H
O
F

7

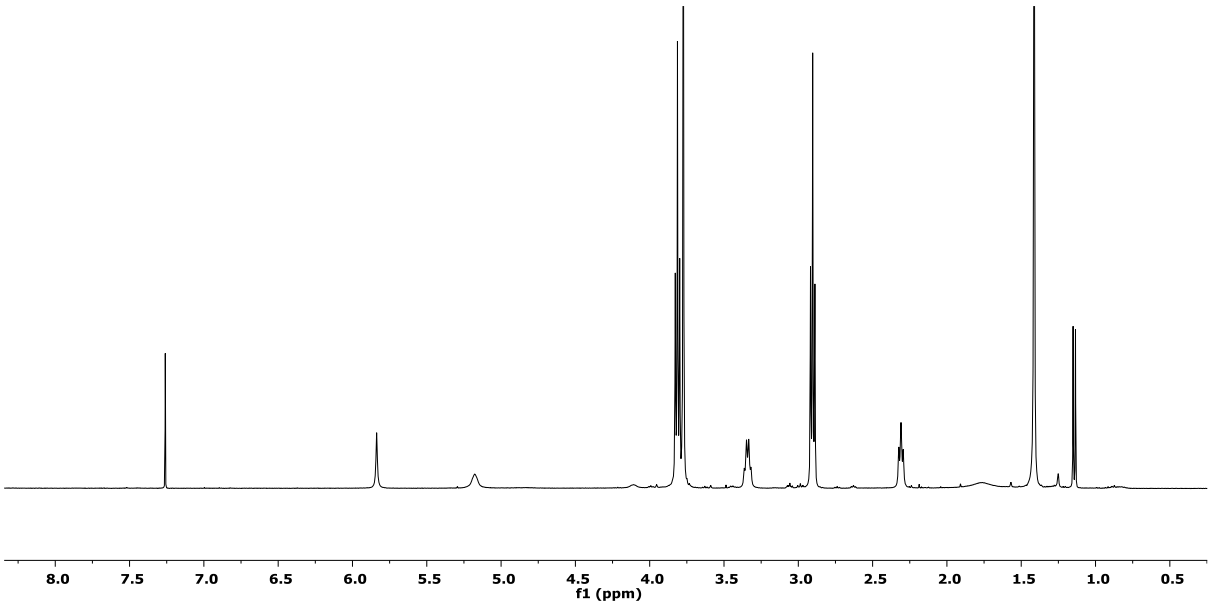
8.0
7.5
7.0
6.5
6.0
5.5
5.0
4.5
4.0
3.5
3.0
2.5
2.0
1.5
1.0
0.5
f1 (ppm)

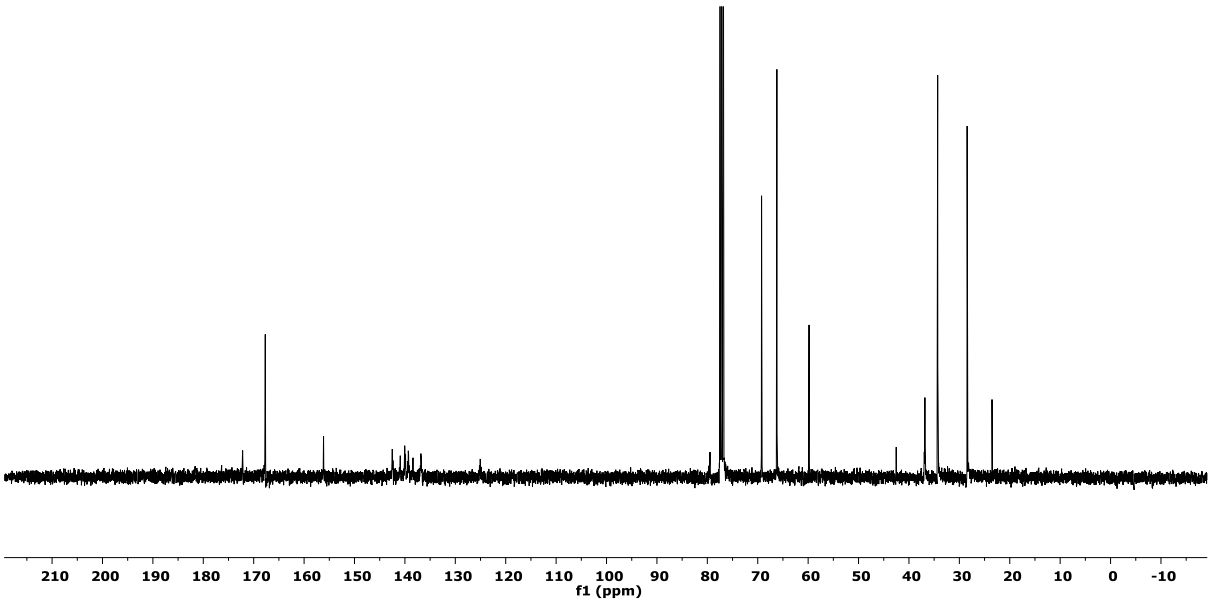
210
200
190
180
170
160
150
140
130
120
110
100
90
80
70
60
50
40
30
20
10
0
-10
f1 (ppm)

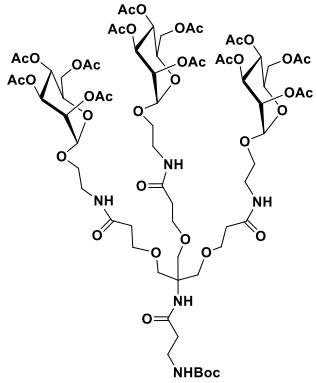
AcO
OAc
NH
O
NHBoc

8

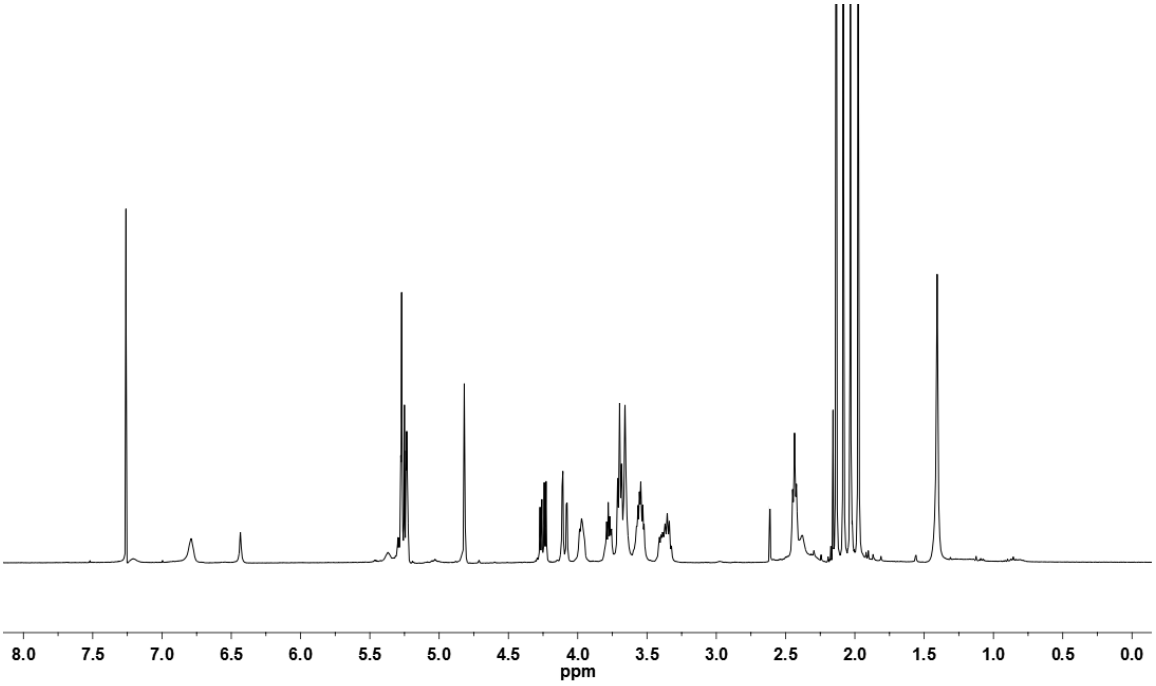
8.0
7.5
7.0
6.5
6.0
5.5
5.0
4.5
4.0
3.5
3.0
2.5
2.0
1.5
1.0
0.5
0.0
ppm

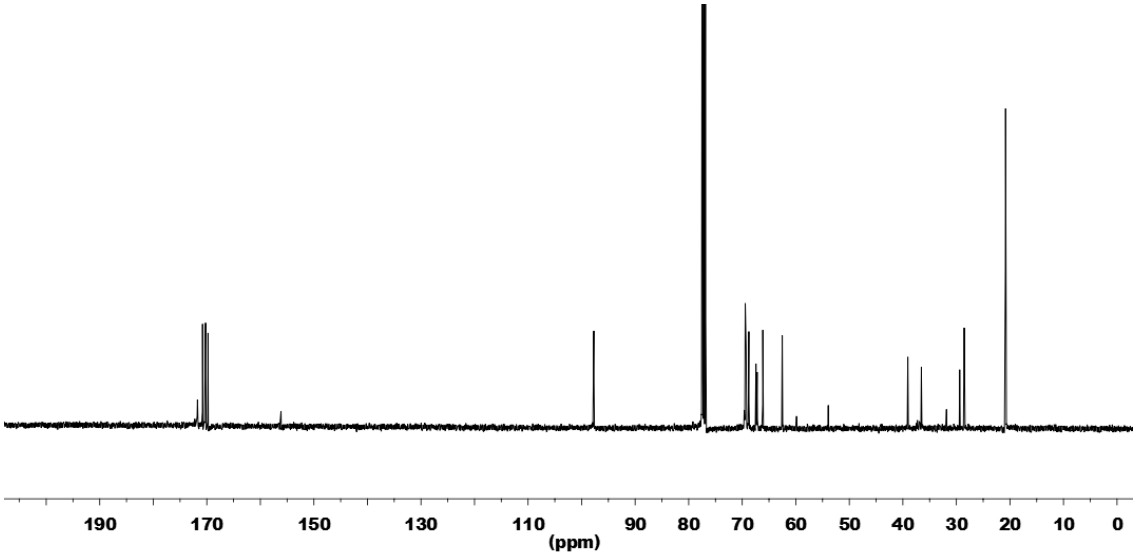
190
170
150
130
110
90
80
70
60
50
40
30
20
10
0
(ppm)

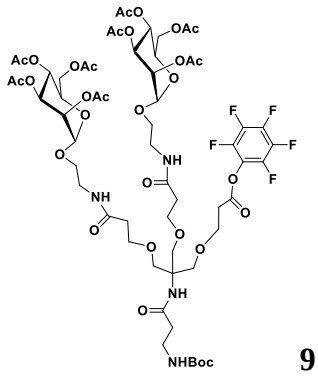
AcO
OAc
NH
O
F
NHBoc

9

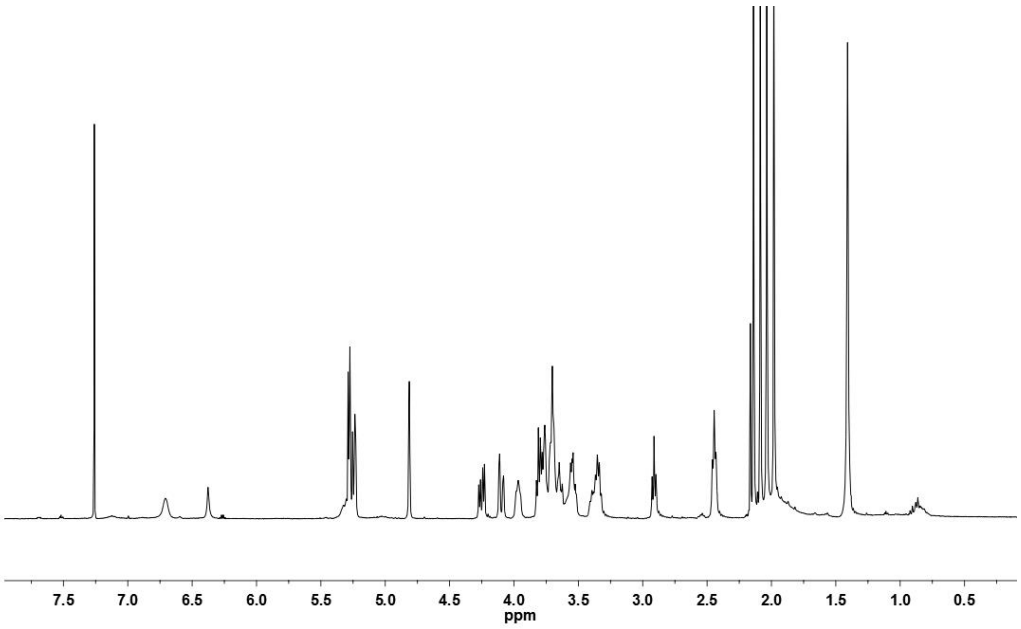
7.5
7.0
6.5
6.0
5.5
5.0
4.5
4.0
3.5
3.0
2.5
2.0
1.5
1.0
0.5
ppm

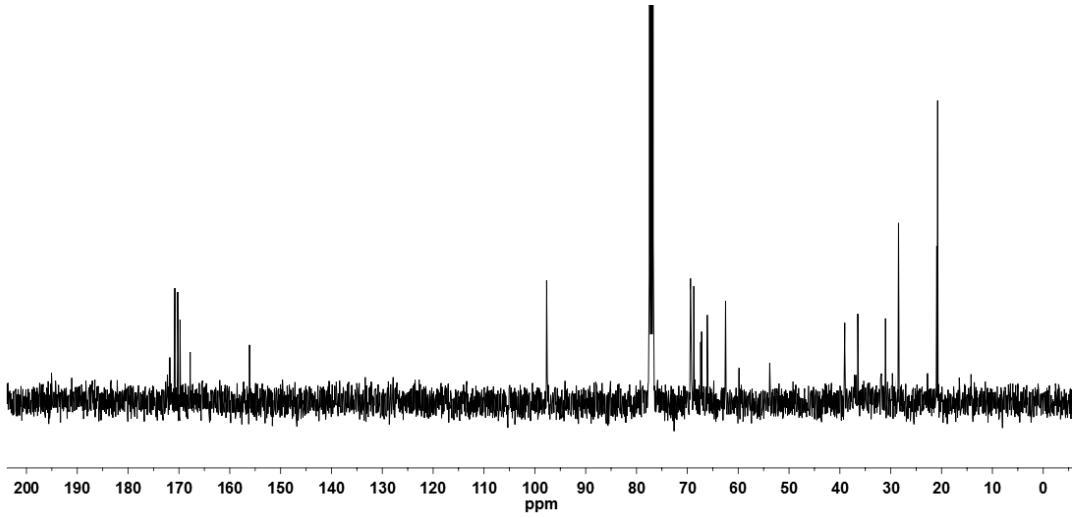
200
190
180
170
160
150
140
130
120
110
100
90
80
70
60
50
40
30
20
10
0
ppm

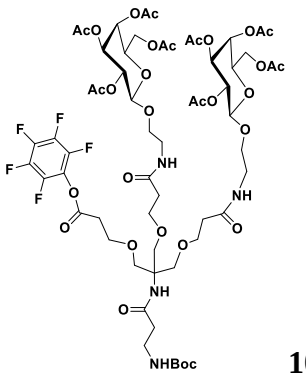
OAc
AcO
OAc
AcO
O
O
NH
O
F
F
F
F
O
O
O
O
O
NH
O
NH
O
NHBoc

10

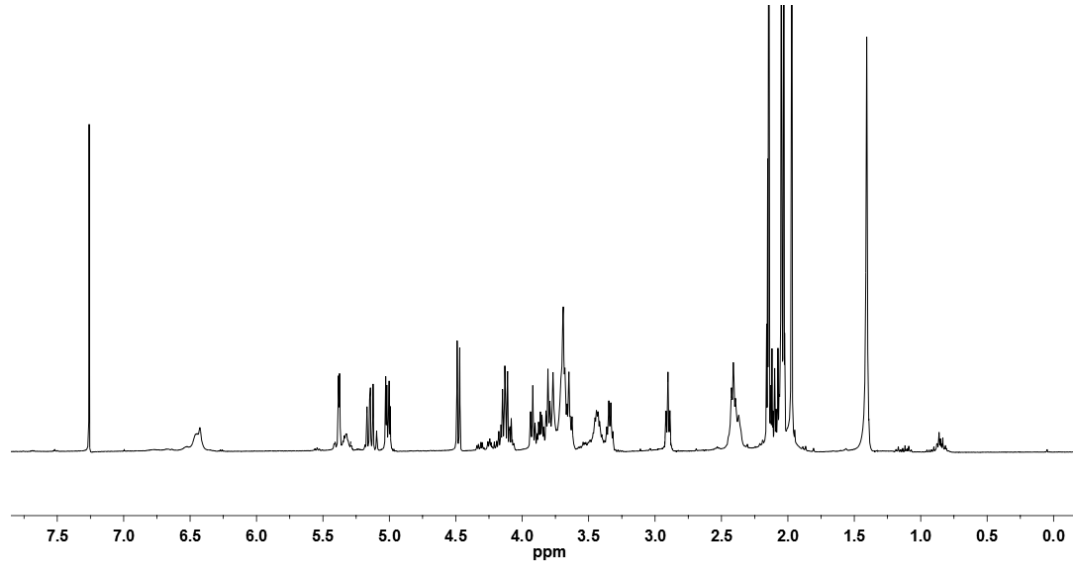
7.5 7.0 6.5 6.0 5.5 5.0 4.5 4.0 3.5 3.0 2.5 2.0 1.5 1.0 0.5 0.0
ppm

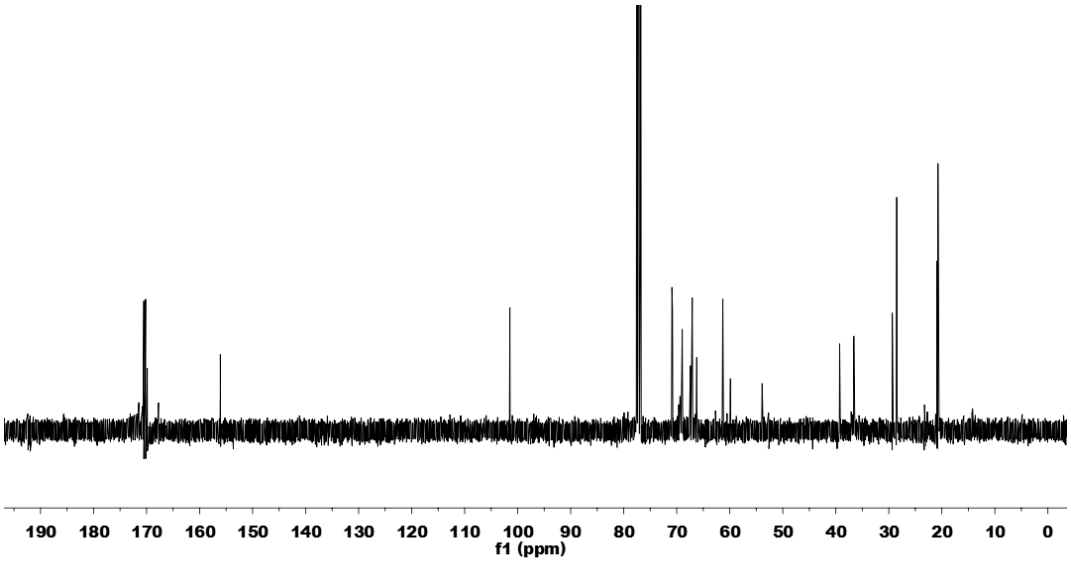
190 180 170 160 150 140 130 120 110 100 90 80 70 60 50 40 30 20 10 0
f1 (ppm)

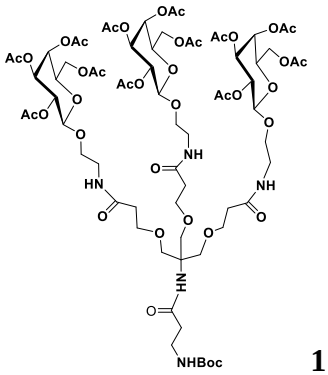
OAc
AcO
OAc
AcO
O
NH
HN
O
NHBoc

11

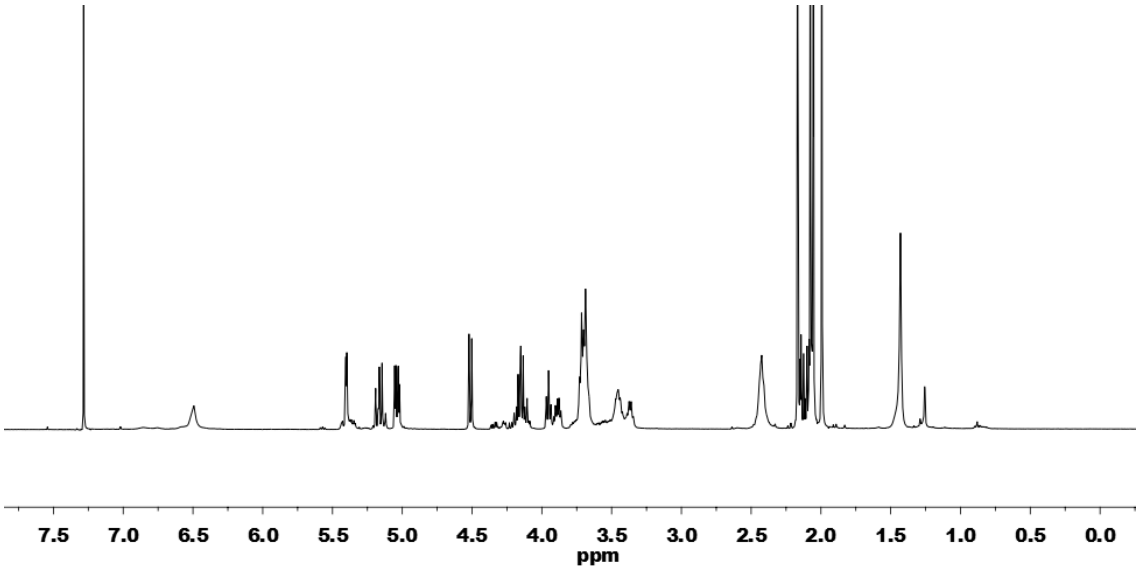
7.5 7.0 6.5 6.0 5.5 5.0 4.5 4.0 3.5 3.0 2.5 2.0 1.5 1.0 0.5 0.0
ppm

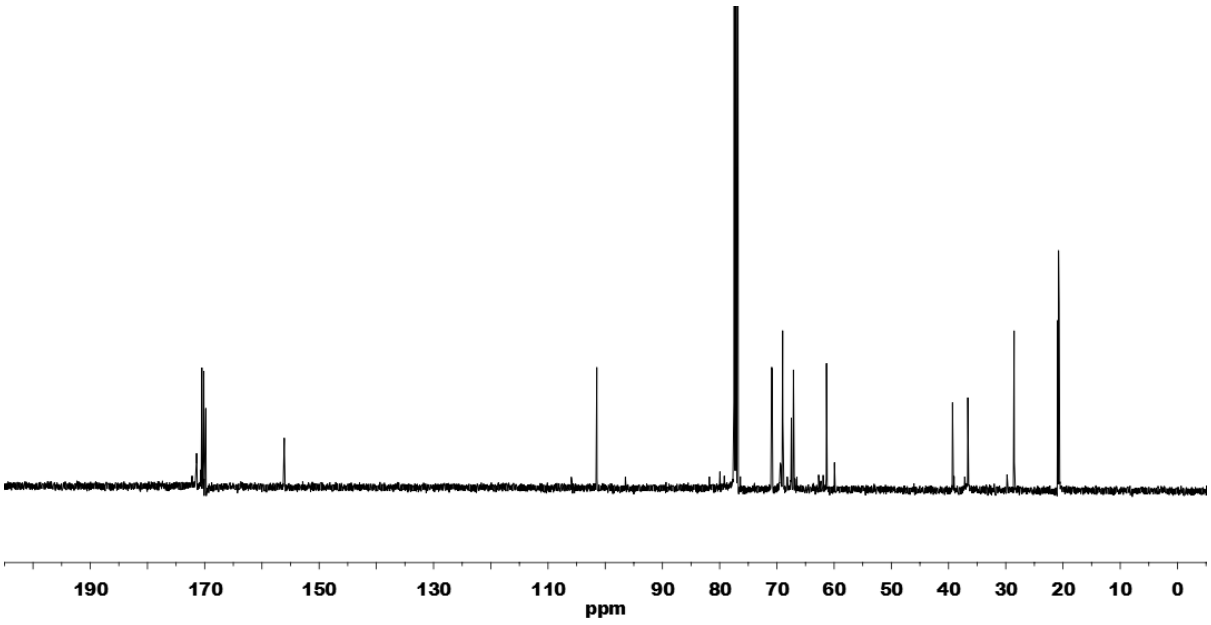
190 170 150 130 110 90 80 70 60 50 40 30 20 10 0
ppm

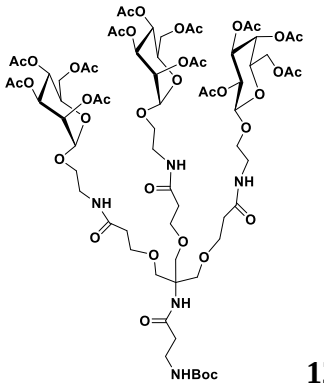
AcO
OAc
NH
O
NHBoc

12

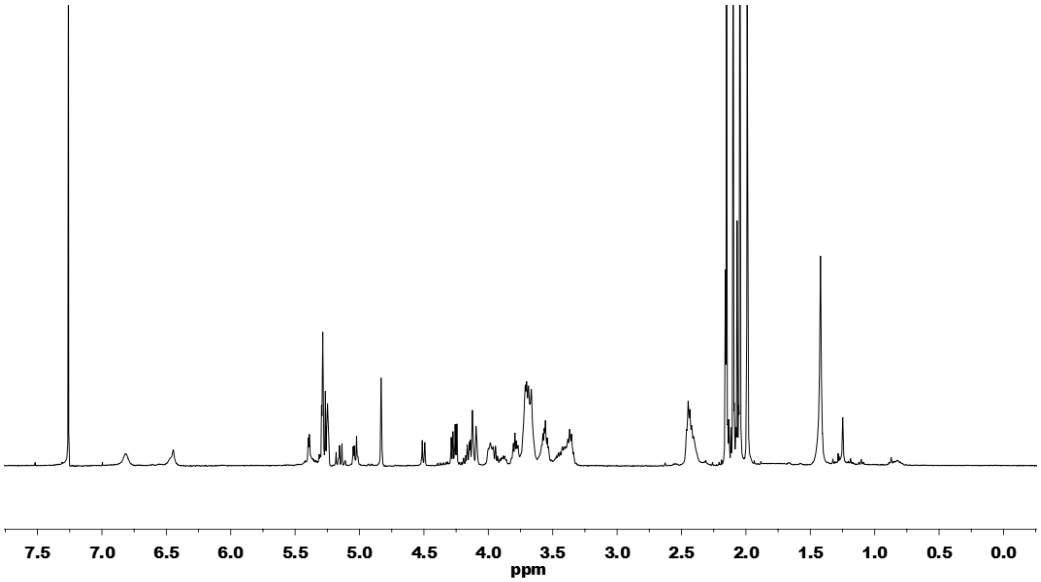
7.5 7.0 6.5 6.0 5.5 5.0 4.5 4.0 3.5 3.0 2.5 2.0 1.5 1.0 0.5 0.0
ppm

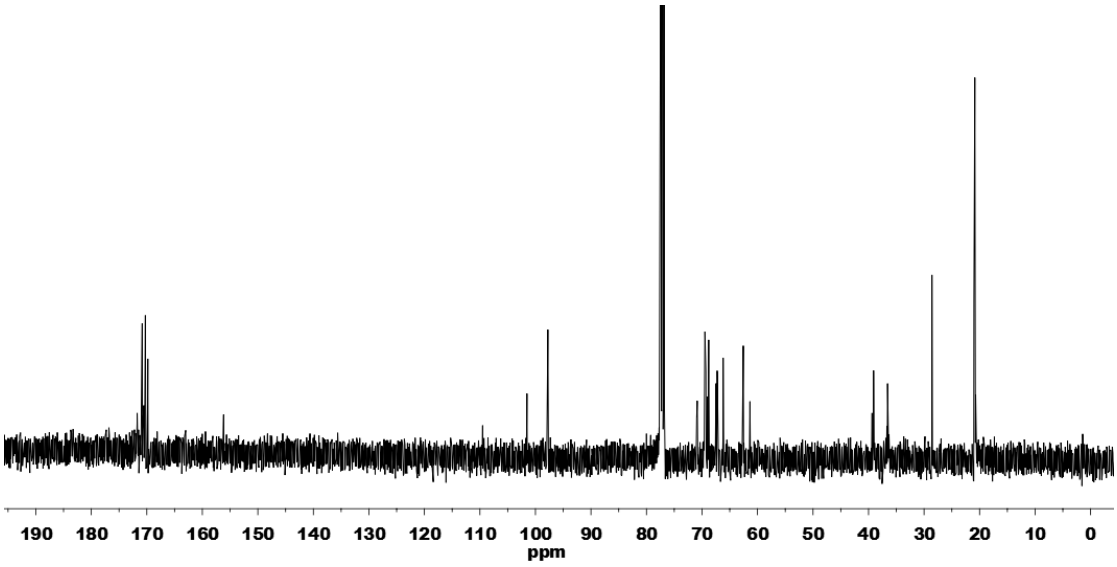
190 180 170 160 150 140 130 120 110 100 90 80 70 60 50 40 30 20 10 0
ppm

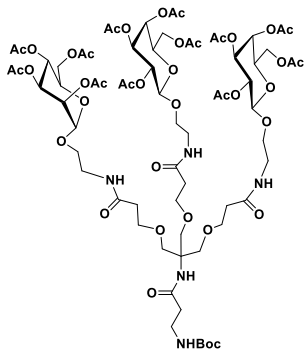
AcO
OAc
NH
O
NHBoc

13

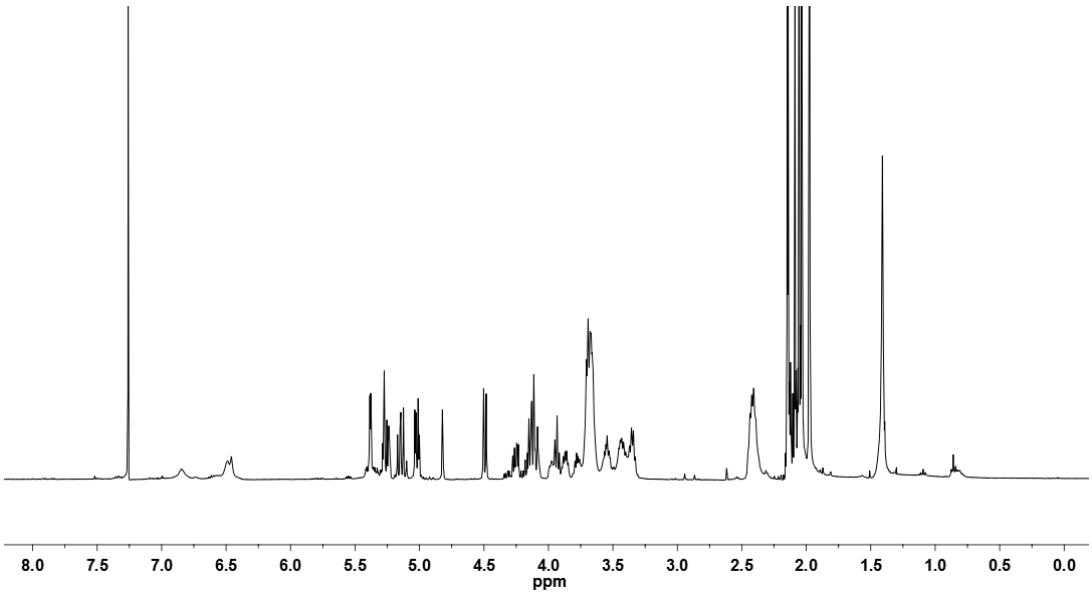
8.0
7.5
7.0
6.5
6.0
5.5
5.0
4.5
4.0
3.5
3.0
2.5
2.0
1.5
1.0
0.5
0.0
ppm

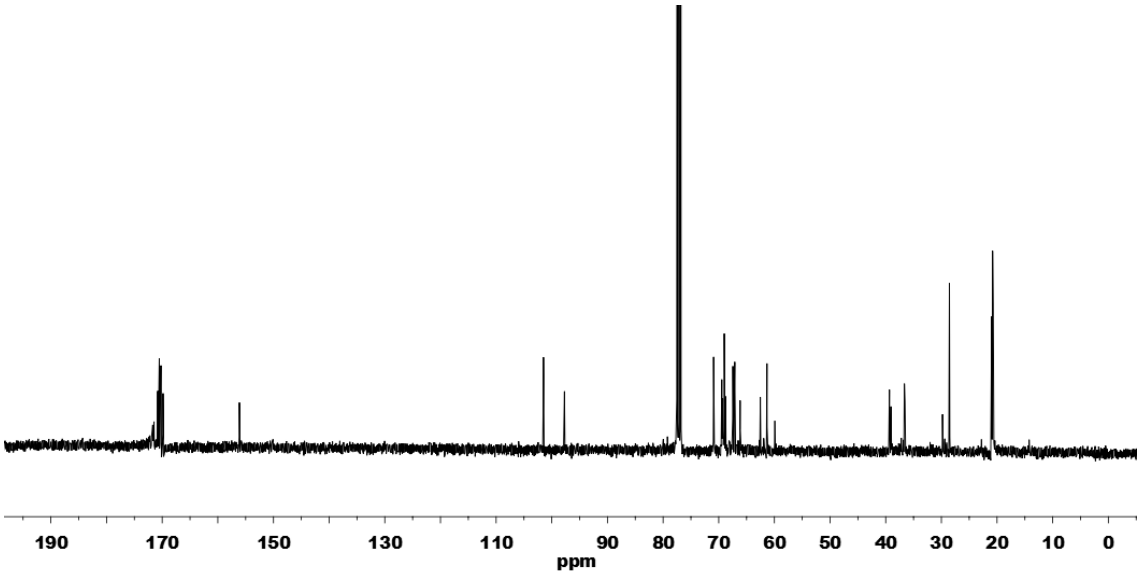
190
170
150
130
110
90
80
70
60
50
40
30
20
10
0
ppm

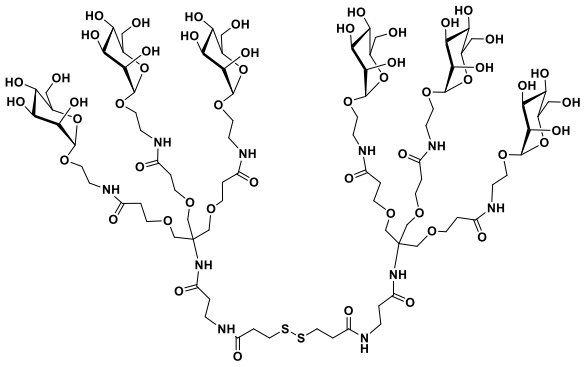

1

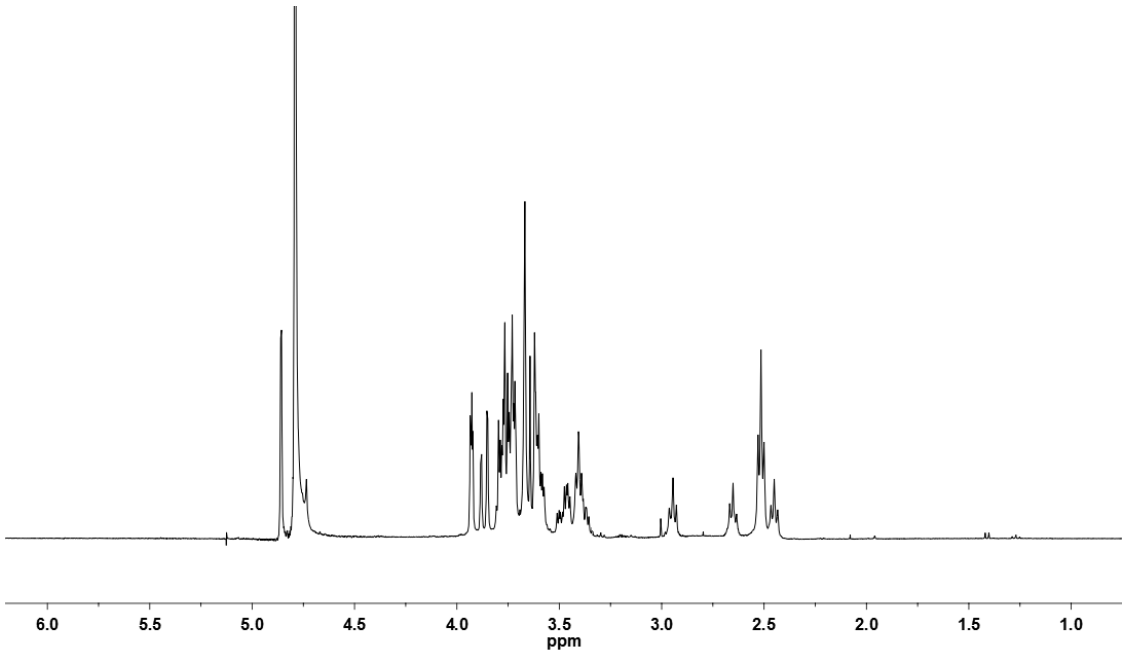
6.0
5.5
5.0
4.5
4.0
3.5
ppm
3.0
2.5
2.0
1.5
1.0

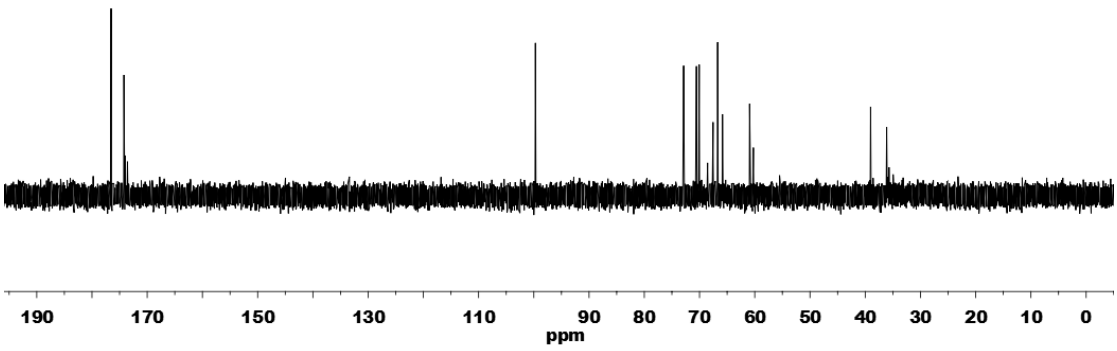
190
170
150
130
110
90
ppm
80
70
60
50
40
30
20
10
0

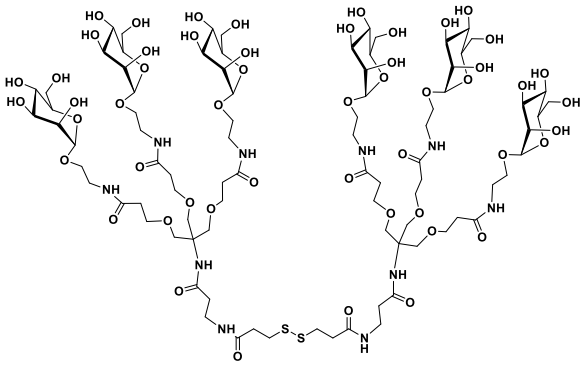

1

HRMS

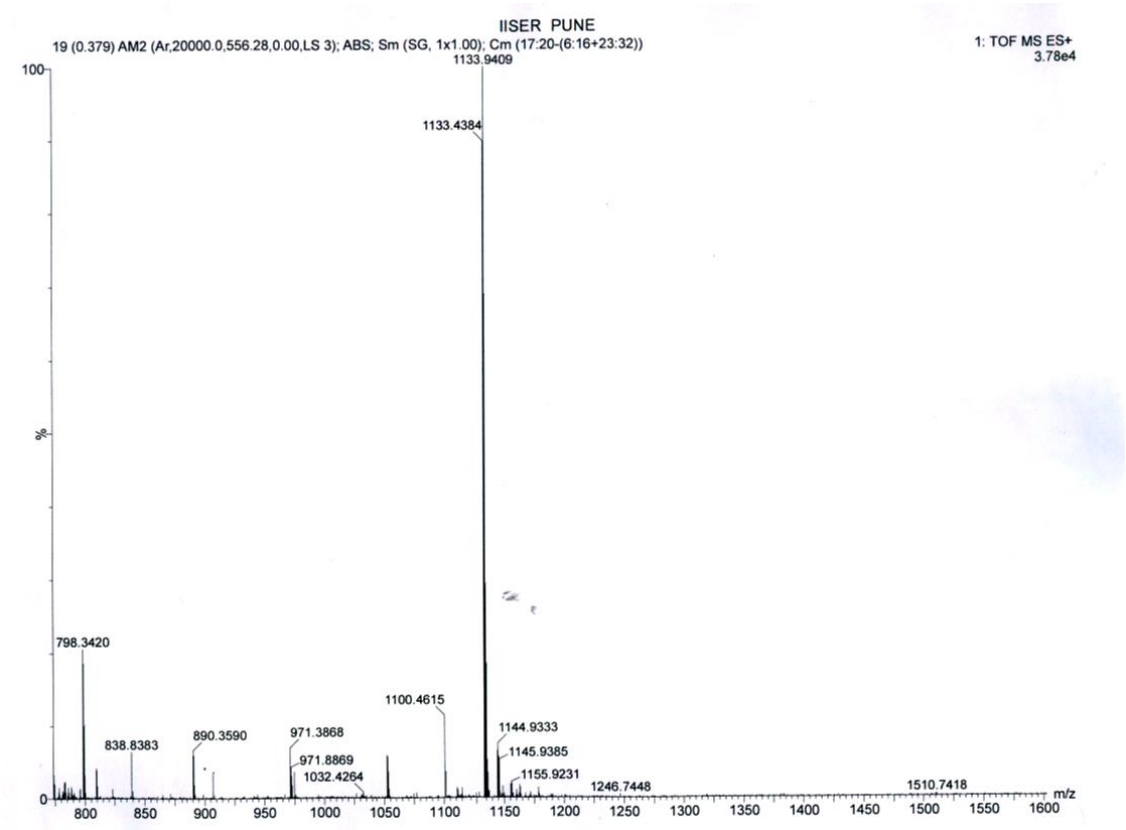
IISER PUNE
19 (0.379) AM2 (Ar,20000.0,556.28,0.00,LS 3); ABS; Sm (SG, 1x1.00); Cm (17:20-(6:16+23:32))
1: TOF MS ES+
3.78e4
1133.9409
1133.4384
798.3420
838.8383
890.3590
971.3868
971.8869
1032.4264
1100.4615
1144.9333
1145.9385
1155.9231
1246.7448
1510.7418
%
m/z

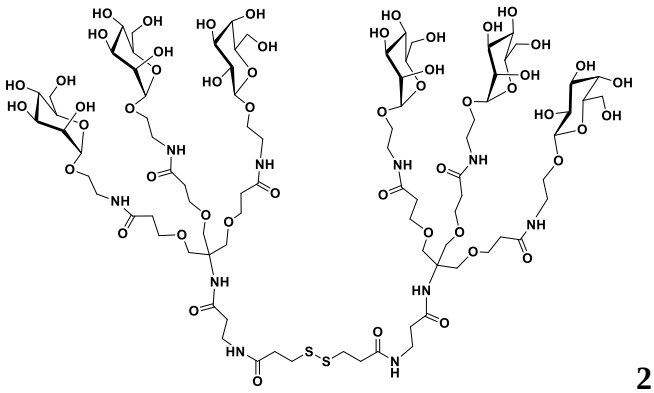

2

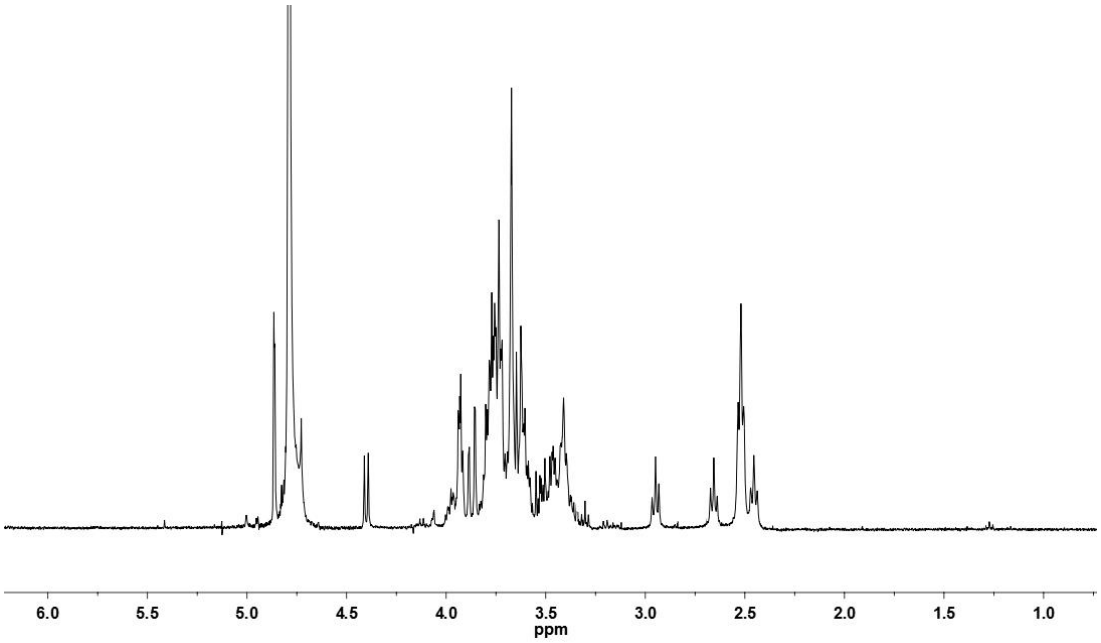
6.0
5.5
5.0
4.5
4.0
3.5
3.0
2.5
2.0
1.5
1.0
ppm

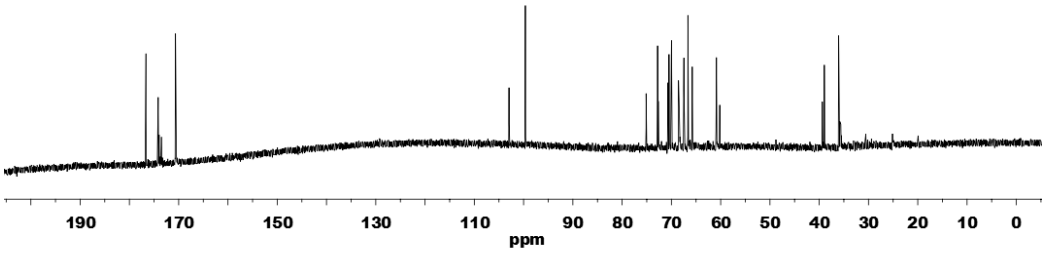
190
170
150
130
110
90
80
70
60
50
40
30
20
10
0
ppm

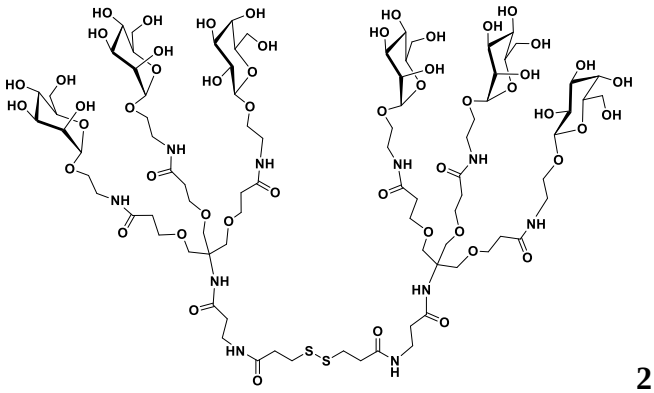

2

HRMS

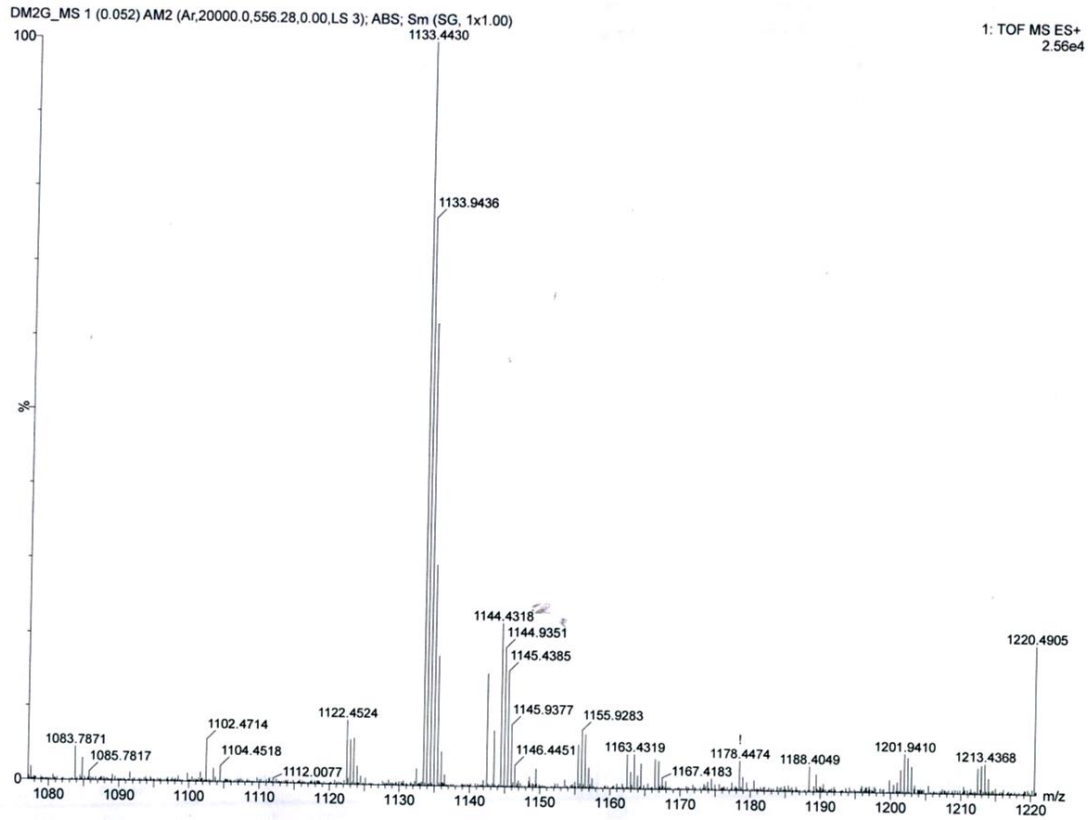
DM2G_MS 1 (0.052) AM2 (Ar,20000.0,556.28,0.00,LS 3); ABS; Sm (SG, 1x1.00)
1: TOF MS ES+
2.56e4
100
%
0
1133.4430
1133.9436
1144.4318
1144.9351
1145.4385
1145.9377
1155.9283
1220.4905
1122.4524
1102.4714
1083.7871
1085.7817
1104.4518
1112.0077
1146.4451
1163.4319
1178.4474
1167.4183
1188.4049
1201.9410
1213.4368
1080
1090
1100
1110
1120
1130
1140
1150
1160
1170
1180
1190
1200
1210
1220
m/z

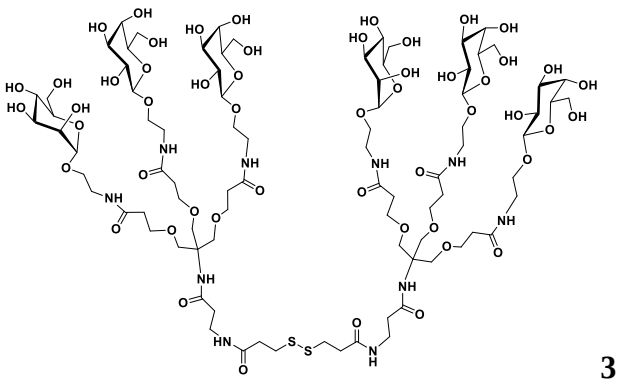

3

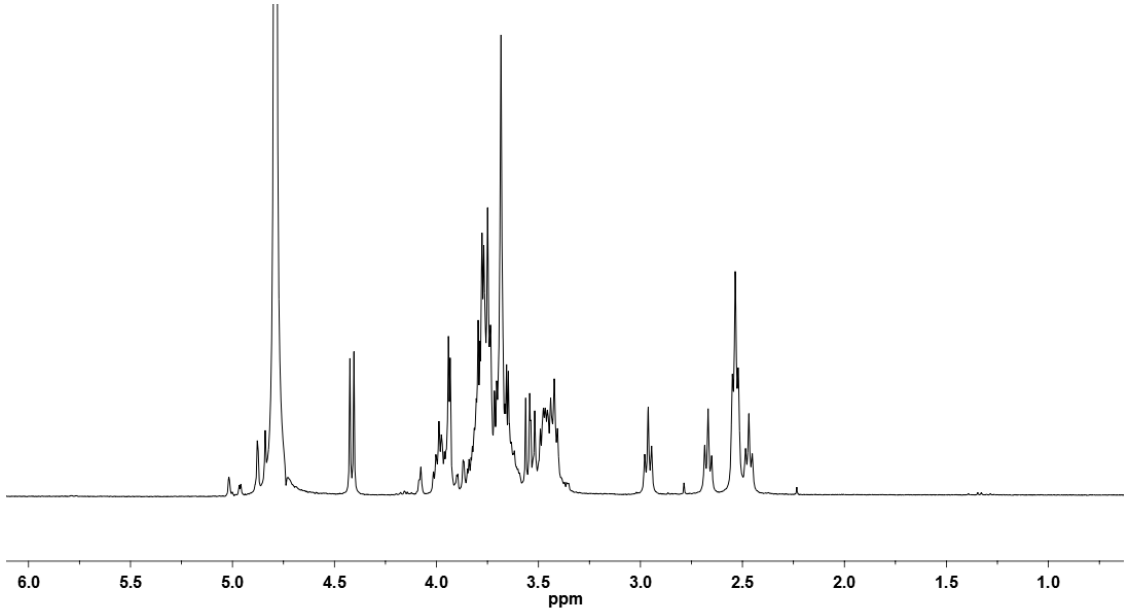
6.0
5.5
5.0
4.5
4.0
3.5
3.0
2.5
2.0
1.5
1.0
ppm

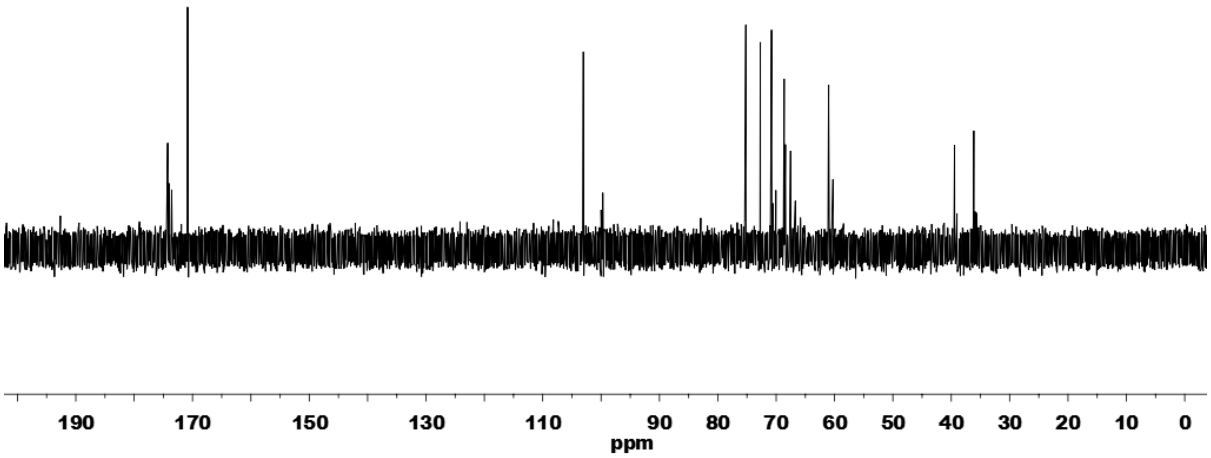
190
170
150
130
110
90
80
70
60
50
40
30
20
10
0
ppm

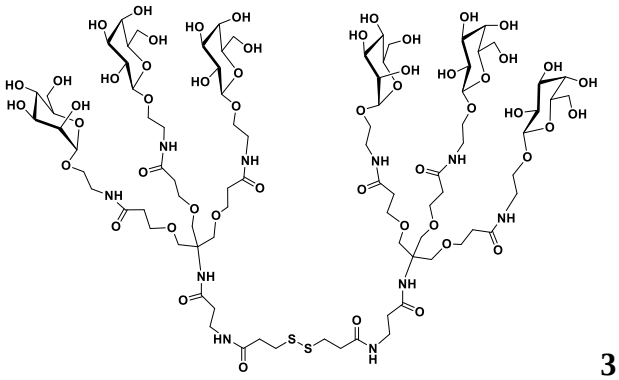

3

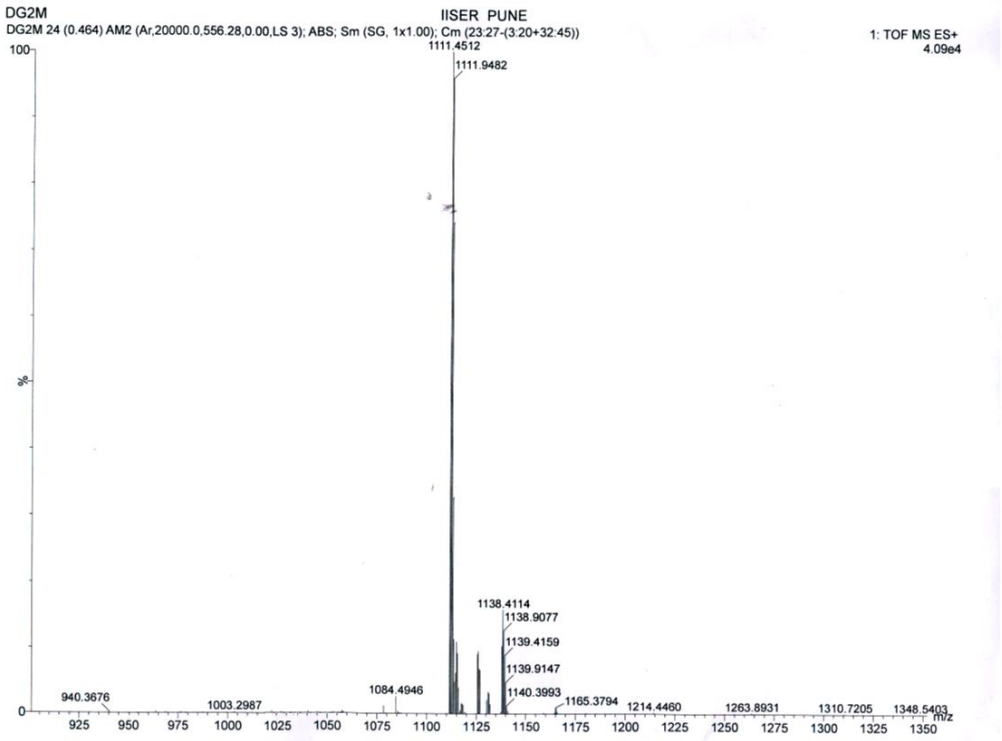
DG2M
IISER PUNE
DG2M 24 (0.464) AM2 (Ar,20000.0,556.28,0.00,LS 3); ABS; Sm (SG, 1x1.00); Cm (23:27-(3:20+32:45))
1: TOF MS ES+
4.09e4
100
%
0
1111.4512
1111.9482
1138.4114
1138.9077
1139.4159
1139.9147
1140.3993
940.3676
1003.2987
1084.4946
1165.3794
1214.4460
1263.8931
1310.7205
1348.5403
925 950 975 1000 1025 1050 1075 1100 1125 1150 1175 1200 1225 1250 1275 1300 1325 1350
m/z

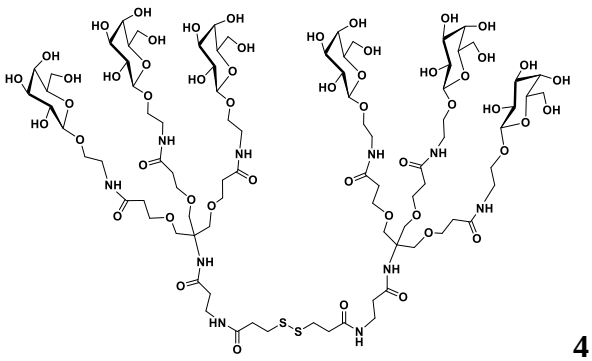

4

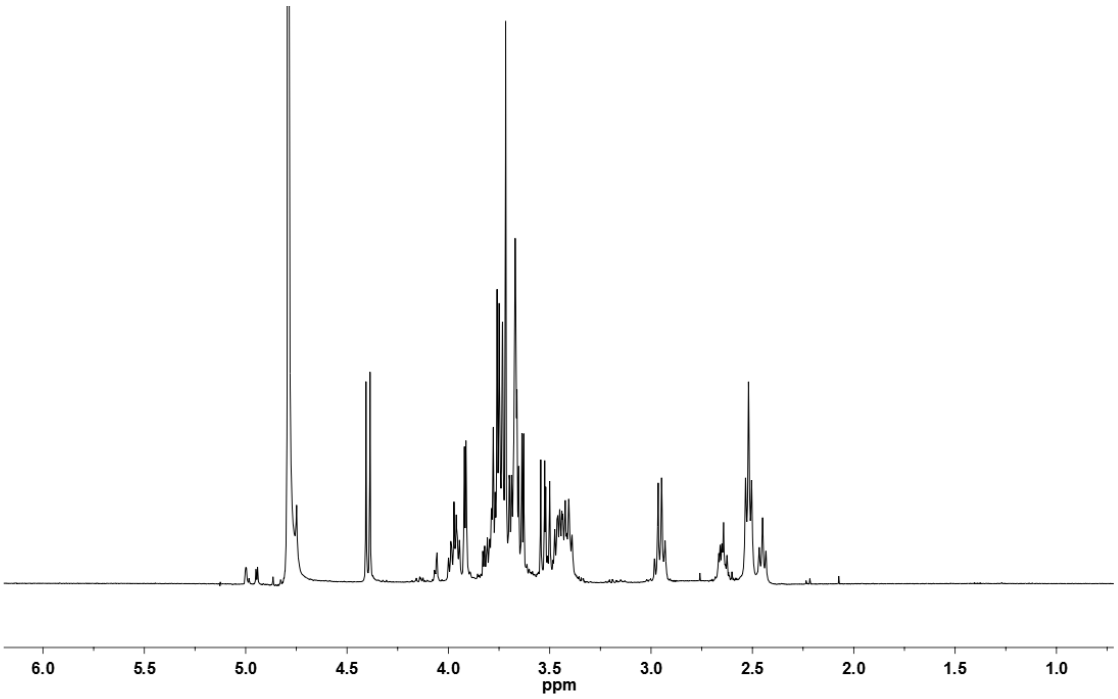
6.0
5.5
5.0
4.5
4.0
3.5
3.0
2.5
2.0
1.5
1.0
ppm

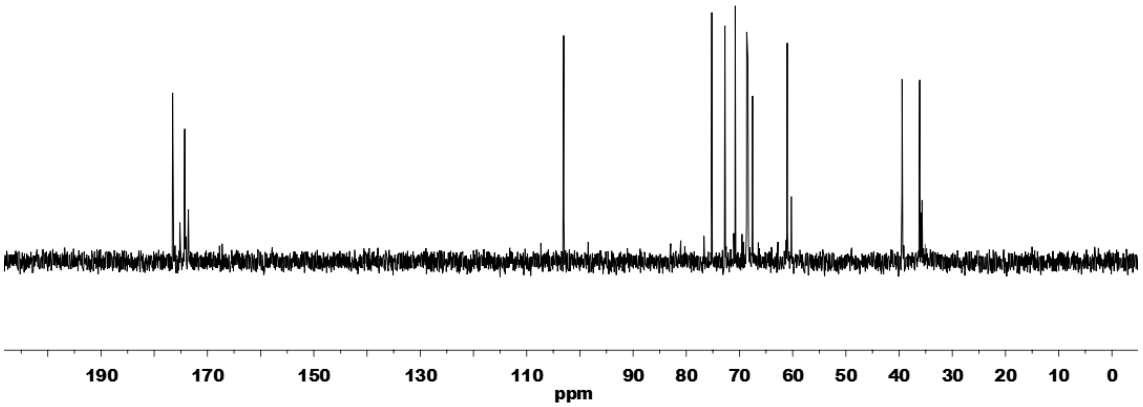
190
170
150
130
110
90
80
70
60
50
40
30
20
10
0
ppm

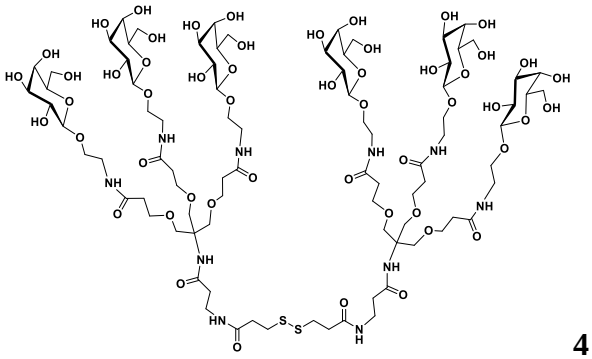

4

HRMS

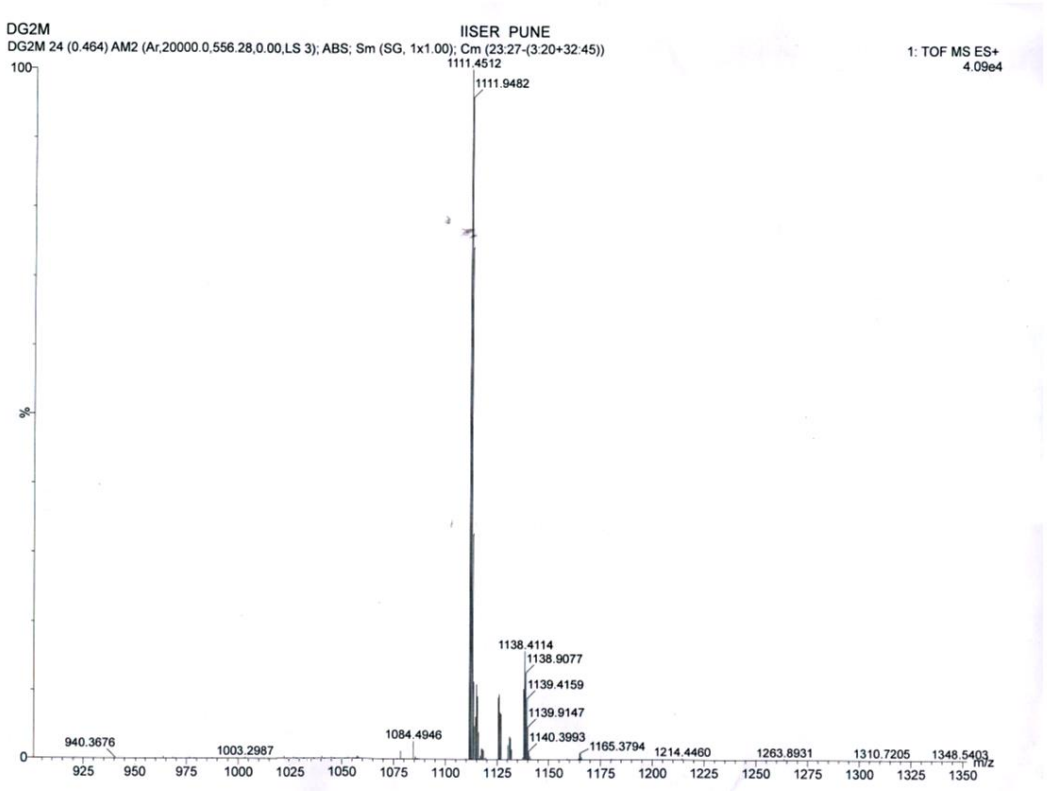
DG2M
IISER PUNE
DG2M 24 (0.464) AM2 (Ar,20000.0,556.28,0.00,LS 3); ABS; Sm (SG, 1x1.00); Cm (23:27-(3:20+32:45))
1: TOF MS ES+
4.09e4
100
%
0
1111.4512
1111.9482
1138.4114
1138.9077
1139.4159
1139.9147
1140.3993
1165.3794
940.3676
1003.2987
1084.4946
1214.4460
1263.8931
1310.7205
1348.5403
925 950 975 1000 1025 1050 1075 1100 1125 1150 1175 1200 1225 1250 1275 1300 1325 1350
m/z

CHAPTER-3

Gold Nanoparticles Mediated Immune modulation of *N*-Glycolylneuraminic acid Glycans.

Abstract

N-Acetylneuraminic acid (Neu5Ac) and *N*-glycolylneuraminic acid (Neu5Gc) glycans are the two predominant Sia forms in most mammals. Interestingly, humans cannot synthesize the common mammalian sialic acid *N*-glycolylneuraminic acid (Neu5Gc) due to an irreversible mutation in the gene. Surprisingly the Neu5Gc is expressed in human malignant tumors and in fetal tissues, which promotes inflammation and risk of cancer. To investigate the immunological properties of Neu5Gc acid glycans, (Neu5Gcα(2-3)galβ(1-4)glcNAc and Neu5Gcα(2-6)galβ(1-4)glcNAc) were synthesized by adopting novel synthetic methods. Next, these glycans were functionalised on the different sizes of sphere gold nanoparticles (15, 30 and 50 nm) and a carrier protein (CRM_{197}). As a control we also synthesised (Neu5Acα(2-3)galβ(1-4)glcNAc and Neu5Acα(2-6)galβ(1-4)glcNAc). Further, the funtionalized gold nanoparticles and carrier protein were immunized to the B6.129X1-*Cmah*^{tm1Avrk}/J mice to investigate the immune responses of Neu5Gc glycans.

3.1 Introduction:

Sialic acids (Sia) are a class of monosaccharides typically found on the outermost ends of glycan chains on glycoproteins and glycolipids expressed by the deuterostome lineage of animals and on certain bacterial species.[1] *N*-Acetylneuraminic acid (Neu5Ac) and its hydroxylated derivative, Neu5Gc, are the two predominant Sia forms in most mammals. Interestingly, humans cannot synthesize the common mammalian sialic acid *N*-glycolylneuraminic acid (Neu5Gc), due to an irreversible mutation in the gene encoding cytidine monophosphate (CMP)-*N*-acetylneuraminic acid (Neu5Ac) hydroxylase (CMAH), the enzyme responsible for the generation of CMP-Neu5Gc from CMP-Neu5Ac.[2] Thus, in comparison to our closest evolutionary relatives such as chimpanzees and gorillas, human blood cells and serum proteins lack Neu5Gc and instead accumulate an excess of the precursor Neu5Ac.[3] Though no alternate pathway for Neu5Gc synthesis in humans is known to date, small amounts of Neu5Gc have been found in cultured human cells (including human embryonic stem cells), and in certain tissue samples from humans. Larger amounts of Neu5Gc were reported in human malignant tumors and in fetal tissues.[4-6] Varki et al. have shown that Neu5Gc accumulation that occurs in the human body arises from dietary sources such as red meat and milk products.[7, 8] This is of biomedical relevance, as there are variable and sometimes high levels of circulating antibodies detectable in human sera that are directed against Neu5Gc.[9] However, Neu5Gc is too small to fill the binding pocket of an antibody, and thus there is also specificity for the underlying glycan chains. Little is known about the specific Neu5Gc-glycan moiety and antibody interactions that are involved in chronic inflammation and carcinoma progression.[10-12] Thus, there is a great deal of research interest to develop monoclonal antibodies against specific Neu5Gc glycans and use them in immunohistochemistry to analyze the antigen expression level on tissues.[13-20] However, poor immunogenicity of Neu5Gc glycans hamper the T-cell dependent immune responses.[21] Recently, It has been shown that nanoparticles alone can induce immunological responses and modulate antigen processing and antibody secretion.[22-24] Previously, Sawa and coworkers showed that the shape and size of the gold nanoparticles effectively modulated west Nile virus antigen processing, cytokine secretion and immune modulation.[25] Similarly, Corzana and coworkers synthesized full length MUC1 conjugated gold nanoparticles to develop antigen specific immune responses.[26] In this chapter, we focused on the size of the gold nanoparticles dependent immune response in vivo. We prepared three different sizes of gold nanoparticles (15, 30, 50 nm diameter) and coated them with Neu5Gc glycans (Neu5Gcα(2-3)galβ(1-4)glcNAc) and (Neu5Gcα(2-6)galβ(1-4)glcNAc). We chose these size because 15-60 nm

AuNPs is known to be internalized into the cells, and (2-3) and (2-6) linked sialic acid glycans are ubiquitous on cell surfaces. As a control we synthesized Neu5Acα(2-3)galβ(1-4)glcNAc) and (Neu5Acα(2-6)galβ(1-4)glcNAc) glycan. The functionalised AuNPs and CRM_{197} carrier protein were immunized to the B6.129X1-*Cmah*^{tm1Avrk}/J mice to investigate immune responses of Neu5Gc.

3.2 Results and Discussion:

3.2.1 Synthesis of Neu5Ac and Neu5Gc glycans:

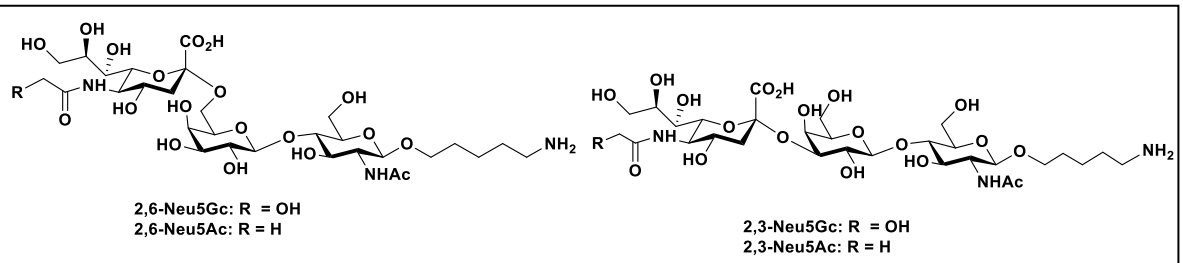

Figure 1. Structutres of sialic acid glycans

The chemical synthesis of sialic acid glycans is a formidable synthetic challenge due to its instability, difficulties in α-glycosylation and low reactivity.[27] The pioneering work from the lab of Danishefsky, David Crich, Makato Kiso, Cristina De Meo, Chi-Huey Wong, Koichi, and Schmidt reported necessary glycosylation conditions to achieve sialic acid glycans.[28-31] Using a similar synthetic strategy with sialic acid donor **8a**, Neu5Ac analogs were also synthesized (**2,6-Nue5Ac** and **2,3-Neu5Ac**) (Figure 1). However, the synthesis of Neu5Gc glycans using these methods is still a challenging task. Therefore, an enzymatic method has been extensively used in the synthesis of complex sialylated-glycans.[32] In the present synthetic strategy, we adopted two key steps to synthesize Neu5Gc glycans: (a) we constructed the sialic acid glycans using allyl ester instead of traditional methyl ester-ligand to avoid harsh deprotection conditions, which may cleave α-sialyl linkage; (b) we have developed a labile method to deprotect oxazolidinone ring to control the selective *N*-glycolyl substitution. Neu5Gc glycans were obtained from orthogonally protected sialic acid donor **8** and sequentially glycosylated to galactose and glucose building blocks under standard glycosylation conditions. The sialic acid donors were obtained by single step percetylation and allyl-esterification of sialic acid, followed by *p*-thiocresol glycosylation and Boc-protection. Deacetylation of **3** in the presence of sodium methoxide and allyl alcohol, followed by oxazolidinone formation and peracetylation yielded desire donor **5**, which was treated with acetoxyacetyl chloride to obtain Neu5Gc **7** thio-

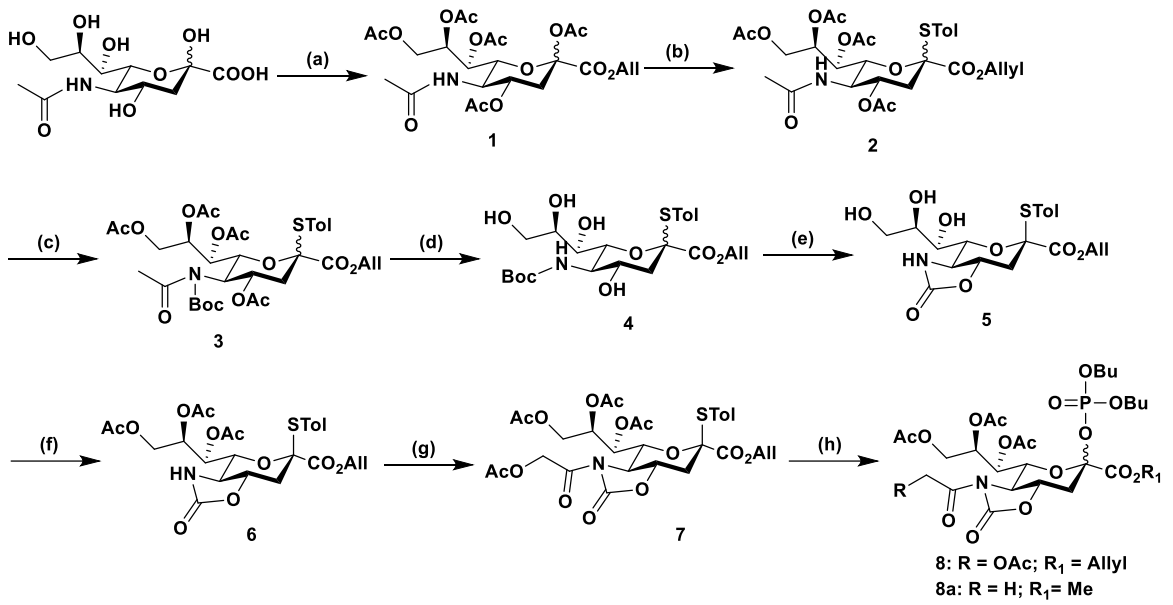

Scheme 1. Synthesis of donor **8**. Reagents and conditions: (a) i) Ac_2O, pyridine, rt, 12 h; ii) Cs_2CO_3, AllylBr, DMF, 40 ºC, 4 h, 69% over two steps; (b) *p*-Thiocresol, $BF_3{\cdot}OEt_2$, CH_2Cl_2, rt, 24 h, 78%; (c) Boc_2O, DMAP, THF, 60 ºC, 4 h, 85%; (d) NaOMe, AllylOH, rt, 4 h, 56 %; (e) i) TFA/CH_2Cl_2 (1:1, v/v), rt, 3 h ii) $NO_2C_6H_4OCOCl$, $NaHCO_3$, H_2O/MeCN (2:1, v/v), 0 ºC, 4 h, 47% over two steps; (f) Ac_2O, pyridine, rt, 12 h, 84%; (g) Acetoxyacetyl chloride, DIPEA, CH_2Cl_2, 0 ºC to rt, 2 h, 83 %; (h) NIS, TfOH, dibutyl phosphate, CH_2Cl_2, 0 ºC, 6 h, 74%.

donor. Finally, glycosylation of **7** with dibutyl phosphate in the presence of *N*-iodosuccinimide (NIS) and trifluoromethanesulfonic acid (TfOH) yielded the desire sialic acid donor **8** in an excellent yield (Scheme 1).

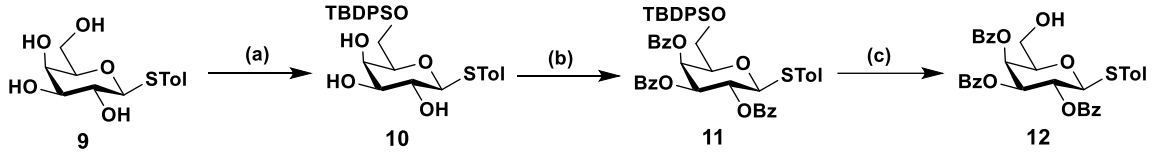

Scheme 2. Synthesis of galactose acceptor **12**. Reagents and conditions: i) (a) TBDPSCl, Imidazole, DMF, rt, 12 h, 77%; (d) BzCl, pyridine, rt, 12 h, 89%; (e) TBAF, AcOH, THF, rt, 36 h, 73%.

To achieve α(2-6) and α(2-3) glycosylated sialic acid disaccharides **20** and **25,** two different galactose building blocks **12** (Scheme 2) and **17** (Scheme 3) were synthesized in 5 and 8 steps from D-galactose. Briefly, D-galactose was percetylated and glycosylated with *p*-thiocresol using boron trifluoride. Diethyl ether ($BF_3.OEt_2$) promotor. This was followed by deacetylation and selective 6-OH protection with t-butyl-diphenyl silyl (TBDPS) group followed by benzoylation and selective TBDPS deprotection using Tetra-n-butylammonium fluoride

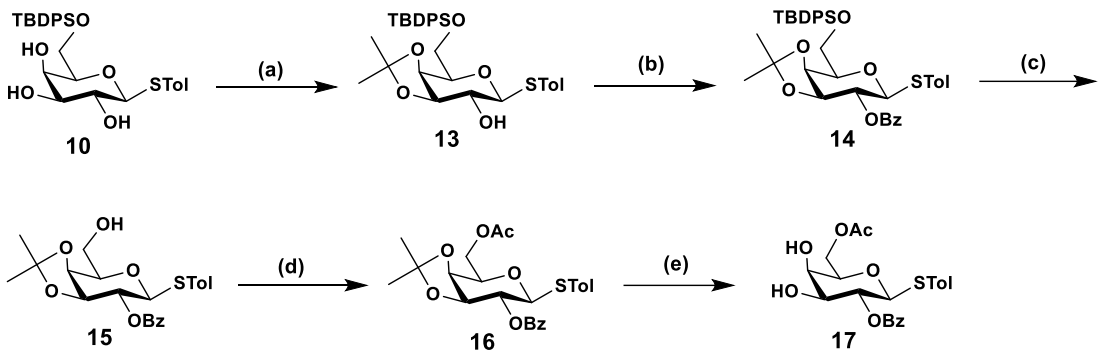

Scheme 3. Synthesis of galactose acceptors **17**. Reagents and conditions: (a) DMP, CSA, acetone, rt, 4 h, 86%; (b) BzCl, pyridine, rt, 12 h, 89%; (c) TBAF, AcOH, THF, rt, 36 h, 74%; (d) Ac_2O, pyridine, rt, 12 h, 88%; (e) AcOH/H_2O (8:2, v/v), 60 ºC, 6 h, 82%.

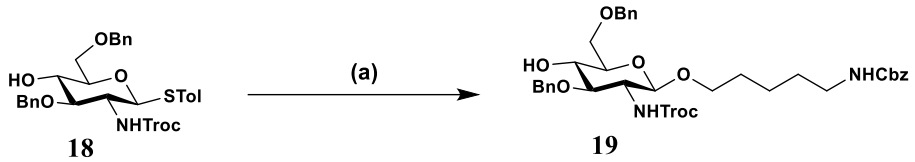

Scheme 4. Synthesis of glucose building block: (a) Linker, NIS, TfOH, -20 °C, 2 h, 82%.

(TBAF) to obtain galactose 6-OH precursor **12** (scheme 2). While, the ketal protection of the 3,4-OH group of **10**, followed by benzoylation of the 2-OH group, yielded galactose precursor **14**. Then, the TBDPS group of **14** was deprotected, followed by acetylation of 6-OH and finally ketal deprotection yielded galactose 3-OH precursor **17** in 19% (5 steps) overall yield (Scheme 3).

The glucose building block **18** was synthesized as reported previously and glycosylated with Cbz-amine protected linker using standard glycosylation conditions to obtain 82% of **19** (Scheme 4). [37] The sialic acid disaccharides (**20**, **25**) was obtained by glycosylating the sialic acid donor **8** with **12** and **17** acceptors in the presence of TMSOTf at -50 °C in DCM solvent. In the case of α(2-3) disaccharides, the glycosylated product was again reacted with acetic anhydride to block 4-OH group on galactose residue. Then glycosylation of disaccharide thio-donors (**20** and **25**) with **19** acceptor was carried out with NIS/TfOH at -20 °C gave protected trisaccharide in moderate to good yield. To accomplish the final deprotected **2,6-Neu5Gc** and **2,3-Neu5Gc**, the correct order of deprotection is critical to obtain Neu5Gc analogs. It was found the oxazolidinone deprotection prior Troc-removal resulted in partial deprotection of Troc. In addition, the global deprotection of oxazolidinone, acetate and benzoyl group using strong basic conditions also resulted complete deproctection of glucose *N*-acetate. Thus, Troc-

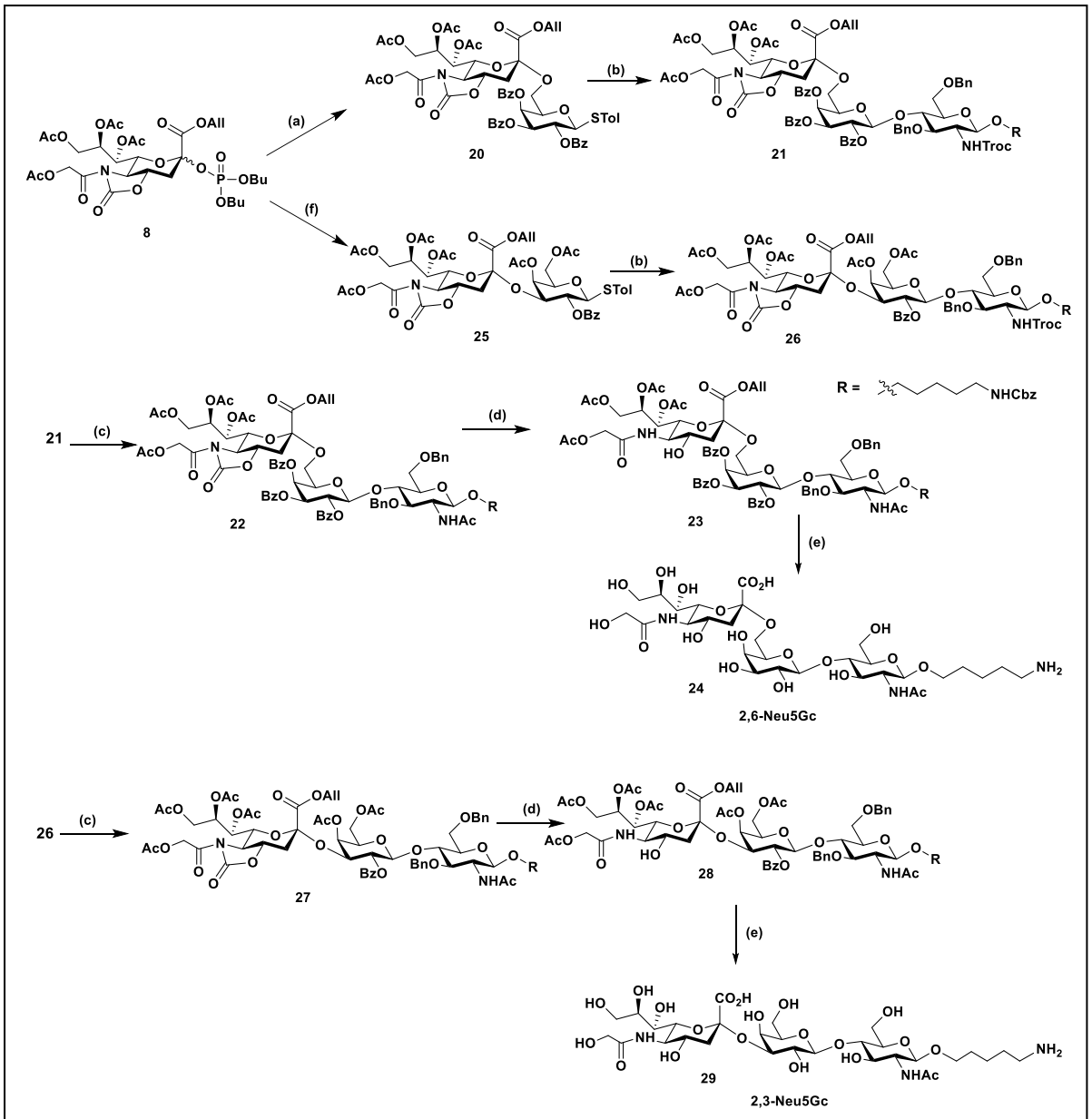

Scheme 5. Synthesis of Neu5Gc trisaccharides. Reagents and conditions: (a) **12**, TMSOTf, CH_2Cl_2, -50 ºC, 2 h, 72%; (b) **19**, NIS, TfOH, CH_2Cl_2, -20 ºC, 2 h, **21**: 71%; **26**: 68%; (c) Zn, THF/AcOH/Ac_2O (3:2:1, v/v), rt, 4 h, **22**: 65%, **27**: 70%; (d) 1,2-ethanedithiol, DBU, CH_2Cl_2, 0 ºC, 2 h, **23**: 74%; **28**: 75%; (e) i) LiOH, THF/H_2O/MeOH (2:2:1, v/v), rt, 12 h; ii) $Pd(OH)_2$/C, H_2, H_2O/MeOH (3:1, v/v), rt, 48 h, **24**: 63%; **29**: 59%, over two steps. (f) i) **17**, TMSOTf, CH_2Cl_2, -50 ºC, 2 h; ii) Ac_2O, pyridine, rt, 12 h, 49% over two steps.

protection removal and acetylation is the first necessary step to maintain the *N*-glycolyl group. This was followed by selective oxazolidinone deprotection using 1,2-ethanethiol and DBU mixture, followed by global deprotection using lithium hydroxide, followed by hydrogenolysis yielded (**2,6-Neu5Gc**) and (**2,3-Neu5Gc**) (Scheme 5). These final Neu5Ac and Neu5Gc trisaccharides were further treated with *N*-hydroxysuccinimide-11-mercaptoundecanoate to yield thio-compounds.

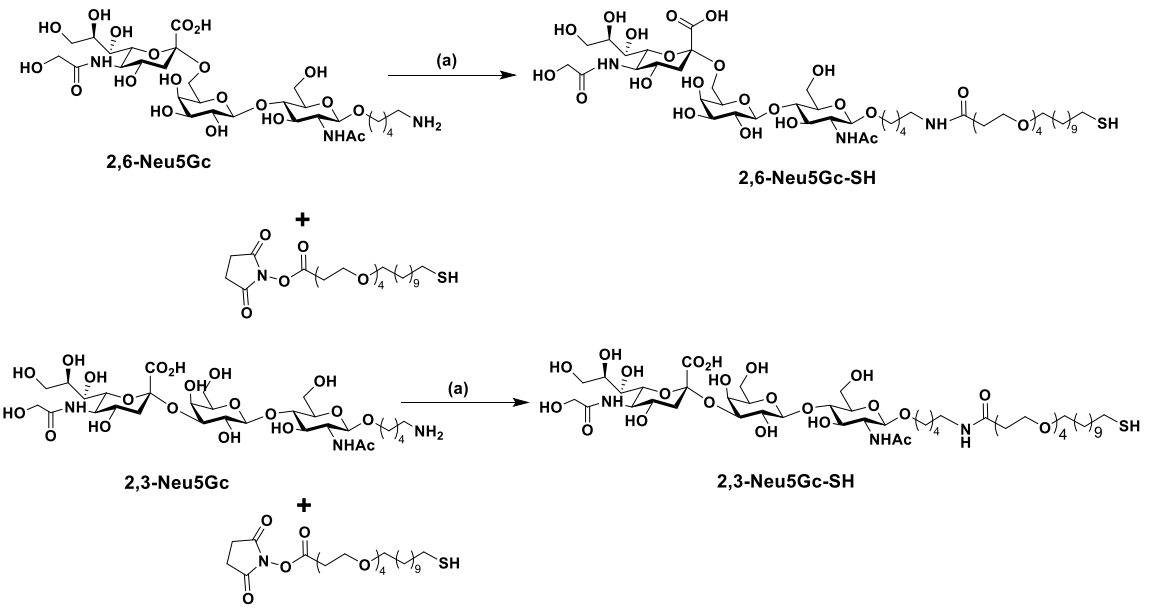

Scheme 5. Synthesis of thio-linker sialic acid glycans: (a) DMF, Et_3N, 3 h, 40 °C, 83-85% yield.

3.2.2 Glyco-gold nanoparticles synthesis and characterization:

Spherical gold nanoparticles of sizes 15, 30 and 50 nm were synthesized by reaction of chloroauric acid with sodium citrate and centrifuge at different time intervals. Then sialic acid glycans were encapsulated by a ligand exchange process (Scheme 5).

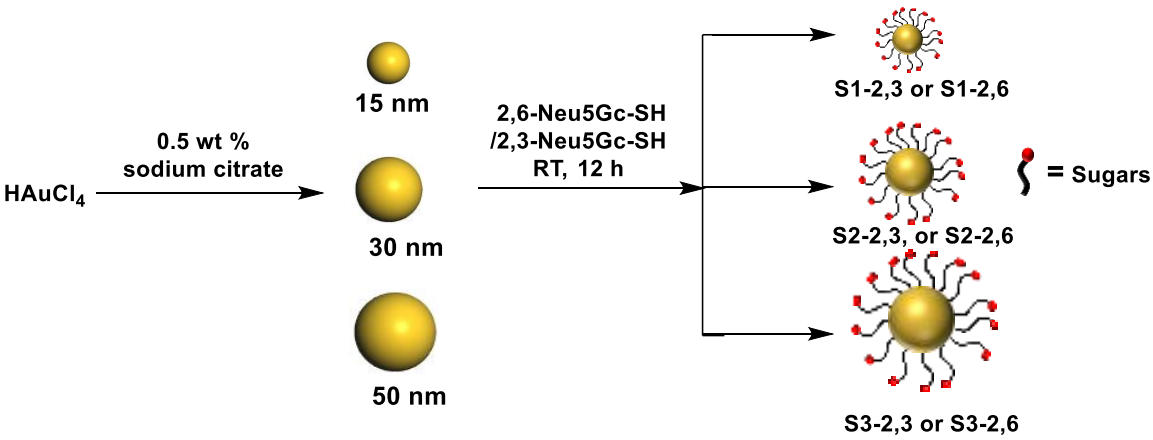

Scheme 5. Synthesis of glyco-gold nanoparticles.

The size of the nanoparticles was confirmed by scanning electron microscopy (SEM) and UV-visible absorption (Figure 2). The functionalization of AuNPs was confirmed by changes in the zeta potential. After sugar ligand exchange, the zeta-potential of spherical shapes AuNPs showed

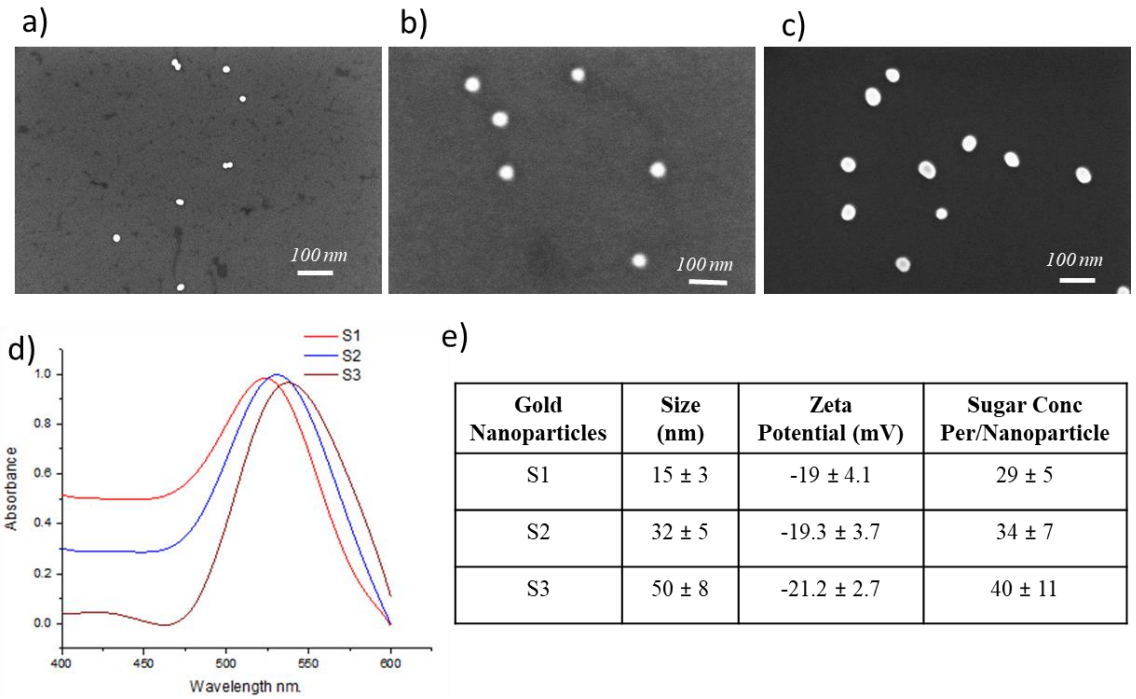

Gold Nanoparticles	Size (nm)	Zeta Potential (mV)	Sugar Conc Per/Nanoparticle
S1	15 ± 3	-19 ± 4.1	29 ± 5
S2	32 ± 5	-19.3 ± 3.7	34 ± 7
S3	50 ± 8	-21.2 ± 2.7	40 ± 11

Figure 2. a) FESEM image of 15 nm sphere AuNPs b) FESEM image of 30 nm AuNPs c) FESEM image of 50 nm sphere AuNPs d) UV-Visible spectra of sphere nanoparticles e) Physical characteristic of gold nanoparticles.

(-26 mV to -19 mV) (Figure 2 e). This may be due to the displacement of negatively changed citrate by the sialic acid scaffolds. Finally, we quantified the sialic acid conjugation by resorcinol-HCl calorimetric method, which indicates 30-40 sugar conjugation on AuNPs (Figure 2 e).

3.2.3 Glycan carrier protein conjugation.

As a positive control for immune studies, we have also synthesized CRM_{197}, a carrier protein sialic acid conjugated system (Scheme 6). Briefly, the 2,3-Neu5Gc and 2,6-Neu5Gc were coupled to disuccinimidyl suberate ester, and then mixed with CRM_{197} and purified by 10 kDa cutoff filter. The conjugation was characterized by gel electrophoresis and MALDI-TOF mass spectrometry (Figure 3). Further, we calculated no of 2,3-Neu5Gc and 2,6-Neu5Gc molecules conjugated on single carrier protein were 6 and 7, respectively.

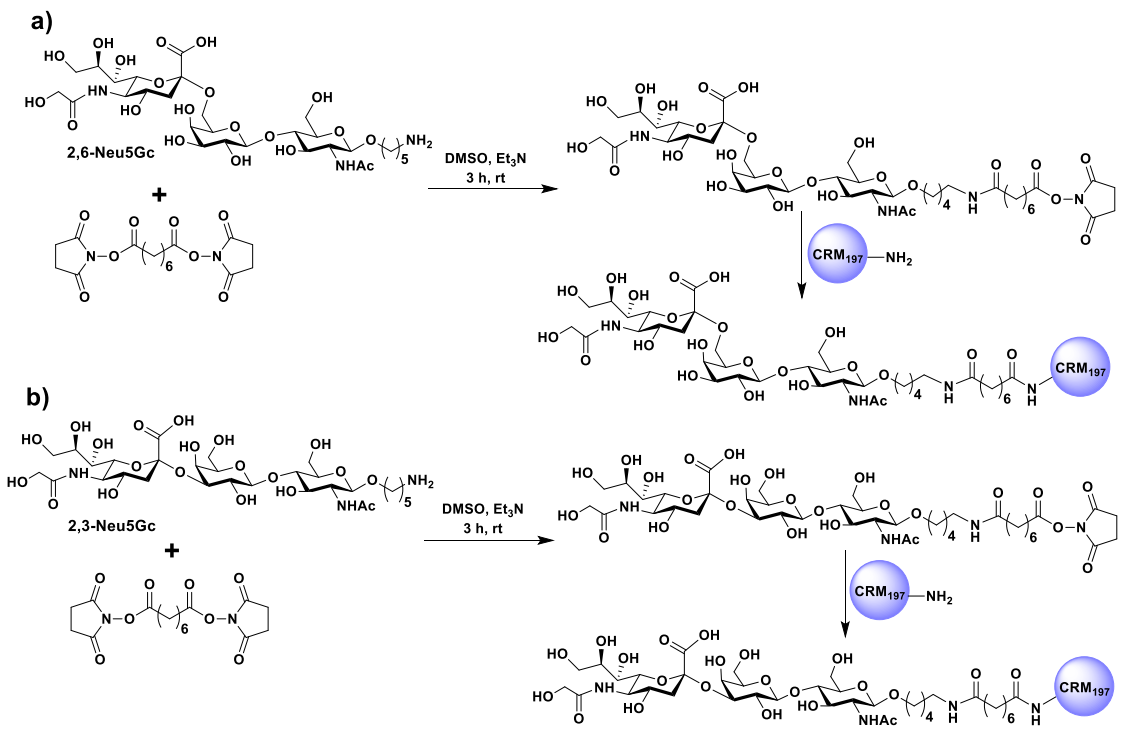

Scheme 6. Glycan carrier protein (CRM_{197}) conjugation.

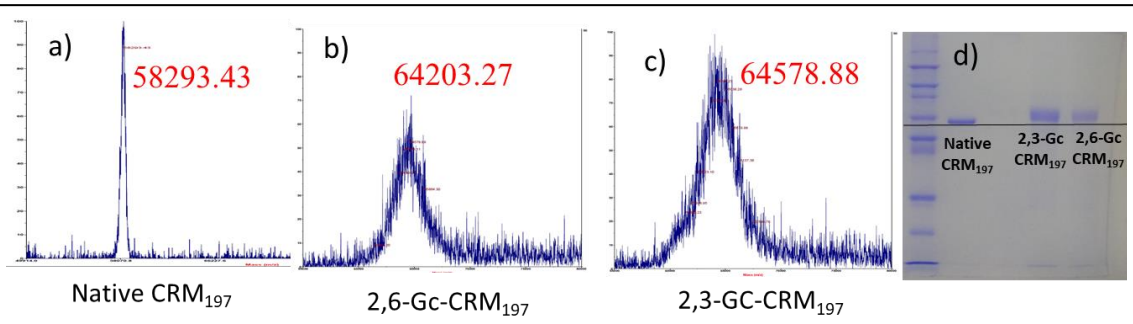

Figure 3. MALDI-TOF spectra and and SDS-PAGE stained with coomassie blue G-250 of glycoconjugate. a) MALDI-TOF of CRM_{197} b) MALDI-TOF of 2,6-Gc-CRM_{197} c) MALDI-TOF of 2,3-Gc-CRM_{197} d) SDS-PAGE of CRM_{197} glycoconjugate.

3.2.4 Immune response of Neu5Gc glycans appended AuNPs and CRM_{197} conjugates:

A group of five female B6.129X1-*Cmah*^{tm1Avrk}/J of 6-8 weeks old was immunized with Neu5Gc conjugated AuNPs (2.5 µg of sugar) weekly for the first two weeks and followed final booster at the end of 30th day and phosphate buffer as control. At the end of the 5th week, animal sera were withdrawn and pooled with respect to the individual group and microarray analysis was performed for IgG antibody response against various sialic acid glycans. Unfortunately, we didn't observe any efficient IgG antibody response against Neu5Gc sialic acid glycans (Figure

4). However, 2,3-Neu5Gc-conjugated CRM_{197} showed a moderate immune response against Gc glycans. These results showed that sugar alone cannot modulate immune responses, glycopeptides and adjuvant conjugation are essential to modulate the immune response.

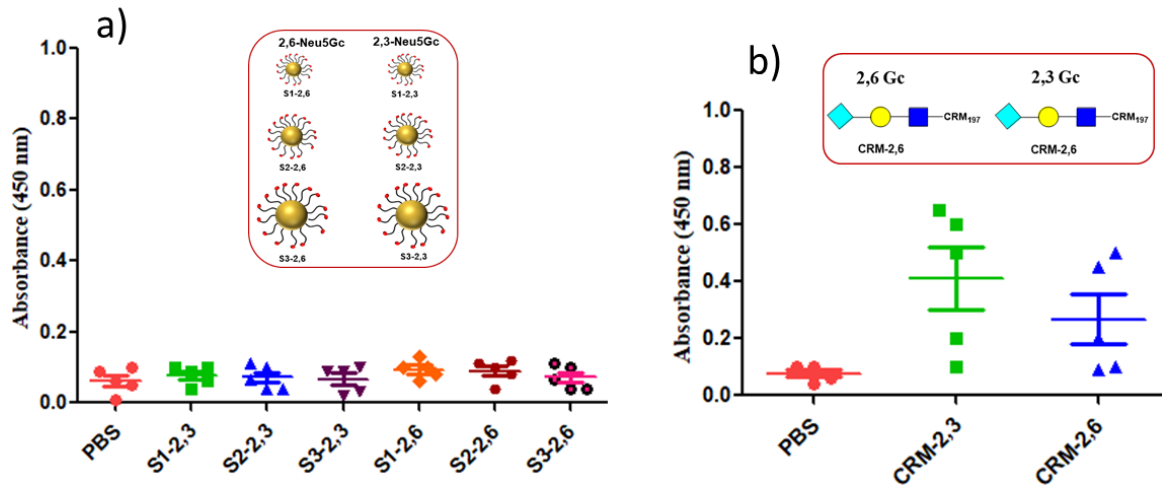

Figure 4. IgG Antibody titre after 5th week of Immunization of Neu5Gc. a) Immune responses of Neu5Gc functionalized AuNPs b) Immune responses Neu5Gc conjugated carrier protein (CRM_{197}).

3.3 Conclusion:

Our work demonstrated the immune responses of the gold nanoparticles conjugated Neu5Gc is very poor. The amount of IgG antibodies generated by nanoparticles is negligible, whereas CRM_{197} glycoconjugates showed promising IgG antibody responses. These results indicated that the incorporation of sugar alone on nanoparticles could not induce immunogenicity to the sialic acid glycans. A suitable combination of adjuvant and glycopeptides are essential for immune modulation.

3.4 Experimental Section:

3.4.1 General information:

All reagents and solvents obtained from suppliers were used without further purification. All reactions were carried out under a nitrogen atmosphere in anhydrous solvents unless otherwise noted. Reactions were monitored by TLC on Merck silica gel 60 F_{254}. The compounds were visualized under UV light or dipping the TLC plate in CAM solution followed by heating. Column chromatography was carried out using the force flow of the indicated solvents on Fluka kieselgel 60 (230-400 mesh). ^{1}H and ^{13}C NMR spectra of the compounds were recorded on Bruker 400 MHz, Bruker 600 MHz and Jeol 400 MHz with cryoprobe using residual solvents as an internal reference ($CDCl_3$ δH 7.26 ppm, δC 77.3 ppm, CD_3OD δH 3.31 ppm, δC 49.0

ppm, and D_2O δH 4.79 ppm). The chemical shifts (δ) are reported in ppm and coupling constants (J) in Hz.

3.4.2 Synthesis of Trisaccharide:

Synthesis of compound 1

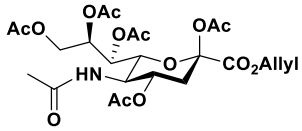

N-Acetylneuraminic acid (1.5 gm, 4.85 mmol) in pyridine (10 mL) was mixed with acetic anhydride (3.67 mL, 38.8 mmol) at 0 ºC and stirred at RT for 12 hours. The reaction mixture was quenched with methanol and concentrated *in vacuo,* and the residue was co-evaporated with toluene and used as such for next step without further purification. Next, the residue in DMF (20 mL), along with cesium carbonate (4.7 gm, 14.55 mmol), allyl bromide (1.2 mL, 14.55 mmol) was stirred at 40 ºC for 4 hours and quenched with methanol. The reaction mixture was filtered through celite bed, and the filtrate was concentrated. The residue was purified by silica gel column chromatography using a mixture of (4:1, v/v) dichloromethane and methanol as eluent to afford compound **1** (1.9 gm, 69% over two steps). ^{1}H NMR (400 MHz, Chloroform-*d*) δ = 5.98-5.82 (m, 1H), 5.45-5.31 (m, 3H), 5.30-5.20 (m, 2H), 5.07 (ddd, *J* = 6.7, 5.0, 2.6 Hz, 1H), 4.74-4.58 (m, 2H), 4.45 (dd, *J* = 12.4, 2.6 Hz, 1H), 4.19-4.05 (m, 3H), 2.55 (dd, *J* = 13.5, 5.0 Hz, 1H), 2.14 (s, 3H), 2.14 (s, 3H), 2.10 (dt, *J* = 4.5, 2.4 Hz, 1H), 2.05 (s, 3H), 2.03 (s, 3H), 2.03 (s, 3H), 1.89 (s, 3H). ^{13}C NMR (101 MHz, Chloroform-*d*) δ = 171.13, 170.71, 170.4, 170.40, 170.38, 168.37, 165.57, 131.28, 119.14, 97.74, 73.04, 71.49, 68.44, 68.02, 66.96, 62.22, 49.50, 36.02, 23.32, 21.05, 20.98, 20.92, 20.89. HRMS (ESI): Calcd for $C_{24}H_{33}NNaO_{14}$ $[M+Na]^+$ 582.1799, found 582.1798.

Synthesis of compound 2

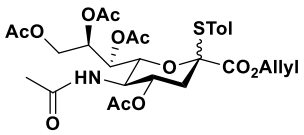

To a stirred solution of compound **1** (1.2 gm, 2.14 mmol) and 4-methylbenzenethiol (0.4 gm, 3.21 mmol) in anhydrous dichloromethane (15 mL) was added boron trifluoride diethyl etherate (0.8 mL, 6.42 mmol) at 0 ºC. The reaction mixture was stirred at room temperature for 24 hours, neutralized with triethylamine and washed with brine solutions. The organic layer was dried over sodium sulphate, concentrated *in vacuo* and purified by silica gel column chromatography using a mixture of (9:1, v/v) dichloromethane and methanol as eluent to afford compound **2** (1.05 gm, 78%, α/β=1:13). *β* anomer: ^{1}H NMR (400 MHz, Chloroform-*d*) δ = 7.33 (d, *J* = 8.1 Hz, 2H), 7.12 (d, *J* = 8.0 Hz, 2H), 5.83-5.70 (m,1H), 5.53 (bs, 1H), 5.45 (t, *J* = 2.5 Hz, 1H), 5.39 (ddd, *J* = 11.6, 10.4, 4.8 Hz, 1H), 5.30-5.17 (m, 2H), 4.95 (dt, *J* = 8.4, 2.4

Hz, 1H), 4.61 (dd, *J* = 10.5, 2.6 Hz, 1H), 4.50 (tddd, *J* = 12.9, 11.6, 5.9, 1.2 Hz, 2H), 4.39 (dd, *J* = 12.3, 2.3 Hz, 1H), 4.19-4.08 (m, 2H), 2.64 (dd, *J* = 13.9, 4.9 Hz, 1H), 2.32 (s, 3H), 2.10 (s, 3H), 2.06 (s, 3H), 2.03 (s, 3H), 1.97 (s, 3H), 1.89 (s, 3H). ^{13}C NMR (101 MHz, Chloroform-*d*) δ = 171.21, 171.06, 170.40, 170.36, 167.51, 140.23, 136.29, 131.42, 130.05, 125.36, 119.25, 88.79, 73.26, 73.10, 69.22, 68.98, 66.64, 62.59, 49.62, 37.49, 23.31, 21.42, 21.21, 21.01, 20.88. HRMS (ESI): Calcd for $C_{29}H_{38}NO_{12}S$ $[M+H]^+$ 624.2115, found 624.2114.

Synthesis of compound 3

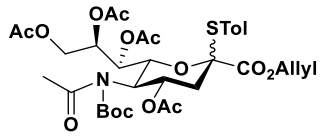

To a stirred solution of compound **2** (1.8 gm, 2.89 mmol) in anhydrous THF (25 mL) was added di-tert-butyl dicarbonate (3.3 mL, 14.45 mmol), DMAP (70 mg, 0.57 mmol) and stirred at 60 ºC for 4 hours. The reaction mixture was cooled, quenched with methanol and concentrated *in vacuo*. The residue was purified by silica gel column chromatography using a mixture of (3:2, v/v) ethyl acetate and hexane as eluent to afford compound **3** (1.78 gm, 85%). *β* anomer: ^{1}H NMR (400 MHz, Chloroform-*d*) δ 7.34 (d, *J* = 8.1 Hz, 2H), 7.12 (d, *J* = 8.0 Hz, 2H), 5.84-5.69 (m, 2H), 5.43 (dd, *J* = 10.1, 2.1 Hz, 1H), 5.34 (dd, *J* = 3.1, 2.0 Hz, 1H), 5.28-5.16 (m, 2H), 5.11 (dt, *J* = 8.0, 2.6 Hz, 1H), 4.85 (t, *J* = 10.5 Hz, 1H), 4.53-4.43 (m, 2H), 4.39 (dd, *J* = 12.4, 2.2 Hz, 1H), 4.16 (dd, *J* = 12.4, 8.0 Hz, 1H), 2.72 (dd, *J* = 13.8, 4.9 Hz, 1H), 2.35 (s, 3H), 2.32 (s, 3H), 2.05 (s, 3H), 2.04 (s, 3H), 1.97 (s, 3H), 1.95 (s, 3H), 1.70 (s, 9H). ^{13}C NMR (101 MHz, Chloroform-*d*) δ 173.94, 170.60, 170.51, 170.32, 169.96, 167.38, 152.11, 140.17, 136.54, 136.36, 131.45, 130.00, 125.77, 119.07, 89.33, 85.42, 72.79, 72.34, 68.66, 66.56, 66.49, 62.33, 52.98, 38.87, 28.28, 26.74, 21.42, 21.13 , 20.95, 20.85, 20.81. HRMS (ESI): Calcd for $C_{34}H_{45}NNaO_{14}S$ $[M+Na]^+$ 746.2458, found 746.2458.

Synthesis of compound 4

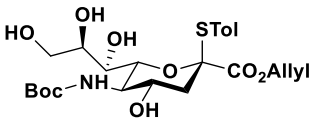

Compound **3** (2.6 gm, 3.59 mmol) in allyl alcohol, was basified with and 1M NaOMe until the pH of the reaction mixture reached 9. The reaction mixture was stirred at room temperature for 4 hours, quenched with acetic acid, and concentrated *in vacuo*. The residue was purified by silica gel column chromatography using a mixture of (4:1, v/v) dichloromethane and methanol as eluent to afford compound **4** (1.05 gm, 56%). *β* anomer: ^{1}H NMR (400 MHz, Methanol-d_4) δ = 7.47 (d, *J* = 8.1 Hz, 2H), 7.16 (d, *J* = 7.9 Hz, 2H), 5.81-5.74 (m, 1H), 5.28 (dq, *J* = 17.3, 1.6 Hz, 1H), 5.20 (dq, *J* = 10.3, 1.3 Hz, 1H), 4.48 (d, *J* = 10.6 Hz, 1H), 4.40-4.42 (m, 2H), 4.06 (ddd, *J* = 11.6, 9.9, 4.6 Hz, 1H), 3.87-3.78 (m, 2H), 3.71-3.66 (m, 2H), 3.60 (t, *J* = 10.2 Hz, 1H), 2.67 (dd, *J* = 13.6, 4.6 Hz, 1H), 2.34 (s, 3H), 1.96 (dd, *J* = 13.6, 11.6 Hz, 1H), 1.48 (s, 9H). ^{13}C

NMR (101 MHz, Methanol-d_4) δ = 170.11, 159.10, 140.93, 137.33, 132.81, 130.63, 127.91, 118.94, 91.22, 80.51, 73.84, 71.51, 70.74, 68.29, 67.30, 65.23, 55.06, 42.31, 28.78, 21.27. HRMS (ESI): Calcd for $C_{24}H_{36}NO_9S$ $[M+H]^+$ 514.2111, found 514.2107.

Synthesis of compound 5

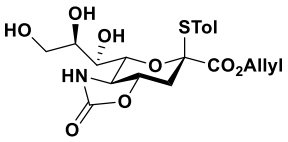

Compound **4** (3.5 gm, 6.81 mmol) in a 1:1 (v/v) mixture of CH_2Cl_2/TFA (30mL) was stirred at room temperature for 3 hours. The reaction mixture was concentrated *in vacuo*, and the residue was co-evaporated with toluene and dried under a high vacuum for 12 hours. Next, the residue in a 1:2 (v/v) mixture of ACN/H_2O (60 mL) was treated with sodium bicarbonate (2.86 gm, 34.05 mmol). The reaction mixture was cooled to 0 ºC, and 4-nitrophynylchloroformate (4.1 gm, 20.43 mmol) was added. Next, the resulting mixture was stirred at 0 ºC for 4 hours and extracted with ethyl acetate (50 mL x 3). The organic layer was dried over sodium sulphate and concentrated *in vacuo*. The residue was purified by silica gel column chromatography using a mixture of (4:1, v/v) ethyl acetate and methanol as eluent to afford compound **5** (1.4 gm, 47% over two steps). ^{1}H NMR (400 MHz, Methanol-d_4) δ = 7.46 (d, *J* = 8.1 Hz, 2H), 7.15 (d, *J* = 8.0 Hz, 2H), 5.83-5.70 (m, 1H), 5.32-5.15 (m, 2H), 4.71 (dd, *J* = 10.5, 0.6 Hz, 1H), 4.42 (dt, *J* = 5.8, 1.2 Hz, 2H), 4.20 (ddd, *J* = 11.6, 10.3, 4.7 Hz, 1H), 4.11-4.01 (m, 1H), 3.81 (dd, *J* = 11.2, 2.8 Hz, 1H), 3.78-3.72 (m, 1H), 3.65 (dd, *J* = 11.2, 5.3 Hz, 1H), 3.49 (d, *J* = 8.9 Hz, 1H), 2.68 (dd, *J* = 13.6, 4.7 Hz, 1H), 2.32 (s, 3H), 1.98 (dd, *J* = 13.6, 11.6 Hz, 1H). ^{13}C NMR (101 MHz, Methanol-d_4) δ = 170.39, 141.32, 137.53, 130.91, 127.84, 119.35, 91.37, 72.72, 71.58, 70.86, 67.81, 67.71, 65.19, 54.61, 42.39, 21.50. HRMS (ESI): Calcd for $C_{20}H_{26}NO_8S$ $[M+H]^+$ 440.1339, found 440.1335.

Synthesis of compound 6

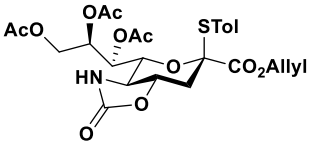

Compound **5** (1.7 gm, 3.87 mmol) in pyridine (20 mL) was added dropwise to acetic anhydride (1.7 mL, 19.35 mmol) at 0 ºC and stirred at room temperature for 12 hours and concentrated *in vacuo*. The residue was purified by silica gel column chromatography using a mixture of (7:3, v/v) ethyl acetate and hexane as eluent to afford compound **6** (1.85 gm, 84%). ^{1}H NMR (400 MHz, Chloroform-*d*) δ = 7.27 (d, *J* = 8.2 Hz, 2H), 7.12 (d, *J* = 8.0 Hz, 2H), 5.84-5.67 (m, 1H), 5.51 (s, 1H), 5.30-5.23 (m, 1H), 5.23-5.18 (m, 2H), 5.15 (td, *J* = 5.7, 2.4 Hz, 1H), 4.73-4.63 (m, 1H), 4.57 (dd, *J* = 9.7, 2.6 Hz, 1H), 4.54-4.42 (m, 2H), 4.35 (dd, *J* = 12.6, 2.4 Hz, 1H), 4.28 (dd, *J* = 12.5, 6.0 Hz, 1H), 3.10 (ddd, *J* = 11.1, 9.7, 1.4 Hz, 1H), 2.79 (dd, *J* = 13.1, 3.8 Hz,

1H), 2.33 (s, 3H), 2.24 (t, *J* = 12.8 Hz, 1H), 2.13 (s, 3H), 2.07 (d, *J* = 1.0 Hz, 3H), 2.01 (d, *J* = 0.8 Hz, 3H). ^{13}C NMR (101 MHz, Chloroform-*d*) δ = 171.37, 170.37, 170.17, 167.01, 159.26, 140.52, 136.09, 131.20, 130.10, 125.31, 119.14, 88.87, 76.96, 73.22, 70.84, 70.29, 66.60, 61.77, 58.55, 36.42, 21.38, 21.04, 20.80, 20.76. HRMS (ESI): Calcd for $C_{26}H_{32}NO_{11}S$ $[M+H]^+$ 566.1696, found 566.1698.

Synthesis of compound 7

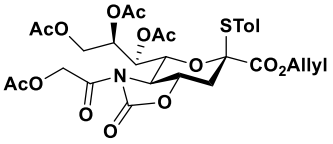

Compound **6** (1.5 gm, 2.65 mmol) in anhydrous dichloromethane (20 mL) was mixed with acetoxyacetyl choride (1.4 mL, 13.5 mmol), DIPEA (3.69 mL, 21.2 mmol) at 0 ºC. The reaction mixture was brought to room temperature and stirred at room temperature for 2 h. The resulting mixture was diluted with dichloromethane, washed with sodium bicarbonate and brine solutions. The organic layer was dried over sodium sulphate and concentrated *in vacuo.* The residue was purified by silica gel chromatography using a mixture of (1:1, v/v) ethyl acetate and hexane as eluent to afford compound **7** (1.46 gm, 83%). ^{1}H NMR (400 MHz, Chloroform-*d*) δ = 7.35 (d, *J* = 8.1 Hz, 2H), 7.13 (d, *J* = 7.9 Hz, 2H), 5.78-5.71 (m, 1H), 5.55 (t, *J* = 2.6 Hz, 1H), 5.34-5.18 (m, 3H), 4.98 (dt, *J* = 7.8, 2.6 Hz, 1H), 4.85 (dd, *J* = 9.1, 2.6 Hz, 2H), 4.76 (ddd, *J* = 12.8, 11.3, 3.7 Hz, 1H), 4.61-4.44 (m, 2H), 4.30 (dd, *J* = 12.1, 2.7 Hz, 1H), 4.02 (dd, *J* = 12.1, 7.9 Hz, 1H), 3.73 (dd, *J* = 11.3, 9.2 Hz, 1H), 2.83 (dd, *J* = 13.0, 3.7 Hz, 1H), 2.50 (s, 3H), 2.33 (s, 3H), 2.29 (t, *J* = 12.9 Hz, 1H), 2.11 (s, 3H), 2.06 (s, 3H), 1.96 (s, 3H).^{13}C NMR (101 MHz, Chloroform-*d*) δ = 172.52, 171.13, 170.44, 169.81, 167.08, 153.71, 140.66, 131.23, 130.13, 124.79, 119.41, 88.05, 75.69, 75.22, 73.70, 72.52, 66.76, 62.81, 59.78, 35.81, 24.81, 21.41, 21.20, 20.84, 20.82. HRMS (ESI): Calcd for $C_{30}H_{35}NNaO_{14}S$ $[M+Na]^+$ 688.1676, found 688.1675.

Synthesis of compound 8

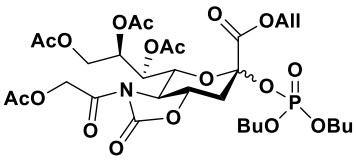

Compound **7** (1.9 gm, 2.85 mole) and dibutyl phosphate (1.7 mL, 8.55 mmol) was dissolved in anhydrous dichloromethane (30 mL) and activated 4 Å molecular sieves was added. The reaction mixture was stirred at room temperature for 2 hours. The resultant mixture was cooled to 0 ºC, and NIS (0.96 gm, 4.27 mmol), TfOH (53 µl, 0.57 mmol) were added. The reaction mixture was stirred at 0 ºC for 6 hours, neutralized with DIPEA and concentrated *in vacuo.* The residue was purified by silica gel column chromatography using a mixture of (3:2, v/v) ethyl acetate and hexane as eluent to afford compound **8** (1.59 gm, 74%, *α/β* = 1:1). ^{1}H NMR (400 MHz, Chloroform-*d*) δ = 5.94 (dddt, *J* = 17.5, 10.3, 7.3, 5.9 Hz, 2H), 5.73 (dd, *J* = 8.1, 1.5 Hz, 1H),

5.64 (dd, *J* = 5.4, 1.9 Hz, 1H), 5.42-5.35 (m, 2H), 5.31-5.24 (m, 4H), 5.15-5.00 (m, 4H), 4.83 (dd, *J* = 9.7, 1.5 Hz, 1H), 4.76-7.64 (m, 6H), 4.42 (dd, *J* = 12.2, 2.8 Hz, 1H), 4.35 (dd, *J* = 12.3, 2.7 Hz, 1H), 4.26 (ddd, *J* = 13.3, 11.2, 4.0 Hz, 1H), 4.17-4.01 (m, 12H), 3.83 (ddd, *J* = 15.2, 11.2, 9.6 Hz, 2H), 2.99 (dd, *J* = 12.3, 4.0 Hz, 1H), 2.90 (dd, *J* = 12.8, 3.7 Hz, 1H), 2.72 (t, *J* = 12.7 Hz, 1H), 2.37 (td, *J* = 12.8, 2.2 Hz, 1H), 2.16 (s, 3H), 2.15 (s, 3H), 2.12 (s, 3H), 2.09 (s, 3H), 2.08 (s, 3H), 2.08 (s, 3H), 2.03 (s, 3H), 2.02 (s, 3H), 1.6-1.61 (m, 8H), 1.38 (m, 8H), 0.95-0.91 (m, 12H). ^{13}C NMR (101 MHz, Chloroform-*d*) δ = 172.25, 171.97, 170.75, 170.70, 170.65, 170.09, 170.05 169.90, 166.62, 166.55, 164.84, 153.64, 153.59, 131.09, 130.91, 120.11, 119.44, 99.05, 99.00, 98.28, 98.21, 76.74, 74.22, 74.12, 72.60, 71.70, 71.64, 70.03, 68.72, 68.66, 68.57, 68.51, 68.32, 68.26, 68.20, 68.14, 67.51, 67.47, 62.83, 62.62, 59.03, 58.43, 36.15, 36.02, 35.98, 32.29, 32.25, 32.22, 32.18, 32.15, 29.80, 24.77, 24.7, 21.12, 21.09, 20.90, 20.86, 18.73, 18.69, 13.69, 13.66. HRMS (ESI): Calcd for $C_{31}H_{47}NO_{18}P$ $[M+H]^+$ 752.2531, found 752.2528.

Synthesis of compound 9

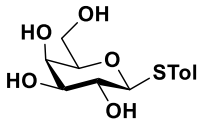

Compound **9** was synthesised by following synthetic reported methods.[33] ^{1}H NMR (400 MHz, Methanol-d_4) δ 7.46 (d, *J* = 8.2 Hz, 2H), 7.13 (d, *J* = 7.9 Hz, 2H), 4.52 (d, *J* = 9.6 Hz, 1H), 3.90 (dd, *J* = 3.3, 1.1 Hz, 1H), 3.77-3.72 (m, 2H), 3.61-3.53 (m, 2H), 3.50 (dd, *J* = 9.2, 3.3 Hz, 1H), 2.32 (s, 3H). ^{13}C NMR (101 MHz, Chloroform-*d*) δ 138.40, 132.88, 132.05, 130.52, 90.64, 80.55, 76.32, 70.99, 70.39, 62.57, 21.07. HRMS (ESI): Calcd for $C_{13}H_{18}NaO_5S$ $[M+Na]^+$ 309.0773, found 309.0773.

Synthesis of compound 10

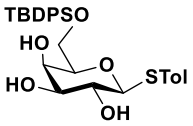

Compound **9** (1.10 gm, 3.84 mmol) in anhydrous DMF (10 mL) was added to ter-butyldiphenylchlorosilane (1.10 mL, 4.22 mmol) and imidazole (0.4 gm, 5.76 mmol). The reaction mixture was stirred at room temperature for 12 hours, quenched with methanol and concentrated *in vacuo*. The residue was purified by silica gel column chromatography using a mixture of (3:2, v/v) ethyl acetate and hexane as eluent to afford compound **10** (1.55 gm, 77%). ^{1}H NMR (400 MHz, Chloroform-*d*) δ = 7.73-7.67 (m, 4H), 7.46-7.35 (m, 8H), 7.05 (d, *J* = 7.7 Hz, 2H), 4.45 (d, *J* = 9.6 Hz, 1H), 4.10 (s, 1H), 3.96-3.93 (m, 2H), 3.66 (t, *J* = 9.3 Hz, 1H), 3.60-3.52 (m, 2H), 3.22 (bs, 1H), 3.06 (bs, 1H), 2.31 (s, 3H), 1.78 (bs, 1H), 1.06 (s, 9H). ^{13}C NMR (101 MHz, Chloroform-*d*) δ = 135.79, 135.71, 133.01, 130.02, 129.87, 127.96, 88.98, 78.27, 75.08, 70.01, 69.58, 63.88, 26.91, 21.28, 19.2. HRMS (ESI): Calcd for $C_{29}H_{36}NaO_5SSi$ $[M+Na]^+$ 547.1950, found 547.1958.

Synthesis of compound 11

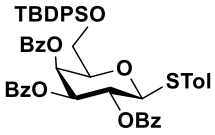

Compound **10** (1.3 gm, 2.48 mmol) in pyridine (10 mL) was mixed with benzoyl chloride (1.44 mL, 12.4 mmol) at 0 ºC. The reaction mixture was stirred at room temperature for 12 h, neutralized with methanol and concentrated *in vacuo*. The residue was purified by silica gel column chromatography using a mixture of (2:3, v/v) ethyl acetate and hexane as eluent to afford compound **11** (1.86 gm, 89%). ^{1}H NMR (400 MHz, Chloroform-*d*) δ = 7.95 (dd, *J* = 8.4, 1.1 Hz, 2H), 7.83 (dd, *J* = 8.1, 1.1 Hz, 2H), 7.75 (dd, *J* = 8.2, 1.2 Hz, 2H), 7.66 (dd, *J* = 7.9, 1.5 Hz, 2H), 7.60 (t, *J* = 7.4 Hz, 1H), 7.54-7.46 (m, 3H), 7.43-7.35 (m, 10H), 7.28 (d, *J* = 7.4 Hz, 1H), 7.22 (t, *J* = 7.8 Hz, 2H), 7.11 (t, *J* = 6.8 Hz, 4H), 6.04-6.00 (m, 1H), 5.66-5.54 (m, 2H), 4.89 (d, *J* = 9.2 Hz, 1H), 4.09 (t, *J* = 6.9 Hz, 1H), 3.86 (dd, *J* = 10.2, 6.0 Hz, 1H), 3.76 (dd, *J* = 10.2, 7.7 Hz, 1H), 2.37 (s, 3H), 0.99 (s, 9H). ^{13}C NMR (101 MHz, Chloroform-*d*) δ = 165.71, 165.34, 165.20, 135.76, 135.61, 134.60, 133.37, 130.10, 129.96, 129.80, 129.71, 129.55, 128.53, 128.35, 127.95, 127.75, 127.43, 86.07, 77.81, 73.51, 68.26, 68.15, 61.57, 26.80, 21.51, 19.15. Calcd for $C_{50}H_{49}O_8SSi$ $[M+H]^+$ 836.2939, found 836.2848.

Synthesis of compound 12

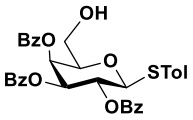

Compound **11** (2.5 gm, 2.99 mmol) in anhydrous THF (30 mL) was mixed with tertabutylammonioum fluoride (2.35 gm, 7.47 mmol) and acidify with acetic acid until the pH reached 6. The resulting mixture was stirred at room temperature for 36 hours at room temperature. The residue was purified by silica gel column chromatography using a mixture of (1:1, v/v) ethyl acetate and hexane as eluent to afford compound **12** (1.31 gm, 73%). ^{1}H NMR (400 MHz, Chloroform-*d*) δ = 7.98 (dd, *J* = 8.5, 1.3 Hz, 2H), 7.90 (dd, *J* = 8.3, 1.3 Hz, 2H), 7.77 (dd, *J* = 8.4, 1.2 Hz, 2H), 7.66-7.55 (m, 1H), 7.53 (t, *J* = 7.4 Hz, 1H), 7.43 (dd, *J* = 14.8, 7.8 Hz, 6H), 7.28-7.17 (m, 3H), 7.14 (d, *J* = 7.9 Hz, 2H), 5.81 (d, *J* = 3.1 Hz, 1H), 5.76 (t, *J* = 9.9 Hz, 1H), 5.56 (dd, *J* = 10.0, 3.2 Hz, 1H), 4.95 (d, *J* = 9.9 Hz, 1H), 4.07 (t, *J* = 6.9 Hz, 1H), 3.84 (dt, *J* = 12.0, 6.8 Hz, 1H), 3.61 (dt, *J* = 12.0, 7.0 Hz, 1H), 2.58 (t, *J* = 7.1 Hz, 1H), 2.37 (s, 3H). ^{13}C NMR (101 MHz, Chloroform-*d*) δ = 166.69, 165.63, 165.32, 138.92, 134.62, 133.90, 133.49, 133.46, 130.24, 129.95, 129.89, 129.82, 129.47, 128.85, 128.76, 128.69, 128.59, 128.45, 127.17, 85.98, 77.96, 73.28, 69.13, 68.17, 60.89, 21.49. HRMS (ESI): Calcd for $C_{34}H_{31}O_8S$ $[M+H]^+$ 599.1740, found 599.1736.

Synthesis of compound 13

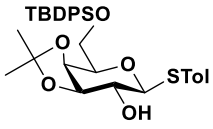

Compound **10** (1.90 gm, 3.62 mmol) in anhydrous acetone (20 mL) was mixed with 2,2-methoxypropane (0.66 mL, 5.43 mmol) and (1S)-(+)-10-camphorsulfonic acid (40 mg, 0.18 mmol) and stirred at room temperature for 4 hours. The reaction mixture was neutralized with triethylamine and concentrated *in vacuo*. The residue was purified by silica gel column chromatography using a mixture of (2:3, v/v) ethyl acetate and hexane as eluent to afford **13** (1.76 gm, 86%).^{1}H NMR (400 MHz, Chloroform-*d*) δ = 7.77-7.70 (m, 4H), 7.48-7.36 (m, 8H), 7.12-7.04 (m, 2H), 4.41 (d, *J* = 10.2 Hz, 1H), 4.30 (dd, *J* = 5.4, 2.1 Hz, 1H), 4.10 (dd, *J* = 6.9, 5.4 Hz, 1H), 3.98 (m, 2H), 3.90 (ddd, *J* = 6.8, 6.0, 2.1 Hz, 1H), 3.56 (ddd, *J* = 10.2, 7.0, 2.3 Hz, 1H), 2.59 (d, *J* = 2.4 Hz, 1H), 2.33 (s, 3H), 1.43 (s, 3H), 1.35 (s, 3H), 1.08 (s, 9H). ^{13}C NMR (101 MHz, Chloroform-*d*) δ = 138.26, 135.75, 135.73, 133.44, 133.02, 129.86, 129.82, 129.80, 128.56, 127.82, 127.75, 110.15, 88.67, 79.11, 77.26, 73.43, 71.68, 63.02, 28.23, 26.88, 26.43, 21.25, 19.33. HRMS (ESI): Calcd for $C_{32}H_{40}NaO_5SSi$ $[M+Na]^+$ 587.2263, found 587.2261.

Synthesis of compound 14

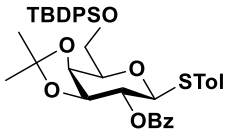

Compound **13** (1.5 gm, 2.36 mmol) in pyridine (10 mL) was mixed with benzoyl chloride (0.9 mL, 7.9 mmol) at 0 ºC and stirred at room temperature for 12 h. The reaction mixture was quenched with methanol and concentrated *in vacuo*. The residue was purified by silica gel column chromatography using a mixture of (2:3, v/v) ethyl acetate and hexane as eluent to afford compound **14** (1.58 gm, 89%). ^{1}H NMR (400 MHz, Chloroform-*d*) δ = 8.09 (dd, *J* = 8.3, 1.2 Hz, 2H), 7.73 (dd, *J* = 7.9, 1.5 Hz, 4H), 7.58 (t, *J* = 7.5 Hz, 1H), 7.48-7.33 (m, 10H), 7.03 (d, *J* = 8.0 Hz, 2H), 5.33-5.23 (m, 1H), 4.73 (d, *J* = 10.1 Hz, 1H), 4.38-4.32 (m, 2H), 4.06-3.94 (m, 3H), 2.30 (s, 3H), 1.57 (s, 3H), 1.35 (s, 3H), 1.09 (s, 9H). ^{13}C NMR (101 MHz, Chloroform-*d*) δ = 165.53, 137.88, 135.78, 133.41, 133.25, 132.57, 130.04, 129.87, 129.75, 128.45, 127.86, 127.80, 110.62, 86.71, 73.62, 72.38, 63.05, 27.87, 26.91, 26.49, 21.26, 19.36. HRMS (ESI): Calcd for Calcd for $C_{39}H_{44}NaO_6SSi$ $[M+Na]^+$ 691.2526, found 691.2526.

Synthesis of compound 15

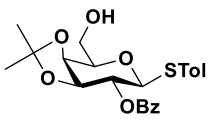

Compound **14** (2.1 gm, 3.14 mmol) in anhydrous THF (20 mL) was mixed with tertabutylammonioum fluoride (2.4 gm, 7.85 mmol) and acidify with acetic acid until the pH reached 6. The reaction mixture was stirred at room temperature for 36 hours, concentrated *in vacuo* and purified by silica gel column

chromatography using a mixture of (1:1, v/v) ethyl acetate and hexane as eluent to afford compound **15** (1.01 gm, 74%). ^{1}H NMR (400 MHz, Chloroform-*d*) δ = 8.07 (dd, *J* = 8.3, 1.2 Hz, 2H), 7.58 (t, *J* = 7.4 Hz, 1H), 7.45 (t, *J* = 7.7 Hz, 2H), 7.34 (d, *J* = 8.1 Hz, 2H), 7.08 (d, *J* = 8.0 Hz, 2H), 5.28 (dd, *J* = 9.9, 7.1 Hz, 1H), 4.74 (d, *J* = 9.9 Hz, 1H), 4.37 (dd, *J* = 7.0, 5.5 Hz, 1H), 4.26 (dd, *J* = 5.4, 2.1 Hz, 1H), 4.03 (ddd, *J* = 10.8, 7.5, 1.9 Hz, 1H), 3.97-3.87 (m, 1H), 3.84 (td, *J* = 12.4, 10.7, 3.9 Hz, 1H), 2.31 (s, 3H), 2.23 (dd, *J* = 9.0, 2.8 Hz, 1H), 1.57 (s, 3H), 1.34 (s, 3H). ^{13}C NMR (101 MHz, Chloroform-*d*) δ = 165.48 , 138.21, 133.35, 132.69, 130.04, 129.86, 129.48, 128.49, 111.04, 86.27, 77.05, 74.03, 72.27, 62.67, 27.75, 26.50, 21.25. HRMS (ESI): Calcd for $C_{23}H_{27}O_6S$ $[M+H]^+$ 431.1528, found 431.1532.

Synthesis of compound 16

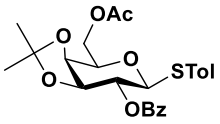

Compound **15** (1.32 gm, 3.07 mmol) in pyridine (10 mL) was mixed with acetic anhydride dropwise (0.86 mL, 9.21 mmol) at 0 ºC and stirred at room temperature for 12 h. Then the reaction mixture was quenched with methanol and concentrated *in vacuo.* The residue was purified by silica gel column chromatography using a mixture of (2:3, v/v) ethyl acetate and hexane as eluent to afford compound **16** (1.28 gm, 88%). ^{1}H NMR (400 MHz, Chloroform-*d*) δ = 8.07 (dd, *J* = 8.4, 1.3 Hz, 2H), 7.58 (t, *J* = 7.4 Hz, 1H), 7.45 (t, *J* = 7.8 Hz, 2H), 7.38 (d, *J* = 8.2 Hz, 2H), 7.07 (d, *J* = 8.4 Hz, 2H), 5.27 (dd, *J* = 9.9, 7.0 Hz, 1H), 4.70 (d, *J* = 9.9 Hz, 1H), 4.40 (d, *J* = 6.2 Hz, 2H), 4.36 (dd, *J* = 7.0, 5.5 Hz, 1H), 4.25 (dd, *J* = 5.4, 2.2 Hz, 1H), 4.04 (td, *J* = 6.0, 2.2 Hz, 1H), 2.31 (s, 3H), 2.10 (s, 3H), 1.57 (s, 3H), 1.34 (s, 3H). ^{13}C NMR (101 MHz, Chloroform-*d*) δ = 170.91, 165.46, 138.13, 133.34, 132.83, 130.03, 129.85, 129.75, 129.66, 128.48, 111.08, 86.29, 77.31, 74.38, 73.70, 72.12, 63.80, 27.70, 26.44, 21.24, 20.98. HRMS (ESI): Calcd for $C_{25}H_{29}O_7S$ $[M+H]^+$ 473.1634, found 473.1632.

Synthesis of compound 17

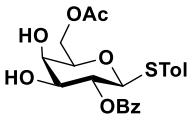

Compound **16** (1.8 gm, 3.81 mmol) was dissolved in an 8:2 (v/v) mixture of AcOH/H_2O (30 mL) and stirred at 60 ºC for 6 h. The reaction mixture was concentrated *in vacuo.* The residue was purified by silica gel column chromatography using a mixture of (1:1, v/v) ethyl acetate and hexane as eluent to afford compound **17** (1.35 gm, 82%). ^{1}H NMR (400 MHz, Chloroform-*d*) δ = 8.08 (dd, *J* = 8.4, 1.4 Hz, 2H), 7.60 (t, *J* = 7.4 Hz, 1H), 7.47 (t, *J* = 7.7 Hz, 2H), 7.37 (d, *J* = 8.2 Hz, 2H), 7.08 (d, *J* = 7.8 Hz, 2H), 5.13 (dd, *J* = 10.0, 9.2 Hz, 1H), 4.73 (d, *J* = 10.0 Hz, 1H), 4.45-4.31 (m, 2H), 3.98 (t, *J* = 3.5 Hz, 1H), 3.82 (ddd, *J* = 9.2, 6.7, 3.4 Hz, 1H), 3.77 (t, *J* = 6.4 Hz, 1H), 3.46 (d,

J = 6.8 Hz, 1H), 2.90 (d, *J* = 4.6 Hz, 1H), 2.32 (s, 3H), 2.10 (s, 3H).^{13}C NMR (101 MHz, Chloroform-*d*) δ = 171.23, 167.24, 138.52, 133.69, 133.42, 130.21, 129.79, 129.51, 128.62, 86.30, 76.10, 73.87, 72.36, 68.97, 63.10, 21.30, 21.00. HRMS (ESI): Calcd for $C_{22}H_{25}O_7S$ $[M+H]^+$ 433.1321, found 433.1322.

Synthesis of compound 18

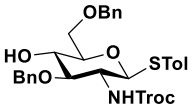

Compound **18** was synthesised by following synthetic reported methods. [34] ^{1}H NMR (400 MHz, Chloroform-*d*) δ = 7.41-7.28 (m, 12H), 7.05 (d, *J* = 7.9 Hz, 2H), 5.12 (d, *J* = 8.3 Hz, 1H), 4.91 (d, *J* = 10.3 Hz, 1H), 4.80-4.72 (m, 4H), 4.61-4.53 (m, 2H), 3.81-3.74 (m, 3H), 3.67 (t, *J* = 9.2 Hz, 1H), 3.51 (dt, *J* = 9.5, 4.7 Hz, 1H), 3.35 (q, *J* = 9.6 Hz, 1H), 2.77 (s, 1H), 2.31 (s, 3H). ^{13}C NMR (101 MHz, Chloroform-*d*) δ = 153.95, 138.38, 138.11, 137.83, 133.34, 129.86, 128.73, 128.61, 128.32, 128.17, 127.99, 127.90, 86.21, 81.91, 77.97, 74.91, 74.58, 73.89, 73.10, 70.70, 56.18, 21.28. HRMS (ESI): Calcd for $C_{30}H_{32}Cl_3NNaO_6S$ $[M+Na]^+$ 662.0914, found 662.0908.

Synthesis of compound 19

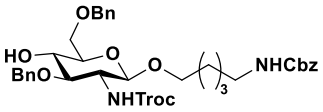

Donor **18** (1.3 gm, 2.03 mmol) and 5-(Z-Amino)-1-pentanol (0.53 gm, 2.23 mmol) were dissolved in anhydrous dichloromethane (20 mL) and activated by 4 Å molecular sieves. The resulting mixture was stirred at room temperature for 2 h. Next, the reaction mixture was cooled to -20 ºC, and NIS (0.59 gm, 2.63 mmol) and TfOH (36 µL, 0.40 mmol) were added and stirred 2 h more. The reaction mixture was neutralized with DIPEA and filtered through celite pad, and the filtrate was concentrated *in vacuo*. The residue was purified by silica gel column chromatography using a mixture of (1:1, v/v) ethyl acetate and hexane as eluent to afford compound **19** (1.24 gm, 81%). ^{1}H NMR (400 MHz, Chloroform-*d*) δ = 7.27-7.41 (m, 15H), 5.40 (bs, 1H), 5.09 (s, 2H), 4.78 (bs, 2H), 4.71 (s, 2H), 4.62-4.54 (m, 3H), 3.87-3.82 (m, 1H), 3.74 (d, *J* = 4.9 Hz, 3H), 3.67 (m, 1H), 3.50-3.41 (m, 2H), 3.36-3.30 (m, 1H), 3.16 (q, *J* = 6.7 Hz, 2H), 2.84 (s, 1H), 1.71 (s, 1H), 1.61.1.53 (m, 2H), 1.49-1.45 (m, 2H), 1.39-1.32 (m, 2H). ^{13}C NMR (101 MHz, Chloroform-*d*) δ = 156.59, 154.20, 138.38, 137.79, 136.75, 128.67, 128.61, 128.22, 128.04, 128.00, 127.90, 100.51, 95.73, 80.61, 74.49, 73.85, 73.75, 73.34, 70.70, 69.63, 66.73, 57.60, 41.04, 29.54, 28.96, 23.19. HRMS (ESI): Calcd for $C_{36}H_{44}Cl_3N_2O_9$ $[M+H]^+$ 753.2112, found 753.2104.

3.4. 3 General Procedure for glycosylation with sialyl phosphate donor:

Sialyl phosphate donor (1.73 mmol) and galactose acceptor (1.73 mmol) were dissolved in anhydrous dichloromethane (20 mL) and activated by 4 Å molecular sieves. The resulting mixture was stirred under an N_2 atmosphere at room temperature for 2 h. Next, the reaction mixture was cooled to -50 ºC, followed by the addition of TMSOTf (2.07 mmol). The reaction mixture was stirred at the same temperature for 2 h, then neutralized with DIPEA, filtered and washed with brine. The organic layer was dried over sodium sulphate, concentrated in vacuo, and the residue was purified by silica gel column chromatography using a mixture of (3:2, v/v) ethyl acetate and hexane as eluent.

3.4.4 General Procedure for glycosylation with disaccharide:

Disaccharide donor (0.49 mmol) and glucose acceptor (0.58 mmol) were dissolved in anhydrous dichloromethane (10 mL), and activated by 4 Å molecular sieves. The resulting mixture was stirred at room temperature for 2 h then cooled to -40 ºC, followed by the addition of NIS (0.58 mmol) and TfOH (0.1 mmol). After being stirred at -20 ºC for 2 h, the reaction mixture was neutralized with DIPEA, filtered through celite pad and the filtrate was concentrated *in vacuo*. The residue was purified by silica gel column chromatography using (7:3, v/v) ethyl acetate and hexane as eluent.

3.4.5 General Procedure for Troc deprotection:

Troc protected trisaccharide (0.23 mmol) was dissolved in a 3:2:1 (v/v) mixture of THF/AcOH/Ac_2O (6 mL) and Zn (4.6 mmol). To this solution, a saturated aqueous solution of $CuSO_4$ (50 µL) was added, and the reaction mixture was stirred at room temperature for 4 h. Next, the reaction mixture was diluted with dichloromethane and filtered through celite pad, and the filtrate was concentrated *in vacuo*. The residue was purified by silica gel column chromatography by using (9:1, v/v) dichloromethane and methanol and as eluent.

3.4.6 General Procedure for oxazolidinone ring deprotection:

Trisaccharide (0.13 mmol) in anhydrous CH_2Cl_2 (5 mL) was mixed with 1,2-ethanedithiol (0.65 mmol) and DBU (0.065 mmol) at 0 ºC and stirred at room temperature for 3 h and concentrated. The residue was purified by silica gel column chromatography using (4:2, v/v) dichloromethane and methanol and as eluent.

3.4.7 General Procedure for global deprotection:

Trisaccharide (43 µmole) in a 2:2:1 (v/v) in a mixture of THF/ H_2O/MeOH (1.5 mL) was mixed with to LiOH (430 µmmol), and stirred at room temperature for 12 h. then the reaction mixture

was neutralized with Amberlite IR120 acidic resin, filtered and concentrated. The crude compound was desalted by using the Bond elute C18 column using water and methanol as eluent. Next, the desalted compound was dissolved in a 3:1 (v/v) mixture of H_2O/MeOH (1.6 mL), and $Pd(OH)_2/C$ (250 mg) was added. The resulting mixture was stirred under a hydrogen atmosphere at room temperature for 48 hours, filtered and concentrated. The residue was purified by the Bond elute C18 column using water as eluent. The combined solvent fraction was pooled and lyophilized to yield a fully deprotected trisaccharide.

Synthesis of compound 20

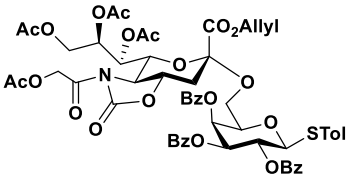

Compound **20** was synthesised from donor **8** and acceptor **12** using the general glycosylation procedure **1** (72%). ^{1}H NMR (400 MHz, Chloroform-*d*) δ = 7.97 (d, *J* = 7.2 Hz, 2H), 7.88 (d, *J* = 7.0 Hz, 2H), 7.73 (d, *J* = 7.1 Hz, 2H), 7.60 (t, *J* = 7.4 Hz, 1H), 7.51 (dd, *J* = 13.7, 7.7 Hz, 3H), 7.45-7.35 (m, 5H), 7.22 (t, *J* = 7.8 Hz, 2H), 7.16 (d, *J* = 8.0 Hz, 2H), 6.02 (d, *J* = 2.7 Hz, 1H), 5.83-5.72 (m, 1H), 5.72-5.67 (m, 2H), 5.66-5.61 (m, 1H), 5.53-5.46 (m, 1H), 5.32-5.19 (m, 2H), 5.15 (d, *J* = 9.4 Hz, 1H), 5.12-5.02 (m, 2H), 4.70 (dd, *J* = 9.6, 1.5 Hz, 1H), 4.57 (dd, *J* = 12.7, 6.3 Hz, 1H), 4.45 (td, *J* = 12.4, 4.4 Hz, 2H), 4.37 (t, *J* = 7.1 Hz, 1H), 4.14-3.99 (m, 2H), 3.92 (dd, *J* = 10.9, 6.1 Hz, 1H), 3.73 (d, *J* = 9.7 Hz, 1H), 3.70-3.62 (m, 1H), 2.76 (dd, *J* = 12.2, 3.6 Hz, 1H), 2.39 (s, 3H), 2.18 (s, 3H), 2.17 (s, 3H), 2.13 (s, 3H), 2.07-2.03 (m, 1H), 1.97 (s, 3H). ^{13}C NMR (101 MHz, Chloroform-*d*) δ = 171.07, 170.66, 170.49, 170.19, 168.22, 167.41, 165.54, 165.28, 153.52, 138.37, 134.12, 133.40, 133.31, 133.22, 130.62, 130.05, 129.96, 129.86, 129.66, 129.12, 128.56, 128.49, 128.35, 127.79, 120.82, 99.79, 85.34, 76.21, 75.46, 75.10, 73.29, 71.44, 68.61, 68.19, 67.11, 63.68, 59.44, 36.57, 21.50, 21.24, 21.04, 20.83, 20.62. HRMS (ESI): Calcd for $C_{57}H_{58}NO_{22}S$ $[M+H]^+$ 1140.3171, found 1140.3164.

Synthesis of compound 21

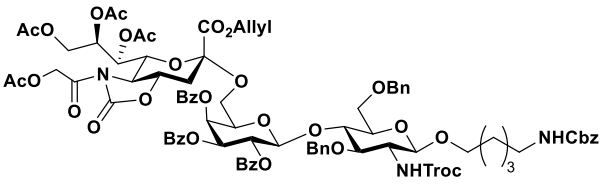

Compound **21** was synthesised from donor **20** and acceptor **19** using the general glycosylation procedure **2** (71%). ^{1}H NMR (400 MHz, Chloroform-*d*) δ = 7.94 (d, *J* = 7.2 Hz, 2H), 7.89 (dd, *J* = 8.3, 1.1 Hz, 2H), 7.76 (dd, *J* = 8.4, 1.1 Hz, 2H), 7.55 (t, *J* = 7.4 Hz, 1H), 7.49 (t, *J* = 7.4 Hz, 1H), 7.41 (dd, *J* = 8.3, 1.7 Hz, 4H), 7.38-7.28 (m, 14H), 7.26 (d, *J* = 6.7 Hz, 2H), 7.23 (d, *J* = 7.7 Hz, 2H), 5.92 (d, *J* = 3.3 Hz, 1H), 5.74-5.63 (m, 3H), 5.52 (dd, *J* = 10.5,

3.5 Hz, 1H), 5.46 (dq, *J* = 9.2, 3.0 Hz, 2H), 5.24-5.12 (m, 2H), 5.12-4.98 (m, 6H), 4.82 (d, *J* = 11.4 Hz, 2H), 4.68 (s, 2H), 4.63 (dd, *J* = 9.6, 1.4 Hz, 1H), 4.59 (d, *J* = 12.2 Hz, 1H), 4.53 (dd, *J* = 12.7, 6.4 Hz, 1H), 4.46 (s, 1H), 4.41-4.33 (m, 2H), 4.23 (dd, *J* = 12.7, 5.9 Hz, 1H), 4.15-3.95 (m, 4H), 3.88 (td, *J* = 10.7, 5.7 Hz, 2H), 3.76 (dt, *J* = 9.5, 6.1 Hz, 1H), 3.68-3.53 (m, 4H), 3.45 (q, *J* = 8.5 Hz, 1H), 3.37 (s, 1H), 3.33-3.25 (m, 1H), 3.14 (q, *J* = 6.6 Hz, 2H), 2.75-2.71 (m, 1H), 2.17 (s, 3H), 2.16-2.12 (m, 1H), 2.08 (s, 3H), 2.07 (s, 3H), 2.00 (s, 3H), 1.48 (m, 4H), 1.32 (q, *J* = 7.1, 6.6 Hz, 2H). ^{13}C NMR (101 MHz, Chloroform-*d*) δ = 171.00, 170.60, 170.22, 170.15, 168.29, 167.15, 165.55, 165.35, 165.32, 156.53, 154.20, 153.54, 138.84, 138.34, 136.85, 133.47, 133.30, 130.64, 129.91, 129.86, 129.64, 129.33, 129.10, 128.71, 128.64, 128.61, 128.44, 128.39, 128.19, 128.13, 128.03, 127.95, 127.65, 120.71, 100.08, 99.63, 76.23, 75.09, 74.80, 74.55, 73.84, 73.50, 72.04, 71.85, 71.59, 70.66, 69.48, 68.70, 68.62, 68.17, 67.08, 66.71, 63.72, 63.48, 63.31, 59.48, 57.14, 41.08, 36.35, 29.60, 29.03, 23.24, 21.19, 20.93, 20.86, 20.57. HRMS (ESI): Calcd for $C_{86}H_{94}Cl_3N_3O_{31}$ $[M+H]^+$ 1768.4859, found 1768.4856

Synthesis of compound 22

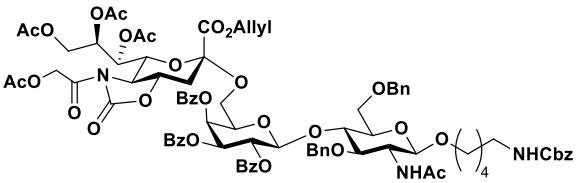

Compound **22** was synthesised from **21** using the general Troc deprotection procedure **3** (65%). ^{1}H NMR (400 MHz, Chloroform-*d*) δ = 7.97 (d, *J* = 7.0 Hz, 2H), 7.90 (d, *J* = 7.0 Hz, 2H), 7.75 (d, *J* = 7.0 Hz, 2H), 7.57 (t, *J* = 7.5 Hz, 1H), 7.50 (t, *J* = 7.6 Hz, 1H), 7.44-7.30 (m, 14H), 7.33-7.26 (m, 5H), 7.29-7.18 (m, 3H), 6.06 (d, *J* = 8.4 Hz, 1H), 5.94 (dd, *J* = 3.3, 1.1 Hz, 1H), 5.77-5.62 (m, 3H), 5.60 (dd, *J* = 10.4, 3.4 Hz, 1H), 5.45 (ddd, *J* = 8.5, 6.7, 3.0 Hz, 1H), 5.26-5.14 (m, 2H), 5.08-5.03 (m, 4H), 5.00 (d, *J* = 7.8 Hz, 1H), 4.91 (d, *J* = 11.6 Hz, 2H), 4.77 (d, *J* = 11.7 Hz, 1H), 4.64 (dd, *J* = 9.6, 1.6 Hz, 1H), 4.60-4.49 (m, 3H), 4.44-4.33 (m, 2H), 4.29 (dd, *J* = 12.7, 6.0 Hz, 1H), 4.15-3.92 (m, 5H), 3.90 (dd, *J* = 10.8, 5.9 Hz, 1H), 3.72-3.57 (m, 6H), 3.51 (dt, *J* = 8.1, 4.5 Hz, 1H), 3.19 (dt, *J* = 9.7, 6.5 Hz, 1H), 3.12 (q, *J* = 6.5 Hz, 2H), 2.73 (dd, *J* = 12.3, 3.6 Hz, 1H), 2.17 (s, 3H), 2.07 (s, 3H), 2.06 (s, 3H), 1.98 (s, 3H), 1.92 (s, 3H), 1.45 (m, 4H), 1.28 (m, 2H). ^{13}C NMR (101 MHz, Chloroform-*d*) δ = 171.02, 170.62, 170.37, 170.25, 170.11, 168.22, 167.15, 165.66, 165.50, 165.34, 156.54, 153.55, 138.98, 138.31, 136.82, 133.54, 133.50, 133.32, 130.60, 129.90, 129.84, 129.60, 129.26, 129.03, 128.71, 128.62 , 128.41, 128.38, 128.20, 128.16, 127.98, 127.96, 127.62, 120.75, 100.31, 99.84, 99.66, 78.04, 76.21, 75.83 , 75.02 74.72, 73.44, 73.33, 72.05, 71.57, 71.50, 70.60, 69.14, 68.57, 68.16, 67.09, 66.64, 63.71, 63.59, 63.34, 59.45, 54.27, 41.06, 36.38, 29.83, 29.60, 28.96, 23.49, 23.32,

21.18, 20.92, 20.85, 20.59. HRMS (ESI): Calcd for HRMS (ESI): Calcd for $C_{85}H_{93}N_3NaO_{30}$ $[M+Na]^+$ 1658.5742, found 1658.5736.

Synthesis of compound 23

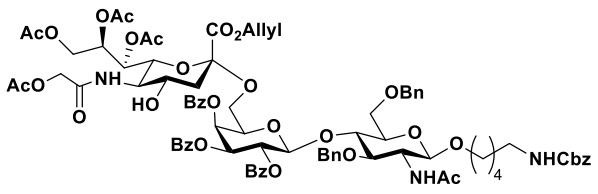

Compound **23** was synthesised from **22** using the general oxazolidinone ring deprotection procedure **4** (74%). ^{1}H NMR (400 MHz, Chloroform-*d*) δ = 7.95 (d, *J* = 7.0 Hz, 2H), 7.90 (d, *J* = 7.0 Hz, 2H), 7.76 (d, *J* = 7.0 Hz, 2H), 7.56-7.47 (m, 2H), 7.42-7.30 (m, 19H), 7.27-7.20 (m, 3H), 6.44 (d, *J* = 7.7 Hz, 1H), 6.03 (d, *J* = 8.5 Hz, 1H), 5.91 (dd, *J* = 3.4, 1.1 Hz, 1H), 5.77-5.61 (m, 2H), 5.54 (dd, *J* = 10.4, 3.4 Hz, 1H), 5.40 (ddd, *J* = 8.9, 4.9, 2.6 Hz, 1H), 5.24-5.10 (m, 3H), 5.07 (s, 2H), 5.01-4.87 (m, 3H), 4.81 (d, *J* = 11.9 Hz, 1H), 4.61-4.46 (m, 4H), 4.45-4.35 (m, 2H), 4.33-4.25 (m, 2H), 4.19-4.07 (m, 3H), 4.06-3.87 (m, 4H), 3.74 (q, *J* = 7.6 Hz, 1H), 3.68-3.62 (m, 3H), 3.57 (dd, *J* = 10.5, 7.7 Hz, 1H), 3.49 (dt, *J* = 6.8, 4.5 Hz, 1H), 3.32 (td, *J* = 10.3, 7.7 Hz, 1H), 3.22-3.06 (m, 4H), 2.62 (dd, *J* = 13.1, 4.4 Hz, 1H), 2.18 (s, 3H), 2.08 (s, 3H), 2.05 (s, 3H), 2.00 (s, 3H), 1.91 (s, 3H), 1.79 (t, *J* = 12.5 Hz, 1H), 1.44 (h, *J* = 7.1, 6.3 Hz, 4H), 1.27 (m, 2H). ^{13}C NMR (101 MHz, Chloroform-*d*) δ = 171.04, 170.71, 170.31, 169.83, 169.80, 168.39, 167.09, 165.56, 165.39, 165.13, 156.46, 138.74, 138.19, 136.72, 133.44, 133.29, 133.17, 130.95, 129.80, 129.73, 129.53, 129.15, 128.98, 128.55, 128.51, 128.36, 128.25, 128.08, 127.91, 127.88, 127.54, 119.72, 100.34, 99.70, 99.46, 75.52, 74.65, 73.38, 73.04, 72.07, 71.61, 71.56, 70.49, 69.00, 68.13, 67.98, 67.86, 66.56, 63.08, 62.58, 62.26, 54.17, 53.96, 40.95, 40.47, 29.46, 28.82, 23.37, 23.20, 20.99, 20.72. HRMS (ESI): Calcd for $C_{84}H_{96}N_3O_{29}$ $[M+H]^+$ 1610.6129, found 1610.6113.

Synthesis of compound 24

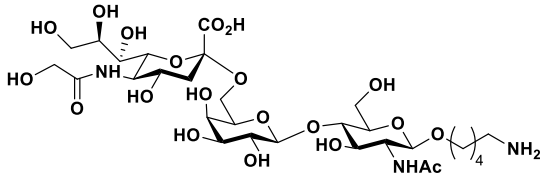

Compound **24** was synthesised from **23** using the general global deprotection procedure **5** (63%).^{1}H NMR (400 MHz, Deuterium Oxide) δ = 4.56 (d, *J* = 8.2 Hz, 1H), 4.46 (d, *J* = 7.9 Hz, 1H), 4.12 (s, 2H), 4.01 (t, *J* = 10.0 Hz, 2H), 3.95-3.91 (m, 2H), 3.90-3.85 (m, 3H), 3.84-3.80 (m, 3H), 3.79-3.71 (m, 3H), 3.70-3.58 (m, 5H), 3.57-3.52 (m, 3H), 3.05-2.95 (m, 2H), 2.69 (dd, *J* = 12.3, 4.6 Hz, 1H), 2.07 (s, 3H), 1.77-1.58 (m, 5H), 1.45-1.38 (m, 2H). ^{13}C NMR (151 MHz, Deuterium Oxide) δ = 175.63, 174.41, 172.72, 103.43, 100.88, 99.65, 80.73, 74.41, 73.60, 72.40, 72.36, 72.32, 71.41, 70.64, 70.00, 68.30, 67.65, 63.34, 62.68, 60.93, 60.29, 54.81, 51.45, 39.74, 39.28,

28.01, 26.31, 22.23, 22.08. HRMS (ESI): Calcd for $C_{30}H_{54}N_3O_{20}$ $[M+H]^+$ 776.3301, found 776.3306.

Synthesis of compound 25

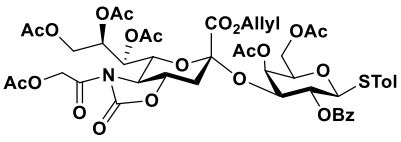

Compound **25** was synthesised from donor **8** and acceptor **17** using the general glycosylation procedure **1**. Next, the compound was dissolved in pyridine (10 mL), and acetic anhydride was added (0.5 mL) at 0 ºC. The resulting mixture was stirred at RT for 12 hours, concentrated *in vacuo* and purified using mixture of (3:2, v/v) ethyl acetate and hexane as eluent to afford compound **25** (49% over two steps). ^{1}H NMR (400 MHz, Chloroform-*d*) δ = 8.24-8.15 (m, 2H), 7.59 (t, *J* = 7.4 Hz, 1H), 7.48 (t, *J* = 7.6 Hz, 2H), 7.35 (d, *J* = 8.1 Hz, 2H), 7.06 (d, *J* = 7.8 Hz, 2H), 5.96 (ddt, *J* = 17.0, 10.3, 6.4 Hz, 1H), 5.61 (ddd, *J* = 9.5, 7.2, 2.4 Hz, 1H), 5.50 (dd, *J* = 9.4, 2.1 Hz, 1H), 5.40 (dq, *J* = 17.2, 1.4 Hz, 1H), 5.35 (dq, *J* = 10.3, 1.1 Hz, 1H), 5.28 (t, *J* = 9.8 Hz, 1H), 5.06-4.88 (m, 4H), 4.81 (dd, *J* = 12.6, 6.5 Hz, 1H), 4.76 (dd, *J* = 9.7, 3.2 Hz, 1H), 4.58 (ddt, *J* = 12.6, 6.1, 1.3 Hz, 1H), 4.35 (dd, *J* = 12.3, 2.5 Hz, 1H), 4.26 (dd, *J* = 9.6, 2.2 Hz, 1H), 4.08 (d, *J* = 6.3 Hz, 2H), 4.02-3.96 (m, 2H), 3.94-3.87 (m, 1H), 3.43 (dd, *J* = 11.4, 9.6 Hz, 1H), 2.91 (dd, *J* = 11.8, 3.5 Hz, 1H), 2.31 (s, 3H), 2.16 (s, 3H), 2.13 (s, 3H), 2.09 (s, 3H), 2.06 (s, 3H), 1.98 (s, 3H), 1.86 (dd, *J* = 13.3, 11.9 Hz, 1H), 1.24 (s, 3H). ^{13}C NMR (101 MHz, Chloroform-*d*) δ = 170.91, 170.82, 170.67, 170.46, 170.28, 169.84, 167.70, 166.85, 165.61, 153.30, 138.29, 133.57, 133.50, 130.75, 130.56, 130.31, 129.56, 128.72, 128.67, 121.08, 97.29, 86.83, 76.98, 73.80, 72.66, 71.38, 69.44, 68.16, 68.05, 67.90, 63.59, 63.50, 62.45, 59.24, 36.18, 21.65, 21.28, 20.87, 20.84, 20.80, 20.57, 20.00. HRMS (ESI): Calcd for $C_{47}H_{54}NO_{22}S$ $[M+H]^+$ 1016.2858, found: 1016.2855.

Synthesis of compound 26

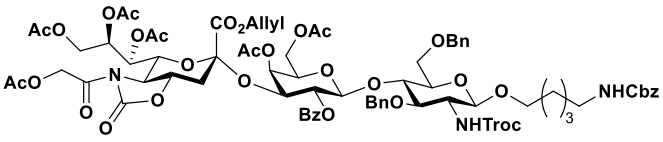

Compound **26** was synthesised from donor **25** and acceptor **19** using the general glycosylation procedure **2** (69%). ^{1}H NMR (400 MHz, Chloroform-*d*) δ = 8.24 (d, *J* = 7.2 Hz, 2H), 7.56 (t, *J* = 7.4 Hz, 1H), 7.46 (t, *J* = 7.6 Hz, 2H), 7.37-7.2 (m, 15H), 5.96 (ddt, *J* = 16.9, 10.2, 6.3 Hz, 1H), 5.69 (ddd, *J* = 10.2, 7.4, 2.5 Hz, 1H), 5.53 (dd, *J* = 9.5, 2.2 Hz, 1H), 5.45-5.29 (m, 4H), 5.11-4.93 (m, 6H), 4.91 (d, *J* = 10.2 Hz, 1H), 4.81 (dd, *J* = 12.4, 6.6 Hz, 2H), 4.72-4.68 (m, 2H), 4.68-4.53 (m, 3H), 4.45-4.35 (m, 4H), 4.26 (dd, *J* = 9.6, 2.2 Hz, 1H), 4.10-3.90 (m, 4H), 3.88-3.74 (m, 3H), 3.71-3.63 (m, 2H), 3.59-3.51 (m, 1H), 3.47-3.35 (m, 3H), 3.21 (s, 1H), 3.12 (q, *J* =

6.8 Hz, 2H), 2.89 (dd, *J* = 11.9, 3.4 Hz, 1H), 2.17 (s, 3H), 2.14 (s, 3H), 2.05 (s, 3H), 1.96 (s, 3H), 1.91 (s, 3H), 1.87 (d, *J* = 11.6 Hz, 1H), 1.53-1.36 (m, 4H), 1.32-1.27 (m, 5H). ^{13}C NMR (101 MHz, Chloroform-*d*) δ = 170.85 , 170.66, 170.55, 170.19, 170.06, 169.69, 167.63, 166.59, 165.48, 153.17, 138.45, 136.65 , 133.54 , 130.61 , 130.38 , 129.86 , 128.67 , 128.51 , 128.21 (d, *J* = 1.4 Hz), 128.06 , 127.75 , 127.49 , 127.38, 127.24, 120.96, 99.86, 97.38, 76.85, 74.69, 73.61, 72.91, 71.85, 71.55, 71.33, 70.77, 69.30, 67.79, 67.68, 66.56, 63.51, 63.38, 61.80, 59.13, 40.91, 38.74, 36.64, 35.94, 31.93, 29.70, 29.44, 29.36, 24.69, 21.48, 20.67, 20.65, 20.58, 20.43, 20.04. HRMS (ESI): Calcd for $C_{76}H_{89}Cl_3N_3O_{31}$ $[M+H]^+$ 1644.4546, found: 1644.4545.

Synthesis of compound 27

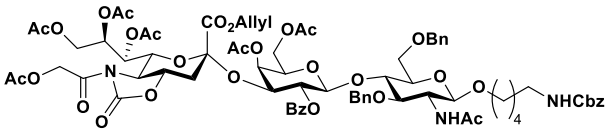

Compound **27** was synthesised from **26** using the general Troc deprotection procedure **3** (70%). ^{1}H NMR (400 MHz, Chloroform-*d*) δ = 8.22 (d, *J* = 1.2 Hz, 2H), 7.57 (t, *J* = 7.4 Hz, 1H), 7.46 (t, *J* = 7.6 Hz, 2H), 7.36-7.20 (m, 15H), 6.01-5.87 (m, 2H), 5.69 (ddd, *J* = 9.9, 7.5, 2.5 Hz, 1H), 5.53 (dd, *J* = 9.5, 2.2 Hz, 1H), 5.40 (dq, *J* = 17.2, 1.4 Hz, 1H), 5.35 (dd, *J* = 10.2, 1.2 Hz, 2H), 5.13-4.90 (m, 7H), 4.81 (ddt, *J* = 12.6, 6.6, 1.1 Hz, 1H), 4.77-4.71 (m, 2H), 4.65 (d, *J* = 11.8 Hz, 1H), 4.59 (ddt, *J* = 12.6, 6.0, 1.2 Hz, 1H), 4.48-4.37 (m, 3H), 4.34 (d, *J* = 6.2 Hz, 1H), 4.27 (dd, *J* = 9.6, 2.2 Hz, 1H), 4.08 (t, *J* = 5.5 Hz, 1H), 4.04-3.97 (m, 2H), 3.96-3.90 (m, 1H), 3.90-3.85 (m, 2H), 3.83 (t, *J* = 5.9 Hz, 1H), 3.71 (td, *J* = 7.7, 4.8 Hz, 2H), 3.59 (tdd, *J* = 12.3, 9.2, 5.7 Hz, 3H), 3.46 (dd, *J* = 11.4, 9.6 Hz, 1H), 3.10 (q, *J* = 6.7 Hz, 2H), 2.98 (dt, *J* = 9.6, 6.5 Hz, 1H), 2.89 (dd, *J* = 11.8, 3.5 Hz, 1H), 2.17 (s, 3H), 2.14 (s, 3H), 2.08 (s, 3H), 1.96 (s, 3H), 1.93 (s, 3H), 1.91 (s, 3H), 1.87 (d, *J* = 12.3 Hz, 1H), 1.42-1.38 (m, 4H), 1.32 (s, 3H), 1.28-1.19 (m, 2H). ^{13}C NMR (101 MHz, Chloroform-*d*) δ = 170.99, 170.82, 170.69, 170.34, 170.20, 169.84, 167.81, 166.71, 166.18, 156.56, 153.29, 138.72, 138.53, 136.82, 133.74, 130.72, 130.46, 129.95, 128.82, 128.61, 128.33, 128.17, 127.72, 127.58, 127.52, 127.37, 121.09, 100.28, 99.39, 97.44, 78.06, 74.46, 73.82, 73.04, 72.79, 71.70, 71.49, 71.38, 70.94, 69.81, 69.09, 67.94, 67.85, 66.62, 63.69, 63.51, 61.88, 59.22, 41.04, 36.08, 29.81, 29.57, 28.91, 23.39, 23.33, 21.62, 20.82, 20.74, 20.70, 20.56, 20.23. HRMS (ESI): Calcd for $C_{75}H_{90}N_3O_{30}$ $[M+H]^+$ 1512.5609, found: 1512.5599.

Synthesis of compound 28

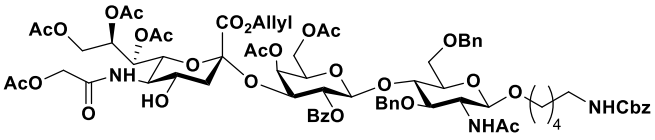

Compound **28** was synthesised from **27** using the general oxazolidinone ring deprotection procedure **4** (75%). ^{1}H NMR (400 MHz, Chloroform-*d*) δ = 8.15 (d, *J* = 7.3 Hz, 2H), 7.56 (t, *J* = 7.3 Hz, 1H), 7.46 (t, *J* = 7.6 Hz, 2H), 7.35-7.28 (m, 12H), 7.27-7.22 (m, 3H), 6.17 (d, *J* = 8.4 Hz, 1H), 6.03-5.88 (m, 2H), 5.66-5.57 (m, 1H), 5.38-5.24 (m, 3H), 5.16 (dd, *J* = 9.4, 2.4 Hz, 1H), 5.06 (s, 2H), 5.03 (d, *J* = 3.4 Hz, 1H), 4.98 (s, 1H), 4.92 (d, *J* = 7.9 Hz, 1H), 4.80-4.68 (m, 3H), 4.64 (d, *J* = 11.7 Hz, 1H), 4.60-4.43 (m, 4H), 4.37-4.26 (m, 3H), 4.10-3.99 (m, 3H), 3.96-3.76 (m, 4H), 3.77 (dd, *J* = 10.7, 2.4 Hz, 1H), 3.71 (dd, *J* = 9.9, 5.0 Hz, 2H), 3.64 (dd, *J* = 10.0, 5.0 Hz, 1H), 3.57 (dt, *J* = 10.1, 5.8 Hz, 2H), 3.24 (q, *J* = 10.1 Hz, 1H), 3.09 (q, *J* = 6.5 Hz, 2H), 3.03-2.87 (m, 2H), 2.62 (dd, *J* = 12.7, 4.5 Hz, 1H), 2.16 (s, 3H), 2.12 (s, 3H), 2.06 (s, 3H), 1.99 (s, 3H), 1.94 (s, 3H), 1.91 (s, 3H), 1.40 (m, 4H), 1.26 (m, 5H). ^{13}C NMR (101 MHz, Chloroform-*d*) δ = 170.78, 170.52, 170.38, 170.30, 170.21, 169.88, 168.51, 167.57, 165.89, 156.56, 138.70, 138.48, 136.78, 133.46, 131.28, 130.21, 130.08, 128.71, 128.57, 128.32, 128.12, 127.75, 127.54, 127.42, 119.89, 100.36, 99.41, 97.22, 78.01, 74.57, 74.38, 73.04, 72.82, 71.67, 70.97, 70.83, 69.54, 69.06, 67.93, 67.48, 67.41, 67.30, 66.58, 63.16, 62.38, 61.92, 53.36, 53.06, 41.01, 40.31. HRMS (ESI): Calcd for $C_{74}H_{92}N_3O_{29}$ $[M+H]^+$ 1486.5816, found: 1486.5808.

Synthesis of compound 29

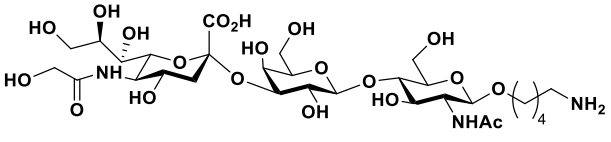

Compound **29** was synthesised from **28** using the general global deprotection procedure **5** (59%). ^{1}H NMR (400 MHz, Deuterium Oxide) δ = 4.56 (d, *J* = 7.9 Hz, 1H), 4.52 (d, *J* = 7.5 Hz, 1H), 4.19-4.07 (m, 3H), 4.04-3.76 (m, 8H), 3.80-3.68 (m, 7H), 3.69-3.53 (m, 5H), 2.99 (dd, *J* = 8.9, 6.4 Hz, 2H), 2.78 (dd, *J* = 12.4, 4.6 Hz, 1H), 2.03 (s, 3H), 1.82 (t, *J* = 12.1 Hz, 1H), 1.74-1.54 (m, 4H), 1.41 (m, 2H). ^{13}C NMR (101 MHz, Deuterium Oxide) δ = 175.75, 174.37, 173.85, 102.54, 101.11, 99.80, 78.30, 75.46, 75.16, 74.74, 72.58, 72.35, 71.80, 70.05, 69.36, 68.05, 67.99, 67.44, 62.53, 61.01, 60.95, 60.02, 55.06, 51.36, 39.67, 39.30, 28.04, 26.33, 22.13, 22.07. HRMS (ESI): Calcd for $C_{30}H_{54}N_3O_{20}$ $[M+H]^+$ 776.3301, found: 776.3310.

Synthesis of compound 8a

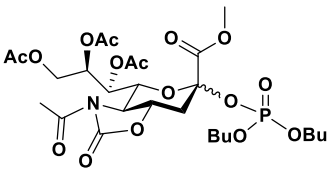

Compound **8a** was synthesised by following synthetic reported methods.[36] ^{1}H NMR (400 MHz, Chloroform-*d*) δ = 5.66 (dd, *J* = 7.5, 1.5 Hz, 1H), 5.32-5.28 (m, 1H), 4.74 (dd, *J* = 9.6, 1.6 Hz, 1H),

4.39 (dd, *J* = 12.3, 2.8 Hz, 1H), 4.20-4.04 (m, 6H), 3.83 (s, 3H), 2.99 (dd, *J* = 12.2, 4.0 Hz, 1H), 2.74 (s, 1H), 2.67 (t, *J* = 12.7 Hz, 1H), 2.49 (s, 3H), 2.13 (s, 3H), 2.09 (s, 3H), 2.03 (s, 3H), 1.70-1.62 (m, 4H), 1.40 (h, *J* = 7.4 Hz, 4H), 0.93 (t, *J* = 7.4 Hz, 6H). ^{13}C NMR (101 MHz, Chloroform-*d*) δ = 171.96, 170.75, 170.11, 170.01, 167.36, 153.65, 98.34, 77.35, 74.31, 71.60, 68.22, 62.63, 58.45, 53.58, 36.00, 32.23, 29.71, 24.76, 21.09, 20.92, 20.87, 18.76, 13.69. HRMS (ESI): Calcd for $C_{27}H_{42}NNaO_{16}P$ $[M+Na]^+$ 690.2139, found 690.2131.

Synthesis of compound 31

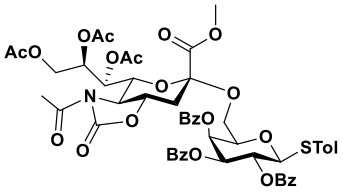

Compound **31** was synthesised from donor **30** and acceptor **12** using the general glycosylation procedure **1** (83%). ^{1}H NMR (400 MHz, Chloroform-*d*) δ = 7.98-7.96 (m, 2H), 7.90-7.87 (m, 2H), 7.75-7.73 (m, 2H), 7.62-7.58 (m, 1H), 7.54-7.48 (m, 3H), 7.45-7.36 (m, 5H), 7.24-7.20 (m, 2H), 7.18-7.15 (m, 2H), 6.01 (q, *J* = 1.2 Hz, 1H), 5.65-5.63 (m, 2H), 5.60 (dd, *J* = 8.3, 1.7 Hz, 1H), 5.49 (ddd, *J* = 8.3, 7.2, 2.7 Hz, 1H), 5.13-5.10 (m, 1H), 4.63 (dd, *J* = 9.4, 1.7 Hz, 1H), 4.50 (dd, *J* = 12.3, 2.8 Hz, 1H), 4.34 (ddd, *J* = 8.4, 5.9, 1.2 Hz, 1H), 4.06 (dd, *J* = 12.3, 7.2 Hz, 1H), 3.97-3.90 (m, 2H), 3.72 (dd, *J* = 11.2, 9.4 Hz, 1H), 3.60 (dd, *J* = 10.5, 8.3 Hz, 1H), 3.52 (s, 3H), 2.74 (dd, *J* = 12.2, 3.5 Hz, 1H), 2.48 (s, 3H), 2.39 (s, 3H), 2.19 (s, 3H), 2.13 (s, 3H), 2.06 (m, 1H), 1.99 (s, 3H). ^{13}C NMR (101 MHz, Chloroform-*d*) δ = 172.16, 171.03, 170.59, 170.22, 168.38, 165.60, 165.26, 165.24, 153.77, 138.50, 134.36, 133.43, 133.34, 133.23, 130.04, 129.96, 129.87, 129.67, 129.64, 129.62, 129.11, 128.58, 128.50, 128.35, 127.63, 99.69, 85.47, 75.96, 75.44, 74.90, 73.34, 71.74, 69.07, 68.12, 63.65, 63.57, 59.08, 53.10, 36.54, 24.86, 21.50, 21.22, 21.09, 20.90. HRMS (ESI): Calcd for $C_{53}H_{54}NO_{20}S$ $[M+H]^+$ 1056.2960, found 1056.2936.

Synthesis of compound 32

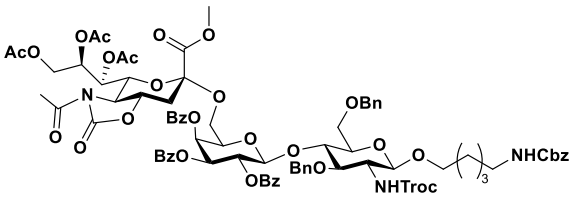

Compound **32** was synthesised from donor **31** and acceptor **19** using the general glycosylation procedure **2** (76%). ^{1}H NMR (400 MHz, Chloroform-*d*) δ = 7.94-7.92 (m, 2H), 7.89-7.87 (m, 2H), 7.77-7.75 (m, 2H), 7.56-7.47 (m, 2H), 7.44-7.38 (m, 5H), 7.37-7.21 (m, 17H), 5.90 (d, *J* = 3.5 Hz, 1H), 5.69 (dd, *J* = 10.4, 8.0 Hz, 1H), 5.58 (dd, *J* = 7.8, 1.7 Hz, 2H), 5.50-5.45 (m, 2H), 5.12-5.04 (m, 4H), 4.86-4.81 (m, 2H), 4.67 (s, 2H), 4.61-4.56 (m, 2H), 4.43 (dd, *J* = 12.2, 2.9 Hz, 2H), 4.35 (d, *J* = 12.2 Hz, 1H), 4.10-4.05 (m, 2H), 3.98-3.86 (m, 4H), 3.79-3.73 (m, 1H), 3.68-3.59 (m, 4H), 3.54-3.42 (m, 1H), 3.37-3.28 (m, 5H), 3.13 (q, *J* = 6.7 Hz, 2H),

2.69 (d, *J* = 3.5 Hz, 1H), 2.47 (s, 3H), 2.09 (s, 3H), 2.08 (s, 3H), 1.99 (s, 3H), 1.54-1.50 (m, 2H), 1.47-1.42 (m, 2H), 1.34-1.27 (m, 2H). ^{13}C NMR (101 MHz, Chloroform-*d*) δ = 172.18, 171.07, 170.33, 170.23, 168.14, 165.58, 165.26, 153.79, 138.85, 138.24, 136.77, 133.48, 133.30, 129.86, 129.83, 129.50, 129.22, 129.02, 128.71, 128.65, 128.63, 128.41, 128.37, 128.20, 128.17, 128.04, 127.98, 127.95, 127.58, 100.03, 99.43, 76.60, 75.93, 74.87, 74.63, 74.44, 73.86, 73.47, 71.82, 70.52, 69.47, 69.11, 68.47, 67.92, 66.66, 63.30, 63.01, 59.10, 53.05, 41.02, 36.38, 29.68, 29.55, 28.97, 24.83, 23.19, 21.17, 21.00, 20.94. HRMS (ESI): Calcd for $C_{82}H_{89}Cl_3N_3O_{29}$ $[M+H]^+$ 1684.4647, found 1684.4641.

Synthesis of compound 33

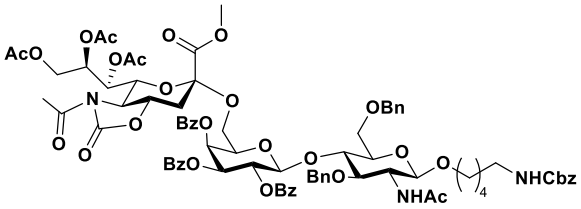

Compound **33** was synthesised from **32** using the general Troc deprotection procedure **3** (69%). ^{1}H NMR (400 MHz, Chloroform-*d*) δ = 7.98-7.95 (m, 2H), 7.91-7.89 (m, 2H), 7.77-7.75 (m, 2H), 7.58-7.54 (m, 1H), 7.52-7.48 (m, 1H), 7.45-7.21 (m, 22H), 6.08 (d, *J* = 8.4 Hz, 1H), 5.92 (dd, *J* = 3.5, 1.1 Hz, 1H), 5.67 (dd, *J* = 10.5, 7.9 Hz, 1H), 5.59-5.53 (m, 2H), 5.46 (ddd, *J* = 8.0, 7.0, 2.9 Hz, 1H), 5.07 (s, 2H), 4.99 (d, *J* = 7.9 Hz, 1H), 4.93 (d, *J* = 11.7 Hz, 1H), 4.78 (d, *J* = 11.8 Hz, 1H), 4.59-4.55 (m, 3H), 4.44 (dd, *J* = 12.2, 2.9 Hz, 1H), 4.37 (d, *J* = 12.1 Hz, 1H), 4.12-3.88 (m, 6H), 3.69-3.61 (m, 5H), 3.56 (dd, *J* = 10.1, 7.6 Hz, 1H), 3.51-3.48 (m, 1H), 3.42 (s, 3H), 3.19 (dt, *J* = 9.7, 6.5 Hz, 1H), 3.12 (q, *J* = 6.7 Hz, 2H), 2.71 (dd, *J* = 12.3, 3.5 Hz, 1H), 2.47 (s, 3H), 2.07 (s, 4H), 2.06 (s, 3H), 1.98 (s, 3H), 1.92 (s, 3H), 1.50-1.41 (m, 4H), 1.31-1.25 (m, 2H). ^{13}C NMR (101 MHz, Chloroform-*d*) δ = 172.12, 170.99, 170.37, 170.31, 170.10, 168.16, 165.61, 165.54, 165.26, 156.54, 153.80, 139.02, 138.30, 136.82, 133.54, 133.50, 133.31, 129.87, 129.83, 129.53, 129.23, 129.01, 128.72, 128.63, 128.60, 128.39, 128.18, 128.15, 127.99, 127.95, 127.89, 127.57, 100.33, 99.82, 99.50, 78.19, 75.90, 74.88, 74.70, 73.45, 73.38, 71.95, 71.75, 71.59, 70.51, 69.16, 69.03, 66.61, 63.32, 63.21, 59.12, 54.52, 53.08, 41.03, 36.40, 29.58, 28.93, 24.83, 23.47, 23.29, 21.15, 20.94, 20.91. HRMS (ESI): Calcd for $C_{81}H_{89}N_3NaO_{28}$ $[M+Na]^+$ 1574.5530, found 1574.5530.

Synthesis of compound 34

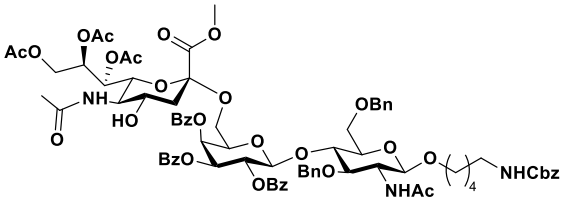

Compound **34** was synthesised from **33** using the general oxazolidinone ring deprotection procedure **4** (81%). ^{1}H NMR (400 MHz, Methanol-d_4) δ = 7.95-7.93 (m, 2H), 7.90-7.87

(m, 2H), 7.76-7.73 (m, 2H), 7.62 (m, 1H), 7.55-7.52 (m, 1H), 7.50-7.44 (m, 5H), 7.43-7.23 (m, 17H), 5.93 (d, *J* = 3.3 Hz, 1H), 5.67 (dd, *J* = 10.4, 7.8 Hz, 1H), 5.57 (dd, *J* = 10.4, 3.3 Hz, 1H), 5.51-5.46 (m, 1H), 5.33 (dd, *J* = 8.4, 2.1 Hz, 1H), 5.19-5.13 (m, 2H), 5.06 (s, 2H), 4.78 (d, *J* = 11.3 Hz, 1H), 4.67 (d, *J* = 12.1 Hz, 1H), 4.40-4.36 (m, 3H), 4.16-4.10 (m, 3H), 4.06 (dd, *J* = 10.7, 2.1 Hz, 1H), 3.93 (dd, *J* = 9.9, 5.3 Hz, 1H), 3.87-3.82 (m, 2H), 3.80-3.65 (m, 3H), 3.46-3.36 (m, 7H), 3.09 (t, *J* = 6.9 Hz, 2H), 2.53 (dd, *J* = 12.9, 4.4 Hz, 1H), 2.13 (s, 3H), 2.06 (s, 3H), 2.00 (s, 3H), 1.93 (s, 3H), 1.88 (s, 3H), 1.75 (t, *J* = 12.6 Hz, 1H), 1.55-1.44 (m, 4H), 1.37-1.32 (m, 2H). ^{13}C NMR (101 MHz, Methanol-d_4) δ = 173.76, 173.13, 172.42, 171.81, 171.46, 169.29, 166.70, 166.59, 158.80, 140.55, 139.51, 138.44, 134.76, 134.58, 134.46, 130.80, 130.70, 130.66, 130.49, 130.30, 130.29, 129.77, 129.75, 129.72, 129.43, 129.29, 129.18, 128.95, 128.91, 128.73, 128.36, 102.53, 101.25, 100.70, 81.45, 79.44, 77.68, 75.75, 74.85, 74.42, 73.93, 73.38, 72.85, 71.98, 70.38, 69.68, 69.34, 69.05, 68.90, 67.24, 63.78, 63.15, 56.10, 53.02, 52.69, 42.00, 41.72, 30.42, 30.13, 24.22, 23.05, 22.90, 21.22, 21.06, 20.88. HRMS (ESI): Calcd for $C_{80}H_{92}N_3O_{27}$ $[M+H]^+$ 1526.5918, found 1526.5905.

Synthesis of compound 35

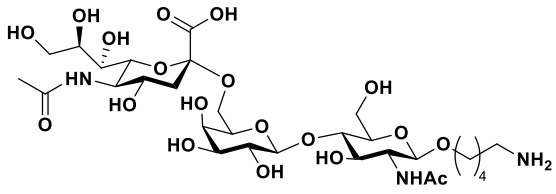

Compound **35** was synthesised from **34** using the general global deprotection procedure **5** (65%). ^{1}H NMR (400 MHz, Deuterium Oxide) δ = 4.56 (d, *J* = 7.9 Hz, 1H), 4.45 (d, *J* = 7.9 Hz, 1H), 4.03-4.00 (m, 2H), 3.95-3.59 (m, 16H), 3.57-3.52 (m, 3H), 3.00 (t, *J* = 7.7 Hz, 2H), 2.67 (dd, *J* = 12.4, 4.7 Hz, 1H), 2.06 (s, 3H), 2.03 (s, 3H), 1.75-1.58 (m, 5H), 1.45-1.36 (m, 2H). ^{13}C NMR (101 MHz, Deuterium Oxide) δ = 174.90, 174.42, 173.41, 103.45, 100.91, 100.06, 80.80, 74.46, 73.68, 72.54, 72.42, 71.65, 70.70, 70.02, 68.39, 68.34, 68.17, 63.35, 62.65, 60.36, 54.86, 51.84, 40.03, 39.32, 28.03, 26.33, 22.26, 22.10, 22.01. HRMS (ESI): Calcd for $C_{30}H_{54}N_3O_{19}$ $[M+H]^+$ 760.3352, found 760.3351.

Synthesis of compound 36

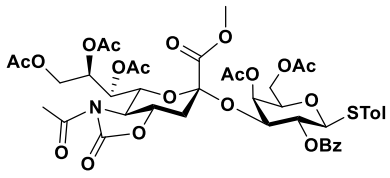

Compound **36** was synthesised from donor **30** and acceptor **17** using the general glycosylation procedure **1**. Next, the compound was dissolved in pyridine (10 mL), and acetic anhydride was added (0.5 mL) at 0 ºC. The resulting mixture was stirred at RT for 12 hours, concentrated *in vacuo* and purified using mixture of (3:2, v/v) ethyl acetate and hexane as eluent to afford compound **36** (54% over two steps). ^{1}H NMR (400

MHz, Chloroform-*d*) δ = 8.21-8.18 (m, 2H), 7.61-7.56 (m, 1H), 7.50-7.46 (m, 2H), 7.35-7.33 (m, 2H), 7.07-7.05 (m, 2H), 5.62 (ddd, *J* = 9.6, 7.3, 2.5 Hz, 1H), 5.45 (dd, *J* = 9.3, 2.1 Hz, 1H), 5.30-5.28 (m, 1H), 4.97-4.94 (m, 2H), 4.75 (dd, *J* = 9.7, 3.2 Hz, 1H), 4.42 (dd, *J* = 12.3, 2.6 Hz, 1H), 4.21 (dd, *J* = 9.4, 2.2 Hz, 1H), 4.08-4.06 (m, 2H), 3.99-3.91 (m, 2H), 3.81 (s, 4H), 3.44 (dd, *J* = 11.4, 9.4 Hz, 1H), 2.88 (dd, *J* = 11.8, 3.4 Hz, 1H), 2.39 (s, 3H), 2.31 (s, 3H), 2.16 (s, 3H), 2.10 (s, 3H), 2.05 (s, 3H), 1.98 (s, 3H), 1.87-1.83 (m, 1H), 1.24 (s, 3H). ^{13}C NMR (101 MHz, Chloroform-*d*) δ = 171.62, 170.91, 170.84, 170.44, 170.39, 170.15, 167.79, 165.63, 153.55, 138.30, 133.59, 133.51, 130.57, 130.32, 129.56, 128.67, 97.37, 86.88, 75.75, 74.49, 74.40, 72.61, 71.48, 69.43, 68.26, 68.08, 63.56, 62.36, 58.92, 53.56, 36.07, 24.65, 21.62, 21.27, 20.84, 20.07. HRMS (ESI): Calcd for $C_{43}H_{50}NO_{20}$ $[M+H]^+$ 932.2647, found 932.2656.

Synthesis of compound 37

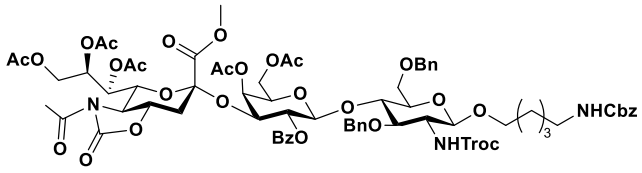

Compound **37** was synthesised from donor **36** and acceptor **19** using the general glycosylation procedure **2** (73%). ^{1}H NMR (400 MHz, Chloroform-*d*) δ = 8.25-8.23 (m, 2H), 7.58-7.54 (m, 1H), 7.48-7.44 (m, 2H), 7.35-7.22 (m, 15H), 5.71 (ddd, *J* = 9.8, 7.4, 2.6 Hz, 1H), 5.49 (dd, *J* = 9.4, 2.2 Hz, 1H), 5.34 (dd, *J* = 10.1, 7.8 Hz, 2H), 5.07-5.03 (m, 3H), 4.92-4.89 (m, 2H), 4.84-4.77 (m, 1H), 4.72-4.69 (m, 2H), 4.66 (m, 2H), 4.48 (dd, *J* = 12.3, 2.6 Hz, 1H), 4.41 (s, 3H), 4.20 (dd, *J* = 9.4, 2.2 Hz, 1H), 4.08-3.96 (m, 3H), 3.87-3.77 (m, 7H), 3.70-3.64 (m, 2H), 3.55 (dd, *J* = 10.7, 5.5 Hz, 1H), 3.47-3.39 (m, 3H), 3.20-3.18 (m, 1H), 3.12 (q, *J* = 6.8 Hz, 2H), 2.87 (dd, *J* = 11.7, 3.5 Hz, 1H), 2.40 (s, 3H), 2.17 (s, 3H), 2.06 (s, 3H), 1.97 (s, 3H), 1.91 (s, 3H), 1.50-1.40 (m, 4H), 1.31-1.24 (m, 5H). ^{13}C NMR (101 MHz, Chloroform-*d*) δ = 171.68, 171.03, 170.80, 170.32, 170.14, 167.67, 165.64, 153.56, 138.59, 136.78, 133.70, 130.55, 130.00, 128.81, 128.65, 128.35, 128.33, 128.20, 127.89, 127.62, 127.51, 127.37, 99.97, 97.59, 75.77, 74.82, 74.39, 73.03, 71.99, 71.63, 71.53, 70.86, 69.43, 67.94, 67.88, 66.69, 63.65, 61.87, 58.94, 53.58, 35.98, 29.70, 29.57, 28.98, 24.67, 23.21, 21.61, 20.86, 20.79, 20.70, 20.26.HRMS (ESI): Calcd for $C_{72}H_{85}Cl_3N_3O_{29}$ $[M+H]^+$ 1560.4334, found 1560.4331.

Synthesis of compound 38

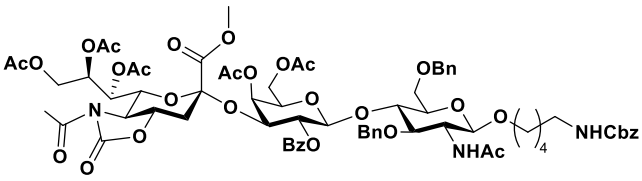

Compound **38** was synthesised from **37** using the general Troc deprotection procedure **3** (77%). ^{1}H NMR (400 MHz, Chloroform-*d*) δ = 8.22-8.20 (m, 2H), 7.55 (t, *J* = 7.4 Hz, 1H), 7.45 (t, *J* = 7.6 Hz, 2H), 7.32-7.22 (m, 15H), 5.99 (d, *J* = 9.5 Hz, 1H), 5.70 (ddd, *J* = 9.9, 7.6, 2.6 Hz, 1H), 5.48 (dd, *J* = 9.4, 2.2 Hz, 1H), 5.33 (dd, *J* = 10.2, 7.9 Hz, 1H), 5.05 (s, 2H), 5.01 (s, 1H), 4.96-4.93 (m, 2H), 4.75-4.71 (m, 2H), 4.64 (d, *J* = 11.7 Hz, 1H), 4.50-4.38 (m, 3H), 4.31 (d, *J* = 6.1 Hz, 1H), 4.20 (dd, *J* = 9.4, 2.2 Hz, 1H), 4.10-4.04 (m, 1H), 4.01-3.95 (m, 1H), 3.87-3.76 (m, 7H), 3.72-3.67 (m, 2H), 3.62-3.53 (m, 3H), 3.46 (dd, *J* = 11.4, 9.4 Hz, 1H), 3.08 (q, *J* = 6.8 Hz, 2H), 2.97 (dt, *J* = 9.7, 6.4 Hz, 1H), 2.86 (dd, *J* = 11.8, 3.4 Hz, 1H), 2.38 (s, 3H), 2.16 (s, 3H), 2.08 (s, 3H), 1.95 (s, 3H), 1.91 (s, 3H), 1.89 (s, 3H), 1.41-1.36 (m, 4H), 1.30 (s, 3H), 1.25-1.20 (m, 2H). ^{13}C NMR (101 MHz, Chloroform-*d*) δ = 171.59, 170.90, 170.70, 170.20, 170.17, 170.13, 170.04, 167.54, 166.07, 156.48, 153.42, 138.63, 138.44, 136.75, 133.64, 130.38, 129.86, 128.72, 128.49, 128.22, 128.03, 127.60, 127.44, 127.25, 100.21, 99.30, 97.43, 78.08, 75.55, 72.90, 72.68, 71.62, 71.47, 71.24, 70.79, 69.68, 68.98, 67.88, 67.78, 66.45, 63.60, 61.70, 58.78, 53.49, 53.27, 40.92, 35.88, 29.44, 28.80, 24.54, 23.26, 23.20, 21.50, 20.70, 20.67, 20.56, 20.19. HRMS (ESI): Calcd for $C_{71}H_{86}N_3O_{28}$ $[M+H]^+$ 1428.5398, found 1428.5391.

Synthesis of compound 39

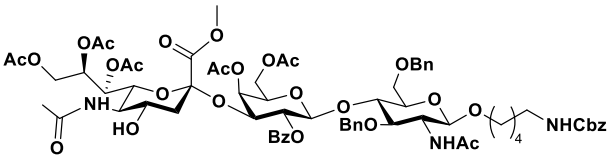

Compound **39** was synthesised from **38** using the general oxazolidinone ring deprotection procedure **4** (79%). ^{1}H NMR (400 MHz, Methanol-d_4) δ = 8.28-8.25 (m, 2H), 7.70-7.65 (m, 1H), 7.59 (dd, *J* = 8.3, 6.9 Hz, 2H), 7.44-7.25 (m, 15H), 5.76 (ddd, *J* = 9.4, 6.4, 2.6 Hz, 1H), 5.30 (dd, *J* = 10.1, 7.9 Hz, 1H), 5.21 (dd, *J* = 9.9, 2.7 Hz, 1H), 5.12 (d, *J* = 8.0 Hz, 1H), 5.08-5.05 (m, 3H), 4.86-4.83 (m, 1H), 4.65-4.62 (m, 2H), 4.53 (d, *J* = 11.6 Hz, 1H), 4.36-4.32 (m, 2H), 4.10-4.02 (m, 2H), 3.99-3.95 (m, 2H), 3.84 (s, 4H), 3.81-3.73 (m, 4H), 3.65 (dd, *J* = 10.6, 2.7 Hz, 1H), 3.60-3.54 (m, 2H), 3.46-3.36 (m, 2H), 3.31-3.28 (m, 1H), 3.09 (t, *J* = 6.9 Hz, 2H), 2.53 (dd, *J* = 12.7, 4.4 Hz, 1H), 2.19 (s, 3H), 2.09 (s, 3H), 1.98 (s, 3H), 1.95 (s, 3H), 1.88 (s, 3H), 1.83 (s, 3H), 1.53-1.44 (m, 7H), 1.38-1.32 (m, 2H). ^{13}C NMR (101 MHz, Methanol-d_4) δ = 173.64, 173.14, 172.37, 172.12, 171.96, 171.77, 171.56, 169.73, 166.89, 158.82, 140.34, 139.73, 138.46, 134.76, 131.32, 131.27, 129.97, 129.43, 129.33, 129.16, 128.91, 128.83, 128.73, 128.68, 128.58, 128.41, 102.44, 101.26, 98.48, 81.70, 79.46, 76.97, 75.78, 75.17, 74.10, 73.26, 72.27, 71.99, 70.36,

69.95, 69.55, 69.29, 68.48, 68.39, 67.24, 63.91, 62.64, 56.15, 53.53, 52.16, 41.71, 41.43, 30.41, 30.12, 24.21, 23.01, 22.87, 21.69, 20.92, 20.81, 20.64. HRMS (ESI): Calcd for $C_{70}H_{88}N_3O_{27}$ $[M+H]^+$ 1402.5605, found 1402.5614.

Synthesis of compound 40

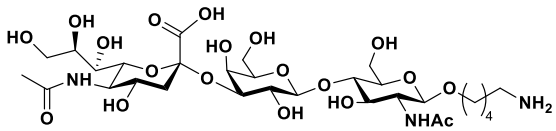

Compound **40** was synthesised from **39** using the general global deprotection procedure **5** (61%). ^{1}H NMR (400 MHz, Deuterium Oxide) δ = 4.56 (d, *J* = 7.9 Hz, 1H), 4.52 (d, *J* = 7.7 Hz, 1H), 4.12 (dd, *J* = 9.9, 3.1 Hz, 1H), 4.01 (dd, *J* = 12.3, 2.3 Hz, 1H), 3.96 (d, *J* = 3.1 Hz, 1H), 3.92-3.88 (m, 5H), 3.76-3.74 (m, 7H), 3.67-3.64 (m, 2H), 3.63-3.57 (m, 4H), 3.01-2.98 (m, 2H), 2.76 (dd, *J* = 12.4, 4.7 Hz, 1H), 2.04 (s, 6H), 1.80 (t, *J* = 12.1 Hz, 1H), 1.72-1.66 (m, 2H), 1.62-1.57 (m, 2H), 1.44-1.38 (m, 2H). ^{13}C NMR (101 MHz, Deuterium Oxide) δ = 175.02, 174.43, 173.90, 102.56, 101.16, 99.81, 78.26, 75.48, 75.20, 74.77, 72.89, 72.39, 71.78, 70.08, 69.39, 68.36, 68.08, 67.46, 62.58, 61.05, 60.02, 55.08, 51.67, 39.62, 39.32, 28.07, 26.36, 22.14, 22.11, 22.03. HRMS (ESI): Calcd for $C_{30}H_{54}N_3O_{19}$ $[M+H]^+$ 760.3352, found 760.3347.

3.4.8 Glycogold nanoparticles synthesis:

Sphere gold nanoparticles were synthesized according to the previously reported method.[41] In brief, 300 µl of 1% chloroauric acid was added to 30 mL of distilled water and brought to boil, and to this solution, 600 µl of 1% citric acid was added to get 15 nm of sphere gold nanoparticles. For 30 and 50 nm sphere gold nanoparticles, 300 and 240 µl of 1% citric acid was added. The resulting solution was refluxed until the colour of the boiling solution changed from dark purple to red vine. The nanoparticles solution was cooled, centrifuged, and the pellet was washed with distilled water. The nanoparticles were characterized by FESEM and UV-vis spectrophotometry. Prior to conjugation, disulphide bond of the linker was reduced with TECEP in water and compounds were purified. The thiol ended sugar molecules were conjugated on the surface of gold nanoparticle. In brief, different size sphere nanoparticles were dispersed in PBS buffer pH 7.4 (1 mL, 0.1 M), to this glycans was added (500 µg). The resulting solution was kept at 25 ºC for 24 h with constant shaking. Then the solution was centrifuged, and the pellet was washed three times with Mili Q water to remove the unbound antigen. A change in zeta potential confirmed the antigen conjugation. The loading quantity of sugar onto the surface of nanoparticles was determined by the phenol sulfuric acid method.

3.4.9 Glycan carrier protein conjugation:

Sugar molecule (1 mg) in 100 µL of anhydrous DMSO dropwise added to the stirring solution containing Suberic acid bis(N-hydroxysuccinimide ester) (13 mole excess) and triethylamine (5 mole excess) in 150 µL of DMSO at RT and further stirred for 2 hours. Next, the reaction mixture was diluted with 500 µL of PBS pH 7.4, and the nonreacted spacer was extracted with chloroform (5 mL X 3 times). Furter the aqueous phase was added to the stirring solution containing CRM_{197} (1 mg) in 500 µL of PBS pH 7.4 and further stirred for 16 h at RT. Finally, the resulting solution was desalted and concentrated by using 10 kDa centrifugal filter (Amicon) and characterized by MALDI-TOF.

3.4.10 Immunization protocol:

All animal studies were performed in the Dr Vered Padler-Karvani Lab (Tel Aviv University, Israel). B6.129X1-*Cmah*^{tm1Avrk}/J mice (6-8 weeks old) were used for the immunization. The groups of mice (n=5) were immunized subcutaneously with 200 µL of immunogen (2.5 µg sugar) and PBS on days 0, 7, 14 and 30. The mice were bled on day 36, and the serum antibody titer was analysed by microarray.

3.4.11 Glycan Microarray:

The IgG antibody titers were quantified using Nanoprint LM-60 Microarray on PolyAn 2D Epoxy covered glass. The glass slides were coated with Nue5Gc glycans as previously described protocol. [39, 40] Next, the glass slides were incubated with diluted sera (1:100) and developed and analysed by following previously reported protocol. [39, 40]

3.5 References:

1. Angata, T.; Varki, A. Chemical diversity in the sialic acids and related alpha-keto acids: an evolutionary perspective. *Chem Rev*. **2002**, *102*, 439-69.
2. Varki, A. Loss of N-glycolylneuraminic acid in humans: Mechanisms, consequences, and implications for hominid evolution. *Am J Phys Anthropol*. **2001**, *Suppl 33*, 54-69.
3. Varki, A. Multiple changes in sialic acid biology during human evolution. *Glycoconj J*. **2009**, *26*, 231-45.
4. Malykh, Y. N.; Schauer, R.; Shaw, L. N-Glycolylneuraminic acid in human tumours. *Biochimie*. **2001**, *83*, 623-34.
5. Samraj, A. N.; Läubli, H.; Varki, N.; Varki, A. Involvement of a non-human sialic Acid in human cancer. *Front Oncol*. **2014**, *4*, 33.
6. Diaz, S. L.; Padler-Karavani, V.; Ghaderi, D.; Hurtado-Ziola, N.; Yu, H.; Chen, X.; Brinkman-Van der Linden, E. C.; Varki, A, Varki, N. M. Sensitive and specific

detection of the non-human sialic Acid N-glycolylneuraminic acid in human tissues and biotherapeutic products. *PLoS One*. **2009**, *4*, e4241.

7. Bardor, M.; Nguyen, D. H.; Diaz, S.; Vark,i A. Mechanism of uptake and incorporation of the non-human sialic acid N-glycolylneuraminic acid into human cells. *J Biol Chem*. **2005**, *280*, 4228-37.
8. Samraj, A. N.; Pearce, O. M.; Läubli, H.; Crittenden, A. N.; Bergfeld, A. K.; Banda, K.; Gregg, C. J.; Bingman, A. E.; Secrest, P.; Diaz, S. L.; Varki, N. M.; Varki, A. A red meat-derived glycan promotes inflammation and cancer progression. *Proc Natl Acad Sci U S A*. **2015**, *112*, 542-7.
9. Zhu, A.; Hurst, R. Anti-N-glycolylneuraminic acid antibodies identified in healthy human serum. *Xenotransplantation*. **2002**, *9*, 376-81.
10. Padler-Karavani, V.; Yu, H.; Cao, H.; Chokhawala, H.; Karp, F.; Varki, N.; Chen, X.; Varki, A. Diversity in specificity, abundance, and composition of anti-Neu5Gc antibodies in normal humans: potential implications for disease. *Glycobiology*. **2008**, *18*, 818-30.
11. Hedlund, M.; Padler-Karavani, V.; Varki, N. M.; Varki, A. Evidence for a human-specific mechanism for diet and antibody-mediated inflammation in carcinoma progression. *Proc Natl Acad Sci U S A*. **2008**, *105*, 18936-41.
12. Samraj, A. N.; Bertrand, K. A.; Luben, R.; Khedri, Z.; Yu, H.; Nguyen, D.; Gregg, C. J.; Diaz, S. L.; Sawyer, S.; Chen, X.; Eliassen, H.; Padler-Karavani, V.; Wu, K.; Khaw, K, T.; Willett, W.; Varki, A. Polyclonal human antibodies against glycans bearing red meat-derived non-human sialic acid N-glycolylneuraminic acid are stable, reproducible, complex and vary between individuals: Total antibody levels are associated with colorectal cancer risk. *PLoS One*. **2018**, *13*, e0197464.
13. Paul, A.; Bachar Abramovitch, S.; Padler-Karavani, V. Specific Detection of Neu5Gc in Animal Tissues by Immunohistochemistry. *Methods Mol Biol*. **2020**, *2110*, 59-72.
14. Soulillou, J. P.; Padler-Karavani, V. Editorial: Human Antibodies Against the Dietary Non-human Neu5Gc-Carrying Glycans in Normal and Pathologic States. *Front Immunol*. **2020**, *11*, 1589.
15. Bashir, S.; Fezeu, L. K.; Leviatan Ben-Arye, S.; Yehuda, S.; Reuven, E, M.; Szabo de Edelenyi, F.; Fellah-Hebia, I.; Le Tourneau, T.; Imbert-Marcille, B. M.; Drouet, E. B.; Touvier, M.; Roussel, J. C.; Yu, H.; Chen, X.; Hercberg, S.; Cozzi, E.; Soulillou, J. P.; Galan, P.; Padler-Karavani, V. Association between Neu5Gc carbohydrate and serum

antibodies against it provides the molecular link to cancer: French NutriNet-Santé study. *BMC Med*. **2020**, *18*, 262.

16. Leviatan Ben-Arye, S.; Schneider, C.; Yu H, Bashir, S.; Chen, X.; von Gunten, S.; Padler-Karavani, V. Differential Recognition of Diet-Derived Neu5Gc-Neoantigens on Glycan Microarrays by Carbohydrate-Specific Pooled Human IgG and IgA Antibodies. *Bioconjug Chem*. **2019**, *30*, 1565-1574.
17. Yehuda, S.; Padler-Karavani, V. Glycosylated Biotherapeutics: Immunological Effects of N-Glycolylneuraminic Acid. *Front Immunol*. **2020**, *11*, 21.
18. Labrada, M.; Dorvignit, D.; Hevia, G.; Rodríguez-Zhurbenko, N.; Hernández, A. M.; Vázquez, A. M.; Fernández, L. E. GM3(Neu5Gc) ganglioside: an evolution fixed neoantigen for cancer immunotherapy. *Semin Oncol*. **2018**, *45*, 41-51.
19. Soulillou, J. P.; Cozzi, E.; Bach, J. M. Challenging the Role of Diet-Induced Anti-Neu5Gc Antibodies in Human Pathologies. *Front Immunol*. **2020**, *11*, 834.
20. Dhar, C.; Sasmal, A.; Varki, A. From "Serum Sickness" to "Xenosialitis": Past, Present, and Future Significance of the Non-human Sialic Acid Neu5Gc. *Front Immunol*. **2019**, *10*, 807.
21. Rappuoli, R.; De Gregorio, E. Costantino, P. On the mechanisms of conjugate vaccines. *Proc Natl Acad Sci U S A*. **2019**, *116*, 14-16.
22. Dykman, L. A.; Khlebtsov, N. G. Immunological properties of gold nanoparticles. *Chem Sci*. **2017**, *8*, 1719-1735.
23. Ferrando, R. M.; Lay, L.; Polito, L. Gold nanoparticle-based platforms for vaccine development. *Drug Discovery Today: Technologies*, **2021**.
24. Dykman, L. A. Gold nanoparticles for preparation of antibodies and vaccines against infectious diseases. *Expert Rev Vaccines*. **2020**, *19*, 465-477.
25. Niikura, K.; Matsunaga, T.; Suzuki, T.; Kobayashi, S.; Yamaguchi, H.; Orba, Y.; Kawaguchi, A.; Hasegawa, H.; Kajino, K.; Ninomiya, T.; Ijiro, K.; Sawa, H. Gold nanoparticles as a vaccine platform: influence of size and shape on immunological responses in vitro and in vivo. *ACS Nano*. **2013**, *7*, 3926-38.
26. Compañón, I.; Guerreiro, A.; Mangini, V.; Castro-López, J.; Escudero-Casao, M.; Avenoza, A.; Busto, J. H.; Castillón, S.; Jiménez-Barbero, J.; Asensio, J. L.; Jiménez-Osés, G.; Boutureira, O.; Peregrina, J. M.; Hurtado-Guerrero, R.; Fiammengo, R.; Bernardes, G. J. L.; Corzana, F. Structure-Based Design of Potent Tumor-Associated Antigens: Modulation of Peptide Presentation by Single-Atom O/S or O/Se Substitutions at the Glycosidic Linkage. *J Am Chem Soc*. **2019**, *141*, 4063-4072.

27. Boons, G. J.; Demchenko, A. V. Recent advances in o-sialylation. *Chem Rev*. **2000**, *100*, 4539-66.
28. De Meo, C.; Jones, B. T. Chemical Synthesis of Glycosides of N-Acetylneuraminic Acid. *Adv Carbohydr Chem Biochem*. **2018**, *75*, 215-316.
29. Komura, N.; Kato, K.; Udagawa, T.; Asano, S.; Tanaka, H. N.; Imamura, A.; Ishida ,H.; Kiso, M.; Ando, H. Constrained sialic acid donors enable selective synthesis of α-glycosides. *Science*. **2019**, *364*, 677-680.
30. Walczak, M. A.; Hayashida, J.; Danishefsky, S. J. Building biologics by chemical synthesis: practical preparation of di- and triantennary N-linked glycoconjugates. *J Am Chem Soc*. **2013**, *135*, 4700-3.
31. Mandhapati, A. R.; Rajender, S.; Shaw, J.; Crich, D. The isothiocyanato moiety: an ideal protecting group for the stereoselective synthesis of sialic acid glycosides and subsequent diversification. *Angew Chem Int Ed Engl*. **2015**, *54*, 1275-8.
32. Kooner, A. S.; Yu, H.; Chen, X. Synthesis of *N*-Glycolylneuraminic Acid (Neu5Gc) and Its Glycosides. *Front Immunol*. **2019**, *10*, 2004.
33. Wang, Z.; Zhou, L.; El-Boubbou, K.; Ye, X. S.; Huang, X. Multi-component one-pot synthesis of the tumor-associated carbohydrate antigen Globo-H based on preactivation of thioglycosyl donors. *J Org Chem*. **2007**, *72*, 6409-20.
34. Mong, T. K.; Huang, C. Y.; Wong, C. H. A new reactivity-based one-pot synthesis of N-acetyllactosamine oligomers. *J Org Chem*. **2003**, *68*, 2135-42.
35. Hsu, C. H.; Chu, K. C.; Lin, Y. S.; Han, J. L.; Peng, Y. S.; Ren, C. T.; Wu, C. Y.; Wong C. H. Highly alpha-selective sialyl phosphate donors for efficient preparation of natural sialosides. *Chemistry*. **2010**, *16*, 1754-60.
36. Wang, Z.; Zhou, L.; El-Boubbou, K.; Ye, X. S.; Huang, X. Multi-component one-pot synthesis of the tumor-associated carbohydrate antigen Globo-H based on preactivation of thioglycosyl donors. *J Org Chem*. **2007**, *72*, 6409-20.
37. Mong, T. K.; Huang, C. Y.; Wong, C. H. A new reactivity-based one-pot synthesis of N-acetyllactosamine oligomers. *J Org Chem*. **2003**, *68*, 2135-42.
38. Hsu, C. H.; Chu, K. C.; Lin, Y. S.; Han, J. L.; Peng, Y. S.; Ren, C. T.; Wu, C. Y.; Wong C. H. Highly alpha-selective sialyl phosphate donors for efficient preparation of natural sialosides. *Chemistry*. **2010**, *16*, 1754-60.
39. Reuven, E. M.; Leviatan Ben-Arye, S.; Yu, H.; Duchi, R.; Perota, A.; Conchon, S.; Bachar Abramovitch, S.; Soulillou, J. P.; Galli, C.; Chen, X.; Padler-Karavani, V.

Biomimetic Glyconanoparticle Vaccine for Cancer Immunotherapy. *ACS Nano*. **2019**, *13*, 2936-2947.

40. Leviatan Ben-Arye, S.; Yu, H.; Chen, X.; Padler-Karavani, V. Profiling Anti-Neu5Gc IgG in Human Sera with a Sialoglycan Microarray Assay. *J Vis Exp*. **2017**, *125*, 56094.
41. Chithrani, B. D.; Ghazani, A. A.; Chan, W. C. Determining the size and shape dependence of gold nanoparticle uptake into mammalian cells. *Nano Lett*. **2006**, *6*, 662-8.

3.6 NMR and HRMS Spectra:

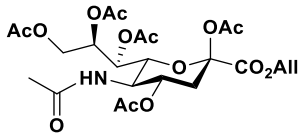

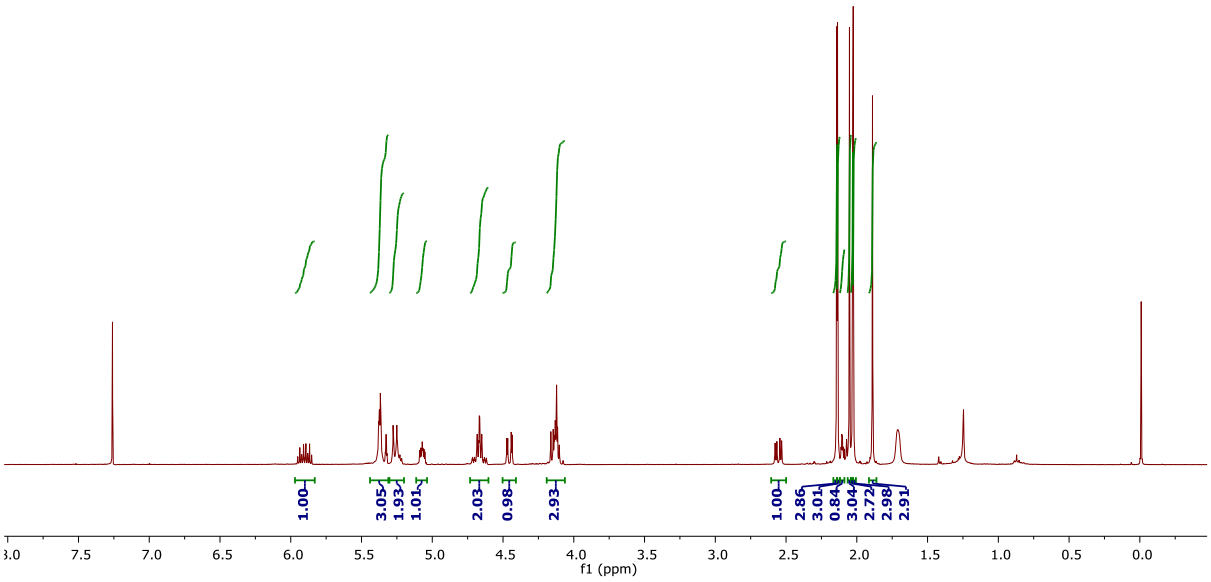

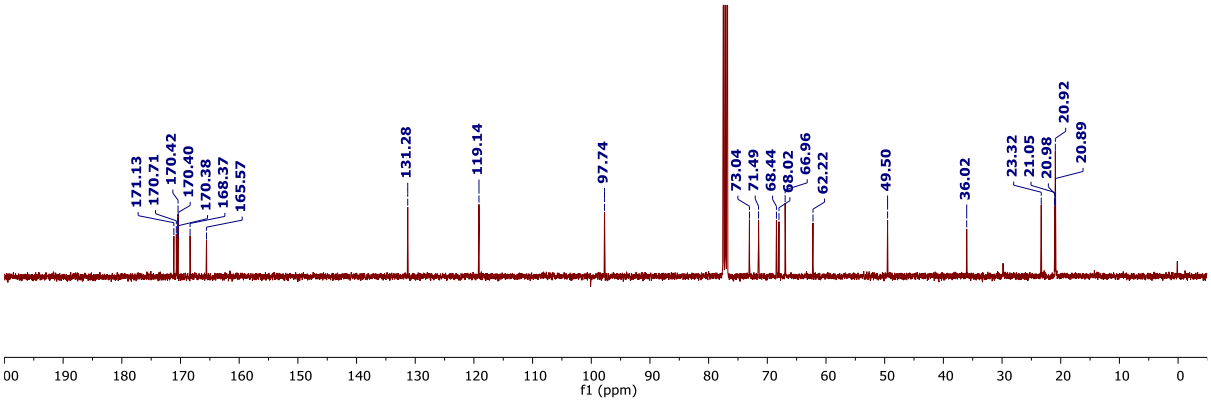

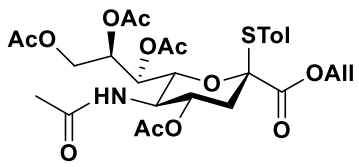
AcO
OAc
OAc
STol
OAll
HN
AcO
O
O
O

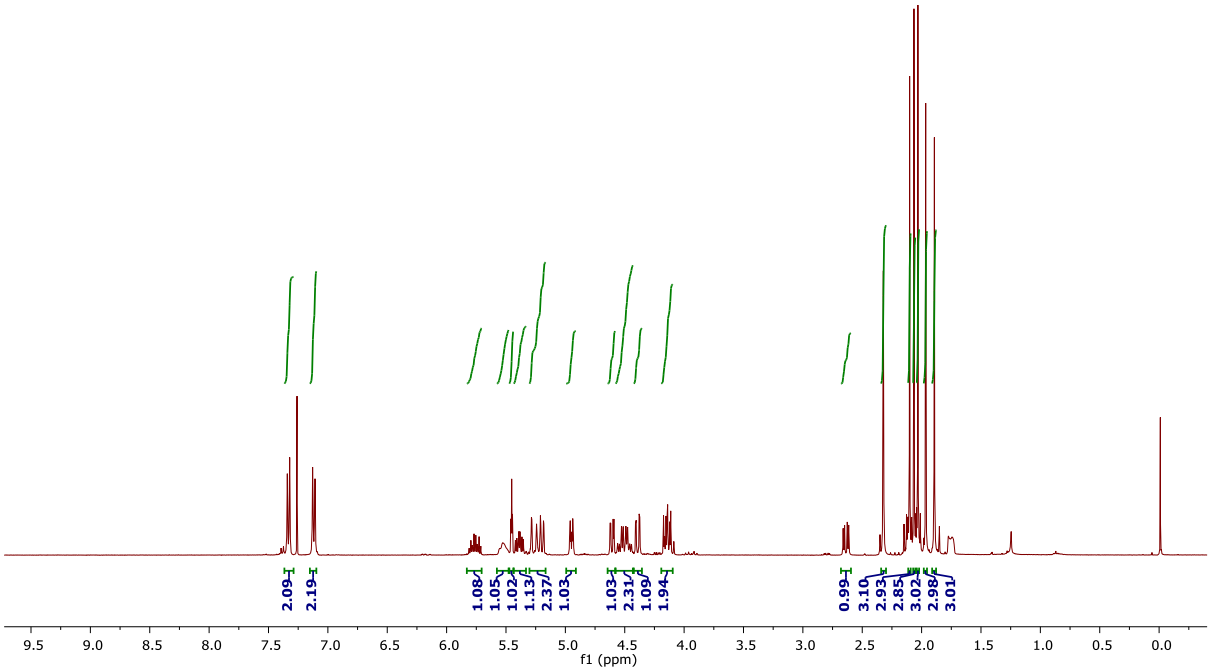
2.09
2.19
1.08
1.05
1.02
1.13
2.37
1.03
1.03
2.31
1.09
1.94
0.99
3.10
2.93
2.85
3.02
2.98
3.01
f1 (ppm)

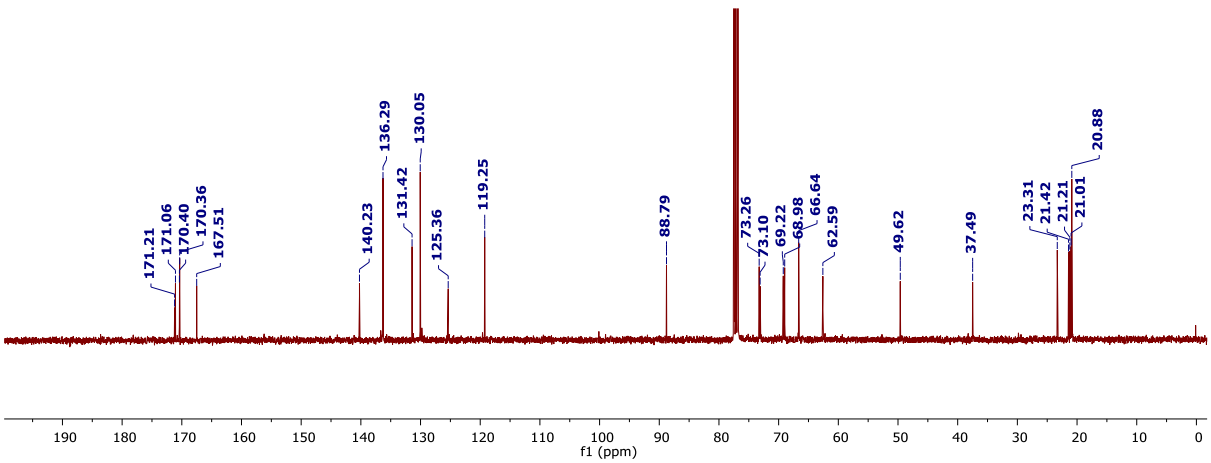
171.21
171.06
170.40
170.36
167.51
140.23
136.29
131.42
130.05
125.36
119.25
88.79
73.26
73.10
69.22
68.98
66.64
62.59
49.62
37.49
23.31
21.42
21.21
21.01
20.88
f1 (ppm)

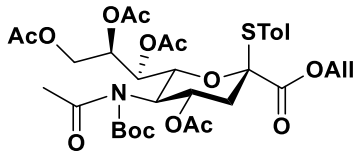
AcO
OAc
OAc
STol
OAll
N
Boc
OAc
O
O
O

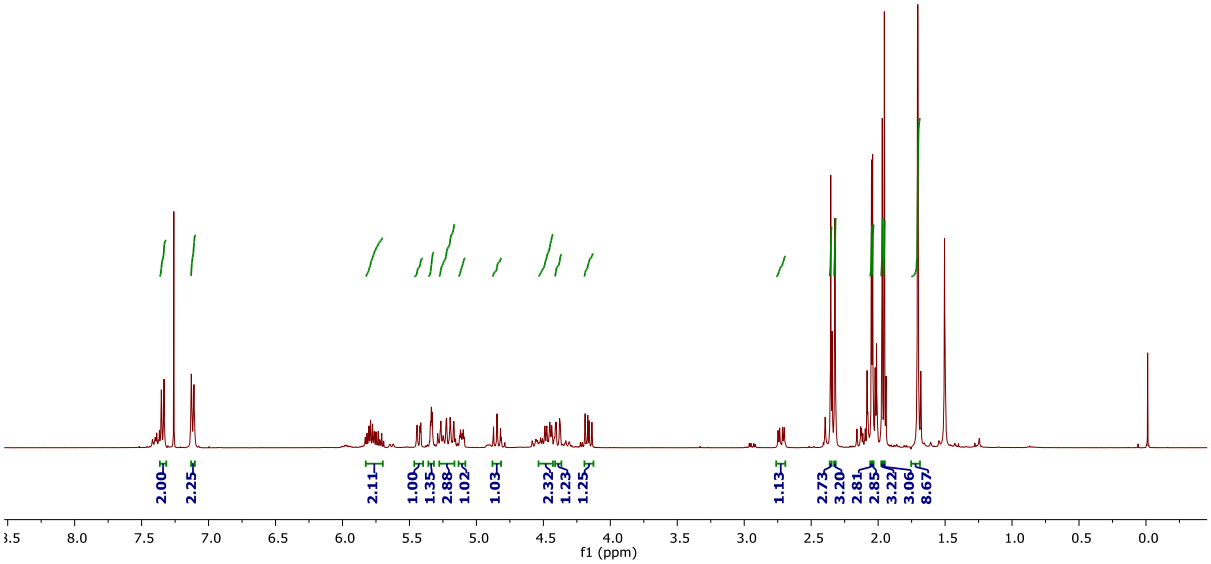
2.00
2.25
2.11
1.00
1.35
2.88
1.02
1.03
2.32
1.23
1.25
1.13
2.73
3.20
2.81
2.85
3.22
3.06
8.67
f1 (ppm)

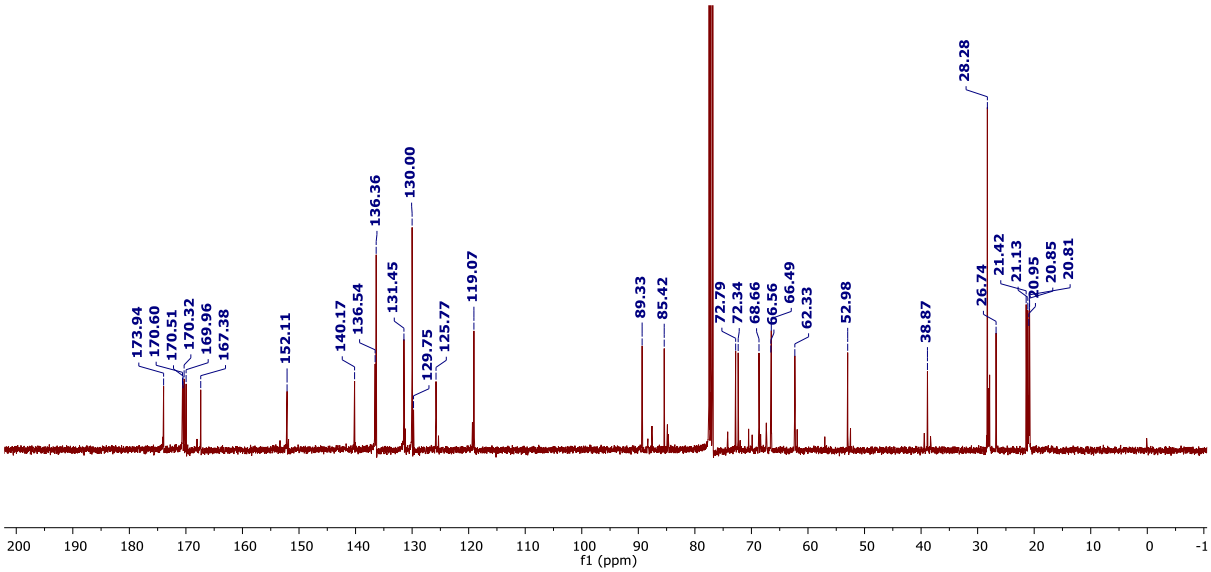
173.94
170.60
170.51
170.32
169.96
167.38
152.11
140.17
136.54
136.36
131.45
130.00
129.75
125.77
119.07
89.33
85.42
72.79
72.34
68.66
66.56
66.49
62.33
52.98
38.87
28.28
26.74
21.42
21.13
20.95
20.85
20.81
f1 (ppm)

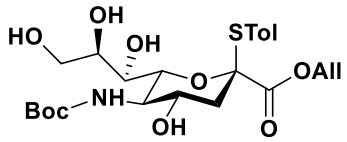
OH
HO
OH
STol
OAll
O
Boc
NH
OH
O

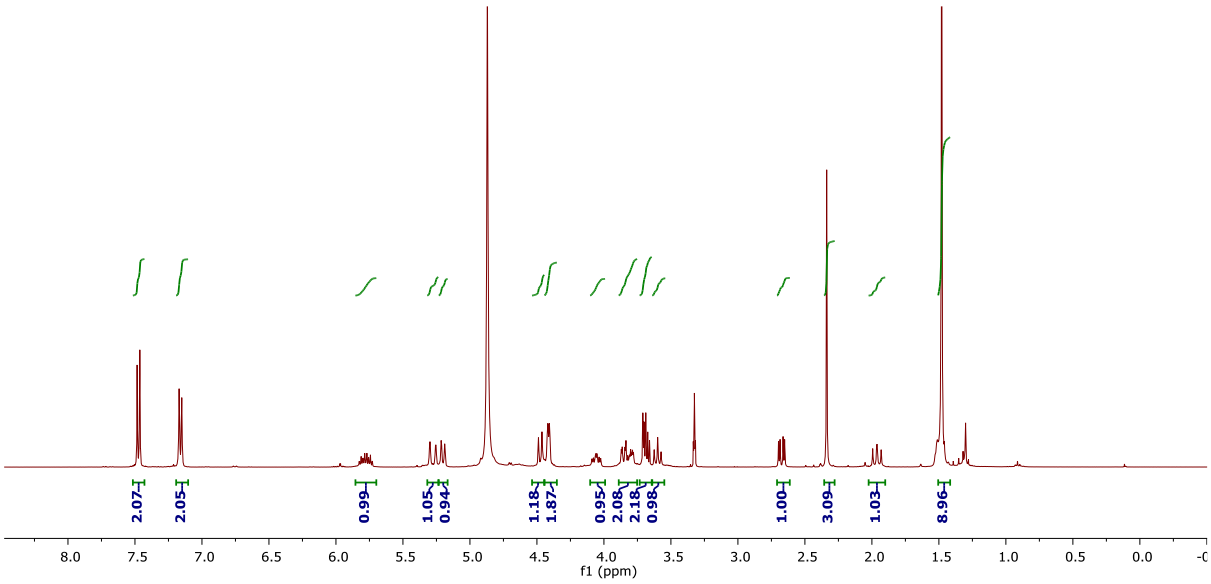
2.07
2.05
0.99
1.05
0.94
1.18
1.87
0.95
2.08
2.18
0.98
1.00
3.09
1.03
8.96
f1 (ppm)

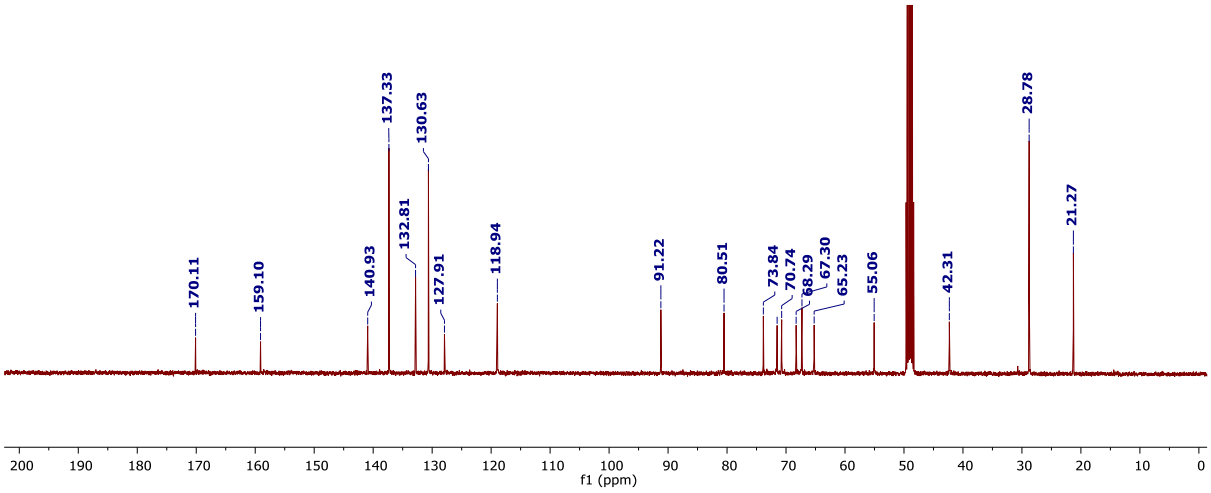
170.11
159.10
140.93
137.33
132.81
130.63
127.91
118.94
91.22
80.51
73.84
70.74
68.29
67.30
65.23
55.06
42.31
28.78
21.27
f1 (ppm)

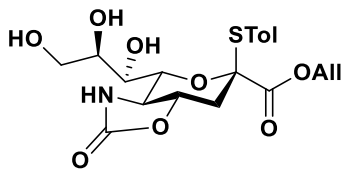
HO
OH
OH
HN
O
O
O
STol
OAll
O

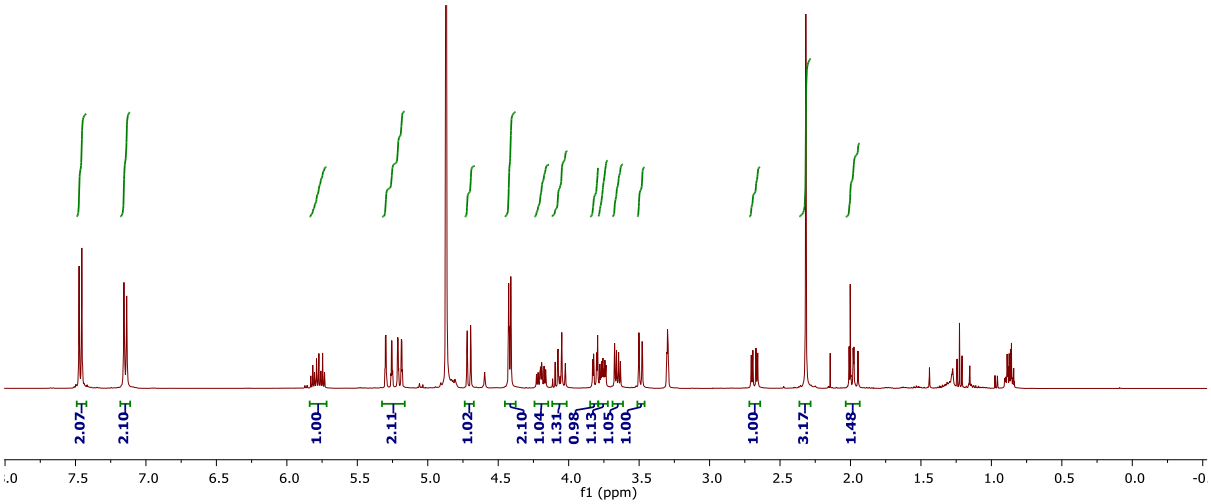
2.07
2.10
1.00
2.11
1.02
2.10
1.04
1.31
0.98
1.13
1.05
1.00
1.00
3.17
1.48
f1 (ppm)

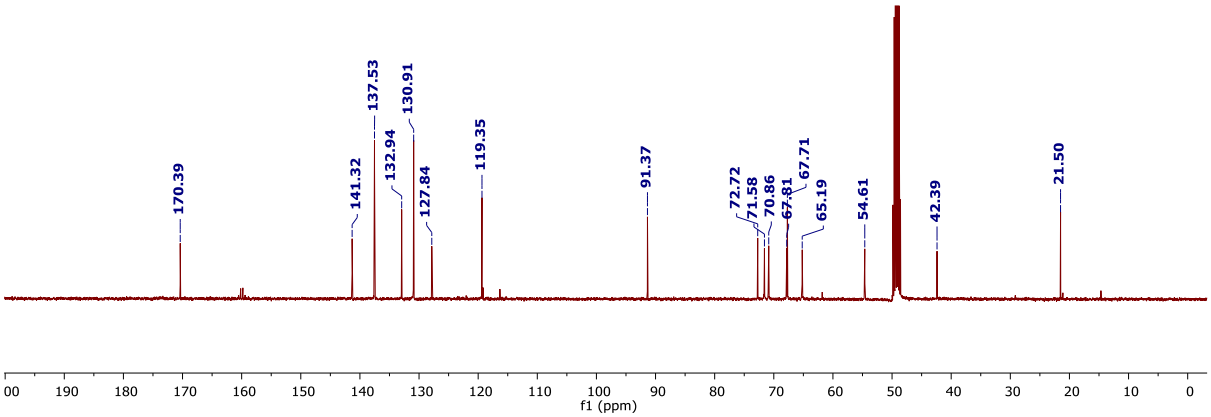
170.39
141.32
137.53
132.94
130.91
127.84
119.35
91.37
72.72
71.58
70.86
67.81
67.71
65.19
54.61
42.39
21.50
f1 (ppm)

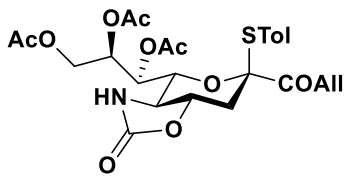
OAc
AcO
OAc
STol
HN
O
COAll
O
O

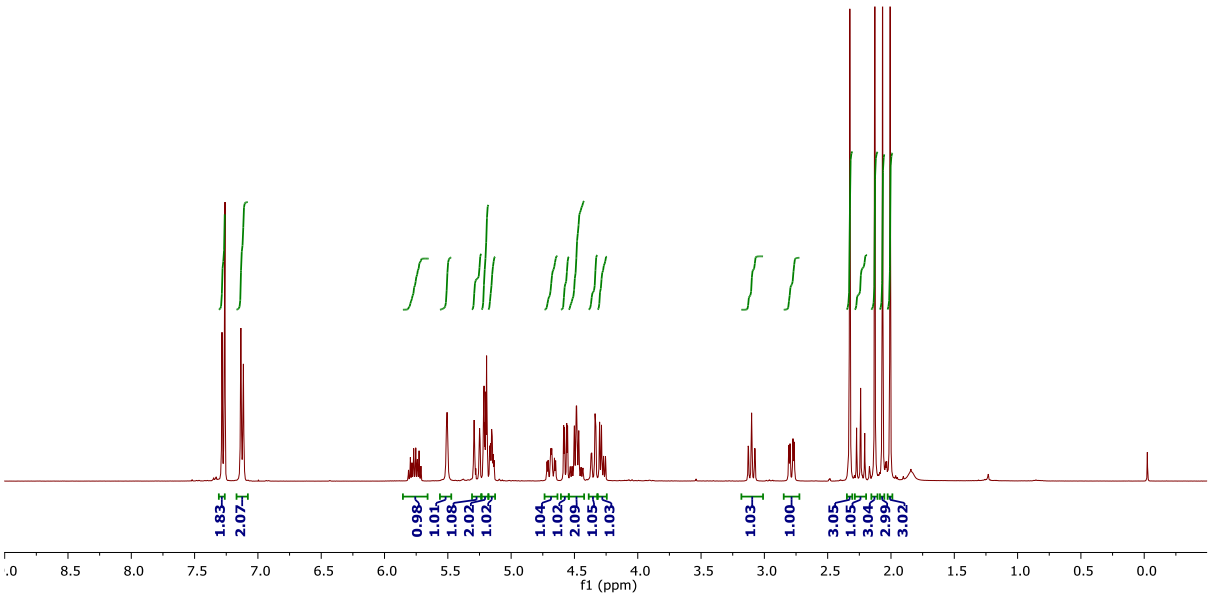
1.83
2.07
0.98
1.01
1.08
2.02
1.02
1.04
1.02
2.09
1.05
1.03
1.03
1.00
3.05
1.05
3.04
2.99
3.02
f1 (ppm)

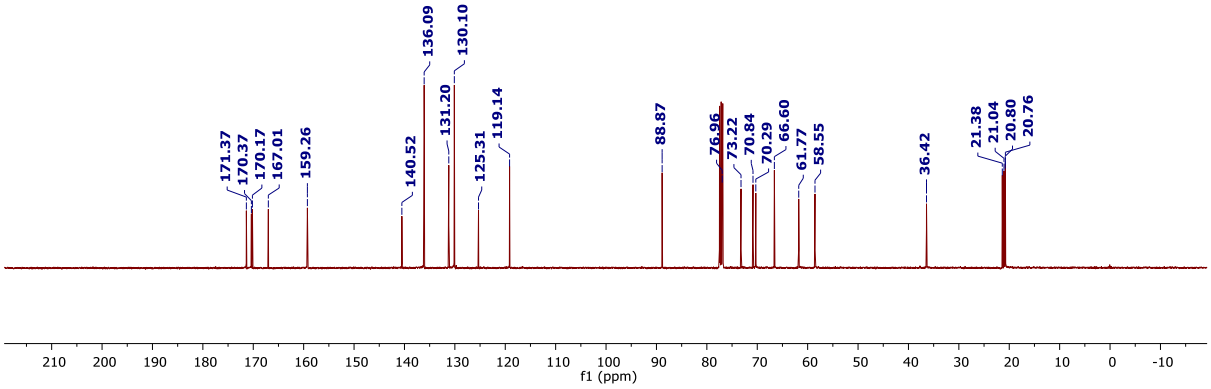
171.37
170.37
170.17
167.01
159.26
140.52
136.09
131.20
130.10
125.31
119.14
88.87
76.96
73.22
70.84
70.29
66.60
61.77
58.55
36.42
21.38
21.04
20.80
20.76
f1 (ppm)

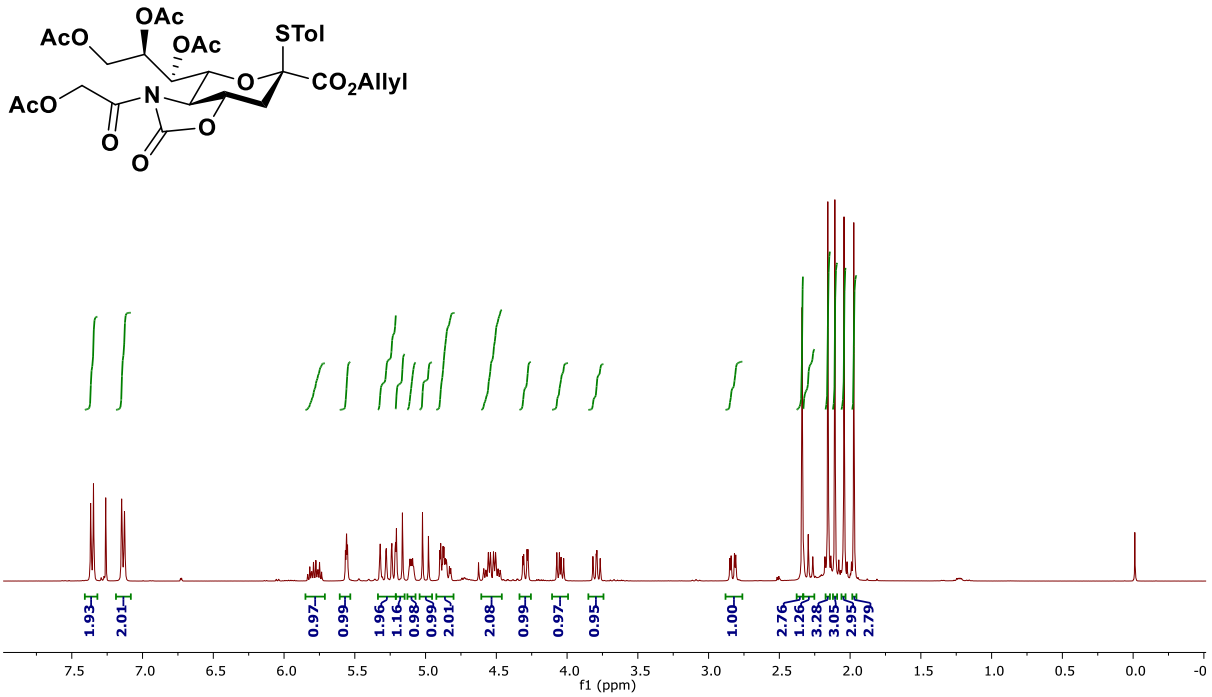
OAc
AcO
OAc
STol
O
CO2Allyl
AcO
N
O
O
O
1.93
2.01
0.97
0.99
1.96
1.16
0.98
0.99
2.01
2.08
0.99
0.97
0.95
1.00
2.76
1.26
3.28
3.05
2.95
2.79
f1 (ppm)

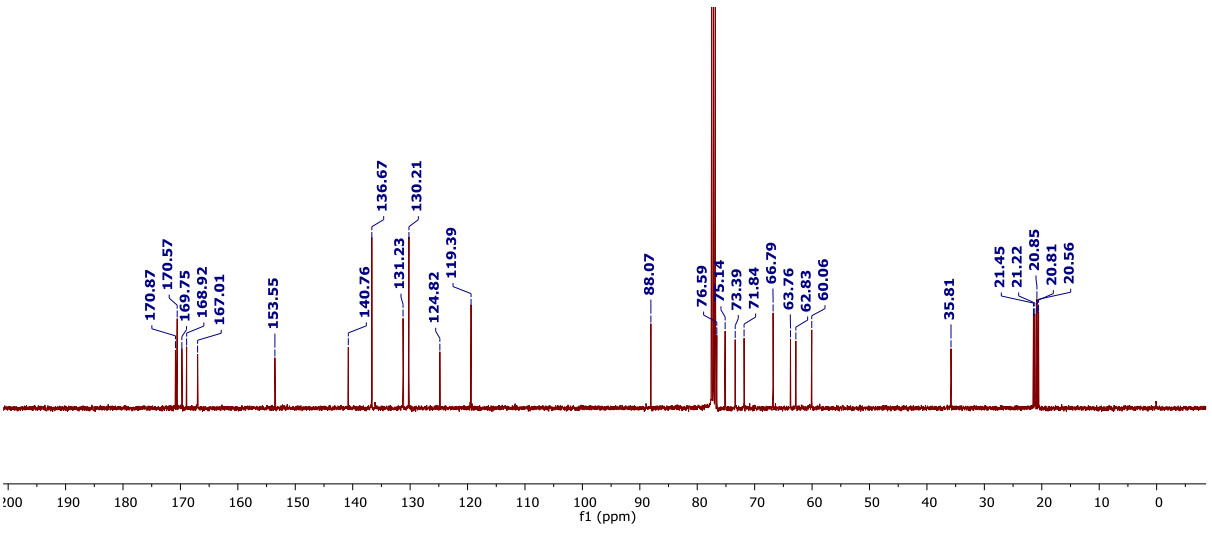
170.87
170.57
169.75
168.92
167.01
153.55
140.76
136.67
131.23
130.21
124.82
119.39
88.07
76.59
75.14
73.39
71.84
66.79
63.76
62.83
60.06
35.81
21.45
21.22
20.85
20.81
20.56
f1 (ppm)

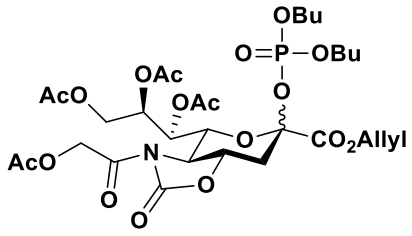
OBu
O=P–OBu
O
OAc
AcO
OAc
O
CO2Allyl
AcO
N
O
O
O

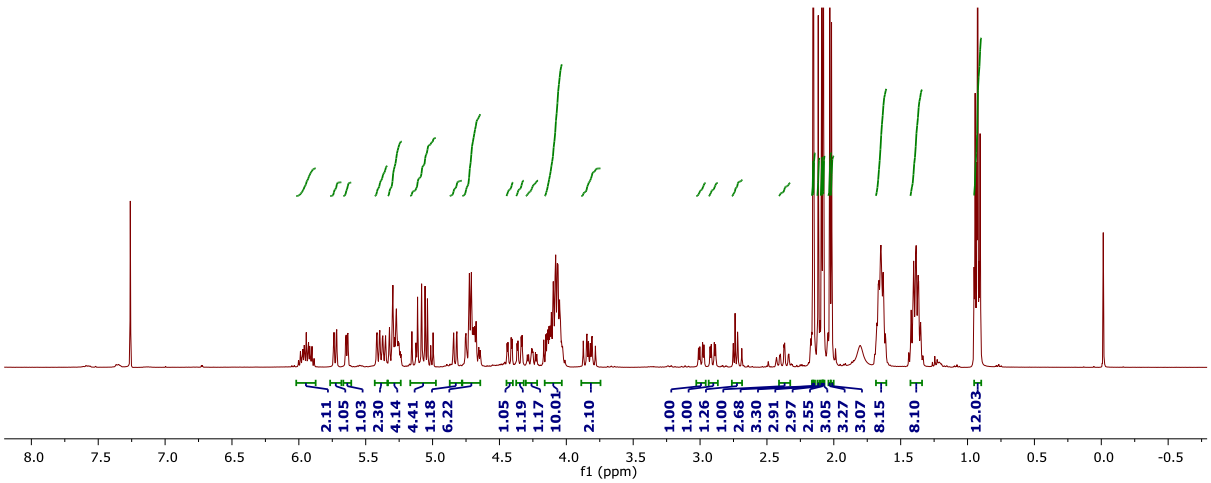
2.11
1.05
1.03
2.30
4.14
4.41
1.18
6.22
1.05
1.19
1.17
10.01
2.10
1.00
1.00
1.26
1.00
2.68
3.30
2.91
2.97
2.55
3.05
3.27
3.07
8.15
8.10
12.03
f1 (ppm)

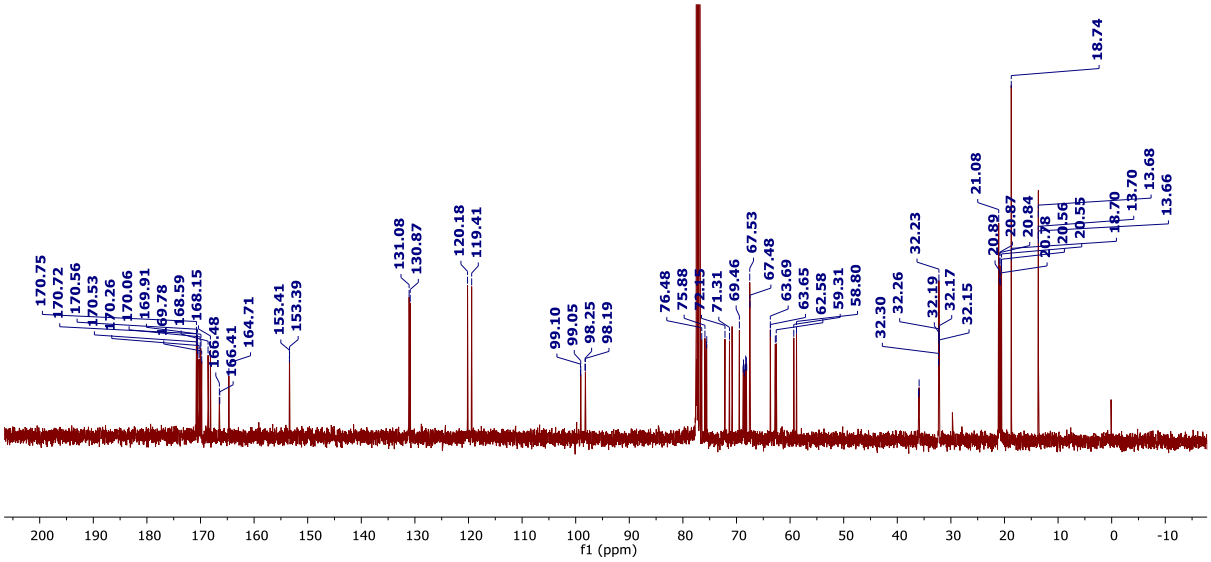
170.75
170.72
170.56
170.53
170.26
170.06
169.91
169.78
168.59
168.15
166.48
166.41
164.71
153.41
153.39
131.08
130.87
120.18
119.41
99.10
99.05
98.25
98.19
76.48
75.88
72.15
71.31
69.46
67.53
67.48
63.69
63.65
62.58
59.31
58.80
32.30
32.26
32.23
32.19
32.17
32.15
21.08
20.89
20.87
20.84
20.78
20.56
20.55
18.74
18.70
13.68
13.66
f1 (ppm)

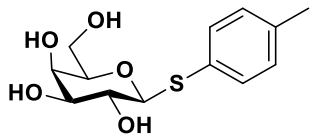
OH
HO
O
S
HO
OH

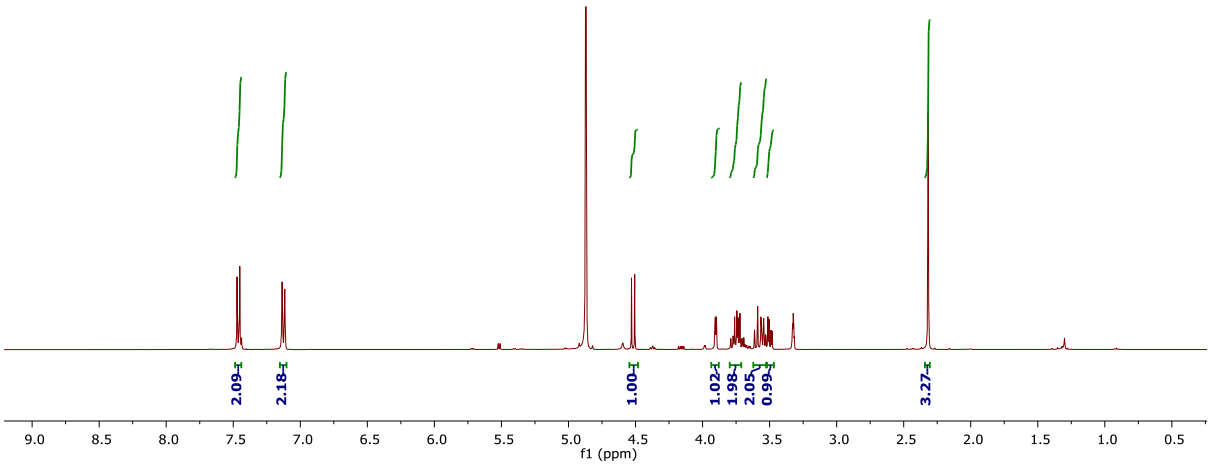
2.09
2.18
1.00
1.02
1.98
2.05
0.99
3.27
9.0
8.5
8.0
7.5
7.0
6.5
6.0
5.5
5.0
4.5
4.0
3.5
3.0
2.5
2.0
1.5
1.0
0.5
f1 (ppm)

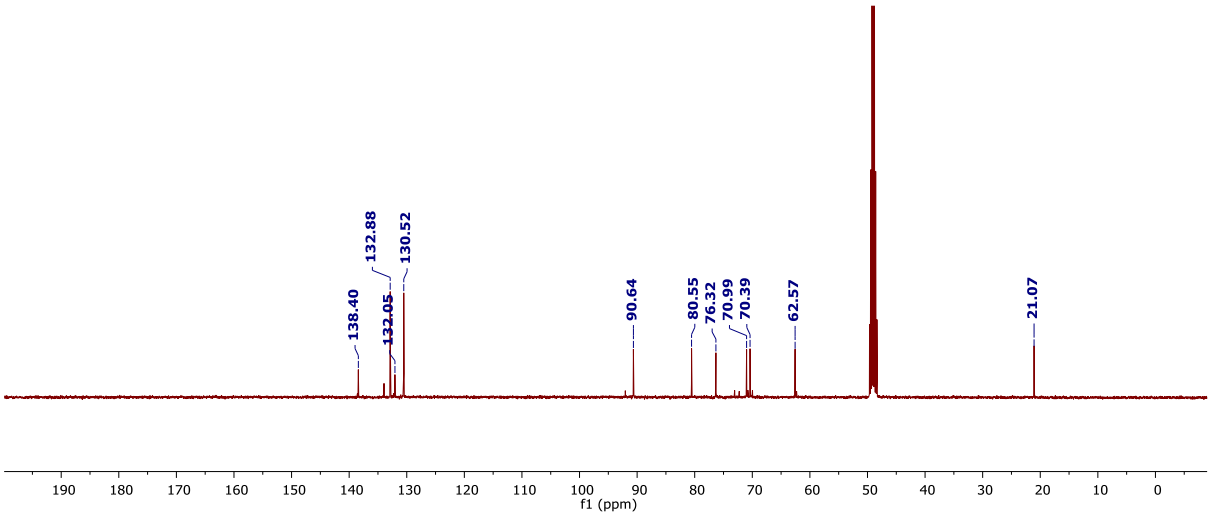
138.40
132.88
132.05
130.52
90.64
80.55
76.32
70.99
70.39
62.57
21.07
190
180
170
160
150
140
130
120
110
100
90
80
70
60
50
40
30
20
10
0
f1 (ppm)

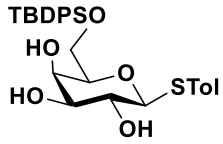
TBDPSO
HO
O
STol
HO
OH

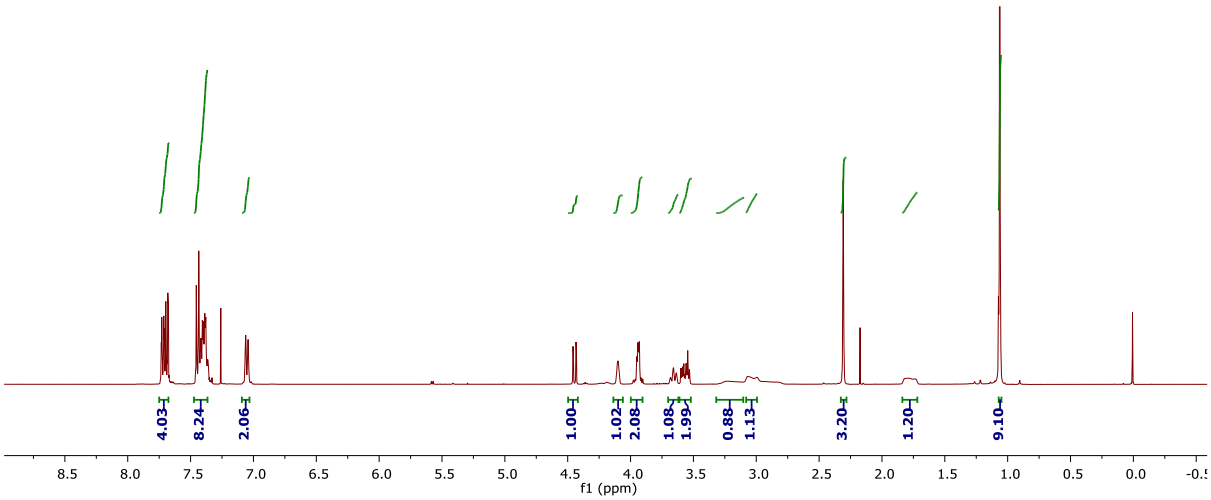
4.03
8.24
2.06
1.00
1.02
2.08
1.08
1.99
0.88
1.13
3.20
1.20
9.10
8.5
8.0
7.5
7.0
6.5
6.0
5.5
5.0
4.5
4.0
3.5
3.0
2.5
2.0
1.5
1.0
0.5
0.0
f1 (ppm)

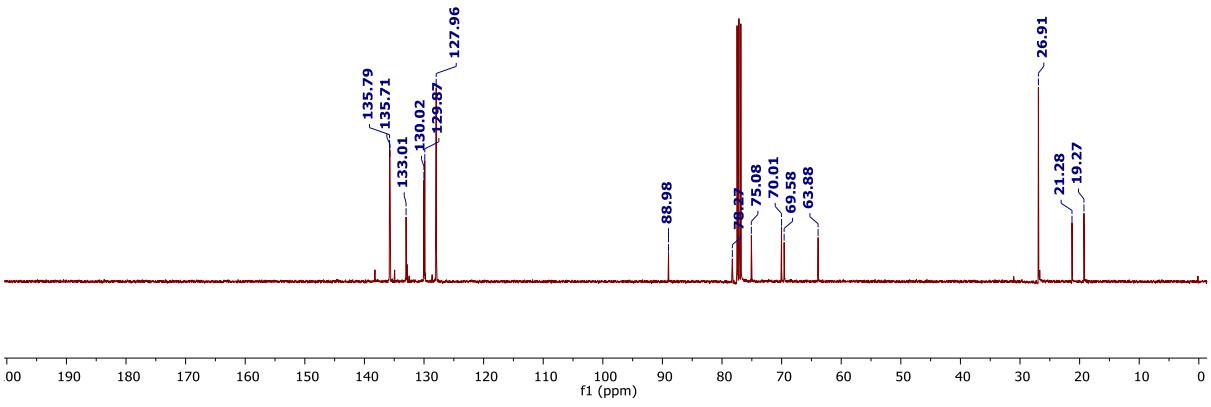
135.79
135.71
133.01
130.02
129.87
127.96
88.98
78.27
75.08
70.01
69.58
63.88
26.91
21.28
19.27
190
180
170
160
150
140
130
120
110
100
90
80
70
60
50
40
30
20
10
0
f1 (ppm)

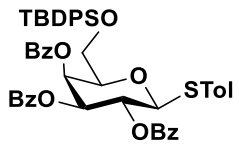
TBDPSO
BzO
O
STol
BzO
OBz

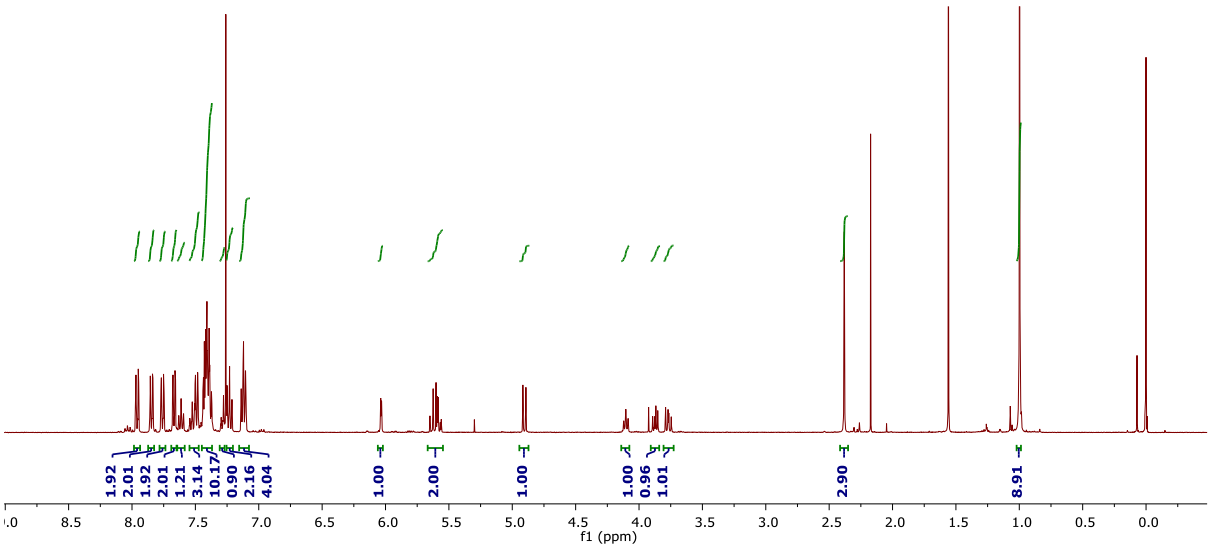
1.92
2.01
1.92
2.01
1.21
3.14
10.17
0.90
2.16
4.04
1.00
2.00
1.00
1.00
0.96
1.01
2.90
8.91
f1 (ppm)

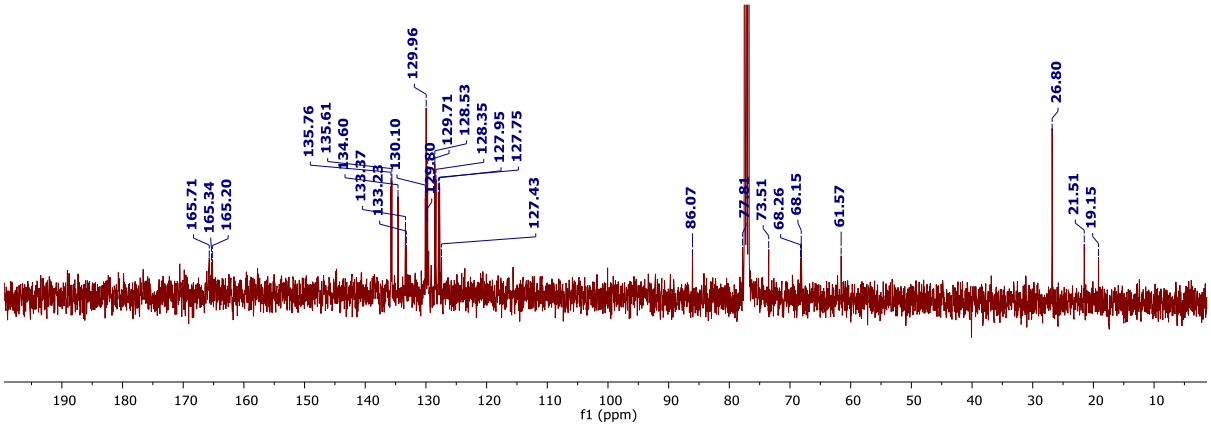
165.71
165.34
165.20
135.76
135.61
134.60
133.37
133.23
130.10
129.96
129.80
129.71
128.53
128.35
127.95
127.75
127.43
86.07
77.84
73.51
68.26
68.15
61.57
26.80
21.51
19.15
f1 (ppm)

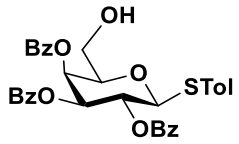
OH
BzO
O
STol
BzO
OBz

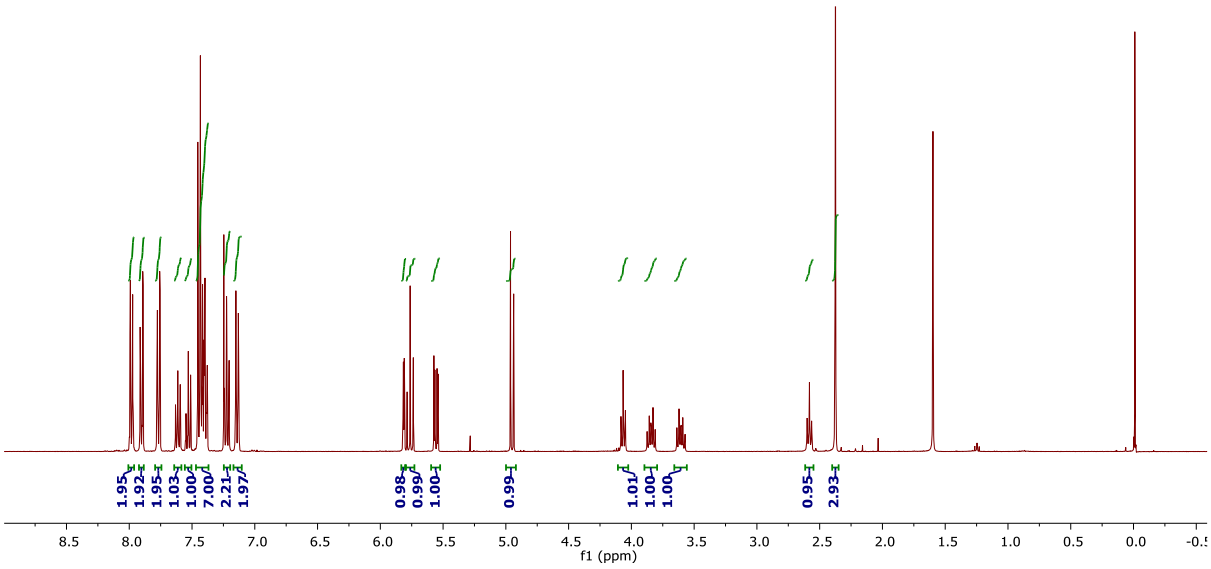
1.95
1.92
1.95
1.03
1.00
7.00
2.21
1.97
0.98
0.99
1.00
0.99
1.01
1.00
1.00
0.95
2.93
8.5
8.0
7.5
7.0
6.5
6.0
5.5
5.0
4.5
4.0
3.5
3.0
2.5
2.0
1.5
1.0
0.5
0.0
f1 (ppm)

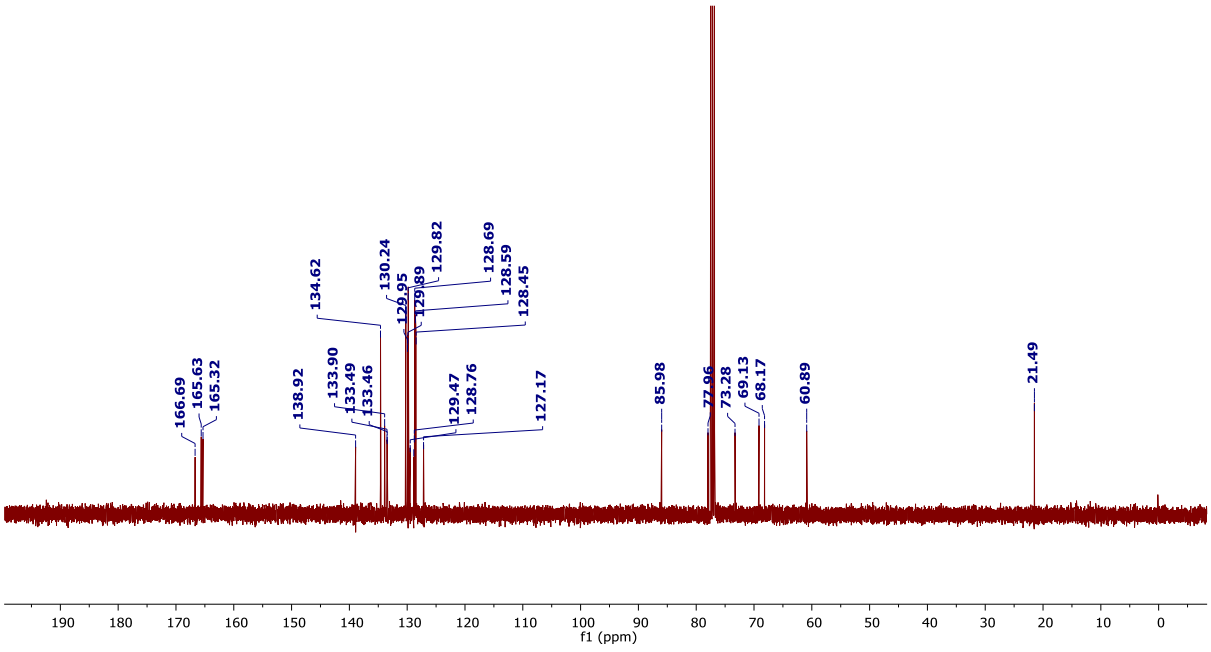
166.69
165.63
165.32
138.92
134.62
133.90
133.49
133.46
130.24
129.95
129.89
129.82
129.47
128.76
128.69
128.59
128.45
127.17
85.98
77.96
73.28
69.13
68.17
60.89
21.49
190
180
170
160
150
140
130
120
110
100
90
80
70
60
50
40
30
20
10
0
f1 (ppm)

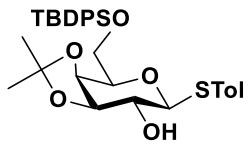
TBDPSO
O
O
O
STol
OH

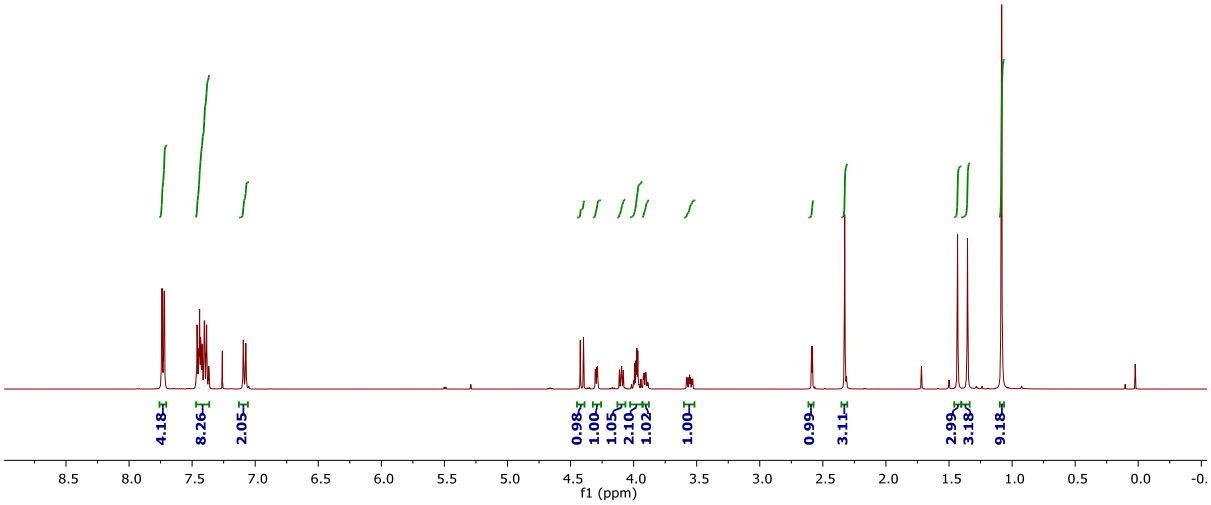
4.18
8.26
2.05
0.98
1.00
1.05
2.10
1.02
1.00
0.99
3.11
2.99
3.18
9.18
f1 (ppm)

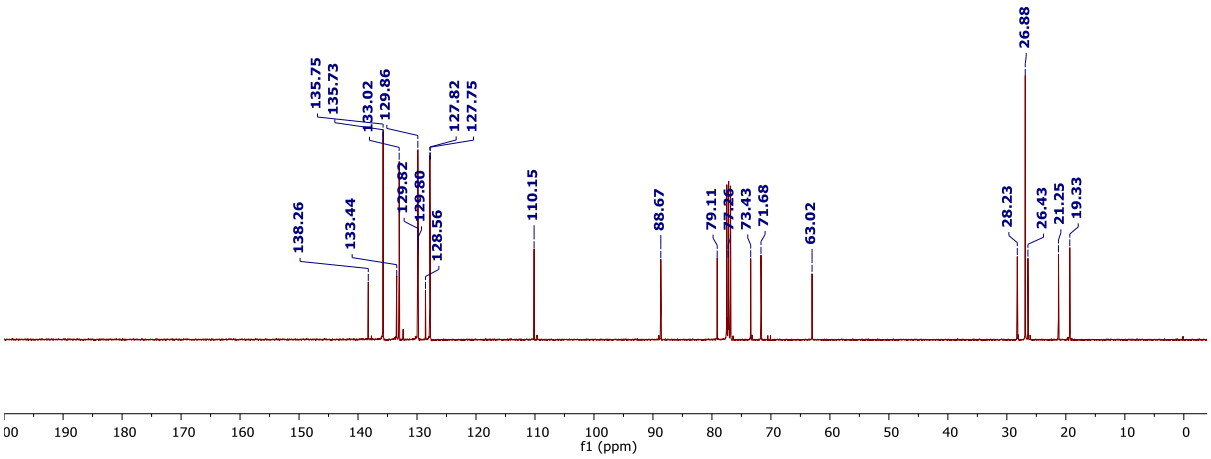
135.75
135.73
133.02
129.86
127.82
127.75
138.26
133.44
129.82
129.80
128.56
110.15
88.67
79.11
77.26
73.43
71.68
63.02
26.88
28.23
26.43
21.25
19.33
f1 (ppm)

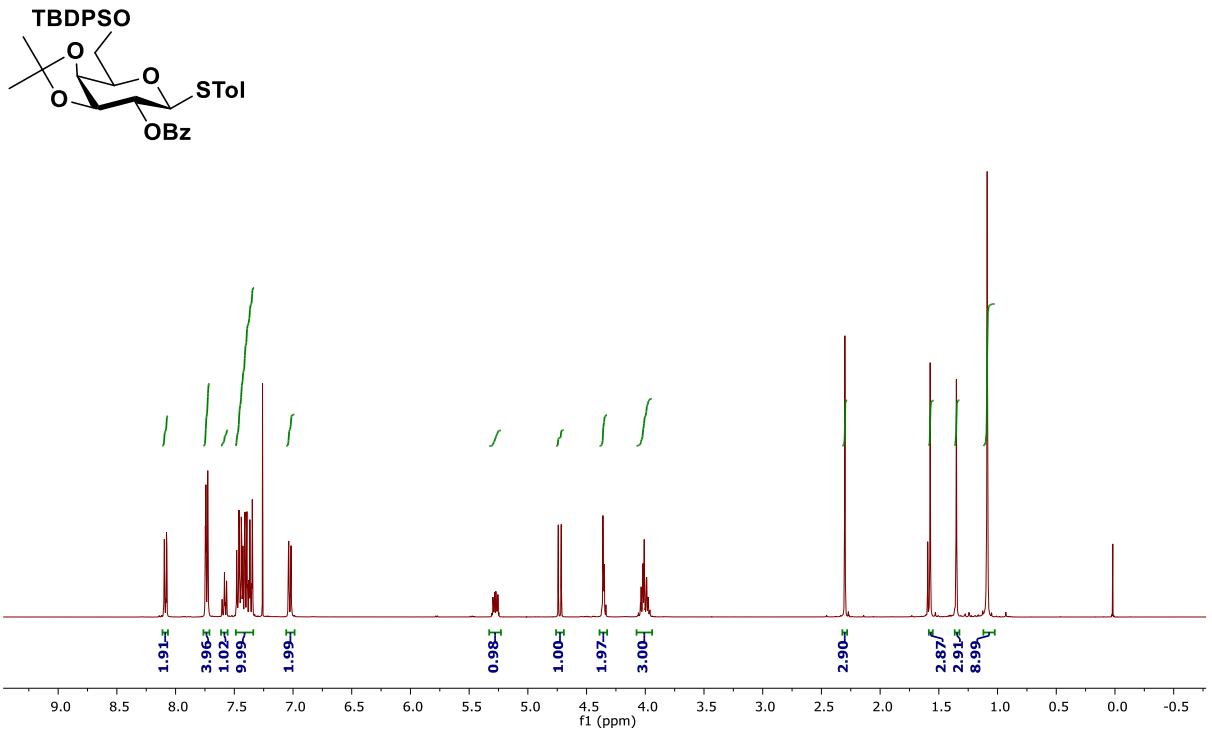
TBDPSO
O
O
O
STol
OBz
1.91
3.96
1.02
9.99
1.99
0.98
1.00
1.97
3.00
2.90
2.87
2.91
8.99
f1 (ppm)

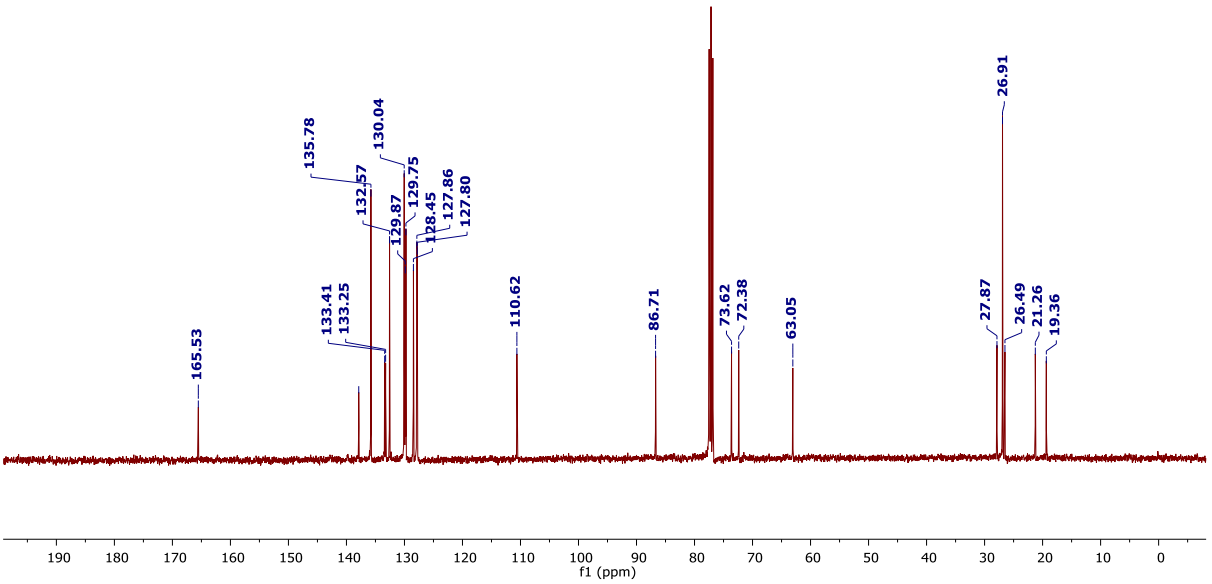
165.53
135.78
133.41
133.25
132.57
130.04
129.87
129.75
128.45
127.86
127.80
110.62
86.71
73.62
72.38
63.05
27.87
26.91
26.49
21.26
19.36
f1 (ppm)

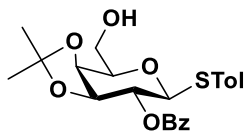
OH
O
O
O
STol
OBz

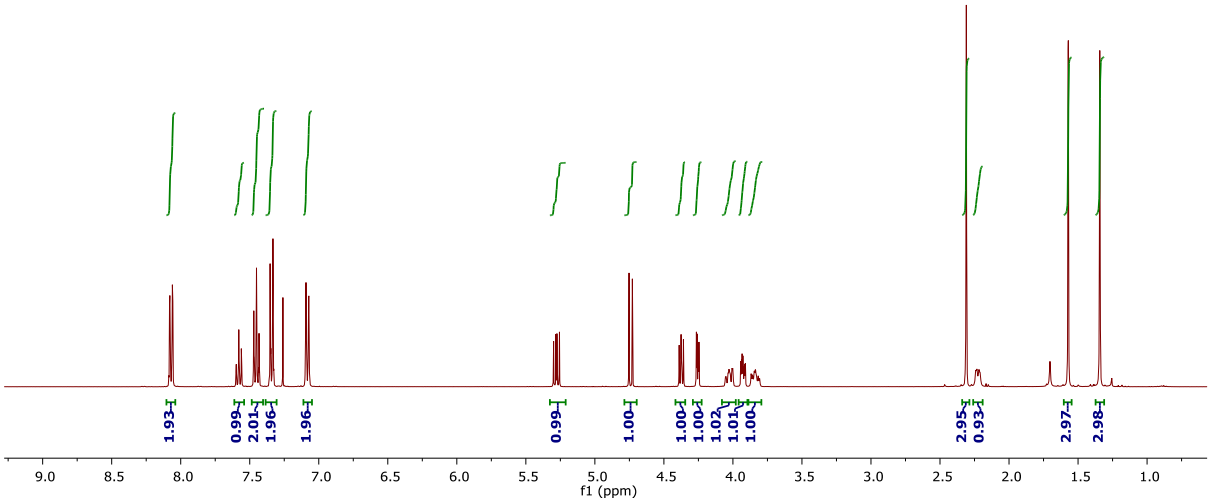
1.93
0.99
2.01
1.96
1.96
0.99
1.00
1.00
1.00
1.02
1.01
1.00
2.95
0.93
2.97
2.98
9.0
8.5
8.0
7.5
7.0
6.5
6.0
5.5
5.0
4.5
4.0
3.5
3.0
2.5
2.0
1.5
1.0
f1 (ppm)

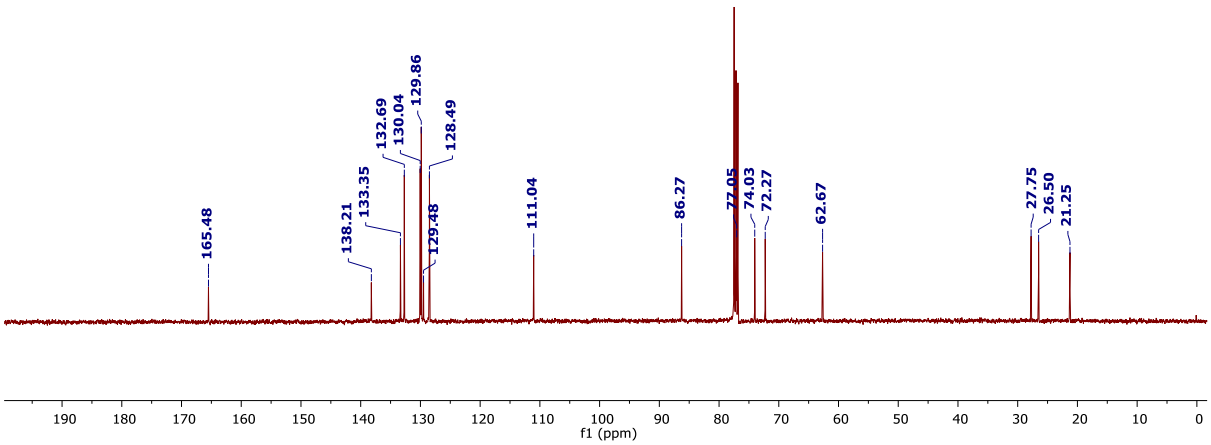
165.48
138.21
133.35
132.69
130.04
129.86
129.48
128.49
111.04
86.27
77.05
74.03
72.27
62.67
27.75
26.50
21.25
190
180
170
160
150
140
130
120
110
100
90
80
70
60
50
40
30
20
10
0
f1 (ppm)

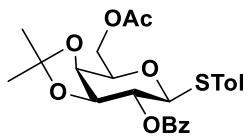
OAc
O
O
O
STol
OBz

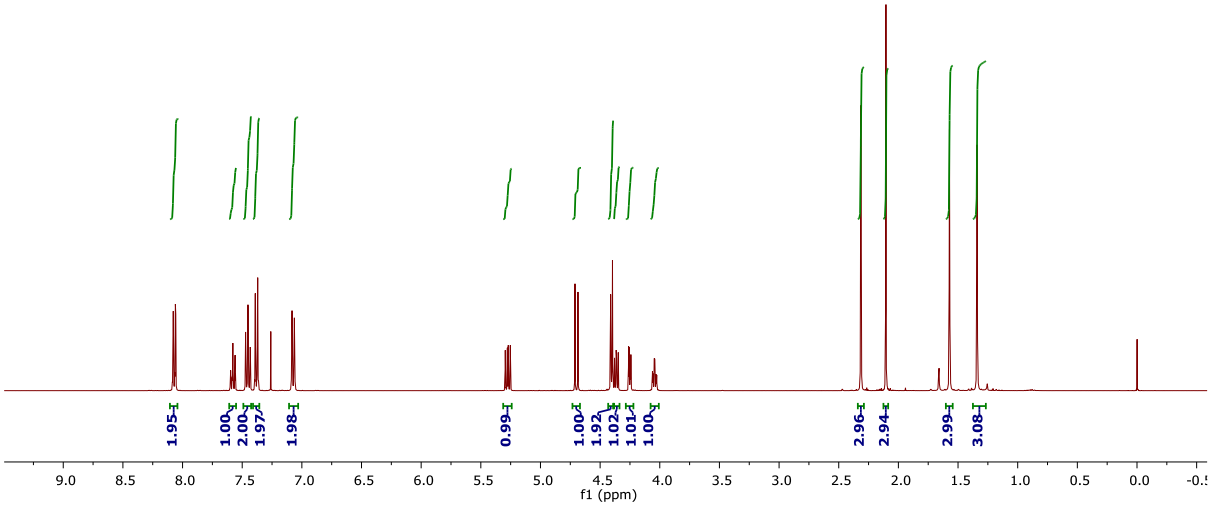
1.95
1.00
2.00
1.97
1.98
0.99
1.00
1.92
1.02
1.01
1.00
2.96
2.94
2.99
3.08
9.0
8.5
8.0
7.5
7.0
6.5
6.0
5.5
5.0
4.5
4.0
3.5
3.0
2.5
2.0
1.5
1.0
0.5
0.0
f1 (ppm)

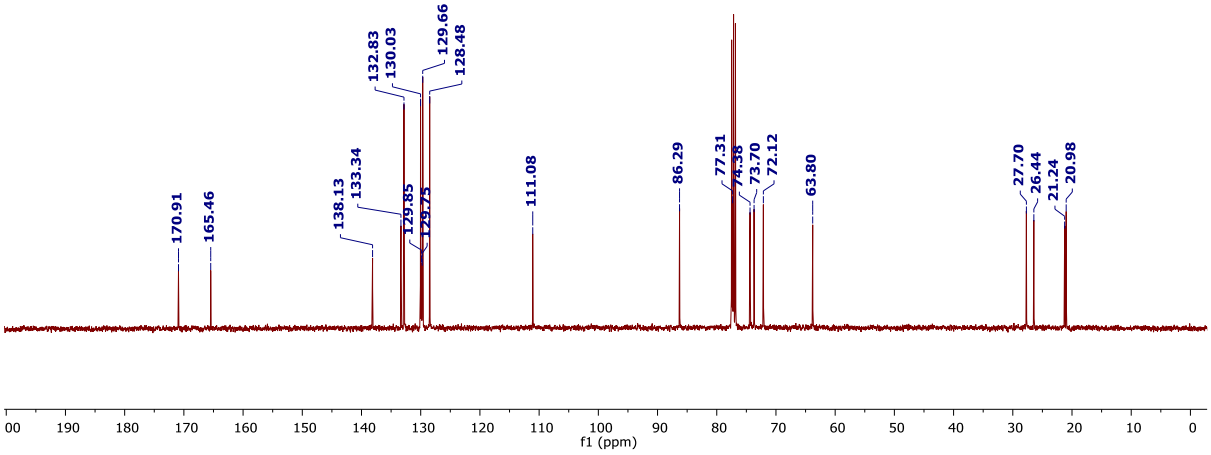
170.91
165.46
138.13
133.34
132.83
130.03
129.85
129.75
129.66
128.48
111.08
86.29
77.31
74.38
73.70
72.12
63.80
27.70
26.44
21.24
20.98
190
180
170
160
150
140
130
120
110
100
90
80
70
60
50
40
30
20
10
0
f1 (ppm)

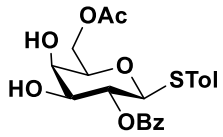
OAc
HO
O
STol
HO
OBz

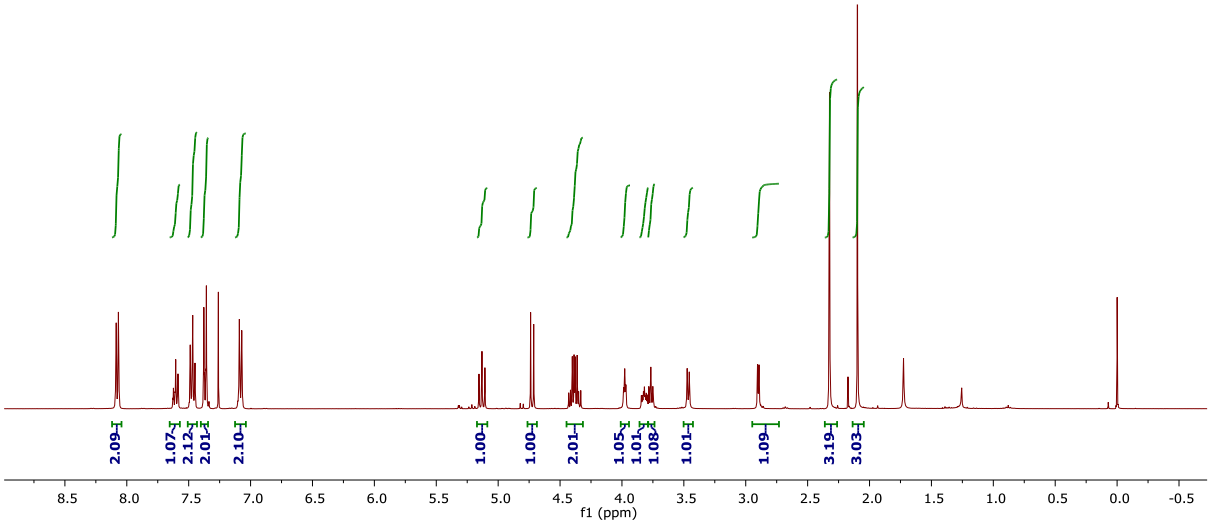
2.09
1.07
2.12
2.01
2.10
1.00
1.00
2.01
1.05
1.01
1.08
1.01
1.09
3.19
3.03
8.5 8.0 7.5 7.0 6.5 6.0 5.5 5.0 4.5 4.0 3.5 3.0 2.5 2.0 1.5 1.0 0.5 0.0 -0.5
f1 (ppm)

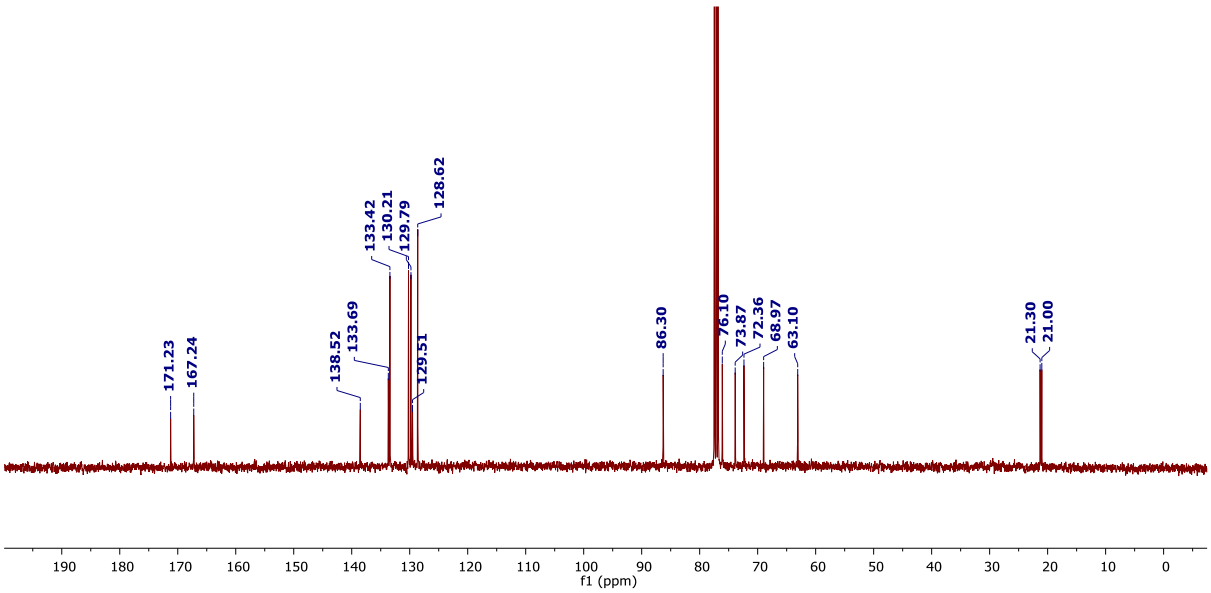
171.23
167.24
138.52
133.69
133.42
130.21
129.79
129.51
128.62
86.30
76.10
73.87
72.36
68.97
63.10
21.30
21.00
190 180 170 160 150 140 130 120 110 100 90 80 70 60 50 40 30 20 10 0
f1 (ppm)

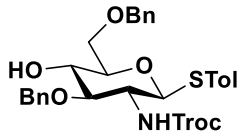
OBn
HO
O
STol
BnO
NHTroc

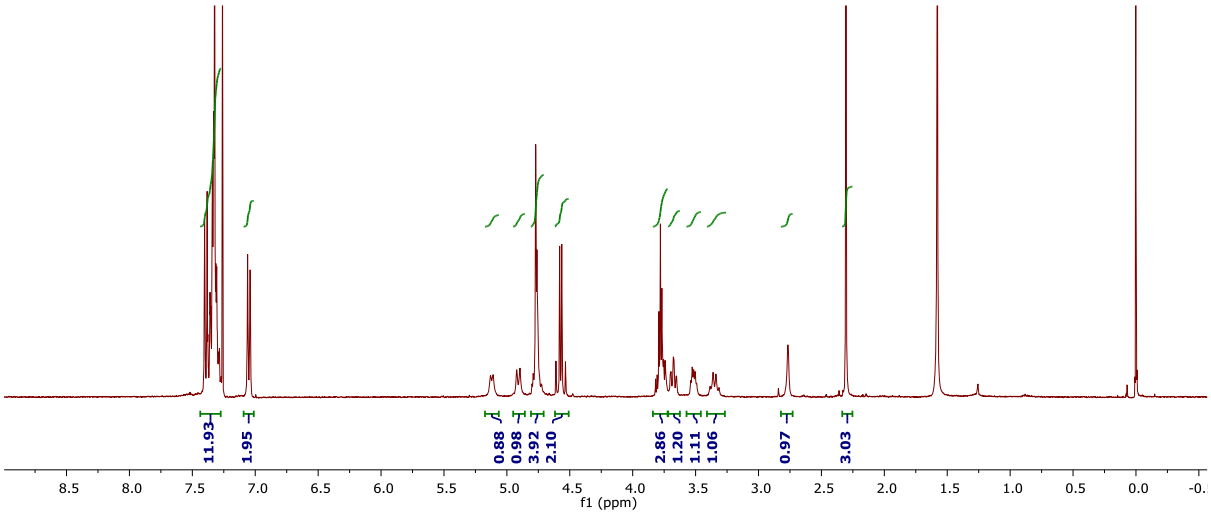
11.93
1.95
0.88
0.98
3.92
2.10
2.86
1.20
1.11
1.06
0.97
3.03
f1 (ppm)

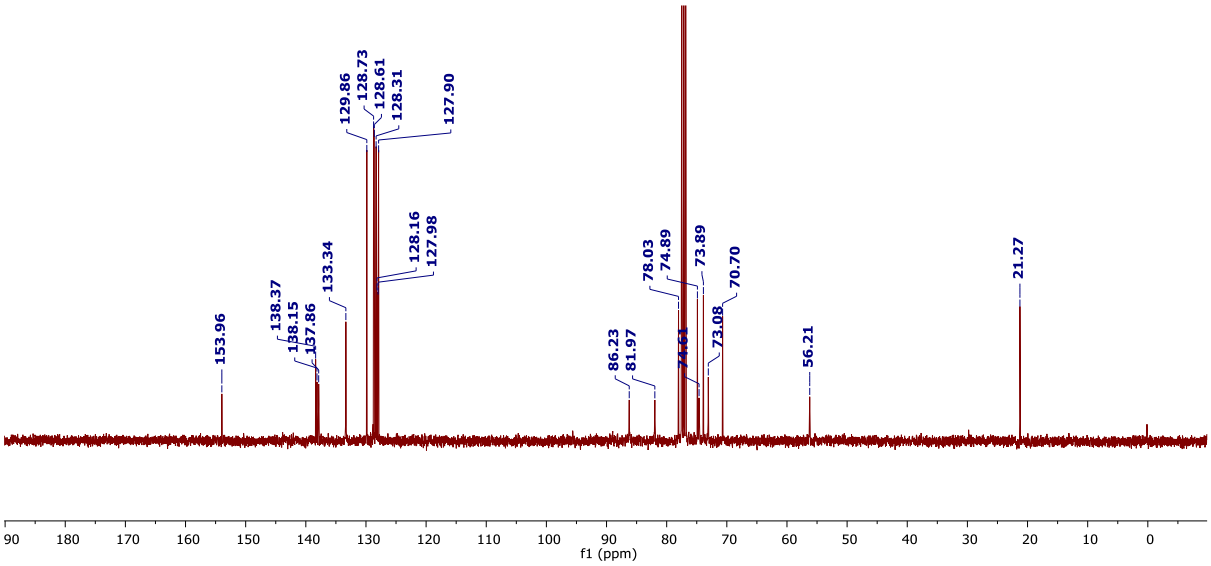
153.96
138.37
138.15
137.86
133.34
129.86
128.73
128.61
128.31
128.16
127.98
127.90
86.23
81.97
78.03
74.89
74.61
73.89
73.08
70.70
56.21
21.27
f1 (ppm)

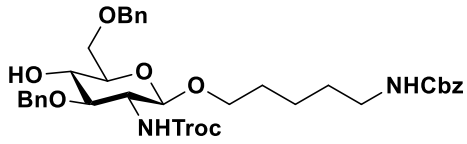
OBn
HO
O
O
NHCbz
BnO
NHTroc

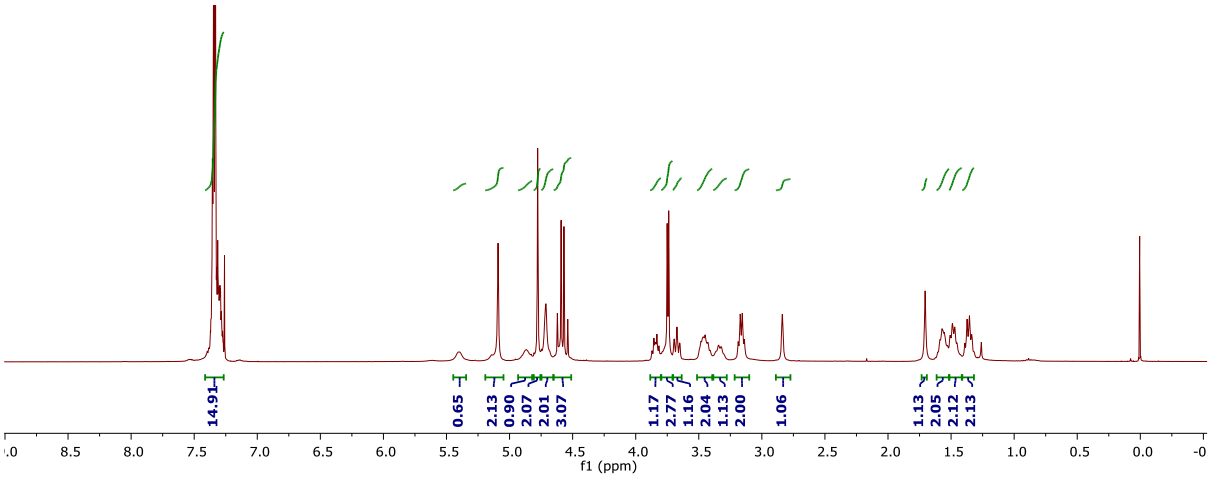
14.91
0.65
2.13
0.90
2.07
2.01
3.07
1.17
2.77
1.16
2.04
1.13
2.00
1.06
1.13
2.05
2.12
2.13
f1 (ppm)

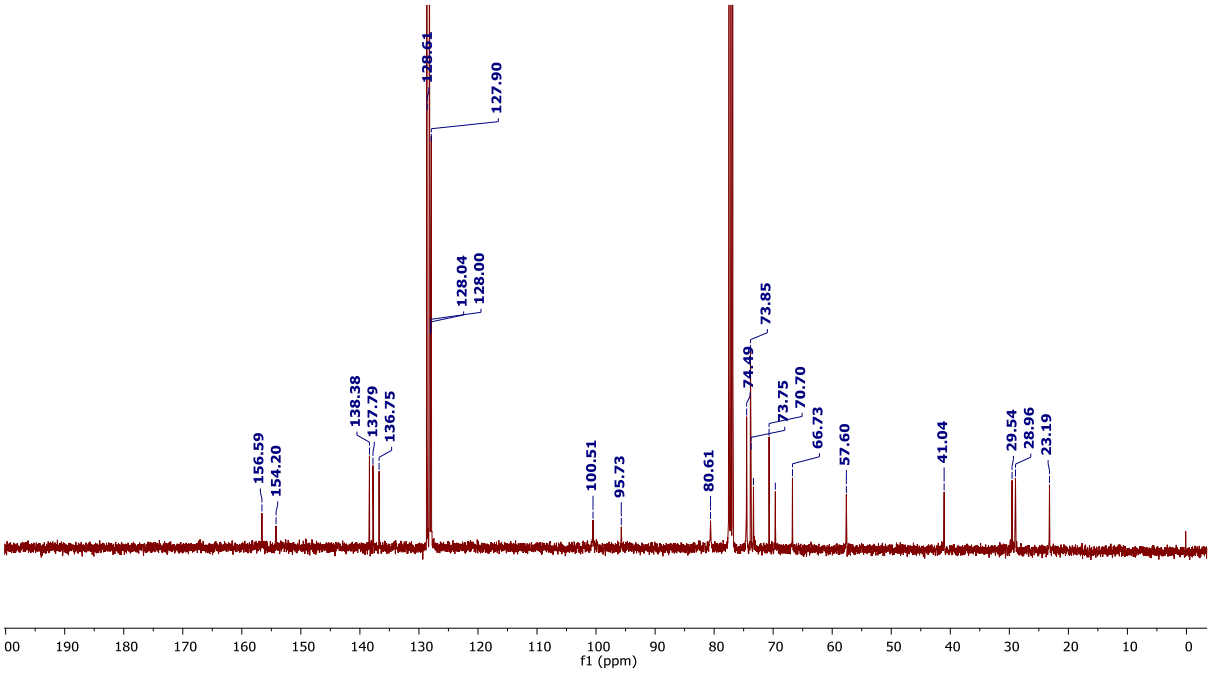
138.61
127.90
128.04
128.00
73.85
74.49
73.75
70.70
66.73
57.60
41.04
29.54
28.96
23.19
156.59
154.20
138.38
137.79
136.75
100.51
95.73
80.61
f1 (ppm)

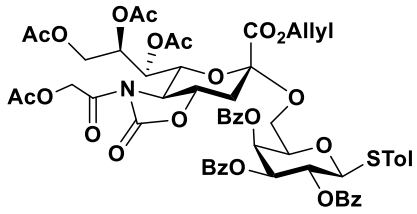
OAc
AcO
OAc
CO2Allyl
AcO
N
O
BzO
O
O
O
O
BzO
STol
OBz

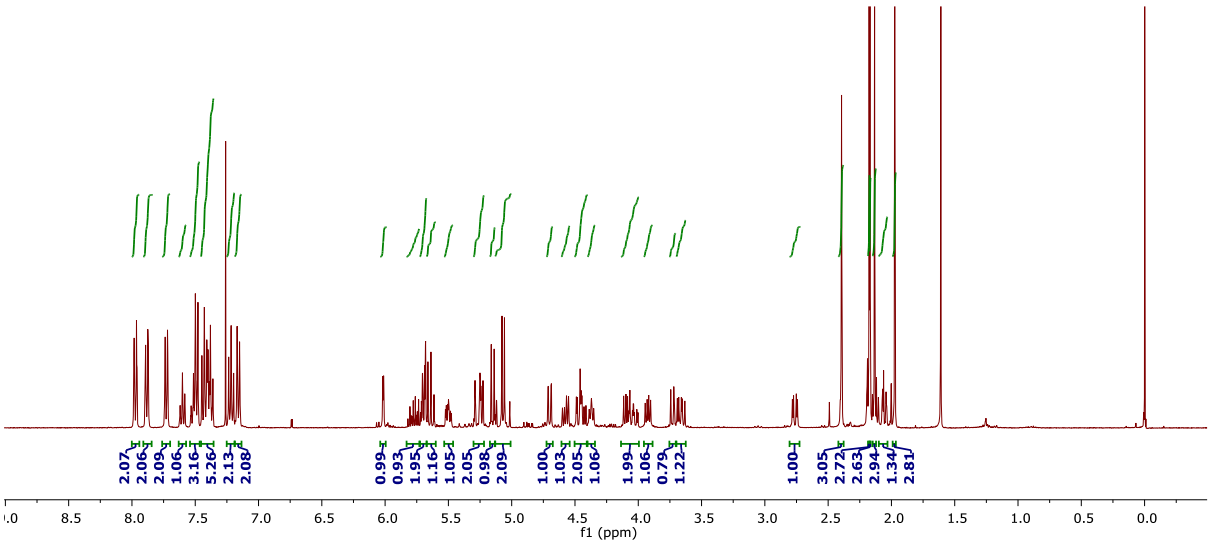
2.07
2.06
2.09
1.06
3.16
5.26
2.13
2.08
0.99
0.93
1.95
1.16
1.05
2.05
0.98
2.09
1.00
1.03
2.05
1.06
1.99
1.06
0.79
1.22
1.00
3.05
2.72
2.63
2.94
1.34
2.81
f1 (ppm)

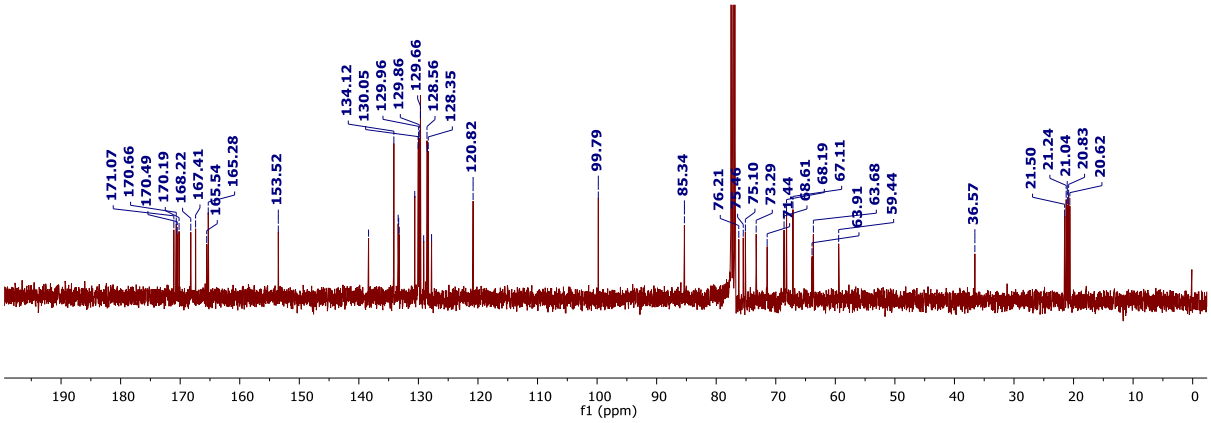
171.07
170.66
170.49
170.19
168.22
167.41
165.54
165.28
153.52
134.12
130.05
129.96
129.86
129.66
128.56
128.35
120.82
99.79
85.34
76.21
75.10
73.29
71.44
68.61
68.19
67.11
63.91
63.68
59.44
36.57
21.50
21.24
21.04
20.83
20.62
f1 (ppm)

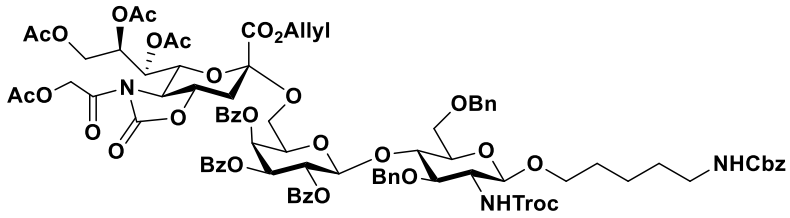
AcO
OAc
OAc
CO2Allyl
AcO
N
O
O
O
O
O
BzO
O
BzO
O
BzO
O
BnO
OBn
O
O
NHTroc
NHCbz

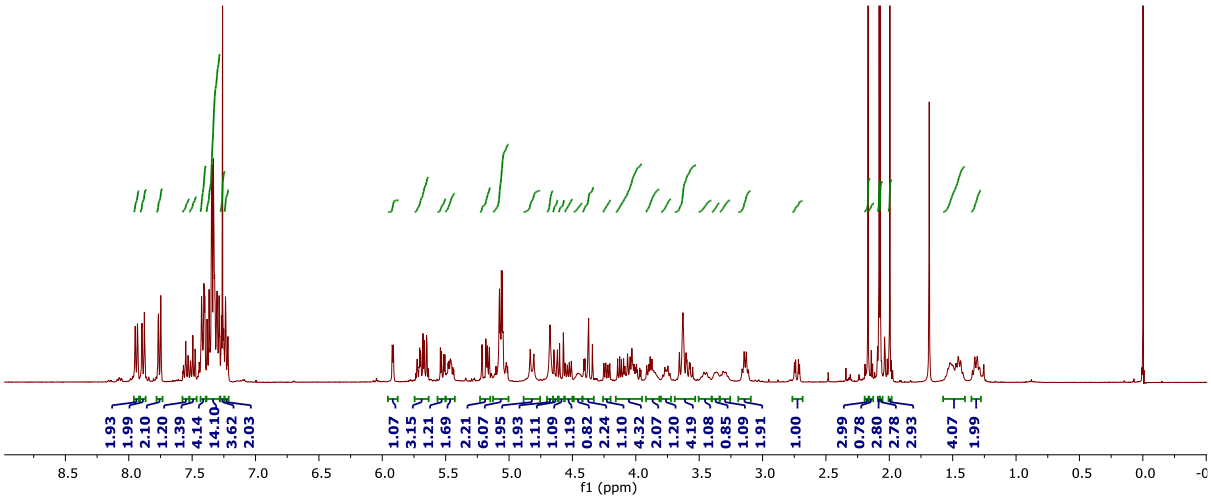
1.93
1.99
2.10
1.20
1.39
4.14
14.10
3.62
2.03
1.07
3.15
1.21
1.69
2.21
6.07
1.95
1.93
1.11
1.09
1.19
0.82
2.24
1.10
4.32
2.07
1.20
4.19
1.08
0.85
1.09
1.91
1.00
2.99
0.78
2.80
2.78
2.93
4.07
1.99
8.5
8.0
7.5
7.0
6.5
6.0
5.5
5.0
4.5
4.0
3.5
3.0
2.5
2.0
1.5
1.0
0.5
0.0
f1 (ppm)

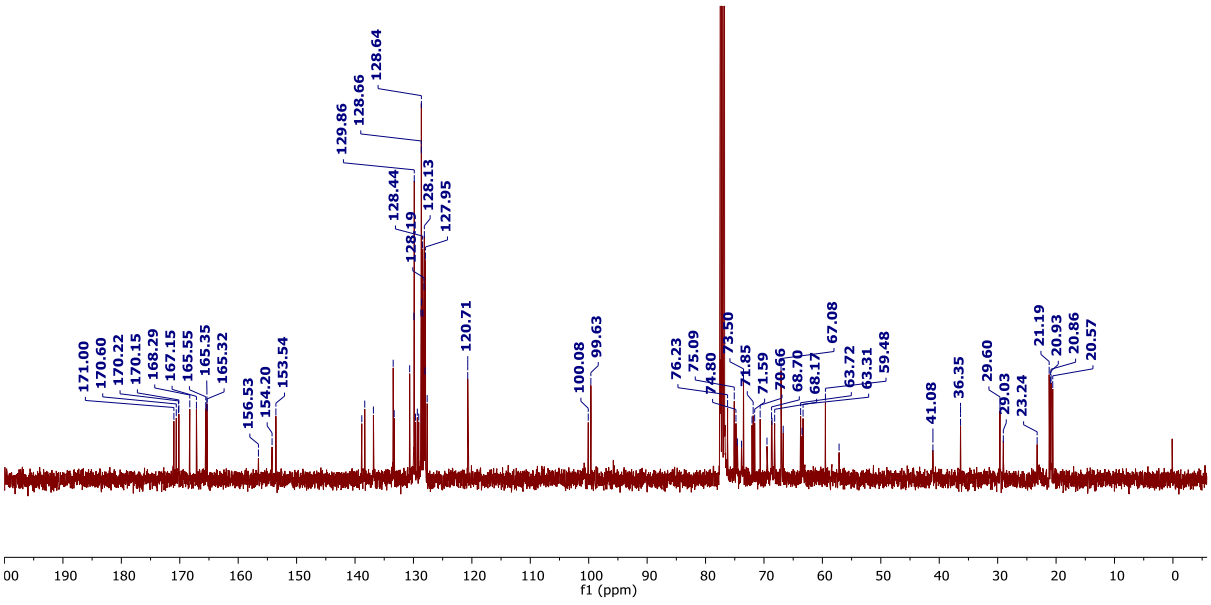
171.00
170.60
170.22
170.15
168.29
167.15
165.55
165.35
165.32
156.53
154.20
153.54
129.86
128.66
128.64
128.44
128.19
128.13
127.95
120.71
100.08
99.63
76.23
75.09
74.80
73.50
71.85
71.59
70.66
68.70
68.17
67.08
63.72
63.31
59.48
41.08
36.35
29.60
29.03
23.24
21.19
20.93
20.86
20.57
190
180
170
160
150
140
130
120
110
100
90
80
70
60
50
40
30
20
10
0
f1 (ppm)

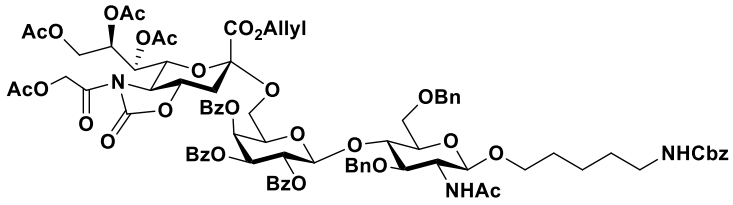
AcO
OAc
OAc
CO2Allyl
AcO
N
O
O
O
O
O
BzO
BzO
BzO
O
O
O
OBn
BnO
O
NHAc
O
NHCbz

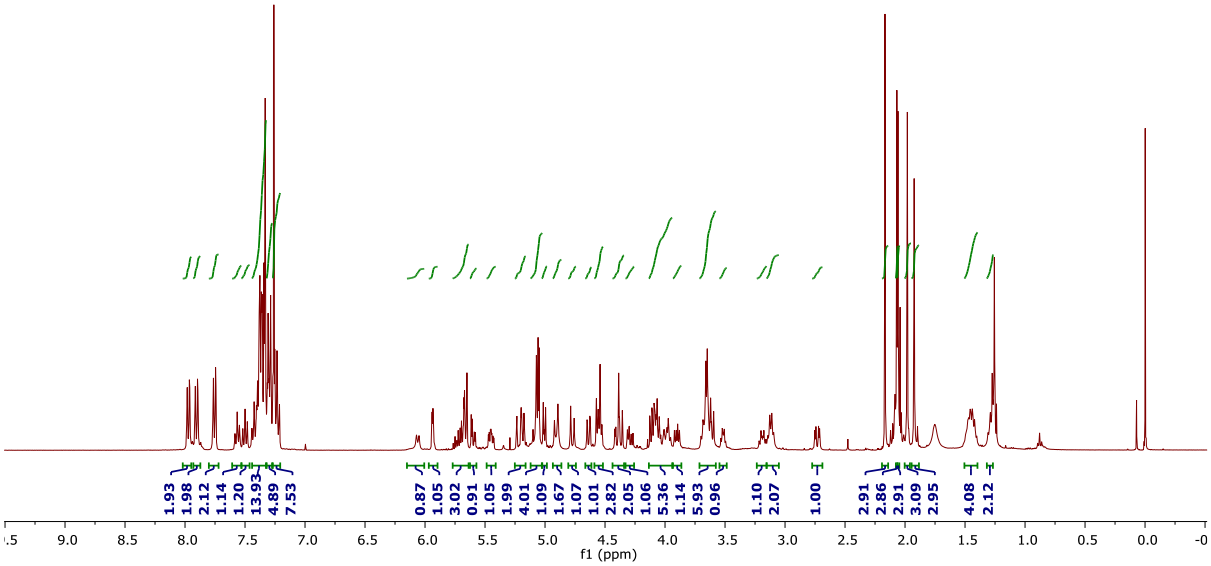
1.93
1.98
2.12
1.14
1.20
13.93
4.89
7.53
0.87
1.05
3.02
0.91
1.05
1.99
4.01
1.09
1.67
1.07
1.01
2.82
2.05
1.06
5.36
1.14
5.93
0.96
1.10
2.07
1.00
2.91
2.86
2.91
3.09
2.95
4.08
2.12
f1 (ppm)

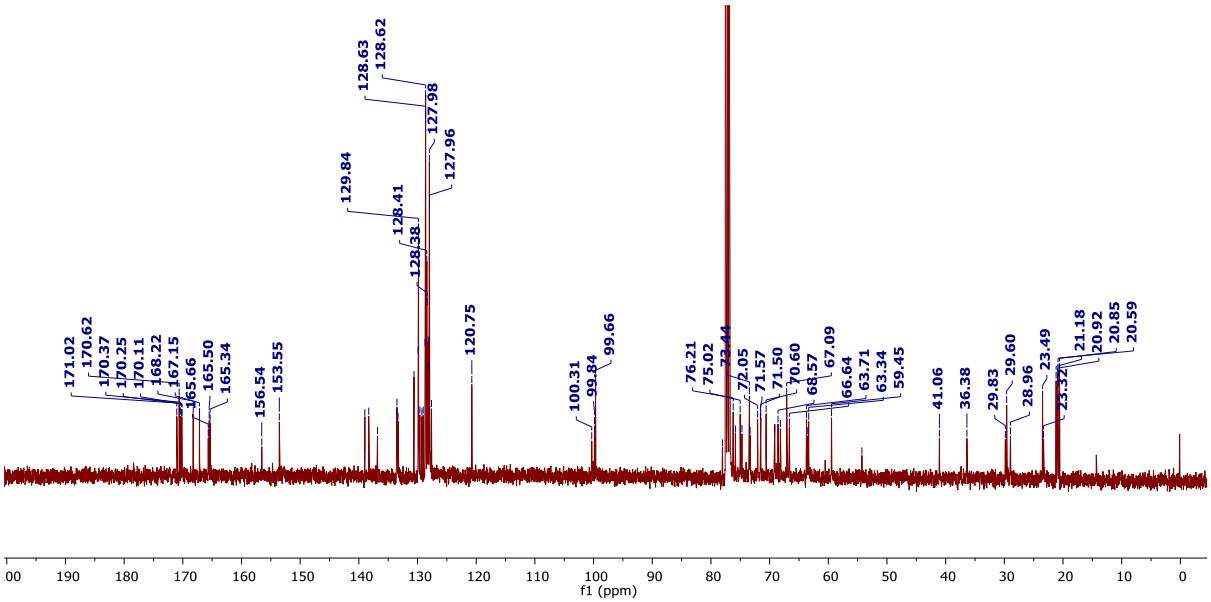
171.02
170.62
170.37
170.25
170.11
168.22
167.15
165.66
165.50
165.34
156.54
153.55
128.63
128.62
127.98
127.96
129.84
128.41
128.38
120.75
100.31
99.84
99.66
76.21
75.02
73.44
72.05
71.57
71.50
70.60
68.57
67.09
66.64
63.71
63.34
59.45
41.06
36.38
29.83
29.60
28.96
23.49
23.32
21.18
20.92
20.85
20.59
f1 (ppm)

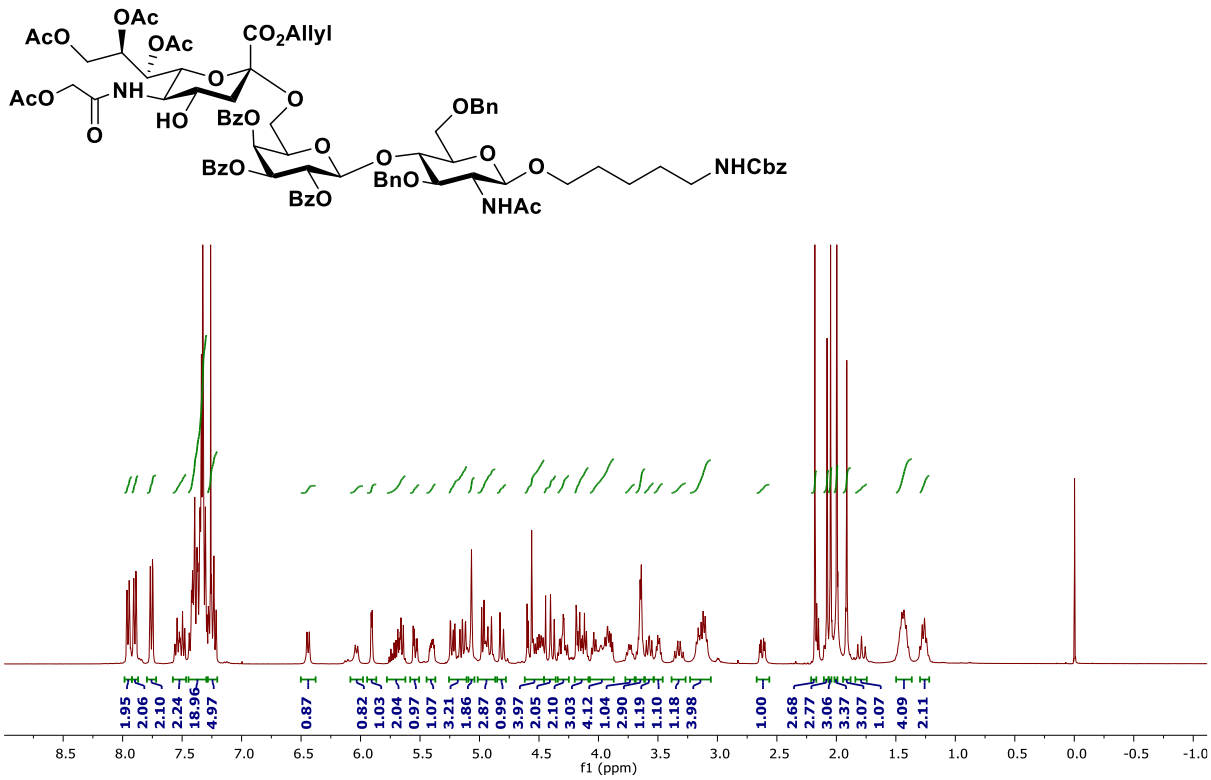
OAc
AcO
OAc
CO2Allyl
AcO
NH
HO
BzO
O
OBn
BzO
BnO
NHAc
NHCbz
BzO
1.95 2.06 2.10 2.24 18.96 4.97 0.87 0.82 1.03 2.04 0.97 1.07 3.21 1.86 2.87 0.99 3.97 2.05 2.10 3.03 4.12 1.04 2.90 1.19 1.10 1.18 3.98 1.00 2.68 2.77 3.06 3.37 3.07 1.07 4.09 2.11
f1 (ppm)

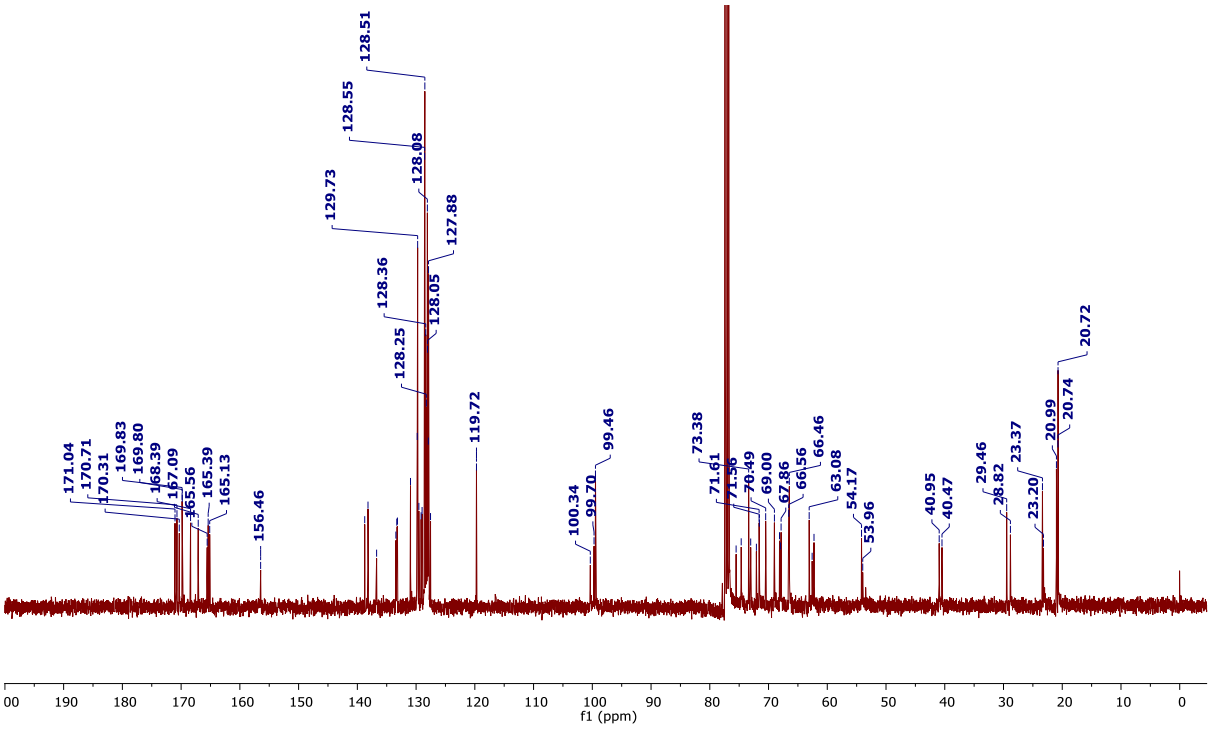
171.04 170.71 170.31 169.83 169.80 168.39 167.09 165.56 165.39 165.13 156.46
128.51 128.55 128.08 129.73 127.88 128.36 128.05 128.25 119.72
100.34 99.70 99.46
73.38 71.61 71.36 70.49 69.00 67.86 66.56 66.46 63.08 54.17 53.96
40.95 40.47
29.46 28.82 23.37 23.20 20.99 20.74 20.72
f1 (ppm)

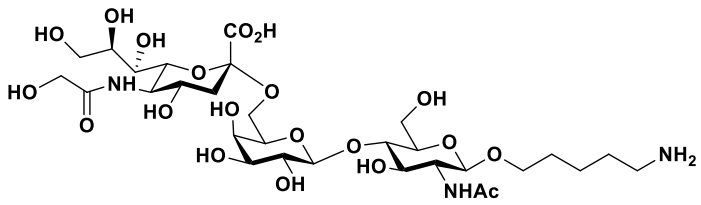
HO
OH
OH
CO2H
NH
HO
HO
O
O
HO
OH
O
O
HO
OH
O
O
NHAc
NH2

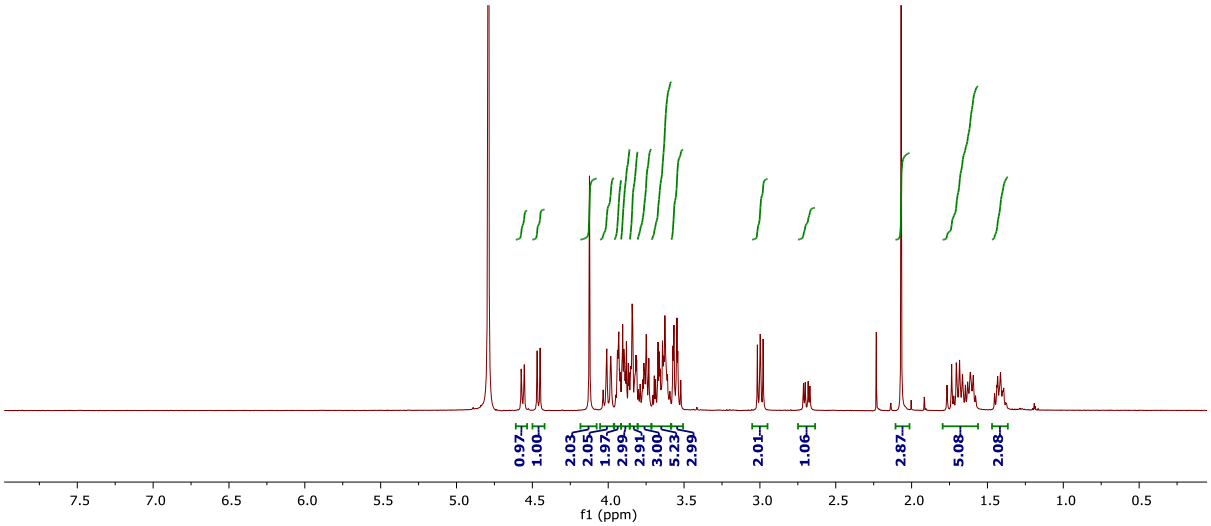
0.97
1.00
2.03
2.05
1.97
2.99
2.91
3.00
5.23
2.99
2.01
1.06
2.87
5.08
2.08
7.5
7.0
6.5
6.0
5.5
5.0
4.5
4.0
3.5
3.0
2.5
2.0
1.5
1.0
0.5
f1 (ppm)

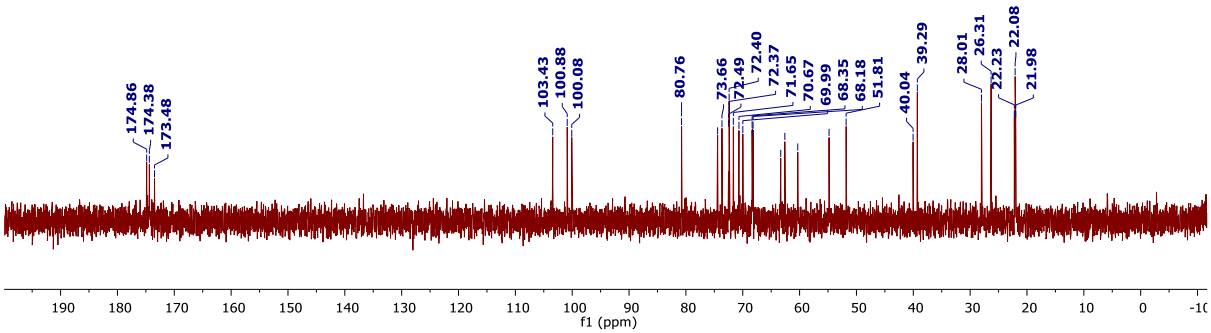
174.86
174.38
173.48
103.43
100.88
100.08
80.76
73.66
72.49
72.40
72.37
71.65
70.67
69.99
68.35
68.18
51.81
40.04
39.29
28.01
26.31
22.23
22.08
21.98
190
180
170
160
150
140
130
120
110
100
90
80
70
60
50
40
30
20
10
0
f1 (ppm)

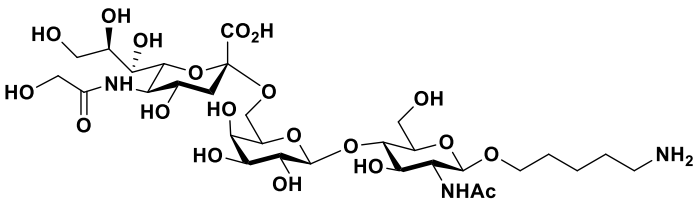
HO
OH
OH
CO2H
NH
HO
HO
O
O
HO
OH
O
O
HO
OH
O
HO
NHAc
O
NH2

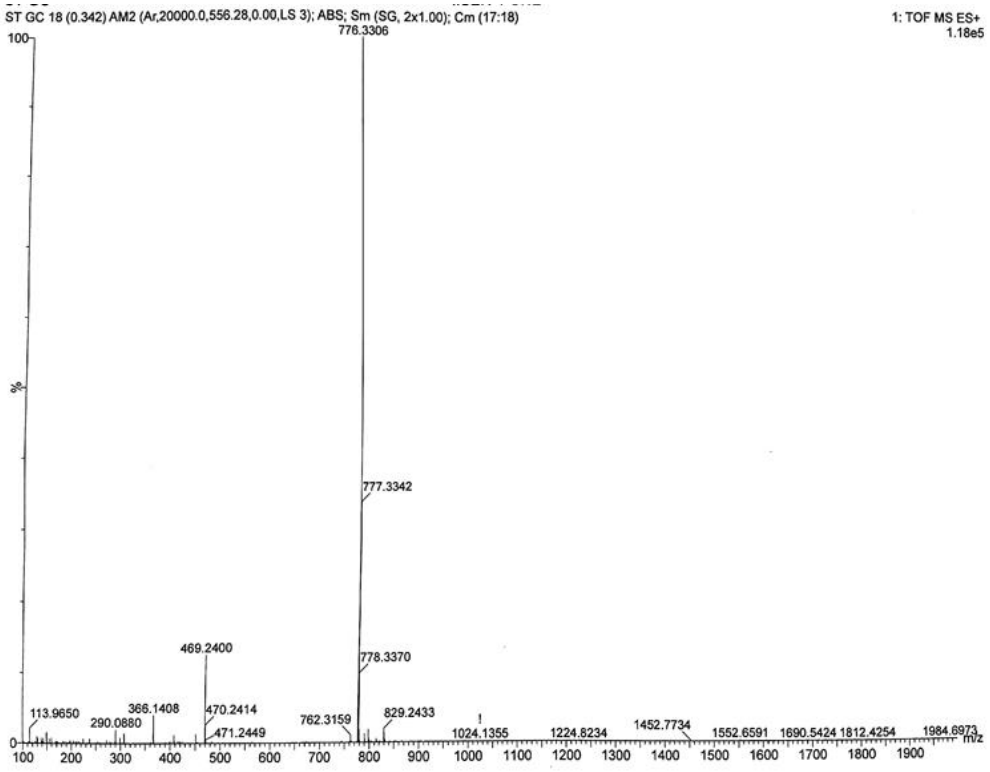
ST GC 18 (0.342) AM2 (Ar,20000.0,556.28,0.00,LS 3); ABS; Sm (SG, 2x1.00); Cm (17:18)
1: TOF MS ES+
1.18e5
100
%
0
776.3306
777.3342
778.3370
469.2400
113.9650
290.0880
366.1408
470.2414
471.2449
762.3159
829.2433
1024.1355
1224.8234
1452.7734
1552.6591
1690.5424
1812.4254
1984.6973
m/z
100 200 300 400 500 600 700 800 900 1000 1100 1200 1300 1400 1500 1600 1700 1800 1900

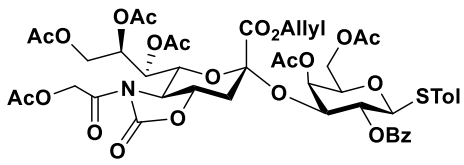
OAc
AcO
OAc
CO2Allyl
OAc
AcO
AcO
N
O
O
O
O
O
O
O
STol
OBz

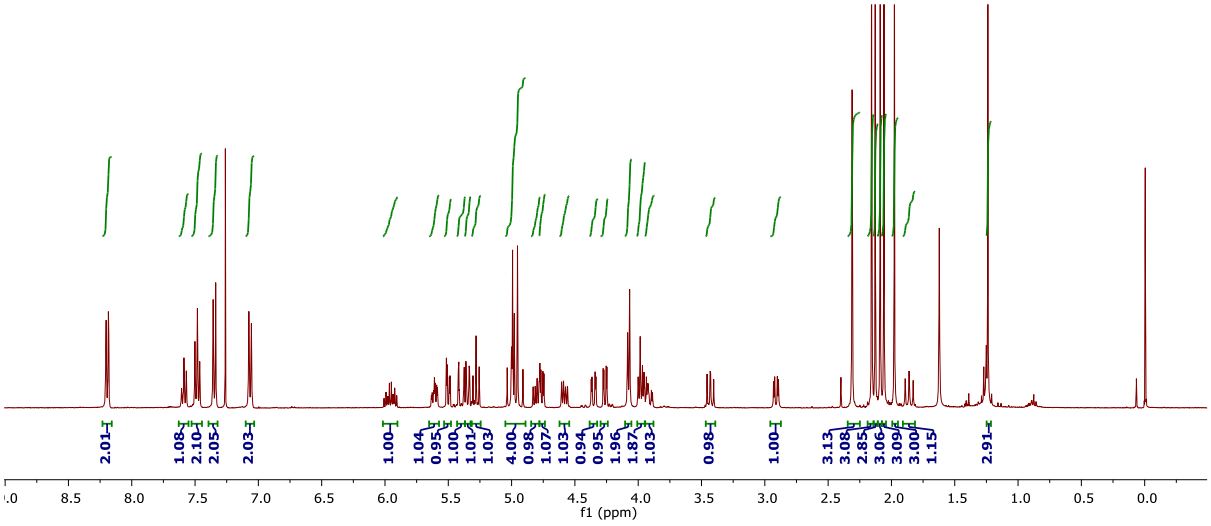
2.01
1.08
2.10
2.05
2.03
1.00
1.04
0.95
1.00
1.01
1.03
4.00
0.98
1.07
1.03
0.94
0.95
1.96
1.87
1.03
0.98
1.00
3.13
3.08
2.85
3.06
3.09
3.00
1.15
2.91
f1 (ppm)

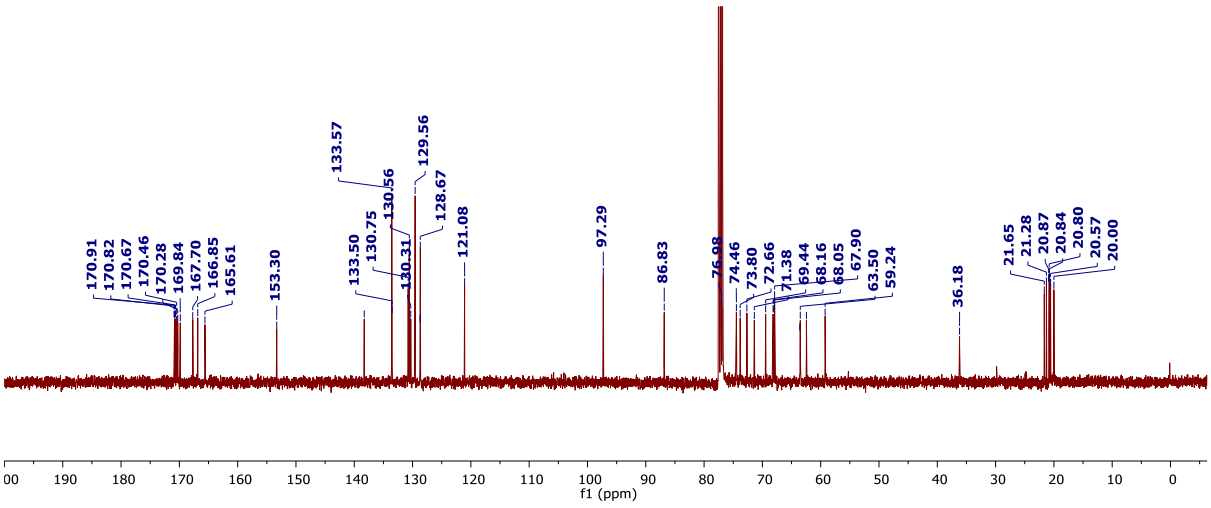
170.91
170.82
170.67
170.46
170.28
169.84
167.70
166.85
165.61
153.30
133.57
133.50
130.75
130.56
130.31
129.56
128.67
121.08
97.29
86.83
76.98
74.46
73.80
72.66
71.38
69.44
68.16
68.05
67.90
63.50
59.24
36.18
21.65
21.28
20.87
20.84
20.80
20.57
20.00
f1 (ppm)

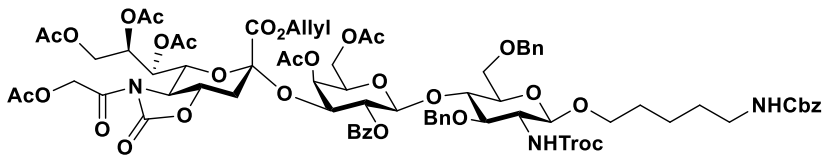
AcO
OAc
OAc
AcO
N
O
O
O
O
O
CO_2Allyl
OAc
AcO
O
O
BzO
O
OBn
O
BnO
NHTroc
O
NHCbz

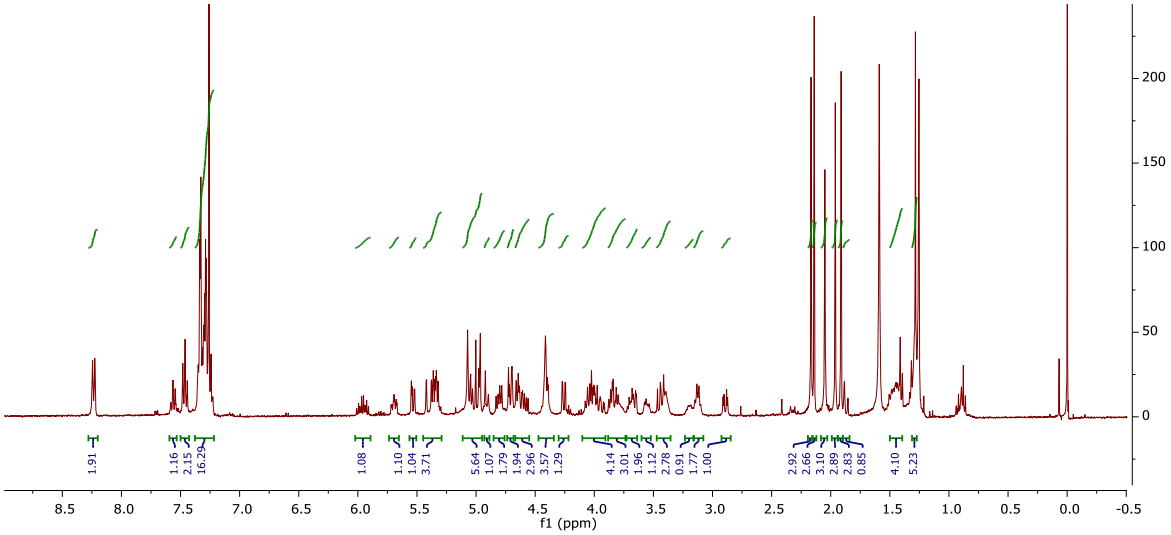
200
150
100
50
0
1.91
1.16
2.15
16.29
1.08
1.10
1.04
3.71
5.64
1.07
1.79
1.94
2.96
3.57
1.29
4.14
3.01
1.96
1.12
2.78
0.91
1.77
1.00
2.92
2.66
3.10
2.89
2.83
0.85
4.10
5.23
8.5
8.0
7.5
7.0
6.5
6.0
5.5
5.0
4.5
4.0
3.5
3.0
2.5
2.0
1.5
1.0
0.5
0.0
-0.5
f1 (ppm)

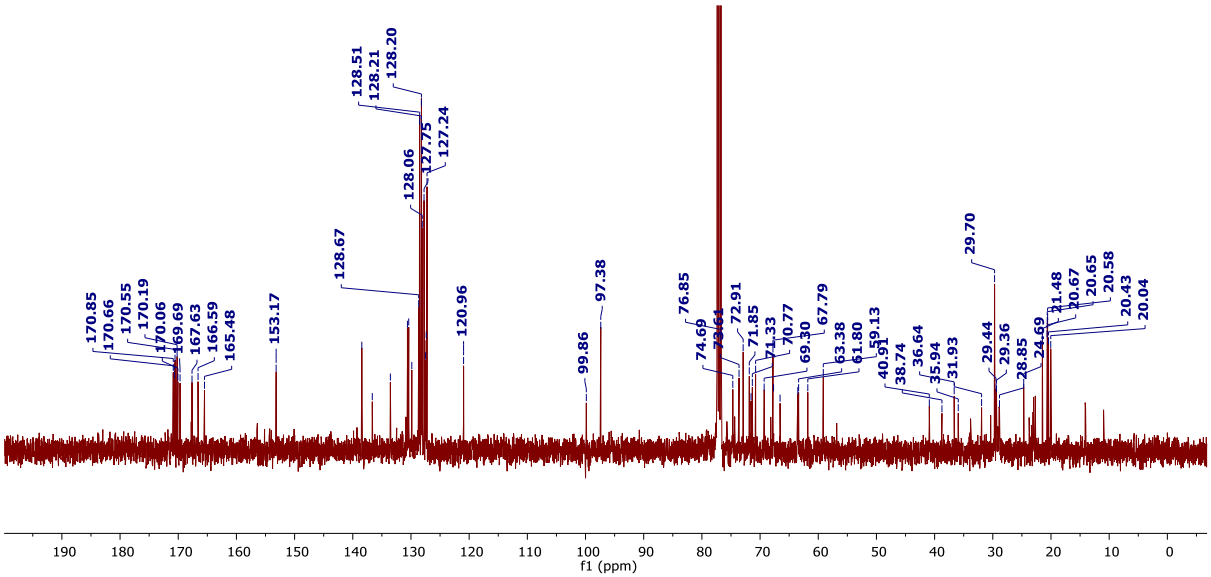
170.85
170.66
170.55
170.19
170.06
169.69
167.63
166.59
165.48
153.17
128.67
128.51
128.21
128.20
128.06
127.75
127.24
120.96
99.86
97.38
76.85
74.69
73.61
72.91
71.85
71.33
70.77
69.30
67.79
63.38
61.80
59.13
40.91
38.74
36.64
35.94
31.93
29.70
29.44
29.36
28.85
24.69
21.48
20.67
20.65
20.58
20.43
20.04
190
180
170
160
150
140
130
120
110
100
90
80
70
60
50
40
30
20
10
0
f1 (ppm)

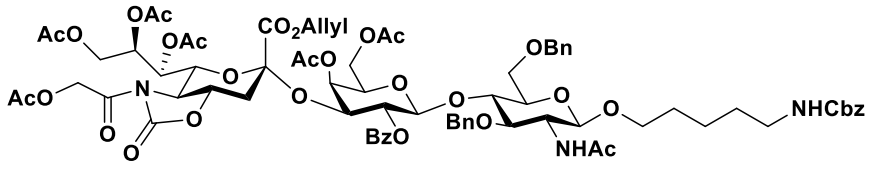
AcO
OAc
OAc
CO2Allyl
OAc
AcO
OBn
AcO
N
O
O
O
O
O
O
O
O
BnO
O
O
NHCbz
BzO
NHAc

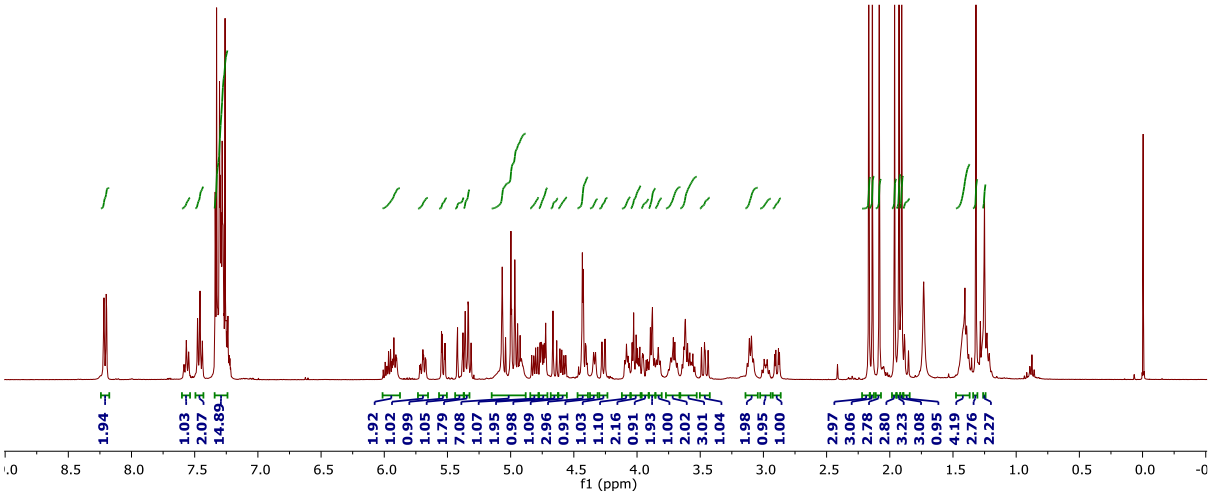
1.94
1.03
2.07
14.89
1.92
1.02
0.99
1.05
1.79
7.08
1.07
1.95
0.98
1.09
2.96
0.91
1.03
1.10
2.16
0.91
1.93
1.00
2.02
3.01
1.04
1.98
0.95
1.00
2.97
3.06
2.78
2.80
3.23
3.08
0.95
4.19
2.76
2.27
8.5
8.0
7.5
7.0
6.5
6.0
5.5
5.0
4.5
4.0
3.5
3.0
2.5
2.0
1.5
1.0
0.5
0.0
f1 (ppm)

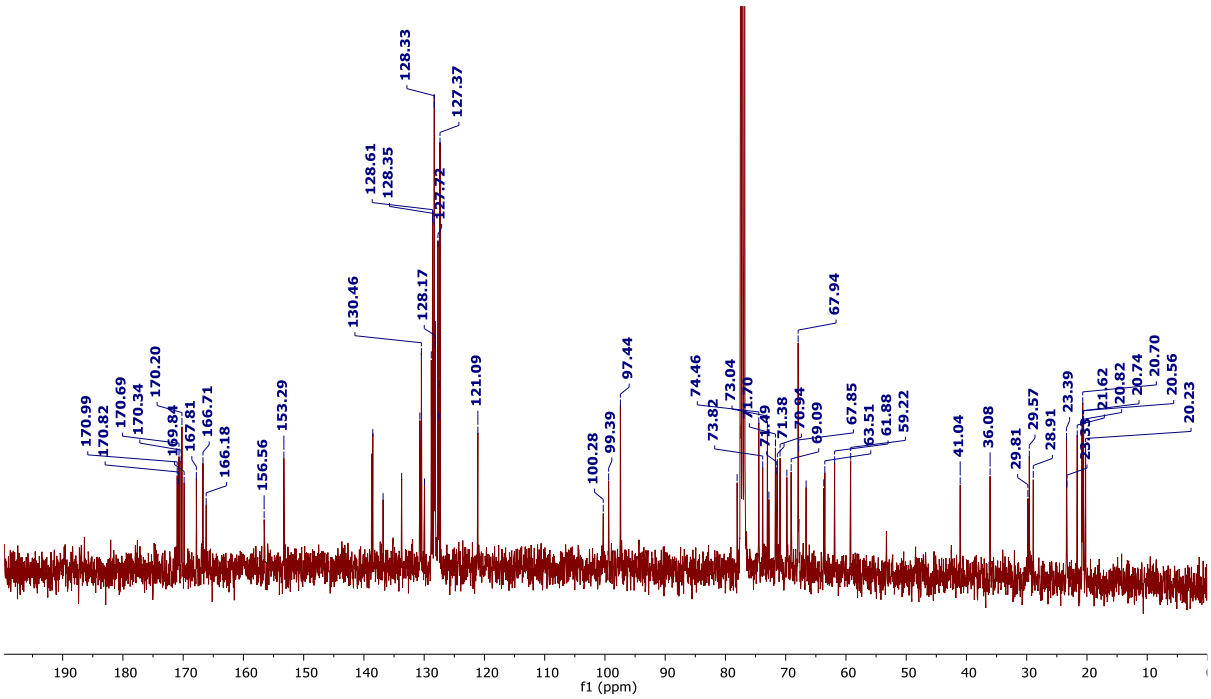
128.33
127.37
128.61
128.35
127.72
130.46
128.17
121.09
97.44
67.94
74.46
73.04
71.70
73.82
71.49
71.38
70.94
69.09
67.85
63.51
61.88
59.22
41.04
36.08
29.81
29.57
28.91
23.39
21.62
20.82
20.74
20.70
20.56
20.23
170.99
170.82
170.69
170.34
170.20
169.84
167.81
166.71
166.18
156.56
153.29
100.28
99.39
190
180
170
160
150
140
130
120
110
100
90
80
70
60
50
40
30
20
10
f1 (ppm)

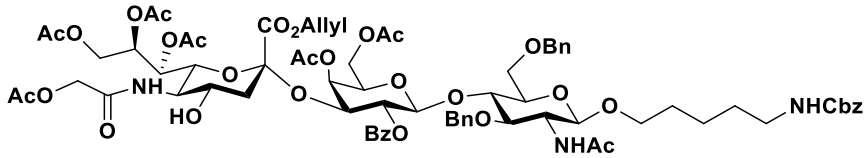
AcO
OAc
OAc
NH
AcO
O
HO
O
CO2Allyl
AcO
OAc
O
O
BzO
O
BnO
OBn
O
NHAc
O
NHCbz

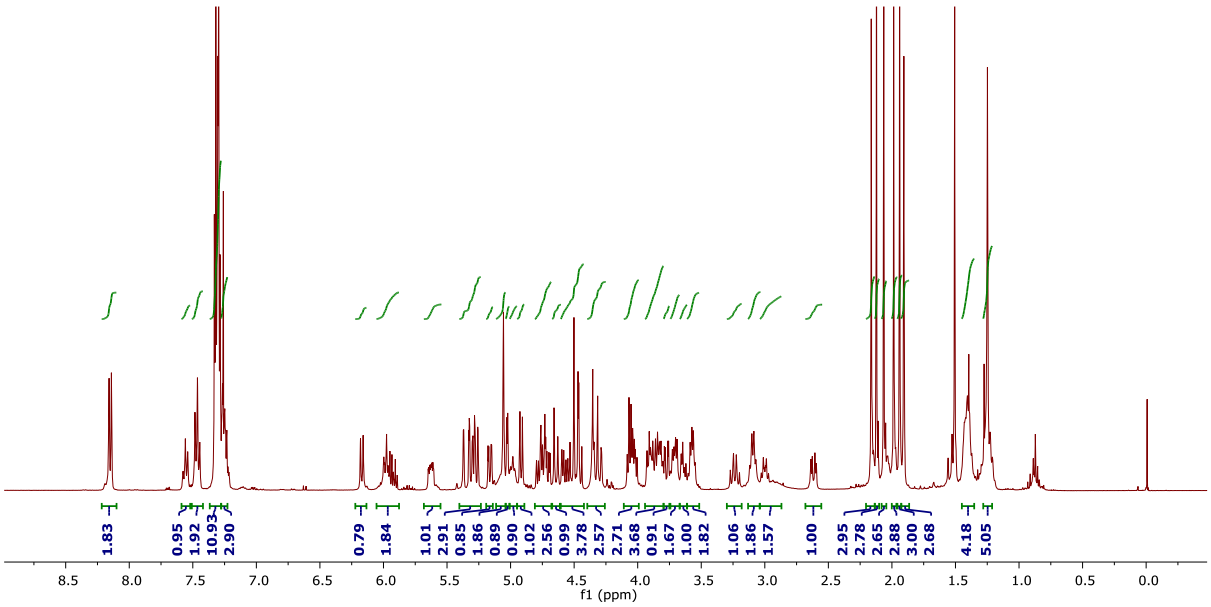
1.83
0.95
1.92
10.93
2.90
0.79
1.84
1.01
2.91
0.85
1.86
0.89
0.90
1.02
2.56
0.99
3.78
2.57
2.71
3.68
0.91
1.67
1.00
1.82
1.06
1.86
1.57
1.00
2.95
2.78
2.65
2.88
3.00
2.68
4.18
5.05
8.5
8.0
7.5
7.0
6.5
6.0
5.5
5.0
4.5
4.0
3.5
3.0
2.5
2.0
1.5
1.0
0.5
0.0
f1 (ppm)

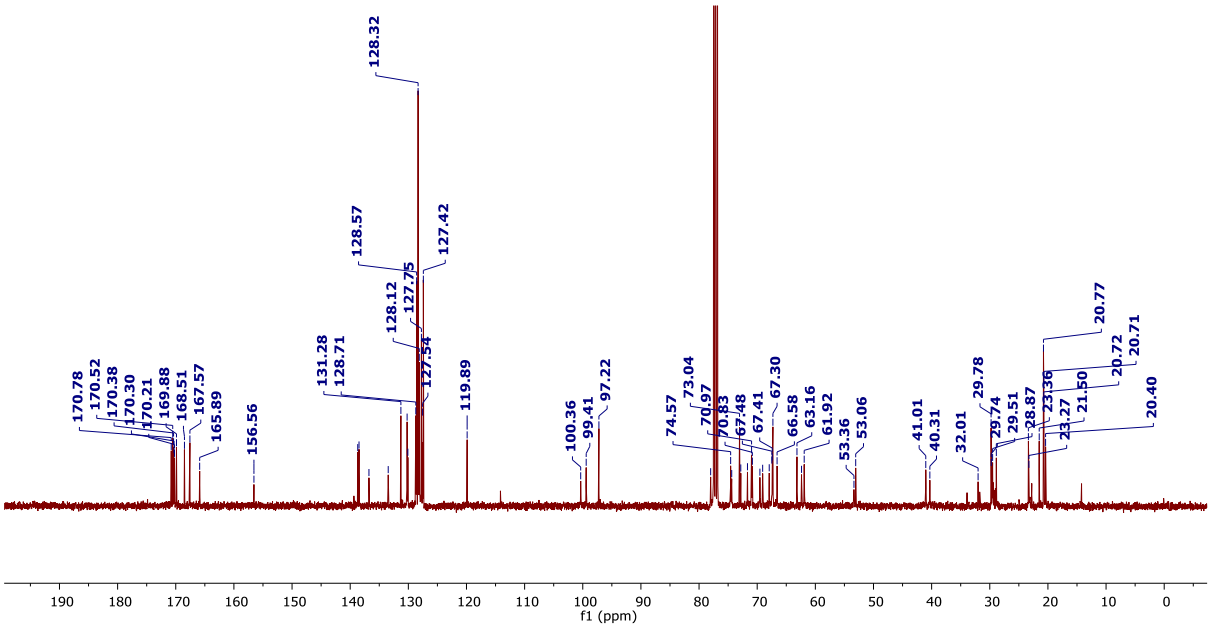
170.78
170.52
170.38
170.30
170.21
169.88
168.51
167.57
165.89
156.56
131.28
128.71
128.32
128.57
128.12
127.75
127.54
127.42
119.89
100.36
99.41
97.22
74.57
73.04
70.97
70.83
67.48
67.41
67.30
66.58
63.16
61.92
53.36
53.06
41.01
40.31
32.01
29.78
29.74
29.51
28.87
23.36
23.27
21.50
20.77
20.72
20.71
20.40
190
180
170
160
150
140
130
120
110
100
90
80
70
60
50
40
30
20
10
0
f1 (ppm)

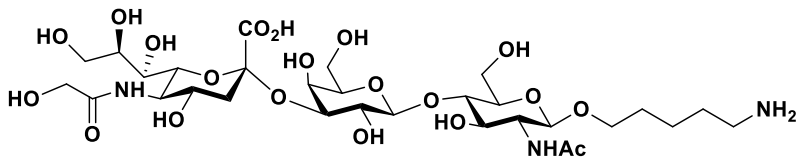
HO
OH
OH
NH
HO
O
CO2H
HO
OH
O
O
OH
O
HO
O
O
NHAc
NH2

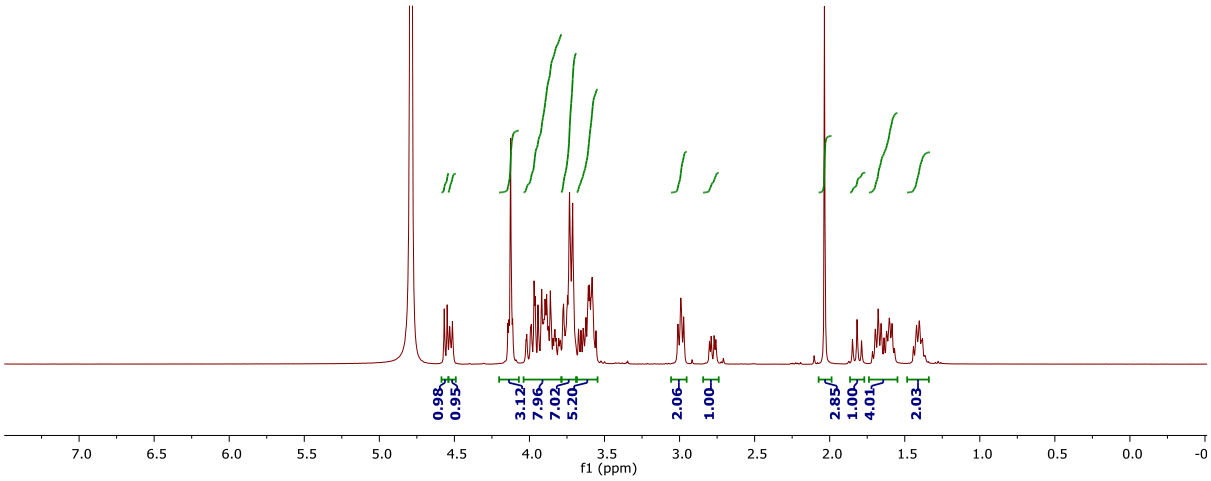
0.98
0.95
3.12
7.96
7.02
5.20
2.06
1.00
2.85
1.00
4.01
2.03
7.0
6.5
6.0
5.5
5.0
4.5
4.0
3.5
3.0
2.5
2.0
1.5
1.0
0.5
0.0
-0
f1 (ppm)

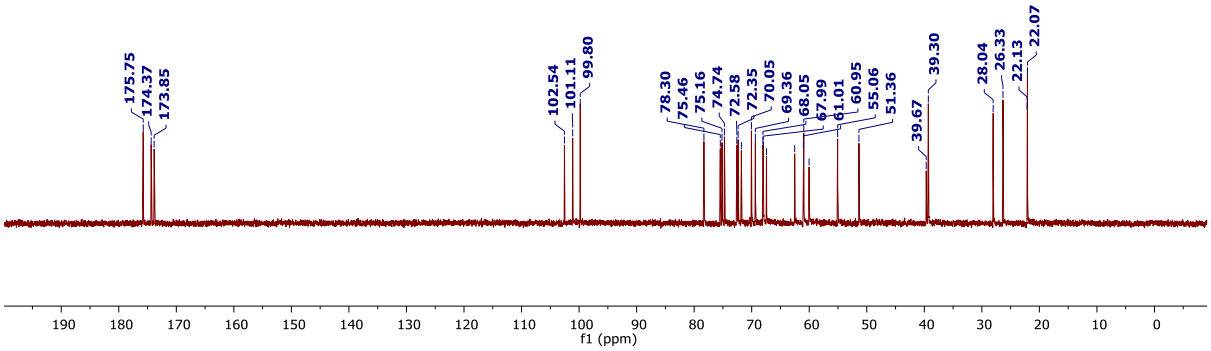
175.75
174.37
173.85
102.54
101.11
99.80
78.30
75.46
75.16
74.74
72.58
72.35
70.05
69.36
68.05
67.99
61.01
60.95
55.06
51.36
39.67
39.30
28.04
26.33
22.13
22.07
190
180
170
160
150
140
130
120
110
100
90
80
70
60
50
40
30
20
10
0
f1 (ppm)

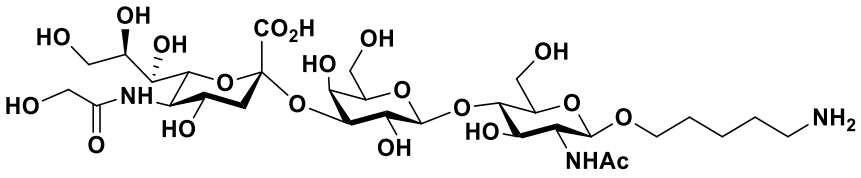
OH
HO
OH
CO2H
OH
HO
OH
NH
O
HO
O
O
O
HO
O
O
HO
OH
NHAc
NH2

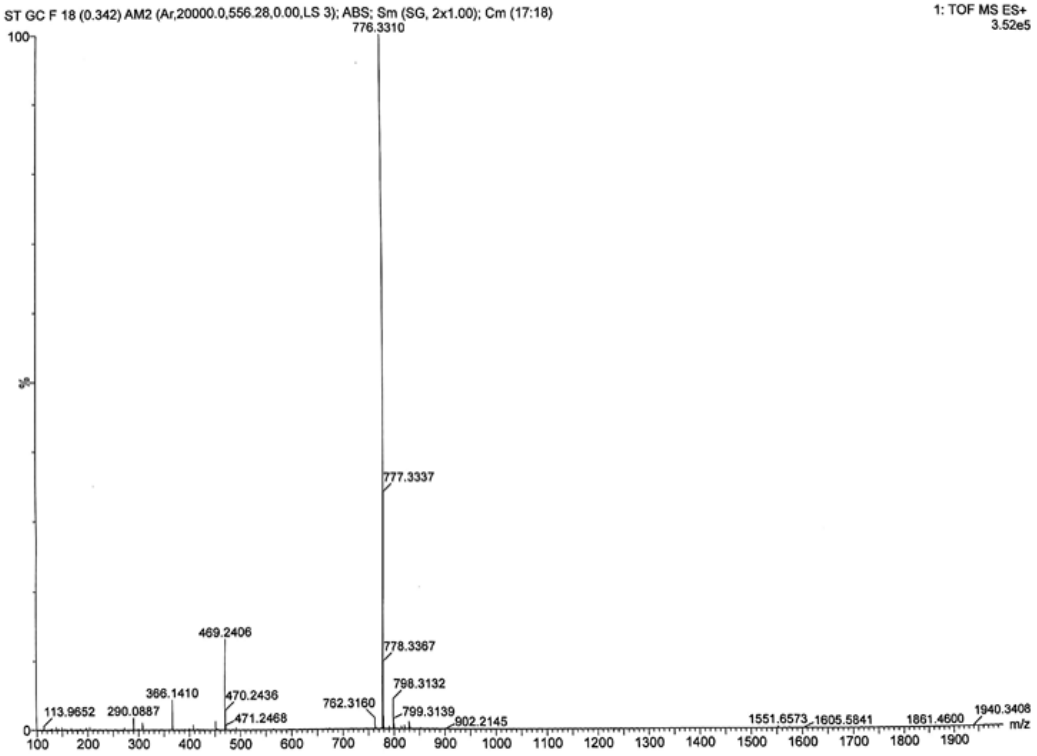
ST GC F 18 (0.342) AM2 (Ar,20000.0,556.28,0.00,LS 3); ABS; Sm (SG, 2x1.00); Cm (17:18)
1: TOF MS ES+
3.52e5
100
%
0
776.3310
777.3337
469.2406
778.3367
798.3132
366.1410
470.2436
762.3160
799.3139
113.9652
290.0887
471.2468
902.2145
1551.6573
1605.5841
1861.4600
1940.3408
m/z
100
200
300
400
500
600
700
800
900
1000
1100
1200
1300
1400
1500
1600
1700
1800
1900

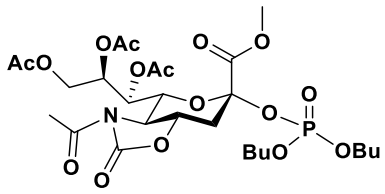
AcO
OAc
OAc
O
O
O
N
O
O
O
O
O
P
BuO
OBu

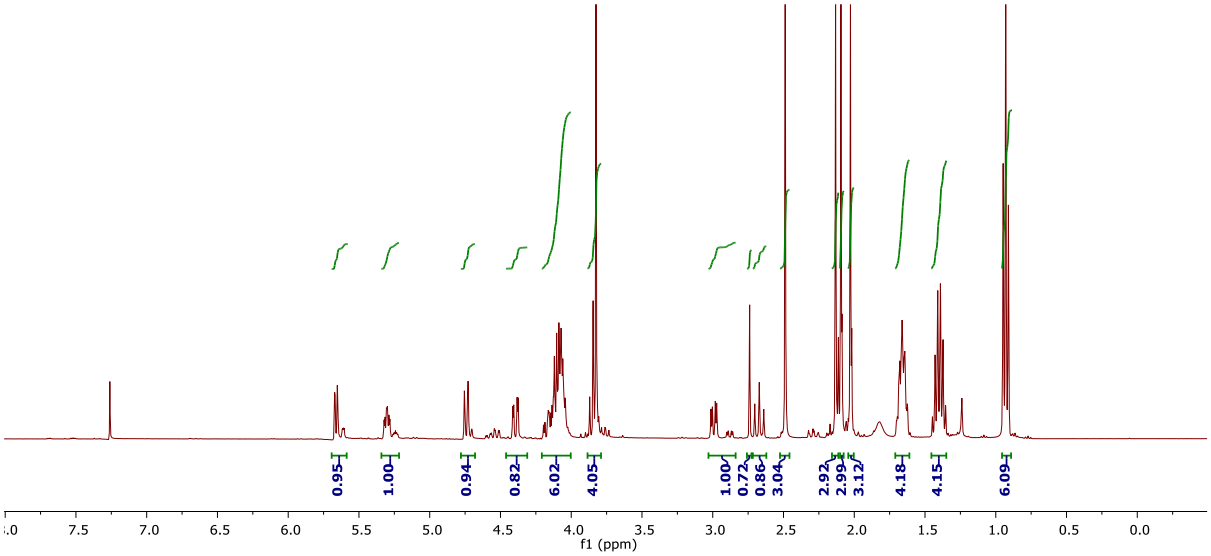
0.95
1.00
0.94
0.82
6.02
4.05
1.00
0.72
0.86
3.04
2.92
2.99
3.12
4.18
4.15
6.09
f1 (ppm)

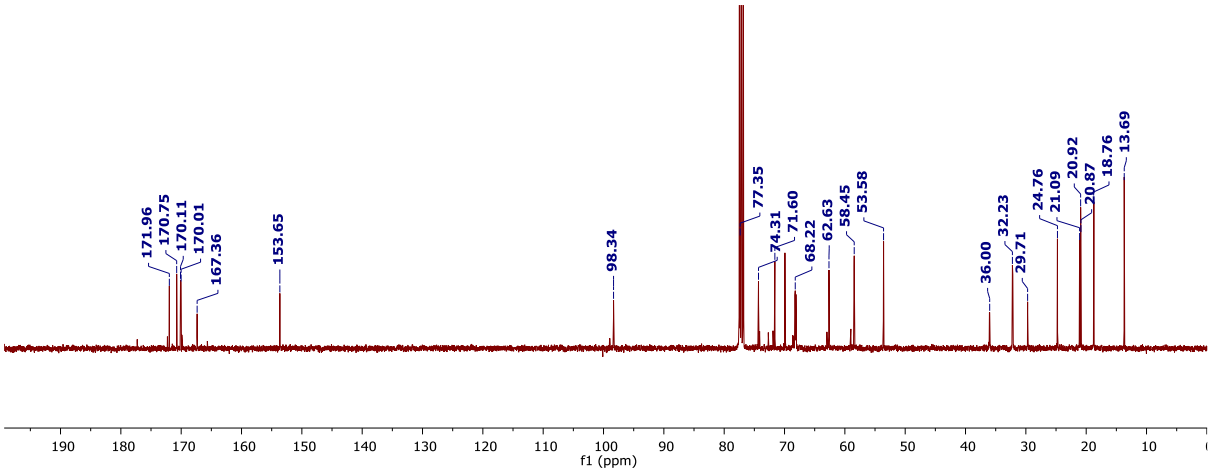
171.96
170.75
170.11
170.01
167.36
153.65
98.34
77.35
74.31
71.60
68.22
62.63
58.45
53.58
36.00
32.23
29.71
24.76
21.09
20.92
20.87
18.76
13.69
f1 (ppm)

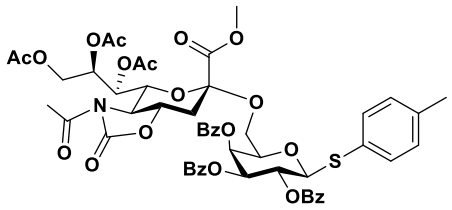
AcO
OAc
OAc
O
O
N
O
O
O
O
O
BzO
BzO
O
S
OBz

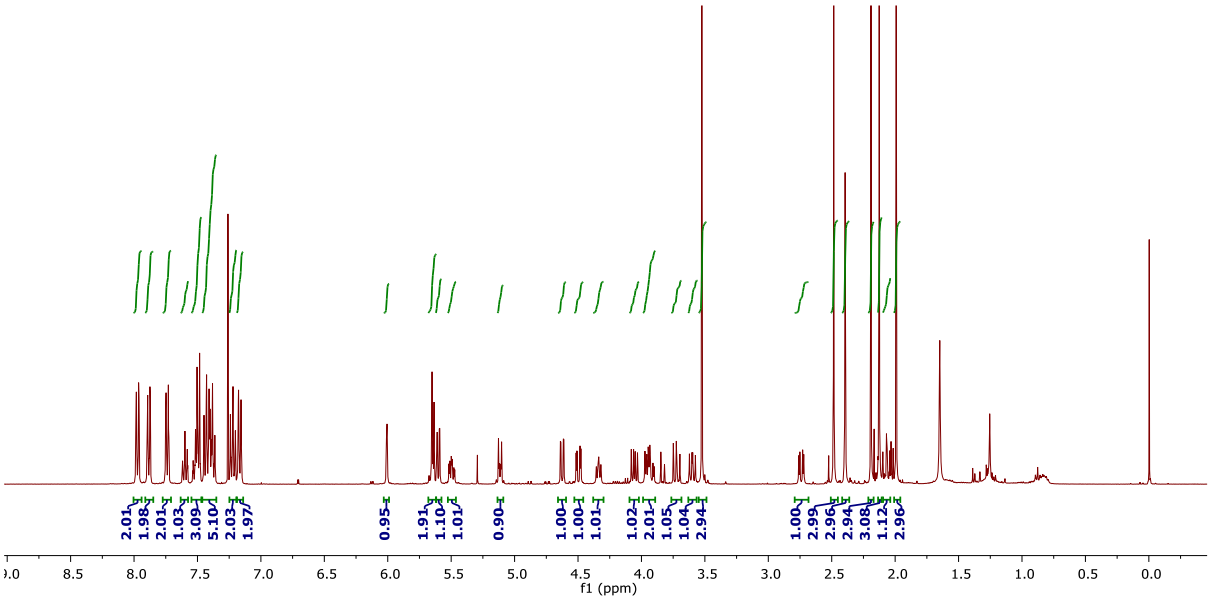
2.01
1.98
2.01
1.03
3.09
5.10
2.03
1.97
0.95
1.91
1.10
1.01
0.90
1.00
1.00
1.01
1.02
2.01
1.05
1.04
2.94
1.00
2.99
2.96
2.94
3.08
1.12
2.96
f1 (ppm)

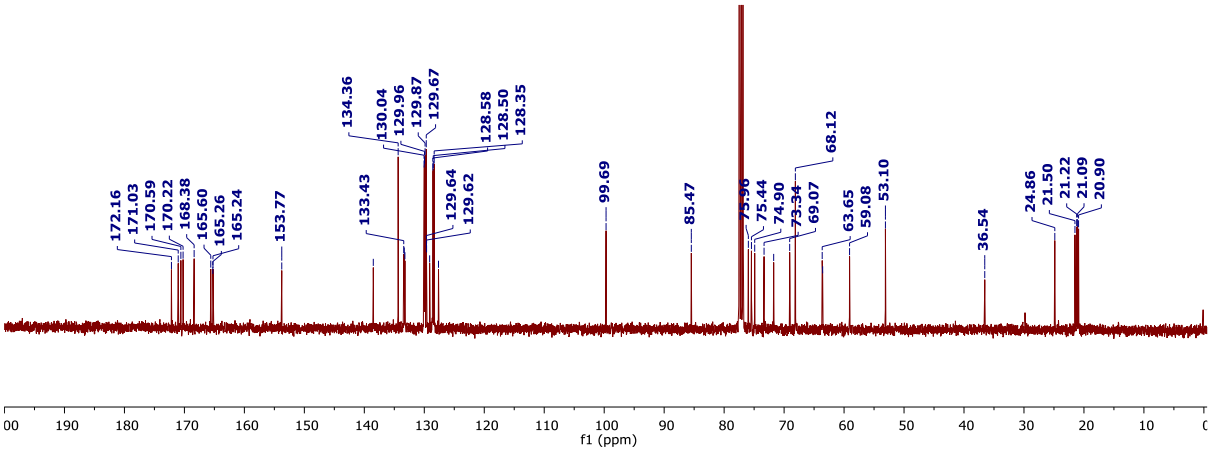
172.16
171.03
170.59
170.22
168.38
165.60
165.26
165.24
153.77
134.36
133.43
130.04
129.96
129.87
129.67
129.64
129.62
128.58
128.50
128.35
99.69
85.47
75.96
75.44
74.90
73.34
69.07
68.12
63.65
59.08
53.10
36.54
24.86
21.50
21.22
21.09
20.90
f1 (ppm)

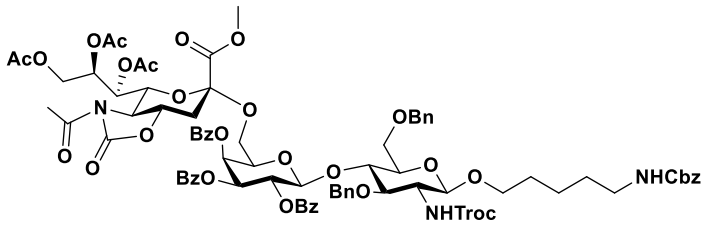
AcO
OAc
OAc
O
O
N
O
O
O
O
O
BzO
BzO
O
O
OBz
O
BnO
OBn
O
O
NHTroc
NHCbz

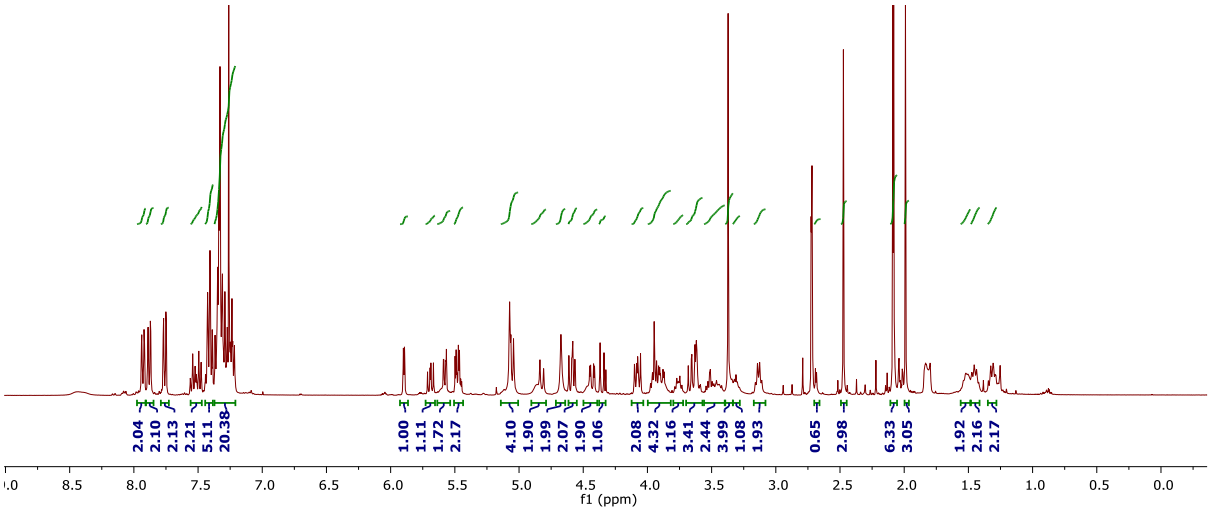
2.04
2.10
2.13
2.21
5.11
20.38
1.00
1.11
1.72
2.17
4.10
1.90
1.99
2.07
1.90
1.06
2.08
4.32
1.16
3.41
2.44
3.99
1.08
1.93
0.65
2.98
6.33
3.05
1.92
2.16
2.17
f1 (ppm)

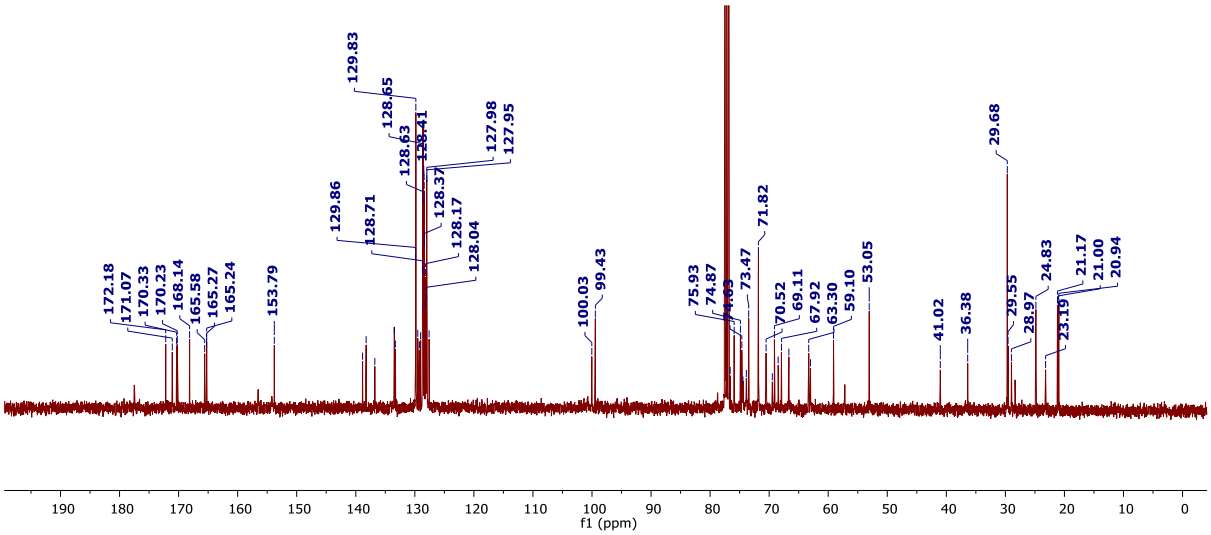
172.18
171.07
170.33
170.23
168.14
165.58
165.27
165.24
153.79
129.86
129.83
128.71
128.65
128.63
128.41
128.37
128.17
128.04
127.98
127.95
100.03
99.43
75.93
74.87
74.63
73.47
71.82
70.52
69.11
67.92
63.30
59.10
53.05
41.02
36.38
29.68
29.55
28.97
24.83
23.19
21.17
21.00
20.94
f1 (ppm)

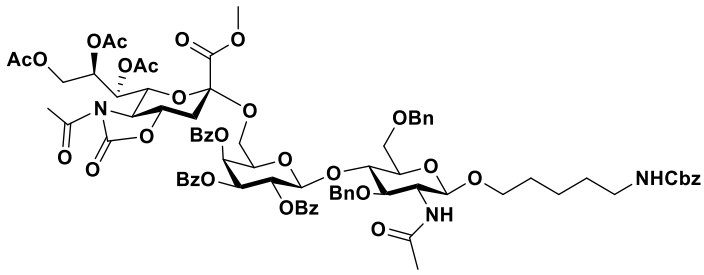
AcO
OAc
OAc
O
O
N
O
O
O
O
BzO
BzO
OBz
O
O
OBn
BnO
O
O
NH
O
O
NHCbz

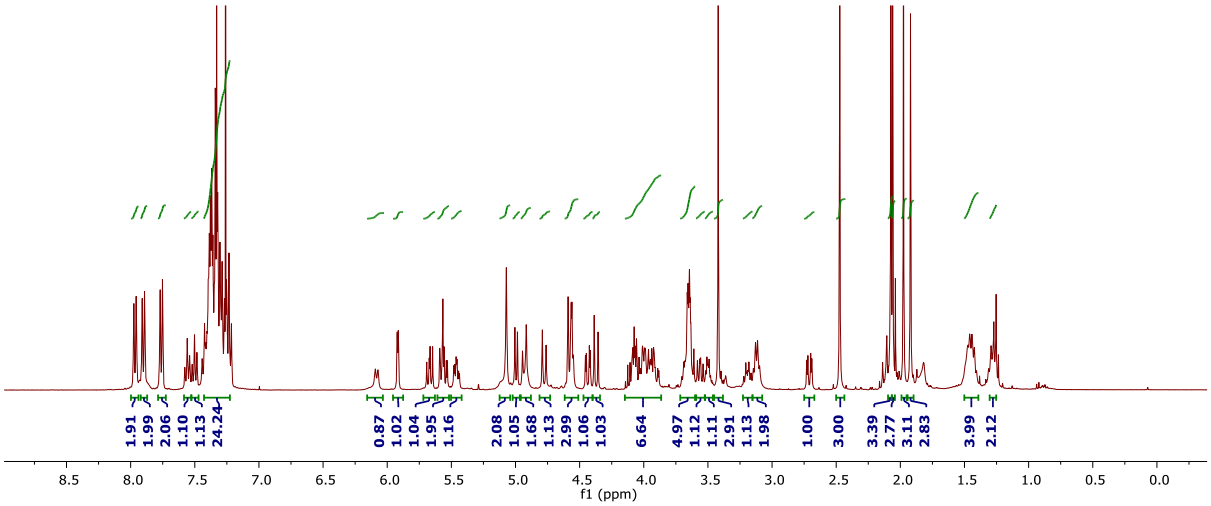
1.91
1.99
2.06
1.10
1.13
24.24
0.87
1.02
1.04
1.95
1.16
2.08
1.05
1.68
1.13
2.99
1.06
1.03
6.64
4.97
1.12
1.11
2.91
1.13
1.98
1.00
3.00
3.39
2.77
3.11
2.83
3.99
2.12
8.5
8.0
7.5
7.0
6.5
6.0
5.5
5.0
4.5
4.0
3.5
3.0
2.5
2.0
1.5
1.0
0.5
0.0
f1 (ppm)

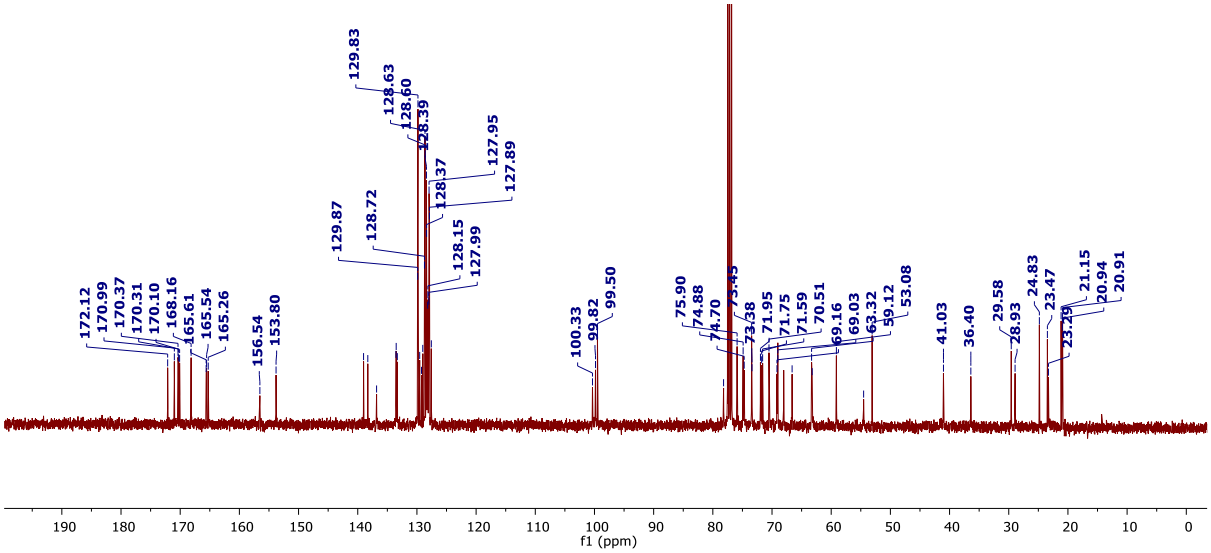
172.12
170.99
170.37
170.31
170.10
168.16
165.61
165.54
165.26
156.54
153.80
129.87
128.72
129.83
128.63
128.60
128.39
128.37
128.15
127.99
127.95
127.89
100.33
99.82
99.50
75.90
74.88
74.70
73.45
73.38
71.95
71.75
71.59
70.51
69.16
69.03
63.32
59.12
53.08
41.03
36.40
29.58
26.93
24.83
23.47
23.29
21.15
20.94
20.91
190
180
170
160
150
140
130
120
110
100
90
80
70
60
50
40
30
20
10
0
f1 (ppm)

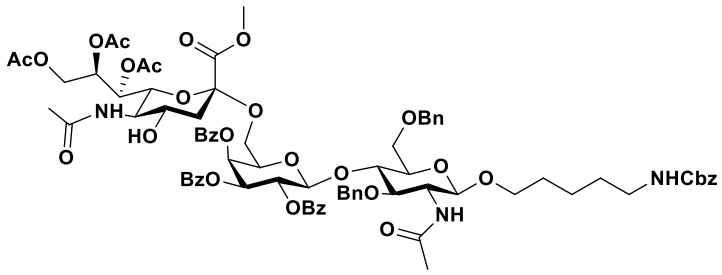
AcO
OAc
OAc
O
O
NH
HO
BzO
O
O
BzO
OBz
O
BnO
OBn
O
O
NH
O
O
NHCbz

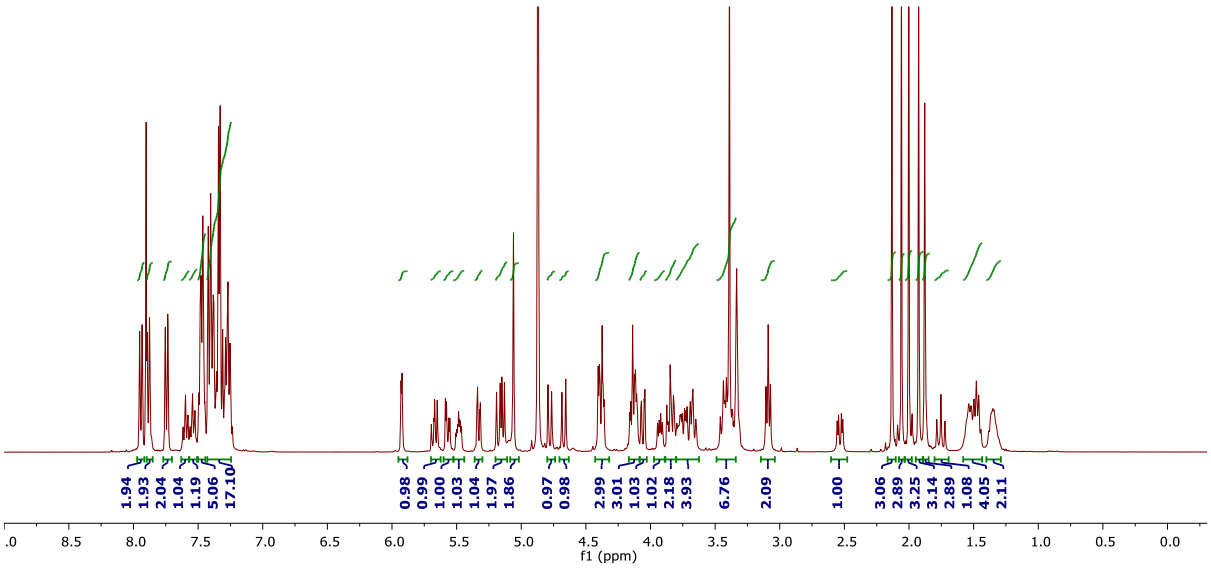
1.94
1.93
2.04
1.04
1.19
5.06
17.10
0.98
0.99
1.00
1.03
1.04
1.97
1.86
0.97
0.98
2.99
3.01
1.03
1.02
2.18
3.93
6.76
2.09
1.00
3.06
2.89
3.25
3.14
2.89
1.08
4.05
2.11
f1 (ppm)

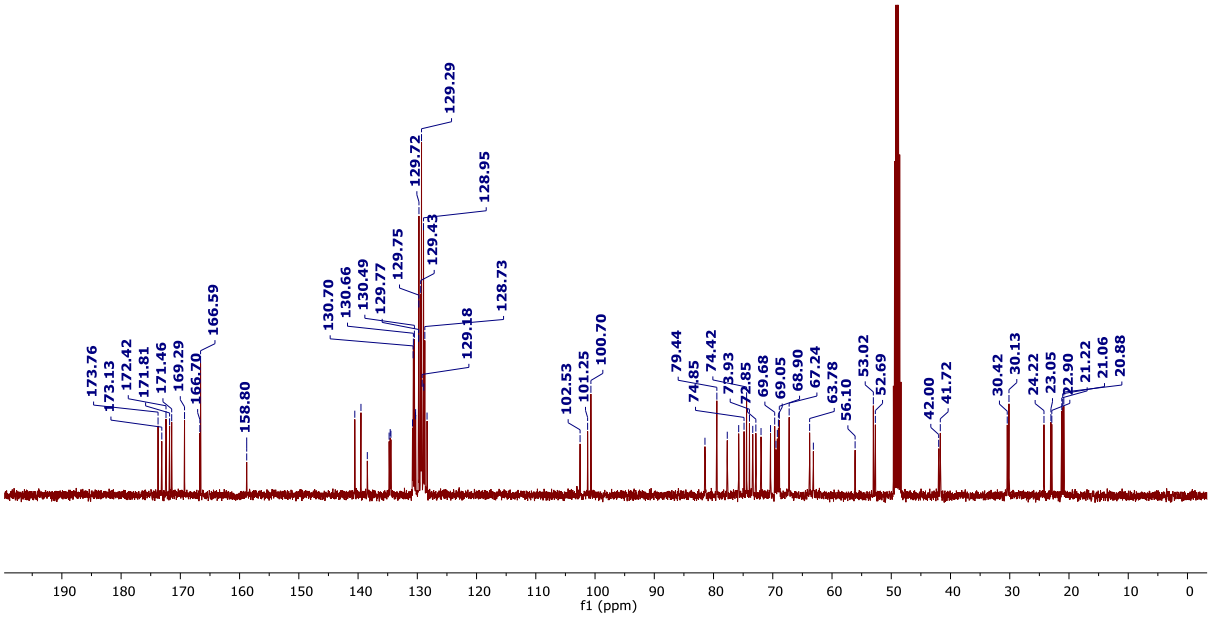
173.76
173.13
172.42
171.81
171.46
169.29
166.70
166.59
158.80
130.70
130.66
130.49
129.77
129.75
129.72
129.43
129.29
129.18
128.95
128.73
102.53
101.25
100.70
79.44
74.85
74.42
73.93
72.85
69.68
69.05
68.90
67.24
63.78
56.10
53.02
52.69
42.00
41.72
30.42
30.13
24.22
23.05
22.90
21.22
21.06
20.88
f1 (ppm)

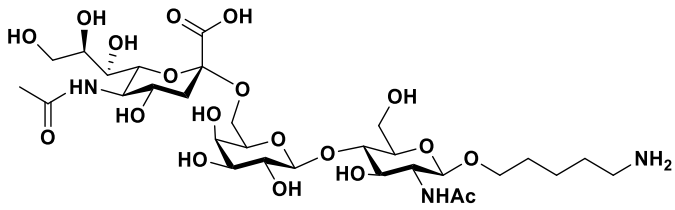
HO
OH
OH
O
OH
HN
O
O
HO
HO
O
HO
OH
O
O
OH
HO
O
NH2
NHAc

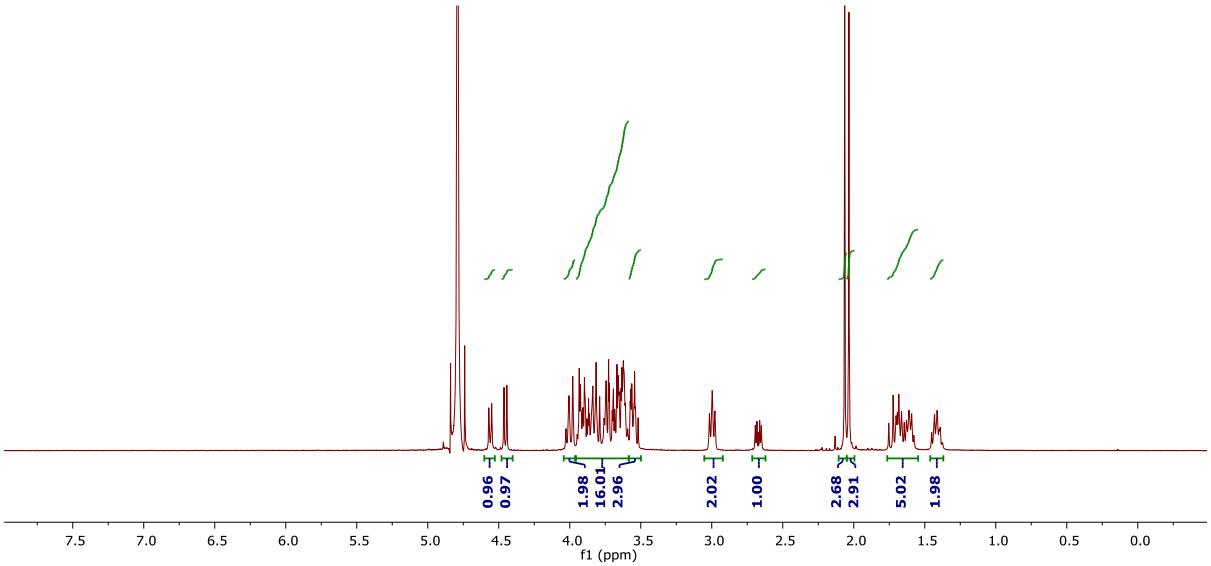
0.96
0.97
1.98
16.01
2.96
2.02
1.00
2.68
2.91
5.02
1.98
7.5
7.0
6.5
6.0
5.5
5.0
4.5
4.0
3.5
3.0
2.5
2.0
1.5
1.0
0.5
0.0
f1 (ppm)

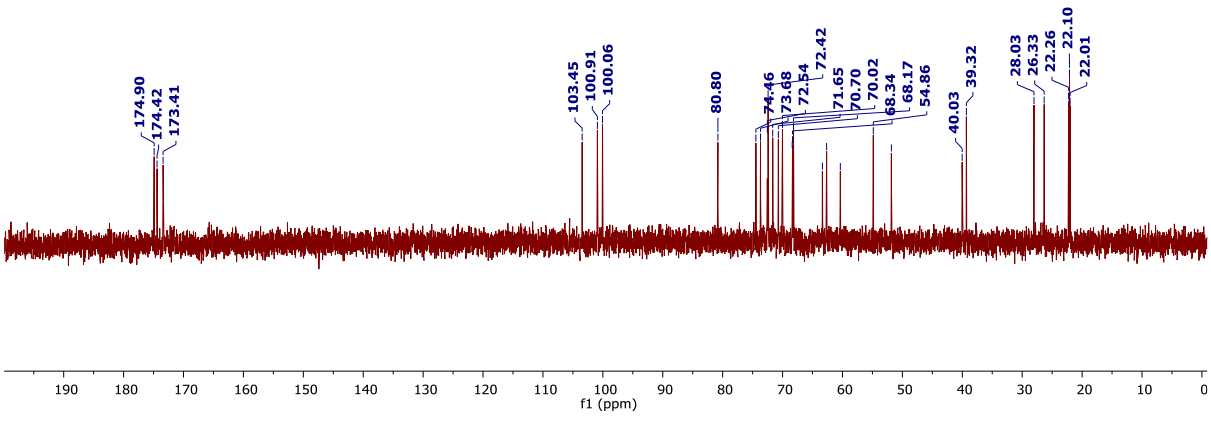
174.90
174.42
173.41
103.45
100.91
100.06
80.80
74.46
73.68
72.54
72.42
71.65
70.70
70.02
68.34
68.17
54.86
40.03
39.32
28.03
26.33
22.26
22.10
22.01
190
180
170
160
150
140
130
120
110
100
90
80
70
60
50
40
30
20
10
0
f1 (ppm)

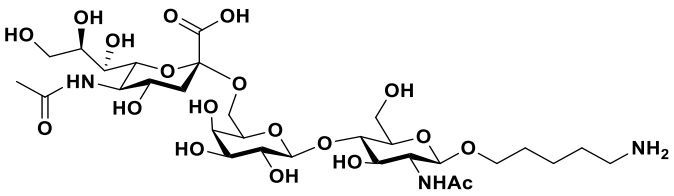
HO
OH
OH
HN
O
HO
O
OH
O
HO
HO
O
OH
O
HO
OH
O
NHAc
NH2

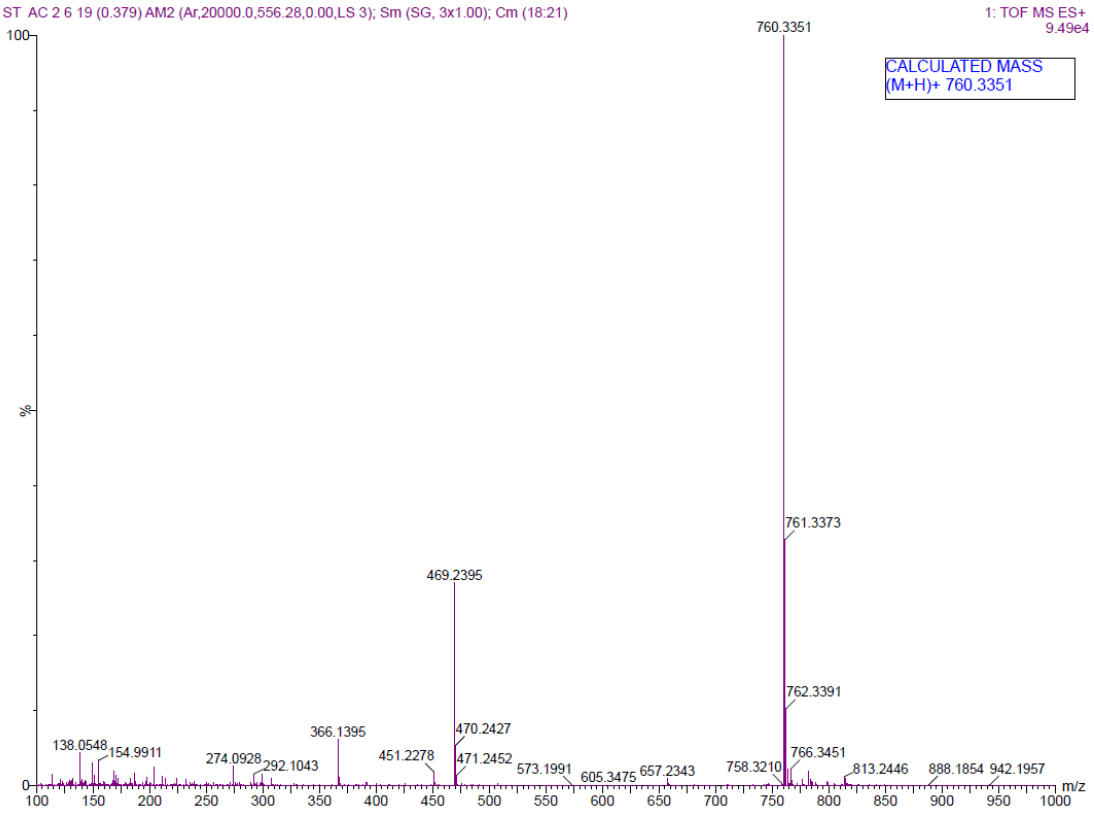
ST AC 2 6 19 (0.379) AM2 (Ar,20000.0,556.28,0.00,LS 3); Sm (SG, 3x1.00); Cm (18:21)
1: TOF MS ES+
9.49e4
CALCULATED MASS
(M+H)+ 760.3351
760.3351
761.3373
469.2395
762.3391
470.2427
366.1395
138.0548
154.9911
274.0928
292.1043
451.2278
471.2452
573.1991
605.3475
657.2343
758.3210
766.3451
813.2446
888.1854
942.1957
100
%
0
m/z
100
150
200
250
300
350
400
450
500
550
600
650
700
750
800
850
900
950
1000

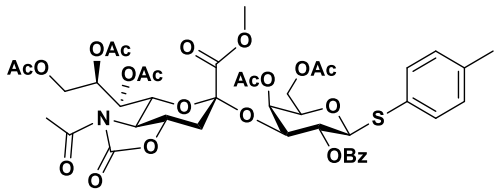
AcO
OAc
OAc
O
O
AcO
OAc
N
O
O
O
O
O
O
S
OBz
O
O

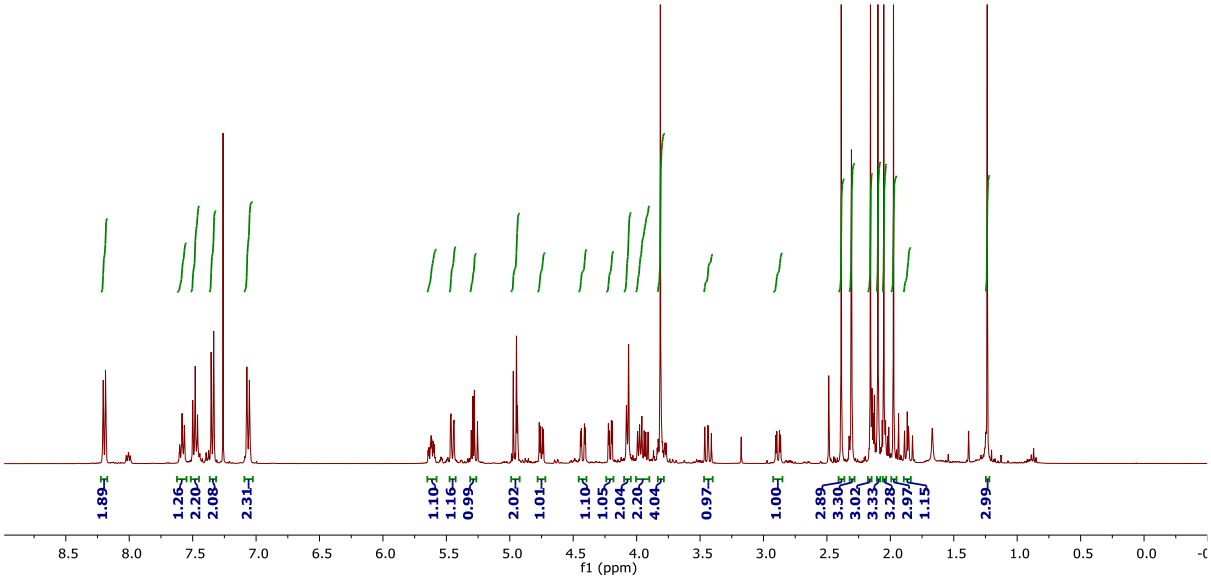
1.89
1.26
2.20
2.08
2.31
1.10
1.16
0.99
2.02
1.01
1.10
1.05
2.04
2.20
4.04
0.97
1.00
2.89
3.30
3.02
3.33
3.28
2.97
1.15
2.99
8.5
8.0
7.5
7.0
6.5
6.0
5.5
5.0
4.5
4.0
3.5
3.0
2.5
2.0
1.5
1.0
0.5
0.0
f1 (ppm)

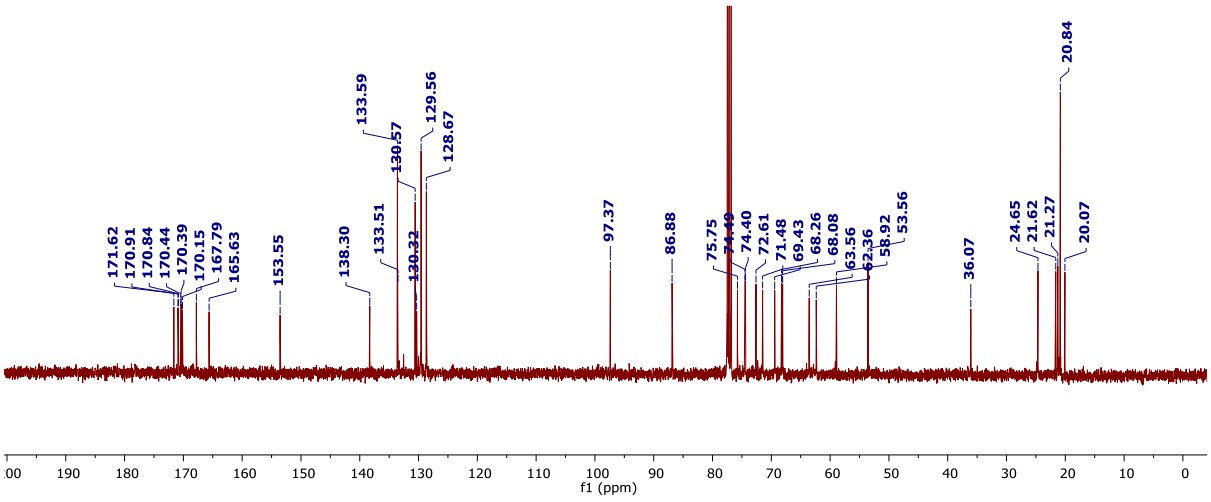
171.62
170.91
170.84
170.44
170.39
170.15
167.79
165.63
153.55
138.30
133.59
133.51
130.57
130.32
129.56
128.67
97.37
86.88
75.75
74.49
74.40
72.61
71.48
69.43
68.26
68.08
63.56
62.36
58.92
53.56
36.07
24.65
21.62
21.27
20.84
20.07
190
180
170
160
150
140
130
120
110
100
90
80
70
60
50
40
30
20
10
0
f1 (ppm)

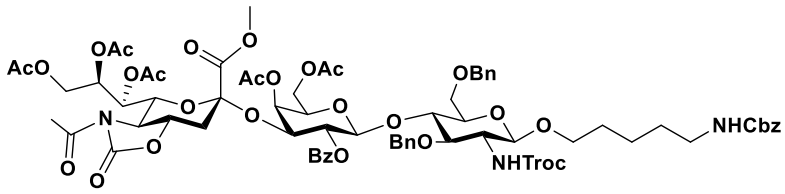
AcO
OAc
OAc
O
O
AcO
OAc
OBn
O
O
O
O
N
O
O
O
BnO
O
NHCbz
BzO
NHTroc
O
O

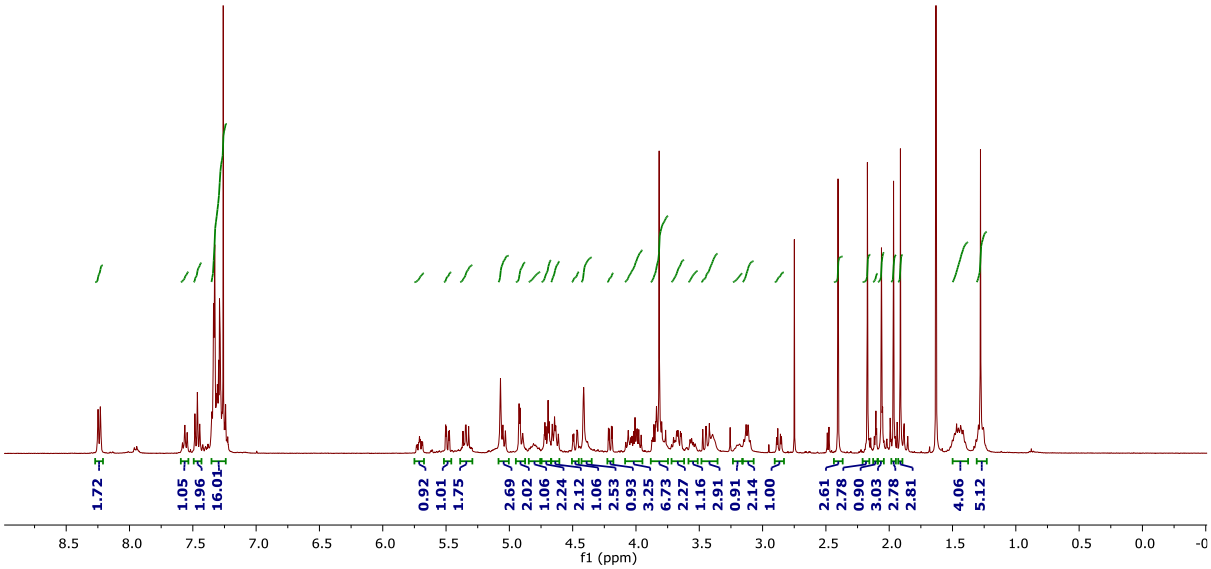
1.72
1.05
1.96
16.01
0.92
1.01
1.75
2.69
2.02
1.06
2.24
2.12
1.06
2.53
0.93
3.25
6.73
2.27
1.16
2.91
0.91
2.14
1.00
2.61
2.78
0.90
3.03
2.78
2.81
4.06
5.12
8.5
8.0
7.5
7.0
6.5
6.0
5.5
5.0
4.5
4.0
3.5
3.0
2.5
2.0
1.5
1.0
0.5
0.0
f1 (ppm)

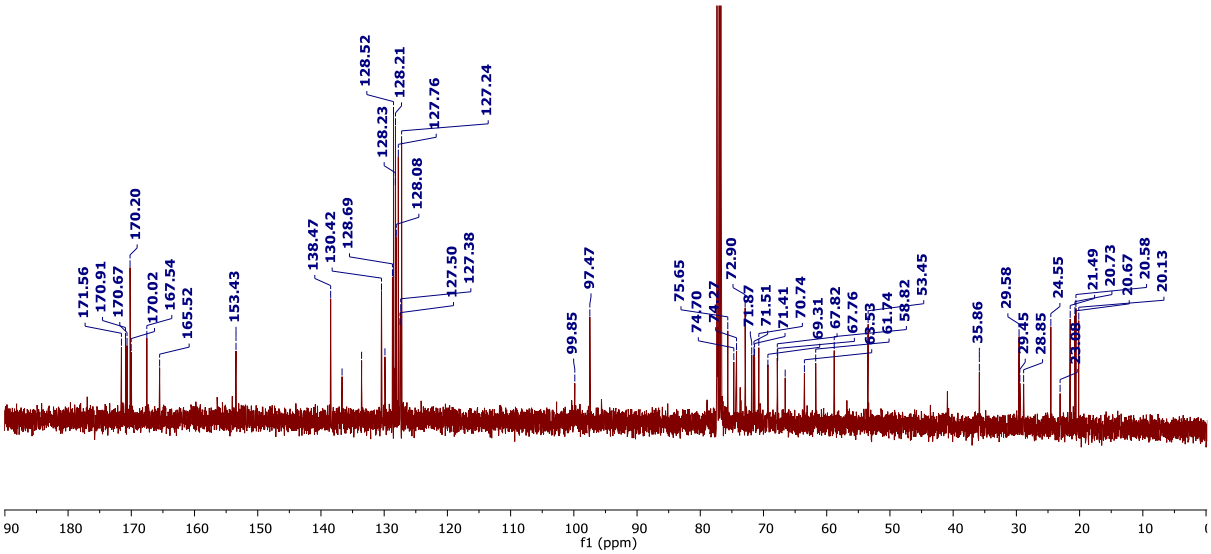
171.56
170.91
170.67
170.20
170.02
167.54
165.52
153.43
138.47
130.42
128.69
128.52
128.23
128.21
127.76
127.24
128.08
127.50
127.38
99.85
97.47
75.65
74.70
74.27
72.90
71.87
71.51
71.41
70.74
69.31
67.82
67.76
65.53
61.74
58.82
53.45
35.86
29.58
29.45
28.85
24.55
23.88
21.49
20.73
20.67
20.58
20.13
90
180
170
160
150
140
130
120
110
100
90
80
70
60
50
40
30
20
10
f1 (ppm)

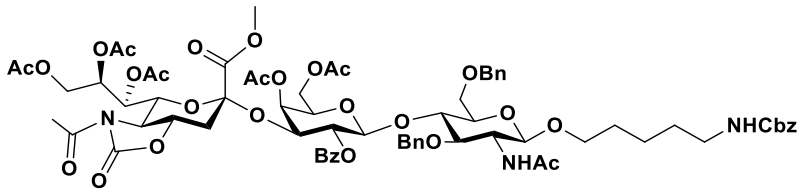
AcO
OAc
OAc
O
O
AcO
OAc
OBn
N
O
O
O
O
O
O
O
O
BnO
O
NHCbz
BzO
NHAc

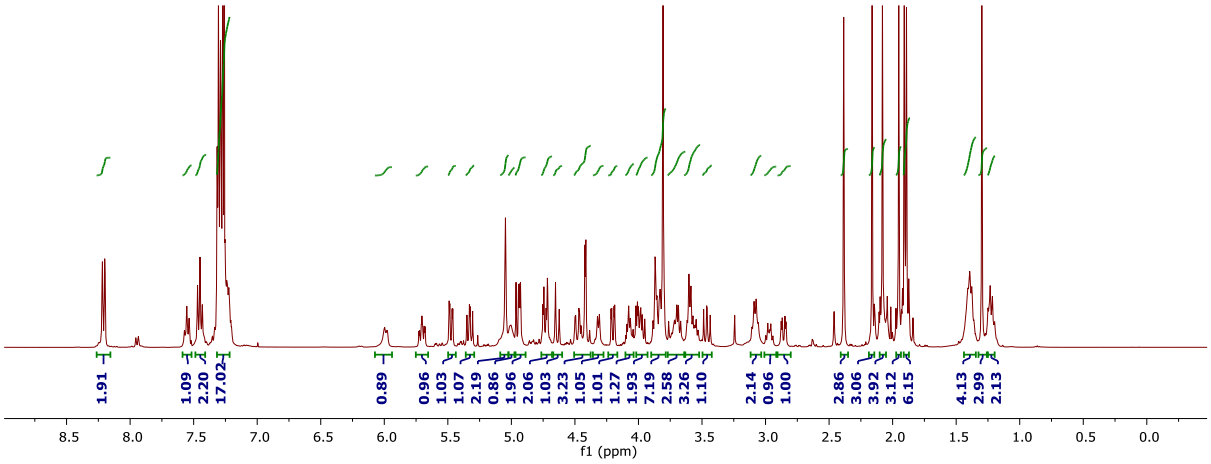
1.91
1.09
2.20
17.02
0.89
0.96
1.03
1.07
2.19
0.86
1.96
2.06
1.03
3.23
1.05
1.01
1.27
1.93
7.19
2.58
3.26
1.10
2.14
0.96
1.00
2.86
3.06
3.92
3.12
6.15
4.13
2.99
2.13
8.5
8.0
7.5
7.0
6.5
6.0
5.5
5.0
4.5
4.0
3.5
3.0
2.5
2.0
1.5
1.0
0.5
0.0
f1 (ppm)

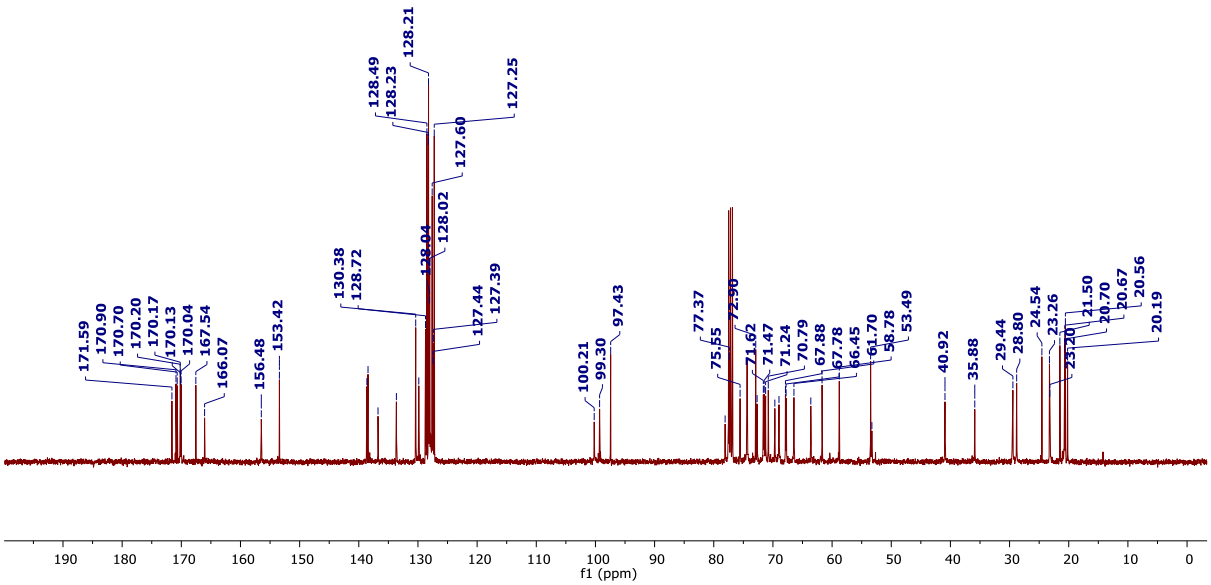
171.59
170.90
170.70
170.20
170.17
170.13
170.04
167.54
166.07
156.48
153.42
130.38
128.72
128.49
128.23
128.21
128.04
128.02
127.60
127.44
127.39
127.25
100.21
99.30
97.43
77.37
75.55
72.90
71.62
71.47
71.24
70.79
67.88
67.78
66.45
61.70
58.78
53.49
40.92
35.88
29.44
28.80
24.54
23.26
23.20
21.50
20.70
20.67
20.56
20.19
190
180
170
160
150
140
130
120
110
100
90
80
70
60
50
40
30
20
10
0
f1 (ppm)

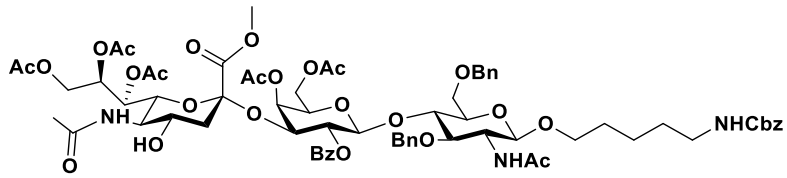
AcO
OAc
OAc
NH
HO
O
O
AcO
OAc
BzO
O
O
O
OBn
BnO
NHAc
O
NHCbz

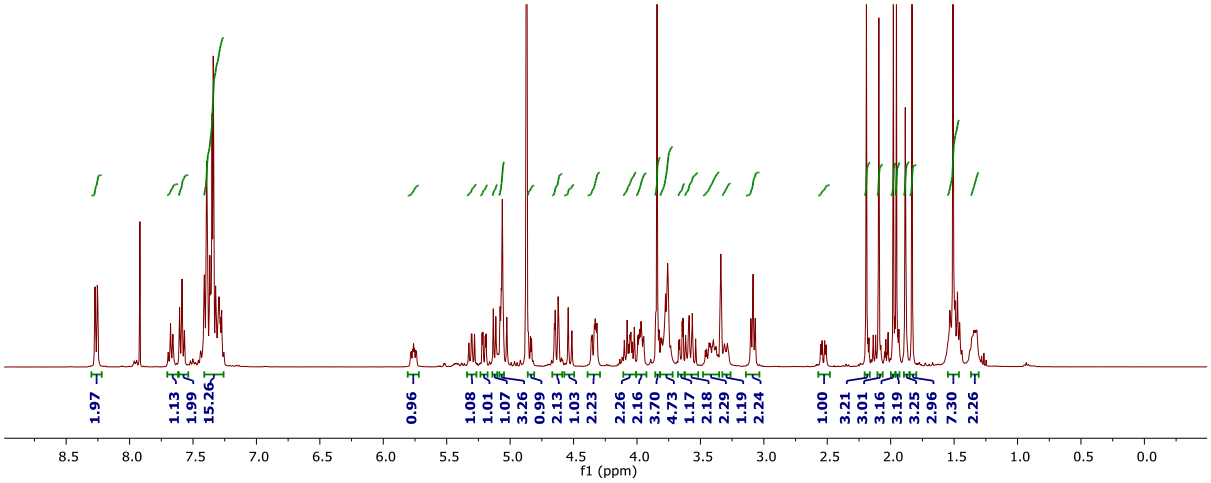
1.97
1.13
1.99
15.26
0.96
1.08
1.01
1.07
3.26
0.99
2.13
1.03
2.23
2.26
2.16
3.70
4.73
1.17
2.18
2.29
1.19
2.24
1.00
3.21
3.01
3.16
3.19
3.25
2.96
7.30
2.26
f1 (ppm)

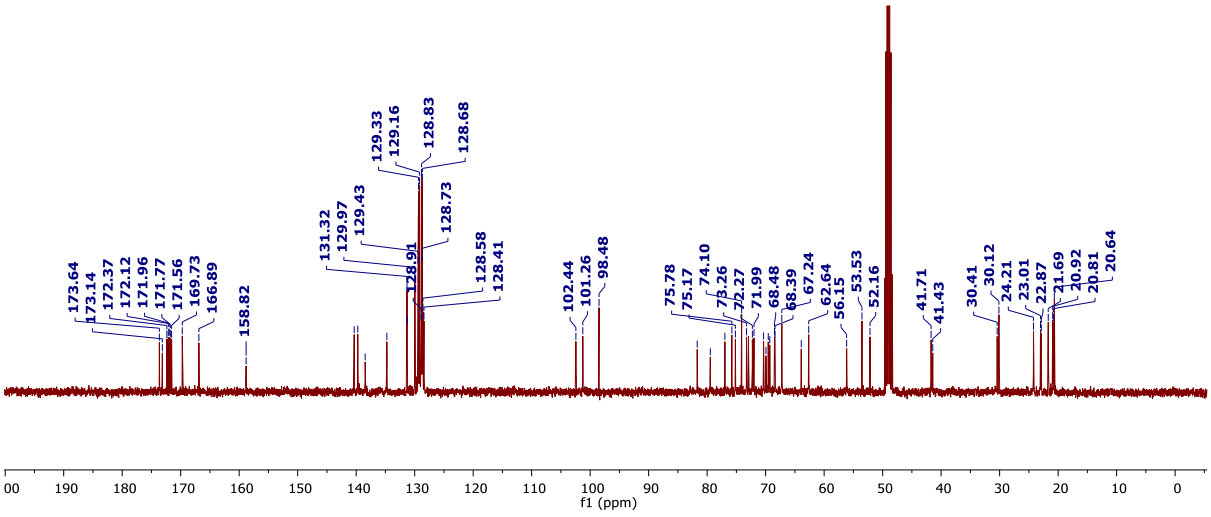
173.64
173.14
172.37
172.12
171.96
171.77
171.56
169.73
166.89
158.82
131.32
129.97
129.43
129.33
129.16
128.83
128.68
128.73
128.91
128.58
128.41
102.44
101.26
98.48
75.78
75.17
74.10
73.26
72.27
71.99
68.48
68.39
67.24
62.64
56.15
53.53
52.16
41.71
41.43
30.41
30.12
24.21
23.01
22.87
21.69
20.92
20.81
20.64
f1 (ppm)

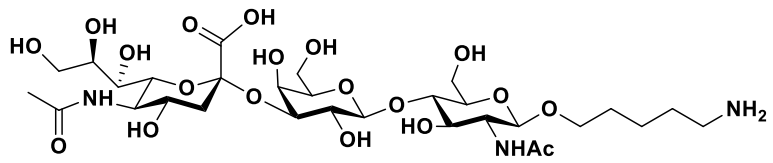
HO
OH
OH
O
OH
NH
O
HO
O
HO
OH
O
O
HO
OH
O
O
NHAc
NH2

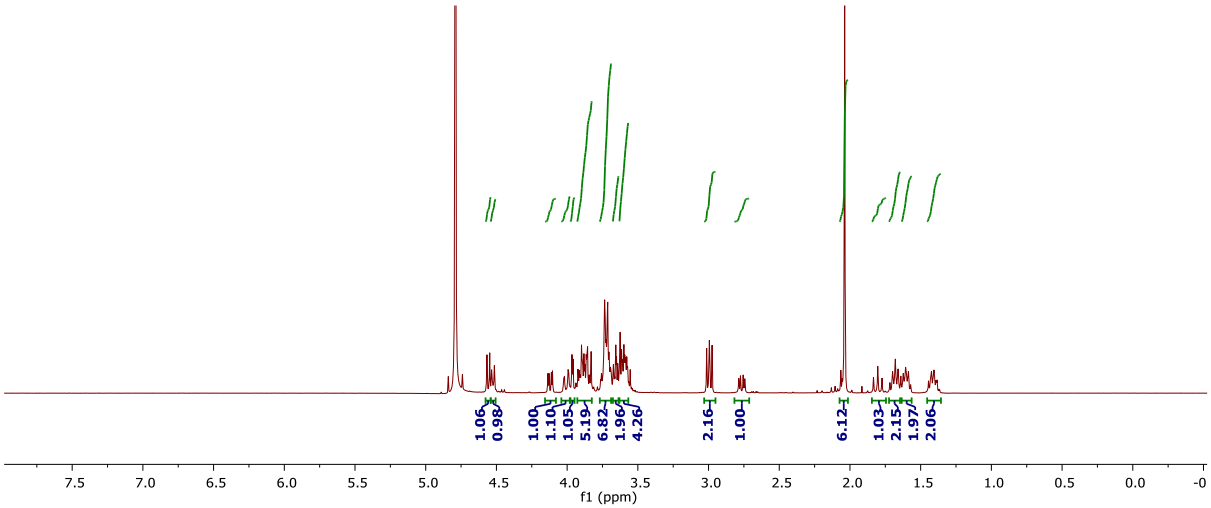
1.06
0.98
1.00
1.10
1.05
5.19
6.82
1.96
4.26
2.16
1.00
6.12
1.03
2.15
1.97
2.06
7.5
7.0
6.5
6.0
5.5
5.0
4.5
4.0
3.5
3.0
2.5
2.0
1.5
1.0
0.5
0.0
-0
f1 (ppm)

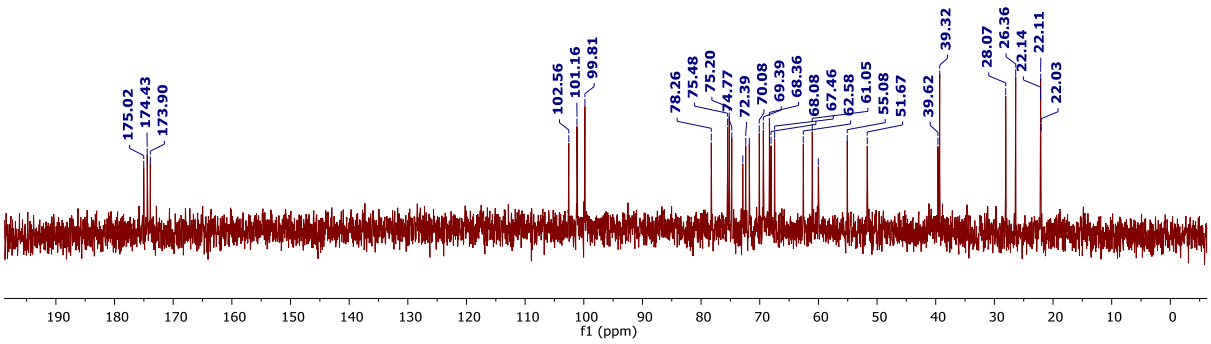
175.02
174.43
173.90
102.56
101.16
99.81
78.26
75.48
75.20
74.77
72.39
70.08
69.39
68.36
68.08
67.46
62.58
61.05
55.08
51.67
39.62
39.32
28.07
26.36
22.14
22.11
22.03
190
180
170
160
150
140
130
120
110
100
90
80
70
60
50
40
30
20
10
0
f1 (ppm)

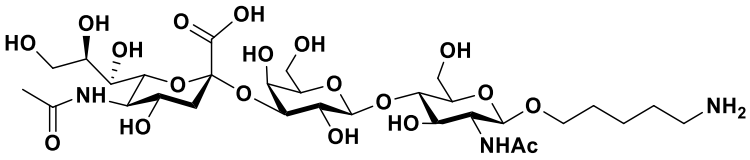
HO
OH
OH
O
OH
NH
O
HO
O
HO
OH
O
O
HO
OH
O
O
O
NH2
NHAc

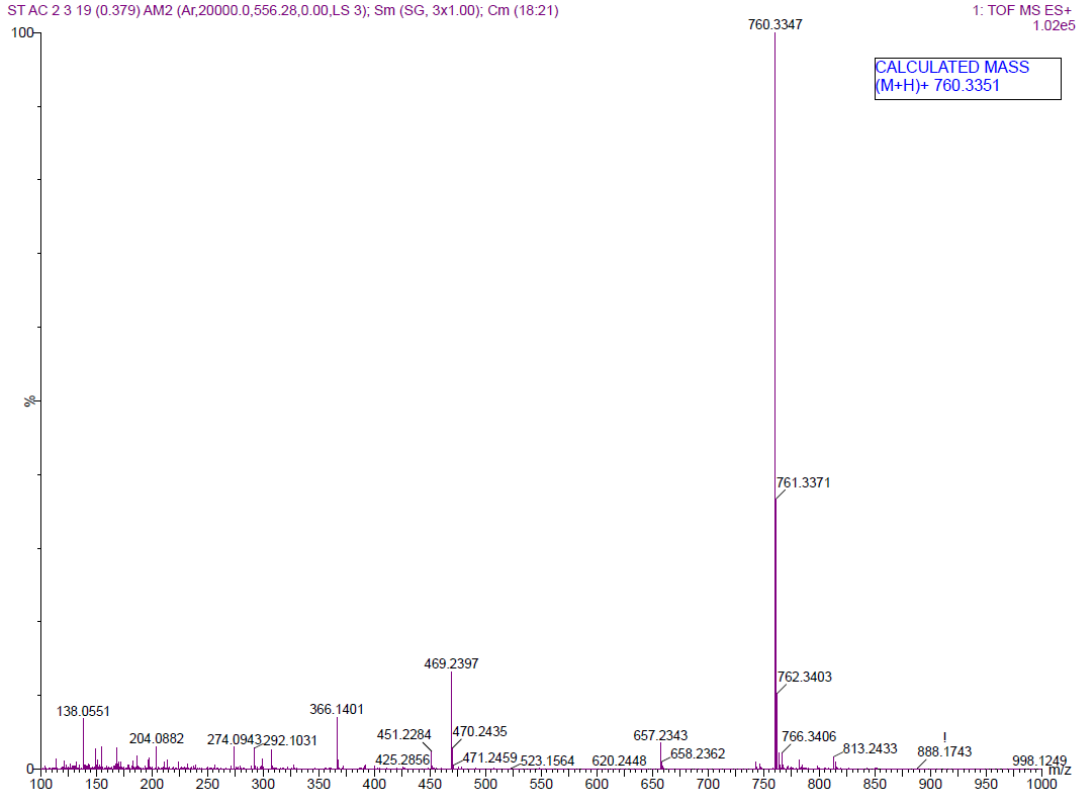
ST AC 2 3 19 (0.379) AM2 (Ar,20000.0,556.28,0.00,LS 3); Sm (SG, 3x1.00); Cm (18:21)
1: TOF MS ES+
1.02e5
100
%
0
760.3347
CALCULATED MASS
(M+H)+ 760.3351
761.3371
762.3403
469.2397
138.0551
366.1401
204.0882
274.0943
292.1031
451.2284
470.2435
425.2856
471.2459
523.1564
620.2448
657.2343
658.2362
766.3406
813.2433
888.1743
998.1249
100
150
200
250
300
350
400
450
500
550
600
650
700
750
800
850
900
950
1000
m/z

S

CHAPTER-4

Shapes of Nanostructures Encode Immunomodulation of Carbohydrate Antigen and Vaccine Development

Abstract:

Carbohydrate-based vaccines have recently emerged as a promising tool for meeting the continued challenge posed by cancer and infectious diseases. However, poor-immunogenicity and T-cell independent immune responses reduced long lasting immune responses. Here, we show that the shape of AuNPs markedly influences carbohydrate-based antigen processing in murine dendritic cells (mDCs) and subsequent T-cell activation. In the study, CpG-adjuvant coated sphere-, rod-, and star-shaped AuNPs were conjugated to the tripodal Tn-glycopeptide antigen to study their DC uptake and the activation of T-cells in the DCs/T-cell co-culture assay. Our results showed that sphere- and star-shaped AuNPs displayed relatively weak receptor-mediated uptake, endosomal sequestration induced a high level of T helper-1 (Th1) biasing immune responses compared with rod-shaped AuNPs, showing that receptor-mediated uptake and cytokine secretion of nanostructures are two independent mechanisms. Significantly, the shapes of AuNPs and antigen/adjuvant conjugation synergistically work together to modulate the effective anti-Tn-glycopeptide immunoglobulin (IgG) antibody response after in vivo administration of the AuNPs. These results show that by varying the shape parameter, one can alter the immunomodulation, leading to the development of carbohydrate vaccines.

4.1 Introduction:

T-cell-dependent (TD) antibody induction is crucial for successfully designing long-lasting immune responses and vaccine development.[1-5] In TD activation, B-cells proliferate, produce immunoglobulin class switching (immunoglobulin M [IgM] to immunoglobulin G [IgG]) and generate memory B-cells, resulting in high affinity with longer living antibodies.[6] Hence, traditional vaccines are composed of antigens, carrier proteins, and co-stimulants, such as toll-like receptor (TLR) adjuvants, to enhance anti-antigen immune responses. Despite sustained efforts by immunologists, there remains a need for a new, versatile method to bring about an effective immune-modulatory system, particularly for such weak immunogenic antigens as carbohydrates.[7-9]

Carbohydrates on the cell surfaces of pathogens and cancer cells are promising antigens for vaccine development.[10, 11] However, because of the immunodominance of carrier proteins over antigens, carbohydrate antigen-carrier protein conjugation methods have typically failed to induce robust humoral and cellular immune responses against self-antigenic tumor-associated carbohydrate antigens (TACAs).[12, 13] Alternatively, nanostructures, virus-like particles, liposomes, and polymers have been used as antigen-carrier platforms to avoid antibody production on scaffolds. [14-19]

Among the various nanostructures used, gold nanoparticles (AuNPs) have received increasing attention because of their nontoxicity and easily tunable physical properties.[20-23] Recently, Corzana and co-workers reported synthesizing AuNPs carrying human mucin 1 (MUC1)-like antigens bearing O/S-glycosidic linkage-displayed immunogenic activity.[24] Westerlind and co-workers investigated AuNPs functionalized with chimeric peptides, containing the MUC1-derived glycopeptide sequence and the P30 sequence of T-cell epitope for selective antibody responses.[25] Similarly, Barchi and co-workers reported developing AuNPs bearing TACAs to develop adjuvant-free immune responses.[26] Furthermore, Barchi and co-workers reported spherical AuNPs bearing 28-mer MUC4 antigens showing IgG responses.[27] However, most AuNPs used for glycan immunogenicity are spherical nanostructures carrying full-length glycopeptides. Thus, the influence of AuNPs with different shapes on the immunomodulation of carbohydrate antigens has not yet been examined. Moreover, shape-dependent immune modulation is fundamental to developing new biomaterials.

Recently, viral antigens have been encapsulated on different shapes of AuNPs to alter immune responses and aid in vaccine development.[28, 29] However, a systematic investigation of

nanostructure shapes modulating the immune response of carbohydrate antigens has not been described. Herein, we report on the synthesis of sphere-, rod-, and star-shaped AuNPs bearing an active part of MUC1 antigen glycopeptide and a CpG adjuvant to study the shape-dependent immune modulation of the MUC1 antigen. Extensive imaging and fluorescence-activated cell sorting (FACS) analysis with murine dendritic cell (mDC) uptake and cytokine secretion in mDC/T-cell co-culture assay established the relation between the physical properties of AuNPs in receptor-mediated mDC uptake and T-cell activation. Finally, we assessed in vivo humoral immune responses to show shape-dependent anti-MUC1 antibody production and representation of a novel platform that can be used for vaccine development.

4.2 Results and Discussion:

4.2.1 Synthesis of antigen/fluorescent conjugate tripod:

With the goal of creating a new nanostructure for glyco-immunomodulation, MUC1, which is overexpressed in cancer cells,[30-32] and the CpG-ODN adjuvant were selected as the immunogenic substrates. The rationale for choosing CpG-ODN as an adjuvant is that it has a strong agonistic nature for TLR9, which induces Th1-biased immune responses.[33, 34] Studies

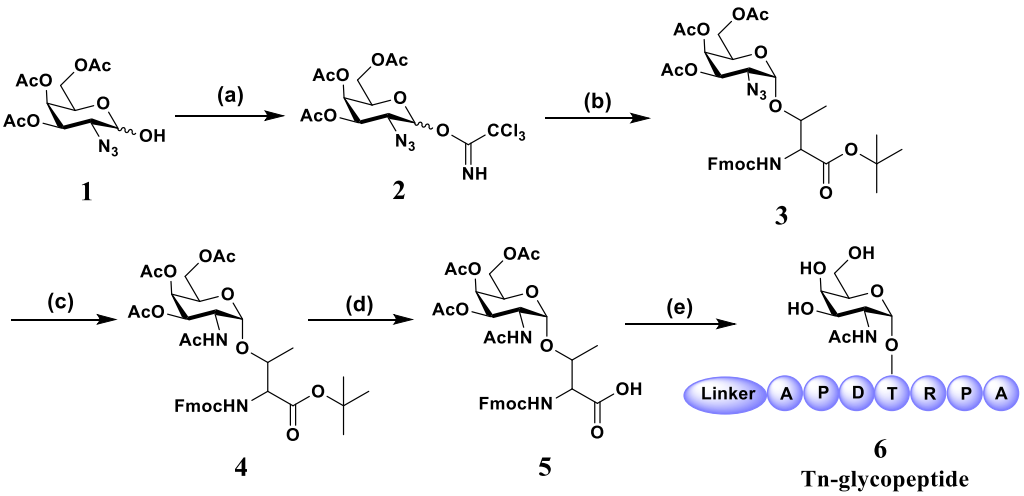

Scheme 1. Synthesis of Tn-glycopeptide **6**: (a) DBU, Cl_3CN, CH_2Cl_2, rt, 2 h, 88%; (b) TMSOTf, Fmoc-Thr-OtBu, CH_2Cl_2, rt, 1 h, 71%; (c) Zn, THF/AcOH/Ac_2O (3:2:1, v/v), rt, 4 h, 61%; (d) TFA/DCM (1:1, v/v), rt, 4 h. (e) Solid Phase Peptide Synthesis.

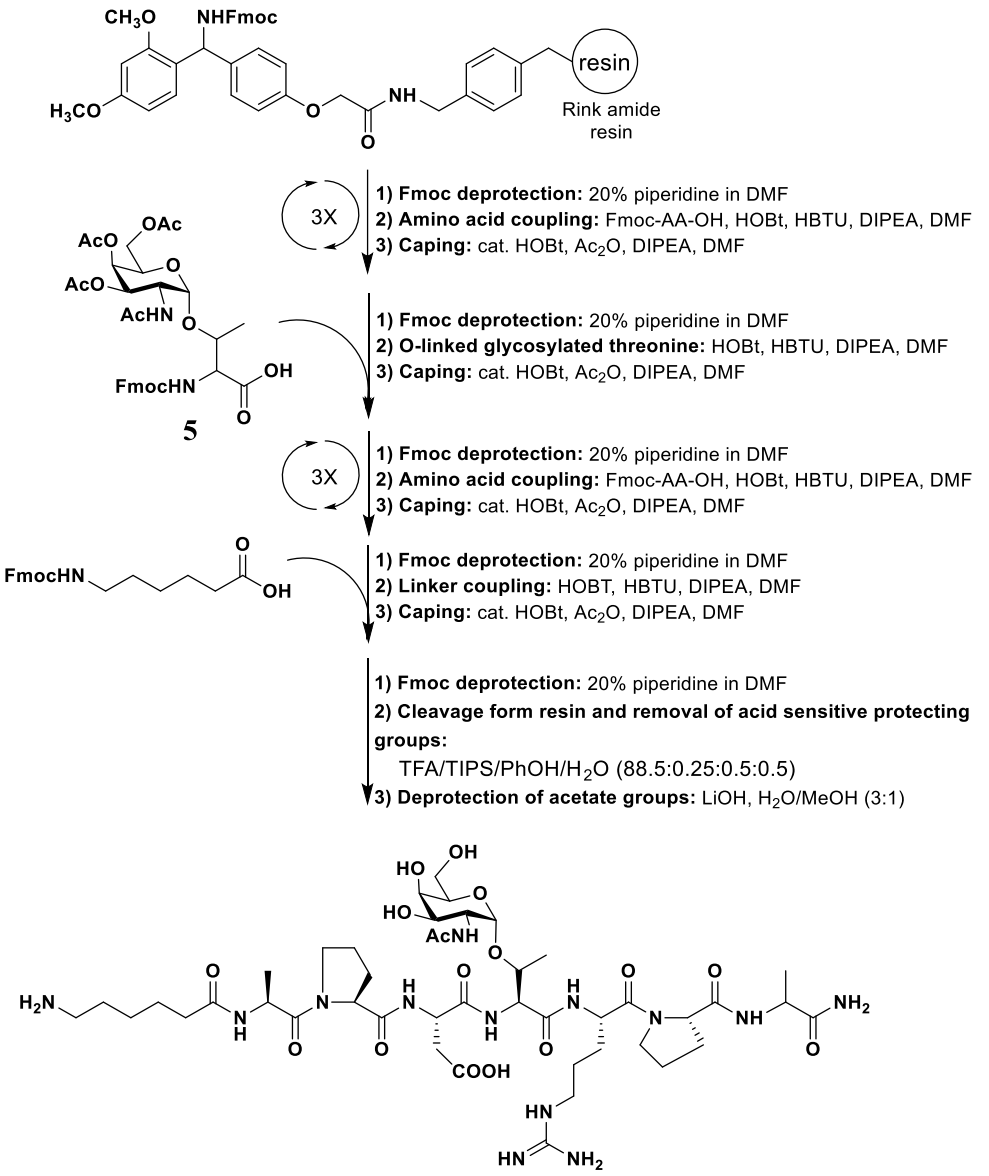

Scheme 2. Solid phase peptide synthesis of Tn-glycopeptide (TnG).

have been conducted to target MUC1 using various innovative platforms,[35-45] findings that the Ala-Pro-Asp-Thr-Arg-Pro (APDTRP) region is the minimum immunogenic epitope of MUC1 responsible for strong tumor cell recognition.[46] Based on this information, we prepared a Tn-glycopeptide (TnG) with an amine linker for nanostructure-mediated immune activity. We used solid-phase peptide synthesis and **5** as the Tn–amino acid residue to synthesize the Tn-glycopeptide **6** (Scheme 1). Compound **5** was synthesized *via* glycosylation of the Fmoc-L-threonine amino acid derivative to **2** using trimethylsilyl trifluoromethanesulfonate (TMSOTf) as a promoter, followed by reducing the azide group of **3** through Zn/AcOH and subsequent

acetylation using acetic anhydride in tetrahydrofuran (THF) solvent. Finally, the *t*-butyl ester group of **4** was deprotected in acidic condition to obtain compound **5.** Then, using rink amide resin and Fmoc-chemistry, TnG **6** was synthesized with an amine linker using 2-(1H-benzotriazol-1-yl)-1,1,3,3-tetramethyluronium hexafluorophosphate/hydroxybenzotrizole (HBTU/HOBt) as the coupling agent (Scheme 2). The final peptide was purified using high-

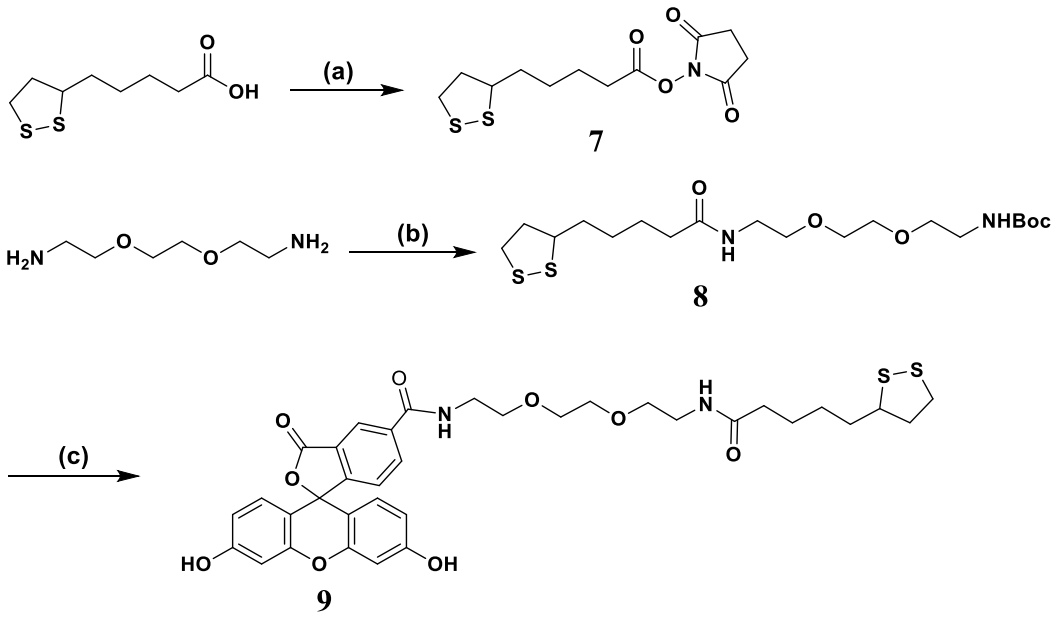

Scheme 3. Synthesis of Carboxylflurescein molcecules **9**. (a) NHS, DCC, CH_2Cl_2, rt, 12 h, 70%; (b) i) Boc_2O, CH_2Cl_2, rt, 12 h, 67%; ii) **7**, CH_2Cl_2, Et_3N, rt, 12 h, 74%; (c) i) TFA/DCM (1:1, v/v), rt, 4 h; ii) Carboxylflurescein diacetate succinimidyl ester, Et_3N, CH_2Cl_2, 40 ºC, 4 h, 87%.

performance liquid chromatography (HPLC) and characterized with nuclear magnetic resonance (NMR) and mass spectroscopic techniques. The fluorescein-linker **9** was synthesized using the previous procedure with slight modifications to obtain a dithiol linker (Scheme 3).[47] We envision conjugating this Tn glycopeptide **6** and florescent tag to well-defined tripod **14** to obtain a multivalent tripod **16** (Scheme 4). The synthesis of tripod **10** was carried out using a previously reported procedure.[48] Further, **11** was obtained by *N,N'*-dicyclohexylcarbodiimide (DCC) coupling of 5-(Boc-amino)pentanoic acid with free amine of **10** followed by Boc deprotection and reaction with DL-α-lipoic acid *N*-hydroxy succinimide. Ester hydrolysis of **12** was followed by active ester formation, giving compound **13**. Later one

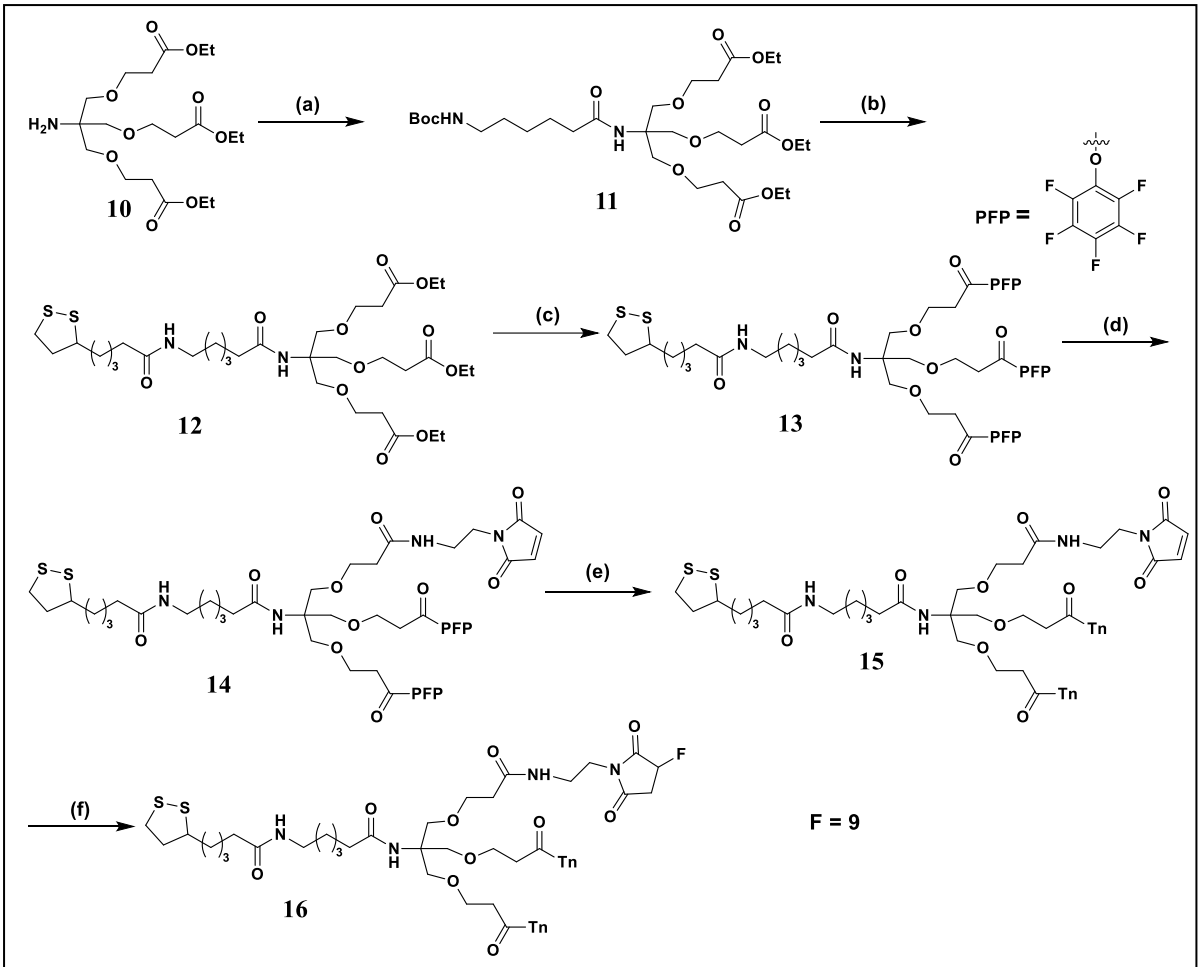

Scheme 4. Synthesis of tripod **16**. (a) DCC, 5-(Boc-amino)pentanoic acid, CH_2Cl_2, rt, 12 h, 69%; (b) i) CH_2Cl_2/TFA (3:1, v/v), rt, 4 h; ii) DIPEA, *N*-Lipoyloxy succinimide, CH_2Cl_2, rt, 4 h, 82% over two steps; (c) i) LiOH, THF/H_2O/Dioxane (2:1:1, v/v), rt, 6 h; ii) Pentaflurophenol, DCC, CH_2Cl_2, 12 h, 47% over two steps; (d) *N*-(2-Aminoethyl)maleimide trifluoroacetate, DIPEA, CH_2Cl_2, rt, 2 h, 31% ;(e) **6** (Tn-glycopeptide), DIPEA, DMF, rt, 4 h, 58%; (f) **9**, DIPEA, DMF, rt, 12 h, 16%.

of the active ester group of tripod **13** was selectively replaced by *N*-(2-aminoethyl)maleimide, and the remaining two active esters were replaced by **6** (Tn-glycopeptide). Next, the Michael addition of the reduced compound **9** to the maleimide group led to the final tripod **16**. The final compound was purified by HPLC and characterized by mass spectroscopy.

4.2.2 Synthesis and characterization of antigen/adjuvant-coated nanoparticles:

To assess the interplay between the Tn antigen, CpG adjuvant, and shapes of AuNPs in immunomodulation, we first synthesized two different sizes of the spheres (S-1: 20 nm and S-2: 45 nm) and rods (R-1: 20 × 6 nm and R-2: 46 × 14 nm), and single-size star-shaped gold nanoparticles (St: 70 nm spike-to-spike), using the previously reported protocol (Table 1).[49-53]

We chose the above sizes of AuNPs because it has been proven that particles of 10–100 nm can regulate effective lymph node targeting and immunomodulation.[54] The NPs' size and shape were confirmed by transmission electron microscopy (HR-TEM) and ultraviolet-visible (UV-vis) absorption (Table 1) . The spheres displayed localized surface plasmon resonance (LSPR) peaks at 524 nm and 548 nm, corresponding to two sizes of sphere AuNPs (20 nm and 45 nm, respectively). The star peaked at 784 nm, and the rods' LSPR peaks were in the near

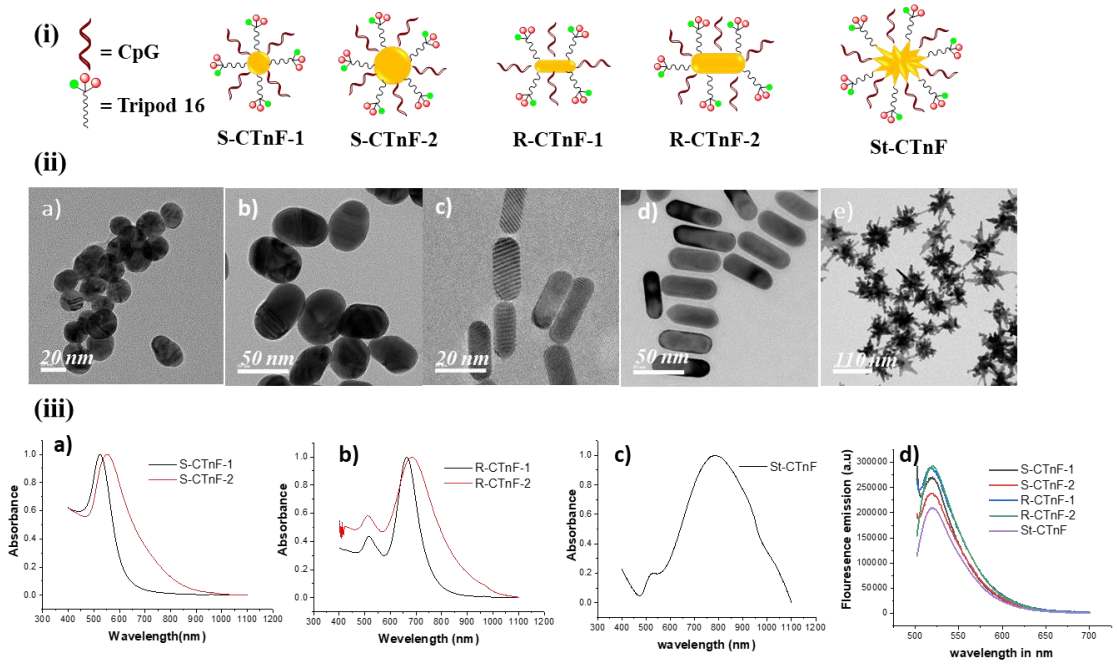

Figure 1. (i) Schematic representation of AuNPs conjugated with tripod **16** and **CpG**; (ii) HR-TEM images of tripod **16** and **CpG** conjugated AuNPs a) S-CTnF-1 b) S-CTnF-1 c) R-CTnF-1 d) R-CTnF-2 e) St-CTnF (iii) UV-visible spectra of CTnF conjugated AuNPs; a) S-CTnF-1 and S-CTnF-1 b) R-CTnF-1 and R-CTnF-2 c) St-CTnF d) Fluorescence spectra of CTnF functionalized AuNPs.

infrared (NIR) region at 660 and 687 nm (Table 1). The AuNPs were encapsulated with the optimum number of CpG adjuvants, which is sufficient to induce immunomodulation by the ligand exchange process. Changes in the zeta (ζ) potentials of AuNPs confirmed the conjugation of the CpG adjuvant. More specifically, after CpG conjugation to rod AuNPs, the ζ-potential of rod AuNPs changed from a positive (+34.5 and +34.8, Table 3) to a negative potential. In contrast, sphere and star AuNPs displayed slight changes in the negative potential, indicating effective CpG conjugation (Table 3). Neither scanning electron microscopy (SEM) nor the UV-vis profile of these AuNPs showed any significant difference from the native nanostructures. The amount of CpG per AuNPs was quantified by a DNA quantification kit (Tables 2 and 3).

Table 1. Physical Characterization of gold nanoparticles.

Sr. No.	Nanoparticles (Nps)	Size (nm)	λ_{max} (nm)	Zeta-potential (mv)
1	**S-1**	20±3	524	-21.0
2	**S-2**	45±6	548	-22.8
3	**R-1**	20±4 X 6±2	660	+34.5
4	**R-2**	46±5 X 14±3	687	+34.8
5	**St**	70±10	784	-26.7

Table 2. Physical Characteristics of CTnF conjugated AuNPs.

Sr. No.	Nanoparticles (NPs)	Zeta-potential (mv)	Total Molecules/NP	CpG Molecules/NP	Tn Molecules/NP
1	**S-CTnF-1**	-17.2	110 ± 10	71 ± 26	45 ± 09
2	**S-CTnF-2**	-21.0	347 ± 49	125 ± 19	198 ± 23
3	**R-CTnF-1**	-11.4	120 ± 21	49 ± 8	75 ± 12
4	**R-CTnF-2**	-17.7	281 ± 30	91 ± 7	174 ± 26
5	**St-CTnF**	-28.7	331 ± 31	140 ± 31	192 ± 30

Table 3. Physical Characteristics of CpG and TnF conjugated AuNPs.

Sr. No.	NPs	ζ -potential (mv)	CpG Molecules/NP	Sr. No.	NPs	ζ -potential (mv)	Tn Molecules/NP
1	**S-CpG-1**	-19.6	82 ± 24	1	**S-TnF-1**	13.6	167±22
2	**S-CpG-2**	-21.0	121 ± 14	2	**S-TnF-2**	13.1	240±31
3	**R-CpG-1**	-16.7	52 ±10	3	**R-TnF-1**	12.4	100±10
4	**R-CpG-2**	-17.2	101 ± 9	4	**R-TnF-2**	11.9	274±28
5	**St-CpG**	-22.8	144 ± 31	5	**St-TnF**	7.1	310±30

Finally, tripod **16** was incorporated directly by mixing the CpG-AuNPs with the known quantity of ligand **16** to obtain S-CTnF-1, S-CTnF-2, R-CTnF-1, R-CTnF-2, and St-CTnF (Figure 1-i and 1-ii). The conjugation of tripod **16** was further confirmed by changes in the zeta potential and quantified using a thiol-detection kit (Table 2). It was observed that, as the size and aspect ratio of the AuNPs increased, the number of **CpG** and tripod **16** per NP also

increased because of the large surface area. As a control, we also synthesized and characterized five fluorescent CpG-adjuvant conjugated AuNPs (S-CpG-1, S-CpG-2, R-CpG-1, R-CpG-2, and St-CpG) and five antigen conjugated AuNPs (S-TnF-1, S-TnF-2, R-TnF-1, R-TnF-2, and St-TnF) (Figure 2).

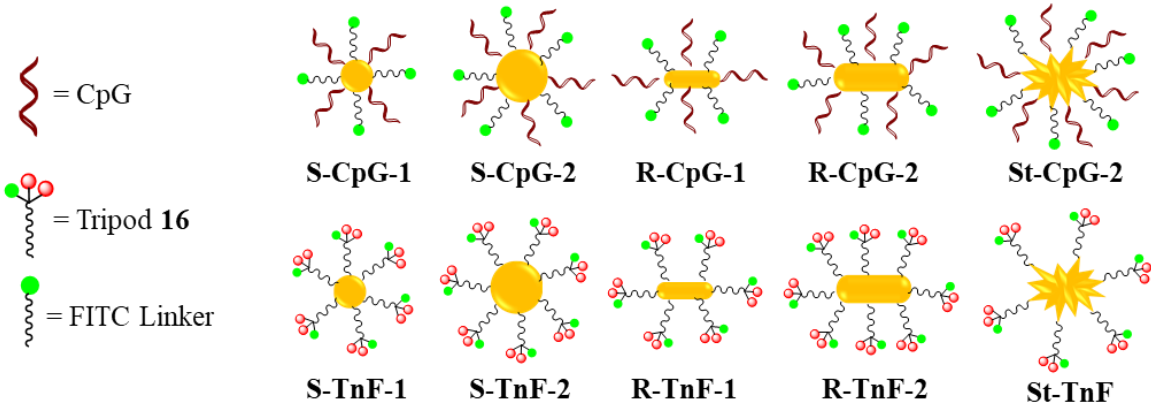

Figure 2. Schematic representation of AuNPs conjugated with tripod **CpG** and tripod **16**.

4.2.3 Nanostructure uptake in murine dendritic cells (mDC):

To address the mechanism underlining the immunomodulation of the nanostructures, we first investigated the cellular internalization of AuNPs using mDCs because MGL (human macrophage galactose and N-acetylgalactosamine-specific C-type lectin) receptors interact with Tn-antigen on mDCs engaged receptor mediated endocytosis.[55] Thus, it is hypothesized that disparity in the aspect ratio, nanostructure contact area, and antigen/adjuvant conjugation modulate the uptake mechanism and sequestration. Since the nanostructures contain different concentrations of CpG and TnF conjugation, we adjusted the amount of AuNPs for *in vitro* and *in vivo* studies. We used 50 nmol of CpG as the optimum concentration for *in vitro* studies. Accordingly, the concentration of functionalized AuNPs was adjusted for experimental studies. Similarly, TnF concentration was quantified on CTnF-nanostructures and similar concentration of TnF-conjugated nanostructures were used. Next, dendritic cells (DCs) and T cells were isolated from mouse spleen by using $CD11c^{+}$ MicroBeads and Pan T cell isolation kit II (Miletnyi) respectively. The purity of DCs and T cells was analysed using FACS by staining with an anti-CD11c and anti-CD-3e antibodies respectively (Figure 3-i). First, the cytotoxicity of AuNPs was investigated using an MTT assay employing mDC isolated from the spleen. As expected, none of the AuNPs showed cytotoxicity up to a concentration of 200 nmol of CpG. Then, AuNPs carrying 50 nmol of CpG concentration were incubated for 1 h and 4 h with mDC and imaged. The results indicated that rod-shaped AuNPs bearing TnF and CTnF ligands exhibited the most effective uptake than CpG conjugated AuNPs for 4 h (Figure-3-ii). In

contrast, sphere- and star-shaped AuNPs displayed weak uptake (Figure 3-ii). This means that the shape of nanostructures promotes different rates of receptor-mediated endocytosis. We then quantified cellular uptake using FACS and developed a hierarchical clustering analysis (HCA). The HCA of the nanostructure displayed several distinct clusters. Although the Tn-antigen on the nanostructures increased the cellular internalization, the shape and size of the nanostructures displayed disparity in this cellular internalization; notably,

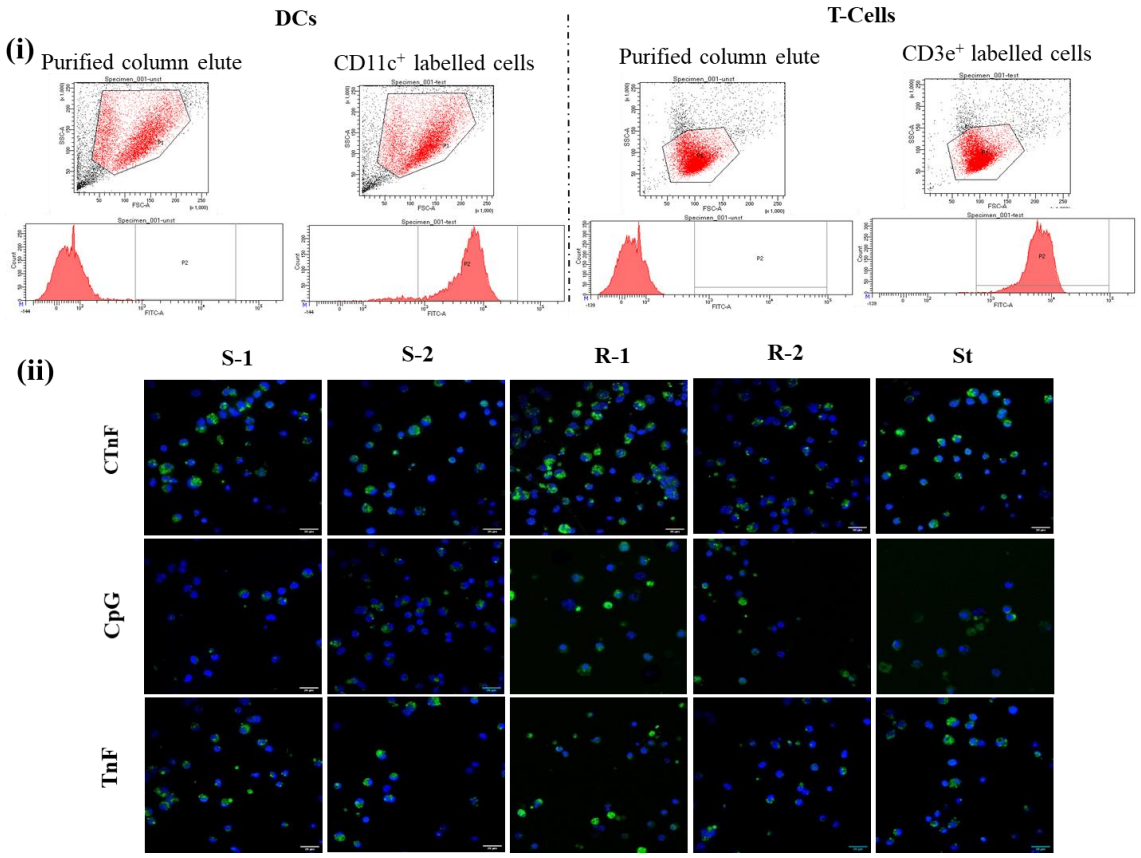

Figure 3. (i) FACS analysis of dendritic cells (DCs) and T cells isolated from mice splenocytes. (ii) Confocal microscopy images for uptake of CTnF, TnF and CpG conjugated AuNPs by dendritic cells at 4 h.

R-TnF-1 showed strong uptake as compared to all other NPs (for 1 h, **S**-TnF-1: 50%; S-TnF-2: 30%; R-TnF-1: 80%; R-TnF-2: 30% and St-TnF: 60%) (Figure 4-i and 4-ii), indicating rod-shaped nanostructures can pear the cell membrane via receptor mediated endocytosis and phagocytosis to induce strong uptake. Similar trend was also observed in CTnF-conjugated nanostructures. In contrast, sphere-shaped AuNPs showed weak and star shaped AuNPs showed moderate uptake. Among different size, R-1 and R-2 conjugates with CTnF and TnF showed a significant disparity in the uptake rate, indicating that aspect ratio and ligand concentrations modulate the uptake rate. Furthermore, CpG-conjugated AuNPs resulted in the least uptake (Figure 4-i), probably due to formidable negative-negative charge repulsion

between the cell-surface oligosaccharides and the oligonucleotides.[56] This trend continued even at 4 h. Based on the results, we hypothesized that the origin of HCA is associated with the shape of the nanostructure and the interactions between the Tn antigen and C-type receptors on the cell surfaces. Moreover, these results correlate with previously published results with shape-dependent nanostructural cellular uptake.

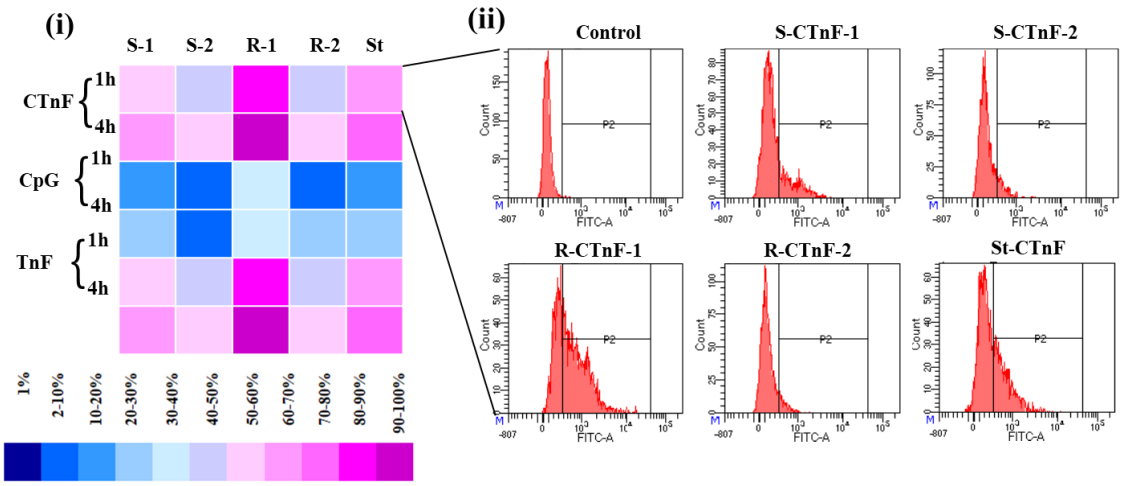

Figure 4. (i) Hierarchical clustering analysis (HCA) for cellular internalization of CTnF, TnF and CpG conjugated AuNPs by dendritic cells at 1 and 4 h interval based on FACS data (Uptake of R-CTnF-1 at 4 h considered as 100%); (ii) Flow cytometry data for CTnF conjugated AuNPs by dendritic cells after 1 h.

4.2.4 Inflammatory activation in DC/T-cell co-culture assay:

Upon cellular internalization of the nanostructure, the CpG adjuvant activates the DCs and processes the antigens as a major histocompatibility complex (MHC), resulting in the activation and differentiation of T-cells into Th1, Th2, and Th17 cells**.** To analyze these adaptive immune responses, we performed a DC/T-cell co-cultivation assay and quantified the level of cytokines secreted in the media in the presence of nanostructures.[57] Stimulation of mDC/T-cells with the nanostructure resulted in nanostructures' shape and adjuvant-dependent enhanced secretion of interleukin (IL)-6, interferon (IFN)-γ, and tumor necrosis factor (TNF)-α; however, IL-10 (Th2-type immune response) was poorly secreted (Figure 5). The cytokine secretion analysis of the AuNPs indicated that CTnF-conjugated AuNPs displayed a stronger Th-1-cytokine response than the TnF-conjugated AuNPs, confirming that antigen/adjuvant conjugated synergistically modulates T-cell activation (Figure 5-i and 5-ii).

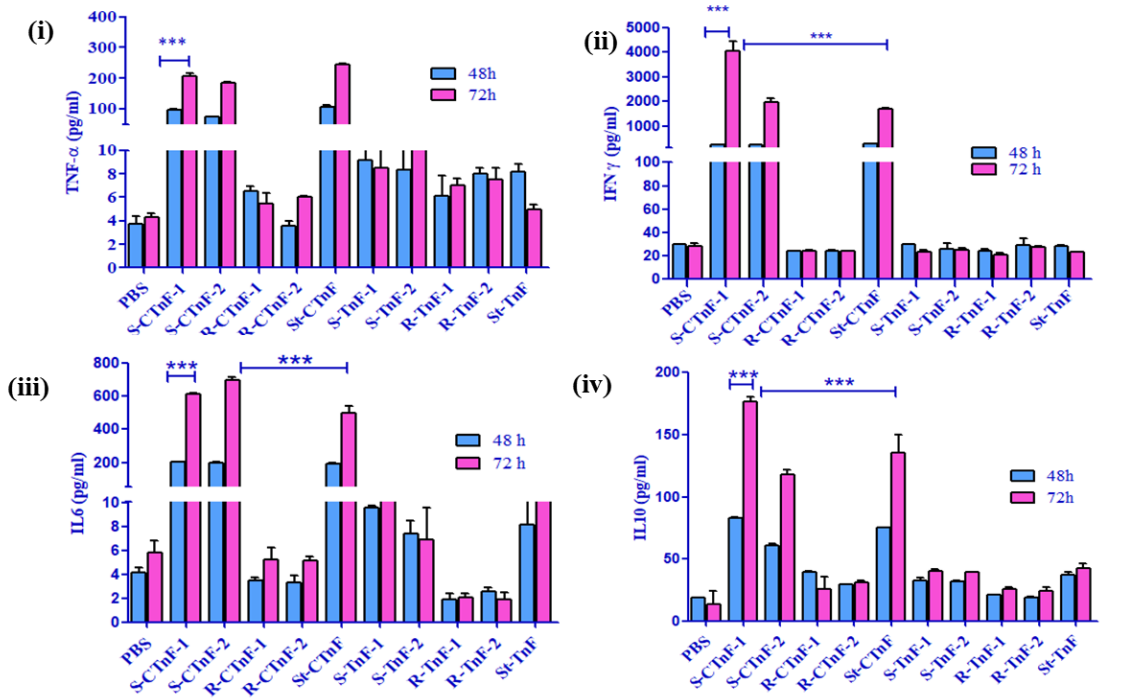

Figure 5. *In vitro* cytokine production by T cells in co-culture with dendritic cells pulsed with **CTnF** and **TnF** conjugated AuNPs. (i) Interleukin-6 (IL-6) production after 48 and 72 h; (ii) Interferon-γ (IFN-γ) production after 48 and 72 h; (iii) Tumor necrosis factor-α (TNF-α) production after 48 and 72 h; (iv) Interleukin-10 (IL-10) production after 48 and 72 h. Asterisks indicate statistically significant differences (***p <0.0001)

Interestingly, the rod-shaped AuNPs showed weak Th1-cytokine secretion as compared to sphere and star shaped AuNPs. This outcome is not entirely surprising, since this type of disparity in cytokine secretion has been reported for nanostructures. Previously, Niikura et al. reported the effect of nanostructure shapes on displaying different rates of sequestration in lysosomes and cytosols to modulate immune responses, and ultimately, antibody production.[28] Lee et al. compared sphere and star-shaped AuNPs sequestration in the endosomes of macrophages and showed that the disparity in the assembly correlates with immune activation.[58] In our case, the R-CTnF-1 impeded TLR9 receptor activation even though they exhibit a great degree of cellular internalization. This may be due to the inherent self-assembly nature of rod-shaped AuNPs and the different rates of sequestration of AuNPs in lysosomes, cytosol, and the endosomal region (Figure 6). Together, these results reiterate that the cellular uptake mechanism and immunomodulation are two independent mechanisms, and the shape of the nanostructures is a crucial factor in controlling the immune process.

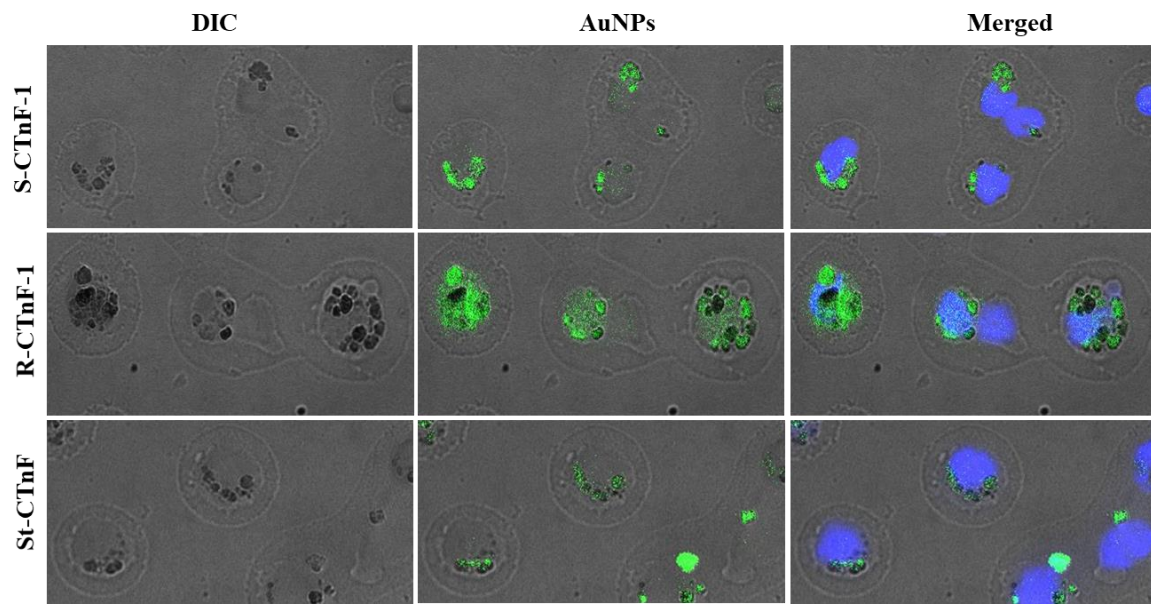

Figure 6. Confocal microscopic images for trafficking of CTnF conjugated AuNPs in dendritic cells.

4.2.5 Antibody response against synthetic Tn-peptide:

As a final component of the study, the in vivo immunogenicity of nanostructures was examined in the C57BL/6 mice model. Groups of five mice were subcutaneously immunized with 100 µl of TnF and CTnF functionalized sphere-, rod- and star-shaped nanostructures (containing 5 nmol of CpG and 7–10 µg of Compound 16) on days 0, 14, and 28. On day 36, the mice were sacrificed; their serum was harvested, and the IgG titer specific to compound TnG was determined by enzyme-linked immunosorbent assay (ELISA). Significantly, S-CTnF-1, R-CTnF-1 and St-CTnF showed the higher antibody induction compared with S-TnF-1, R-TnF-1 or St-TnF nanostructures (Figure 7). Notably, S-CTnF-1 showed the highest immune responses of all six structures. Among three CTnF conjugated AuNPs, R-CTnF-1 showed least IgG titer. These results indicate that the shape of AuNPs has a pivotal role in modulating immune responses and further vaccine development.

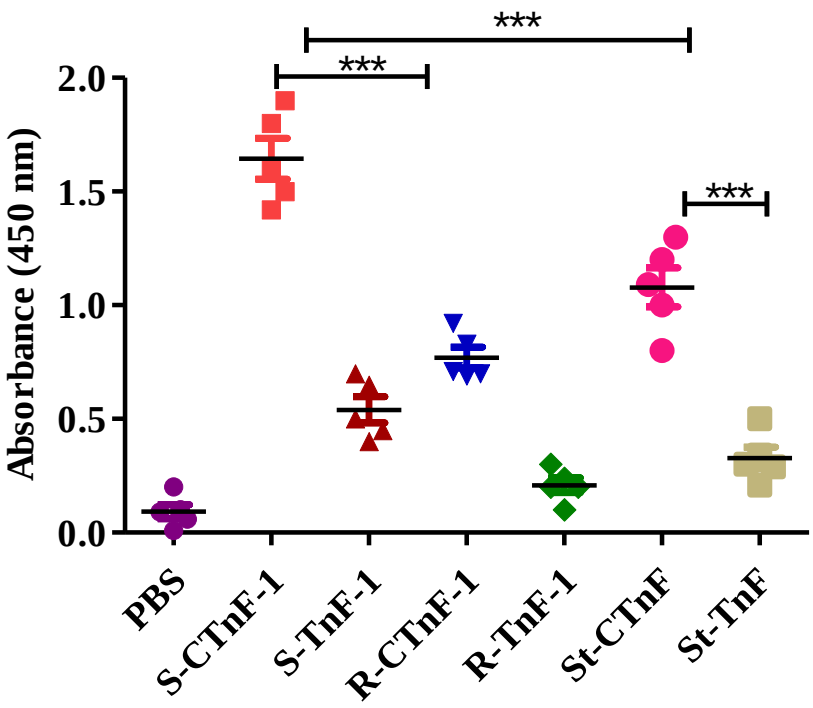

Figure 7. Total IgG antibody titer after immunization of C57BL/6 mice with CTnF and TnF functionalized sphere, rod and star AuNPs. Asterisks indicate statistically significant differences (***p <0.0001)

4.3 Conclusion:

Different shapes and sizes of AuNPs were used to fine-tune the immune responses of the Tn antigen in the presence of CpG adjuvant. Validated by a series of imaging techniques, cytokine secretion and *in vivo* antibody secretion studies, the results showed that cellular internationalization and cytokine secretion are two independent mechanisms. Furthermore, although sphere- and star-shaped nanostructures showed ineffective cellular uptake compared with rod-shaped nanostructures, they were observed to secrete Th1 bias immune responses, resulting in a potential platform to develop T-cell dependent immune modulation of weak immunogenic antigens. Finally, the simplicity and effectiveness of nanotechnology may hold the key to accelerating glycol-nanotechnology in vaccine research.

4.4 Experimental Section:

4.4.1 General information:

All chemicals were reagent grade and used without further purification unless otherwise noted. Reactions were carried out in anhydrous solvents under a nitrogen atmosphere. Reaction progress was monitored by analytical thin-layer chromatography (TLC) on Merck silica gel 60 F_{254}. Spots on TLC plate were visualized under UV light or dipping the TLC plate in

CAM/ninhydrin solution followed by heating. Column chromatography was carried out using Fluka kieselgel 60 (230-400 mesh). Thiol modified oligodeoxynucleotide CpG ODN 1826 (5'-C6SS-TCCATGACGTTCCTGACGTT-3') was purchased from Genemed Synthesis Inc. USA. ^{1}H and ^{13}C NMR spectra of compounds were measured with Bruker 400 MHz, Bruker 600 MHz and Jeol 400 MHz using residual solvents as an internal reference ($CDCl_3$ δH 7.26 ppm, δC 77.3 ppm, CD_3OD δH 3.31 ppm, δC 49.0 ppm, and D_2O δH 4.79 ppm). The chemical shifts (δ) are reported in ppm and coupling constants (J) in Hz. UV-visible measurements were performed with Evolution 300 UV-visible spectrophotometer (Thermo Fisher Scientific, USA). Fluorescence spectra were measured with FluoroMax-4 spectrofluorometer (Horiba Scientific, U.S.A.). Isolation of Dendritic cells and T cells from mice splenocytes were carried out using CD11c+ microbeads and Pan T cells isolation kit II mouse respectively from Miltenyi Bitec. The dendritic and T cells' purity was confirmed using CD11c Monoclonal Antibody (N418), FITC, eBioscience™ and CD3e Monoclonal Antibody (145-2C11), FITC, eBioscience™ respectively. All microscopy images were captured using Leica SP8 confocal microscope and processed using Image J software.

4.4.2 Synthesis of Tn-glycopeptide:

_N_-[(9_H_-Fluoren-9-ylmethoxy)carbonyl]-L-threonine-_tert_-butyl ester

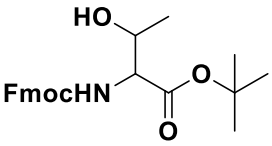

Fmoc-L-threonine (1 gm, 2.93 mmol) in anhydrous ethyl acetate (15 mL) was mixed with *tert*-butyl 2,2,2-trichloroacetimidate (1.06 mL, 5.86 mmol) dropwise. The reaction mixture was stirred at room temperature for 15 h, washed with saturated sodium bicarbonate and brine solutions. The organic layer was dried over Na_2SO_4 and concentrate. The crude compound was purified by silica gel column chromatography using a mixture of (9:1, v/v) dichloromethane and methanol as eluent to afford the desired product (1.01 gm, 2.54 mmol, 87%) as a white solid. ^{1}H NMR (400 MHz, Chloroform-*d*) δ = 7.77 (dq, *J* = 7.6, 0.9 Hz, 2H), 7.61 (d, *J* = 7.3 Hz, 2H), 7.44-7.36 (m, 2H), 7.32 (tt, *J* = 7.4, 1.4 Hz, 2H), 5.56 (d, *J* = 8.9 Hz, 1H), 4.42 (d, *J* = 7.2 Hz, 2H), 4.36-4.14 (m, 3H), 2.00 (d, *J* = 5.5 Hz, 1H), 1.49 (s, 9H), 1.25 (d, *J* = 6.5 Hz, 3H). ^{13}C NMR (101 MHz, Chloroform-*d*) δ = 163.68, 143.88, 141.45, 127.87, 127.23, 125.27, 120.13, 82.90, 68.50, 67.32, 59.65, 47.32, 28.17, 20.07. HR-ESI-MS (m/z): Calcd for $C_{23}H_{27}NNaO_5$ $[M+Na]^+$ 420.1787, found: 420.1784.

3,4,6-Tri-_O_-acetyl-2-deoxy-2-azido-α-D-galactopyranosyl-1-O-trichloroacetimidate (2)

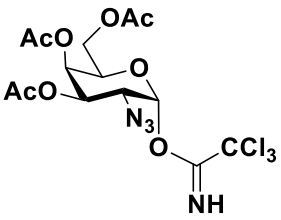

Compound **1** (1.3 gm, 3.92 mmol) in anhydrous dichloromethane (20 mL) was mixed with trichloroacetonitrile (2.00 mL, 19.6 mmol), DBU (0.11 mL, 0.78 mmol) at 0 ˚C and stirred at room temperature for 2 h, and concentrated. The crude compound was purified by silica gel column chromatography using a mixture of (1:1, v/v) ethyl acetate and hexane as eluent to afford the product **2** (1.64 gm, 3.45 mmol, 88 %). ^{1}H NMR (400 MHz, Chloroform-*d*) δ = 8.80 (s, 1H), 6.51 (d, *J* = 3.6 Hz, 1H), 5.54 (dd, *J* = 3.3, 1.3 Hz, 1H), 5.38 (dd, *J* = 11.1, 3.2 Hz, 1H), 4.42 (td, *J* = 6.6, 1.3 Hz, 1H), 4.15 (dd, *J* = 11.3, 6.7 Hz, 1H), 4.10-4.01 (m, 2H), 2.17 (s, 3H), 2.08 (s, 3H), 2.01 (s, 3H). ^{13}C NMR (101 MHz, Chloroform-*d*) δ=170.43, 170.07, 169.84, 160.84, 94.62, 69.26, 68.83, 67.06, 61.34, 57.18, 20.76.

_N_-[(9_H_-Fluoren-9-ylmethoxy)carbonyl]-_O_-(3,4,6-tri-_O_-acetyl-2-azido-2-deoxy-α-D-galactopyranosyl)-L-threonine-_tert_-butyl ester (3)

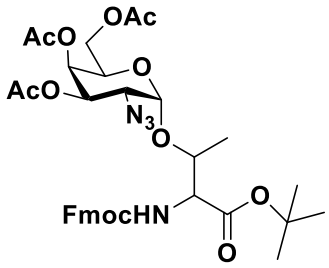

A solution of compound **2** (0.85 gm, 1.79 mmol), Fmoc-Thr-OtBu (0.56 gm, 1.43 mmol) and 4 Å molecular sieves in anhydrous 1:1 (v/v) DCM/Et_2O (20 mL) was stirred under N_2 atmosphere at room temperature for an hour. Next, the reaction mixture was cooled to 0 ˚C, and TMSOTf (32 µl, 0.17 mmol) was added and stirred for an hour. After complete consumption of starting materials, the reaction mixture was quenched with a saturated sodium bicarbonate solution. The organic layer was washed with water, brine and dried over Na_2SO_4 and concentrated. The crude compound was purified by silica gel column chromatography using a mixture of (1:1, v/v) ethyl acetate and hexane as eluent to afford the product **3** (0.9 gm, 1.27 mmol, 71%). ^{1}H NMR (400 MHz, Chloroform-*d*) δ = 7.76 (d, *J* = 7.5 Hz, 2H), 7.63 (d, *J* = 7.5 Hz, 2H), 7.44-7.36 (m, 2H), 7.35-7.28 (m, 2H), 5.68 (d, *J* = 9.6 Hz, 1H), 5.47 (dd, *J* = 3.4, 1.3 Hz, 1H), 5.34 (dd, *J* = 11.2, 3.3 Hz, 1H), 5.11 (d, *J* = 3.7 Hz, 1H), 4.53-4.21 (m, 6H), 4.10 (d, *J* = 6.5 Hz, 2H), 3.64 (dd, *J* = 11.2, 3.7 Hz, 1H), 2.15 (s, 3H), 2.08 (s, 3H), 2.05 (s, 3H), 1.50 (s, 9H), 1.35 (d, *J* = 6.5 Hz, 3H). ^{13}C NMR (101 MHz, Chloroform-*d*) δ = 170.51, 170.15, 170.02, 169.34, 156.98, 144.01, 141.41, 127.84, 127.24, 125.43, 120.08, 99.37, 83.05, 76.53, 68.17, 67.66, 67.19, 61.93, 59.35, 57.84, 47.25, 28.12, 20.81, 20.79, 20.77, 19.08. HR-ESI-MS (m/z): Calcd for $C_{35}H_{43}N_4O_{12}$ $[M+H]^+$ 711.2877, found: 711.2876.

***N*-[(9*H*-Fluoren-9-ylmethoxy)carbonyl]-*O*-(2-acetamido-3,4,6-tri-*O*-acetyl-2-deoxy-α-D-galactopyranosyl)-L-threonine-*tert*-butyl ester (4)**

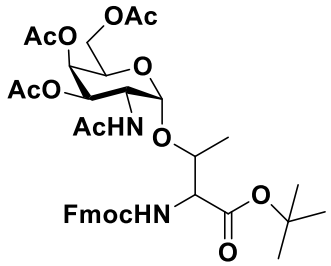

Compound **3** (0.10 gm, 0.14 mmol) was dissolved in 3:2:1 (v/v) mixture of THF/AcOH/Ac_2O (5 mL) and to this solution, Zn (350 mg), saturated $CuSO_4$ (50 µL) were added. The resulting mixture was stirred at room temperature for 4 hours, diluted with ethyl acetate and filtered through celite pad. The organic layer was washed with saturated sodium bicarbonate, brine and dried over Na_2SO_4. The crude compound was purified by silica gel column chromatography using a mixture of (3:2, v/v) ethyl acetate and hexane as eluent to afford the desired product **4** (63 mg, 0.086 mmol, 61%) as a white solid. ^{1}H NMR (400 MHz, Chloroform-*d*) δ = 7.78 (d, *J* = 7.5 Hz, 2H), 7.64 (d, *J* = 7.4 Hz, 2H), 7.44-7.38 (m, 2H), 7.36-7.30 (m, 2H), 5.99 (d, *J* = 9.9 Hz, 1H), 5.56 (d, *J* = 9.4 Hz, 1H), 5.39 (s, 1H), 5.09 (dd, *J* = 11.3, 3.2 Hz, 1H), 4.89 (d, *J* = 3.7 Hz, 1H), 4.62 (td, *J* = 10.6, 3.6 Hz, 1H), 4.53-4.40 (m, 2H), 4.31-4.15 (m, 4H), 4.14-4.04 (m, 2H), 2.17 (s, 3H), 2.04 (s, 3H), 2.00 (s, 3H), 2.00 (s, 3H), 1.46 (s, 9H), 1.32 (d, *J* = 6.3 Hz, 3H). ^{13}C NMR (101 MHz, Chloroform-*d*) δ = 171.11, 170.51, 170.46, 170.14, 156.64, 143.92, 143.88, 141.47, 127.91, 127.26, 125.24, 125.19, 120.16, 100.13, 83.35, 68.82, 67.57, 67.50, 67.38, 62.26, 59.07, 47.46, 47.34, 28.23, 23.39, 20.92, 20.89, 20.79, 18.74.

***N*-[(9*H*-Fluoren-9-ylmethoxy)carbonyl]-*O*-(2-acetamido-3,4,6-tri-*O*-acetyl-2-deoxy-α-D-galactopyranosyl)-L-threonine (5)**

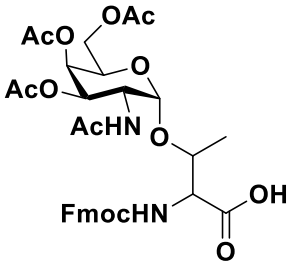

Compound **4** (0.5 gm, 0.68 mmol) was dissolved in 1:1 (v/v) mixture of DCM/TFA (10 mL) and stirred at room temperature for 4 hours. The reaction mixture was concentrated, and the residue was co-evaporated with toluene and dried under a high vacuum for 12 h and used in SPPS without further purification.

Solid phase peptide synthesis

The commercially available Rink amide resin with loading value 0.5-0.6 mmol/g and standard Fmoc chemistry was employed to synthesize the Tn-glycopeotide. The resin-bound Fmoc group was first deprotected using 20% piperidine in DMF. Then, the coupling reaction was carried out using the *in situ* active ester method, using HBTU as a coupling reagent, HOBt as a racemization suppresser, and DIPEA as a base. All the materials used were of peptide synthesis grade (Sigma-Aldrich) and was used without further purification.

Tn-glyocpeptide was synthesized using standard Fmoc chemistry protocol. The resin was pre-swollen in dichloromethane for 12 hours then washed with DMF. Each step of Fmoc deprotection was done by using 20% piperidine in DMF. Each amino acid coupling was carried out using HBTU (3 eq), HOBT (3 eq) and DIPEA (7-8 eq) cocktail solution in DMF for 2 h at room temperature. The coupling reaction was repeated in NMP for better yield. The fully synthesized glyco-peptide was cleaved and partially deprotected using cocktail solution (10 mL) of TFA/H_2O/Phenol/TIPS [8.5:5:5:2.5 (v/v)] at room temperature.

Deacetylation and purification of Tn-glycopeptide (6)

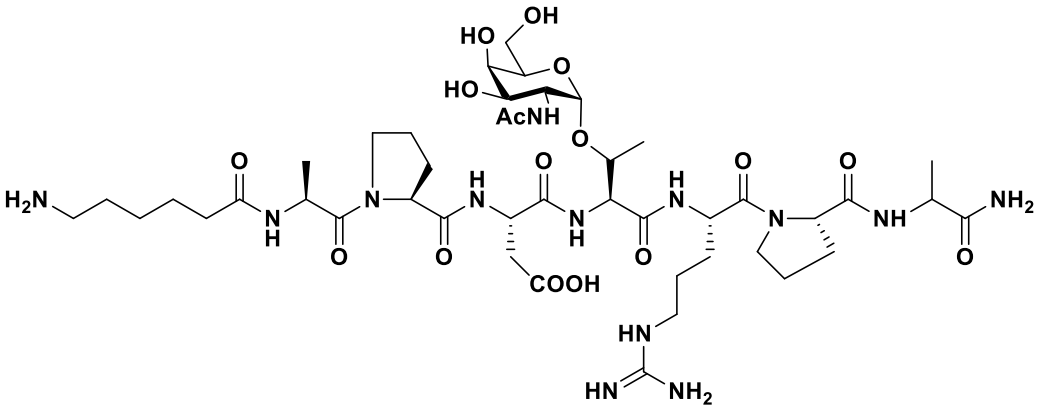

The crude glycopeptide was deacytelated using lithium hydroxide in a mixture of 3:1 (v/v) H_2O/MeOH at room temperature for 12 h. The reaction mixture was quenched with acetic acid, concentrated and purified by RP-HPLC on a semi-preparative C-18 reverse phase column using a linear gradient of 0-100 solvent B (95% acetonitrile + 5% water + 0.1% TFA) and A (95% water + 5% water + 0.1 % TFA) over 45 min. The purified fraction was lyophilized to afford Tn glycopeptide as a white solid. ^{1}H NMR (600 MHz, Deuterium Oxide) δ = 4.59-4.54 (m, 2H), 4.52 (d, *J* = 1.9 Hz, 1H), 4.44 (dd, *J* = 8.5, 5.5 Hz, 1H), 4.37-4.33 (m, 2H), 4.21 (q, *J* = 7.2 Hz, 1H), 4.08 (dd, *J* = 11.0, 3.8 Hz, 1H), 4.00 (dd, *J* = 7.4, 5.1 Hz, 1H), 3.96 (d, *J* = 3.1 Hz, 1H), 3.86 (dd, *J* = 11.0, 3.2 Hz, 1H), 3.84-3.81 (m, 1H), 3.78-3.71 (m, 3H), 3.67 (dt, *J* = 10.2, 6.8 Hz, 1H), 3.62 (dt, *J* = 10.0, 7.1 Hz, 1H), 3.21 (t, *J* = 6.3 Hz, 2H), 3.00-2.96 (m, 3H), 2.87 (dd, *J* = 17.1, 6.9 Hz, 1H), 2.34-2.26 (m, 4H), 2.08-1.09 (m, 7H), 1.91 (tt, *J* = 13.1, 6.5 Hz, 2H), 1.86-1.83 (m, 1H), 1.69-1.64 (m, 5H), 1.60 (dt, *J* = 15.2, 7.6 Hz, 2H), 1.40 (d, *J* = 7.3 Hz, 3H), 1.38-1.34 (m, 5H), 1.24 (d, *J* = 6.4 Hz, 3H). ^{13}C NMR (151 MHz, Deuterium Oxide) δ = 177.90, 176.43, 173.95, 173.78, 173.45, 172.72, 171.15, 170.94, 163.09, 162.86, 156.78, 98.60, 75.55, 71.44, 68.56, 68.18, 61.31, 60.32, 60.12, 57.11, 51.13, 49.88, 49.63, 47.76, 47.68, 40.47, 39.28, 35.15, 34.72, 29.41, 29.25, 27.45, 26.40, 25.07, 24.74, 24.64, 24.55, 24.17, 22.31, 18.41,

16.54, 15.34. HR-ESI-MS (m/z) Calcd for $C_{44}H_{77}N_{13}O_{16}$ $[M+2H]^{2+}$ 521.7805, found: 521.7807.

2,5-dioxopyrrolidin-1-yl 5-(1,2-dithiolan-3-yl)pentanoate (7)

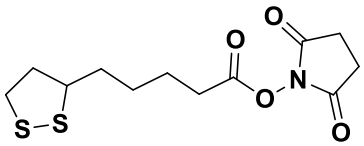

To a stirred solution of DL-6,8-thioctic acid (0.6 gm, 2.91 mmol) in anhydrous DMF (10 mL) were added N-hydroxysuccinamide (0.5 gm, 4.36 mmol), DCC (0.6 gm, 2.91 mmol). The reaction mixture was stirred at room temperature for 12 h, filtered, concentrated and purified by silica gel column chromatography using a mixture of (1:3, v/v) ethyl acetate and hexane as eluent to afford **7** (0.62 gm, 2.04 mmol, 70%) as a yellow oil. ^{1}H NMR (400 MHz, Chloroform-*d*) δ = 3.56 (dq, *J* = 8.2, 6.4 Hz, 1H), 3.22-3.04 (m, 2H), 2.81 (s, 4H), 2.61 (t, *J* = 7.3 Hz, 2H), 2.52-2.39 (m, 1H), 1.91 (dq, *J* = 13.5, 6.8 Hz, 1H), 1.81-1.64 (m, 4H), 1.59-1.45 (m, 2H).^{13}C NMR (101 MHz, Chloroform-*d*) δ = 169.26, 168.50, 56.17, 40.23, 38.59, 34.48, 30.85, 28.38, 25.68, 24.43.

tert-butyl (2-(2-(2-(5-(1,2-dithiolan-3-yl)pentanamido)ethoxy)ethoxy)ethyl)carbamate (8)

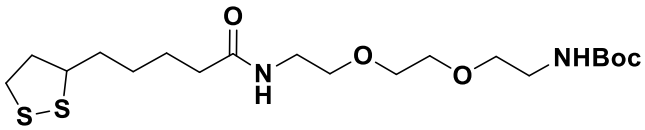

Di-tert-butyl dicarbonate (0.92 mL, 4.05 mmol) in anhydrous dichloromethane (30 mL) was mixed with 2,2-(ethylenedioxy)bis(ethylamine) (1.2 mL, 8.10 mmol) at 0 ˚C. The reaction mixture was stirred at room temperature for 12 h, washed five times with brine and the organic layer dried over sodium sulphate, concentrated to afford a viscous colourless oil (1.34 gm, 5.40 mmol, 67%). Next, the obtained crude compound (0.53 gm, 2.13 mmol) was dissolved in anhydrous dichloromethane, and compound **7** (0.43 gm, 1.42 mmol), triethylamine (1 mL, 7.1 mmol) were added. The reaction mixture was stirred at room temperature for 12 h, concentrated. The crude compound was purified by column chromatography using a mixture of (1:9, v/v) dichloromethane and methanol as eluent to afford desired product **8** (0.46 gm, 1.05 mmol, 74%). ^{1}H NMR (400 MHz, Chloroform-*d*) δ = 6.17 (bs, 1H), 5.02 (bs, 1H), 3.61-3.49 (m, 9H), 3.42 (q, *J* = 5.2 Hz, 2H), 3.28 (s, 2H), 3.18-3.02 (m, 2H), 2.41 (dq, *J* = 12.4, 6.2 Hz, 1H), 2.17 (t, *J* = 7.5 Hz, 2H), 1.86 (dq, *J* = 13.6, 6.9 Hz, 1H), 1.72-1.53 (m, 4H), 1.40 (s, 11H).

N-(2-(2-(2-(5-(1,2-dithiolan-3-yl)pentanamido)ethoxy)ethoxy)ethyl)-3',6'-dihydroxy-3-oxo-3H-spiro[isobenzofuran-1,9'-xanthene]-5-carboxamide (9)

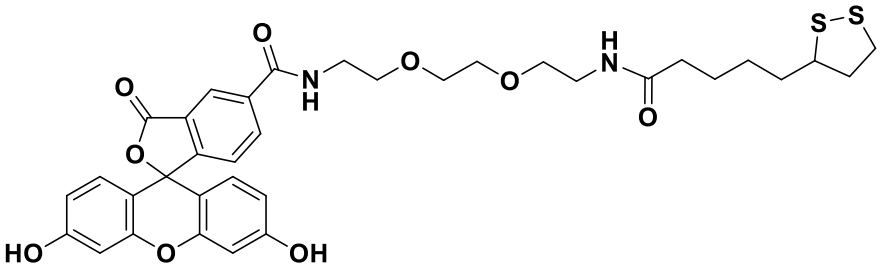

Compound **8** (0.63 gm, 1.44 mmol) was dissolved in 1:1 (v/v) mixture of DCM/TFA (10 mL) and stirred at room temperature for 4 h. The reaction mixture was concentrated and co-evaporated with toluene to afford viscous colourless oil. To a stirred solution of crude compound (0.24 gm, 0.44 mmol) in anhydrous DMF (5 mL) Carboxylflurescein diacetate succinimidyl ester (0.18 gm, 0.52 mmol), triethylamine (0.3 mL, 2.2 mmol) were added. The reaction mixture was stirred at 40 °C for 2 h and concentrated. The residue was purified by silica gel column chromatography using a mixture of (4:1, v/v) ethyl acetate and methanol as eluent to afford product **9** (0.27 gm, 0.39 mmol, 87 %). ^{1}H NMR (400 MHz, Methanol-d_4) δ = 8.47 (d, *J* = 1.6 Hz, 1H), 8.15 (dd, *J* = 8.0, 1.6 Hz, 1H), 7.31 (d, *J* = 8.0 Hz, 1H), 6.76 (d, *J* = 8.9 Hz, 2H), 6.69 (d, *J* = 2.3 Hz, 2H), 6.57 (dd, *J* = 8.9, 2.4 Hz, 2H), 3.74-3.62 (m, 8H), 3.58-3.45 (m, 3H), 3.34 (t, *J* = 5.5 Hz, 2H), 3.16-3.00 (m, 2H), 2.40 (dq, *J* = 12.5, 6.6 Hz, 1H), 2.18 (t, *J* = 7.4 Hz, 2H), 1.83 (dq, *J* = 13.5, 6.9 Hz, 1H), 1.71-1.53 (m, 4H), 1.48-1.31 (m, 2H).^{13}C NMR (101 MHz, Methanol-d_4) δ = 176.10, 171.23, 168.73, 155.67, 137.49, 133.53, 130.91, 127.40, 126.42, 116.40, 112.42, 103.77, 71.35, 71.32, 70.67, 70.53, 57.55, 41.28, 41.10, 40.27, 39.31, 36.81, 35.70, 29.83, 26.69. HR-ESI-MS (m/z) Calcd for $C_{35}H_{39}N_2O_9S_2$ $[M+H]^+$ 695.2097, found: 695.2093.

N-(2-[(t-Boc)amino]ethyl Maleimide

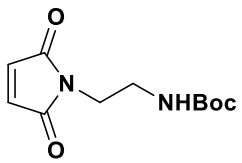

N-Boc-2-maleimidoethylamine was synthesized according to the previously reported procedure.[59] ^{1}H NMR (400 MHz, Chloroform-*d*) δ = 6.71 (s, 2H), 4.73 (bs, 1H), 3.65 (dd, *J* = 6.4, 4.8 Hz, 2H), 3.33 (q, *J* = 5.8 Hz, 2H), 1.39 (s, 9H). ^{13}C NMR (101 MHz, Chloroform-*d*) δ = 170.96, 156.08, 134.31, 79.69, 39.51, 38.12, 28.44. HR-ESI-MS (m/z) Calcd for $C_{11}H_{16}N_2O_4$ $[M+Na]^+$ 263.1008, found: 263.1009.

N-{tris[(3-[ethylcarboxyl-ethoxy)methyl]}methylamine (10)

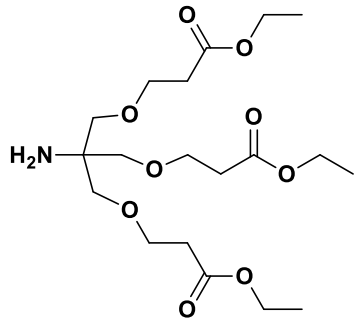

Compound **10** was synthesized according to the previously reported procedure.[47] ^{1}H NMR (400 MHz, Chloroform-*d*) δ = 4.07 (q, *J* = 7.1 Hz, 6H), 3.61 (t, *J* = 6.4 Hz, 6H), 3.24 (s, 6H), 2.47 (t, *J* = 6.4 Hz, 6H), 1.60 (s, 2H), 1.19 (t, *J* = 7.1 Hz, 9H). ^{13}C NMR (101 MHz, Chloroform-*d*) δ = 171.55, 72.77, 66.84, 60.39, 55.94, 35.10, 14.22. HR-ESI-MS (m/z) Calcd for $C_{19}H_{36}NO_9$ $[M+H]^+$ 422.2390, found: 422.2398.

Synthesis of compound (11)

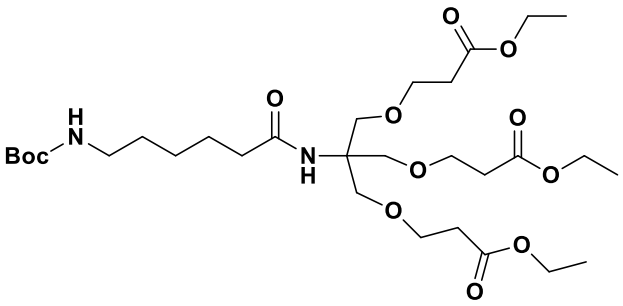

To a stirred solution of compound **10** (2.1 gm, 4.98 mmol) in anhydrous dichloromethane (30 mL) were added DCC (1.23 gm, 5.98 mmol), 5-(Boc-amino)pentanoic acid (1.26 gm, 5.48 mmol). The reaction mixture was stirred at room temperature for 12 h, filtered and concentrated. The residue was purified by silica gel column chromatography using a mixture of (1:1, v/v) ethyl acetate and hexane as eluent to afford the product **11** (2.2 gm, 3.47 mmol, 69%) as a colourless viscous oil. ^{1}H NMR (400 MHz, Chloroform-*d*) δ = 5.94 (s, 1H), 4.64 (bs, 1H), 4.12 (q, *J* = 7.1 Hz, 6H), 3.68-3.65 (m, 12H), 3.09 (q, *J* = 6.4 Hz, 2H), 2.51 (t, *J* = 6.3 Hz, 6H), 2.13 (t, *J* = 7.4 Hz, 2H), 1.58 (p, *J* = 7.3 Hz, 2H), 1.51-1.41 (m, *J* = 7.1 Hz, 2H), 1.41 (s, 9H), 1.35-1.29 (m, 2H), 1.24 (t, *J* = 7.1 Hz, 9H). ^{13}C NMR (101 MHz, Chloroform-*d*) δ = 173.26, 171.75, 156.09, 79.04, 69.30, 66.89, 60.56, 59.71, 40.52, 37.07, 35.11, 29.83, 28.54, 26.39, 25.33, 14.35. HR-ESI-MS (m/z) Calcd for $C_{30}H_{55}N_2O_{12}$ $[M+H]^+$ 635.3755, found: 635.3756.

Synthesis of compound (12)

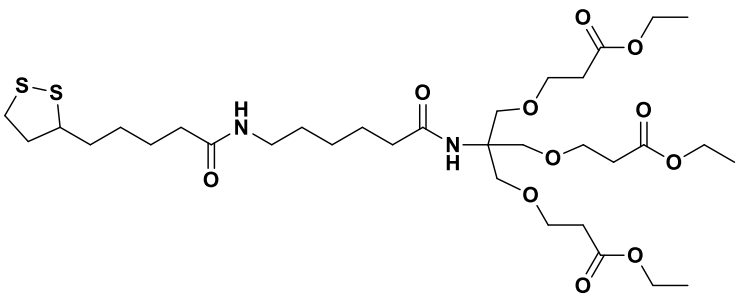

Compound **11** (1.9 gm, 2.99 mmol) was dissolved in a 3:1 (v/v) mixture of DCM/TFA (40 mL) and stirred at room temperature for 4 hours. The resulting mixture was concentrated, and the residue was co-evaporated with toluene and dried under a high vacuum. The crude compound was dissolved in anhydrous dichloromethane (20 mL), and DIPEA (1.4

mL, 7.48 mmol), *N*-Lipoyloxy succinimide (1 gm, 3.29 mmol) were added. The resulting reaction mixture was stirred at room temperature for 4 h, concentrated, and the residue was purified by silica gel column chromatography using (1:1, v/v) ethyl acetate and hexane as eluent to afford product **12** (1.77 gm, 2.45 mmol, 64%) as a yellowish viscous oil. ^{1}H NMR (400 MHz, Chloroform-*d*) δ = 5.95 (s, 1H), 5.86 (t, *J* = 5.7 Hz, 1H), 4.11 (qd, *J* = 7.2, 0.7 Hz, 6H), 3.67-3.63 (m, 12H), 3.53 (dq, *J* = 8.5, 6.4 Hz, 1H), 3.21 (q, *J* = 6.8 Hz, 2H), 3.16-3.04 (m, 2H), 2.50 (t, *J* = 6.2 Hz, 6H), 2.42 (dq, *J* = 12.7, 6.4 Hz, 1H), 2.13 (q, *J* = 7.2 Hz, 4H), 1.91-1.83 (m, 1H), 1.69-1.53 (m, 6H), 1.49-1.39 (m, 4H), 1.34-1.28 (m, 2H), 1.23 (t, *J* = 7.1 Hz, 9H). ^{13}C NMR (101 MHz, Chloroform-*d*) δ = 173.23, 172.76, 171.74, 69.21, 66.83, 60.55, 59.66, 56.49, 40.29, 39.27, 38.51, 36.83, 36.53, 35.05, 29.20, 29.00, 26.35, 25.52, 25.04, 14.30. HR-ESI-MS (m/z) Calcd for $C_{33}H_{59}N_2O_{11}S_2$ $[M+H]^+$ 723.3560, found: 723.3574.

Synthesis of compound (13)

Compound **12** (1.25 gm, 1.73 mmol) was dissolved in a 2:1:1 (v/v) mixture of THF/H_2O/Dioxane (20, mL) and LiOH (166 mg) was added. The reaction mixture was stirred at room temperature for 6 h, quenched with 1N HCl and concentrated. The aqueous layer was extracted with ethyl acetate, and the organic layer was dried over Na_2SO_4 and concentrated.

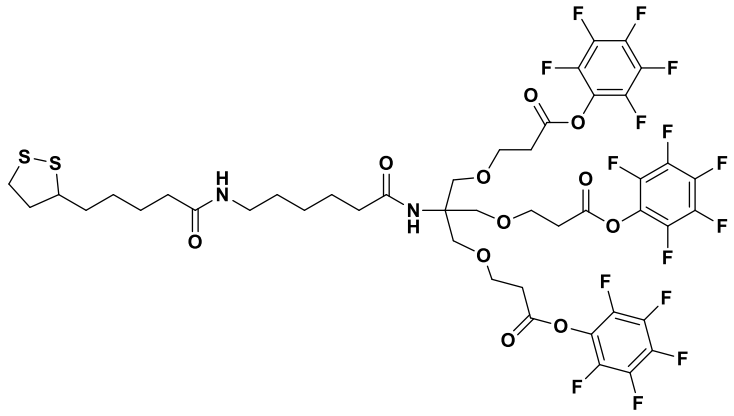

Next, the obtained crude compound was dissolved in anhydrous dichloromethane (20 mL), and DCC (1.25 gm, 6.05 mmol), pentafluorophenol (1.11 gm, 6.05 mmol) were added. The resulting reaction mixture was stirred at room temperature for 12 h, filtered and concentrated. The residue was purified by silica gel column chromatography using a mixture of (2:3, v/v) ethyl acetate and hexane as eluent to afford product **13** (0.9 gm, 0.79 mmol, 46%) as a colourless oil. ^{1}H NMR (400 MHz, Chloroform-*d*) δ = 5.73 (s, 1H), 5.68 (t, *J* = 5.7 Hz, 1H), 3.81-3.76 (m, 12H), 3.54 (dq, *J* = 8.6, 6.4 Hz, 1H), 3.23-3.05 (m, 4H), 2.88 (t, *J* = 5.9 Hz, 6H), 2.47-2.40 (m, 1H), 2.14 (t, *J* = 7.8 Hz, 2H), 2.09 (t, *J* = 7.4 Hz, 2H), 1.88 (dq, *J* = 12.6, 6.9 Hz, 1H), 1.72-1.52 (m, 6H), 1.50-1.40 (m, 4H), 1.33-1.26 (m, 2H). ^{13}C NMR (101 MHz, Chloroform-*d*) δ = 173.40, 172.84, 167.70, 142.42, 140.83, 139.89, 139.23, 138.30, 136.71,

69.23, 66.13, 59.56, 56.53, 40.32, 39.29, 38.54, 36.78, 36.55, 34.71, 34.32, 29.25, 29.00, 26.36, 25.52, 24.96. HR-ESI-MS (m/z) Calcd for $C_{45}H_{44}F_{15}N_2O_{11}S_2$ $[M+H]^+$ 1137.2147, found: 1137.2142.

Synthesis of compound (14)

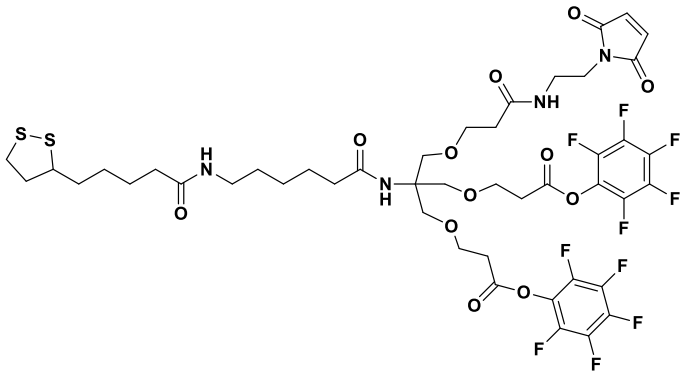

Compound **13** (0.6 gm, 0.53 mmol) in anhydrous dichloromethane (10 mL) was mixed with DIPEA (0.23 mL, 1.33 mmol), 2-Maleimidoethylamine trifluoroacetate (96 mg, 0.689 mmol). The reaction mixture was stirred at room temperature for 2 h, concentrated, and the residue was purified by silica gel column chromatography using a mixture of (4:1, v/v) ethyl acetate and acetone as eluent to afford the desired product **14** (180 mg, 0.16 mmol, 31%) as a colourless viscous oil. ^{1}H NMR (400 MHz, Chloroform-*d*) δ = 6.69 (s, 2H), 6.61 (t, *J* = 6.0 Hz, 1H), 5.96 (s, 1H), 5.73 (t, *J* = 5.8 Hz, 1H), 3.83-3.77 (m, 6H), 3.71-3.66 (m, 6H), 3.63 (t, *J* = 5.8 Hz, 2H), 3.55 (dt, *J* = 8.6, 6.3 Hz, 1H), 3.43 (q, *J* = 5.8 Hz, 2H), 3.24-3.07 (m, 4H), 2.90 (t, *J* = 5.9 Hz, 4H), 2.49-2.42 (m, 1H), 2.38 (t, *J* = 5.7 Hz, 2H), 2.17-2.14 (m, 2H), 2.11 (t, *J* = 7.3 Hz, 2H), 1.90 (dq, *J* = 12.7, 6.9 Hz, 1H), 1.74-1.52 (m, 6H), 1.50-1.44 (m, 4H), 1.34-1.28 (m, 2H). ^{13}C NMR (101 MHz, Chloroform-*d*) δ = 173.45, 172.86, 171.92, 171.02, 167.77, 134.31, 69.70, 69.61, 67.27, 66.24, 59.52, 56.58, 40.38, 39.36, 38.58, 38.51, 37.82, 36.94, 36.71, 36.60, 34.75, 34.37, 29.36, 29.04, 26.37, 25.56, 25.19. HR-ESI-MS (m/z) Calcd for $C_{45}H_{51}F_{10}N_4O_{12}S_2$ $[M+H]^+$ 1093.2785, found: 1093.2794.

Synthesis of compound (15)

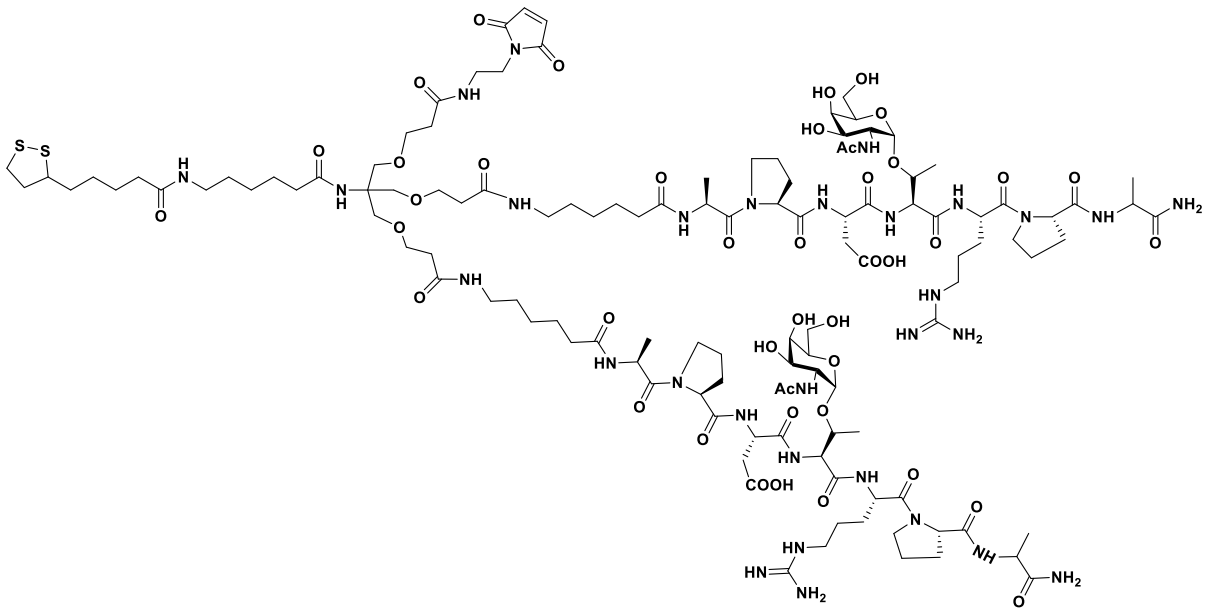

To a stirred solution of **14** (1 mg, 0.91 µmol) in anhydrous DMF (100 µL) were added DIPEA (1 µl, 6.34 µmol), Tn-glycopeptide **6** (2 mg, 1.9 µmol). The reaction mixture was stirred at room temperature for 3 h and concentrated. The residue was purified using Bond elute C-18 column chromatography using a mixture of (1:1, v/v) water and acetonitrile as eluent. The purified fraction was lyophilized to afford the **15** (1.5 mg, 0.53 µmol, 58%) as a white solid. ^{1}H NMR (400 MHz, Deuterium Oxide) δ = 6.88 (s, 2H), 4.62-4.51 (m, 4H), 4.52 (d, *J* = 1.5 Hz, 2H), 4.47-4.44 (m, 2H), 4.41-4.37 (m, 4H), 4.23 (q, *J* = 7.2 Hz, 2H), 4.12-4.08 (m, 2H), 4.04 (t, *J* = 6.3 Hz, 2H), 3.99 (s, 2H), 3.92 (dd, *J* = 11.2, 3.0 Hz, 2H), 3.86-3.63 (m, 25H), 3.42-3.39 (m, 2H), 3.37 (s, 2H), 3.23 (t, *J* = 6.3 Hz, 4H), 3.19 (t, *J* = 6.7 Hz, 6H), 2.79 (dd, *J* = 16.4, 8.1 Hz, 2H), 2.66-2.62 (m, 2H), 2.54-2.51 (m, 2H), 2.47 (t, *J* = 5.8 Hz, 4H), 2.42 (t, *J* = 6.0 Hz, 2H), 2.38-2.21 (m, 13H), 2.09-2.02 (m, 12H), 1.98-1.86 (m, 8H), 1.79-1.70 (m, 7H), 1.66-1.50 (m, 15H), 1.42-1.34 (m, 19H), 1.27 (d, *J* = 6.4 Hz, 6H). ^{13}C NMR (151 MHz, Deuterium Oxide) δ = 177.89, 177.66, 177.65, 173.95, 173.83, 173.75, 173.71, 173.27, 173.25, 172.84, 156.77, 134.42, 72.85, 71.39, 68.53, 67.80, 67.50, 61.33, 60.26, 60.10, 60.01, 58.67, 57.08, 56.59, 56.58, 51.07, 51.01, 49.70, 49.57, 47.71, 47.47, 40.45, 40.28, 39.23, 39.10, 39.06, 38.60, 38.59, 38.09, 38.07, 37.66, 37.15, 36.26, 36.23, 36.18, 36.12, 35.97, 35.52, 34.95, 33.71, 29.36, 29.19, 29.14, 28.11, 28.05, 27.82, 25.63, 25.60, 25.11, 24.94, 24.81, 24.72, 24.60, 24.06, 24.01, 22.29, 18.34, 17.11, 16.48, 15.50. MALDI-TOF (m/z) Calcd for $[M-2H]^{+}$ 2805.35, found: 2805.84.

Synthesis of compound (16)

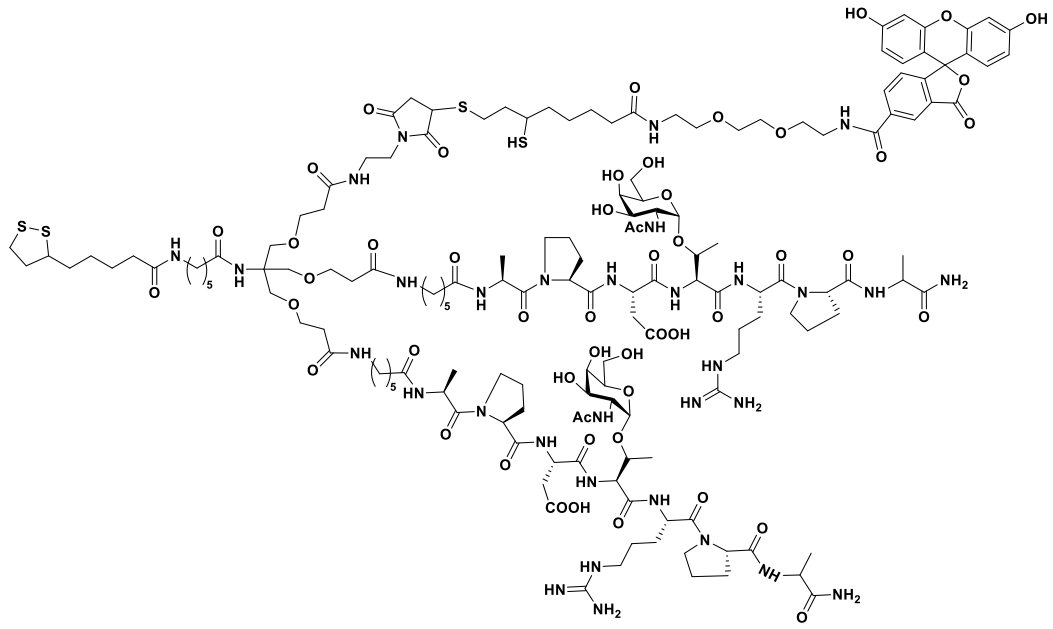

Compound **9** (10 mg, 14.4 µmole) was dissolved in a 1:1 (v/v) mixture of DMF/H_2O (0.5 mL) and TCEP (18 mg, 72 µmol) was added. The reaction mixture was stirred at room temperature for 1 h, concentrated and diluted with ethyl acetate. The organic layer was washed with water, brine and dried over Na_2SO_4 and concentrated. Next, the obtained crude compound (0.5 mg, 0.7 µmol) was dissolved in anhydrous DMF (100 µL), and DIPEA (1.2 µL, 7.12 µmol), **15** (1 mg, 0.36 µmol) were added. The resulting reaction mixture was stirred at room temperature for 24 h and concentrated. The residue was purified by Bond elute C-18 column chromatography using a mixture of (1:4, v/v) water and acetonitrile as eluent. The purified fraction was lyophilized to afford product **16** (0.21 mg, 0.53 nmol, 16%). MALDI-TOF (m/z) Calcd for [M+3H] 3507.61, found: 3507.29. Calcd for [M+Na+CH_3CN] 3569.61, found 3569.79.

4.4.3 Synthesis of gold nanoparticles:

Synthesis of sphere gold nanoparticles

Sphere gold nanoparticles were synthesized according to the previously reported method.[49] In brief, 300 µl of 1% chloroauric acid was added to 30 mL of distilled water and brought to boil, and to this solution, 300 µl of 1% citric acid was added to get 22 nm of sphere gold nanoparticles. For 45 nm sphere gold nanoparticles, 240 µl of 1% citric acid was added. The resulting solution was refluxed until the colour of the boiling solution changes from dark purple to the red vine. The nanoparticles solution was cooled, centrifuged, and the pellet was washed with distilled water. The nanoparticles were characterized by HRTEM and UV-vis spectrophotometry.

Synthesis of rod gold nanoparticles

Small size nanorods were synthesized using the reported procedure.[60] Preparation of seed solution: To a stirred solution of CTAB (9.75 mL) were added $HAuCl_4$ (0.25 mL, 0.01 M), ice-cold solution of freshly prepared $NaBH_4$ (0.6 mL, 0.0 1M). The resulting solution was vigorously stirred for 2 min and kept undisturbed at room temperature for 3 hours.

Preparation of growth solution: Growth solution was prepared by sequential addition of $HAuCl_4$ (0.2 mL, 0.01 M), $AgNO_3$ (0.1 mL, 0.01 M) and HCl (0.2 mL, 1.0 M) to CTAB (8.0 mL, 0.1M). Next, ascorbic acid solution (0.08 mL, 0.1 M) was added with vigorous stirring. Further, the seed solution (2 mL) was added to the growth solution with vigorous stirring and stirred for 2 min. The resulting solution was kept undisturbed for 12 h, centrifuged, and the pellet of 21 nm gold nanorods was washed with distilled water and characterized by HRTEM and UV-vis spectrophotometry.

Large size nanorods were synthesized according to the previously reported method by Khanal et al.[61]

Preparation of seed solution: CTAB solution (5 mL, 0.2 M) was added to $HAuCl_4.3H_2O$ solution (5mL, 0.0005 M) with moderate stirring at 25 ºC. Then an ice-cold solution of $NaBH_4$ (0.6 mL, 0.001 M) was added and vigorously stirred for 2 min. Then the solution was kept at 25 ºC and used for the next step after 15 min.

Preparation of growth solution: $AgNO_3$ solution (0.846 mL, 0.004 M) was added to a stirring solution of CTAB (10 mL, 0.2 M) at 28 ºC. Then $HAuCl_4.3H_2O$ solution (10 mL, 0.002 M) and ascorbic acid solution (0.23 mL, 0.0788 M) were added. Finally, the seed solution (0.032 mL) was added, stirred for 2 min, and kept undisturbed at 27-30 º C for an hour. The nanoparticle solution was centrifuged, and the pellet of 45 nm gold nanorods was washed with distilled water and characterized by HRTEM and UV-vis spectrophotometry.

Synthesis of star nanoparticles

Star gold nanoparticles were synthesized by using the reported literature method.[62]

Preparation of seed solution: Citrate solution (1%, 15 mL) was added to boiling solution of $HAuCl_4$ (100 mL), the resultant solution was boiled for 15 min, then cooled and filtered by a 0.22 µm nitrocellulose membrane and used for the next step.

Synthesis of Star nanoparticles: Seed solution (100 µl) and HCl (10 µl, 1 M) were added to stirring solution of $HAuCl_4$ (10 mL, 0.25 mM) at 25 ºC. Quickly, silver nitrate (100 µl, 20 µM) and ascorbic acid (50 µl, 100 mM) were added simultaneously. The resulting solution was stirred for 25 seconds as its colour was rapidly changed from light blue to greenish-black. Then the nanoparticles solution was immediately centrifuged to stop the nucleation. The pellet of

nanoparticles was washed with distilled water and characterized by HRTEM and UV-vis spectrophotometry.

4.4.4 CpG and tripod 16 functionalization on gold nanoparticle surface:

Thiol-modified tripodal Tn glycopeptide and CpG ODNs were directly conjugated onto the surface of different shapes and sizes of gold nanoparticles using a simple ligand exchange method. Conjugation of these molecules and handling were done in sterile conditions.

CpG-ODNs conjugation

Prior to conjugation, the disulfide bond of CpG was reduced to thiol group in a TCEP solution (10 mM, 1 mL H_2O) at RT for an hour with constant shaking. Then the reaction mixture was centrifuged with an amicon ultra centrifugal filter (cutoff size was 3 kD) to remove TCEP and linker by-product. The reduced CpG-ODN (100 µg) was mixed with gold nanoparticles in PBS pH 7.4 (0.5 mL, 0.1 M) at RT for 12 h with constant shaking, further the concentration of NaCl in the solution was slowly increased to 0.1 M over 2 h time window by stepwise addition of 2 M NaCl. The solution was further kept at RT for 12 h with constant shaking. Then the resulting solution was centrifuged, and pellet was washed three times with Mili Q water to remove the unbound antigen. The loading quantity of CpG-ODNs onto the surface of nanoparticles were determined by ssDNA assay kit (Thermo Fisher). Briefly, nanoparticles were digested with a gold etching solution containing I_2 (0.16 M) and KI (1 M) for 15 min; further, this solution was treated with a reducing solution containing $NaBH_4$ (2 M) and DTT (0.3 M) for 30 min. The resulting solution was centrifuged at 20000g, and the supernatant was analysed.

These CpG conjugated nanoparticles were further dispersed in PBS pH 7.4, and FITC linker **9** (50 µg) was added and kept for 24 h with constant shaking. The solution was centrifuged to get **S-CpG-1, S-CpG-2, R-CpG-1, R-Cpg-2** and **St-CpG** nanoparticles.

Tripod 16 conjugation

In brief, CpG loaded nanoparticles (1000 µg) were dispersed in PBS buffer pH 7.4 (1 mL, 0.1 M), to this tripod **16** (50 µg) was added. The resulting solution was kept at 25 ºC for 24 h with constant shaking. Then the solution was centrifuged, and the pellet was washed three times with Mili Q water to remove the unbound antigen. A change in zeta potential confirmed the antigen (Tripod **16**) conjugation. The loading quantity of antigen onto the surface of nanoparticles was determined by a thiol detection kit (Cayman chemicals, USA).

In a similar way to get **S-TnF-1, S-TnF-2, R-TnF-1, R-TnF-2** and **St-TnF** nanoparticles the tripod **16** (50 µg) was mixed with gold nanoparticles (500 µg) in PBS pH 7.4 (0.5 mL, 0.1 M) and kept at RT for 24 h with constant shaking followed by centrifugation.

4.4.5 Isolation of T cells and dendritic cells from mice splenocytes:

Mice model

All animal studies were performed with the approved protocol from the institutional animal ethical committee. Before the experiment, female C57BL/6 mice (6-8 weeks old) were maintained in pathogen-free condition with proper food supplements and day and night cycles. Dendritic cells and T cells were isolated from spleens of 6-8 weeks old female C57BL/6 mice.

Isolation of splenocytes

Spleens were flushed with complete IMDM medium (Containing 2 mM L-glutamine, 5 % penstrep, 10% FBS) on ice to get cells suspension. The suspension was passed through 40 µm cell strainer, centrifuged at 300*g* for 10 min at 4 ºC. The pellet was suspended in 5 % erythrocyte lysis buffer (5 mL) and incubated at 4 ºC for 2 min. The cell suspension was centrifuged, and the pellet was washed with IMDM medium twice and finally suspended in freshly prepared MACS buffer (PBS, 0.5 % BSA, 2mM EDTA).

Isolation of dendritic cells

Dendritic cells were isolated from the suspension of spleen cells by using $CD11c^+$ MicroBeads (Miltenyi). In detail, the suspension of cells was incubated with $CD11c^+$ beads for 10 min and loaded on a MACS column in a magnetic field. The column was washed with MACS buffer to remove unbound cells. The magnetically labelled $CD11c^+$ cells were retained within the column. The labelled cells were eluted by MACS buffer by removing the magnetic field and applying pressure on the column. The cell isolation process was repeated to get a high purity of cells. The purified cells were suspended in IMDM medium and used for counting. Flow cytometry analysis was used to check the purity of isolated CD11c+ cells by staining with an anti-CD11c antibody.

T cell isolation

T cells were isolated from the spleen cells suspension using Pan T cell isolation kit II (Miletnyi). The cells suspension was magnetically labelled with a cocktail of biotin-conjugated antibodies, followed by incubation with the anti-biotin monoclonal antibodies conjugated with MicroBeads for 10 min at 4 ºC. Next, the labelled cells suspension was loaded on the MACS column in a magnetic field. The labelled cells were retained within the column, while unlabelled T cells were passed through the column. The cell isolation process was repeated to

get high purity cells. Finally, the isolated T cells were suspended in IMDM medium, and the purity of the T cells was analysed by flow cytometry by staining cells with anti-CD-3e antibody.

4.4.6 Confocal imaging:

Dendritic cells (2×10^6 cells) were seeded on poly-D-lysine coated coverslip in complete IMDM medium and incubated at 37 ºC for overnight. The cells were incubated with CTnF, CpG and TnF functionalised AuNPs (50 nmol of CpG) for different time intervals 1 h and 4h. Then the cells were washed with the cold PBS and fixed with 4% paraformaldehyde at room temperature for 20 min. Next, the coverslips were washed with PBS and water and mounted on a slide using medium (Vectashield). The fluorescent images were taken using Leica sp8 microscope.

4.4.7 FACS analysis:

Dendritic cells (2×10^6 cells) were seeded in 96 well plates in IMDM media and incubated for 30 min. The cells were pulsed with CTnF, CpG and TnF functionalized AuNPs (50 nmole of CpG) for 1 h and 4h. Then the cells were washed with cold PBS and resuspended in FACS buffer and proceeded for analysis. Quantification of uptake was done by using Flowjo software.

4.4.8 mDC/T-cell co-culture assay:

Dendritic cells (2×10^6 cells/well) were seeded in 96 well-plate in IMDM medium at 37 ºC for 30 min. Then cells were pulsed with the CTnF and TnF functionalised AuNPs (50 nmol of CpG) and incubated further for an hour. Next, the purified T-cells (60 µl of 7×10^6/well) were added and incubated for 48 and 72 h. Cytokine (IL6, IL10, TNFα, IFNγ) level in the supernatant was determined after 48 and 72 h of stimulation using ELISA (R&D Systems).

4.4.9 Immunization protocol:

Immunization studies were carried out using 6 to 8 weeks old females (C57BL/6) mice as per protocol approved by the institutional ethical committee. Five groups of mice (n=5) were immunized subcutaneously with 100 µl of each S-CTnF-1, R-CTnF-1, St-CTnF, S-TnF-1, R-

TnF, St-TnF (contains 7 to 10 µg of Tn and 5 nmol of CpG) and PBS on days 0, 14, 28. The mice were bled on days 36 and serum antibody titer was analysed by ELISA.

4.4.10 ELISA for evaluation of IgG antibody titer:

The IgG antibody titers were quantified using maleic anhydride activated 96 well plates.[58] The plates were coated with Tn glycopeptide (Comp **6**) (3 µg/ml in 0.1 M carbonate buffer pH 9.2) at room temperature for 1 h followed by incubation at 4 ºC for overnight. The coated plates were washed with washing buffer (PBS + 0.1 % Tween-20) and blocked with blocking buffer (2 % BSA) for 1h at room temperature. Next, the plates were washed, mice anti-serum (1:1000 diluted) was added and incubated for 2 h at room temperature followed by washing. HRP-coated secondary goat anti-mouse antibody (1:2000 diluted, Thermofisher) was added to the plate and incubated for 2 h at room temperature. The plates were washed, TMB substrate solution was added, and the reaction was stopped by adding 0.5 M H_2SO_4. The absorbance was recorded at 450 nm.

4.5 References:

1. Mond, J. J.; Lees, A.; Snapper, C. M. T cell-independent antigens type 2. *Annu Rev Immunol.* **1995**, *13*, 655-92.
2. Jeurissen, A.; Ceuppens, J. L.; Bossuyt, X. T lymphocyte dependence of the antibody response to 'T lymphocyte independent type 2' antigens. *Immunology*. **2004**, *111*, 1-7.
3. Nishat, S.; Andreana, P. R.; Entirely Carbohydrate-Based Vaccines: An Emerging Field for Specific and Selective Immune Responses. *Vaccines (Basel)*. **2016**, *4*, 19.
4. Billadeau, D. D.; Nolz, J. C.; Gomez, T. S. Regulation of T-cell activation by the cytoskeleton. *Nat Rev Immunol*. **2007**, *7*, 131-43.
5. Jawa, V. Terry, F.; Gokemeije, J.; Mitra-Kaushik, S.; Roberts, B. J.; Tourdot, S.; De Groot, A. S. T-Cell Dependent Immunogenicity of Protein Therapeutics Pre-clinical Assessment and Mitigation-Updated Consensus and Review 2020. *Front Immunol*. **2020**, *30*, 1301.
6. Grewal, I. S.; Flavell, R. A. CD40 and CD154 in cell-mediated immunity. *Annu Rev Immunol.* **1998**, *16*, 111-35.
7. Wilson, R. M.; Danishefsky, S. J. A vision for vaccines built from fully synthetic tumor-associated antigens: from the laboratory to the clinic. *J Am Chem Soc*. **2013**, *135*, 14462-72.
8. Li, W. H.; Li, Y. M. Chemical Strategies to Boost Cancer Vaccines. *Chem Rev.* **2020**, *120*, 11420-11478.

9. Jones, L. H. Recent advances in the molecular design of synthetic vaccines. *Nat Chem.* **2015**, *7*, 952-60.
10. Astronomo, R. D.; Burton, D. R. Carbohydrate vaccines: developing sweet solutions to sticky situations? *Nat Rev Drug Discov*. **2010**, *9*, 308-24.
11. Lang, S.; Huang, X. Carbohydrate Conjugates in Vaccine Developments. *Front Chem.* **2020**, *8*, 284.
12. Gefen, T.; Vaya, J.; Khatib, S.; Rapoport, I.; Lupo, M.; Barnea, E.; Admon, A.; Heller, E. D.; Aizenshtein, E.; Pitcovski, J. The effect of haptens on protein-carrier immunogenicity. *Immunology.* **2015**, *144*, 116-26.
13. Gaidzik, N.; Westerlind, U.; Kunz, H. The development of synthetic antitumour vaccines from mucin glycopeptide antigens. *Chem Soc Rev*. **2013**, *42*, 4421-42.
14. Alam, M. M.; Jarvis, C. M.; Hincapie, R.; McKay, C. S.; Schimer, J.; Sanhueza, C. A.; Xu, K.; Diehl, R. C.; Finn, M. G.; Kiessling, L. L. Glycan-Modified Virus-like Particles Evoke T Helper Type 1-like Immune Responses. *ACS Nano*. **2021**, *15*, 309-321.
15. Wu, X.; McKay, C.; Pett, C.; Yu, J.; Schorlemer, M.; Ramadan, S.; Lang, S.; Behren, S.; Westerlind, U.; Finn, M. G.; Huang X. Synthesis and Immunological Evaluation of Disaccharide Bearing MUC-1 Glycopeptide Conjugates with Virus-like Particles. *ACS Chem Biol.* **2019**, *14*, 2176-2184.
16. Huang, X.; Wang, X.; Zhang, J.; Xia, N.; Zhao, Q. *Escherichia coli*-derived virus-like particles in vaccine development. *NPJ Vaccines*. **2017**, *2*, 3.
17. Broecker, F.; Götze, S.; Hudon, J.; Rathwell, D. C. K.; Pereira, C. L.; Stallforth, P.; Anish, C.; Seeberger, P. H. Synthesis, Liposomal Formulation, and Immunological Evaluation of a Minimalistic Carbohydrate-α-GalCer Vaccine Candidate. *J Med Chem.* **2018**, *61*, 4918-4927.
18. Lang, S.; Huang, X. Carbohydrate Conjugates in Vaccine Developments. *Front Chem.* **2020**, *8*, 284.
19. Wibowo, D.; Jorritsma, S. H. T.; Gonzaga, Z. J.; Evert, B.; Chen, S.; Rehm, B. H. A. Polymeric nanoparticle vaccines to combat emerging and pandemic threats. *Biomaterials.* **2021**, *268*, 120597.
20. Chen, Y. S.; Hung, Y. C.; Lin, W. H.; Huang, G. S. Assessment of gold nanoparticles as a size-dependent vaccine carrier for enhancing the antibody response against synthetic foot-and-mouth disease virus peptide. *Nanotechnology*. **2010**, *21*, 195101.
21. Zhu, M.; Du, L.; Zhao, R.; Wang, H. Y.; Zhao, Y.; Nie, G.; Wang, R. F. Cell-Penetrating Nanoparticles Activate the Inflammasome to Enhance Antibody Production by Targeting

Microtubule-Associated Protein 1-Light Chain 3 for Degradation. *ACS Nano.* **2020**, *14*, 3703-3717.

22. Deng, L.; Wang, B. Z. A Perspective on Nanoparticle Universal Influenza Vaccines. *ACS Infect Dis.* **2018**, *4*, 1656-1665.
23. Lee, D.; Huntoon, K.; Wang, Y.; Jiang, W.; Kim, B. Y. S. Harnessing Innate Immunity Using Biomaterials for Cancer Immunotherapy. *Adv Mater.* **2021**, *33*, e2007576.
24. Compañón, I.; Guerreiro, A.; Mangini, V.; Castro-López, J.; Escudero-Casao, M.; Avenoza, A.; Busto, J. H.; Castillón, S.; Jiménez-Barbero, J.; Asensio, J. L.; Jiménez-Osés, G.; Boutureira, O.; Peregrina, J. M.; Hurtado-Guerrero, R.; Fiammengo, R.; Bernardes, G. J. L.; Corzana, F. Structure-Based Design of Potent Tumor-Associated Antigens: Modulation of Peptide Presentation by Single-Atom O/S or O/Se Substitutions at the Glycosidic Linkage. *J Am Chem Soc*. **2019**, *141*, 4063-4072.
25. Cai, H.; Degliangeli, F.; Palitzsch, B.; Gerlitzki, B.; Kunz, H.; Schmitt, E.; Fiammengo, R.; Westerlind, U. Glycopeptide-functionalized gold nanoparticles for antibody induction against the tumor associated mucin-1 glycoprotein. *Bioorg Med Chem.* **2016**, *24*, 1132-5.
26. Trabbic, K. R.; Whalen, K.; Abarca-Heideman, K.; Xia, L.; Temme, J. S.; Edmondson, E. F.; Gildersleeve, J. C.; Barchi, J. J. Jr. A Tumor-Selective Monoclonal Antibody from Immunization with a Tumor-Associated Mucin Glycopeptide. *Sci Rep.* **2019**, *9*, 5662.
27. Brinãs, R. P.; Sundgren, A.; Sahoo, P.; Morey, S.; Rittenhouse-Olson, K.; Wilding, G. E.; Deng, W.; Barchi, J. J. Jr. Design and synthesis of multifunctional gold nanoparticles bearing tumor-associated glycopeptide antigens as potential cancer vaccines. *Bioconjug Chem.* **2012**, *23*, 1513-23.
28. Niikura, K.; Matsunaga, T.; Suzuki, T.; Kobayashi, S.; Yamaguchi, H.; Orba, Y.; Kawaguchi, A.; Hasegawa, H.; Kajino, K.; Ninomiya, T.; Ijiro, K.; Sawa, H. Gold nanoparticles as a vaccine platform: influence of size and shape on immunological responses in vitro and in vivo. *ACS Nano.* **2013**, *7*, 3926-38.
29. Dykman, L. A.; Staroverov, S. A.; Fomin, A. S.; Khanadeev, V. A.; Khlebtsov, B. N.; Bogatyrev, V. A. Gold nanoparticles as an adjuvant: Influence of size, shape, and technique of combination with CpG on antibody production. *Int Immunopharmacol.* **2018**, *54*, 163-168.
30. Nath, S.; Mukherjee, P. MUC1: a multifaceted oncoprotein with a key role in cancer progression. *Trends Mol Med.* **2014**, *20*, 332-42.
31. Hattrup, C. L.; Gendler, S. J. Structure and function of the cell surface (tethered) mucins. *Annu Rev Physiol*. **2008**, *70*, 431-57.

32. Singh, R.; Bandyopadhyay, D. MUC1: a target molecule for cancer therapy. *Cancer Biol Ther*. **2007**, *6*, 481-6.
33. Bode, C.; Zhao, G.; Steinhagen, F.; Kinjo, T.; Klinman, D. M. CpG DNA as a vaccine adjuvant. *Expert Rev Vaccines*. **2011**, *4*, 499-511.
34. Luchner, M.; Reinke, S.; Milicic, A. TLR Agonists as Vaccine Adjuvants Targeting Cancer and Infectious Diseases. *Pharmaceutics.* **2021**, *13*, 142.
35. Beatson, R.; Maurstad, G.; Picco, G.; Arulappu, A.; Coleman, J.; Wandell, H. H.; Mandel, U.; Taylor-Papadimitriou, J.; Sletmoen, M.; Burchell, J. M. The Breast Cancer-Associated Glycoforms of MUC1, MUC1-Tn and sialyl-Tn, Are Expressed in COSMC Wild-Type Cells and Bind the C-Type Lectin MGL. *PLoS One*. **2015**, *10*, e0125994.
36. Stergiou, N.; Gaidzik, N.; Heimes, A. S.; Dietzen, S.; Besenius, P.; Jäkel, J.; Brenner, W.; Schmidt, M.; Kunz, H.; Schmitt, E. Reduced Breast Tumor Growth after Immunization with a Tumor-Restricted MUC1 Glycopeptide Conjugated to Tetanus Toxoid. *Cancer Immunol Res.* **2019**, *7*, 113-122.
37. Stergiou, N.; Glaffig, M.; Jonuleit, H.; Schmitt, E.; Kunz, H. Immunization with a Synthetic Human MUC1 Glycopeptide Vaccine against Tumor-Associated MUC1 Breaks Tolerance in Human MUC1 Transgenic Mice. *ChemMedChem.* **2017**, *12*, 1424-1428.
38. Thompson, P.; Lakshminarayanan, V.; Supekar, N. T.; Bradley, J. M.; Cohen, P. A.; Wolfert, M. A.; Gendler, S. J.; Boons, G. J. Linear synthesis and immunological properties of a fully synthetic vaccine candidate containing a sialylated MUC1 glycopeptide. *Chem Commun (Camb)*. **2015**, *51*, 10214-7.
39. Wilkinson, B. L.; Day, S.; Malins, L. R.; Apostolopoulos, V.; Payne, R. J. Self-adjuvanting multicomponent cancer vaccine candidates combining per-glycosylated MUC1 glycopeptides and the Toll-like receptor 2 agonist Pam3CysSer. *Angew Chem Int Ed Engl*. **2011**, *50*, 1635-9.
40. Cai, H.; Sun, Z. Y.; Chen, M. S.; Zhao, Y. F.; Kunz, H.; Li, Y. M. Synthetic multivalent glycopeptide-lipopeptide antitumor vaccines: impact of the cluster effect on the killing of tumor cells. *Angew Chem Int Ed Engl*. **2014**, *53*, 1699-703.
41. Hoffmann-Röder, A.; Kaiser, A.; Wagner, S.; Gaidzik, N.; Kowalczyk, D.; Westerlind, U. Synthetic antitumor vaccines from tetanus toxoid conjugates of MUC1 glycopeptides with the Thomsen-Friedenreich antigen and a fluorine-substituted analogue. *Angew Chem Int Ed Engl*. **2010**, *49*, 8498-503.

42. Hoffmann-Röder, A.; Johannes, M. Synthesis of a MUC1-glycopeptide-BSA conjugate vaccine bearing the 3'-deoxy-3'-fluoro-Thomsen-Friedenreich antigen. *Chem Commun (Camb)*. **2011**, *47*, 9903-5.
43. Nativi, C.; Papi, F.; Roelens, S. Tn antigen analogues: the synthetic way to "upgrade" an attracting tumour associated carbohydrate antigen (TACA). *Chem Commun (Camb)*. **2019**, *5*, 7729-7736.
44. Bermejo, I. A.; Navo, C. D.; Castro-López, J.; Guerreiro, A.; Jiménez-Moreno, E.; Sánchez Fernández, E. M.; García-Martín, F.; Hinou, H.; Nishimura, S. I.; García Fernández, J. M.; Mellet, C. O.; Avenoza, A.; Busto, J. H.; Bernardes, G. J. L.; Hurtado-Guerrero, R.; Peregrina, J. M.; Corzana, F. Synthesis, conformational analysis and in vivo assays of an anti-cancer vaccine that features an unnatural antigen based on an sp2-iminosugar fragment. *Chem Sci.* **2020**, *11*, 3996-4006.
45. Martínez-Sáez, N.; Castro-López, J.; Valero-González, J.; Madariaga, D.; Compañón, I.; Somovilla, V. J.; Salvadó, M.; Asensio, J. L.; Jiménez-Barbero, J.; Avenoza, A.; Busto, J. H.; Bernardes, G. J.; Peregrina, J. M.; Hurtado-Guerrero, R.; Corzana, F. Deciphering the Non-Equivalence of Serine and Threonine O-Glycosylation Points: Implications for Molecular Recognition of the Tn Antigen by an anti-MUC1 Antibody. *Angew Chem Int Ed Engl*. **2015**, *54*, 9830-4.
46. Sangabathuni, S.; Murthy, R. V.; Chaudhary, P. M.; Subramani, B.; Toraskar, S.; Kikkeri, R. Mapping the Glyco-Gold Nanoparticles of Different Shapes Toxicity, Biodistribution and Sequestration in Adult Zebrafish. *Sci Rep*. **2017**, *7*, 4239.
47. Kikkeri, R.; Hossain, L. H.; Seeberger, P. H. Supramolecular one-pot approach to fluorescent glycodendrimers. *Chem Commun (Camb)*. **2008**, *18*, 2127-9.
48. Chaudhary, P. M.; Sangabathuni, S.; Murthy, R. V.; Paul, A.; Thulasiram, H. V.; Kikkeri, R. Assessing the effect of different shapes of glyco-gold nanoparticles on bacterial adhesion and infections. *Chem Commun (Camb)*. **2015**, *51*, 15669-72.
49. Sangabathuni, S.; Vasudeva Murthy, R.; Chaudhary, P. M.; Surve, M.; Banerjee, A.; Kikkeri, R. Glyco-gold nanoparticle shapes enhance carbohydrate-protein interactions in mammalian cells. *Nanoscale*. **2016**, *8*, 12729-35.
50. Jia, H.; Fang, C.; Zhu, X. M.; Ruan, Q.; Wang, Y. X.; Wang, J. Synthesis of Absorption-Dominant Small Gold Nanorods and Their Plasmonic Properties. *Langmuir*. **2015**, *31* (26), 7418-26.
51. Khanal, B. P.; Zubarev, E. R. Gram-Scale Synthesis of Isolated Monodisperse Gold Nanorods. *Chemistry*. **2019**, *25*, 1595-1600.

52. Yuan, H.; Khoury, C. G.; Hwang, H.; Wilson, C. M.; Grant, G. A.; Vo-Dinh, T. Gold nanostars: surfactant-free synthesis, 3D modelling, and two-photon photoluminescence imaging. *Nanotechnology*. **2012**, *23*, 075102.
53. Schudel, A.; Francis, D. M.; Thomas, S. N. Material design for lymph node drug delivery. *Nat Rev Mater*. **2019**, *4*, 415-428.
54. Gabba, A.; Bogucka. A.; Luz, J. G.; Diniz, A.; Coelho, H.; Corzana, F.; Cañada, F. J.; Marcelo, F.; Murphy, P. V.; Birrane, G. Crystal Structure of the Carbohydrate Recognition Domain of the Human Macrophage Galactose C-Type Lectin Bound to GalNAc and the Tumor-Associated Tn Antigen. *Biochemistry*. **2021**, *60*, 1327-1336.
55. Palte, M. J.; Raines, R. T. Interaction of nucleic acids with the glycocalyx. *J Am Chem Soc*. **2012**, *134*, 6218-23.
56. Brzezicka, K.; Vogel, U.; Serna, S.; Johannssen, T.; Lepenies, B.; Reichardt, N. C. Influence of Core β-1,2-Xylosylation on Glycoprotein Recognition by Murine C-type Lectin Receptors and Its Impact on Dendritic Cell Targeting. *ACS Chem Biol*. **2016**, *11*, 2347-56.
57. Lee, K.; Huang, Z. N.; Mirkin, C. A.; Odom, T. W. Endosomal Organization of CpG Constructs Correlates with Enhanced Immune Activation. *Nano Lett*. **2020**, *20*, 6170-6175.
58. Trabbic, K. R.; Bourgault, J. P.; Shi, M.; Clark, M.; Andreana, P. R. Immunological evaluation of the entirely carbohydrate-based Thomsen-Friedenreich - PS B conjugate. *Org Biomol Chem*. **2016**, *14*, 3350-5.
59. Tang, F.; Yang, Y.; Tang, Y.; Tang, S.; Yang, L.; Sun, B.; Jiang, B.; Dong, J.; Liu, H.; Huang, M.; Geng, M. Y.; Huang, W. One-pot N-glycosylation remodeling of IgG with non-natural sialylglycopeptides enables glycosite-specific and dual-payload antibody-drug conjugates. *Org Biomol Chem*. **2016**, *14*, 9501-9518.
60. Jia, H. Fang, C.; Zhu, X. M.; Ruan, Q.; Wang, Y. X.; Wang, J. Synthesis of Absorption-Dominant Small Gold Nanorods and Their Plasmonic Properties. *Langmuir*. **2015**, *31*, 7418-26.
61. Khanal, B. P.; Zubarev, E. R. Gram-Scale Synthesis of Isolated Monodisperse Gold Nanorods. *Chemistry*. **2019**, *25*, 1595-1600.
62. Yuan, H.; Khoury, C. G.; Hwang, H.; Wilson, C. M.; Grant, G. A.; Vo-Dinh, T. Gold nanostars: surfactant-free synthesis, 3D modelling, and two-photon photoluminescence imaging. *Nanotechnology*. **2012**, *23*, 075102.

4.6 NMR and HRMS Spectra:

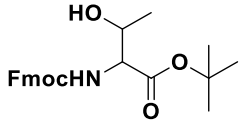

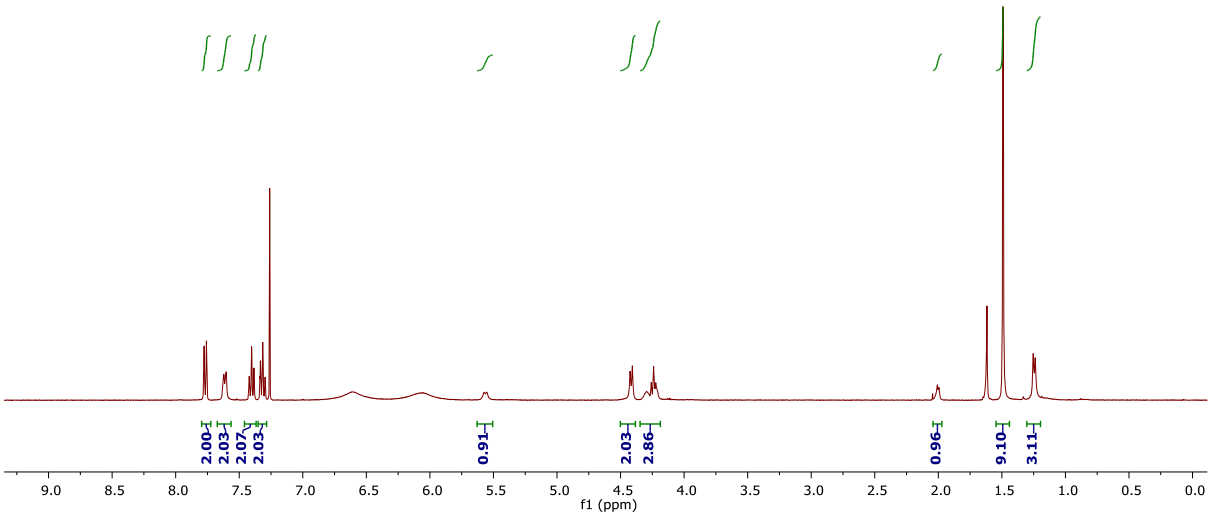

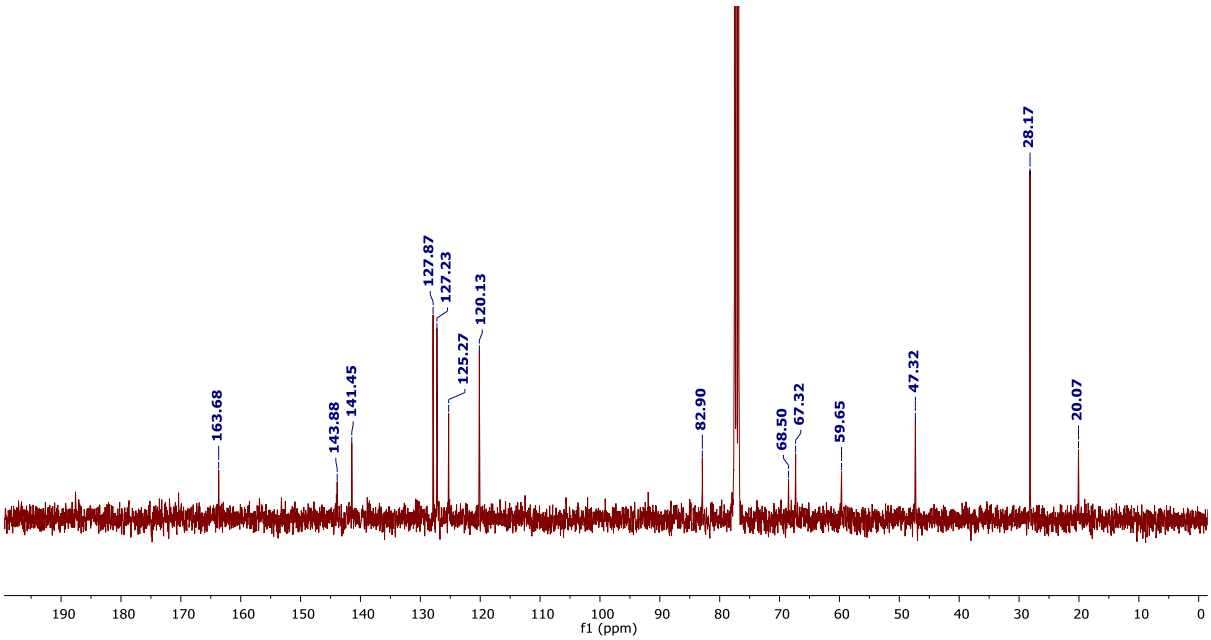

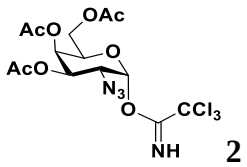
AcO
OAc
AcO
O
N3
O
CCl3
NH

2

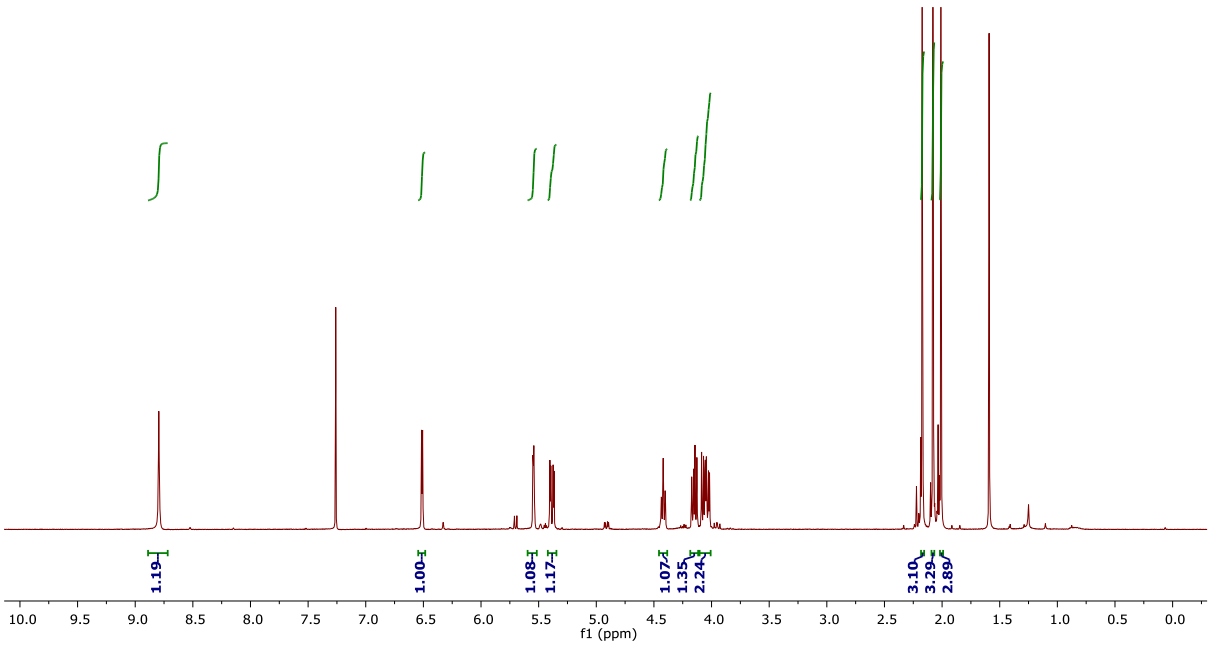
1.19
1.00
1.08
1.17
1.07
1.35
2.24
3.10
3.29
2.89
10.0 9.5 9.0 8.5 8.0 7.5 7.0 6.5 6.0 5.5 5.0 4.5 4.0 3.5 3.0 2.5 2.0 1.5 1.0 0.5 0.0
f1 (ppm)

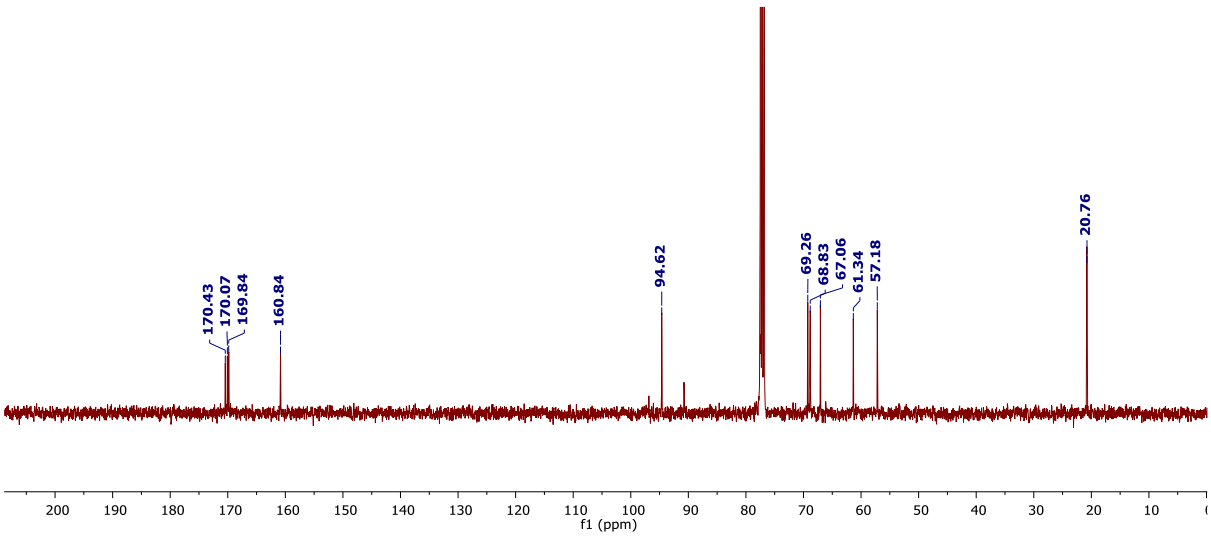
170.43
170.07
169.84
160.84
94.62
69.26
68.83
67.06
61.34
57.18
20.76
200 190 180 170 160 150 140 130 120 110 100 90 80 70 60 50 40 30 20 10
f1 (ppm)

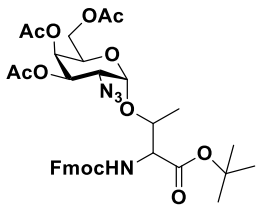
AcO
OAc
AcO
O
N3
O
FmocHN
O
O

3

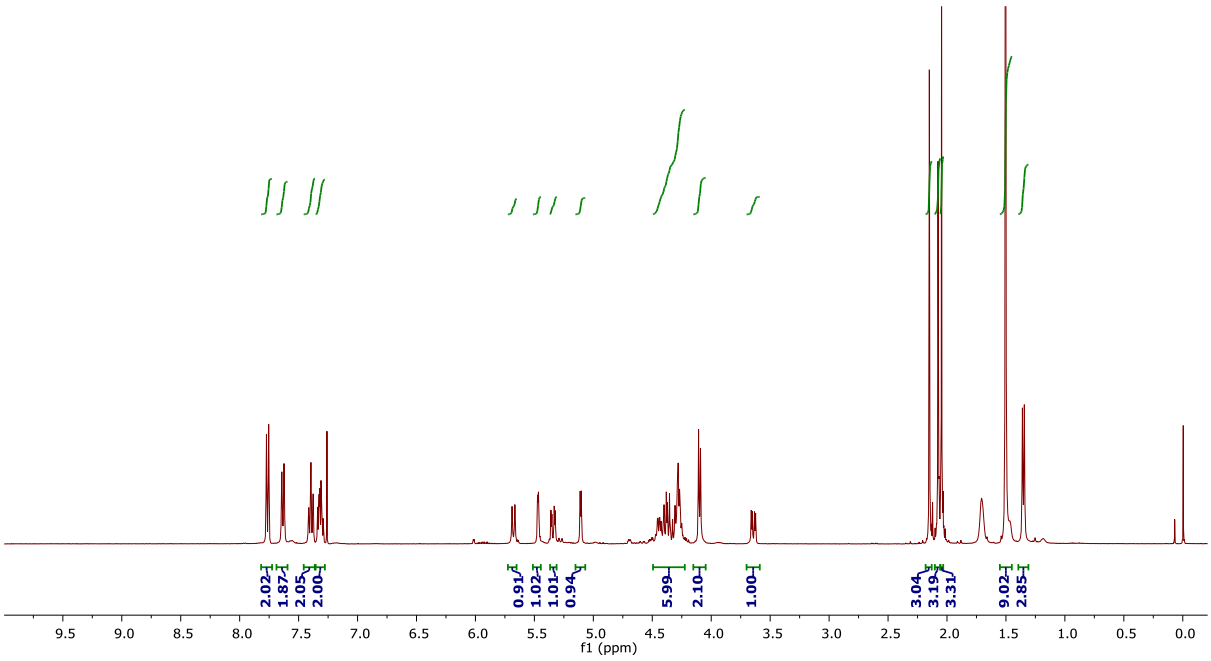
2.02
1.87
2.05
2.00
0.91
1.02
1.01
0.94
5.99
2.10
1.00
3.04
3.19
3.31
9.02
2.85
f1 (ppm)

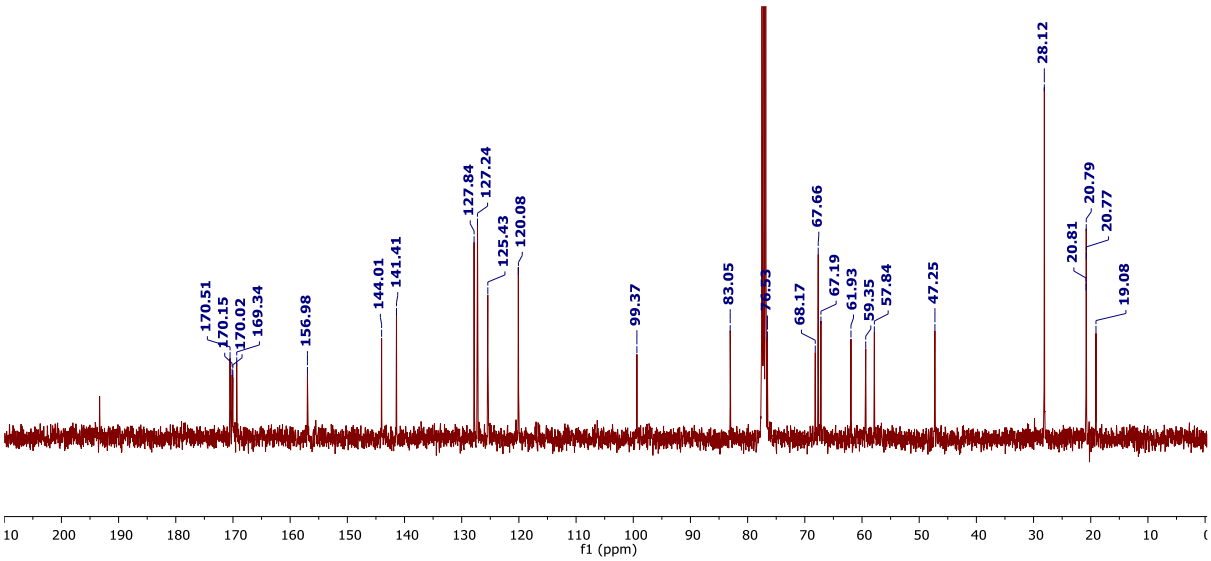
170.51
170.15
170.02
169.34
156.98
144.01
141.41
127.84
127.24
125.43
120.08
99.37
83.05
76.53
68.17
67.66
67.19
61.93
59.35
57.84
47.25
28.12
20.81
20.79
20.77
19.08
f1 (ppm)

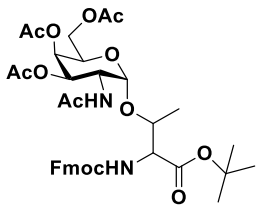
AcO
OAc
O
AcO
AcHN
O
FmocHN
O
O

4

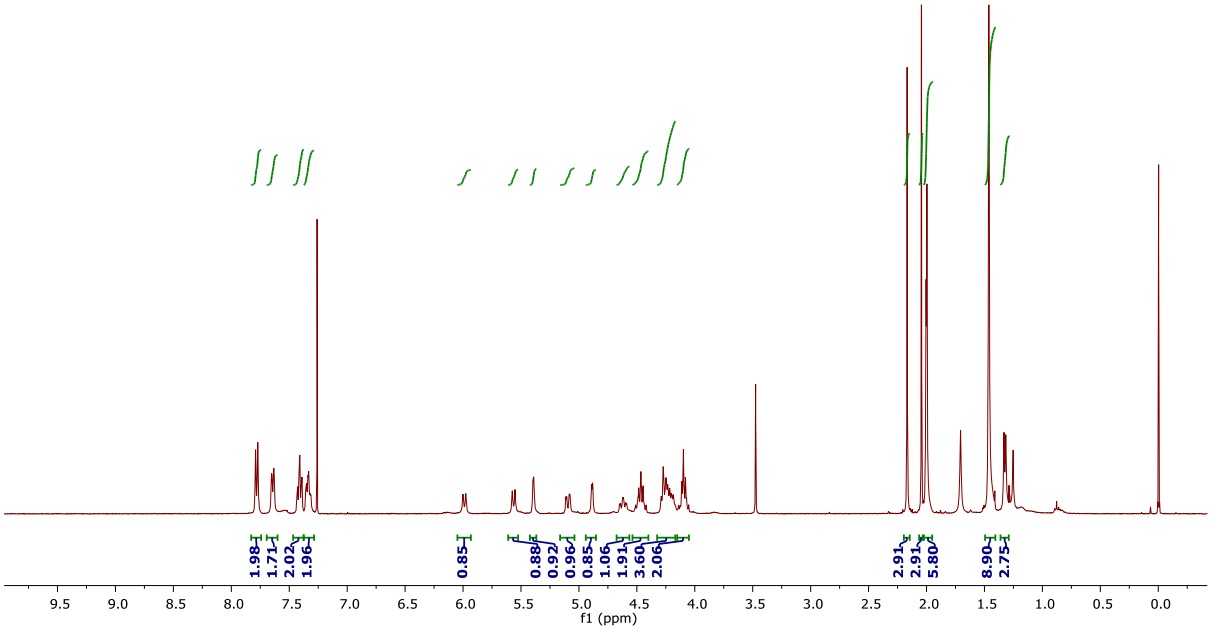
1.98
1.71
2.02
1.96
0.85
0.88
0.92
0.96
0.85
1.06
1.91
3.60
2.06
2.91
2.91
5.80
8.90
2.75
f1 (ppm)

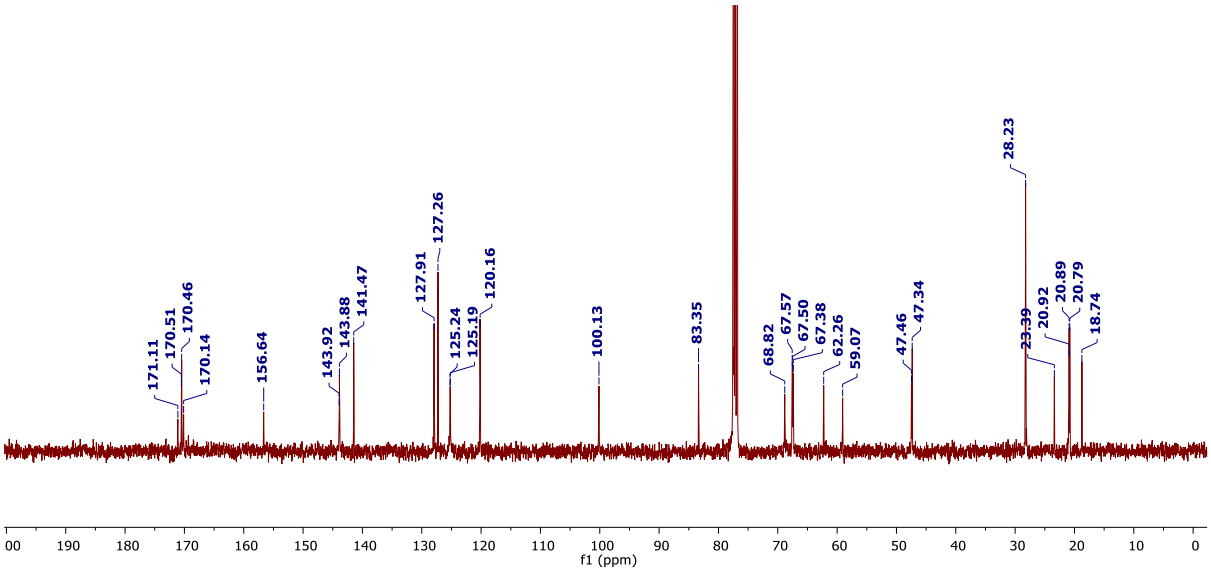
171.11
170.51
170.46
170.14
156.64
143.92
143.88
141.47
127.91
127.26
125.24
125.19
120.16
100.13
83.35
68.82
67.57
67.50
67.38
62.26
59.07
47.46
47.34
28.23
23.39
20.92
20.89
20.79
18.74
f1 (ppm)

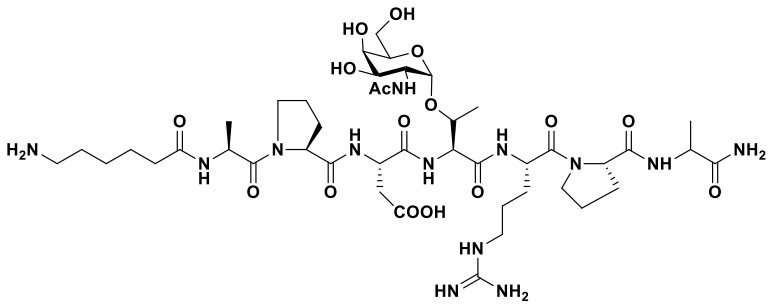

6

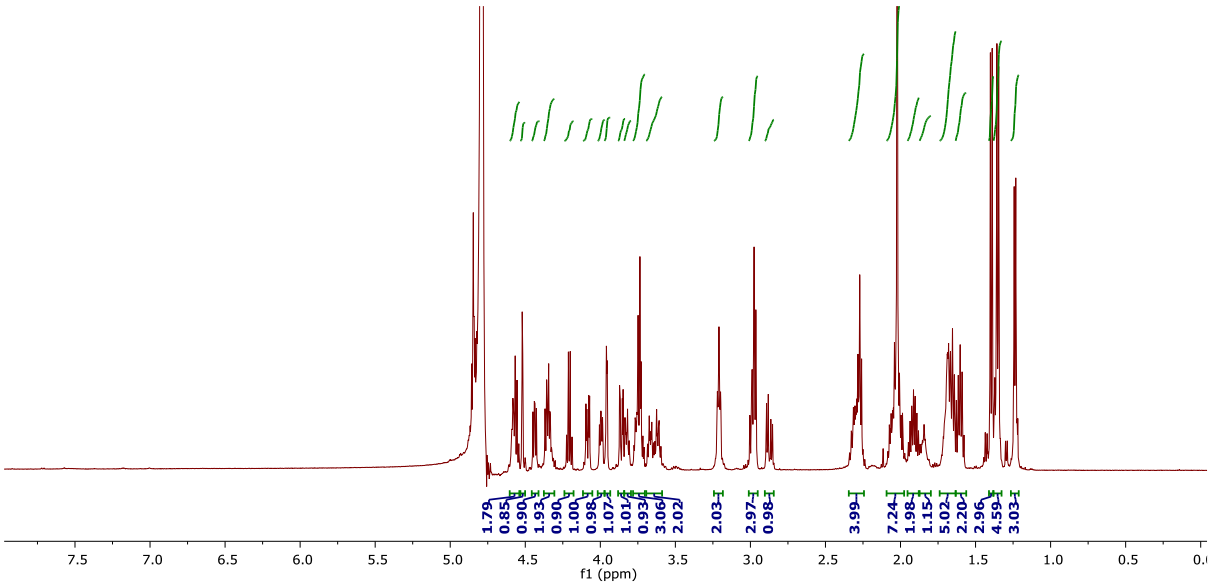
1.79
0.85
0.90
1.93
0.90
1.00
0.98
1.07
1.01
0.93
3.06
2.02
2.03
2.97
0.98
3.99
7.24
1.98
1.15
5.02
2.20
2.96
4.59
3.03
f1 (ppm)

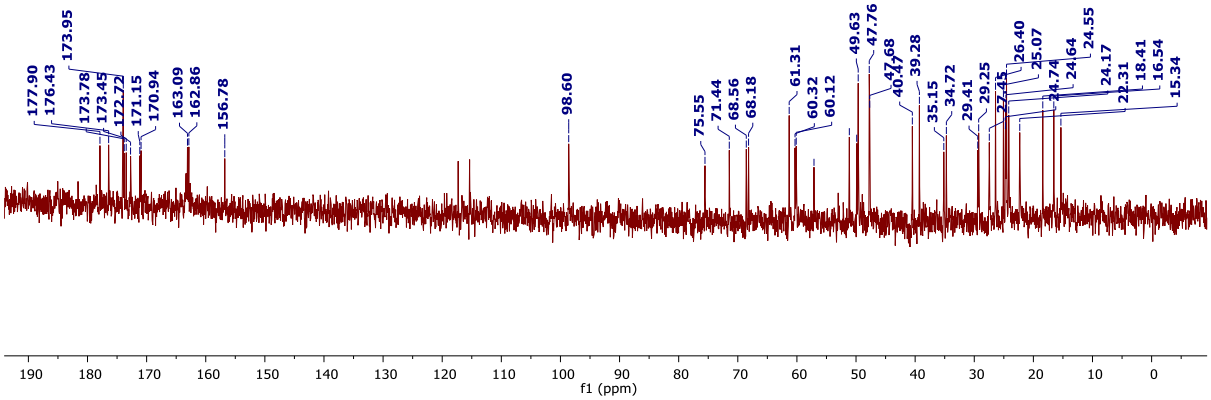
177.90
176.43
173.95
173.78
173.45
172.72
171.15
170.94
163.09
162.86
156.78
98.60
75.55
71.44
68.56
68.18
61.31
60.32
60.12
49.63
47.76
47.68
40.47
39.28
35.15
34.72
29.41
29.25
27.45
26.40
25.07
24.74
24.64
24.55
24.17
23.31
18.41
16.54
15.34
f1 (ppm)

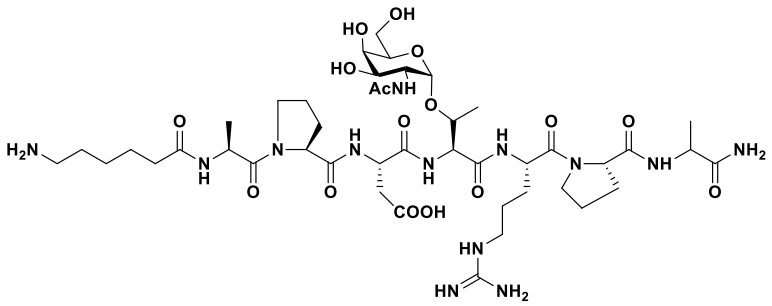

6

DEPT-135

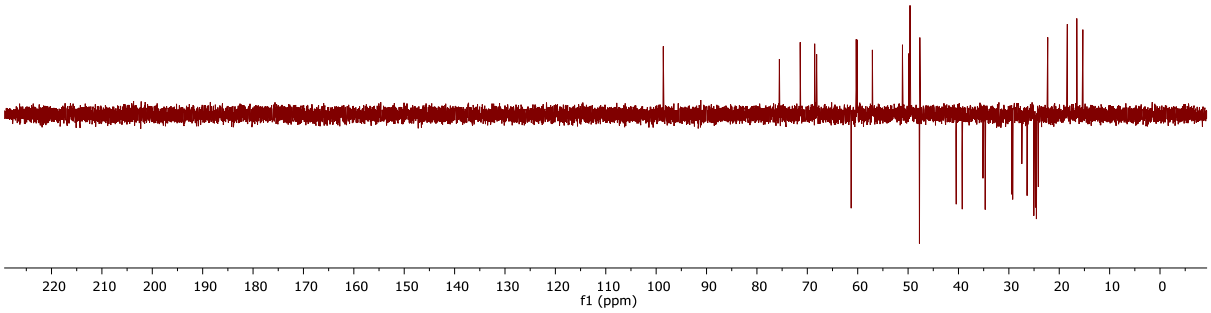

HRMS

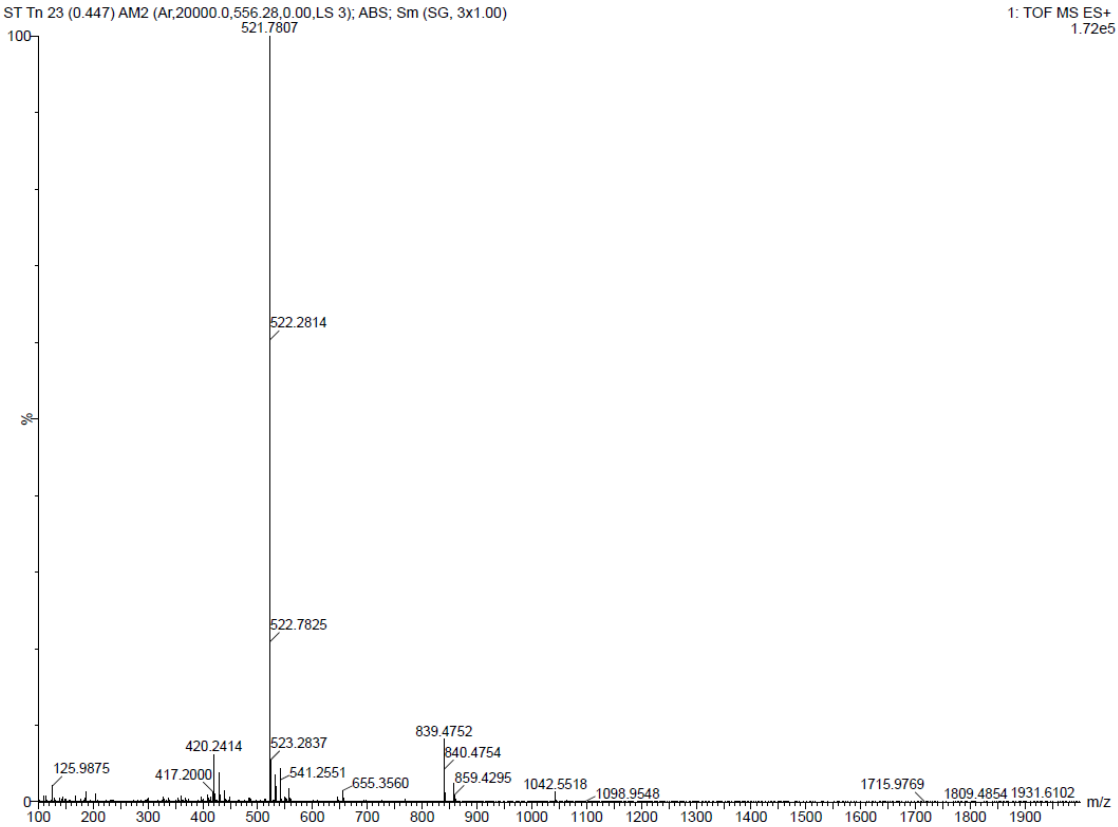

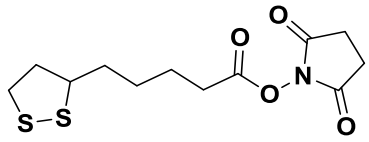
O
O
N
O
O
S
S

7

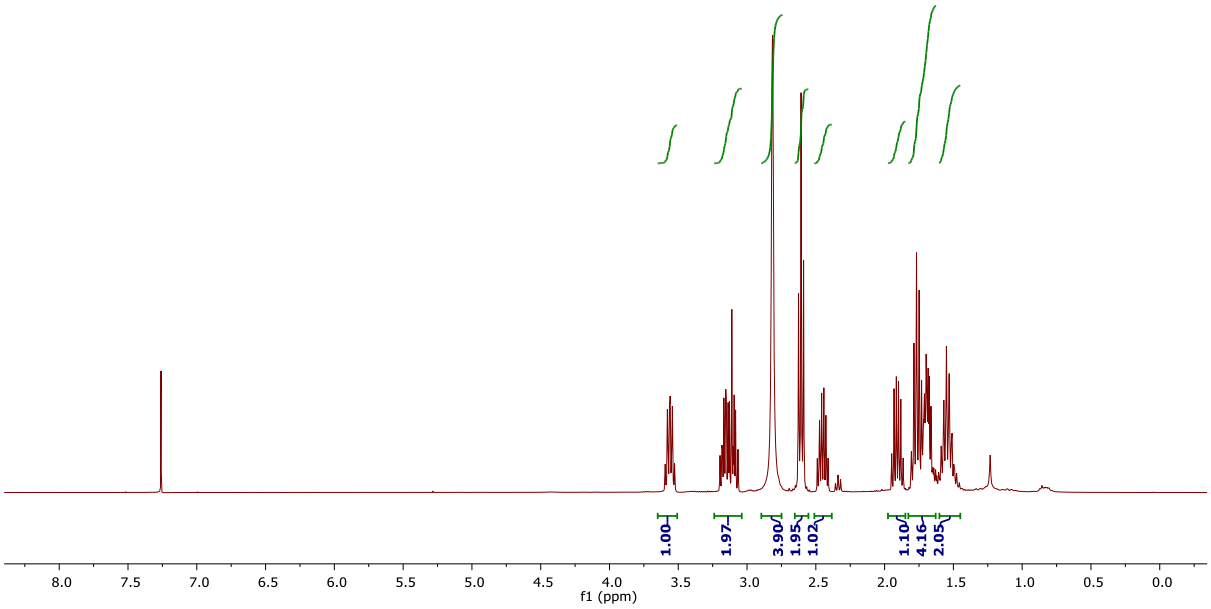
1.00
1.97
3.90
1.95
1.02
1.10
4.16
2.05
8.0
7.5
7.0
6.5
6.0
5.5
5.0
4.5
4.0
3.5
3.0
2.5
2.0
1.5
1.0
0.5
0.0
f1 (ppm)

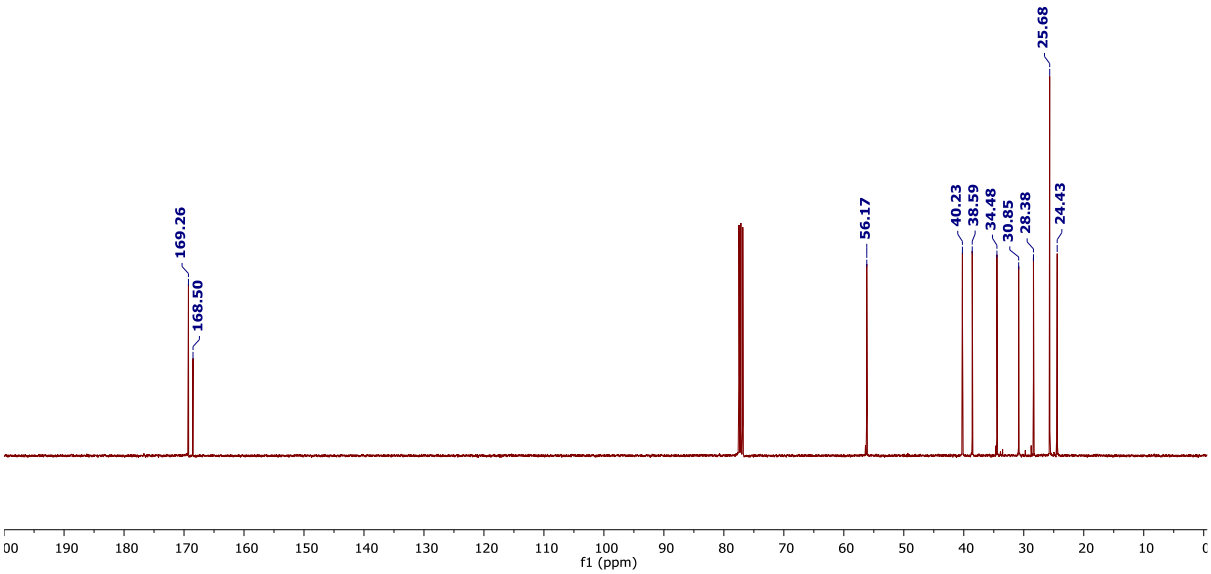
169.26
168.50
56.17
40.23
38.59
34.48
30.85
28.38
25.68
24.43
190
180
170
160
150
140
130
120
110
100
90
80
70
60
50
40
30
20
10
f1 (ppm)

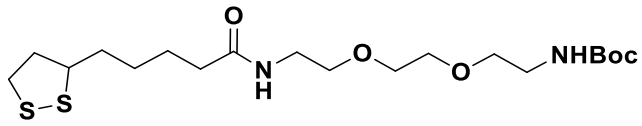
O
N
H
O
O
NHBoc
S
S

8

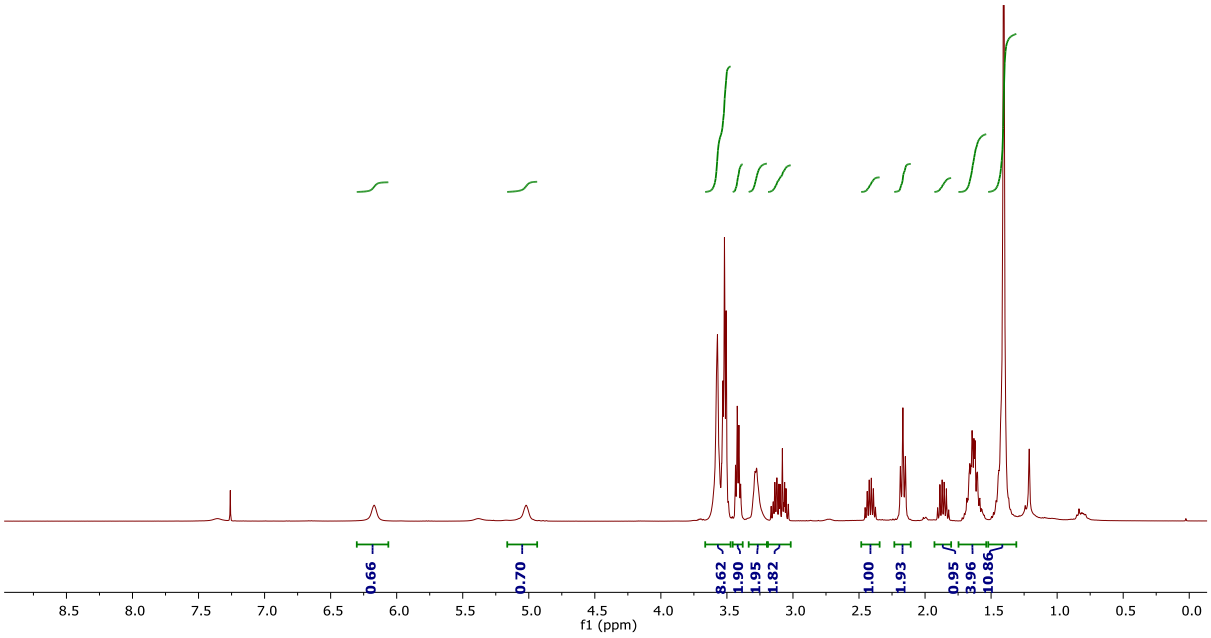
0.66
0.70
8.62
1.90
1.95
1.82
1.00
1.93
0.95
3.96
10.86
8.5
8.0
7.5
7.0
6.5
6.0
5.5
5.0
4.5
4.0
3.5
3.0
2.5
2.0
1.5
1.0
0.5
0.0
f1 (ppm)

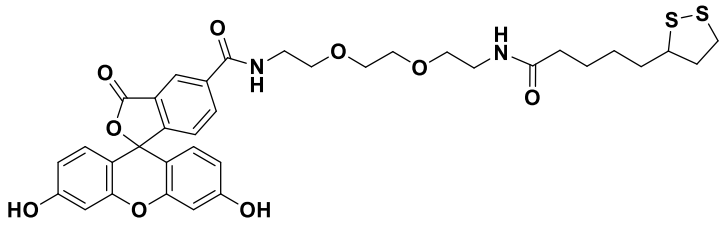

9

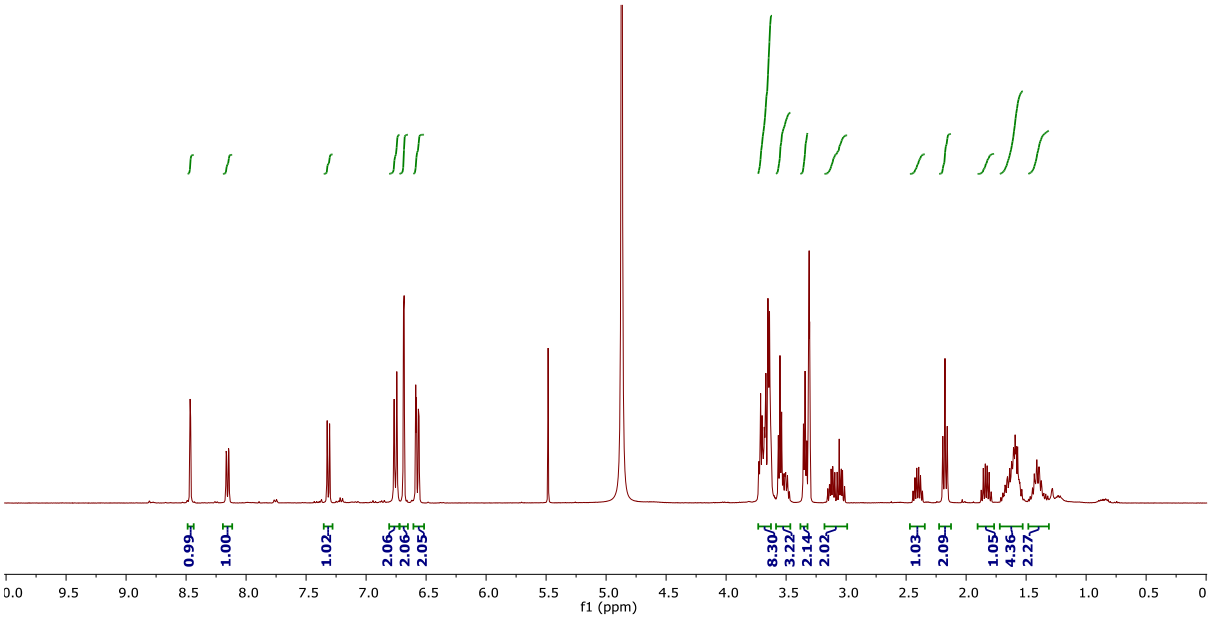
0.99
1.00
1.02
2.06
2.06
2.05
8.30
3.22
2.14
2.02
1.03
2.09
1.05
4.36
2.27
f1 (ppm)

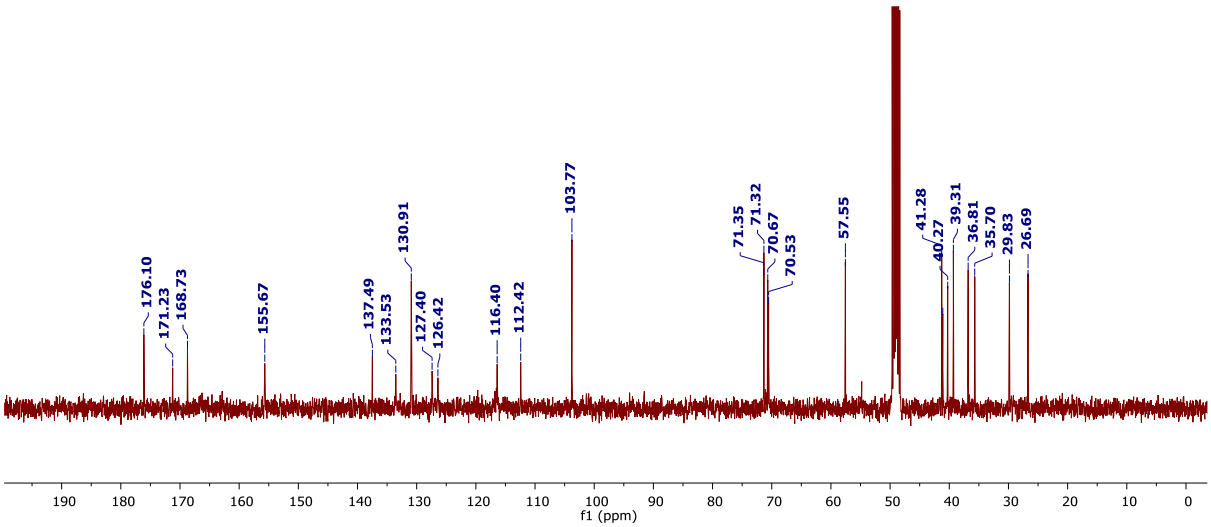
176.10
171.23
168.73
155.67
137.49
133.53
130.91
127.40
126.42
116.40
112.42
103.77
71.35
71.32
70.67
70.53
57.55
41.28
40.27
39.31
36.81
35.70
29.83
26.69
f1 (ppm)

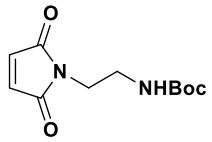
O
N
NHBoc
O

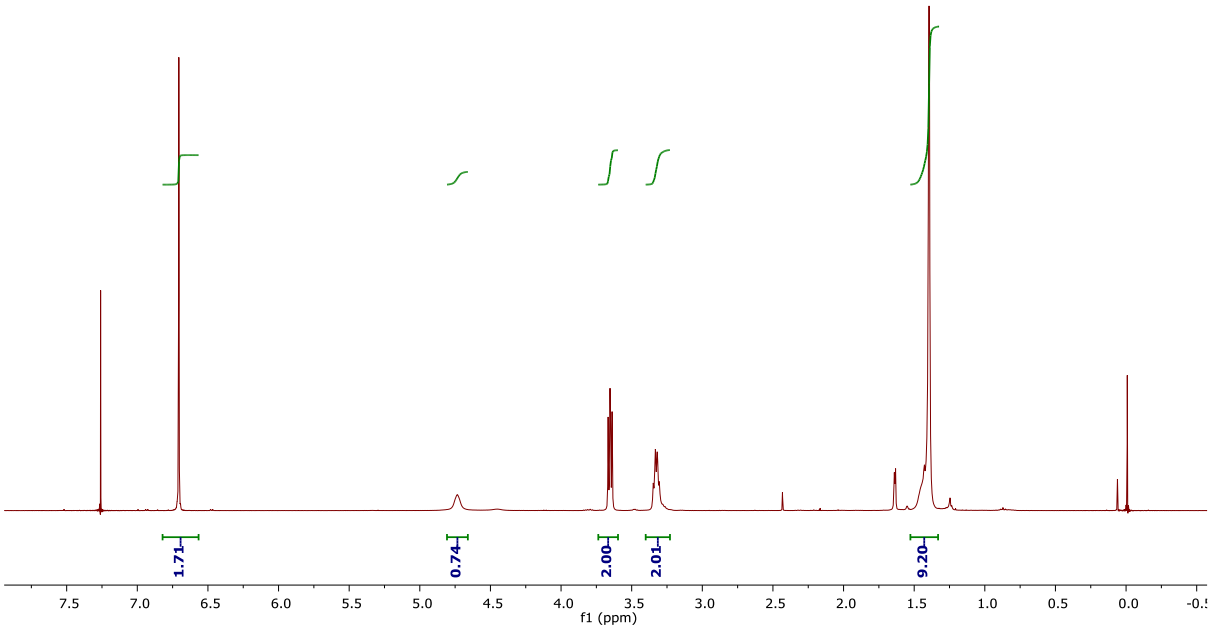
1.71
0.74
2.00
2.01
9.20
7.5
7.0
6.5
6.0
5.5
5.0
4.5
4.0
3.5
3.0
2.5
2.0
1.5
1.0
0.5
0.0
f1 (ppm)

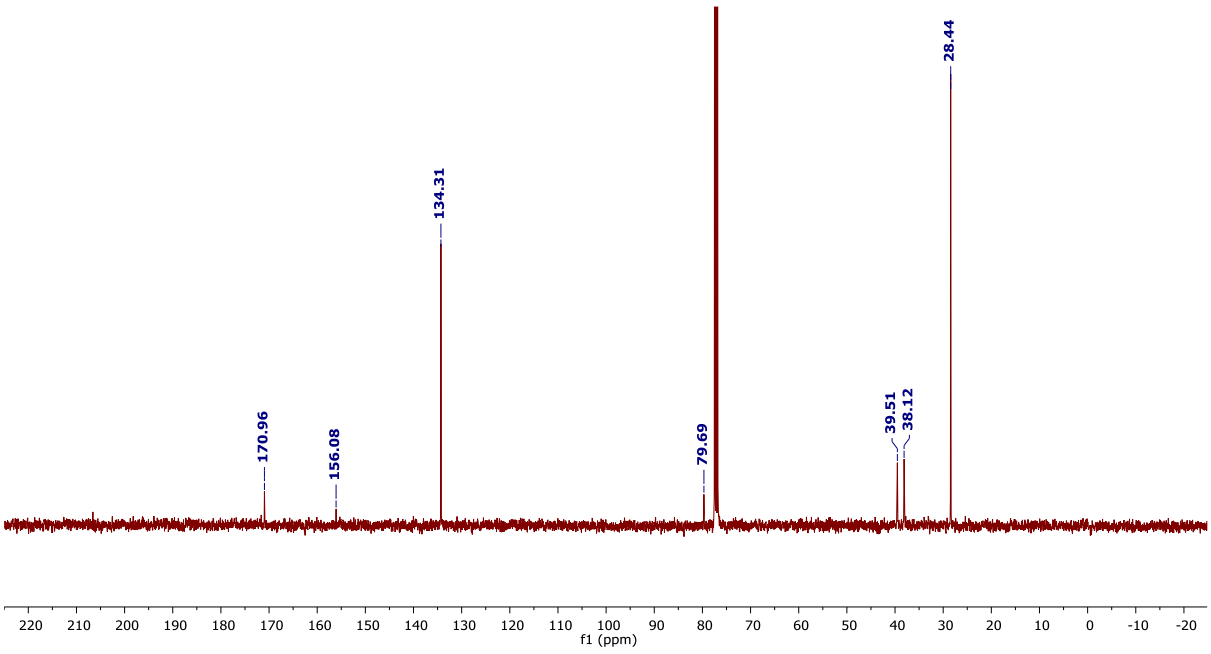
170.96
156.08
134.31
79.69
39.51
38.12
28.44
220
210
200
190
180
170
160
150
140
130
120
110
100
90
80
70
60
50
40
30
20
10
0
-10
-20
f1 (ppm)

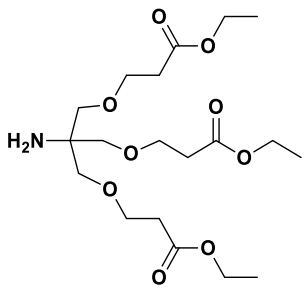

10

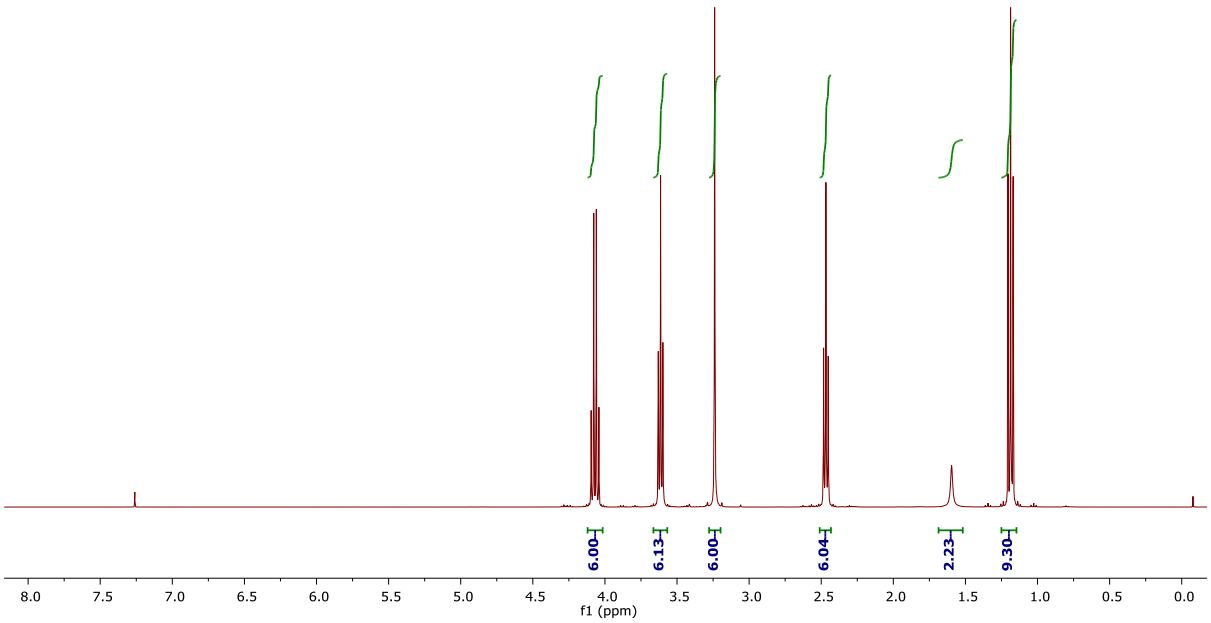
6.00
6.13
6.00
6.04
2.23
9.30
8.0
7.5
7.0
6.5
6.0
5.5
5.0
4.5
4.0
3.5
3.0
2.5
2.0
1.5
1.0
0.5
0.0
f1 (ppm)

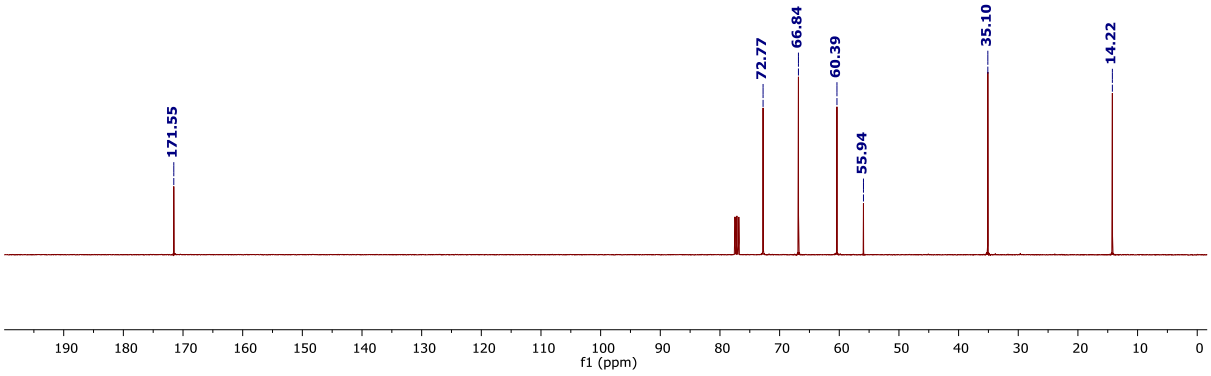
171.55
72.77
66.84
60.39
55.94
35.10
14.22
190
180
170
160
150
140
130
120
110
100
90
80
70
60
50
40
30
20
10
0
f1 (ppm)

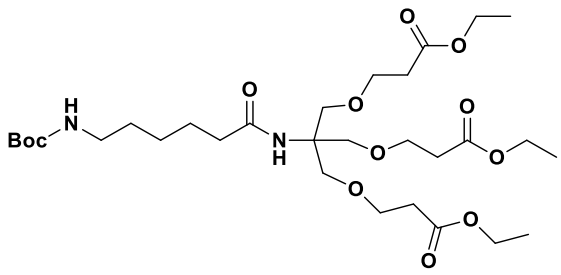

11

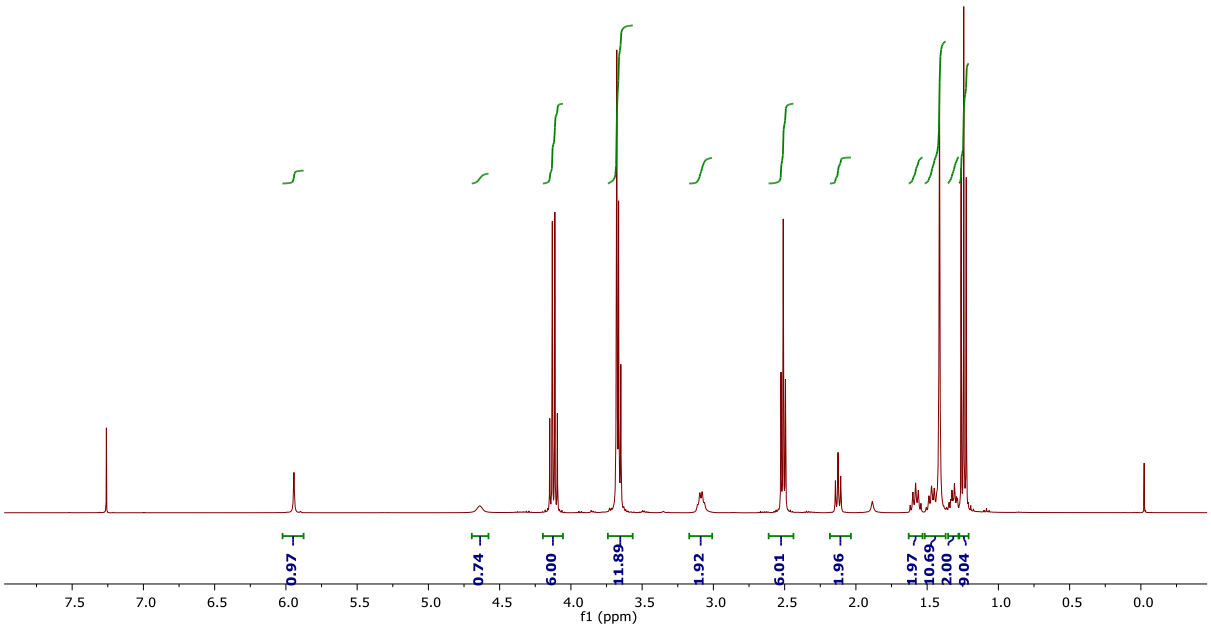
0.97
0.74
6.00
11.89
1.92
6.01
1.96
1.97
10.69
2.00
9.04
7.5
7.0
6.5
6.0
5.5
5.0
4.5
4.0
3.5
3.0
2.5
2.0
1.5
1.0
0.5
0.0
f1 (ppm)

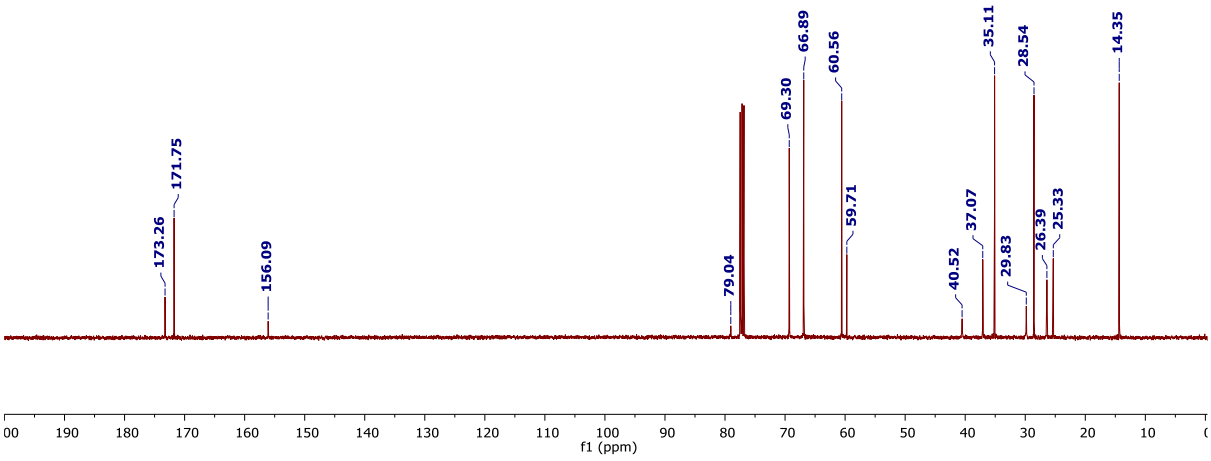
173.26
171.75
156.09
79.04
69.30
66.89
60.56
59.71
40.52
37.07
29.83
35.11
28.54
26.39
25.33
14.35
190
180
170
160
150
140
130
120
110
100
90
80
70
60
50
40
30
20
10
f1 (ppm)

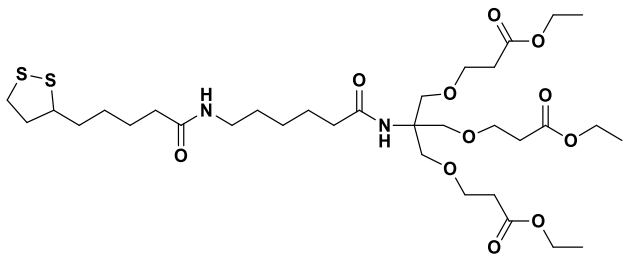

12

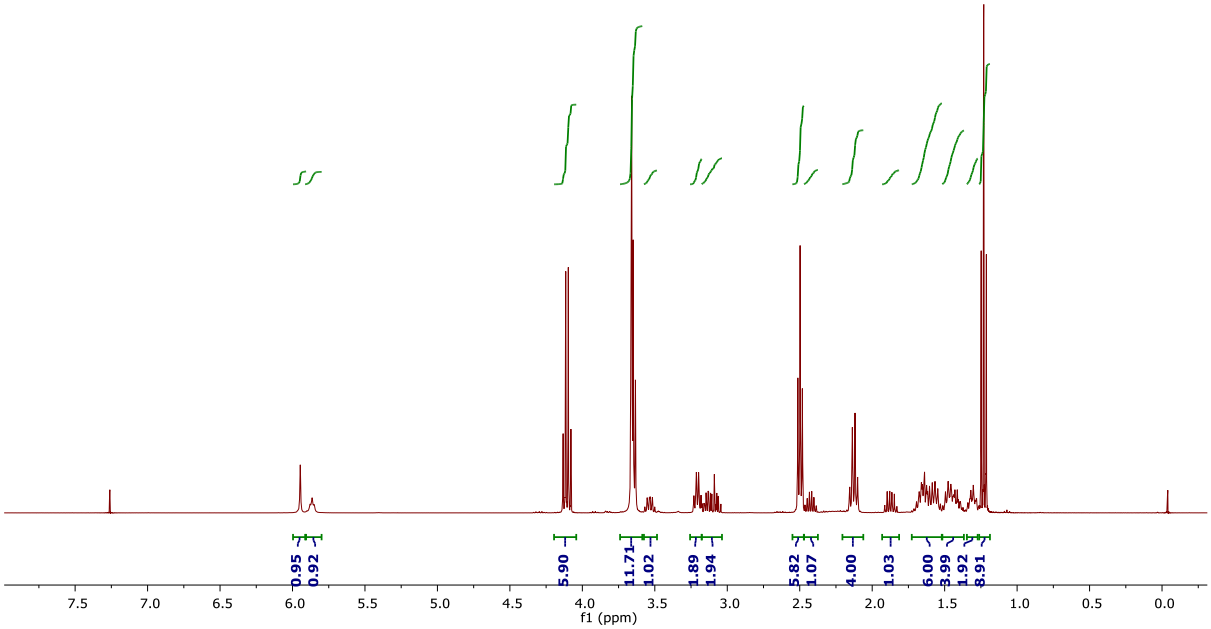
0.95
0.92
5.90
11.71
1.02
1.89
1.94
5.82
1.07
4.00
1.03
6.00
3.99
1.92
8.91
f1 (ppm)

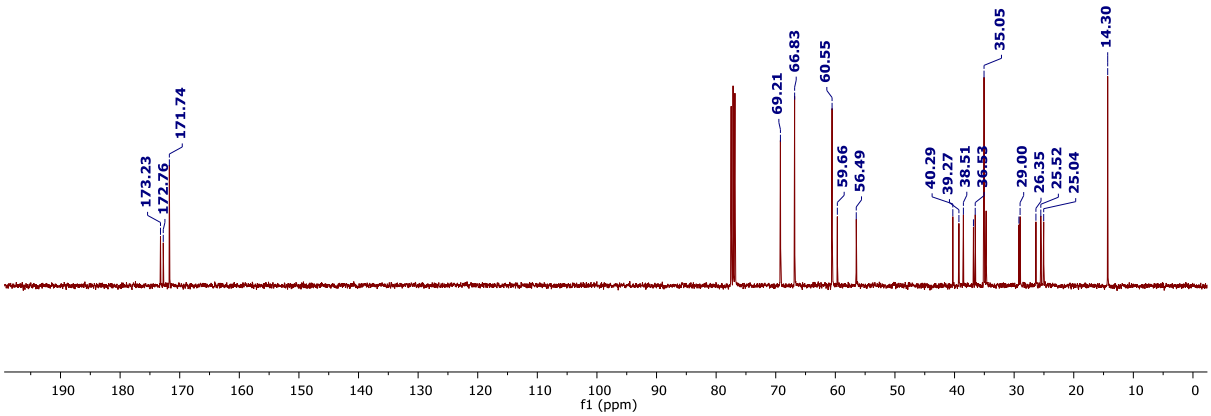
173.23
172.76
171.74
69.21
66.83
60.55
59.66
56.49
40.29
39.27
38.51
36.53
35.05
29.00
26.35
25.52
25.04
14.30
f1 (ppm)

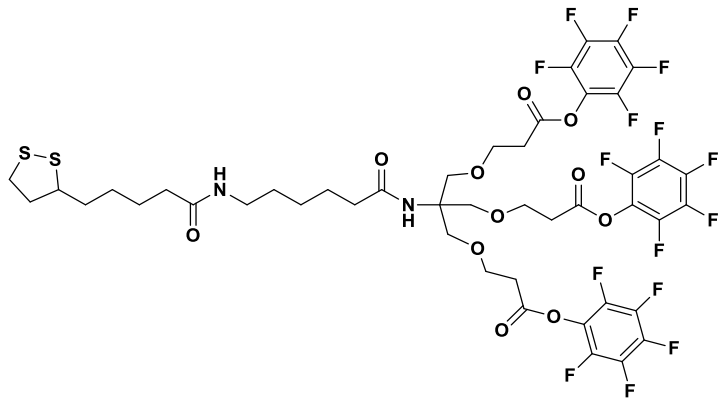

13

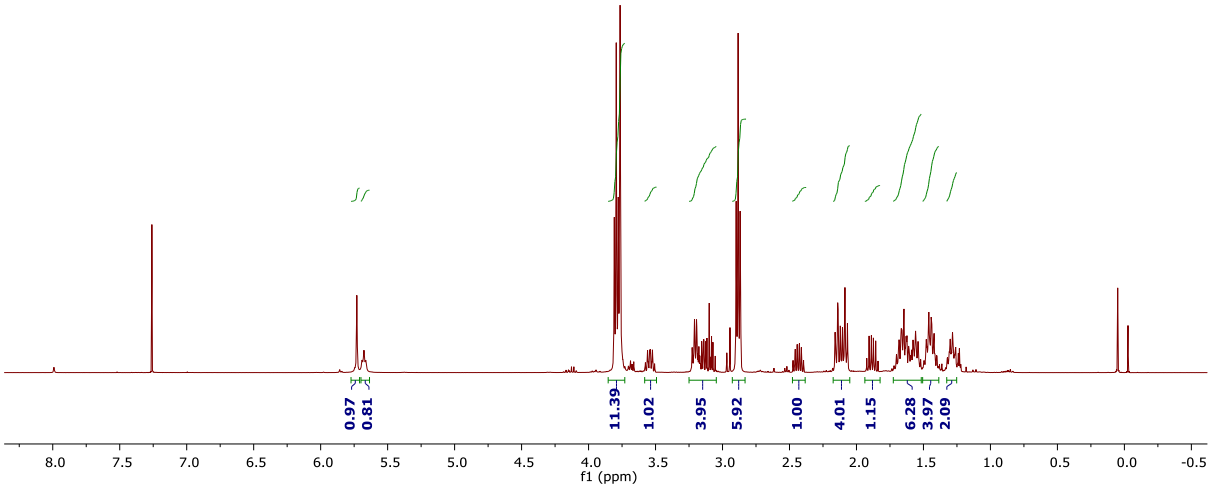
0.97
0.81
11.39
1.02
3.95
5.92
1.00
4.01
1.15
6.28
3.97
2.09
f1 (ppm)

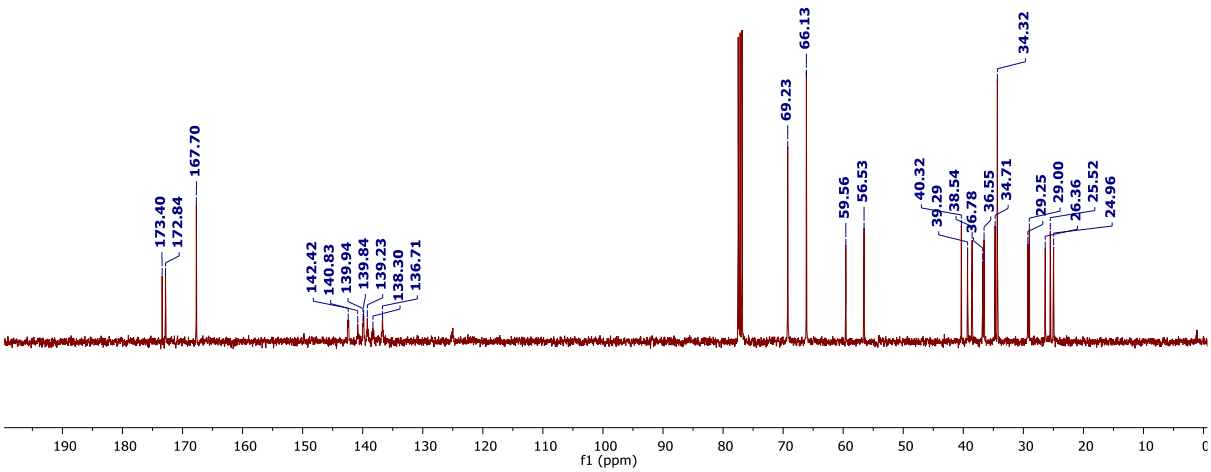
173.40
172.84
167.70
142.42
140.83
139.94
139.84
139.23
138.30
136.71
69.23
66.13
59.56
56.53
40.32
39.29
38.54
36.78
36.55
34.71
34.32
29.25
29.00
26.36
25.52
24.96
f1 (ppm)

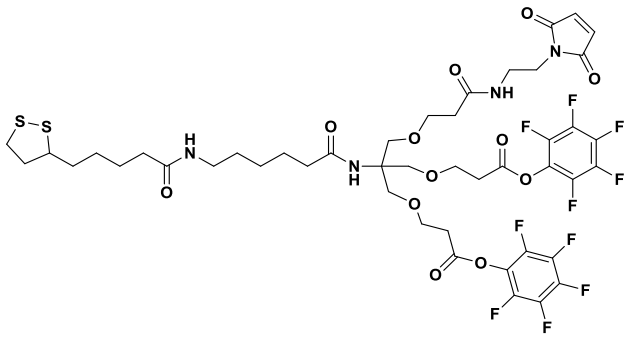

14

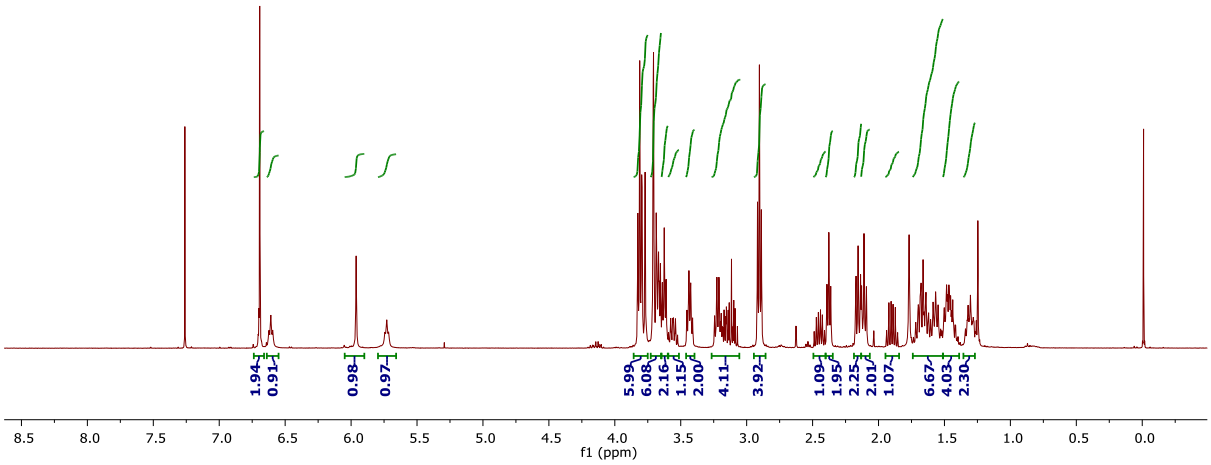
1.94
0.91
0.98
0.97
5.99
6.08
2.16
1.15
2.00
4.11
3.92
1.09
1.95
2.25
2.01
1.07
6.67
4.03
2.30
f1 (ppm)

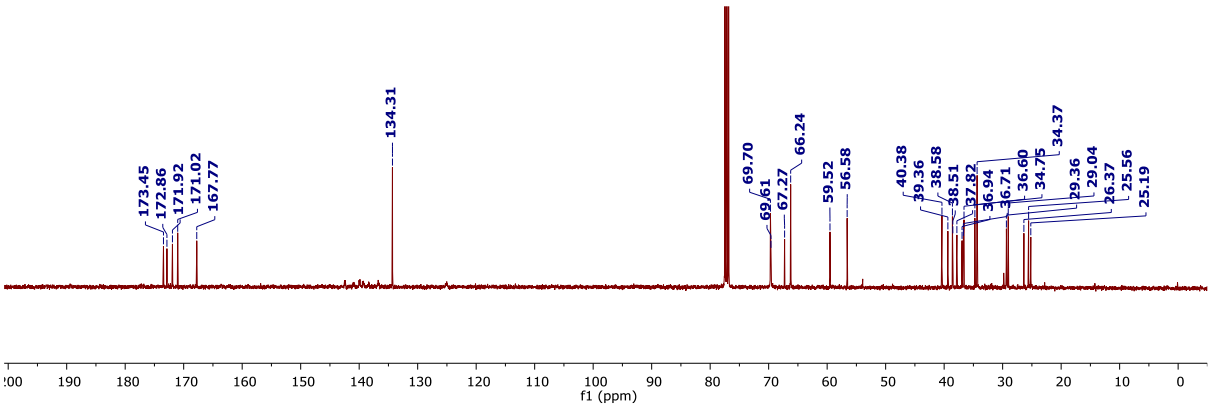
173.45
172.86
171.92
171.02
167.77
134.31
69.70
69.61
67.27
66.24
59.52
56.58
40.38
39.36
38.58
38.51
37.82
36.94
36.71
36.60
34.75
34.37
29.36
29.04
26.37
25.56
25.19
f1 (ppm)

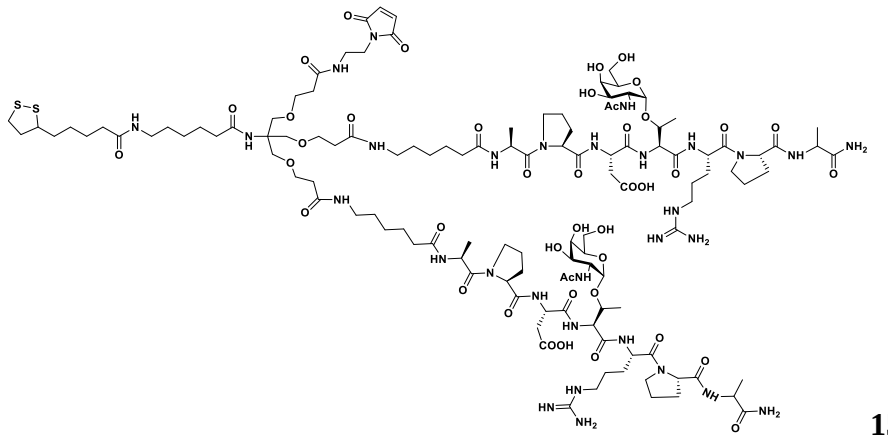

15

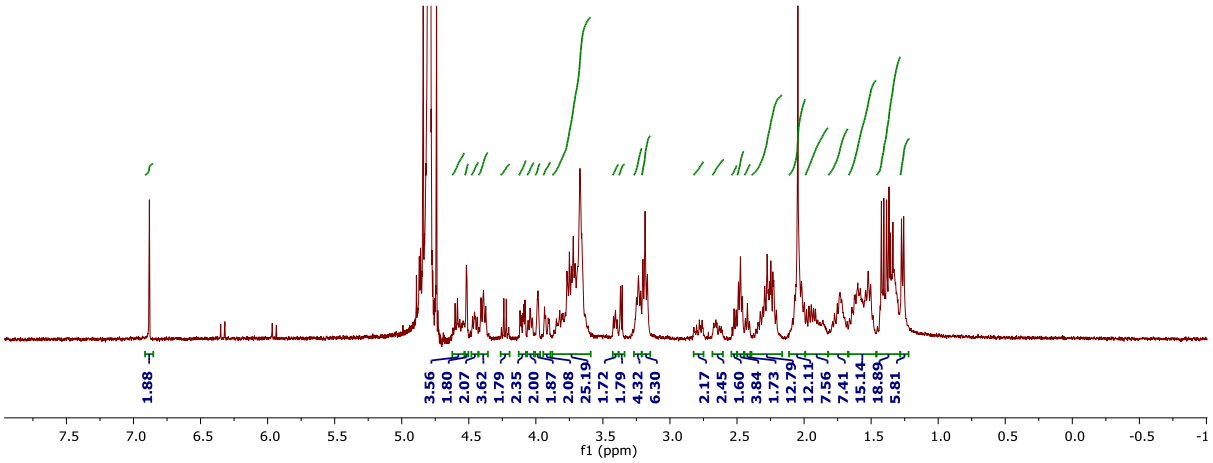
1.88
3.56
1.80
2.07
3.62
1.79
2.35
2.00
1.87
2.08
25.19
1.72
1.79
4.32
6.30
2.17
2.45
1.60
3.84
1.73
12.79
12.11
7.56
7.41
15.14
18.89
5.81
f1 (ppm)

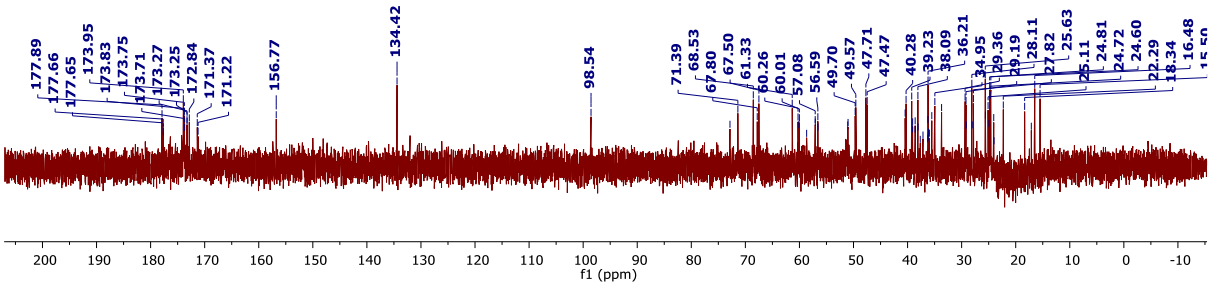
177.89
177.66
177.65
173.95
173.83
173.75
173.71
173.27
173.25
172.84
171.37
171.22
156.77
134.42
98.54
71.39
68.53
67.80
67.50
61.33
60.26
60.01
57.08
56.59
49.70
49.57
47.71
47.47
40.28
39.23
38.09
36.21
34.95
29.36
29.19
28.11
27.82
25.63
25.11
24.81
24.72
24.60
22.29
18.34
16.48
f1 (ppm)

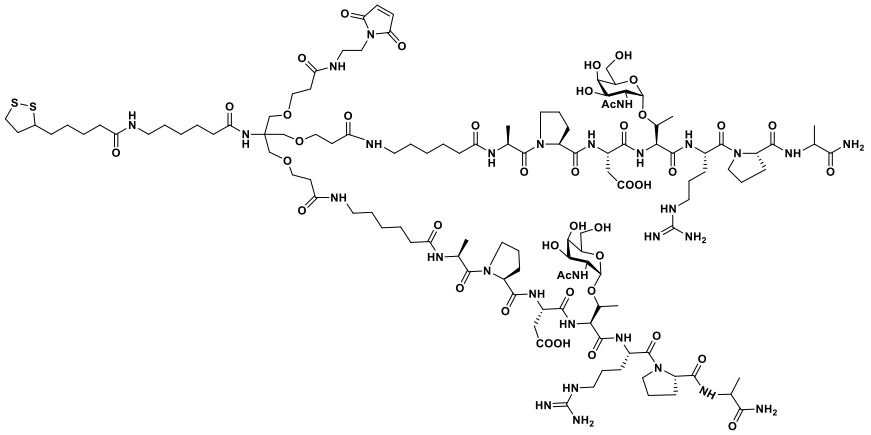

15

MALDI-TOF

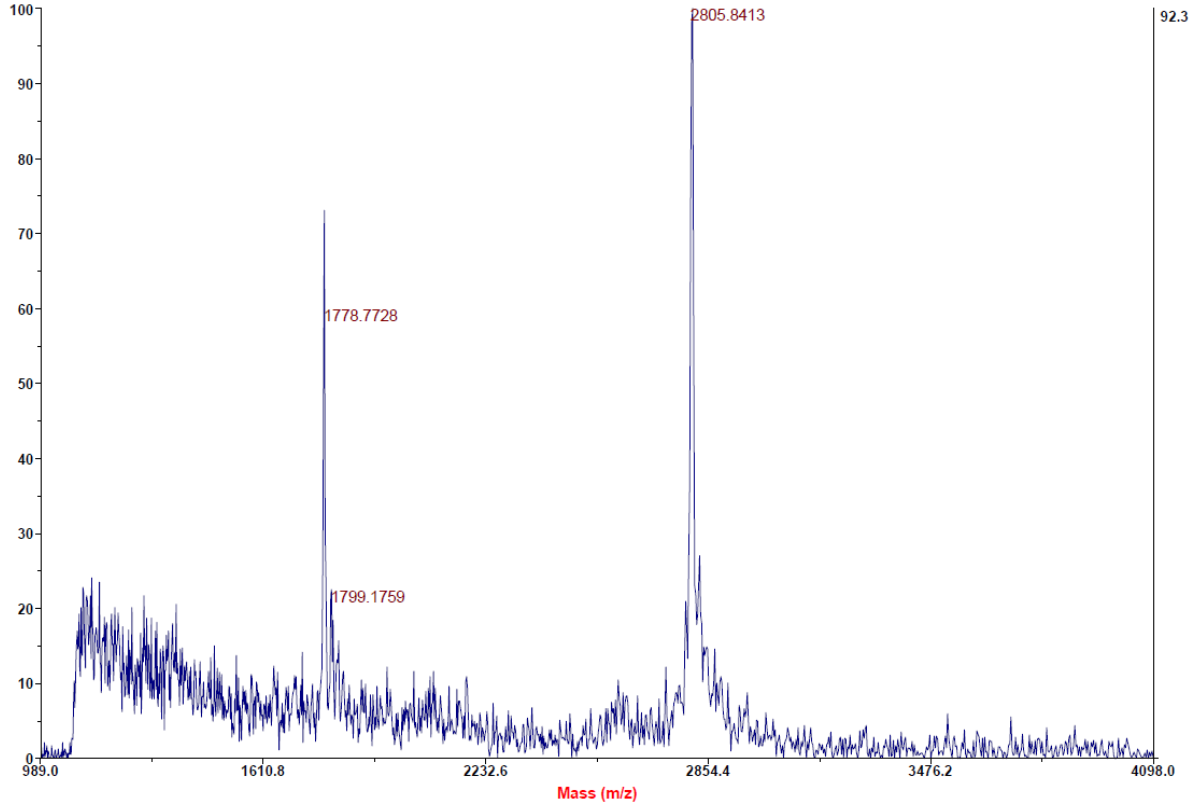
2805.8413
92.3
1778.7728
1799.1759
100
90
80
70
60
50
40
30
20
10
0
989.0
1610.8
2232.6
2854.4
3476.2
4098.0
Mass (m/z)

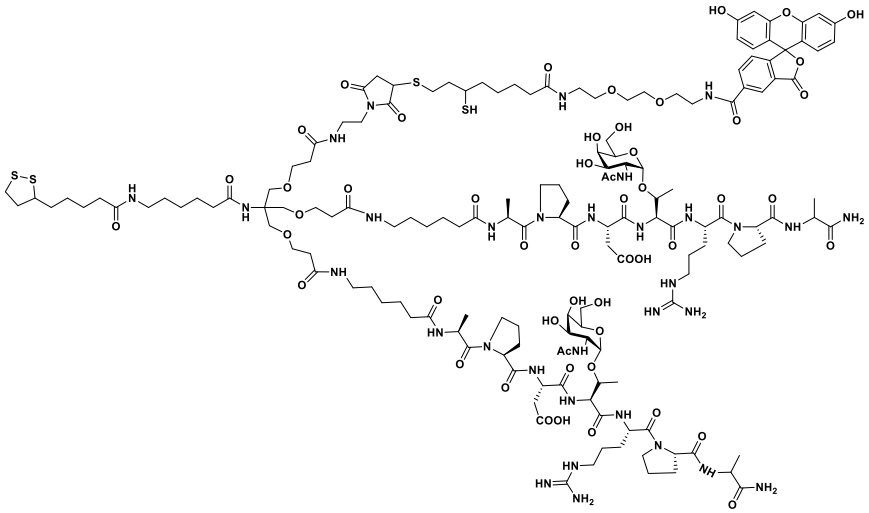

16

HPLC Profile

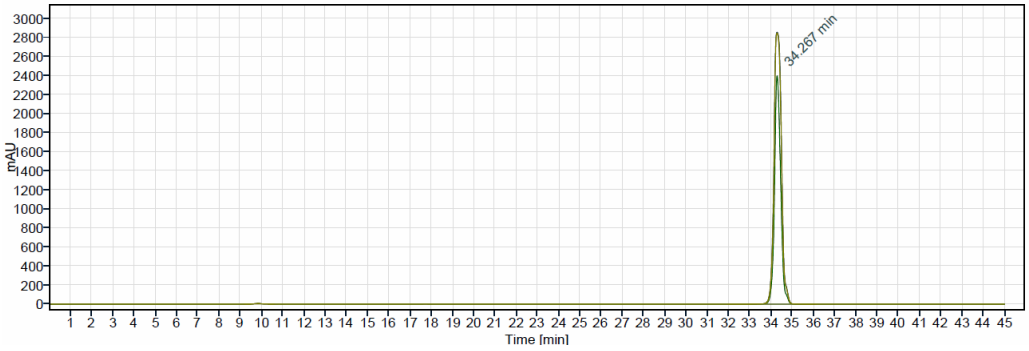

HPLC Purification conditions: C-18 reverse phase column, linear gradient of 0-100 solvent B (95% acetonitrile + 5% water + 0.1% TFA) and A (95% water + 5% water + 0.1 % TFA) over 40 min.

CHAPTER-5

Immunomodulation of STn Antigen Using Glyconanotechnolgy

5.1 Introduction:

Cell surface glycans are critical to tissue homeostasis and cell signalling. These glycans reshape in normal and pathological processes. For instance, the dense *N-glycan-based* mucin undergoes a series of structural remodelling by glycosidase enzyme to alter the binding affinity with various growth factors during embryonic development and cancer metastasis and proliferation.[1-4] Several carbohydrate antigens are overexpressed on cancer cell surface due to abnormal glycosylation process.[5-7] Sialyl-Tn (STn) antigen is an attractive therapeutic target for various cancer. STn has long been associated with tumor initiation, propagation, and metastasis. Hence, several research groups tried to develop T-cell dependent antibody responses against STn antigen.[8-14] However, these antibodies failed in the clinic for multiple reasons, primarily because these antigens failed to process through the T-cell dependent immune system. They could not activate a complementary system to kill cancer cells. Motivated by the shape of the nanoparticles dependent immune modulation of carbohydrate antigens, We synthesized STn antigen and small molecule adjuvant conjugated nanoparticles to develop T-cell-dependent immune response and IgG antibody against STn antigen. These antibodies are expected to be potential biomarkers for cancer cells and inhibit cancer cell growth and metastasis.

5.2 Synthesis of STn Precursor:

The STn disaccharide precursor **8** preparation started with the synthesis of two building blocks (**4** and **1**) from D-galactose and sialic acid, respectively (Scheme 1). Compound **1** was readily synthesized from per acetylated 2-azido glucose **3** in a nine-steps reactions using the standard reported procedure.[15] Synthesis of sialic acid donor was reported in chapter 3. Finally, glycosylation of sialic acid donor **4** and galactose acceptor **1** in the presence of TMSOTf as promoter yielded 66% of disaccharide precursor **5**, which was reduced by using Zn dust and acetic acid and acetic anhydride solution to obtain STn precursor **8**.

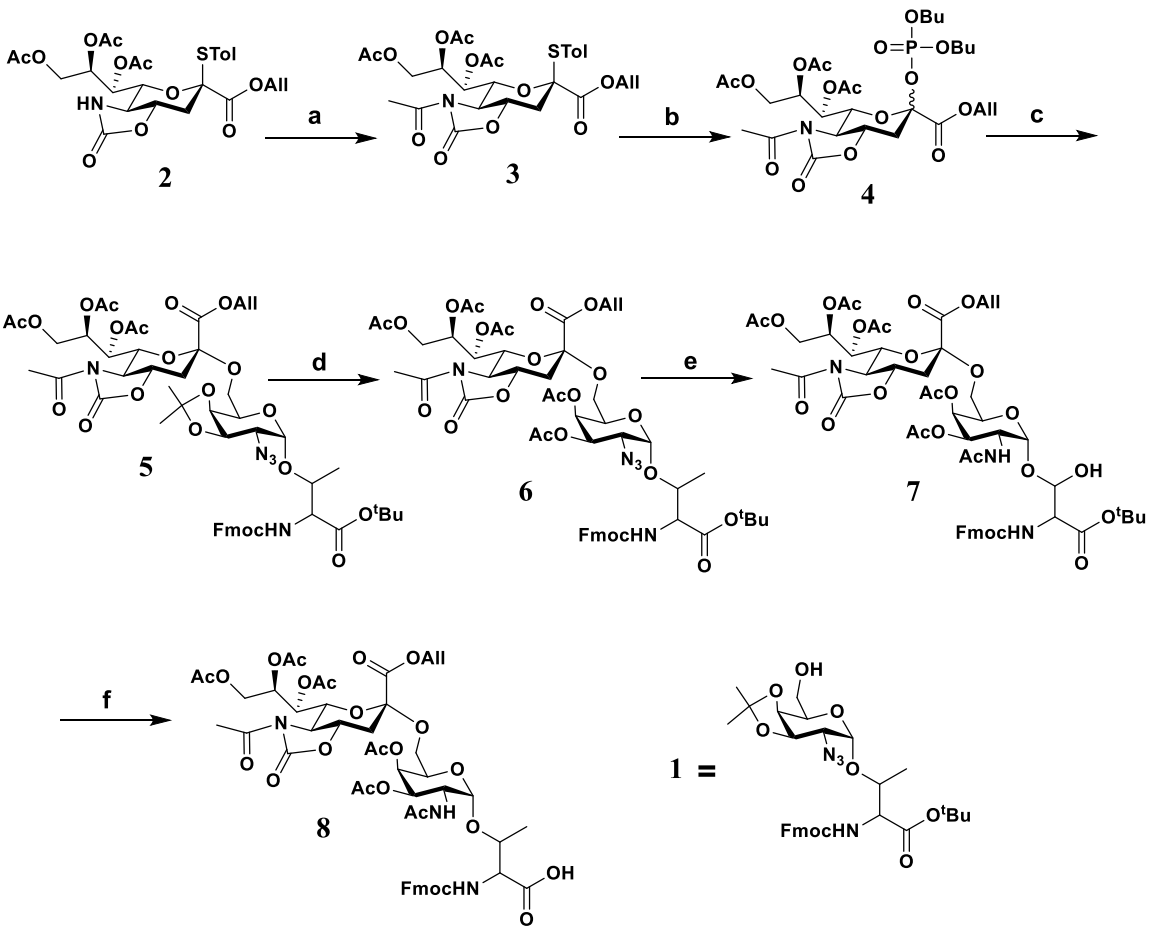

Scheme 1. Synthesis of STn precursor: (a) Ac_2O, pyridine, RT, 12 h, 86% ; (b) Dibutyl phosphate, NIS, TfOH, DCM, 0 °C, 4 h, 71%; (c) **1**, TMSOTf, DCM, -45 °C, 2 h, 66%; (d) i) AcOH/H_2O, RT, 12 h; ii) Ac_2O, pyridine, RT, 12 h, 70% over two steps; (e) Zn, THF/AcOH/Ac_2O, RT, 4 h, 69%; (f) TFA/DCM, RT, 4 h

Once we have STn precursor **8** in hand, we next synthesized the STn glycopeptides using a solid phase peptide synthesizer following standard Fmoc protocol. Briefly, The rink amide bound Fmoc group was first deprotected with 20 % piperidine in DMF. The coupling reactions were carried out using *the in situ active ester method, HBTU as a coupling reagent, HOBt as a racemization suppresser,* and DIPEA as a base (Scheme 2). Peptide GPAPRTDPAS-amine linker was synthesized, purified by reverse phase semi-preparative HPLC and characterized by MALDI-TOF data. We are now synthesizing STn and TLR8/9 adjuvant conjugate gold nanoparticles for further immune studies.

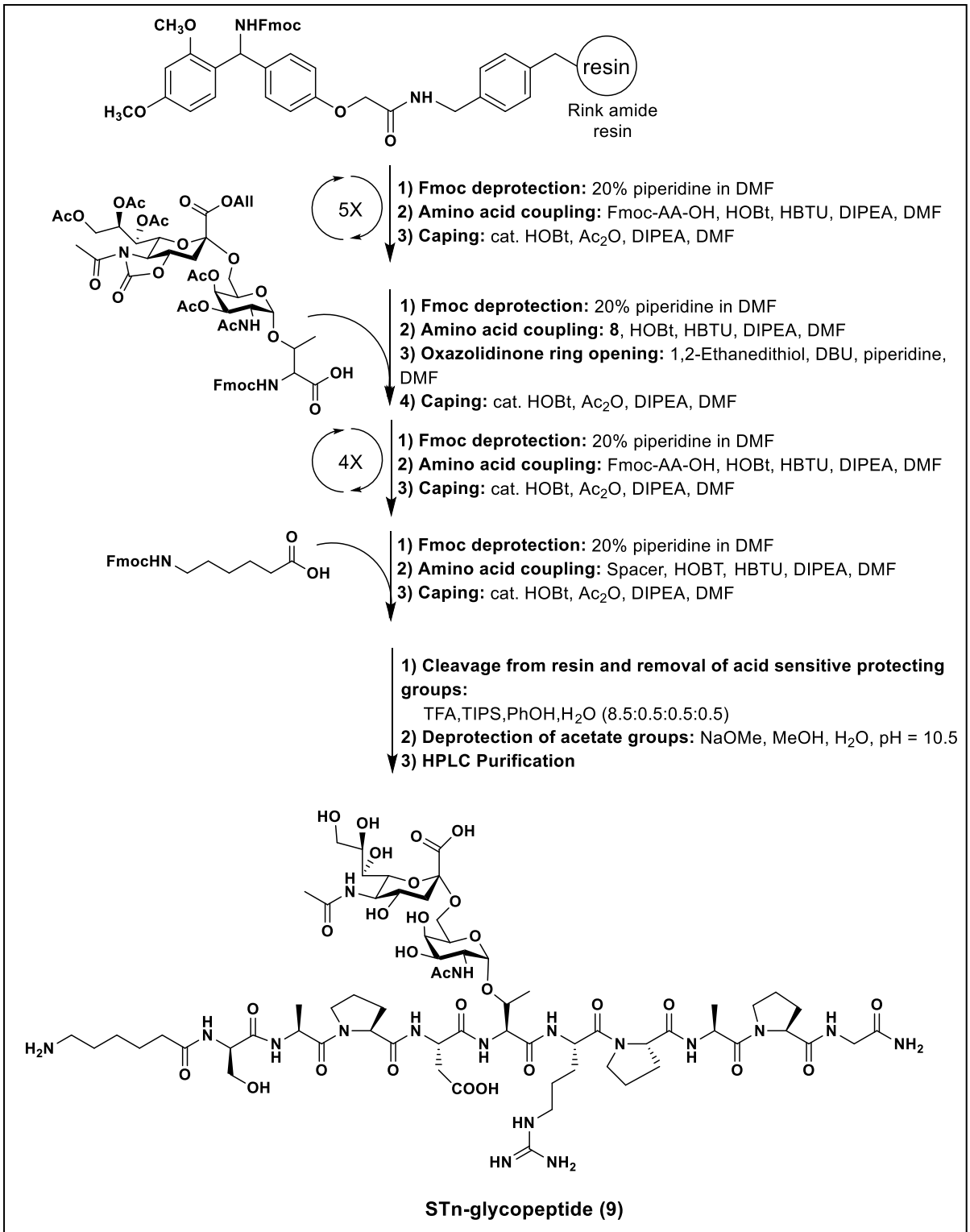

Scheme 2. Solid phase peptide synthesis of STn glycopeptide.

5.3 Conclusion:

In summary, we have successfully optimized STn-glycopeptides synthetic protocol. All intermediates and final compounds are characterized by using standard spectroscopic techniques. Currently, we are synthesizing STn/TLR8 hybrid tripodal system and nanoparticles conjugation. Finally, these nanoparticles will be used to study their immune responses, T-cell dependent IgG antibody production and vaccine development.

5.4 Experiment Section:

Compound 3

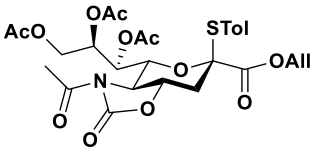

Compound **2** (1.3 gm, 2.30 mmol) in anhydrous dichloromethane (20 mL) was mixed with acetyl choride (0.82 mL, 11.5 mmol) and DIPEA (1.2 mL, 6.9 mmol) at 0 ºC. Further the reaction mixture was brought to room temperature and stirred for 2 h. The resulting mixture was diluted with dichloromethane, washed with sodium bicarbonate and brine solutions. The organic layer was dried over sodium sulphate and concentrated *in vacuo.* The residue was purified by silica gel chromatography using a mixture of (1:1, v/v) ethyl acetate and hexane as eluent to afford compound **3** (1.2 gm, 86%). ^{1}H NMR (400 MHz, Chloroform-*d*) δ = 7.35 (d, *J* = 8.1 Hz, 2H), 7.13 (d, *J* = 7.9 Hz, 2H), 5.7.84-5.71 (m, 1H), 5.55 (t, *J* = 2.6 Hz, 1H), 5.34-5.18 (m, 2H), 4.98 (dt, *J* = 7.8, 2.6 Hz, 1H), 4.85 (dd, *J* = 9.1, 2.6 Hz, 1H), 4.76 (ddd, *J* = 12.8, 11.3, 3.7 Hz, 1H), 4.61-4.44 (m, 2H), 4.30 (dd, *J* = 12.1, 2.7 Hz, 1H), 4.02 (dd, *J* = 12.1, 7.9 Hz, 1H), 3.73 (dd, *J* = 11.3, 9.2 Hz, 1H), 2.83 (dd, *J* = 13.0, 3.7 Hz, 1H), 2.50 (s, 3H), 2.33 (s, 3H), 2.29 (t, *J* = 12.9 Hz, 1H), 2.11 (s, 3H), 2.06 (s, 3H), 1.96 (s, 3H).^{13}C NMR (101 MHz, Chloroform-*d*) δ = 172.52, 171.13, 170.44, 169.81, 167.08, 153.71, 140.66, 131.23, 130.13, 124.79, 119.41, 88.05, 75.69, 75.22, 73.70, 72.52, 66.76, 62.81, 59.78, 35.81, 24.81, 21.41, 21.20, 20.84, 20.82. HR-ESI-MS (m/z) Calcd for $C_{28}H_{34}NO_{12}S$ $[M+H]^+$ 608.1802, found: 608.1815.

Compound 4

Compound **3** (1.1 gm, 1.81 mole) and dibutyl phosphate (1.14 mL, 5.43 mmol) was dissolved in anhydrous dichloromethane (20 mL) and activated 4 Å molecular sieves was added. The reaction mixture was stirred at room temperature for 2 hours. Further the resultant reaction mixture was cooled to 0 ºC, and NIS (0.49 gm, 2.17 mmol), TfOH (32 µl, 0.36 mmol) were added and stirred at 0 ºC for 6 hours. The reaction was neutralized with DIPEA and concentrated *in vacuo.* The residue was purified by silica gel column chromatography using a

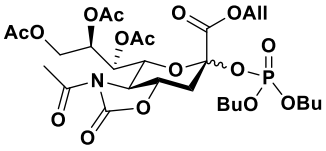

mixture of (3:2, v/v) ethyl acetate and hexane as eluent to afford compound **4** (0.9 gm, 71%). (*α/β* isomer 1:1) ^{1}H (NMR 400 MHz, Chloroform-*d*) δ = 6.01-5.87 (m, 2H), 5.67 (dd, *J* = 7.4, 1.6 Hz, 1H), 5.63 (dd, *J* = 4.3, 2.0 Hz, 1H), 5.44-5.34 (m, 2H), 5.33-5.27 (m, 3H), 5.24-5.26-5.22 (m, 1H), 4.79 (dd, *J* = 9.5, 1.7 Hz, 1H), 4.75-4.67 (m, 4H), 4.63-4.35 (m, 1H), 4.48 (dd, *J* = 12.2, 2.7 Hz, 1H), 4.40 (dd, *J* = 12.3, 2.8 Hz, 1H), 4.20-3.99 (m, 12H), 3.85 (dd, *J* = 11.3, 9.5 Hz, 1H), 3.77 (dd, *J* = 11.3, 9.6 Hz, 1H), 3.02 (dd, *J* = 12.2, 4.0 Hz, 1H), 2.88 (dd, *J* = 12.7, 3.7 Hz, 1H), 2.67 (dd, *J* = 13.2, 12.3 Hz, 1H), 2.49 (s, 6H), 2.32 (td, *J* = 12.7, 2.7 Hz, 1H), 2.14 (s, 3H), 2.11 (d, *J* = 1.4 Hz, 3H), 2.09 (s, 3H), 2.08 (s, 3H), 2.03 (s, 3H), 2.01 (s, 3H), 1.69-1.59 (m, 8H), 1.44-1.34 (m, 8H), 0.99-0.89 (m, 12H). ^{13}C NMR (101 MHz, Chloroform-*d*) δ = 172.25 , 171.97 , 170.75 , 170.70 , 170.65 , 170.09 , 170.05 , 169.90 , 166.62 , 166.55, 164.84, 153.64, 153.59, 131.09, 130.91, 120.11, 119.44, 99.05, 99.00, 98.28, 98.21, 76.74, 74.22, 74.12, 72.60, 71.70, 71.64, 70.03, 68.72, 68.66, 68.57, 68.51, 68.32, 68.26, 68.20, 68.14, 67.51, 67.47, 62.83, 62.62, 59.03, 58.43, 36.15, 36.02, 35.98, 32.29, 32.25, 32.22, 32.18, 32.15, 29.80, 24.77, 24.75, 21.12, 21.09, 20.90, 20.86, 18.73, 18.69, 13.69, 13.66. HR-ESI-MS (m/z) Calcd for $C_{29}H_{45}N_{17}O_{16}P$ $[M+H]^+$ 694.2476, found: 694.2487.

Compound 1

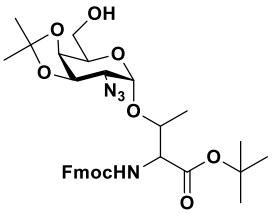

Compound **1** was synthesised by following synthetic reported methods.[15] ^{1}H NMR (400 MHz, Chloroform-*d*) δ = 7.77 (d, *J* = 7.6 Hz, 2H), 7.63 (d, *J* = 7.5 Hz, 2H), 7.40 (t, *J* = 7.7 Hz, 2H), 7.31 (t, *J* = 7.5 Hz, 2H), 5.68 (d, *J* = 9.5 Hz, 1H), 5.03 (d, *J* = 3.6 Hz, 1H), 4.44-4.38 (m, 3H), 4.33 (dd, *J* = 10.4, 7.4 Hz, 1H), 4.29-4.23 (m, 3H), 4.19-4.14 (m, 1H), 3.99-3.92 (m, 1H), 3.84 (s, 1H), 3.41 (dd, *J* = 8.2, 3.6 Hz, 1H), 2.25 (bs, 1H), 1.52 (s, 3H), 1.50 (s, 9H), 1.37 (s, 3H), 1.33 (d, *J* = 6.5 Hz, 3H). ^{13}C NMR (101 MHz, Chloroform-*d*) δ = 169.46, 156.87, 143.9, 141.41, 127.84, 127.21, 125.38, 120.10, 110.44, 98.36, 83.03, 76.13, 73.70, 73.37, 68.49, 67.43, 62.81, 61.25, 59.13, 47.26, 28.25, 28.11, 26.32, 19.06. HR-ESI-MS (m/z) Calcd for $C_{32}H_{41}N_4O_9$ $[M+H]^+$ 625.2874, found: 625.2868.

Compound 5

Sialyl phosphate donor **3** (1.25 gm, 1.80 mmol) and galactose acceptor **1** (1.3 gm, 2.16 mmol) were dissolved in anhydrous dichloromethane (30 mL) and 4 Å molecular sieves were added. The resulting mixture was stirred under a N_2 atmosphere at room temperature for 2 h. Further, the reaction mixture was cooled to -50 ºC, followed by the addition of TMSOTf (0.36 mL, 1.98

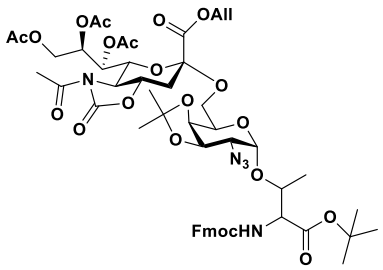

mmol). After 2 h the reaction mixture was neutralized with DIPEA, filtered and washed with brine. The organic layer was dried over sodium sulphate, concentrated in *vacuo*, and the residue was purified by silica gel column chromatography using a mixture of (3:2, v/v) ethyl acetate and hexane as eluent to afford compound **5** (1.3 gm, 66%). ^{1}H NMR (400 MHz, Chloroform-*d*) δ = 7.74 (d, *J* = 7.5 Hz, 2H), 7.63-7.57 (m, 2H), 7.38 (t, *J* = 7.4 Hz, 2H), 7.29 (t, *J* = 7.5 Hz, 2H), 6.02-5.83 (m, 1H), 5.66-5.50 (m, 2H), 5.46-5.34 (m, 1H), 5.37-5.26 (m, 1H), 4.98 (d, *J* = 3.8 Hz, 1H), 4.76-4.54 (m, 4H), 4.51-4.28 (m, 4H), 4.31-4.16 (m, 3H), 4.18-4.09 (m, 1H), 4.13-3.96 (m, 3H), 3.93 (dd, *J* = 10.5, 7.2 Hz, 1H), 3.81-3.64 (m, 2H), 3.47 (dd, *J* = 7.4, 3.8 Hz, 1H), 2.87 (dd, *J* = 12.0, 3.4 Hz, 1H), 2.48 (d, *J* = 4.9 Hz, 3H), 2.11 (s, 3H), 2.10 (s, 3H), 2.01 (s, 3H), 1.48 (s, 9H), 1.47 (s, 3H), 1.36 (d, *J* = 6.4 Hz, 3H), 1.32 (s, 3H). ^{13}C NMR (101 MHz, Chloroform-*d*) δ = 172.11, 170.52, 170.23, 169.93, 169.29, 167.59, 156.77, 153.68, 143.92, 143.76, 141.26, 130.80, 127.71, 127.10, 125.30, 125.23, 120.25, 119.97, 119.30, 110.15, 99.04, 98.90, 82.74, 76.62, 76.06, 74.82, 72.92, 72.57, 72.17, 69.74, 67.51, 67.31, 66.89, 64.45, 62.91, 60.49, 59.39, 59.03, 47.12, 36.03, 27.98, 27.81, 26.03, 24.72, 21.12, 20.76, 19.13, 18.57. HR-ESI-MS (m/z) Calcd for $C_{53}H_{66}N_5O_{21}$ $[M+H]^+$ 1108.4250, found: 1108.4264.

Compound 6

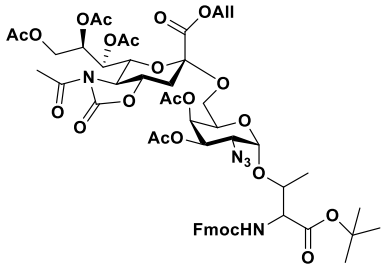

Compound **5** (1.7 gm, 1.53 mmol) was dissolved in a mixture of AcOH/H_2O (4:1, 28 mL) and stirred at RT for 12 h. The reaction mixture was concentrated and the residue was co-evaporated with toluene 3 times. Further the residue was dissolved in a mixture of pyridine/Ac_2O (4:1, 20 mL) and stirred at RT for 12 h. The reaction mixture was concentrated and the residue was purified by silica gel column chromatography using a mixture of ethyl acetate and hexane (3:2) s as an eluent to afford **6** (1.24 gm, 70% over two steps). ^{1}H NMR (400 MHz, Chloroform-*d*) δ = 7.76 (d, *J* = 7.4 Hz, 2H), 7.63 (d, *J* = 7.4 Hz, 2H), 7.39 (t, *J* = 7.5 Hz, 2H), 7.31 (tdd, *J* = 7.4, 3.2, 1.2 Hz, 2H), 5.89 (ddt, *J* = 16.6, 10.2, 6.2 Hz, 1H), 5.67 (d, *J* = 9.6 Hz, 1H), 5.56 (dd, *J* = 8.4, 1.8 Hz, 1H), 5.42-5.34 (m, 4H), 5.31 (dd, *J* = 11.3, 3.3 Hz, 1H), 5.12 (d, *J* = 3.8 Hz, 1H), 4.68-4.61 (m, 3H), 4.48-4.31 (m, 4H), 4.30-4.24 (m, 2H), 4.23-4.17 (m, 1H), 4.05-3.93 (m, 2H), 3.89 (dd, *J* = 10.5, 7.2 Hz, 1H), 3.69 (dd, *J* = 11.2, 9.4 Hz, 1H), 3.62 (dd, *J* = 11.2, 3.7 Hz, 1H), 3.32 (dd, *J* = 10.5, 4.5 Hz, 1H), 2.79 (dd, *J* = 12.1, 3.5 Hz, 1H), 2.48 (s, 3H), 2.14 (s, 6H), 2.11 (d, *J* = 3.4 Hz, 1H), 2.08 (s, 3H), 2.07 (s, 3H), 2.01 (s, 3H), 1.50 (s, 9H), 1.38 (d, *J* = 6.4 Hz,

3H). ^{13}C NMR (101 MHz, Chloroform-*d*) δ = 172.10, 170.61, 170.25, 170.14, 170.09, 169.96, 169.28, 167.82, 156.95, 153.70, 143.98, 143.94, 141.35, 130.60, 127.79, 127.21, 127.18, 125.40, 121.17, 120.05, 99.72, 98.96, 82.95, 76.69, 75.78, 74.82, 71.79, 68.69, 68.41, 68.20, 67.95, 67.59, 67.12, 64.55, 63.28, 59.49, 59.04, 57.75, 47.19, 36.39, 28.07, 24.81, 21.20, 21.09, 20.82, 20.68, 19.07. HR-ESI-MS (m/z) Calcd for $C_{54}H_{66}N_5O_{23}$ $[M+H]^+$ 1152.4149, found: 1152.4157.

Compound 7

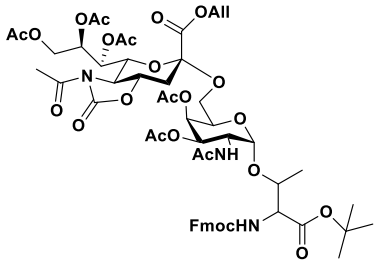

Compound **7** (1.4 gm, 1.22 mmol) was dissolved in 3:2:1 (v/v) mixture of THF/AcOH/Ac_2O (5 mL) and to this solution, Zn (350 mg), saturated $CuSO_4$ (50 µL) were added. The resulting mixture was stirred at room temperature for 4 hours, diluted with ethyl acetate and filtered through celite pad. The organic layer was washed with saturated sodium bicarbonate, brine and dried over Na_2SO_4. The crude compound was purified by silica gel column chromatography using a mixture of (3:2, v/v) ethyl acetate and hexane as eluent to afford the desired product **8** (0.97 gm, 69%) as a white solid. ^{1}H NMR (400 MHz, Chloroform-*d*) δ = 7.77 (d, *J* = 7.5 Hz, 2H), 7.63 (d, *J* = 5.9 Hz, 2H), 7.40 (t, *J* = 7.4 Hz, 2H), 7.32 (t, *J* = 7.4 Hz, 2H), 5.99 (d, *J* = 9.9 Hz, 1H), 5.89 (ddt, *J* = 16.7, 10.3, 6.2 Hz, 1H), 5.65 (d, *J* = 9.3 Hz, 1H), 5.58 (dd, *J* = 8.2, 1.8 Hz, 1H), 5.40-5.31 (m, 4H), 5.05 (dd, *J* = 11.4, 3.1 Hz, 1H), 4.89 (d, *J* = 3.7 Hz, 1H), 4.66-4.59 (m, 4H), 4.45 (dd, *J* = 7.0, 2.2 Hz, 2H), 4.35 (dd, *J* = 12.3, 2.8 Hz, 1H), 4.27-4.19 (m, 3H), 4.16 (t, *J* = 6.2 Hz, 1H), 4.07-3.93 (m, 2H), 3.86 (dd, *J* = 10.4, 7.0 Hz, 1H), 3.68 (dd, *J* = 11.2, 9.4 Hz, 1H), 3.36 (dd, *J* = 10.4, 4.8 Hz, 1H), 2.79 (dd, *J* = 12.1, 3.6 Hz, 1H), 2.47 (s, 3H), 2.14 (s, 3H), 2.12 (s, 3H), 2.08 (s, 3H), 2.01 (s, 3H), 1.99 (s, 3H), 1.98 (s, 3H), 1.45 (s, 9H), 1.35 (d, *J* = 6.3 Hz, 3H). ^{13}C NMR (101 MHz, Chloroform-*d*) δ = 172.04, 171.08, 170.69, 170.45, 170.37, 170.20, 170.09, 170.03, 167.67, 156.63, 153.73, 143.90, 143.81, 141.40, 130.62, 127.87, 127.20, 125.17, 121.07, 120.14, 100.19, 99.02, 83.22, 75.77, 74.83, 71.75, 69.06, 68.89, 68.65, 67.74, 67.34, 67.11, 64.48, 63.18, 59.17, 59.05, 47.27, 36.30, 28.19, 24.80, 23.39, 21.19, 21.03, 20.93, 20.83, 20.79, 18.72. HR-ESI-MS (m/z) Calcd for $C_{56}H_{70}N_3O_{24}$ $[M+H]^+$ 1168.4349, found: 1168.4353.

Compound 8

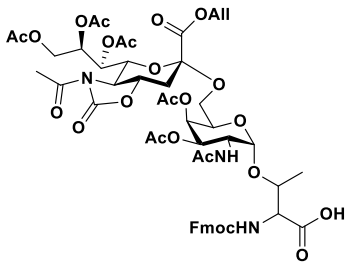

Compound **8** (0.5 gm, 0.43 mmol) was dissolved in 1:1 (v/v) mixture of DCM/TFA (10 mL) and stirred at room temperature for 4 hours. The reaction mixture was concentrated, and the residue was co-evaporated with toluene and dried under a high vacuum for 12 h and used in SPPS without further purification.

Solid phase peptide synthesis

The commercially available Rink amide resin with loading value 0.3-0.4 mmol/g and standard Fmoc chemistry was employed to synthesize the STn-glycopeotide. The resin-bound Fmoc group was first deprotected using 20% piperidine in DMF. Then, the coupling reaction was carried out using the *in situ* active ester method, using HBTU as a coupling reagent, HOBt as a racemization suppresser, and DIPEA as a base. All the materials used were of peptide synthesis grade (Sigma-Aldrich) and was used without further purification.

STn-glyocpeptide was synthesized using standard Fmoc chemistry protocol. The resin was pre-swollen in dichloromethane for 12 hours then washed with DMF. Each step of Fmoc deprotection was done by using 20% piperidine in DMF. Each amino acid coupling was carried out using HBTU (3 eq), HOBT (3 eq) and DIPEA (7-8 eq) cocktail solution in DMF for 2 h at room temperature. The coupling reaction was repeated in NMP for better yield. The fully synthesized glyco-peptide was cleaved and partially deprotected using cocktail solution (10 mL) of TFA/H_2O/Phenol/TIPS [8.5:5:5:2.5 (v/v)] at room temperature.

Compound 9

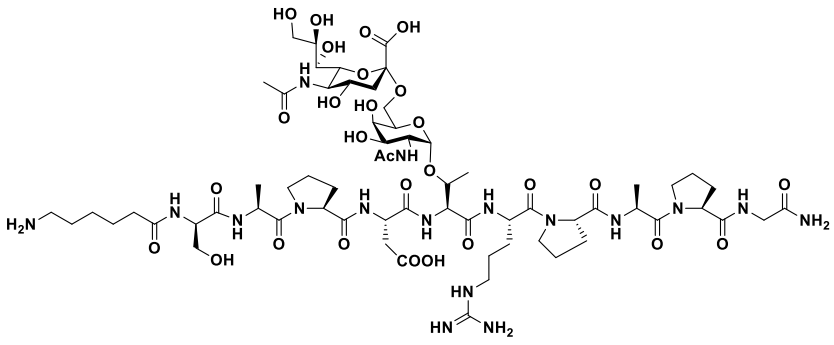

The crude glycopeptide was deacytelated using lithium hydroxide in a mixture of 3:1 (v/v) H_2O/MeOH at room temperature for 12 h. The reaction mixture was quenched with acetic acid, concentrated and purified by RP-HPLC on a semi-preparative C-18 reverse phase column using a linear gradient of 0-100 solvent B (95% acetonitrile + 5% water + 0.1% TFA) and A (95% water + 5% water + 0.1 % TFA) over 45 min. The purified fraction was lyophilized to afford STn glycopeptide as a white solid. ^{1}H NMR (600 MHz, Deuterium

Oxide) δ = 4.68 (t, *J* = 7.2 Hz, 1H), 4.57 (q, *J* = 7.0 Hz, 1H), 4.51-4.45 (m, 3H), 4.38-4.26 (m, 5H), 4.01 (ddd, *J* = 27.5, 9.6, 3.7 Hz, 2H), 3.90-3.67 (m, 12H), 3.64-3.54 (m, 6H), 3.51-3.49 (m, 2H), 3.15 (hept, *J* = 7.0 Hz, 2H), 2.92 (t, *J* = 7.6 Hz, 2H), 2.71 (dd, *J* = 16.1, 7.5 Hz, 1H), 2.64 (dd, *J* = 12.4, 4.6 Hz, 1H), 2.54 (dd, *J* = 16.1, 6.9 Hz, 1H), 2.30-2.20 (m, 5H), 2.03-1.87 (m, 13H), 1.85-1.78 (m, 3H), 1.69-1.55 (m, 8H), 1.35-1.29 (m, 8H), 1.22 (d, *J* = 6.3 Hz, 3H). ^{13}C NMR (151 MHz, Deuterium Oxide) δ = 177.59, 176.95, 174.83, 174.78, 174.05, 173.80, 173.53, 173.24, 172.59, 171.21, 171.08, 171.03, 156.64, 100.11, 98.72, 75.83, 72.40, 71.65, 69.89, 68.53, 68.15, 67.71, 63.90, 62.46, 61.02, 60.63, 60.16, 59.76, 57.02, 55.26, 51.72, 51.18, 51.03, 49.52, 47.70, 47.57, 41.93, 40.35, 40.03, 39.13, 38.44, 34.86, 29.33, 29.18, 29.13, 27.10, 26.31, 24.91, 24.61, 24.55, 24.45, 23.97, 22.22, 21.91, 18.33, 15.49, 14.95. HR-ESI-MS (m/z) Calcd for $C_{65}H_{108}N_{17}O_{28}$ $[M+H]^+$ 1574.7550, found: 1574.7559.

5.5 References:

1. Ohtsubo, K.; Marth, J. D. Glycosylation in cellular mechanisms of health and disease. *Cell*. **2006**, *126*, 855-67.
2. Varki, A.; Cummings, R. D.; Esko, J. D.; Freeze, H. H.; Stanley, P.; Bertozzi, C. R.; Hart, G. W.; Etzler, M. E. *Essentials of Glycobiology*. 2nd ed. Cold Spring Harbor New York. 2009.
3. Varki, A. Biological roles of glycans. *Glycobiology*. **2017**, *27*, 3-49.
4. Reily, C.; Stewart, T. J.; Renfrow, M. B.; Novak, J. Glycosylation in health and disease. *Nat Rev Nephrol*. **2019**, *15*, 346-366.
5. Hakomori, S. Tumor-associated carbohydrate antigens defining tumor malignancy: basis for development of anti-cancer vaccines. *Adv Exp Med Biol*. **2001**, *491*, 369-402.
6. Cazet, A.; Julien, S.; Bobowski, M.; Burchell, J.; Delannoy, P. Tumour-associated carbohydrate antigens in breast cancer. *Breast Cancer Res*. **2010**, *12*, 204.
7. Astronomo, R. D.; Burton, D. R. Carbohydrate vaccines: developing sweet solutions to sticky situations? *Nat Rev Drug Discov*. **2010**, *9*, 308-24.
8. Julien, S.; Picco, G.; Sewell, R.; Vercoutter-Edouart, A. S.; Tarp, M.; Miles, D.; Clausen, H.; Taylor-Papadimitriou, J.; Burchell, J. M. Sialyl-Tn vaccine induces antibody-mediated tumour protection in a relevant murine model. *Br J Cancer*. **2009**, *100*, 1746-54.
9. Song, C,; Zheng, X. J.; Liu, C. C.; Zhou, Y.; Ye, X. S. A cancer vaccine based on fluorine-modified sialyl-Tn induces robust immune responses in a murine model. *Oncotarget*. **2017**, *8*, 47330-47343.

10. Shi, M,; Kleski, K. A.; Trabbic, K. R.; Bourgault, J. P.; Andreana, P. R. Sialyl-Tn Polysaccharide A1 as an Entirely Carbohydrate Immunogen: Synthesis and Immunological Evaluation. *J Am Chem Soc.* **2016**, *138*, 14264-14272.
11. Lang, S,; Huang, X. Carbohydrate Conjugates in Vaccine Developments. *Front Chem.* **2020**, *8*, 284.
12. Kaiser, A.; Gaidzik, N.; Westerlind, U.; Kowalczyk, D.; Hobel, A.; Schmitt, E.; Kunz, H. A synthetic vaccine consisting of a tumor-associated sialyl-T(N)-MUC1 tandem-repeat glycopeptide and tetanus toxoid: induction of a strong and highly selective immune response. *Angew Chem Int Ed Engl*. **2009**, *48*, 7551-5.
13. McDonald, D. M.; Byrne, S. N.; Payne, R. J. Synthetic self-adjuvanting glycopeptide cancer vaccines. *Front Chem*. **2015**, *3*, 60.
14. Beckwith, D, M.; Cudic, M. Tumor-associated O-glycans of MUC1: Carriers of the glyco-code and targets for cancer vaccine design. *Semin Immunol*. **2020**, *47*, 101389.
15. Corcilius, L.; Payne, R. J. Stereoselective synthesis of sialylated tumor-associated glycosylamino acids. *Org Lett*. **2013**, *15*, 5794-7.

5.6 NMR and HRMS Spectra:

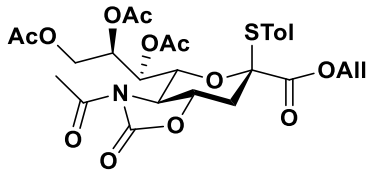

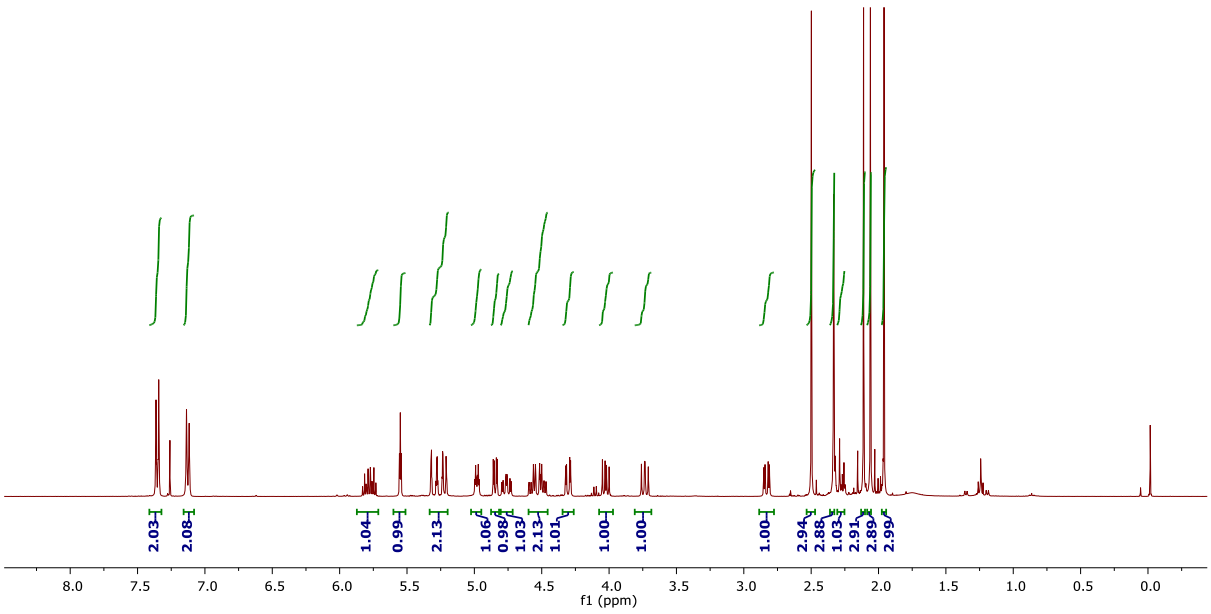

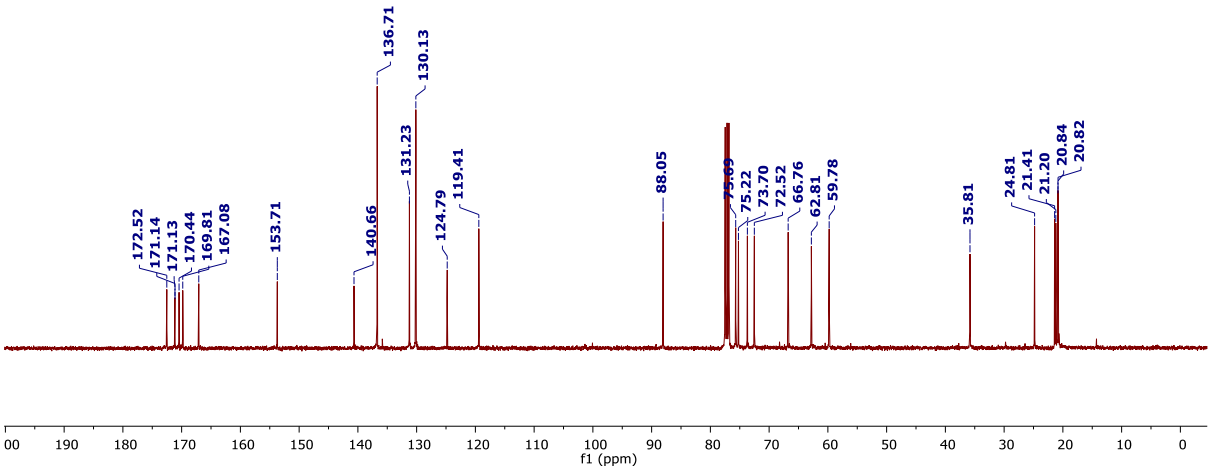

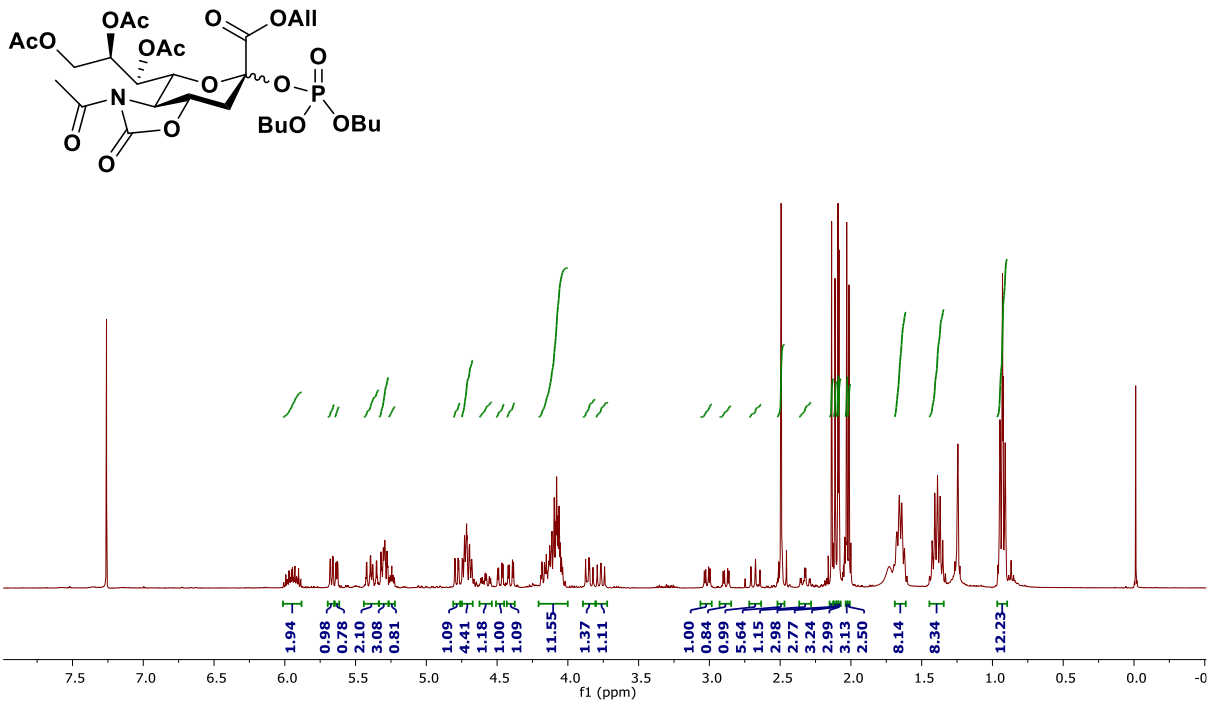
1.94
0.98
0.78
2.10
3.08
0.81
1.09
4.41
1.18
1.00
1.09
11.55
1.37
1.11
1.00
0.84
0.99
5.64
1.15
2.98
2.77
3.24
2.99
3.13
2.50
8.14
8.34
12.23
f1 (ppm)

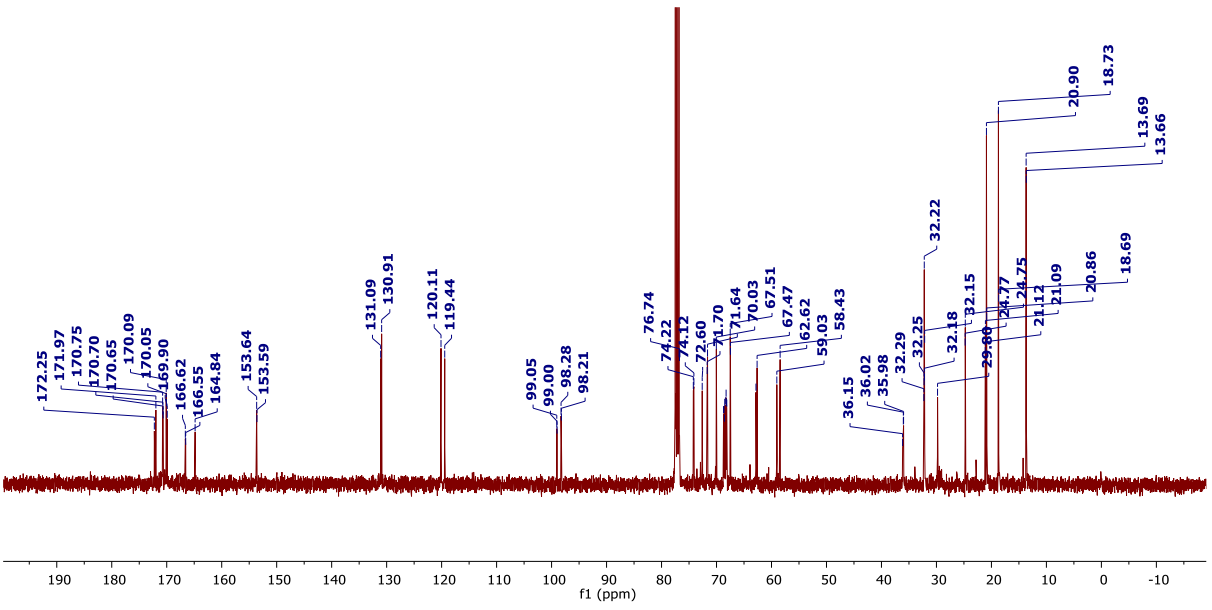
172.25
171.97
170.75
170.70
170.65
170.09
170.05
169.90
166.62
166.55
164.84
153.64
153.59
131.09
130.91
120.11
119.44
99.05
99.00
98.28
98.21
76.74
74.22
74.12
72.60
71.70
71.64
70.03
67.51
67.47
62.62
59.03
58.43
36.15
36.02
35.98
32.29
32.25
32.22
32.18
32.15
29.80
24.77
24.75
21.12
21.09
20.90
20.86
18.73
18.69
13.69
13.66
f1 (ppm)

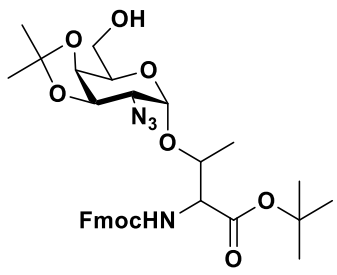
OH
O
O
O
N3
O
FmocHN
O
O

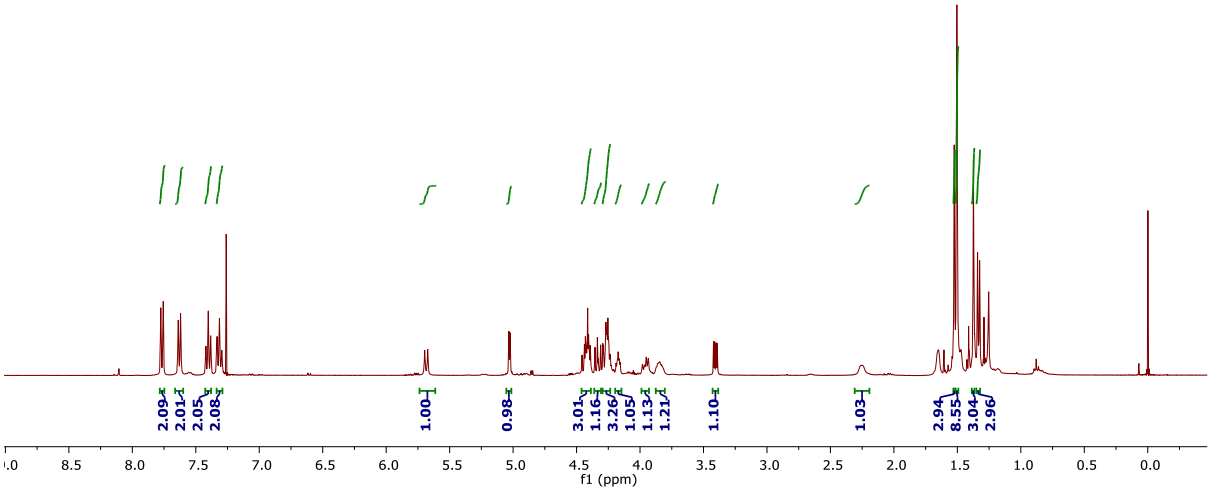
2.09
2.01
2.05
2.08
1.00
0.98
3.01
1.16
3.26
1.05
1.13
1.21
1.10
1.03
2.94
8.55
3.04
2.96
f1 (ppm)

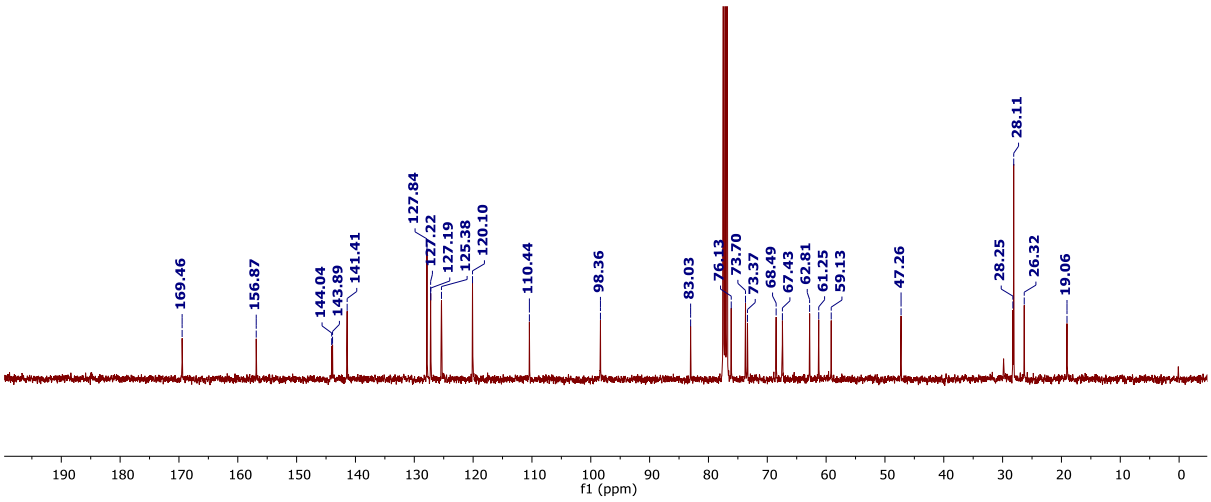
169.46
156.87
144.04
143.89
141.41
127.84
127.22
127.19
125.38
120.10
110.44
98.36
83.03
76.13
73.70
73.37
68.49
67.43
62.81
61.25
59.13
47.26
28.25
28.11
26.32
19.06
f1 (ppm)

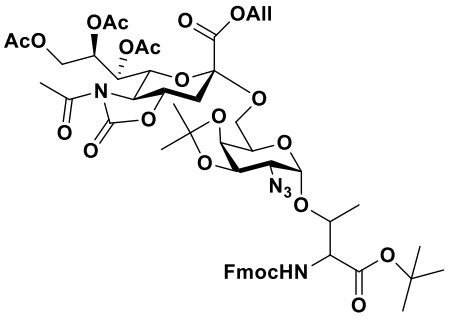
AcO
OAc
OAc
O
OAll
O
N
O
O
O
O
O
O
O
O
O
N3
O
FmocHN
O
O

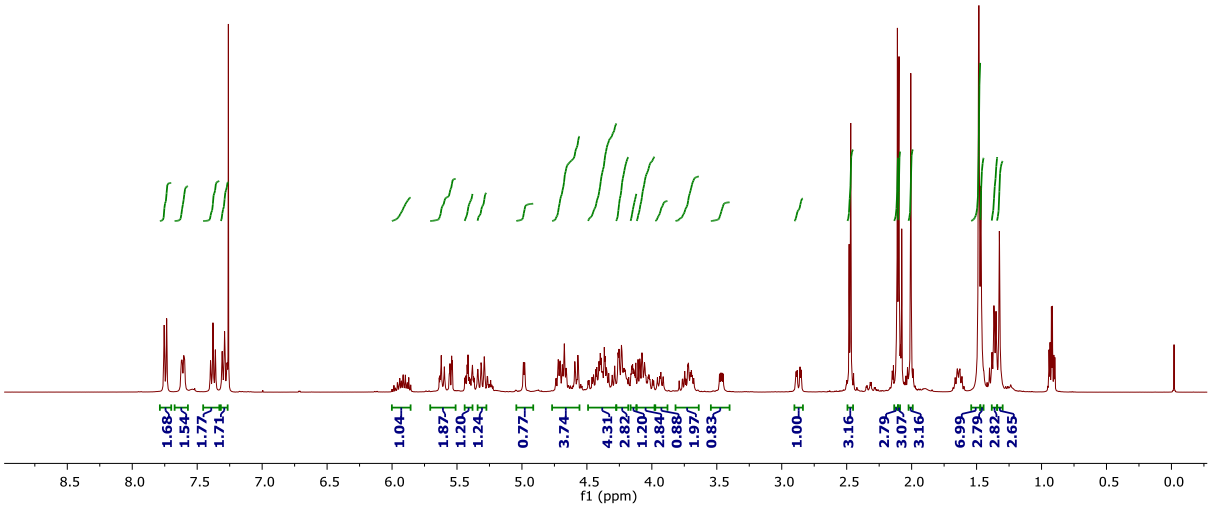
1.68
1.54
1.77
1.71
1.04
1.87
1.20
1.24
0.77
3.74
4.31
2.82
1.20
2.84
0.88
1.97
0.83
1.00
3.16
2.79
3.07
3.16
6.99
2.79
2.82
2.65
8.5
8.0
7.5
7.0
6.5
6.0
5.5
5.0
4.5
4.0
3.5
3.0
2.5
2.0
1.5
1.0
0.5
0.0
f1 (ppm)

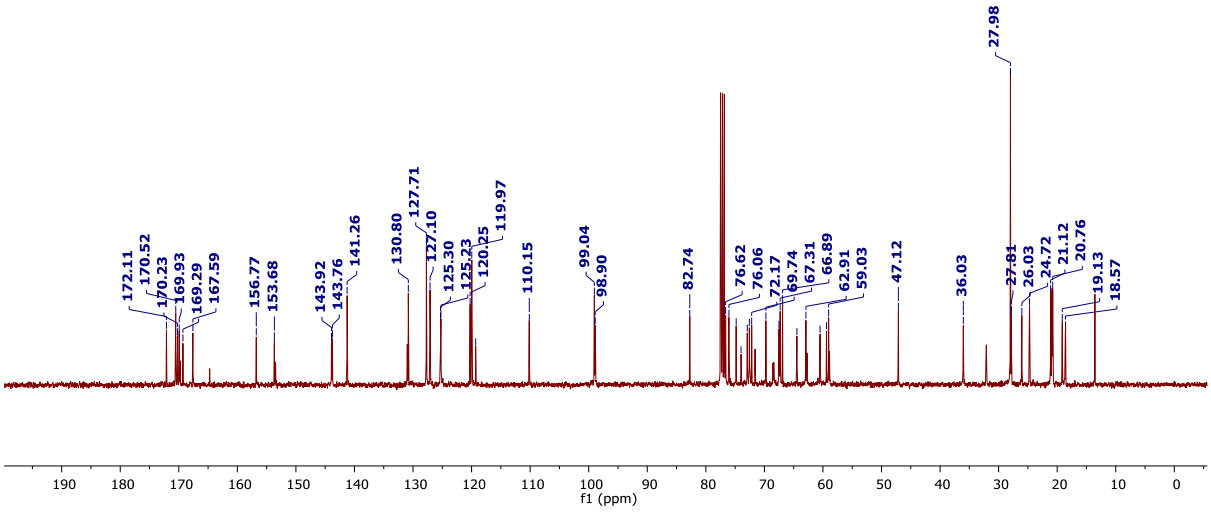
172.11
170.52
170.23
169.93
169.29
167.59
156.77
153.68
143.92
143.76
141.26
130.80
127.71
127.10
125.30
125.23
120.25
119.97
110.15
99.04
98.90
82.74
76.62
76.06
72.17
69.74
67.31
66.89
62.91
59.03
47.12
36.03
27.98
27.81
26.03
24.72
21.12
20.76
19.13
18.57
190
180
170
160
150
140
130
120
110
100
90
80
70
60
50
40
30
20
10
0
f1 (ppm)

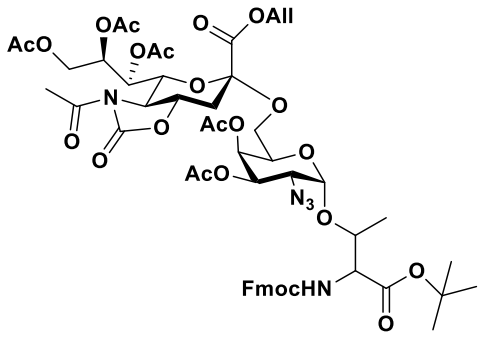
OAc
AcO
OAc
O
OAll
N
O
O
AcO
O
O
AcO
N3
O
FmocHN
O
O

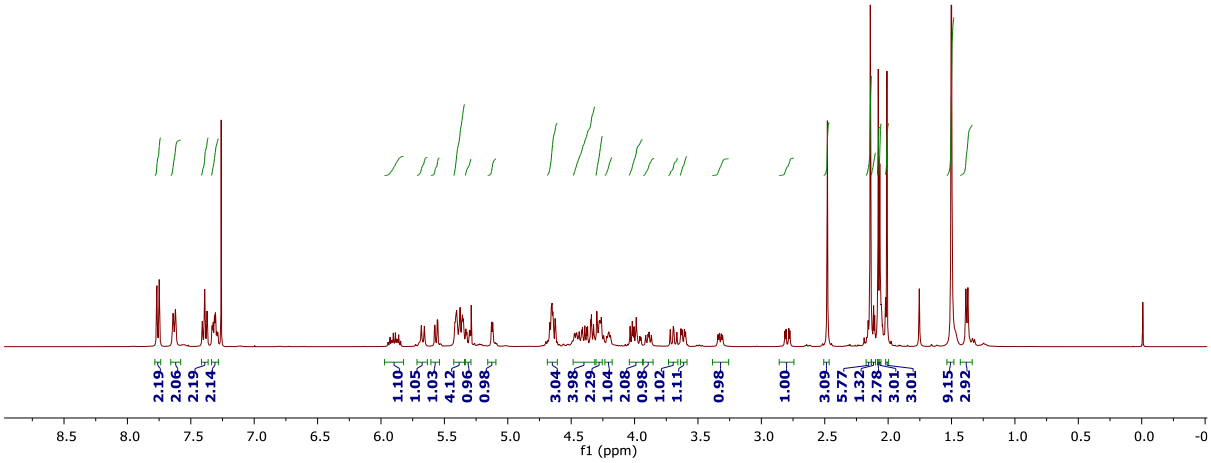
2.19
2.06
2.19
2.14
1.10
1.05
1.03
4.12
0.96
0.98
3.04
3.98
2.29
1.04
2.08
0.98
1.02
1.11
0.98
1.00
3.09
5.77
1.32
2.78
3.01
3.01
9.15
2.92
f1 (ppm)

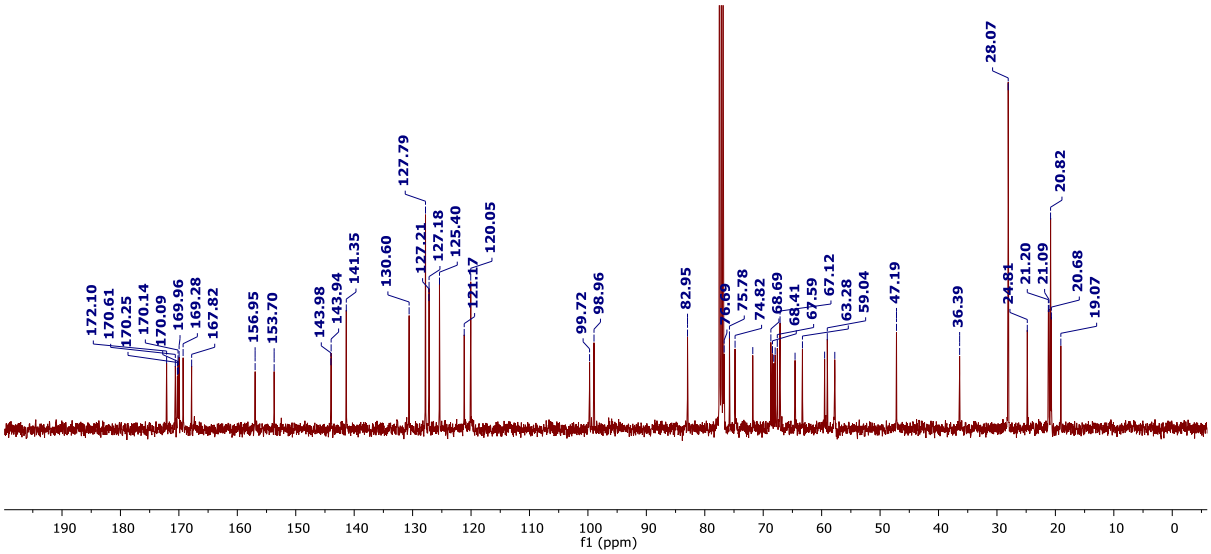
172.10
170.61
170.25
170.14
170.09
169.96
169.28
167.82
156.95
153.70
143.98
143.94
141.35
130.60
127.79
127.21
127.18
125.40
121.17
120.05
99.72
98.96
82.95
76.69
75.78
74.82
68.69
68.41
67.59
67.12
63.28
59.04
47.19
36.39
28.07
24.81
21.20
21.09
20.82
20.68
19.07
f1 (ppm)

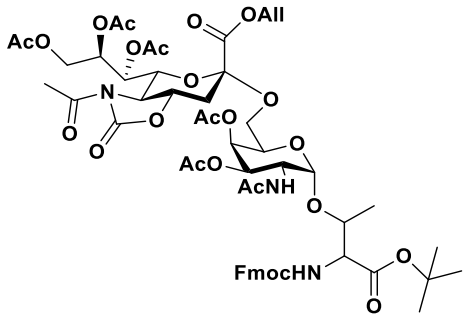
AcO
OAc
OAc
O
OAll
O
N
O
O
O
O
AcO
AcO
O
AcNH
O
FmocHN
O
O

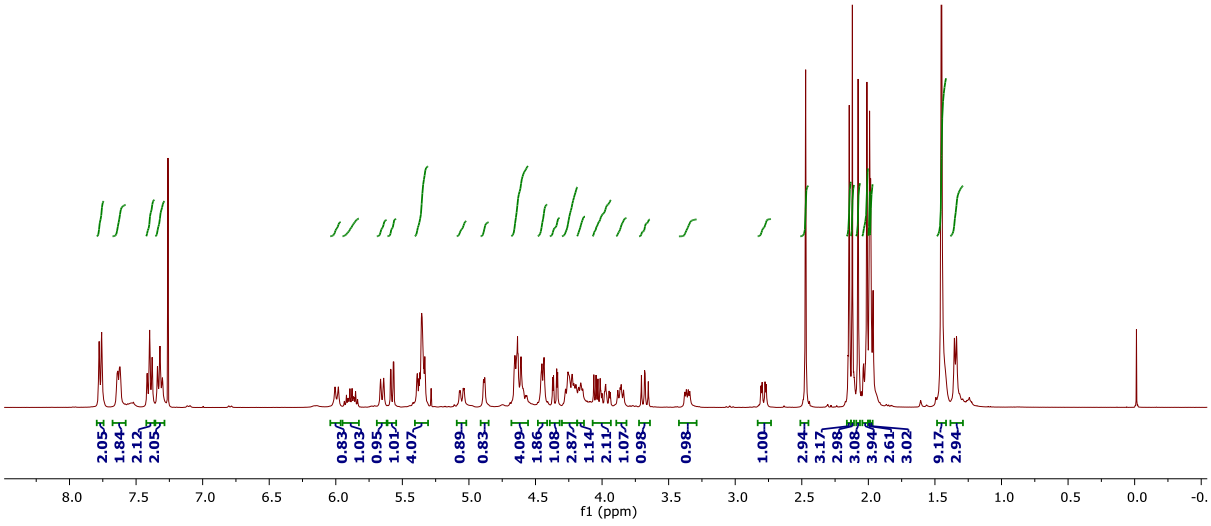
2.05
1.84
2.12
2.05
0.83
1.03
0.95
1.01
4.07
0.89
0.83
4.09
1.86
1.08
2.87
1.14
2.11
1.07
0.98
0.98
1.00
2.94
3.17
2.98
3.08
3.94
2.61
3.02
9.17
2.94
f1 (ppm)

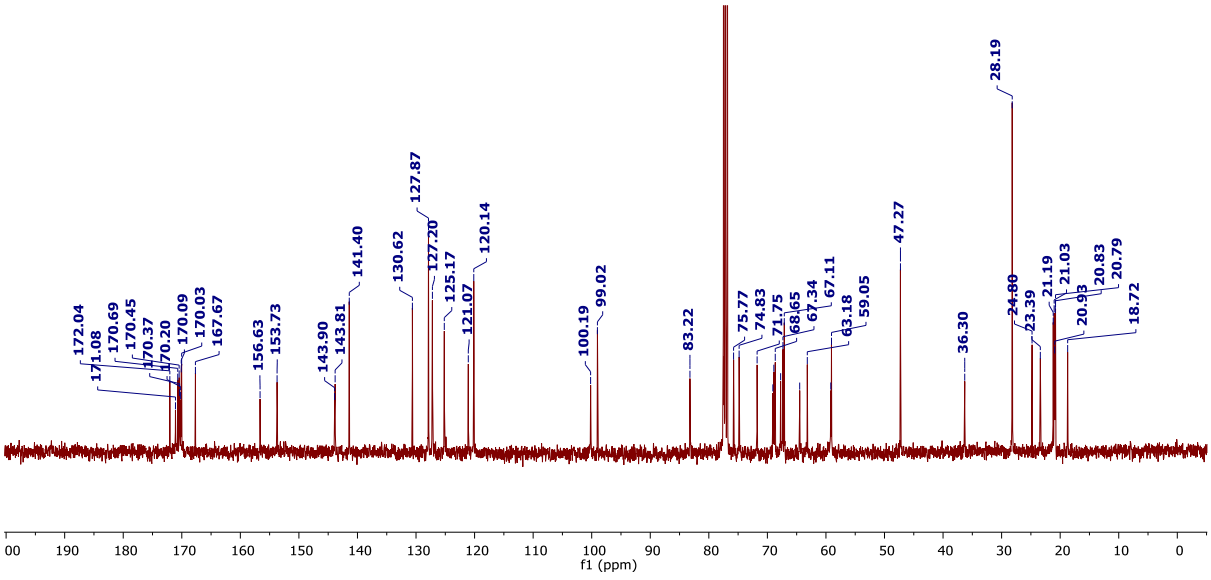
172.04
171.08
170.69
170.45
170.37
170.20
170.09
170.03
167.67
156.63
153.73
143.90
143.81
141.40
130.62
127.87
127.20
125.17
121.07
120.14
100.19
99.02
83.22
75.77
74.83
71.75
68.65
67.34
67.11
63.18
59.05
47.27
36.30
28.19
24.80
23.39
21.19
21.03
20.93
20.83
20.79
18.72
f1 (ppm)

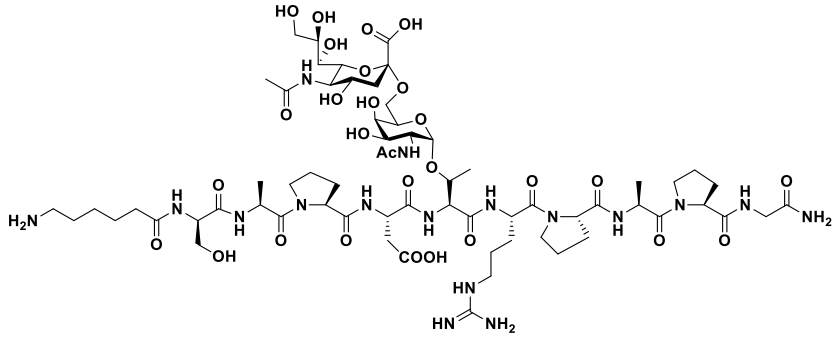

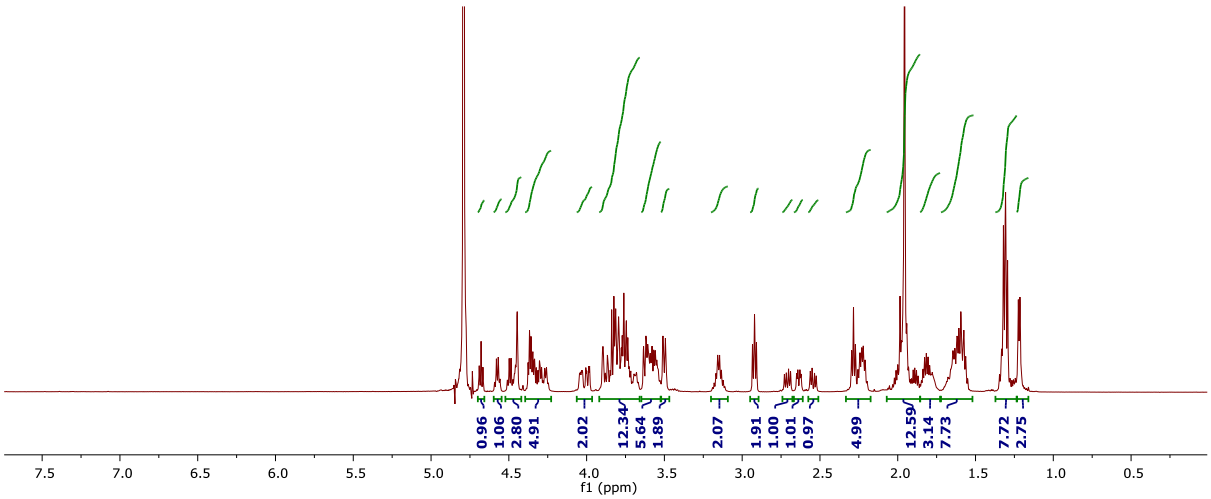
0.96
1.06
2.80
4.91
2.02
12.34
5.64
1.89
2.07
1.91
1.00
1.01
0.97
4.99
12.59
3.14
7.73
7.72
2.75
f1 (ppm)

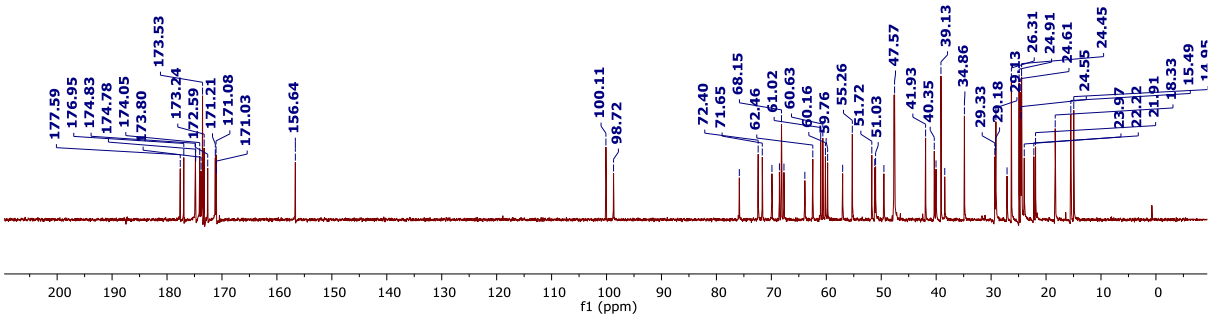
177.59
176.95
174.83
174.78
174.05
173.80
173.53
173.24
172.59
171.21
171.08
171.03
156.64
100.11
98.72
72.40
71.65
68.15
62.46
61.02
60.63
60.16
59.76
55.26
51.72
51.03
47.57
41.93
40.35
39.13
34.86
29.33
29.18
29.13
26.31
24.91
24.61
24.55
24.45
23.97
22.22
21.91
18.33
15.49
f1 (ppm)

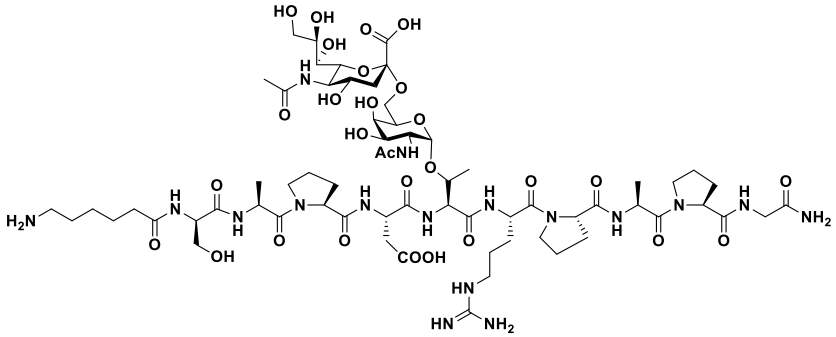

HRMS

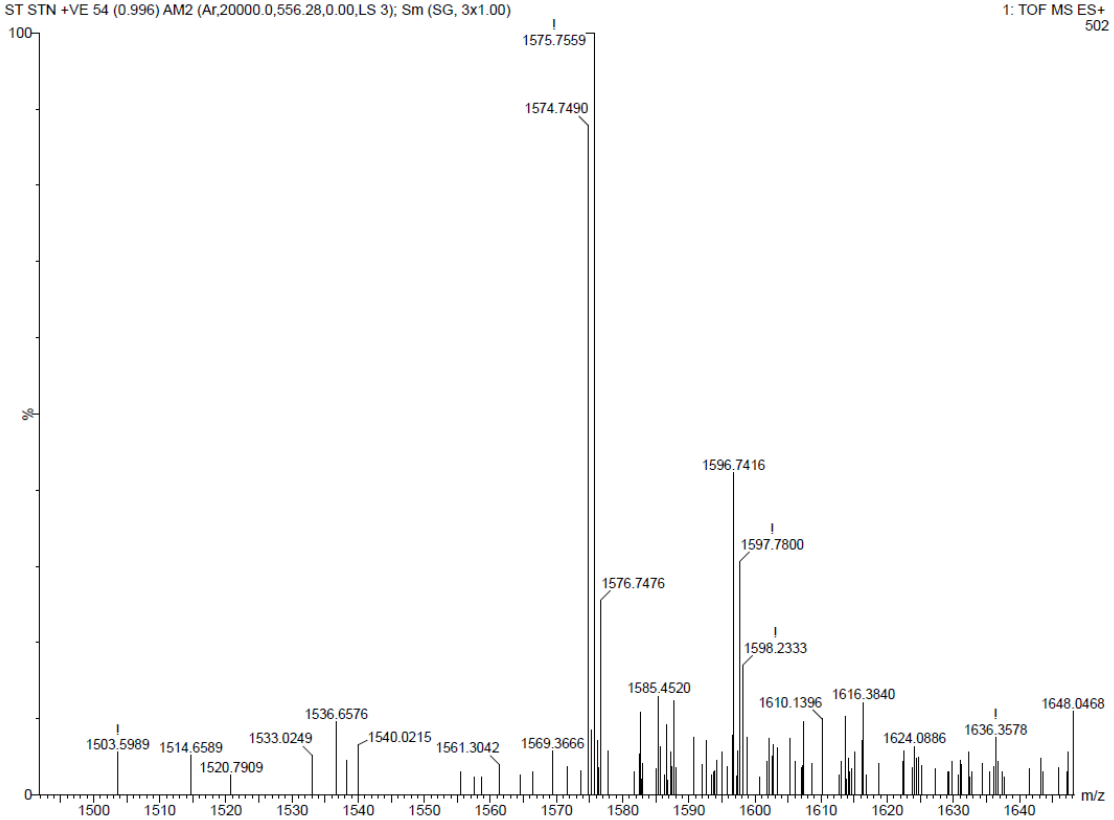
ST STN +VE 54 (0.996) AM2 (Ar,20000.0,556.28,0.00,LS 3); Sm (SG, 3x1.00)
1: TOF MS ES+
502
100
%
0
1575.7559
1574.7490
1596.7416
1597.7800
1576.7476
1598.2333
1585.4520
1610.1396
1616.3840
1648.0468
1636.3578
1624.0886
1536.6576
1503.5989
1514.6589
1533.0249
1540.0215
1561.3042
1569.3666
1520.7909
1500
1510
1520
1530
1540
1550
1560
1570
1580
1590
1600
1610
1620
1630
1640
m/z